UNIVERSITÉ DE STRASBOURG

EDSC
École Doctorale des
Sciences Chimiques

ÉCOLE DOCTORALE DES SCIENCES CHIMIQUES

Institut de Chimie UMR 7177

THÈSE présentée par :

Bruno SENJEAN

soutenue le : **24 septembre 2018**

pour obtenir le grade de : **Docteur de l'université de Strasbourg**

Discipline/ Spécialité : Chimie / Chimie Théorique

Development of new embedding techniques for strongly correlated electrons: from in-principle-exact formulations to practical approximations.

THÈSE dirigée par :	
M. FROMAGER Emmanuel	Maître de Conférences, Université de Strasbourg, France
RAPPORTEURS :	
Mme. GORI-GIORGI Paola	Professeur, Vrije Universiteit Amsterdam, The Netherlands
M. AYERS Paul	Professeur, McMaster University, Hamilton, Canada
EXAMINATEURS :	
Mme. REINING Lucia	Directrice de recherche au CNRS, ETSF Palaiseau, Paris, France
M. SAVIN Andreas	Chercheur émérite, UPMC Sorbonne Université, Paris, France
M. ROBERT Vincent	Professeur, Université de Strasbourg, France

Université de Strasbourg

Bruno SENJEAN

EDSC
École Doctorale des
Sciences Chimiques

Development of new embedding techniques for strongly correlated electrons: from in-principle-exact formulations to practical approximations.

Résumé

Ce mémoire traite du développement et de l'implémentation de nouvelles méthodes visant à décrire la corrélation électronique forte dans les molécules et les solides. Après avoir introduit l'état de l'art des méthodes utilisées en chimie quantique et en physique de la matière condensée, une nouvelle méthode hybride combinant théorie de la fonction d'onde et théorie de la fonctionnelle de la densité (DFT) est présentée et s'intitule "site-occupation embedding theory" (SOET). Celle-ci est appliquée au modèle de Hubbard à une dimension. Ensuite, le problème du gap fondamental est revisité en DFT pour les ensembles, où la dérivée discontinue est réécrite comme une fonctionnelle de la densité de l'état fondamental. Enfin, une extension à la chimie quantique est proposée, basée sur une fonction d'onde de séniorité zéro complémentée par une fonctionnelle de la matrice densité, et exprimée dans la base des orbitales naturelles.

Mots clefs: Chimie Quantique – Physique de la matière condensée – corrélation forte – théorie de la fonction d'onde – théorie de la fonctionnelle de la densité – méthode d'embedding – modèle de Hubbard.

Résumé en anglais

The thesis deals with the development and implementation of new methods for the description of strong electron correlation effects in molecules and solids. After introducing the state of the art in quantum chemistry and in condensed matter physics, a new hybrid method so-called "site-occupation embedding theory" (SOET) is presented and based on the merging of wavefunction theory and density functional theory (DFT). Different formulations of this theory are described and applied to the one-dimensional Hubbard model. In addition, a novel ensemble density functional theory approach has been derived to extract the fundamental gap exactly. In the latter approach, the infamous derivative discontinuity is reformulated as a derivative of a weight-dependent exchange-correlation functional. Finally, a quantum chemical extension of SOET is proposed and based on a seniority-zero wavefunction, completed by a functional of the density matrix and expressed in the natural orbital basis.

Keywords: Quantum chemistry – condensed matter physics – strongly correlated electrons – wavefunction theory – density functional theory – embedding methods – Hubbard model.

“In these bodies we will live, in these bodies we will die,
Where you invest your love, you invest your life”
Mumford & Sons, Gentlemen of the road.

Remerciements

Après ces trois belles années passées dans le laboratoire de chimie quantique de Strasbourg, il est enfin temps de remercier toutes les personnes qui m'ont aidé dans la réalisation de cette thèse. Que ce soit dans le travail ou dans les loisirs, essentiels pour garder ma bonne humeur ! Tout d'abord, merci aux membres du jury d'avoir accepté de juger mon travail. Merci à toi, Paul Ayers, d'avoir bien voulu faire ce long voyage depuis le Canada ! Merci également à vous, Paola Gori Giorgi, Lucia Reining et Andreas Savin. J'apprécie grandement votre implication pour cette soutenance, malgré tout le travail que vous avez déjà. Je suis persuadé que nous aurons de belles discussions scientifiques durant votre séjour. Merci aussi à toi Vincent, de faire partie de mon jury mais avant tout pour toute ta gentillesse, ton soutien, et ta présence positive durant toutes ces 5 dernières années. Tes calambours et contrepèteries me manqueront !

Je ne remercierai jamais assez mon directeur de thèse, Emmanuel Fromager. Manu, c'est d'abord en première année de Master que je suis arrivé au laboratoire pour faire un stage sous ta tutelle. L'enthousiasme que tu partages en parlant de ton travail m'a immédiatement marqué, et s'est avéré être contagieux. Chaque discussion scientifique que l'on avait me motivait à avancer. C'est pour cette raison, combinée à mon goût prononcé pour la théorie, que j'ai décidé de continuer à travailler avec toi en Master 2 et en thèse. Tu as toujours été de bon conseil, et tu as toujours été présent pour répondre à mes questions, aussi simples soient elles. Tu as su me rendre indépendant en me laissant suffisamment de liberté pour concrétiser mes idées, tout en contrôlant l'avancée du projet de thèse. Bref, ton encadrement était parfait pour moi, il n'aurait pas pu mieux se passer. Mais assez parlé de travail. Tu es également pour moi un ami, nous avons partagé de nombreuses discussions amicales et trinqué de nombreuses fois à notre santé. Je n'ai jamais eu l'impression que tu étais mon "supérieur hiérarchique", je te vois plus comme un ami qui en connait bien plus que moi en physique et en chimie quantique. J'espère de tout coeur que notre collaboration scientifique se poursuivra, et qu'on aura encore de nombreuses occasions pour boire à la santé de ta famille !

En parlant de collaboration, je tiens également à remercier très chaleureusement mes amis japonais Masahisa Tsuchiizu et Naoki Nakatani. Vous avez rendu mes voyages au Japon inoubliables. Un peu moins loin (Montpellier), merci à toi Matthieu Saubanère, pour tous tes conseils, toutes les discussions skype, et ton intérêt pour nos travaux. Vous avez tous les trois contribué à la richesse de cette thèse, et je souhaite que notre collaboration continue autant que possible.

Revenons-en au laboratoire, où je remercie Paola (Sager), que ce soit pour le côté administratif dans lequel je suis très rapidement perdu, pour les pauses cafés, pour l'organisation de tous nos repas de labo, pour ton aide dans toutes les galères qu'on a eues pendant nos voyages, et pour être restée tard au labo pour l'impression de ma thèse ! Merci Sylvie pour ton aide en informatique, et pour ta bonne humeur. Merci à tous les autres membres du laboratoire, Christophe, Chantal, Etienne et Roberto, avec qui j'ai passé de bons moments. Vous avez tous contribué à ce que ces années au laboratoire se passent merveilleusement bien. Merci à mes jeunes collègues et amis Killian et Laurent. Sans vous, j'aurai été bien seul dans ce grand bureau ! Merci Mauricio pour toute ton aide sur la RDMFT, c'était un plaisir d'avoir ri et travaillé avec toi !

Enfin, je remercie l'Alcanes qui fait tourner la Kfet de chimie. C'est pour moi le meilleur endroit du campus ! Ça va me manquer de ne plus donner de tutoriels aux étudiants de licence en chimie quantique... Merci aussi à mon club de badminton, essentiel pour garder une bonne condition physique et mentale ! On a bien rigolé, et j'espère que vous réussirez à vous maintenir en prénat !! Je remercie aussi ma famille, en particulier mes parents qui sont formidables, et mes amis pour leur soutien. La meilleure pour la fin... Merci Hana pour tout, pour ta patience, ton amour, ton soutien, et ta gentillesse... Et merci de me suivre à Amsterdam pour mon postdoc !

Table of Contents

Liste des publications

Only the articles denoted in **bold** are discussed in this thesis. Note that the article **[BS3]** has received the Molecular Physics Longuet-Higgins Early Career Researcher Prize 2017.

[BS1] B. Senjean, S. Knecht, H. J. A. Jensen, E. Fromager. "Linear interpolation method in ensemble Kohn-Sham and range-separated density-functional approximations for excited states". *Phys. Rev. A*, **2015** 92(1), 012518.

[BS2] B. Senjean, E. D. Hedegard, M. M. Alam, S. Knecht, E. Fromager. "Combining linear interpolation with extrapolation methods in range-separated ensemble density functional theory". *Mol. Phys.* **2016**, 114, 968.

[BS3] B. Senjean, M. Tsuchiizu, V. Robert, E. Fromager. "Local density approximation in site-occupation embedding theory". *Mol. Phys.* **2017**, 115, 48.

[BS3-bis] B. Senjean. "Molecular Physics Longuet-Higgins Early Career Researcher Prize 2017 winner profile", *Mol. Phys.*. **2018**, 116, 2145.

[BS4] B. Senjean, N. Nakatani, M. Tsuchiizu, E. Fromager. "Site-Occupation Embedding Theory using Bethe Ansatz Local Density Approximations". *Phys. Rev. B* **2018**, 97, 235105

[BS5] K. Deur, L. Mazouin, B. Senjean, E. Fromager, "Exploring weight-dependent density-functional approximations for ensembles in the Hubbard dimer". *Eur. Phys. J. B* **2018**, 91, 162.

[BS6] B. Senjean, E. Fromager. "Unified formulation of fundamental and optical gap problems in density-functional theory for ensembles". *Phys. Rev. A* **2018**, 98, 022513.

[BS7] B. Senjean, N. Nakatani, M. Tsuchiizu, E. Fromager. "Multiple impurities and combined local density approximations in Site-Occupation Embedding Theory". **2018**, arXiv:1806.06057

Notations

To avoid confusion, the same notations will be used throughout the whole thesis:

Table 1: Notations

Symbol	Refers to
$\mathbf{x}$	Space and spin coordinates $\mathbf{x} \equiv (\mathbf{r}, \sigma)$
σ	Spin of the electron (either $\alpha \equiv\uparrow$ or $\beta \equiv\downarrow$)
$\mathbf{r}$	Space coordinates $\mathbf{r} \equiv (x, y, z)$
$\phi(\mathbf{x})$	One-electron molecular spin orbital.
$\varphi(\mathbf{r})$	One-electron molecular orbital
$\varphi^{\sigma}(\mathbf{x})$	One-electron molecular spin orbital for spin σ.
$\chi(\mathbf{r})$	One-electron atomic orbital.
$\Phi \equiv \Phi(\mathbf{x}_1, \ldots, \mathbf{x}_N)$	N-electron Slater determinant
$\Psi \equiv \Psi(\mathbf{x}_1, \ldots, \mathbf{x}_N)$	N-electron wavefunction

Acronyms

Acronyms, if correctly employed, can ease the reading. I give here a list of acronyms that will be used throughout the thesis:

Table 2: Acronyms

Acronyms	Meaning
BA	Bethe Ansatz
BALDA	Bethe Ansatz Local Density Approximation
iBALDA(M)	M-impurity Bethe ansatz local density approximation
2L-BALDA	two-level Bethe ansatz local density approximation
CAS	Complete Active Space
CASSCF	Complete Active Space Self-Consistent Field
DFT	Density-Functional Theory
DMET	Density Matrix Embedding Theory
DMFT	Dynamical Mean-Field Theory
eDFT	Ensemble Density Functional Theory
(F)CI	(Full) Configuration Interaction
GF	Green's Function
GOK	Gross–Oliveira–Kohn
KS	Kohn–Sham (leading to KS-DFT and KS-SOFT)
LDA	Local Density Approximation
MCSCF	Multi-Configurational Self-Consistent Field
NI	Non Interacting bath formulation in DMET
P-SOET	Projected Site-Occupation Embedding Theory
RDMFT	Reduced Density Matrix Functional Theory
1RDM and 2RDM	One- and Two-particle Reduced Density Matrices
SIAM	Single-impurity Anderson model
SOET	Site-Occupation Embedding Theory
SOFT	Site-Occupation Functional Theory
SOPT	Second-Order Perturbation Theory
(U)HF	(un)restricted Hartree-Fock
WFT	Wavefunction Theory

Résumé en Français

Introduction

La chimie quantique est une discipline qui applique la mécanique quantique à l'étude théorique des systèmes chimiques. Par l'étude de la structure et de la dynamique de ces systèmes, elle vise à comprendre les différents mécanismes des réactions chimiques régies par leurs propriétés thermodynamiques et cinétiques. Par ailleurs, le but de la physique de la matière condensée est de rationaliser les phénomènes naturels dans les phases condensées (comme les solides), par exemple par la description de la transition entre un métal et un isolant, engendrée par la variation de plusieurs paramètres tels que la pression ou l'introduction d'impuretés dans le matériau. Plusieurs méthodes et modèles ont été développés dans ces deux disciplines, permettant non seulement de reproduire les résultats expérimentaux, mais également de faire des prédictions ensuite vérifiées par l'expérience. La qualité d'une théorie est jugée sur ces deux critères. Cependant (et malgré les progrès continuellement effectués) certains systèmes restent extrêmement difficiles à décrire, comme les systèmes dits *fortement corrélés*. Les systèmes à forte corrélation électronique font l'objet d'une intense recherche depuis de nombreuses années, à travers le développement et la synthèse de matériaux toujours plus innovants, réunissant les chimistes et les physiciens, aussi bien expérimentaux que théoriciens. Ce sujet de recherche recouvre de nombreuses problématiques en théorie quantique, passant par la simple description d'une rupture de liaison chimique à la description des complexes de métaux de transition présentant des propriétés magnétiques et électroniques très intéressantes. Par exemple, certains matériaux manifestent des transitions métal-isolant (NiO et V_2O_3), des transitions de phases induites par la température comme les superconducteurs à haute température critique (La_2CuO_4), ou encore une magnétorésistance colossale ($LaMnO_3$) [1]. Ces propriétés originales ont permis de concevoir de nouveaux nanomatériaux ayant des applications potentielles dans la conversion d'énergie, le transport électronique pour les cellules photovoltaïques, les champs magnétiques forts, et le stockage magnétique de l'information. Les oxydes de métaux de transition sont également employés dans les catalyses homogènes et hétérogènes, et jouent un rôle essentiel en biologie chimique par leur présence dans les sites actifs des protéines.

Alors que le nombre de découvertes de nouveaux matériaux continue d'augmenter, le manque de méthodes théoriques suffisamment précises et efficaces pour décrire de tels matériaux se fait ressentir. Le développement de nouvelles méthodes permettrait de mieux comprendre et même de prédire de nouvelles structures manifestant des propriétés intéressantes, et prend une place importante dans la conception de technologies futuristes.

D'un point de vue théorique, le terme "fortement corrélé" vient du fait que la théorie dite de champ moyen n'est pas capable de décrire les phénomènes et transitions mentionnés précédemment. En effet, cette théorie ne décrit pas la corrélation électronique, dictée par l'interaction entre les électrons. Quand cette interaction joue un rôle prédominant, on parle de corrélation électronique *forte*, et celle-ci reste très difficile à traiter que ce soit en chimie ou en physique des états solides. À ce jour, aucune méthode ne fait autorité pour la description de tels systèmes. La formulation et l'implémentation d'une méthode universelle capable de les décrire restent un véritable challenge.

Alors que certaines méthodes (en théorie de la fonction d'onde, WFT en anglais pour *wavefunction theory*) seraient en principe suffisamment précises [2], elles restent bien trop chères en temps de calcul, si bien que d'autres méthodes moins coûteuses ont été développées. Par exemple, la théorie de la fonctionnelle de la densité (DFT en anglais, pour *density functional theory*) qui est une des méthodes les plus utilisées à ce jour. Cependant, la DFT ne décrit pas correctement les systèmes à forte corrélation électronique [3]. Intuitivement, il paraît naturel de vouloir mixer les théories WFT et DFT pour obtenir une méthode performante à moindre coût. Les méthodes dites d'"embedding" font partie de cette nouvelle famille hybride, où seulement une partie du système est traitée en WFT et le reste en DFT [4]. À présent que la loi de Moore a atteint sa limite, les méthodes de faible coût permettant la description de systèmes de grandes tailles avec suffisamment de précision prennent de l'importance. C'est pourquoi un intérêt grandissant concernant les approches de type embedding est observé. Ces dernières sont devenues populaires aussi bien en chimie quantique, pour les atomes et les molécules, qu'en physique de la matière condensée pour les solides.

Cette thèse vise au développement de nouvelles théories hybrides, à l'interface entre la chimie quantique et la physique de la matière condensée. Dans cette dernière communauté, il est courant d'utiliser des modèles fictifs simplifiés décrivant les principaux effets physiques manifestés par le système réel. Le modèle de Hubbard sera particulièrement employé.

Ce résumé se focalise sur le développement de la théorie hybride dénommée SOET (pour "site-occupation embedding theory") appliquée au modèle de Hubbard. Pour comprendre cette théorie, l'état de l'art de la chimie quantique et la présentation du modèle de Hubbard seront détaillés. Les autres théories présentées dans cette thèse, comme la théorie de la fonctionnelle de la densité pour les ensembles permettant l'extraction du gap fondamental, et la théorie de la fonctionnelle de la matrice densité basée sur une fonction d'onde de séniorité zéro, ne seront pas expliquées dans le résumé.

Théorie de la structure électronique en Chimie Quantique

L'évolution dans le temps d'un système physique contenant d'importants effets quantiques est mathématiquement décrite par l'équation de Schrödinger (Prix nobel de Physique en 1933). Si le système évolue dans un potentiel indépendant du temps et où les effets relativistes sont négligeables, alors cette équation se réduit à l'équation de Schrödinger indépendante du temps:

$$\hat{H}|\Psi\rangle = E|\Psi\rangle, \tag{1}$$

où Ψ est la fonction d'onde décrivant l'état stationnaire du système quantique ayant pour énergie totale E. Pour un système moléculaire contenant N électrons de masse m_e, charge e et positions $\{\mathbf{r}_i\}_{i=1,N}$ et M noyaux de masse $\{M_A\}_{A=1,M}$, charge $Z_A \times e$ et positions $\{R_A\}_{A=1,M}$, l'Hamiltonien de l'Eq. (1) est donné par, dans les unités du système international,

$$\begin{aligned}
\hat{H} &= \hat{T}_{\mathrm{n}} + \hat{T}_{\mathrm{e}} + \hat{V}_{\mathrm{ne}} + \hat{W}_{\mathrm{ee}} + \hat{V}_{\mathrm{n}} \\
&= -\sum_{A=1}^{M} \frac{\hbar^2}{2M_A}\nabla_A^2 - \sum_{i=1}^{N} \frac{\hbar^2}{2m_{\mathrm{e}}}\nabla_i^2 - \sum_{i=1}^{N}\sum_{A=1}^{M} \frac{Z_A e^2}{4\pi\varepsilon_0|\mathbf{R}_A - \mathbf{r}_i|} \\
&\quad + \sum_{i=1}^{N}\sum_{j>i}^{N} \frac{e^2}{4\pi\varepsilon_0|\mathbf{r}_i - \mathbf{r}_j|} + \sum_{A=1}^{M}\sum_{B>A}^{M} \frac{Z_A Z_B e^2}{4\pi\varepsilon_0|\mathbf{R}_A - \mathbf{R}_B|},
\end{aligned} \tag{2}$$

où $\hat{T}_n$ et $\hat{T}_e$ sont les opérateurs d'énergie cinétique des noyaux et des électrons, respectivement, et $\hat{V}_{\mathrm{ne}}$, $\hat{W}_{\mathrm{ee}}$ et $\hat{V}_{\mathrm{n}}$ sont les opérateurs d'énergie potentielle correspondant à l'attraction coulombienne électron-noyaux, et à la répulsion coulombienne électron-électron et noyaux-noyaux, respectivement. En chimie quantique, l'un des principaux objectifs est la bonne description des réactions chimiques, impliquant la formation et la rupture de liaisons chimiques. Ces derniers processus sont dus aux interactions entre les électrons du système. Puisque la masse d'un noyau est au moins 1836 fois supérieure à celle d'un électron, une approximation judicieuse consiste à négliger les mouvements des noyaux par rapport aux mouvements des électrons. Autrement dit, les noyaux sont *gelés*: c'est l'approximation de Born–Oppenheimer proposée en 1927 [5]. L'équation de Schrödinger peut alors être réécrite en découplant la partie électronique de la partie nucléaire:

$$\hat{H}_{\mathrm{e}}|\Psi_{\mathrm{e}}\rangle = E_{\mathrm{e}}|\Psi_{\mathrm{e}}\rangle, \tag{3}$$

où l'indice e correspond à "électronique", et ne sera plus employé dans la suite par simplicité. En utilisant les unités atomiques, l'Hamiltonien électronique devient simplement:

$$\hat{H} \longrightarrow \hat{T} + \hat{W}_{\text{ee}} + \hat{V}_{\text{ne}} = -\sum_{i=1}^{N} \frac{1}{2}\nabla_i^2 + \sum_{i=1}^{N}\sum_{j>i}^{N} \frac{1}{r_{ij}} - \sum_{i=1}^{N}\sum_{A=1}^{M} \frac{Z_A}{r_{iA}}, \tag{4}$$

où r_{iA} et r_{ij} sont respectivement les distances entre l'électron i et le noyau A, et entre l'électron i et l'électron j. Malgré la simplification apportée par l'approximation de Born–Oppenheimer, l'Eq. (3) n'a été résolue analytiquement que pour très peu de systèmes pédagogiques simples. Elle peut néanmoins être résolue numériquement pour certains atomes et molécules diatomiques. Pour de plus gros systèmes, une telle résolution reste infaisable, bien que de récents progrès aient vu le jour de par l'utilisation de la méthode de Monte Carlo Quantique (QMC) [6].

Théories de la fonction d'onde

Dans cette thèse, nous nous intéresserons à l'état fondamental du système, c'est-à-dire l'état de plus basse énergie. Cette énergie peut être déterminée par le principe variationnel de Rayleight–Ritz:

$$E_0 = \langle \Psi_0 | \hat{H} | \Psi_0 \rangle \leqslant \langle \Psi | \hat{H} | \Psi \rangle, \tag{5}$$

où Ψ_0 est la fonction d'onde de l'état fondamental (généralement indéterminée), et Ψ est n'importe quelle fonction d'onde d'essai. En théorie de la fonction d'onde, de nombreuses méthodes ont été développées et visent à approcher le plus possible la fonction d'onde de l'état fondamental. Grâce au principe variationnel [Eq. (5)], l'énergie associée à cette fonction d'onde approchée sera toujours de plus haute énergie que celle de l'état fondamental. Pour que la fonction d'onde (électronique) corresponde bien à un système physique fermionique, elle doit décrire un système où les électrons sont indiscernables et doivent respecter le principe d'exclusion de Pauli, c'est-à-dire que deux électrons ne peuvent pas se trouver simultanément dans le même état quantique. Autrement dit, deux électrons de même spin ne peuvent pas occuper la même orbitale spatiale. Ce principe revient à imposer l'antisymétrie de la fonction d'onde par rapport à la permutation de deux électrons. Considérons un système à N électrons à répartir dans N spin-orbitales moléculaires $\{\varphi_i\}_{i=1,N}$. La fonction d'onde la plus simple respectant les conditions précédemment mentionnées nous est alors donnée par un déterminant de Slater:

$$\Phi(\mathbf{x}_1, \mathbf{x}_2, \ldots, \mathbf{x}_N) = \frac{1}{\sqrt{N!}} \begin{vmatrix} \phi_1(\mathbf{x}_1) & \phi_2(\mathbf{x}_1) & \ldots & \phi_N(\mathbf{x}_1) \\ \phi_1(\mathbf{x}_2) & \phi_2(\mathbf{x}_2) & \ldots & \phi_N(\mathbf{x}_2) \\ \vdots & \vdots & \ddots & \vdots \\ \phi_1(\mathbf{x}_N) & \phi_2(\mathbf{x}_N) & \ldots & \phi_N(\mathbf{x}_N) \end{vmatrix}, \tag{6}$$

où $1/\sqrt{N!}$ est un facteur de normalisation. Il est clair que si deux électrons sont dans le même état quantique, alors deux lignes du déterminant sont identiques et la fonction d'onde est égale à 0. Si deux électrons sont permutés, cela revient à changer deux lignes du déterminant, et donc à changer son signe. Le principe de Pauli est ainsi respecté. Les méthodes où la fonction d'onde peut être écrite comme un unique déterminant de Slater ne peuvent décrire qu'une seule configuration électronique. Elles sont appelées *méthodes monoconfigurationelles*, et la plus connue est la méthode Hartree–Fock (HF) [7, 8]. Pour plus de simplicité, considérons un système à couches fermées contenant un nombre pair N d'électrons dans un ensemble d'orbitales spatiales orthonormées $\{\varphi_i\}_{i=1,N/2}$. L'équation autocohérente Hartree–Fock est donnée par:

$$\left(-\frac{1}{2}\nabla^2 + \hat{v}^{\mathrm{HF}}\left[\{\varphi_j\}_{j=1,N/2}\right] - \sum_A^M \frac{Z_A}{|\mathbf{r} - \mathbf{R}_A|}\right)\varphi_i(\mathbf{r}) = \varepsilon_i \varphi_i(\mathbf{r}) \tag{7}$$

où

$$\hat{v}^{\mathrm{HF}} = \sum_{j=1}^{N/2} \left(2\hat{J}_j - \hat{K}_j\right) \tag{8}$$

est l'opérateur potentiel HF (effectif) monoélectronique, décrivant le champ moyen généré par les $N-1$ autres électrons, avec

$$\hat{J}_j \varphi_i(\mathbf{r}_1) = \left(\int \mathrm{d}\mathbf{r}_2 \frac{\varphi_j^*(\mathbf{r}_2)\varphi_j(\mathbf{r}_2)}{|\mathbf{r}_1 - \mathbf{r}_2|}\right) \times \varphi_i(\mathbf{r}_1) \tag{9}$$

l'opérateur monoélectronique local décrivant la répulsion coulombienne classique, et

$$\hat{K}_j \varphi_i(\mathbf{r}_1) = \int \mathrm{d}\mathbf{r}_2 \frac{\varphi_j^*(\mathbf{r}_2)\varphi_i(\mathbf{r}_2)}{|\mathbf{r}_1 - \mathbf{r}_2|}\varphi_j(\mathbf{r}_1) \tag{10}$$

l'opérateur monoélectronique non local décrivant l'intéraction d'échange électron-électron. L'Eq. (7) est résolue de manière itérative, car le champ généré par l'opérateur HF dépend des orbitales, elles-mêmes déterminées par résolution de l'équation HF. Le déterminant de Slater construit par les orbitales

HF convergées est ensuite utilisé pour déterminer l'énergie HF:

$$E_{\mathrm{HF}} = \langle \Phi_{\mathrm{HF}} | \hat{H} | \Phi_{\mathrm{HF}} \rangle = 2 \sum_{i=1}^{N/2} \langle \varphi_i | \hat{h} | \varphi_i \rangle + \sum_{i=1}^{N/2} \sum_{j=1}^{N/2} (2J_{ij} - K_{ij}) \geqslant E_0, \tag{11}$$

où

$$\begin{aligned} J_{ij} = \langle ij | ij \rangle &= \langle \varphi_i \varphi_j | \varphi_i \varphi_j \rangle = \iint \mathrm{d}\mathbf{r}_1 \mathrm{d}\mathbf{r}_2 \frac{\varphi_i^*(\mathbf{r}_1)\varphi_j^*(\mathbf{r}_2)\varphi_i(\mathbf{r}_1)\varphi_j(\mathbf{r}_2)}{r_{12}}, \\ K_{ij} = \langle ij | ji \rangle &= \langle \varphi_i \varphi_j | \varphi_j \varphi_i \rangle = \iint \mathrm{d}\mathbf{r}_1 \mathrm{d}\mathbf{r}_2 \frac{\varphi_i^*(\mathbf{r}_1)\varphi_j^*(\mathbf{r}_2)\varphi_i(\mathbf{r}_2)\varphi_j(\mathbf{r}_1)}{r_{12}}, \end{aligned} \tag{12}$$

sont respectivement les intégrales de Coulomb et d'échange. Il est clair d'après l'Eq. (11) que l'énergie HF n'est pas une simple somme des énergies orbitalaires, ce qui signifie que la méthode HF décrit l'interaction entre les électrons $1/r_{ij}$, qui est traitée par le champ moyen généré par le potentiel HF non local.

Cependant, cette approche reste une approximation. Pour retrouver l'énergie fondamentale exacte du système, il faut corriger l'énergie HF par une énergie de corrélation:

$$E_{\mathrm{c}} = E - E_{\mathrm{HF}}. \tag{13}$$

Cette énergie de corrélation peut être divisée en deux contributions. La première est appelée corrélation dynamique (ou corrélation faible), et peut être retrouvée en considérant une fonction d'onde constituée d'un mélange de déterminants: le déterminant HF et des déterminants excités d'ordre supérieur. Bien que cette fonction d'onde soit multidéterminantale, elle demeure monoconfigurationelle. Ces déterminants excités ont habituellement une contribution très faible à l'énergie, mais celle-ci est nécessaire pour atteindre la précision chimique (≈ 1 kcal/mol). Par exemple, la corrélation dynamique est essentielle pour décrire proprement la dissociation du dimère d'Helium [9]. La deuxième est appelée corrélation statique (ou corrélation forte) et constitue le principal objet de cette thèse. Celle-ci apparaît quand des configurations de faibles énergies sont presque dégénérées avec le déterminant de Slater de référence [10]. si bien qu'il n'y a plus une seule configuration dominante. Un mélange de ces configurations est alors nécessaire: la fonction d'onde est dite multiconfigurationelle. Un exemple pédagogique simple est donné par la dissociation ($R \to +\infty$) de la molécule de dihydrogène, où la fonction d'onde est donnée par une combinaison moyennée de deux configurations électroniques: $1\sigma_g^2$ et $1\sigma_u^2$, où $1\sigma_g$ est l'orbitale moléculaire liante, et $1\sigma_u$ l'orbitale moléculaire antiliante.

Les méthodes mixant ainsi plusieurs déterminants sont appelées les méthodes post-HF. En écrivant la fonction d'onde comme une combinaison linéaire de déterminants de Slater Φ_I, nous obtenons la fonction d'onde d'*intéraction de configuration* (CI en anglais, pour "configuration interaction"):

$$|\Psi(\mathbf{C})\rangle = \sum_I C_I \Phi_I, \tag{14}$$

où les coefficients CI ($\mathbf{C} = \{C_I\}_I$) sont à optimiser. Si la fonction d'onde contient tous les déterminants possibles, construits à partir d'un ensemble donné d'orbitales, alors on parle de fonction d'onde FCI (pour "Full configuration interaction"). Le nombre de déterminants à considérer est donné par

$$N_{\text{det}} = \binom{M}{N} = \frac{M!}{N!(M-N)!}, \tag{15}$$

où N est le nombre d'électrons et M le nombre de spin-orbitales. Par exemple, pour $N = 20$ et $M = 40$, il faudrait considérer 137 846 528 800 déterminants, ce qui est actuellement impossible à cause du temps de calcul nécessaire pour traiter autant de combinaisons. FCI est donc utilisée comme méthode de référence pour de très petits systèmes uniquement. En pratique, pour étudier de plus gros systèmes, ce nombre de déterminants est tronqué pour ne garder, par exemple, que les déterminants obtenus par simple et double excitation du déterminant HF:

$$|\Psi\rangle \approx |\Phi_{\text{HF}}\rangle + \sum_{ia} c_i^a |\Phi_i^a\rangle + \sum_{ijab} c_{ij}^{ab} |\Phi_{ij}^{ab}\rangle + \dots, \tag{16}$$

où i,j dénotent les orbitales occupées et a,b les orbitales non occupées du déterminant HF, de sorte que le déterminant Ψ_i^a corresponde à l'excitation de l'électron de l'orbitale i à l'orbitale a, et le déterminant Ψ_{ij}^{ab} corresponde à la double excitation de l'électron de l'orbitale i à l'orbitale a, et de l'électron de l'orbitale j à l'orbitale b. L'énergie obtenue par cette fonction d'onde tronquée ne peut être qu'une approximation de la fonction d'onde exacte.

Pour ajouter plus de flexibilité, il est possible d'optimiser non seulement les coefficients CI, mais aussi ceux des orbitales moléculaires, qui sont exprimées comme une combinaison linéaire d'orbitales atomiques (CLOA). Cela consiste à faire une rotation des orbitales moléculaires. Permettre cette réoptimisation des orbitales dans un calcul CI tronqué donne lieu à une nouvelle approche s'intitulant *champ autocohérent multiconfigurationel* (MCSCF en anglais, pour "multiconfigurational self-consistent field"). Plutôt que de considérer les déterminants simplement et doublement excités, il serait intéressant de considérer tous les déterminants possibles mais uniquement dans une espace orbitalaire restreint, appelé espace actif complet (CAS en anglais, pour "complete active space"). L'énergie associée à cette fonction d'onde CASSCF est donnée par

$$E_{\mathrm{CAS}} = \min_{\boldsymbol{\kappa},\mathbf{C}} \left\{ \langle \Psi^{\mathrm{CAS}}(\boldsymbol{\kappa},\mathbf{C}) | \hat{T} + \hat{W}_{\mathrm{ee}} + \hat{V}_{\mathrm{ne}} | \Psi^{\mathrm{CAS}}(\boldsymbol{\kappa},\mathbf{C}) \rangle \right\}, \tag{17}$$

où $\boldsymbol{\kappa}$ est la matrice contenant les paramètres à optimiser pour faire tourner les orbitales. Cette méthode permet le bon traitement de la corrélation statique, mais manque de corrélation dynamique. Celle-ci peut être décrite par une théorie des perturbations. Aussi, au maximum 18 électrons dans 18 orbitales peuvent être traités, ce qui est insuffisant pour décrire des système très complexes [11]. Pour aller au-delà de cette limite, la méthode DMRG [12, 13] (en anglais, pour "density matrix renormalization group") est utilisée et peut décrire jusqu'à 40 électrons dans 40 orbitales [14, 15]. L'idée de cette méthode est de tronquer les coefficients CI. Pour cela, la DMRG exprime les coefficients sous forme matricielle, puis effectue une succession de décompositions en valeur singulière (SVD) et de décompositions de Schmidt, jusqu'à ce que la fonction d'onde soit exprimée comme un état de produits de matrices. La troncation s'effectue à chaque décomposition en valeur singulière, où seulement les m plus grandes valeurs singulières sont conservées.

Théorie de la fonctionnelle de la densité

Nous avons vu précédemment qu'il est difficile d'obtenir une bonne approximation de la fonction d'onde du système tout en conservant un temps de calcul relativement faible. On peut alors se demander si chercher cette fonction d'onde est le seul moyen de décrire un système à plusieurs particules manifestant des effets quantiques. En effet, une fonction d'onde est un objet d'une extrême complexité. Une illustration amusante a été donné par Hardy Gross[1] sur l'atome d'oxygène possèdant 8 électrons. Si l'on veut représenter la surface d'énergie potentielle de cet atome, donnée par

$$\int \mathrm{d}\mathbf{r}_1 \int \mathrm{d}\mathbf{r}_2 \ \ldots \int \mathrm{d}\mathbf{r}_N \Psi^*(\mathbf{r}_1, \mathbf{r}_2, \ldots, \mathbf{r}_N) \hat{H} \Psi(\mathbf{r}_1, \mathbf{r}_2, \ldots, \mathbf{r}_N), \tag{18}$$

il faut alors pouvoir stocker la fonction d'onde. Pour ce faire, chaque coordonnée (3 par électron, soit 24 coordonnées) va être discrétisée par 10 valeurs. Ainsi, 10^{24} valeurs doivent être stockées. Pour cela, un tableau à 10^{24} entrées est nécessaire. Si une entrée correspond à un byte, alors il faudra bien sûr 10^{24} bytes pour enregistrer toutes ces données. Maintenant, considérons un DVD ayant une capacité de 5 GB (5×10^9 bytes). Pour pouvoir stocker la fonction d'onde de l'oxygène (pour seulement 10 valeurs par coordonnées), 2×10^{14} DVD seront nécessaires. Soit 200 000 milliards de DVD. Si un DVD

---

[1] pendant une école d'été à Los Angeles en Août 2016, intitulée "mathematical foundations of density functional theory"

pèse environ 10 grammes, cela équivaut à 2 milliards de tonnes de DVD. Pour pallier à ce problème, des méthodes se basant sur d'autres variables que la fonction d'onde existent, et utilisent la densité électronique, la matrice densité, ou encore les fonctions de Green. Dans ce résumé, seule la théorie basée sur la densité électronique sera présentée.

Utiliser la densité électronique comme variable est un concept introduit par Thomas en 1927 [16], suivi indépendamment par Fermi [17], donnant lieu à la méthode de Thomas–Fermi. Celle-ci consiste à représenter l'opérateur Hamiltonien comme une fonctionnelle de la densité électronique

$$n(\mathbf{r}) = N \sum_{\sigma} \int \mathrm{d}\mathbf{x}_2 \int \mathrm{d}\mathbf{x}_3 \ \ldots \ \int \mathrm{d}\mathbf{x}_N \left|\Psi(\mathbf{r}, \sigma, \mathbf{x}_2, \ldots, \mathbf{x}_N)\right|^2, \tag{19}$$

de sorte que la fonction d'onde n'a pas besoin d'être construite. Basée sur le gaz homogène d'électrons, l'expression analytique de l'énergie cinétique du système non interagissant a donné lieu à la première approximation locale de la densité (LDA en anglais, pour “local density approximation”):

$$T^{\mathrm{TF}}[n] = \frac{3}{10}\left(3\pi^2\right)^{2/3} \int \mathrm{d}\mathbf{r} \ n^{5/3}(\mathbf{r}). \tag{20}$$

Cependant, cette énergie est bien loin de refléter la réalité d'un système chimique complexe, où les électrons sont en interaction et ne forment pas un gaz homogène. Pour améliorer cette théorie, Dirac [18] a proposé un terme supplémentaire d'échange:

$$E_{\mathrm{x}}[n] = -\frac{3}{4}\left(\frac{3}{\pi}\right)^{1/3} \int \mathrm{d}\mathbf{r} \ n^{4/3}(\mathbf{r}), \tag{21}$$

exact dans le cas du gaz homogène d'électrons. Malgré cette correction, les résultats obtenus par cette méthode restent trop imprécis. Cette méthode a donc été mise de côté jusqu'au milieu des années 1960, où Hohenberg et Kohn (Walter Kohn, prix Nobel en chimie en 1998) ont formulé les deux théorèmes qui firent renaître cette théorie, maintenant appelée théorie de la fonctionnelle de la densité (DFT en anglais, pour “density functional theory”) qui est l'une des méthodes les plus utilisées en chimie quantique. Le premier théorème démontre la correspondance bi-univoque qui existe entre le potentiel local externe $v(\mathbf{r})$, à une constante près, et la densité de l'état fondamental $n_0(\mathbf{r})$. Ainsi, si la densité $n_0(\mathbf{r})$ est connue, alors le potentiel externe l'est également et avec lui l'Hamiltonien et ses valeurs et fonctions propres associées,

$$n_0(\mathbf{r}) \longleftrightarrow v(\mathbf{r}) = v[n_0](\mathbf{r}) \longleftrightarrow \Psi_0[v] = \Psi_0[v[n_0]] = \Psi_0[n_0]. \tag{22}$$

De ce fait, toutes les propriétés du système deviennent des fonctionnelles de la densité électronique de l'état fondamental. Le second théorème est l'analogue du principe variationnel pour les fonctions d'onde, mais appliqué à la densité électronique:

$$E_0[v] = \min_n \Big\{ E_v[n] \Big\} = E_v[n_0], \tag{23}$$

où

$$\begin{aligned} E_v[n] &= T[n] + W_{\mathrm{ee}}[n] + V[n], \\ &= F[n] + \int \mathrm{d}\mathbf{r}\; v(\mathbf{r}) n(\mathbf{r}), \end{aligned} \tag{24}$$

et, d'après le formalisme de recherche sous contraintes de Levy–Lieb [19],

$$F[n] = \min_{\Psi \to n} \Big\{ \langle \Psi | \hat{T} + \hat{W}_{\mathrm{ee}} | \Psi \rangle \Big\}. \tag{25}$$

L'énergie fondamentale est alors donnée par l'expression variationnelle suivante:

$$\begin{aligned} E_0[v] &= \min_n \left[\min_{\Psi \to n} \Big\{ \langle \Psi | \hat{T} + \hat{W}_{\mathrm{ee}} | \Psi \rangle \Big\} + \int \mathrm{d}\mathbf{r}\; v(\mathbf{r}) n(\mathbf{r}) \right] \\ &= \min_n \left[\min_{\Psi \to n} \Big\{ \langle \Psi | \hat{T} + \hat{W}_{\mathrm{ee}} | \Psi \rangle \Big\} + \int \mathrm{d}\mathbf{r}\; v(\mathbf{r}) n^{\Psi}(\mathbf{r}) \right], \end{aligned} \tag{26}$$

qui est équivalente au principe variationnel pour les fonctions d'onde,

$$E_0[v] = \min_{\Psi} \Big\{ \langle \Psi | \hat{T} + \hat{W}_{\mathrm{ee}} | \Psi \rangle + \int \mathrm{d}\mathbf{r}\; v(\mathbf{r}) n^{\Psi}(\mathbf{r}) \Big\}. \tag{27}$$

Pour l'instant, DFT ne semble pas plus simple que WFT, car la fonctionnelle $F[n]$ dépendant explicitement de la densité électronique n'est pas connue. Celle-ci pourrait être déterminée numériquement par la minimisation décrite par l'Eq. (25), mais cela revient à connaître l'ensemble des fonctions d'onde donnant la densité $n(\mathbf{r})$.

C'est en 1965 que Kohn et Sham (KS) ont eu l'idée de construire la densité de l'état fondamental par le biais d'un système non interagissant, bien plus simple à résoudre. Pour un tel système, la fonctionnelle de Levy–Lieb devient équivalente à l'énergie cinétique non interagissante,

$$T_{\mathrm{s}}[n] = \min_{\Phi \to n} \Big\{ \langle \Phi | \hat{T} | \Phi \rangle \Big\}, \tag{28}$$

où les fonctions d'onde d'un système non interagissant peuvent toujours être écrites comme un déterminant de Slater Φ. En KS-DFT, la fonctionnelle universelle est alors décomposée comme suit,

$$F[n] = T_{\mathrm{s}}[n] + E_{\mathrm{Hxc}}[n], \tag{29}$$

où $E_{\mathrm{Hxc}}[n]$ est l'énergie d'Hartree-échange-corrélation (Hxc), fonctionnelle de la densité. L'énergie fondamentale s'écrit alors

$$E_0 = \min_{\Phi} \left\{ \langle \Phi | \hat{T} | \Phi \rangle + E_{\mathrm{Hxc}}[n^{\Phi}] + \int \mathrm{d}\mathbf{r} v_{\mathrm{ne}}(\mathbf{r}) n^{\Phi}(\mathbf{r}) \right\}. \tag{30}$$

En comparant l'Eq. (30) à l'Eq. (27), il est clair que la fonctionnelle Hxc décrit implicitement l'interaction entre les électrons, plutôt que de traiter $1/r_{ij}$ explicitement. Le déterminant KS Φ^{KS} minimisant l'Eq. (30) reproduit la densité fondamentale $n_0(\mathbf{r})$, et est construit (dans un formalisme restreint à couches fermées) par les $N/2$ plus basses orbitales KS, doublement occupées, satisfaisant l'équation autocohérente suivante:

$$\left(-\frac{1}{2}\nabla^2 + v_{\mathrm{ne}}(\mathbf{r}) + \frac{\delta E_{\mathrm{Hxc}}[n^{\Phi^{\mathrm{KS}}}]}{\delta n(\mathbf{r})} \right) \varphi_i^{\mathrm{KS}}(\mathbf{r}) = \varepsilon_i^{\mathrm{KS}} \varphi_i^{\mathrm{KS}}(\mathbf{r}), \tag{31}$$

où la densité électronique est donnée par

$$n^{\Phi^{\mathrm{KS}}}(\mathbf{r}) = 2 \sum_{i=1}^{N/2} \left| \varphi_i^{\mathrm{KS}}(\mathbf{r}) \right|^2. \tag{32}$$

La KS-DFT est en principe exacte. Malheureusement, l'énergie Hxc, fonctionnelle de la densité, reste pour le moment inconnue bien que de nombreuses approximations existent [20, 21].

Théories hybrides combinant WFT et DFT

Malgré toutes les approximations existantes pour la fonctionnelle Hxc, la DFT reste incapable de traiter correctement les systèmes multiconfigurationnels (où la corrélation statique domine). Chercher la fonctionnelle exacte et universelle est un véritable challenge, si bien que d'autres approches hybrides ont vu le jour, combinant WFT et DFT. En effet, les méthodes en WFT sont capables de traiter la corrélation statique mais sont très chères en temps de calcul, alors que la KS-DFT est très peu coûteuse mais ne décrit actuellement pas bien la corrélation statique. Il paraît donc naturel d'extraire le meilleur de ces deux approches en les combinant. Cependant, WFT et DFT sont deux approches formulées dans des langages totalement différents. En effet, alors que l'une nécessite la construction de fonctions d'onde multiélectroniques, l'autre n'utilise que la densité électronique. Bien qu'une combinaison rigoureuse de ces méthodes soit également un challenge, un gain d'intérêt est tout de même observé depuis la fin des années 1990. En particulier, trouver une combinaison qui ne compte pas plusieurs fois les mêmes effets de corrélation (appelé le problème de "double comptage") s'avère compliqué, car la séparation entre WFT et DFT n'est pas unique, et peut être faite de nombreuses manières différentes. Cette thèse traite principalement de cette problématique.

Une manière de combiner WFT et DFT a été proposée par Savin en 1996 [22, 23], et consiste à diviser la répulsion électronique dans l'espace réel en utilisant la fonction erreur:

$$\frac{1}{r_{12}} = \frac{\mathrm{erf}(\mu r_{12})}{r_{12}} + \frac{1-\mathrm{erf}(\mu r_{12})}{r_{12}}, \tag{33}$$

où $\mathrm{erf}(\mu r_{12}) = 2/\sqrt{\pi}\int_0^{\mu r_{12}} e^{-t^2}\mathrm{d}t$, et le premier terme dans la partie de droite de l'Eq. (33) est dit de longue portée (lr, pour "long range"), tandis que l'autre est dit de courte portée (sr, pour "short range"). L'idée est alors de traiter la partie de longue portée en WFT alors que la courte portée sera traitée en DFT par une énergie Hxc, fonctionnelle de la densité. Ainsi, quand $\mu = 0$, toute l'interaction électronique sera traitée en DFT, à l'opposé de $\mu \to +\infty$. L'énergie de l'état fondamental devient

$$E_0[v] = \min_{\Psi}\left\{\langle\Psi|\hat{T} + \hat{W}_{\mathrm{ee}}^{\mathrm{lr},\mu} + \hat{V}|\Psi\rangle + E_{\mathrm{Hxc}}^{\mathrm{sr},\mu}[n^{\Psi}]\right\}, \tag{34}$$

où la fonction d'onde minimisante Ψ^μ satisfait l'équation autocohérente suivante:

$$\left(\hat{T} + \hat{W}_{\mathrm{ee}}^{\mathrm{lr},\mu} + \int \mathrm{d}\mathbf{r}\left[v(\mathbf{r}) + \frac{\delta E_{\mathrm{Hxc}}^{\mathrm{sr},\mu}[n^{\Psi^\mu}]}{\delta n(\mathbf{r})}\right]\hat{n}(\mathbf{r})\right)|\Psi^\mu\rangle = \mathcal{E}^\mu|\Psi^\mu\rangle. \tag{35}$$

Contrairement à la KS-DFT, où le système de référence est non interagissant, Ψ^μ est multiconfigurationnelle car la répulsion électronique de longue portée est traitée explicitement. Cette méthode s'appelle la DFT à séparation de portée. Bien que cette méthode (en principe exacte) soit prometteuse, la construction de fonctionnelle Hxc de courte portée reste une tâche très complexe. Par exemple, la corrélation statique (supposée être traitée en WFT) n'est pas purement de longue portée [24, 25]. En effet, la corrélation statique trouve sa définition dans l'espace orbitalaire, ce qui rend la séparation de l'interaction en courte et longue portées discutable.

Une séparation alternative consiste à séparer l'interaction dans l'espace orbitalaire. Un CAS est alors considéré, où l'interaction sera traitée en WFT, tandis que les orbitales hors du CAS seront traitées en DFT, donnant lieu à une nouvelle méthode nommée CAS-DFT. L'expression variationnelle de l'énergie fondamentale en CAS-DFT est donnée par [26, 27]:

$$E_0[v] = \min_{\boldsymbol{\kappa},\mathbf{S}} \Big\{ \langle \Psi^{\mathrm{CAS}}(\boldsymbol{\kappa},\mathbf{S}) | \hat{T} + \hat{W}_{\mathrm{ee}} + \hat{V} | \Psi^{\mathrm{CAS}}(\boldsymbol{\kappa},\mathbf{S}) \rangle + E_{\mathrm{c}}^{\mathrm{CAS}}[n^{\Psi^{\mathrm{CAS}}(\boldsymbol{\kappa},\mathbf{S})}] \Big\}, \tag{36}$$

où la fonctionnelle Hxc doit dépendre du CAS considéré pour éviter tout problème de double comptage de la corrélation électronique, et ne peut donc pas être universelle. En pratique, cette méthode est donc très compliquée à implémenter [28]. Il est bon de noter que d'autres méthodes similaires ont été proposées par Savin, combinant CI et DFT [29, 30]. Que ce soit en CAS-DFT ou en CI-DFT, le problème de double comptage est extrêmement difficile à traiter, car l'énergie Hxc doit dépendre de l'espace orbitalaire dans lequel les interactions sont traitées explicitement en WFT. Or, cette énergie est fonctionnelle de la densité électronique qui, elle, est définie dans l'espace réel. Récemment, Fromager a proposé une nouvelle méthode où l'énergie de corrélation est définie non plus comme une fonctionnelle de la densité électronique, mais comme une fonctionnelle des occupations des orbitales [25]. Ainsi, le problème de double comptage pourrait être plus facile à éviter en pratique.

Toutes les méthodes hybrides présentées jusque là ne sont pas standard en chimie quantique, pour deux raisons. La première est que ces méthodes restent chères en temps de calcul. La deuxième est que de nouvelles fonctionnelles doivent être développées pour éviter les problèmes de double comptage, ce qui est loin d'être une tâche facile. Plutôt que de séparer l'interaction en utilisant une séparation de portée, considérons un système plus grand où seule une petite partie de ce système serait traitée en WFT, tandis que le reste du système serait traité en DFT. Ce type de méthode est désigné par le terme "embedding" (signifiant ici que la partie traitée en WFT est "plongée" dans le reste du système traité en DFT). Ce type d'approche est par exemple utilisé pour décrire des problèmes généralement mal décrits en DFT, comme la chimisorption (adsorbat lié à la surface par des liaisons chimiques) [31] ou la présence d'impureté(s) dans un semiconducteur [32]. La division du système entre WFT et DFT est définie par l'utilisateur, et n'est pas unique. Il peut être difficile de vraiment savoir où faire cette séparation entre les deux méthodes. Ce problème devient bien plus clair en considérant des Hamiltoniens modèles, pour lesquels l'espace devient un nombre de sites dont l'occupation joue le rôle de densité électronique. Dans l'esprit de l'embedding, seuls certains sites seront interagissants, tandis que l'interaction des autres sites sera traitée par une fonctionnelle de l'occupation des sites. Cette méthode est la théorie d'embedding de l'occupation des sites (SOET en anglais, pour "site occupation embedding theory") [25, 33–35], qui est la méthode principalement développée durant cette thèse. Avant de parler plus précisément de la SOET, il est important d'introduire le concept d'Hamiltoniens modèles utilisés dans la physique de la matière condensée.

Modèle de Hubbard et la théorie de la fonctionnelle de l'occupation des sites

Dans le but de développer de nouvelles méthodes capables de décrire la forte corrélation électronique, il est important de commencer avec des modèles simplifiés. En effet, bien qu'une théorie qui marche sur un modèle ne soit pas directement transférable aux systèmes réels, une théorie qui ne marche pas sur un modèle est certaine de ne pas non plus pouvoir décrire la physique d'un système réel. Et vu la complexité de l'Hamiltonien moléculaire, il est préférable de commencer par traiter des modèles plus simples. Il est important de comprendre que même si le modèle considéré est fictif, il peut cependant décrire un phénomène physique particulier. Par exemple, le modèle de Hubbard considéré dans cette thèse contient la physique nécessaire pour décrire des superconducteurs à haute température critique ($\mathrm{LaCuO_4}$), et des phénomènes comme la transition de Mott (transition métal-isolant due à l'interaction entre les électrons, qui ne peut pas être décrite par une théorie de champ moyen). L'Hamiltonien de Hubbard est décrit comme suit [36–39]:

$$\begin{aligned} \hat{H} &\longrightarrow \hat{T} + \hat{U} - \hat{\mu}, \\ &= -t \sum_{\langle ij \rangle} \sum_{\sigma} (\hat{c}^{\dagger}_{i\sigma} \hat{c}_{j\sigma} + \hat{c}^{\dagger}_{j\sigma} \hat{c}_{i\sigma}) + U \sum_i \hat{n}_{i\uparrow} \hat{n}_{i\downarrow} - \mu \sum_i \hat{n}_i, \end{aligned} \tag{37}$$

où $\hat{n}_i = \hat{n}_{i\uparrow} + \hat{n}_{i\downarrow}$ est l'opérateur d'occupation sur le site i avec $\hat{n}_{i\sigma} = \hat{c}^{\dagger}_{i\sigma} \hat{c}_{i\sigma}$, et μ est le potentiel chimique définissant le remplissage en électrons du modèle. Ce modèle peut être considéré dans plusieurs dimensions. Dans cette thèse, seule une dimension sera traitée, comme le montre la figure 1. Sur cette figure, nous voyons que la répulsion électronique, dénotée par le paramètre U, est uniquement sur site (deux électrons sur différents sites n'interagissent pas entre eux), et l'énergie cinétique est dénotée par le paramètre t, qui correspond au saut d'un électron d'un site à son plus proche voisin uniquement. Ces restrictions rendent le modèle bien plus simple que la réalité, bien qu'il reste toujours très compliqué à traiter. Dans le cas du demi-remplissage (un électron par site), l'interaction U empêche les électrons de sauter de sites en sites, ce qui rend le modèle isolant. L'introduction d'une impureté permet de passer d'un isolant à un conducteur (un métal), dénotant une transition de Mott. La valeur du ratio U/t définit si le modèle est fortement corrélé ou non. Si $U/t \gg 1$, alors les électrons sont localisés sur le réseau de sites, et on dit qu'ils sont fortement corrélés. Si $U/t \ll 1$, alors les électrons sont délocalisés et faiblement corrélés.

La DFT appliquée au modèle de Hubbard est appelée la théorie de la fonctionnelle de l'occupation des sites (SOFT en anglais, pour "site-occupation functional theory"). Ainsi, la densité électronique en

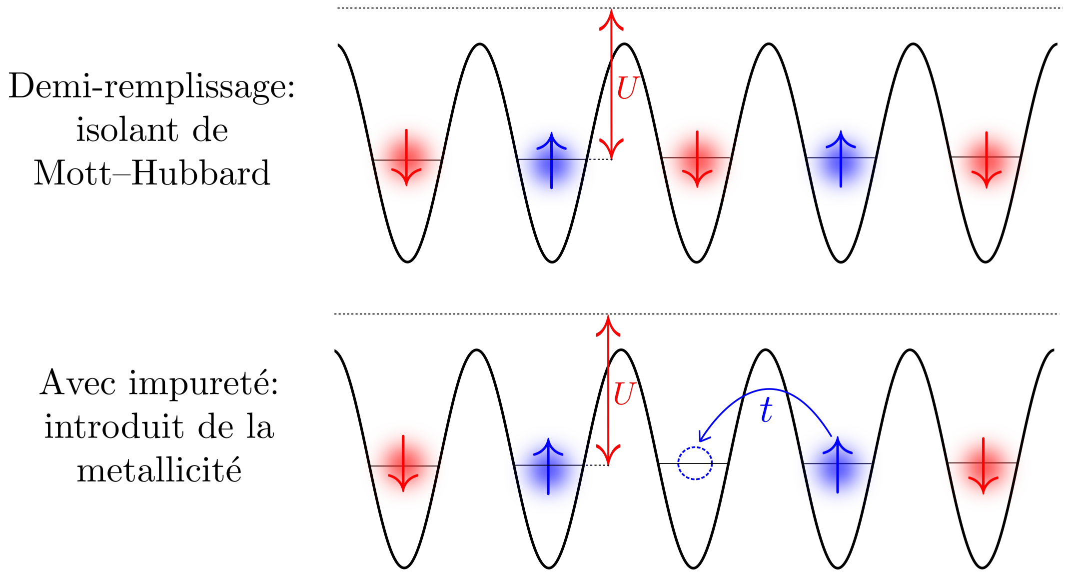

Figure 1: Modèle de Hubbard en une dimension à demi-remplissage (au haut, correspondant à un isolant). L'introduction d'une impureté (d'un électron ou d'un trou) rend le modèle métallique (en bas).

DFT est définie dans l'espace réel, alors qu'en SOFT l'occupation des sites joue le rôle de la densité. Plutôt que d'avoir une fonction de l'espace $n(\mathbf{r})$, nous avons une collection de nombres (ou vecteur) d'occupation $\mathbf{n} \equiv \{n_i\}_i$. Tout comme en DFT standard, une formulation KS existe pour la SOFT, de sorte qu'une fonction $E_{\rm Hxc}(\mathbf{n})$ décrit l'interaction entre les électrons. L'expression variationnelle de l'énergie fondamentale s'écrit alors

$$E_0(\mathbf{v}) = \min_{\Psi} \left\{ \langle \Psi | \hat{T} | \Psi \rangle + \sum_i v_i n_i + E_{\rm Hxc}(\mathbf{n}^{\Psi}) \right\}. \tag{38}$$

où $\mathbf{v} \equiv \{v_i\}_i$ est un potentiel externe, et $\Phi^{\rm KS}$ est la fonction d'onde monodéterminantale minimisant l'énergie, et satisfaisant l'équation autocohérente suivante:

$$\left(\hat{T} + \sum_i \left[v_i + \frac{\partial E_{\rm Hxc}(\mathbf{n}^{\Phi^{\rm KS}})}{\partial n_i} \right] \hat{n}_i \right) |\Phi^{\rm KS}\rangle = \mathcal{E}^{\rm KS} |\Phi^{\rm KS}\rangle. \tag{39}$$

La fonctionnelle utilisée dans cette thèse sera BALDA (pour "Bethe ansatz local density approximation") [40–42], dont l'expression est

$$E_{\rm Hxc}^{\rm BALDA}(\mathbf{n}) = \sum_i \left(\frac{U}{4} n_i^2 + e_{\rm c}^{\rm BALDA}(n_i) \right), \tag{40}$$

avec

$$e_{\rm c}^{\rm BALDA}(n,U) = e^{\rm BALDA}(n,U) - e^{\rm BALDA}(n,U=0) - \frac{U}{4}n^2, \tag{41}$$

où

$$e^{\rm BALDA}(U, n \leq 1) = \frac{-2t\beta(U/t)}{\pi} \sin\left(\frac{\pi n}{\beta(U/t)}\right), \tag{42}$$

et la fonction β est définie par

$$\frac{-2\beta(U/t)}{\pi} \sin\left(\frac{\pi}{\beta(U/t)}\right) = -4\int_0^\infty \frac{dx}{x} \frac{J_0(x)J_1(x)}{1+\exp\left(\frac{U}{2t}x\right)}. \tag{43}$$

BALDA s'est montrée très perfomante pour décrire les profils de densité et d'énergie du modèle de Hubbard à une dimension [40–42].

Théorie d'embedding de l'occupation des sites

Dans l'esprit des théories d'embedding, nous voulons développer une méthode où seuls certains sites seront traités en WFT et les autres en SOFT. Cette méthode est la SOET [25, 33–35]. Ainsi, un système de référence partiellement interagissant sera considéré à la place du système non interagissant de la SOFT. Les sites interagissants seront appelés les sites d'"impureté" (abbrégé par "imp" dans les équations), tandis que le "bain" ("bath" en anglais) fera référence aux sites non interagissants. Pour faire cette séparation, la fonctionnelle universelle est séparée en un terme d'impureté et une fonctionnelle Hxc du bain:

$$F(\mathbf{n}) = F_M^{\rm imp}(\mathbf{n}) + \overline{E}_{{\rm Hxc},M}^{\rm bath}(\mathbf{n}), \tag{44}$$

où M dénote le nombre d'impuretés du modèle et

$$F_M^{\rm imp}(\mathbf{n}) = \min_{\Psi\rightarrow\mathbf{n}} \left\{\langle\Psi|\hat{T}+\hat{U}_M|\Psi\rangle\right\}, \tag{45}$$

avec $\hat{U}_M = U\sum_{i=0}^{M-1}\hat{n}_{i\uparrow}\hat{n}_{i\downarrow}$. Comme en CAS-DFT, la fonctionnelle Hxc doit dépendre du nombre d'impureté(s) pour éviter tout problème de double comptage. L'énergie fondamentale en SOET se réduit à l'expression variationnelle suivante:

$$E(\mathbf{v}) = \min_{\Psi}\Big\{\langle\Psi|\hat{T}+\hat{U}_M|\Psi\rangle + \overline{E}_{{\rm Hxc},M}^{\rm bath}\left(\mathbf{n}^\Psi\right) + \left(\mathbf{v}|\mathbf{n}^\Psi\right)\Big\}, \tag{46}$$

où la fonction d'onde d'impureté $\Psi_M^{\rm imp}$ minimisant cette équation satisfait l'équation autocohérente:

$$\left(\hat{T} + \hat{U}_M + \sum_i \left[v_i + \frac{\partial \overline{E}^{\rm bath}_{{\rm Hxc},M}\left(\mathbf{n}^{\Psi_M^{\rm imp}}\right)}{\partial n_i} \right]\right) |\Psi_M^{\rm imp}\rangle = \mathcal{E}_M^{\rm imp} |\Psi_M^{\rm imp}\rangle, \tag{47}$$

où $v_i + \partial \overline{E}^{\rm bath}_{{\rm Hxc},M}(\mathbf{n})/\partial n_i = v^{\rm emb}_{M,i}(\mathbf{n})$ est le potential d'embedding permettant de reproduire la densité exacte du système physique. Tournons-nous à présent vers l'expression de la fonctionnelle Hxc du bain. Tout d'abord, exprimons la fonctionnelle d'impureté dans la décomposition KS:

$$F_M^{\rm imp}(\mathbf{n}) = T_{\rm s}(\mathbf{n}) + E^{\rm imp}_{{\rm Hxc},M}(\mathbf{n}), \tag{48}$$

où une fonctionnelle Hxc d'impureté est introduite, décrivant implicitement les interactions sur les sites d'impureté. Il est ensuite très facile de démontrer que la fonctionnelle du bain s'écrit comme:

$$\overline{E}^{\rm bath}_{{\rm Hxc},M}(\mathbf{n}) = E_{\rm Hxc}(\mathbf{n}) - E^{\rm imp}_{{\rm Hxc},M}(\mathbf{n}). \tag{49}$$

Ainsi, pour trouver la fonctionnelle du bain, nous pouvons utiliser les fonctionnelles en SOFT et développer de nouvelles fonctionnelles pour $E^{\rm imp}_{{\rm Hxc},M}$. Les systèmes non interagissants, partiellement interagissants et entièrement interagissants sont alors connectés par ces trois fonctionnelles, comme le montre la figure 2. Dans le cas du modèle uniforme ($\mathbf{v} = 0$), l'approximation locale est exacte et nous pouvons exprimer la fonctionnelle du bain par site, mesurant la déviation de la fonctionnelle d'impureté par rapport à la fonctionnelle standard, comme:

$$\overline{e}^{\rm bath}_{{\rm c},M}(\mathbf{n}) = \frac{1}{M}\left[\left(\sum_{i=0}^{M-1} e_c(n_i)\right) - E^{\rm imp}_{{\rm c},M}(\mathbf{n})\right], \tag{50}$$

tel que

$$\overline{E}^{\rm bath}_{{\rm c},M}(\mathbf{n}) = \sum_{i=M}^{L-1} e_{\rm c}(n_i) + M\overline{e}^{\rm bath}_{{\rm c},M}(\mathbf{n}), \tag{51}$$

où BALDA sera utilisée pour décrire l'énergie de corrélation par site $e_{\rm c}(n)$.

Pour résumer, trois résultats importants ont été trouvés dans cette thèse:

1. Il est nécessaire que la fonctionnelle du bain par site $\overline{e}^{\rm bath}_{{\rm c},M}(\mathbf{n})$ doive dépendre de toutes les occupations des sites. Autrement, l'embedding ne peut pas être exact.

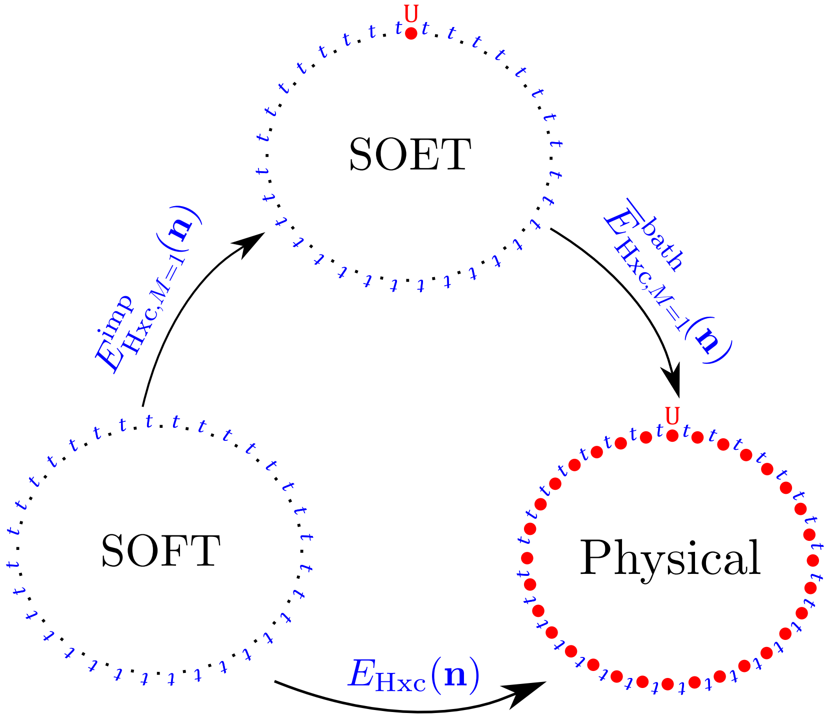

Figure 2: Illustration de la connexion entre le système physique, le système à une impureté, et le système non interagissant pour le modèle de Hubbard à 32 sites, à une dimension avec des conditions périodiques.

2. L'expression exacte de l'énergie par site du modèle uniforme est donnée par:

$$e = \frac{1}{M}\sum_{i=0}^{M-1}\left(t_{\mathrm{s}}(n_i^{\Psi_M^{\mathrm{imp}}}) + t\frac{\partial e_{\mathrm{c}}(n_i^{\Psi_M^{\mathrm{imp}}})}{\partial t} + U d^{\mathrm{imp}}_{M,i}\right) + \frac{\partial \overline{e}^{\mathrm{bath}}_{\mathrm{c},M}(\mathbf{n}^{\Psi_M^{\mathrm{imp}}})}{\partial U}, \tag{52}$$

où $d^{\mathrm{imp}}_{M,i} = \langle \Psi^{\mathrm{imp}}_M | \hat{n}_{i\uparrow}\hat{n}_{i\downarrow} | \Psi^{\mathrm{imp}}_M \rangle$.

3. L'expression exacte de la double occupation du modèle uniforme est donnée par:

$$d = \frac{1}{M}\sum_{i=0}^{M-1} d^{\mathrm{imp}}_{M,i} + \frac{\partial \overline{e}^{\mathrm{bath}}_{\mathrm{c},M}(\mathbf{n}^{\Psi_M^{\mathrm{imp}}})}{\partial U}. \tag{53}$$

D'après les deux expressions des Eqs. (52) et (53), il est clair que nous avons bien une combinaison de termes déterminés par la fonction d'onde d'impureté, et de termes venant de la fonctionnelle des occupations des sites: donc une méthode hybride mixant WFT et SOFT.

Ensuite, pour appliquer la SOET en pratique, des fonctionnelles de corrélation de l'impureté ont été développées. La première, la plus simple, utilise BALDA sur le(s) site(s) d'impureté, donnant naissance à l'approximation iBALDA (pour "impurity BALDA"):

$$E^{\mathrm{imp}}_{\mathrm{Hxc},M}(\mathbf{n}) \xrightarrow{\mathrm{iBALDA}(M)} \sum_{i=0}^{M-1} e_{\mathrm{c}}^{\mathrm{BALDA}}(n_i), \tag{54}$$

ce qui revient à négliger la contribution de l'énergie de corrélation par site du bain:

$$\overline{e}^{\mathrm{bath}}_{\mathrm{c},M}(\mathbf{n}) \xrightarrow{\mathrm{iBALDA}(M)} 0. \tag{55}$$

Une autre consiste à utiliser la fonctionnelle d'impureté exacte du dimère de Hubbard, dénotée par "2L":

$$E^{\mathrm{imp}}_{\mathrm{c},M=1}(\mathbf{n}) \longrightarrow E^{\mathrm{imp,2L}}_{\mathrm{c},M=1}(U, n_0) = E_{\mathrm{c}}^{\mathrm{2L}}(U/2, n_0), \tag{56}$$

où la relation de scaling en $U/2$ de l'égalité précédente a été prouvée dans un précédent travail sur le dimère [33], et la fonctionnelle $E_{\mathrm{c}}^{\mathrm{2L}}(U, n_0)$ possède une expression paramétrée par Carrascal *et al.* [43, 44] (n_0 correspond à l'occupation du site d'impureté). Combinée à BALDA, utilisée pour la fonctionnelle standard [voir Eq. (49)], l'approximation s'intitulera 2L-BALDA. Enfin, des fonctionnelles basées sur le modèle d'Anderson (SIAM, pour "single impurity Anderson model) ont également été développées, grâce à la grande similarité entre le modèle d'impureté de Hubbard et le SIAM:

$$E^{\mathrm{imp}}_{\mathrm{c},M=1}(\mathbf{n}) \longrightarrow E_{\mathrm{c}}^{\mathrm{SIAM}}(n_0). \tag{57}$$

Combinées à BALDA décrivant la fonctionnelle standard, ces approximations sont dénotées par l'acronyme SIAM-BALDA. Dans ce résumé, seule l'approximation SIAM-BALDA[n=1] (qui est une interpolation de deux fonctionnelles, l'une valide dans le régime faiblement corrélé et l'autre dans le régime fortement corrélé) sera présentée.

Passons à présent aux résultats obtenus par la résolution de l'Eq. (47) en fonction des différentes approximations. Cette résolution nous donne la fonction d'onde d'impureté Ψ^{imp}_M, et donc l'occupation convergée des sites, $\mathbf{n}^{\Psi^{\mathrm{imp}}_M}$, ainsi que la double occupation des sites de l'impureté, $d^{\mathrm{imp}}_{M,i}$. Il suffit d'utiliser ces valeurs dans les Eqs. (52) et (53) pour obtenir les résultats des figures 3 et 4 pour le modèle de Hubbard à 32 sites, respectivement. Il est important de noter qu'à demi-remplissage, le potentiel d'embedding exact est connu et est égal à $-U/2$ sur les sites d'impureté et 0 dans le bain. Ce potentiel restaure donc l'occupation exacte des sites, et aucune erreur due à la densité n'est observée. Il est clair d'après ces deux figures que l'approximation iBALDA pour $M = 1$ n'est pas

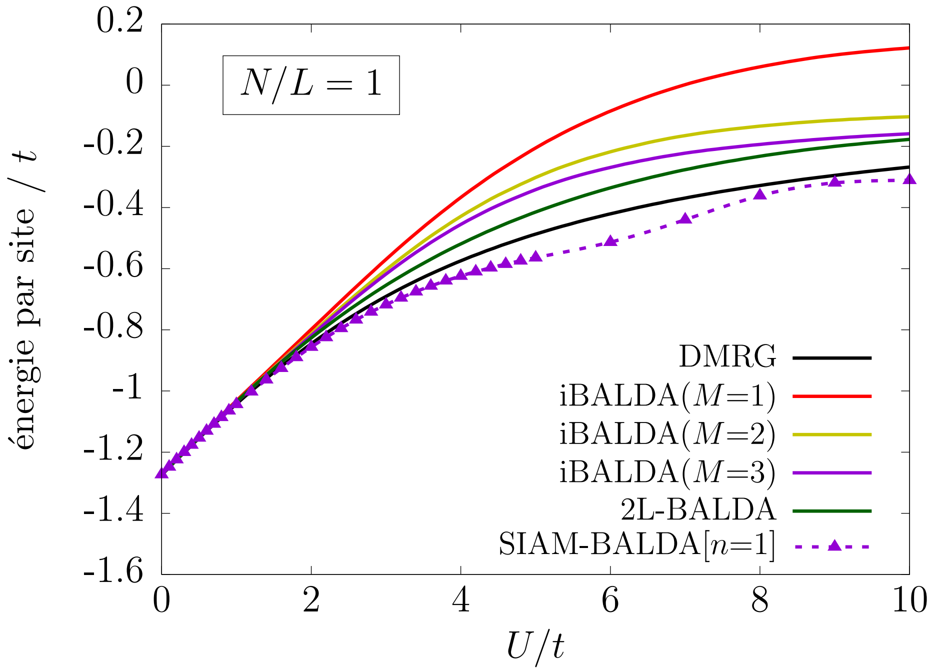

Figure 3: Énergie par site à demi-remplissage en fonction de U/t. L'énergie obtenue par calcul DMRG sur le système physique entièrement interagissant est la référence.

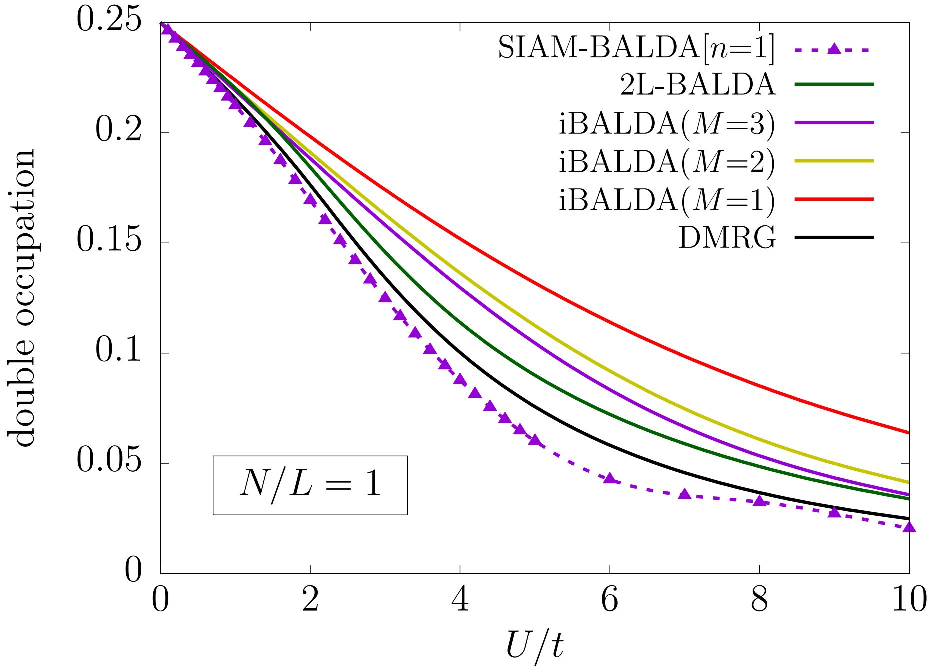

Figure 4: Pareil que la figure 3 mais pour la double occupation.

très performante. Il existe deux manières possibles pour améliorer les résultats en SOET. La première manière est d'augmenter le nombre d'impuretés dont l'interaction est traitée explicitement en WFT, conduisant aux approximations iBALDA(M=2) et iBALDA(M=3). L'amélioration est visible mais n'est pas significative, or le temps de calcul augmente avec le nombre d'impuretés considéré. La deuxième manière est de considérer une fonctionnelle $\overline{e}^{\rm bath}_{{\rm c},M}(\mathbf{n})$ non nulle. Les approximations 2L-BALDA et SIAM-BALDA[n=1] sont de telles fonctionnelles, et elles fournissent de meilleurs résultats que iBALDA(M=3) bien qu'une seule impureté soit considérée. Ainsi, il semble plus important de développer de meilleures fonctionnelles en gardant un nombre d'impuretés faible, plutôt que d'augmenter le nombre d'impuretés.

Vers une implementation performante de la SOET

Contrairement aux autres méthodes de type embedding, l'information sur l'occupation des sites du bain n'est pas perdue en SOET. Cependant, bien que ce point semble avantageux, il génère également des problèmes, notamment dans l'implémentation de la SOET dont la résolution nécessite un temps de calcul élevé. Or, seulement certains sites sont explicitement interagissants. Il est donc naturel de se demander si une implémentation différente de la SOET, nécessitant un temps de calcul faible, existe. Dans cette partie, nous allons montrer qu'il est en effet possible de résoudre les équations de la SOET en un temps très court, tout en conservant d'excellents résultats. Dans l'esprit de la DMET ("density matrix embedding theory") [45], cette nouvelle implémentation de la SOET consiste à employer la décomposition de Schmidt (également utilisée en DMRG). Dans une première étape, le système est divisé en deux parties: un fragment F et le reste du système E, appelé environnement. L'espace de Hilbert du système s'écrit alors comme un produit tensoriel de celui de F et de E, $\mathcal{H} = \mathcal{H}_F \otimes \mathcal{H}_E$. La taille de $\mathcal{H}_F$ ($\mathcal{H}_E$) est $N_F = 4^{L_F}$ ($N_E = 4^{L_E}$) et $\{|F_i\rangle\}_i$ ($\{|E_i\rangle\}_j$) représente une base d'états multicorps. L_F et L_E sont respectivement le nombre d'orbitales (ou ici, le nombre de sites) du fragment et de l'environnement, et le nombre 4 vient du fait qu'un site est décrit par 4 états différents: $|rmvac\rangle$, $|\uparrow\rangle$, $|\downarrow\rangle$ et $|\uparrow\downarrow\rangle$. La fonction d'onde de l'état fondamental du système peut alors s'écrire

$$|\Psi_0\rangle = \sum_i^{N_F}\sum_j^{N_E} C_{ij}|F_i\rangle|E_j\rangle, \tag{58}$$

et peut être simplifiée en appliquant une décomposition en valeur singulière:

$$|\Psi_0\rangle = \sum_i^{N_F}\sum_j^{N_E}\sum_\alpha^{\min(N_F,N_E)} \tilde{U}_{i\alpha}\lambda_\alpha\tilde{V}^\dagger_{\alpha j}|F_i\rangle|E_j\rangle \tag{59}$$

$$= \sum_\alpha^{N_F}\lambda_\alpha|F_\alpha\rangle|B_\alpha\rangle, \tag{60}$$

où on a supposé que $N_F < N_E$. $\tilde{U}_{i\alpha}$ ($\tilde{V}^\dagger_{\alpha j}$) transforme la base $\{|F_i\rangle\}_i$ ($\{|E_j\rangle\}_j$) en une nouvelle base $\{|F_\alpha\rangle\}_\alpha$ ($\{|B_\alpha\rangle_\alpha\}$):

$$\sum_i^{N_E}\tilde{U}^\dagger_{i\alpha}|F_i\rangle = |F_\alpha\rangle, \qquad \left(\sum_j^{N_E}\tilde{V}^\dagger_{\alpha j}|E_j\rangle = |B_\alpha\rangle\right), \tag{61}$$

appelée la base du fragment. Quand cette dernière est combinée à la base du bain [entre parenthèse dans l'Eq. (61)], une nouvelle base dîte de Schmidt de dimension N_F^2 est construite. En effet, il est clair d'après l'Eq. (59) que le nombre d'états à considérer pour l'environnement a été réduit à N_F états du bain, alors que le nombre d'états du fragment est resté inchangé. Ensuite, un projecteur sur cette base de Schmidt est construit grâce aux nouveaux états du fragment et du bain tel que $\hat{P} = \sum_{\alpha\beta}^{N_F}|F_\alpha B_\beta\rangle\langle F_\alpha B_\beta|$. On peut montrer facilement que la fonction d'onde de l'état fondamental Ψ_0 est invariante sous cette projection, et que l'Hamiltonien projeté (dit Hamiltonien d'embedding), $\hat{H}' = \hat{P}\hat{H}\hat{P}$, partage la même énergie d'état fondamentale que le système physique. Ainsi, la décomposition de Schmidt permet de réduire considérablement le nombre d'états à considérer dans la fonction d'onde, tout en conservant les propriétés de l'état fondamental. Cependant, celle-ci nécessite la connaissance *a priori* de la fonction d'onde Ψ_0, qui est bien entendu inconnue. En DMET, un calcul Hartree–Fock est utilisé pour obtenir une approximation à Ψ_0. La décomposition de Schmidt est ensuite appliquée sur le déterminant de HF, pour construire des états du bain simple corps au lieu d'états multicorps. En SOET, un calcul SOFT est effectué à la place. La décomposition de Schmidt est donc appliquée sur le déterminant KS, permettant de construire les états du bain (approximés) et donc le projecteur $\hat{P}$. La grande différence avec la formulation précédente de la SOET est que l'information sur l'environnement est perdue, puisque celui-ci est projeté pour former les états du bain. Reconsidérons l'Hamiltonien en SOET pour un système uniforme:

$$\hat{H}^{\rm SOET} = \hat{T} + \hat{U}_M + \sum_{i=0}^{L-1}\left[\left.\frac{\partial\overline{E}^{\rm bath}_{{\rm Hxc},M}(\mathbf{n})}{\partial n_i}\right|_{\mathbf{n}=\underline{n}_0^{\Psi_M^{\rm imp}}}\right]\hat{n}_i. \tag{62}$$

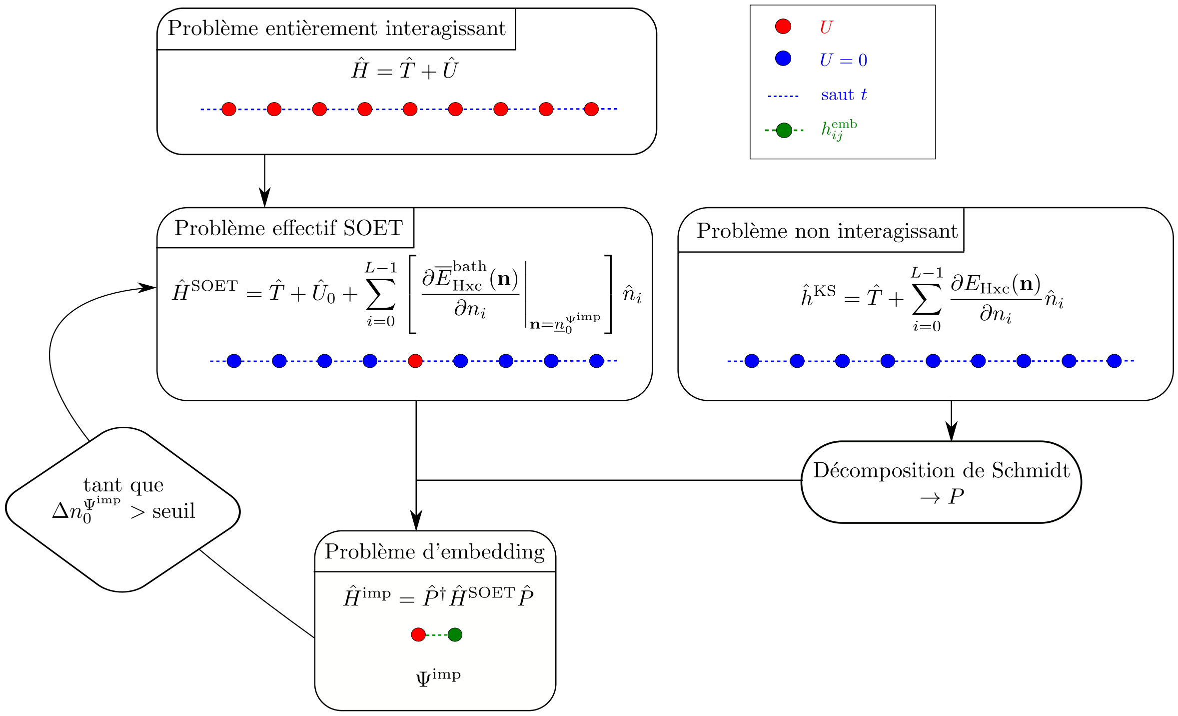

Figure 5: Étapes de la P-SOET pour une seule impureté dénotée par 0. Le projecteur est calculé une seule fois grâce à la décomposition de Schmidt sur la fonction d'onde obtenue en appliquant KS-SOFT sur le modèle de Hubbard.

Ce dernier est projeté pour construire l'Hamiltonien d'embedding. Pour ce faire, seule la partie monoélectronique de $\hat{H}^{\text{SOET}}$ est projetée (la répulsion électronique traitée explicitement sur les impuretés reste inchangée), c'est-à-dire l'opérateur d'énergie cinétique et le potentiel d'embedding, pour former $\hat{h}^{\text{emb}} = \hat{P}\hat{h}^{\text{SOET}}$. L'Hamiltonien SOET projeté devient alors

$$\hat{H}^{\text{imp}} = \hat{h}^{\text{emb}} + \hat{U}_M = \sum_{ij=0}^{2M-1} \sum_{\sigma} h_{ij}^{\text{emb}} \left(\hat{c}_{i\sigma}^{\dagger} \hat{c}_{j\sigma} + \text{h.c.} \right) + U \sum_{i=0}^{M-1} \hat{n}_{i\uparrow} \hat{n}_{i\downarrow}. \tag{63}$$

Dans le cas d'une seule impureté, ce nouveau problème d'embedding se réduit à un site d'impureté et un site de bain uniquement, c'est-à-dire un dimère de Hubbard à une impureté qui peut être résolu analytiquement. Une fois le problème résolu, une nouvelle occupation du site de l'impureté est obtenue et réinsérée dans le potentiel d'embedding de l'Hamiltonien de l'Eq. (62), lui-même à nouveau projeté, et ainsi de suite jusqu'à ce que l'occupation converge. Pour résumer, la figure 5 décrit les différentes étapes de cette nouvelle implémentation, nommée P-SOET (pour "Projected-SOET"). Plus généralement, pour M impuretés, le problème d'embedding à résoudre est de taille $2M$.

La P-SOET nous permet d'étudier un modèle de Hubbard bien plus grand qu'avec la première implémentation de la SOET, pour un temps de calcul encore plus petit. De ce fait, 400 sites seront à présent considérés au lieu de 32 sites. Dans ce résumé, seule la description de la transition de Mott en fonction du remplissage [46] sera présentée. Cette transition de Mott est manifestée par l'ouverture d'un gap de charge entre la bande de valence et la bande de conduction. Dans le modèle de Hubbard, l'ouverture du gap se fait dans le cas du demi-remplissage. Autrement, aucun gap n'est observé. Pour voir l'apparition de cette transition, nous traçons la densité en fonction du potentiel chimique μ qui correspond à un déplacement du potentiel externe, et qui fixe le nombre d'électrons dans le système:

$$\hat{H} \longrightarrow \hat{H}(\mu) = \hat{H} - \mu\hat{N}, \tag{64}$$

où $\hat{N} = \sum_i \hat{n}_i$ est l'opérateur de comptage. Le nombre total d'électrons varie avec μ tant que μ ne se situe pas à l'intérieur du gap. Dans le cas contraire, la variation de μ à l'intérieur du gap n'induit aucun changement du nombre d'électrons, qui restera égal au nombre d'électrons remplissant entièrement la bande de valence (c'est-à-dire $n = N/L = 1$ pour le modèle de Hubbard). Pour trouver le nombre d'électrons correspondant à une valeur du potentiel chimique, il suffit de résoudre l'Hamiltonien $\hat{H}(\mu)$ pour un μ donné en faisant varier le nombre d'électrons du système. Autrement dit, la minimisation suivante doit être résolue:

$$\min_N \left\{ e^{\text{P-SOET}}(n) - \mu N/L \right\}, \tag{65}$$

où n est la densité exacte $n = N/L$. Pour voir l'effet de l'autocohérence et l'erreur sur la densité due aux différentes approximations en P-SOET, la densité convergée a aussi été utilisée, $n = n_0^{\Psi_M^{\text{imp}}}$. Puisque seulement des nombres pairs d'électrons sont considérés, et que le modèle contient 400 sites, un ensemble de 200 valeurs de N est pris en compte pour la minimisation. Cette minimisation n'aurait pas été qualitativement correcte dans la formulation précédente de la SOET, où le modèle contenait uniquement 32 sites. La densité minimisante, $n(\mu) = N(\mu)/L$ [où $N(\mu)$ est le nombre d'électrons qui minimise le terme dans l'Eq. (65)] est tracée sur la figure 6 en fonction du potentiel chimique. D'après la figure 6, la densité augmente avec le potentiel chimique de façon monotone jusqu'à atteindre le demi-remplissage $n = 1$. À cette valeur, la densité reste constante bien que le potentiel chimique continue d'augmenter, indiquant l'ouverture du gap de charge. En utilisant la densité exacte $n = N/L$ dans l'Eq. (65) (lignes pleines sur la figure 6), iBALDA (M=1) est quasiment superposée à la courbe exacte (légendée par BA). Du coup, augmenter le nombre d'impuretés n'améliore pas les résultats, bien que cela ne les détériore pas non plus. Si la densité convergée est utilisée, alors de fortes erreurs sont observées plus on s'approche du demi-remplissage. Il est intéressant de noter que l'approximation 2L-BALDA sous-estime largement la valeur du gap de charge par rapport à iBALDA. Cependant, il est déjà impressionnant que ces approximations en P-SOET permettent de décrire l'ouverture du gap

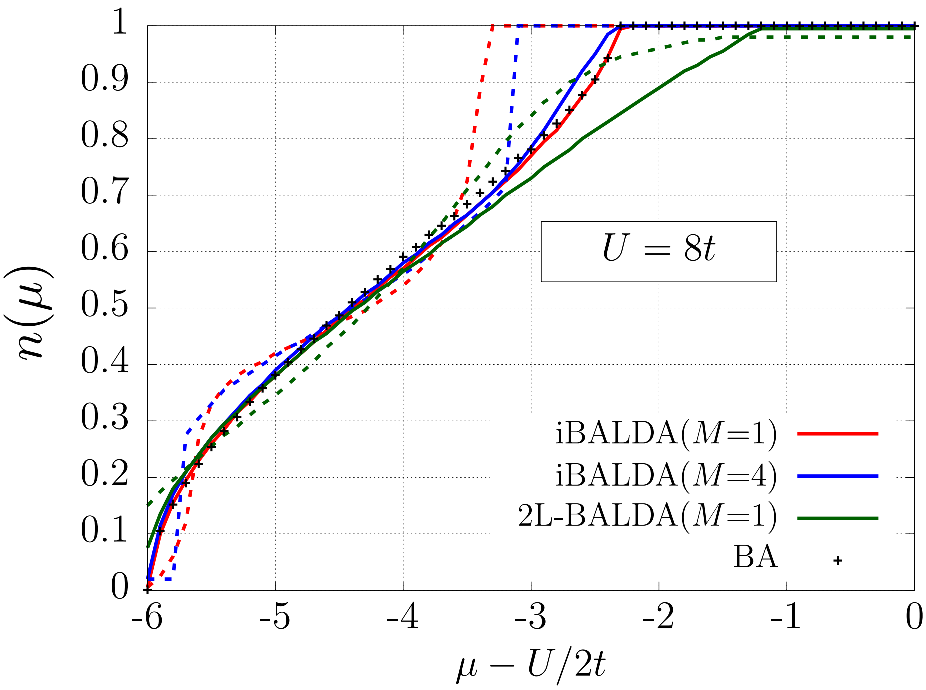

Figure 6: Variation du remplissage en fonction du potentiel chimique pour $U/t = 8$ obtenue en résolvant Eq. (65) en utilisant la densité exacte $[e^{\text{P-SOET}}(n = N/L)]$ (lignes pleines), et la densité convergée $[e^{\text{P-SOET}}(n = n_0^{\Psi_M^{\text{imp}}})]$ (lignes pointillées). BA est l'acronyme de "Bethe Ansatz" et est la courbe de référence exacte.

avec une seule impureté. En effet, cette transition de Mott (en fonction du remplissage) n'est décrite ni par la DMET [45, 47], ni par la DMFT [46] (pour "dynamical mean-field theory") avec une seule impureté. L'ouverture de ce gap avec une seule impureté est le résultat le plus marquant de la SOET, en plus des autres résultats très prometteurs pour la double occupation et l'énergie par site.

Conclusions et Perspectives

Ce résumé nous a permis de voir succintement le développement et les résultats principaux de la SOET, et également de la P-SOET. Nous avons montré que cette théorie était bien une théorie hybride, mélangeant WFT et DFT pour obtenir les résultats les plus précis possible en un temps relativement court. La SOET (et sa version projetée) s'est montrée très prometteuse, et peut jouer un rôle très important dans le développement de nouvelles méthodes hybrides. De par sa formulation en principe exacte, celle-ci permet d'avoir une compréhension plus approfondie des méthodes de type embedding, où les problèmes de double comptage ne sont pas toujours évidents à identifier. Pour que la SOET devienne plus populaire et soit utilisée par la communauté scientifique, il faudrait l'appliquer à des modèles plus complexes, comme les modèles de Hubbard à deux (pour la description des supraconducteurs $LaCuO_4$) ou trois dimensions. Pour cela, de nouvelles fonctionnelles sont nécessaires, et un moyen d'en développer de façon automatique serait très attrayant. Dans le cadre de la chimie quantique, une généralisation de la SOET a été proposée dans le dernier chapitre de cette thèse (non montrée dans ce résumé), et est encore en cours de développement.

Bibliography

[1] Y. Tokura, N. Nagaosa, *Science* **2000**, *288*, 462–468.

[2] T. Helgaker, P. Jorgensen, J. Olsen, *Molecular electronic-structure theory*, John Wiley & Sons, **2014**.

[3] A. J. Cohen, P. Mori-Sánchez, W. Yang, *Chem. Rev.* **2011**, *112*, 289–320.

[4] Q. Sun, G. K.-L. Chan, *Acc. Chem. Res.* **2016**, *49*, 2705–2712.

[5] M. Born, R. Oppenheimer, *Ann. Phys.* **1927**, *389*, 457.

[6] B. L. Hammond, W. A. Lester, P. J. Reynolds, *Monte Carlo methods in ab initio quantum chemistry*, *Vol. 1*, World Scientific, **1994**.

[7] J. C. Slater, *Phys. Rev.* **1930**, *35*, 210.

[8] V. Fock, *Z. Phys.* **1930**, *61*, 126–148.

[9] Ł. Mentel, X. Sheng, O. Gritsenko, E. Baerends, *J. Chem. Phys.* **2012**, *137*, 204117.

[10] A. D. Becke, *J. Chem. Phys.* **2013**, *138*, 074109.

[11] K. H. Marti, I. M. Ondik, G. Moritz, M. Reiher, *J. Chem. Phys.* **2008**, *128*, 014104.

[12] S. R. White, *Phys. Rev. Lett.* **1992**, *69*, 2863.

[13] S. R. White, *Phys. Rev. B* **1993**, *48*, 10345.

[14] S. Wouters, D. Van Neck, *Eur. Phys. J. D* **2014**, *68*, 272.

[15] N. Nakatani, S. Guo, *J. Chem. Phys.* **2017**, *146*, 094102.

[16] L. H. Thomas in Mathematical Proceedings of the Cambridge Philosophical Society, *Vol. 23*, Cambridge University Press, **1927**, pp. 542–548.

[17] E. Fermi, *Rend. Accad. Naz. Lincei* **1927**, *6*, 32.

[18] P. A. Dirac in Mathematical Proceedings of the Cambridge Philosophical Society, *Vol. 26*, Cambridge University Press, **1930**, pp. 376–385.

[19] M. Levy, *Proc. Natl. Acad. Sci.* **1979**, *76*, 6062–6065.

[20] M. A. L. Marques, M. J. T. Oliveira, T. Burnus, *Computer Physics Communications* **2012**, *183*, 2272–2281.

[21] N. Mardirossian, M. Head-Gordon, *Mol. Phys.* **2017**, *115*, 2315–2372.

[22] A. Savin, *Recent Developments and Applications of Modern Density Functional Theory*, Elsevier, Amsterdam, **1996**, p. 327.

[23] T. Leininger, H. Stoll, H.-J. Werner, A. Savin, *Chem. Phys. Lett.* **1997**, *275*, 151.

[24] P. Gori-Giorgi, A. Savin, *Int. J. Quantum Chem.* **2009**, *109*, 1950–1961.

[25] E. Fromager, *Mol. Phys.* **2015**, *113*, 419.

[26] B. B. Miehlich, H. Stoll, A. Savin, *Mol. Phys.* **1997**, *91*, 527–536.

[27] J. Gräfenstein, D. Cremer, *Chem. Phys. Lett.* **1999**, *316*, 569.

[28] Y. Kurzweil, K. V. Lawler, M. Head-Gordon, *Mol. Phys.* **2009**, *107*, 2103–2110.

[29] A. Savin, *Int. J. Quantum Chem.* **1988**, *34*, 59.

[30] C. Gutlé, A. Savin, *Phys. Rev. A* **2007**, *75*, 032519.

[31] C. Huang, M. Pavone, E. A. Carter, *J. Chem. Phys.* **2011**, *134*, 154110.

[32] K. Yu, F. Libisch, E. A. Carter, *J. Chem. Phys.* **2015**, *143*, 102806.

[33] B. Senjean, M. Tsuchiizu, V. Robert, E. Fromager, *Mol. Phys.* **2017**, *115*, 48–62.

[34] B. Senjean, N. Nakatani, M. Tsuchiizu, E. Fromager, *Phys. Rev. B* **2018**, *97*, 235105.

[35] B. Senjean, N. Nakatani, M. Tsuchiizu, E. Fromager, *arXiv:1806.06057* **2018**.

[36] J. Hubbard, *Proc. R. Soc. London A* **1963**, *276*, 238–257.

[37] J. Hubbard, *Proc. R. Soc. London A* **1964**, *277*, 237–259.

[38] J. Hubbard, *Proc. R. Soc. London A* **1964**, *281*, 401.

[39] J. Hubbard, *Proc. R. Soc. London A* **542-560**, *285*, 238–257.

[40] N. Lima, L. Oliveira, K. Capelle, *Europhys. Lett.* **2002**, *60*, 601.

[41] N. A. Lima, M. F. Silva, L. N. Oliveira, K. Capelle, *Phys. Rev. Lett.* **2003**, *90*, 146402.

[42] K. Capelle, N. Lima, M. Silva, L. Oliveira in *The Fundamentals of Electron Density, Density Matrix and Density Functional Theory in Atoms, Molecules and the Solid State*, Springer, **2003**, p. 145.

[43] D. J. Carrascal, J. Ferrer, J. C. Smith, K. Burke, *J. Phys. Condens. Matter* **2015**, *27*, 393001.

[44] D. Carrascal, J. Ferrer, J. Smith, K. Burke, *J. Phys. Condens. Matter* **2016**, *29*, 019501.

[45] G. Knizia, G. K.-L. Chan, *Phys. Rev. Lett.* **2012**, *109*, 186404.

[46] M. Capone, M. Civelli, S. Kancharla, C. Castellani, G. Kotliar, *Phys. Rev. B* **2004**, *69*, 195105.

[47] I. W. Bulik, G. E. Scuseria, J. Dukelsky, *Phys. Rev. B* **2014**, *89*, 035140.

Introduction

Quantum chemistry applies quantum mechanics to the theoretical study of chemical systems. It aims at understanding the mechanisms of chemical reactions (driven by thermodynamic and kinetic properties of chemical systems) by the study of chemical structure and chemical dynamics. On the other hand, the purpose of condensed matter physics is to rationalize natural phenomena in condensed phases, like the transition between a metal and an insulator driven by the variation of various parameters (such as pressure or the introduction of impurities, so-called "doping"). Several methods and models have been developed in both fields. Not only they were able to reproduce experimental results, but they can also make predictions which are then verified by new observations. The quality of a theory is judged on both these criteria. Nevertheless (and despite the numerous progress made since the last decades) some systems remain extremely challenging to describe, for instance the so-called *strongly correlated* materials.

Strongly correlated systems are the object of intense research since many years now. The development and synthesis of innovative materials gather both chemists and physicists, experimentalists or theoreticians. This topic covers several long-standing issues in quantum theory, starting from the theoretical modelling of a simple bond-breaking in chemistry to the description of transition metal complexes, featuring magnetic and electronic properties of high interest. For instance, strongly correlated materials can exhibit metal-insulator transitions (NiO and V_2O_3), temperature induced phase transition leading to high-T_c superconductors (La_2CuO_4 and the doped $La_{2-x}Sr_xCuO_4$) or colossal magnetoresistance ($LaMnO_3$) in condensed matter physics [1]. These exotic properties have led to the design of new nanodevices, with applications to energy conversion and electronic transport for solar cells, magnetic storage, and superconducting magnets generating strong magnetic fields. Transition metal oxides are also employed in homogeneous and heterogeneous catalysis, and are present in chemical biology where the active part of a protein is composed of metallic centers. While the discovery of novel materials continues to grow, there is a profound need for the development of new theoretical approaches. New methods should be able to give a better understanding of these existing materials and, ultimately, to predict new structures featuring such interesting properties, which promise to shape the technology of the future.

From a theoretical point of view, the name “strongly correlated” originates from the fact that mean-field theory (or band theory for solids) is not able to describe the aforementioned systems. The reason is that mean-field theory (in a sense of Hartree–Fock theory) misses the description of correlation effects, driven by the interaction between the electrons. When this correlation plays a prominent role, it is the so-called *strong* electron correlation which remains a tremendous problem in both quantum chemistry and solid state physics. Indeed, no method has yet emerged as the method of choice for modelling such materials. While the standard low-cost methods such as *density functional theory* (DFT) usually fail to describe strong correlation effects [2], more involved wavefunction-based approaches (WFT) [3] could in principle be applied, but they remain out of reach in terms of computational cost. A natural and intuitive idea is to merge the two methods to build a new one that gathers all advantages: a low computational cost and good accuracy. One specific class of these hybrid methods features is the class of “embedding” theories [4]. They rely on the separation of the whole system into small subsystems, where only the active part of interest is treated by a high-level (WFT) method while the rest of the system is treated by a low-level approach (such as DFT or mean-field theory). Embedding techniques are gaining more and more interest, above all because Moore’s law is now reaching its limit, thus lending weight to the development of low-cost approaches able to model large systems with sufficient accuracy. They are now popular in both quantum chemistry, for atoms and molecules, and condensed matter physics for extended systems like solids. In the latter community, it is common to start with a simple model (which still contains the key physical effects of the realistic material) in order to develop new approaches. For example, the Hubbard model features the competition between localization (induced by a strong repulsion between the electrons, interpreted as the strongly correlated regime) and delocalization (interpreted as the weakly correlated regime) of the electrons, and is one of the worst case scenarios for mean-field theories.

This thesis aims to develop and implement novel and in-principle-exact hybrid methods at the interface between physics and chemistry. Focusing on the description of strong correlation effects, the methods will first be applied to the Hubbard model, and then generalized to the *ab-initio* molecular Hamiltonian. The thesis is organized as follows.

Chapter 1 gives the state of the art of the electronic structure theory in quantum chemistry. Sec. 1.1 starts from the foundation of quantum chemistry through the Schrödinger equation, for which several approximate solutions are discussed. The Hartree–Fock theory is briefly explained as well as the definition of the electronic correlation. Then, post-Hartree–Fock approaches are considered to account for correlation effects. Due to their high scaling with respect to the number of electrons, these methods become rapidly not tractable as the size of the system increases. Alternatively, methods based on reduced quantities as basic variable, instead of the complicated many-body wavefunction, are presented in Sec. 1.2. They consist of DFT, *reduced density matrix functional theory* (RDMFT) and one-body Green's function theory. Finally, various hybrid methods that merge WFT and DFT are introduced in Sec. 1.3.

Turning to the electronic structure theory in condensed matter physics in Chapter 2, model Hamiltonians (in particular the Hubbard model) and their relations with real materials are discussed in Sec. 2.1. Applying DFT in this context leads to the so-called *site occupation functional theory* (SOFT), described in Sec. 2.2. Then, the *single impurity Anderson model* (SIAM) is introduced in Sec. 2.3 as well as embedding techniques employed in condensed matter physics in Sec. 2.4.

Chapters 1 and 2 provide a large overview of the current state of the art in both quantum chemistry and condensed matter physics, respectively. They are both really helpful to understand the four following Chapters, which are all dedicated to new methods developed in this thesis.
Chapter 3 deals with the main topic of this thesis, i.e. the development and implementation of a new embedding scheme, so-called *site-occupation embedding theory* (SOET) applied to the one-dimensional Hubbard model. Starting with the in-principle exact formulation of SOET in Sec. 3.1, exact expressions for the per-site energy and the double occupation have been derived in the uniform case (Sec. 3.2). Then, exact properties that the functional in SOET should fulfil are given in Sec. 3.3. Finally, after introducing the approximate analytic functionals in Sec. 3.4, the SOET self-consistent equation is solved. The resulting per-site energy and double occupation are discussed extensively in Sec. 3.5.

Then, efficient implementations of the self-consistent impurity problem in SOET are discussed in Chapter 4. A transformation of the SOET Hamiltonian into the SIAM is made in Sec. 4.1, and is then solved using Green's function techniques. Another implementation in Sec. 4.2 consists in using the Schmidt decomposition, thus allowing a drastic decrease of the computational cost. As an important result, this projected version of SOET is able to describe the "density-driven" Mott–Hubbard transition, related to the opening of a gap.

Turning to another long-standing issue in DFT, Chapter 5 provides a complete reformulation of the infamous derivative discontinuity, necessary to extract the exact fundamental gap in DFT. This formulation is based on ensemble DFT, originally formulated for excited states to extract the optical gap, as described in Sec. 5.1. After introducing the fundamental gap problem within DFT in Sec. 5.2, we present our new formulation, so-called N-centered ensemble DFT, in Sec. 5.3.

To conclude, the extension of SOET to the quantum chemical Hamiltonian is discussed in Sec. 6.1 of Chapter 6. An alternative approach is then developed based on geminals, i.e. pair-electron functions.

The notion of seniority-zero and theories based on geminals are first briefly introduced in Sec. 6.2, then followed by the new hybrid method formulated in the natural orbital basis, where a reference seniority-zero wavefunction is complemented by a functional of the reduced one-particle density matrix (Sec. 6.3). Conclusions and perspectives are finally ending this work.

Chapter 1

Electronic Structure Theory in Quantum Chemistry

The correct description of the total ground-state energy of a molecule is essential in chemistry and material science. Indeed, the understanding and the prediction of a given chemical reaction obviously involve the knowledge of the ground-state energy of the electrons [5], as it gives informations about the reaction barrier which has to be overcome to obtain a given chemical product. It often appears that only a very small energy difference determines the geometries and qualitative properties of molecules [6], such as a transition state or the adsorption of a molecule on a surface.

Hence, one needs highly accurate theoretical methods to reach this chemical accuracy (≈ 1 kcal/mol). This is the main goal of quantum chemistry. However, systematically improvable methods are usually extremely expensive in terms of computational cost so that only very small systems can be considered. Because of the growing interest in supramolecular science, as well as the need to understand biological processes or the modelling of real size materials (such as batteries or photovoltaic cells), more than a thousand of atoms is commonly studied. This can be achieved by using the mean-field theory, but the gain in computational cost usually comes with a decrease in chemical accuracy.

In this Chapter, I will review some of the quantum chemical methods that are needed to understand the development and the context of our new methods described in Chapters 3, 4, 5 and 6. First, the Schrödinger equation which is the central equation in quantum chemistry is introduced. Because this equation is impossible to solve generally, approximations have to be employed such as the mean-field theory. However, such a theory does not describe the electron correlation, essential to describe chemical processes involving creation or breaking of the bonds, for instance. To go beyond this approximation, several post-mean-field methods have been developed and are described in this chapter, which is organized as follows. Sec. 1.1 lays the basics of the electronic structure theory which relies on the explicit calculation of a many-body wavefunction. Starting from the mean-field approximation with a single Slater determinant wavefunction, more involved methods employing a multiconfigurational wavefunction (which are approximate solutions of the Schrödinger equation) are introduced. Then, alternative treatments of the electronic problem are considered in Sec. 1.2, where the whole many-body complexity is transferred from the wavefunction to reduced quantities, such as the electron density, the one-particle density matrix or the one-particle Green's function. Finally, Sec. 1.3 introduces hybrid methods which combine wavefunction theory with density functional theory.

1.1 Wavefunction Theory

1.1.1 Schrödinger Equation and Born-Oppenheimer Approximation

The evolution in time of a physical system containing significant quantum effects is mathematically described by the Schrödinger equation, derived in 1925 by Erwin Schrödinger (Nobel Prize in Physics, 1933). Considering a system evolving in a time-independent potential and where relativistic effects are negligible, this equation reduces to one of the most famous eigenvalue equations, the time-independent Schrödinger equation,

$$\hat{H}|\Psi\rangle = E|\Psi\rangle, \tag{1.1}$$

where Ψ is the stationary state wavefunction of the quantum system with associated total energy E. For a given molecular system containing N electrons of mass m_e, charge e and positions $\{\mathbf{r}_i\}_{i=1,N}$ and M nuclei of mass $\{M_A\}_{A=1,M}$, charge $Z_A \times e$ and positions $\{\mathbf{R}_A\}_{A=1,M}$, the Hamiltonian in Eq. (1.1) reads (in SI units)

$$\begin{aligned}\hat{H} &= \hat{T}_\mathrm{n} + \hat{T}_\mathrm{e} + \hat{V}_\mathrm{ne} + \hat{W}_\mathrm{ee} + \hat{V}_\mathrm{n} \\ &= -\sum_{A=1}^{M} \frac{\hbar^2}{2M_A}\nabla_A^2 - \sum_{i=1}^{N} \frac{\hbar^2}{2m_\mathrm{e}}\nabla_i^2 - \sum_{i=1}^{N}\sum_{A=1}^{M} \frac{Z_A e^2}{4\pi\varepsilon_0|\mathbf{R}_A - \mathbf{r}_i|} \\ &\quad + \sum_{i=1}^{N}\sum_{j>i}^{N} \frac{e^2}{4\pi\varepsilon_0|\mathbf{r}_i - \mathbf{r}_j|} + \sum_{A=1}^{M}\sum_{B>A}^{M} \frac{Z_A Z_B e^2}{4\pi\varepsilon_0|\mathbf{R}_A - \mathbf{R}_B|},\end{aligned} \tag{1.2}$$

where $\hat{T}_\mathrm{n}$ and $\hat{T}_\mathrm{e}$ are the nuclear and electron kinetic energy operators, respectively, and $\hat{V}_\mathrm{ne}$, $\hat{W}_\mathrm{ee}$ and $\hat{V}_\mathrm{n}$ are the potential energy operators corresponding to Coulomb electron-nuclei attraction, electron-electron and nuclei-nuclei repulsions, respectively. In quantum chemistry, one of the main targets is the correct description of chemical reactions. In other words, the forming and breaking of chemical bonds between atoms. These processes involve interactions between the electrons in the system, so that the part of interest of the Hamiltonian in Eq. (1.2) is the electronic part. Considering the ratio in mass between nuclei and electrons ($M_A/m_{\mathrm{e}} \approx 1836$), a first sound approximation is to consider the electronic motion decoupled from the motion of the nuclei. Equivalently, it means that the electrons accommodate almost instantaneously to any change in the positions of the nuclei, so that one can study the electronic part of a system while keeping the nuclei frozen. This is the so-called Born–Oppenheimer approximation proposed in 1927 [7]. The Schrödinger equation in Eq. (1.1) is then reduced to an electronic part decoupled from the nuclear part,

$$\hat{H}_{\mathrm{e}}|\Psi_{\mathrm{e}}\rangle = E_{\mathrm{e}}|\Psi_{\mathrm{e}}\rangle, \tag{1.3}$$

where E_{e} is the electronic energy associated to the electronic wavefunction Ψ_{e}. From a mathematical point of view, both are respectively the eigenvalue and eigenfunction of the electronic Hamiltonian

$$\hat{H}_{\mathrm{e}} = \hat{H} - \hat{T}_{\mathrm{n}} - \hat{V}_{\mathrm{n}} = \hat{T}_{\mathrm{e}} + \hat{W}_{\mathrm{ee}} + \hat{V}_{\mathrm{ne}}, \tag{1.4}$$

where the nuclear kinetic energy operator in Eq. (1.2) has been neglected and the nuclear-nuclear repulsive potential has become a constant for a given geometry, that has to be added after solving the electronic problem. This approximation is used in the whole thesis as well as the use of atomic units, so that the subscript "e" (standing for "electronic") will be dropped. From now on, atomic units will be used, which simply consists in using unitless energy $\tilde{E} = E/E_h$ and coordinates $\tilde{x} = x/a_0$, $\tilde{y} = y/a_0$ and $\tilde{z} = z/a_0$, where $E_h = \hbar^2/(m_{\mathrm{e}}a_0^2)$ ($= 1$ hartree) corresponds to two times the ionization energy of the hydrogen atom and $a_0 = 4\pi\varepsilon_0\hbar^2/(m_{\mathrm{e}}e^2)$ is the Bohr radius. Within the atomic units, the following N-electron Hamiltonian reads

$$\hat{H} \longrightarrow \hat{T} + \hat{W}_{\mathrm{ee}} + \hat{V}_{\mathrm{ne}} = -\sum_{i=1}^{N}\frac{1}{2}\nabla_i^2 + \sum_{i=1}^{N}\sum_{j>i}^{N}\frac{1}{r_{ij}} - \sum_{i=1}^{N}\sum_{A=1}^{M}\frac{Z_A}{r_{iA}}, \tag{1.5}$$

where r_{iA} and r_{ij} are the distances between the ith electron and the Ath nucleus, and the ith and the jth electrons, respectively. Note that the tilde notation that has been introduced to denote atomic units will be dropped for convenience. Although the number of degrees of freedom has been reduced from $3(N+M)$ to $3N$ using the Born–Oppenheimer approximation, finding the solution of the electronic Schrödinger equation remains an extremely difficult task due to the electron-electron repulsion term in Eq. (1.5). Only few physical systems exist for which their eigenvalues and eigenstates are found analytically. Some (pedagogical) examples are the particle in a box, the hydrogen atom and the quantum harmonic oscillator. Otherwise, the electronic Schrödinger equation has to be solved numerically. Highly accurate numerical solutions have been obtained for atoms and diatomic molecules containing a small number of electrons by including the interelectronic distance r_{ij} explicitly in the wavefunction. For instance, the Helium atom by Hylleraas in 1929 [8], the hydrogen molecule by James and Coolidge in 1933 [9] and the Beryllium atom by Sims and Hagstrom in 1971 [10]. While such numerical solutions were unfeasible for more than a few electrons at the time, lots of progress have been made recently, in particular by the development of the *quantum Monte Carlo* (QMC) method in quantum chemistry [11].

1.1.2 Variational Principle

The state having the lowest energy is called the ground state of the system. This associated ground-state energy can be determined variationally through the Rayleigh-Ritz variational principle:

$$E_0 = \langle \Psi_0 | \hat{H} | \Psi_0 \rangle \leqslant \langle \Psi | \hat{H} | \Psi \rangle \tag{1.6}$$

where Ψ denotes any trial normalized wavefunction. The equality holds only for the ground-state wavefunction Ψ_0. Based on this variational principle, the ground-state energy of the system can be found by minimizing the expectation value of the Hamiltonian over Ψ:

$$E_0 = \min_{\Psi} \Big\{ \langle \Psi | \hat{T} + \hat{W}_{\text{ee}} + \hat{V}_{\text{ne}} | \Psi \rangle \Big\}. \tag{1.7}$$

Unfortunately, the exact minimization is not possible in practice as one would need the whole set of normalized many-body wavefunctions. As mentioned in the previous section, solving the Schrödinger equation exactly for a general many-body system is unfeasible. Therefore, approximate parametrizations of the wavefunction have been proposed to approach the ground-state wavefunction, and the energies resulting from these wavefunctions will always be an upper bound to the true ground-state energy, if determined variationally. In the following, the standard approximations used by quantum chemists to approach the exact ground-state wavefunction are introduced.

1.1.3 Molecular Orbital Theory

The difficulty of finding the exact solution to the electronic Schrödinger equation comes from the interelectronic term $1/r_{ij}$ of the Hamiltonian in Eq. (1.5). To bypass this issue, one could approximate this interaction by an effective one-body potential, so-called a mean-field approximation. In such an approach, the many-electron wavefunction will be defined by a set of one-electron functions, so-called spin orbitals. The simplest approximate wavefunction was proposed by D. R. Hartree [12] and takes the form of a product of orbitals: this is the so-called Hartree product. For a system containing N electrons with a set of molecular spin-orbitals $\{\phi_i\}_{i=1,N}$, the approximate many-particle Hartree wavefunction reads

$$\Phi^{\mathrm{H}}(\mathbf{x}_1, \mathbf{x}_2, \ldots, \mathbf{x}_N) = \phi_1(\mathbf{x}_1)\phi_2(\mathbf{x}_2)\ldots\phi_N(\mathbf{x}_N), \tag{1.8}$$

where $\mathbf{x} \equiv (\mathbf{r}, \sigma)$ denotes the spatial coordinate vector $\mathbf{r}_i \equiv (x_i, y_i, z_i)$ and the spin state $\sigma = \pm 1/2$, which corresponds to a spin up $(+1/2)$ or a spin down $(-1/2)$. The molecular spin orbital is defined by $\phi_i(\mathbf{x}) \equiv \varphi_i^{\sigma_i}(\mathbf{x}) = \varphi_i(\mathbf{r})\delta_{\sigma_i\sigma}$, where $\varphi_i(\mathbf{r})$ is the corresponding spatial orbital, δ is the Kronecker delta ($\delta_{\sigma_i\sigma} = 1$ if $\sigma_i = \sigma$, $\delta_{\sigma_i\sigma} = 0$ otherwise) and σ_i is the spin state of the ith orbital. In practice, the molecular orbitals are determined by a *linear combination of atomic orbitals* (LCAO). For a set of K non-orthonormal atomic orbitals $\chi_\mu(\mathbf{r})$ centered at each nucleus, K orthonormal molecular orbitals are constructed as follows:

$$\varphi_i(\mathbf{r}) = \sum_{\mu=1}^{K} C_{\mu i}\chi_\mu(\mathbf{r}). \tag{1.9}$$

The atomic orbitals are defined with basis functions such as Slater-type or the more standard Gaussian-type functions, forming the so-called basis set (see Appendix H). According to the variational principle [Eq. (1.7)], the coefficients $C_{\mu i}$ are determined so that the set of molecular orbitals minimizes the energy. The wavefunction written as a Hartree product describes the electron-electron interaction implicitly in an effective manner. Indeed, each electron evolves in a mean-field (described by a one-electron potential operator) created by the nuclei and all the other electrons in the system, as described by Hartree in 1957 (p.18, Ref. [13]):

> *"Each one of these functions … should be determined as a solution of Schrödinger's equation for one electron in the field of the nuclei and of the total average charge distribution of the electrons in the other wavefunctions. In such a treatment, the field of the average electron distribution derived from the wavefunctions … must be the same as the field used in evaluating these wavefunctions".*

The first sentence of this quotation describes a mean-field, while the second sentence introduces the idea of self-consistency, i.e. the mean-field has to be evaluated in an iterative manner. This is the Hartree method.

The problem with this wavefunction is that it does not ensure the Pauli exclusion principle [14] proposed by Wolfgang Pauli in 1925, which states that two electrons cannot have the same values of the four quantum number (the principal quantum number n, the angular momentum quantum number l, the magnetic quantum number m_l and the spin quantum number m_s). In addition, each electron is attached to one particular spin orbital $\phi_i(\mathbf{x})$ such that they are not indistinguishable. In order to enforce the Pauli exclusion principle *and* have indiscernible electrons, the wavefunction has to fulfil the fermionic antisymmetry condition, i.e. the sign of the wavefunction should change when permuting two electrons. This can be done by considering all possible electron permutations in the Hartree product, thus leading to the Slater determinant [15]:

$$\Phi(\mathbf{x}_1, \mathbf{x}_2, \ldots, \mathbf{x}_N) = \frac{1}{\sqrt{N!}} \begin{vmatrix} \phi_1(\mathbf{x}_1) & \phi_2(\mathbf{x}_1) & \ldots & \phi_N(\mathbf{x}_1) \\ \phi_1(\mathbf{x}_2) & \phi_2(\mathbf{x}_2) & \ldots & \phi_N(\mathbf{x}_2) \\ \vdots & \vdots & \ddots & \vdots \\ \phi_1(\mathbf{x}_N) & \phi_2(\mathbf{x}_N) & \ldots & \phi_N(\mathbf{x}_N) \end{vmatrix}, \tag{1.10}$$

where $1/\sqrt{N!}$ is a normalization factor. Permuting two electrons would be equivalent to permuting two lines in the determinant, such that

$$\Phi(\mathbf{x}_1, \mathbf{x}_2, \ldots, \mathbf{x}_i, \ldots, \mathbf{x}_j, \ldots, \mathbf{x}_N) = -\Phi(\mathbf{x}_1, \mathbf{x}_2, \ldots, \mathbf{x}_j, \ldots, \mathbf{x}_i, \ldots, \mathbf{x}_N), \tag{1.11}$$

and if two orbitals are the same, two columns would be identical and the determinant would be equal to 0. Hence, the structure of a Slater determinant fulfils the Pauli principle and the antisymmetry condition by construction. For convenience, a lighter expression of a Slater determinant is introduced,

$$\Phi(\mathbf{x}_1, \mathbf{x}_2, \ldots, \mathbf{x}_N) \equiv |\phi_1\phi_2 \ldots \phi_N|, \tag{1.12}$$

and can be expressed in second quantization as (see Appendix C):

$$|\phi_1\phi_2 \ldots \phi_N| \equiv \hat{c}_1^\dagger \hat{c}_2^\dagger \ldots \hat{c}_N^\dagger |\text{vac}\rangle, \tag{1.13}$$

where $\hat{c}_i^\dagger$ is the creation operator of one electron in the ith spin-orbital ϕ_i and $|\text{vac}\rangle$ is the vacuum state (no electrons). The methods for which the wavefunction can be written as a single Slater determinant describe a single configuration only, and are therefore called single-configuration methods.

1.1.4 Hartree–Fock method

In 1930, Slater and Fock [16, 17] applied the Slater determinant Φ to the Hartree method, leading to one of the core theories in quantum chemistry: the so-called *Hartree–Fock* (HF) method. For simplicity, a closed-shell system containing an even number of electrons N in the set of spatial orbitals $\{\varphi_i\}_{i=1,N/2}$ will be considered. The orthonormalization condition

$$\langle\varphi_i|\varphi_j\rangle = \delta_{ij} = \begin{cases} 1 & , \quad i = j \\ 0 & , \quad i \neq j \end{cases} \tag{1.14}$$

is set by considering the following Lagrangian:

$$\mathcal{L}[\Phi] = \langle\Phi|\hat{H}|\Phi\rangle - \sum_{ij} \varepsilon_{ij} \left(\langle\varphi_i|\varphi_j\rangle - \delta_{ij}\right). \tag{1.15}$$

Imposing $\delta\mathcal{L} = 0$ upon a small variation $\varphi_i(\mathbf{r}) \to \varphi_i(\mathbf{r}) + \delta\varphi_i(\mathbf{r})$ leads to the famous Hartree–Fock equations,

$$\hat{F}\varphi_i(\mathbf{r}) = \varepsilon_i\varphi_i(\mathbf{r}), \tag{1.16}$$

where $\hat{F}$ is the one-electron Fock operator, defined by

$$\hat{F} = \hat{h} + \hat{v}^{\mathrm{HF}}. \tag{1.17}$$

$\hat{h}$ is the one-electron operator containing the kinetic energy operator and the attractive electron-nuclei potential operator,

$$\hat{h} = -\frac{1}{2}\nabla^2 - \sum_{A=1}^{M} \frac{Z_A}{|\mathbf{r} - \mathbf{R}_A|}, \tag{1.18}$$

and $\hat{v}^{\mathrm{HF}}$ is the one-electron nonlocal Hartree–Fock (effective) potential describing the mean field generated by the $(N-1)$ other electrons. The latter potential takes into account the classical coulomb repulsion (which is *local*) and the electron-electron exchange interaction:

$$\hat{v}^{\mathrm{HF}} = \sum_{j=1}^{N/2} \left(2\hat{J}_j - \hat{K}_j\right), \tag{1.19}$$

where

$$\hat{J}_j\varphi_i(\mathbf{r}_1) = \left(\int \mathrm{d}\mathbf{r}_2 \frac{\varphi_j^*(\mathbf{r}_2)\varphi_j(\mathbf{r}_2)}{|\mathbf{r}_1 - \mathbf{r}_2|}\right) \times \varphi_i(\mathbf{r}_1) \tag{1.20}$$

is a one-electron local operator and

$$\hat{K}_j\varphi_i(\mathbf{r}_1) = \int \mathrm{d}\mathbf{r}_2 \frac{\varphi_j^*(\mathbf{r}_2)\varphi_i(\mathbf{r}_2)}{|\mathbf{r}_1 - \mathbf{r}_2|}\varphi_j(\mathbf{r}_1) \tag{1.21}$$

is a one-electron non local operator. Note that the summation runs over the N occupied spin-orbitals only or, equivalently, the first $N/2$ spatial orbitals which are occupied twice in a spin-restricted closed-shell formalism. It is clear from Eqs. (1.20) and (1.21) that the Fock operator depends explicitly on the orbitals, themselves eigenfunctions of the Fock operator in Eq. (1.16). Hence, the Hartree–Fock solution is given by solving

$$\left(-\frac{1}{2}\nabla^2 + \hat{v}^{\mathrm{HF}}\left[\{\varphi_j\}_{j=1,N/2}\right] - \sum_A^M \frac{Z_A}{|\mathbf{r} - \mathbf{R}_A|}\right)\varphi_i(\mathbf{r}) = \varepsilon_i\varphi_i(\mathbf{r}) \tag{1.22}$$

self-consistently with an iterative method:

1. Start with a set of trial orbitals $\{\tilde{\varphi}_i\}_i$
2. Compute the (orbital dependent) Fock operator
3. Solve Eq. (1.22) to obtain new orbitals $\{\varphi_i\}_i$
4. If the difference between the sets $\{\varphi_i\}_i$ and $\{\tilde{\varphi}_i\}_i$ is smaller than a given threshold, then $\{\varphi_i\}_i$ are solutions to the Hartree–Fock equation forming the Hartree–Fock determinant. Otherwise, return to step 2 with the new set $\{\varphi_i\}_i$ until convergence is reached.

Note that in practice, damping factors are used in order to facilitate the convergence process. Convergence can also be reached for a local minima instead of the global one.

Another formalism consists in rewriting the Hartree–Fock eigenvalue problem [Eq. (1.16)] in the non orthonormal basis of atomic orbitals [Eq. (1.9)]. The optimization of the LCAO coefficient vector $\mathbf{C}$ is reached when the following stationary condition is satisfied,

$$\frac{\partial E(\mathbf{C})}{\partial \mathbf{C}} = \frac{\partial}{\partial \mathbf{C}} \frac{\langle \Phi(\mathbf{C})|\hat{H}|\Phi(\mathbf{C})\rangle}{\langle \Phi(\mathbf{C})|\Phi(\mathbf{C})\rangle} = 0, \tag{1.23}$$

thus leading to the famous Roothan equations:

$$\mathbf{FC} = \boldsymbol{\varepsilon}\mathbf{SC}, \tag{1.24}$$

where $\mathbf{F}$ is the Fock matrix, $\mathbf{S}$ is the metric also called overlap matrix and $\boldsymbol{\varepsilon}$ is the diagonal matrix giving the orbital energies. The optimized Hartree–Fock molecular orbitals can be obtained by means of unitary transformations, within the so-called exponential parametrization written in second quantization as [3]:

$$|\Phi(\boldsymbol{\kappa})\rangle = e^{-\hat{\kappa}}|\Phi_0\rangle, \tag{1.25}$$

where $\hat{\kappa}^\dagger = -\hat{\kappa}$ is anti-Hermitian, and $|\Phi_0\rangle$ is the Slater determinant constructed from the unrotated orbitals. The singlet excitation operator $\hat{\kappa}$ that allows for orbital rotations is defined as

$$\hat{\kappa} = \sum_{p>q}\sum_{\sigma} \kappa_{pq}\left(\hat{c}^\dagger_{p\sigma}\hat{c}_{q\sigma} - \hat{c}^\dagger_{q\sigma}\hat{c}_{p\sigma}\right), \tag{1.26}$$

where $\hat{c}^\dagger_{p\sigma}$ ($\hat{c}_{q\sigma}$) is the creation (annihilation) operator of an electron of spin σ in the pth spatial orbital, and $\boldsymbol{\kappa} \equiv \{\kappa_{pq}\}_{pq}$ is the matrix containing all the parameters κ_{pq} to be optimized. The Hartree–Fock energy expression therefore reads

$$E(\boldsymbol{\kappa}) = \langle\Phi(\boldsymbol{\kappa})|\hat{H}|\Phi(\boldsymbol{\kappa})\rangle, \tag{1.27}$$

and the Hartree–Fock molecular orbitals satisfy the following stationary condition:

$$\frac{\partial E(\boldsymbol{\kappa})}{\partial \boldsymbol{\kappa}} = \frac{\partial\langle\Phi(\boldsymbol{\kappa})|\hat{H}|\Phi(\boldsymbol{\kappa})\rangle}{\partial \boldsymbol{\kappa}} = 0. \tag{1.28}$$

As readily seen in Eq. (1.26) the orbital optimization consists in doing single excitations, thus creating a *multideterminantal* wavefunction in the given orbital basis set. Then, the orbital rotates to form a new single Slater determinant in the transformed basis, highlighting the fact that the wavefunction still describes a single configuration only. This should not be confused with a *multiconfigurational* wavefunction, which *cannot* be written as a single Slater determinant, in any molecular orbital basis. The term *multiconfigurational* usually refer to multideterminantal wavefunction in which more than one determinant dominates.

By comparing the one-body Hamiltonian in Eq. (1.22) and the two-body one in Eq. (1.5), it becomes clear that the explicit electron-electron repulsion $1/r_{ij}$ has been replaced by an effective Hartree–Fock potential containing the classical Coulomb repulsion as well as the exchange interaction, also called the Fermi correlation. Therefore, the physical two-body Hamiltonian can be rewritten as

$$\hat{H} = \hat{H}_0 + \sum_{i}^{N}\sum_{j>i}^{N}\frac{1}{r_{ij}} - \sum_{i}^{N}\hat{v}_i^{\mathrm{HF}}, \tag{1.29}$$

where

$$\hat{H}_0 = \sum_i^N \hat{h}_i + \sum_i^N \hat{v}_i^{\mathrm{HF}}, \tag{1.30}$$

is a one-electron operator containing the mean-field Hartree–Fock potential. The difference between $\hat{H}$ and $\hat{H}_0$ is usually called the fluctuation operator and denotes the difference between the explicit and the mean-field treatment of the electronic repulsion. The Hartree–Fock energy E_{HF} is therefore not equal to the exact ground-state one, except if this fluctuation term is equal to 0 (which is not the case except for one electron). Due to the variational principle, which states that any trial wavefunction Ψ will have an energy greater or equal to the energy E_0 of the exact ground-state wavefunction Ψ_0 [Eq. (1.6)], the Hartree–Fock energy can only be an upper bound to the true ground-state energy. Its expression for a closed-shell system with the first $N/2$ doubly-occupied spatial orbitals reads

$$E_{\mathrm{HF}} = \langle \Phi_{\mathrm{HF}} | \hat{H} | \Phi_{\mathrm{HF}} \rangle = 2 \sum_{i=1}^{N/2} \langle \varphi_i | \hat{h} | \varphi_i \rangle + \sum_{i=1}^{N/2} \sum_{j=1}^{N/2} (2J_{ij} - K_{ij}) \geqslant E_0, \tag{1.31}$$

where Φ_{HF} is the Slater determinant constructed from the self-consistently converged HF molecular orbitals, and

$$\begin{aligned} J_{ij} = \langle ij|ij \rangle &= \langle \varphi_i \varphi_j | \varphi_i \varphi_j \rangle = \iint \mathrm{d}\mathbf{r}_1 \mathrm{d}\mathbf{r}_2 \frac{\varphi_i^*(\mathbf{r}_1)\varphi_j^*(\mathbf{r}_2)\varphi_i(\mathbf{r}_1)\varphi_j(\mathbf{r}_2)}{r_{12}}, \\ K_{ij} = \langle ij|ji \rangle &= \langle \varphi_i \varphi_j | \varphi_j \varphi_i \rangle = \iint \mathrm{d}\mathbf{r}_1 \mathrm{d}\mathbf{r}_2 \frac{\varphi_i^*(\mathbf{r}_1)\varphi_j^*(\mathbf{r}_2)\varphi_i(\mathbf{r}_2)\varphi_j(\mathbf{r}_1)}{r_{12}}, \end{aligned} \tag{1.32}$$

are the Coulomb and exchange integrals, respectively. As readily seen in Eq. (1.31) and in contrast to the non-interacting case ($1/r_{ij} \to 0$), the HF energy is *not* a simple sum over occupied orbital energies, simply because it describes the electron interaction. However, this description remains approximate such that the lowest Hartree–Fock solution is not exact and is called the Hartree–Fock limit, which is obtained when the orbital basis set reaches completeness. Going beyond this limit means accounting for the fluctuation term in Eq. (1.29). This fluctuation can be treated as a perturbation, thus leading to the Møller-Plesset second-order perturbation theory (MP2) [18]. Note that the Hartree–Fock energy is recovered by adding the first-order energy correction on top of the zeroth-order one (given by $2\sum_{i=1}^{N/2} \varepsilon_i$) in MP2. MP2 therefore accounts for electronic correlation through second-order exactly.

1.1.5 Electron Correlation

The electronic correlation energy is defined as the difference between the exact energy and the Hartree–Fock one. It quantifies the corrections applied to the mean-field approximation in order to recover the exact solution of the Schödinger equation,

$$E_{\mathrm{c}} = E - E_{\mathrm{HF}}. \tag{1.33}$$

In Hartree–Fock, the wavefunction is written as a single Slater determinant. Note that the exchange contribution is also called Fermi correlation. The latter gives rise to the Fermi hole, i.e. the zero probability of finding two electrons with the same spin at the same point in space. Hence, from a mathematical point of view, Hartree–Fock already contains some correlation. However, electrons with different spins remain uncorrelated such that the mean-field treatment of the repulsion is an approximation. It can be proved by showing that a Slater determinant *cannot* be the exact solution of the Schrödinger equation. Consider a two-electron wavefunction written in the following ansatz, where the antisymmetrization is included in the spin part of the wavefunction (not shown),

$$\Psi(\mathbf{r}_1, \mathbf{r}_2) = \varphi(\mathbf{r}_1)\varphi(\mathbf{r}_2), \tag{1.34}$$

and assume that we can find an orbital $\varphi(\mathbf{r})$ such that $\varphi(\mathbf{r}_1)\varphi(\mathbf{r}_2)$ is a solution of the Schrödinger equation,

$$\hat{H}\left(\varphi(\mathbf{r}_1)\varphi(\mathbf{r}_2)\right) = E\varphi(\mathbf{r}_1)\varphi(\mathbf{r}_2), \tag{1.35}$$

for any $\mathbf{r}_1$ and $\mathbf{r}_2$ values. Given that $\hat{H} = \hat{T} + \hat{W}_{\mathrm{ee}} + \hat{V}_{\mathrm{ne}}$, we obtain

$$\hat{W}_{\mathrm{ee}}\left(\varphi(\mathbf{r}_1)\varphi(\mathbf{r}_2)\right) = E\varphi(\mathbf{r}_1)\varphi(\mathbf{r}_2) - \left(\hat{T} + \hat{V}_{\mathrm{ne}}\right)\varphi(\mathbf{r}_1)\varphi(\mathbf{r}_2). \tag{1.36}$$

Then, using the definition of the operators in Eq. (1.5) and dividing by $\varphi(\mathbf{r}_1)\varphi(\mathbf{r}_2)$ leads to

$$\frac{1}{|\mathbf{r}_1 - \mathbf{r}_2|} = E + \frac{1}{2}\frac{\nabla^2_{\mathbf{r}_1}\varphi(\mathbf{r}_1)}{\varphi(\mathbf{r}_1)} + \frac{1}{2}\frac{\nabla^2_{\mathbf{r}_2}\varphi(\mathbf{r}_2)}{\varphi(\mathbf{r}_2)} - v_{\mathrm{ne}}(\mathbf{r}_1) - v_{\mathrm{ne}}(\mathbf{r}_2). \tag{1.37}$$

In the particular limit $\mathbf{r}_2 \to \mathbf{r}_1 = \mathbf{r}$, it comes

$$E + \frac{\nabla^2_{\mathbf{r}}\varphi(\mathbf{r})}{\varphi(\mathbf{r})} - 2v_{\mathrm{ne}}(\mathbf{r}) \to \infty, \tag{1.38}$$

which is absurd because it has no reason to diverge. Indeed, $\varphi(\mathbf{r})$ could be zero for some distance but not everywhere in space. As a consequence, the Schrödinger equation cannot be solved by a single Slater determinant. To account for the electron correlation originating from the electronic repulsion $1/r_{ij}$, one has to go beyond the Hartree–Fock approximation. Before introducing post-Hartree–Fock methods, let us give more insights about this electron correlation, which has been commonly divided in two different contributions: the dynamic correlation and the nondynamic (static) correlation [19, 20]. The short range part of the former gives rise to the Coulomb hole when the electrons are close to each other ($\mathbf{r}_2 \to \mathbf{r}_1$), which induces a cusp in the electronic wavefunction. Its long rang part corresponds to dispersion correlation [21], responsible for weak interaction such as van der Waals interaction. The dynamical correlation is usually referred to as *weak* correlation effects and can be recovered by mixing the dominating Hartree–Fock reference Slater determinant with higher-order excited determinants [21–23]. Such a (multideterminantal) wavefunction is said to be *monoconfigurational.* Even though these excited determinants are not dominating, their energy contribution is essential to reach the chemical accuracy, for instance in the description of the Helium dimer dissociation curve [24].

On the contrary, static correlation arises when low-energy configurations are nearly degenerate with the reference Slater determinant [21], such that no single configuration dominates and a mixing of these configurations is needed. The wavefunction is then said to be *multiconfigurational.* This correlation, also referred to as *strong* correlation, is the main contribution that arises in bond-breaking of a molecule and in transition metal oxides with localized d- or f-orbitals, for instance. This thesis focuses on this type of correlation.

A simple pedagogical example featuring static correlation is the hydrogen molecule $H_A \cdots H_B$ in a minimal orthonormal basis set containing the $1s$ spatial atomic orbitals centered on each atom, $\chi_{1s_A}(\mathbf{r})$ and $\chi_{1s_B}(\mathbf{r})$. The linear combination of these spatial atomic orbitals leads to the well-known bonding and antibonding molecular orbitals, respectively:

$$\varphi_{1\sigma_g}(\mathbf{r}) = \frac{\chi_{1s_A}(\mathbf{r}) + \chi_{1s_B}(\mathbf{r})}{\sqrt{2}}, \qquad \varphi_{1\sigma_u}(\mathbf{r}) = \frac{\chi_{1s_A}(\mathbf{r}) - \chi_{1s_B}(\mathbf{r})}{\sqrt{2}}, \tag{1.39}$$

where the subscripts g stands for *gerade* (symmetric) and u for *ungerade* (antisymmetric). The most natural two-electron Slater determinant to consider is the one containing two electrons in the orbital having the lowest energy, i.e. the bonding orbital $\varphi_{1\sigma_g}(\mathbf{r})$, $|\Phi_{\text{HF}}\rangle \equiv |\varphi^\alpha_{1\sigma_g}\varphi^\beta_{1\sigma_g}|$ where $\varphi^\alpha_{1\sigma_g}(\mathbf{x}) = \varphi^\alpha_{1\sigma_g}(\mathbf{r},\sigma) = \varphi_{1\sigma_g}(\mathbf{r})\delta_{\sigma\alpha}$ and $\varphi^\beta_{1\sigma_g}(\mathbf{x}) = \varphi^\beta_{1\sigma_g}(\mathbf{r},\sigma) = \varphi_{1\sigma_g}(\mathbf{r})\delta_{\sigma\beta}$. Using Eq. (1.39), it can be shown that the HF Slater determinant becomes

$$|\Phi_{\text{HF}}\rangle \equiv \frac{1}{2}\left(\underbrace{|\chi^\alpha_{1s_A}\chi^\beta_{1s_A}| + |\chi^\alpha_{1s_B}\chi^\beta_{1s_B}|}_{\text{ionic forms}} + \underbrace{|\chi^\alpha_{1s_A}\chi^\beta_{1s_B}| + |\chi^\alpha_{1s_B}\chi^\beta_{1s_A}|}_{\text{neutral forms}}\right). \tag{1.40}$$

Hence, the Hartree–Fock wavefunction contains ionic forms ${}^\ominus H_A \cdots H_B^\oplus$ and ${}^\oplus H_A \cdots H_B^\ominus$ which contribute equally with the neutral forms ${}^\uparrow H_A \cdots H_B^\downarrow$ and ${}^\downarrow H_A \cdots H_B^\uparrow$. This is obviously completely wrong when considering the dissociation limit $R_{AB} \to \infty$, for which the exact ground-state wavefunction should only contain the neutral forms, equally weighted. By calculating the ratio $\rho(R_{\text{AB}})$ between the ionic and the neutral form as a function of the interatomic distance R_{AB}, one finds $\rho_{\text{HF}}(R_{\text{AB}}) = 1$ for any R_{AB}, in total contradiction with $\rho(R_{AB} \to \infty) = 0$. How can we get rid of these ionic contributions? In the dissociation limit, the molecular orbitals $\varphi_{1\sigma_g}$ and $\varphi_{1\sigma_u}$ are nearly degenerate. Hence, it is not obvious if one should take $|\varphi^{\alpha}_{1\sigma_g}\varphi^{\beta}_{1\sigma_g}|$ or $|\varphi^{\alpha}_{1\sigma_u}\varphi^{\beta}_{1\sigma_u}|$ as a single determinant. Indeed, in order to get rid of the ionic contributions, one can check that the exact wavefunction

$$|\Psi_{R_{AB}\to\infty}\rangle \equiv \frac{1}{\sqrt{2}}\left(|\chi^{\alpha}_{1s_A}\chi^{\beta}_{1s_B}| - |\chi^{\alpha}_{1s_B}\chi^{\beta}_{1s_A}|\right) \tag{1.41}$$

is obtained by combining the 2 configurations as follows,

$$|\Psi_{R_{AB}\to\infty}\rangle \equiv \frac{1}{\sqrt{2}}\left(|\varphi^{\alpha}_{1\sigma_g}\varphi^{\beta}_{1\sigma_g}| - |\varphi^{\alpha}_{1\sigma_u}\varphi^{\beta}_{1\sigma_u}|\right), \tag{1.42}$$

such that a mixing of two Slater determinants needs to be taken into account in order to recover the exact wavefunction or, equivalently, the missing correlation energy in the Hartree–Fock method. It is clear from this illustration that a single Slater determinant representing a single electronic configuration (here, $1\sigma_g^2$) is not enough to describe the correct physics of a many-electron wavefunction, when static correlation dominates. To account for this missing correlation, one can use a linear combination of Slater determinants as done in Eq. (1.42) to get a multiconfigurational wavefunction. It is worth mentioning that the unrestricted Hartree–Fock method (UHF) [25], developed to treat open shell systems, describes the H_2 dissociation correctly. In the UHF formalism, the wavefunction is not required to be a spin eigenfunction and the spatial orbitals are different for α and β electrons. However, there is no guarantee that this wavefunction remains a singlet, in contrast to the restricted HF wavefunction. Indeed, the expectation value of the total spin squared $\langle \hat{S}^2 \rangle$ tends to 1 as the hydrogen molecule dissociates, and the wavefunction reads [3]

$$|\Phi_{\text{UHF}}\rangle \equiv |\chi^{\alpha}_{1s_A}\chi^{\beta}_{1s_B}|. \tag{1.43}$$

Therefore, although UHF enables a better description of the bond dissociation, it also contains the so-called spin contamination which leads to a discontinuity in the dissociation curve of H_2 [26]. In this illustration, the UHF Slater determinant is contaminated by the triplet state instead of describing a pure singlet state, and is therefore not an eigenfunction of the total spin operator $\hat{S}^2$.

1.1.6 Configuration Interaction and Exact Diagonalization

As mentioned in the previous section, a single Slater determinant cannot be a solution of the Schrödinger equation, because it does not contain any correlation. Instead, a better approximation consists in writing the wavefunction as a linear combination of Slater determinants Φ_I constructed from the HF orbitals. This leads to a post-HF method so-called the *configuration interaction* (CI) wavefunction,

$$|\Psi(\mathbf{C})\rangle = \sum_I C_I |\Phi_I\rangle, \tag{1.44}$$

where the CI coefficients $\mathbf{C} = \{C_I\}_I$ (to be distinguished to the LCAO coefficients) can be obtained from the variational principle [Eq. (1.6)] following the stationary condition:

$$\frac{\partial E(\mathbf{C})}{\partial \mathbf{C}} = \frac{\partial}{\partial \mathbf{C}} \frac{\langle \Psi(\mathbf{C})|\hat{H}|\Psi(\mathbf{C})\rangle}{\langle \Psi(\mathbf{C})|\Psi(\mathbf{C})\rangle} = 0. \tag{1.45}$$

Note that only the CI coefficients are optimized, while the LCAO coefficients in Eq. (1.9) are fixed, in contrast to the Hartree–Fock method [see Eqs. (1.23) and (1.28)], meaning that there is no rotation of the orbitals. An equivalent formulation of this optimization can be considered by using an exponential parametrization, in analogy with the orbital rotation:

$$|\Psi(\mathbf{S})\rangle = e^{-\hat{S}} |\Psi^{(0)}\rangle, \tag{1.46}$$

where $|\Psi^{(0)}\rangle = \sum_I C_I^{(0)} |\Phi_I\rangle$ is a given starting multideterminantal wavefunction with fixed coefficients $C_I^{(0)}$. $\hat{S}$ is the operator that controls rotations in the configuration space $\mathcal{S} = \{|\Phi_I\rangle\}_I$,

$$\hat{S} = \sum_{I \in \mathcal{S}} S_I \left(|\Phi_I\rangle\langle\Psi^{(0)}| - |\Psi^{(0)}\rangle\langle\Phi_I| \right), \tag{1.47}$$

with $\langle \Phi_i | \Phi_j \rangle = \delta_{ij}$. The stationary condition becomes

$$\frac{\partial E(\mathbf{S})}{\partial \mathbf{S}} = \frac{\langle \Psi(\mathbf{S})|\hat{H}|\Psi(\mathbf{S})\rangle}{\partial \mathbf{S}} = 0, \tag{1.48}$$

where $\Psi(\mathbf{S})$ is normalized. If all the possible determinants constructed from a given basis set are considered to build the wavefunction in Eq. (1.44), then the wavefunction is exact in this particular basis set [1] and is called the *full configuration interaction* (FCI) wavefunction. The number of determinants

---

[1] Considering higher-order excited determinants to build a multideterminantal wavefunction has been suggested to describe the short-range dynamical correlation or, equivalently, the Coulomb cusp. It is interesting to note that even the FCI wavefunction in a complete basis set of one-electron orbitals cannot describe the Coulomb cusp, due to the two-electron repulsion $1/r_{12}$. Because a basis of atomic orbitals is considered, only bound states are described and FCI is not exact. FCI is exact in a given and fixed basis set only. An alternative strategy consists in incorporating r_{12} explicitely in the wavefunction, leading to the so-called explicitly electronic correlated method.

Table 1.1: Number of all Slater determinants N_{det} and singlet states Slater determinants N^1_{det} obtained by distributing N electrons in N spatial orbitals (or $2N$ spin orbitals).

N	N_{det}	N^1_{det}
2	6	4
4	70	36
6	924	400
8	12 870	4 900
10	184 756	63 504
12	2 704 156	853 776
14	40 116 600	11 778 624
16	601 080 390	165 636 900
18	9 075 135 300	2 363 904 400
20	137 846 528 800	34 134 779 536

to be considered is given by

$$N_{\text{det}} = \binom{M}{N} = \frac{M!}{N!(M-N)!}, \tag{1.49}$$

where N is the number of electrons and M the number of spin-orbitals forming the basis set. A tabulation of the number of determinants necessary to build a FCI wavefunction is given in Tab. 1.1. In a case of singlet states with an even number of electrons and m spatial orbitals, the number of determinants increases exponentially with N as m^N. Hence, FCI is in general not applicable and is most of the time used as a benchmark for small systems. Relatively recently, Alavi and co-workers have developed *quantum monte carlo* (QMC) method applied in the FCI space, so-called FCIQMC, enabling to converge towards the FCI energy for much larger spaces [27].

For a given basis set, the configuration interaction in Eq. (1.44) can be expanded as follows,

$$|\Psi\rangle \approx |\Phi_0\rangle + \sum_{ia} c_i^a |\Phi_i^a\rangle + \sum_{ijab} c_{ij}^{ab} |\Phi_{ij}^{ab}\rangle + \dots, \tag{1.50}$$

where i, j denotes occupied orbitals and a, b unoccupied ones in the HF determinant Φ_0. Φ_i^a and Φ_{ij}^{ab} are the determinants corresponding to the single excitation from the ith to the ath orbital, and to the double excitation from the ith to the ath and from the jth to the bth orbitals, respectively. Because of the intractability of such an expansion for large systems, one usually truncates the expansion to the double excited determinants (CISD, for "configuration interaction with single and double excited determinants"), thus leading to size-inconsistency,

$$E(A+B) \overset{R_{\text{AB}}\to+\infty}{\neq} E(A) + E(B), \tag{1.51}$$

where A and B are two subsystems (such as two atoms in a diatomic molecule). Note that it is also not size-extensive (linear scaling of the energy with the number of electrons, the size of the molecule) [28]. The size-extensivity [29–31] can be recovered by construction when using an exponential ansatz, giving birth to the standard *coupled cluster* (CC) theory [32]. Together with MP2, the CISD and CCSD are good approximations when dynamical correlation dominates, but they tend to fail for the description of strongly correlated systems, when static correlation is important. The reason is that static correlation arises when a single electronic configuration is not sufficient to describe the system. However, both CISD or CCSD are based on a single reference Slater determinant which is used to construct other low-excited Slater determinants, thus leading to a description of a single electronic configuration.

1.1.7 Multiconfigurational Self Consistent Field

The FCI energy is invariant under orbital rotation, in contrast to truncated CI expansion. Although the CI coefficients are optimized [Eq. (1.45)], the orbitals are frozen to the Hartree–Fock ones. Allowing for the reoptimization of the orbitals in a truncated CI calculation leads to the so-called *multiconfigurational self-consistent field* (MCSCF) method. This additional flexibility can be achieved by using the same exponential parametrization as in the Hartree–Fock method:

$$|\Psi(\boldsymbol{\kappa},\mathbf{S})\rangle = e^{-\hat{\kappa}}|\Psi(\mathbf{S})\rangle = e^{-\hat{\kappa}}e^{-\hat{S}}|\Psi^{(0)}\rangle. \tag{1.52}$$

Note that the exponential parametrization is usually not used for single state in practice, but is very convenient for response theory and state-average calculation. The convergence is reached when the stationarity conditions are fulfilled:

$$\frac{\partial E(\boldsymbol{\kappa},\mathbf{S})}{\partial \boldsymbol{\kappa}} = \frac{\partial E(\boldsymbol{\kappa},\mathbf{S})}{\partial \mathbf{S}} = 0, \tag{1.53}$$

where

$$E(\boldsymbol{\kappa},\mathbf{S}) = \langle \Psi(\boldsymbol{\kappa},\mathbf{S})|\hat{H}|\Psi(\boldsymbol{\kappa},\mathbf{S})\rangle. \tag{1.54}$$

Depending on the composition of the configuration space, the energy will of course take different values. The multiconfigurational form of the MCSCF wavefunction is particularly interesting to treat static correlation, which arises when near degeneracy of states appears. Hence, one usually selects only a specific orbital space (expected to be small) based on chemical intuition (this orbital space, called active space, has to be composed by the orbitals responsible for such a correlation). For instance, in the case of stretched H_2, the active space would be composed by two electrons in the two molecular orbitals $1\sigma_g$ and $1\sigma_u$. In the minimal basis set, this is equivalent to FCI. If all the possible determinants constructed from this active space are taken into account in the MCSCF calculation, we talk about *complete active space self-consistent field* (CASSCF), which is FCI in the active space. Otherwise, the method is called *restricted active space self-consistent field* (RASSCF). An automated selection of a relevant and optimal active space has been recently proposed by Stein and Reiher [33] and is based on orbital entanglement in quantum information theory. This selection is a step towards making CASSCF a black box approach, which was unthinkable 10 years ago. The CASSCF ground-state energy is obtained variationally as follows:

$$E_{\text{CAS}} = \min_{\boldsymbol{\kappa},\mathbf{S}} \left\{ \langle \Psi^{\text{CAS}}(\boldsymbol{\kappa}, \mathbf{S}) | \hat{T} + \hat{W}_{\text{ee}} + \hat{V}_{\text{ne}} | \Psi^{\text{CAS}}(\boldsymbol{\kappa}, \mathbf{S}) \rangle \right\}, \tag{1.55}$$

where $\Psi^{\text{CAS}}(\boldsymbol{\kappa}, \mathbf{C})$ is the wavefunction built from all possible Slater determinants constructed from the orbitals contained in the CAS. The inactive and virtual orbitals outside the CAS are involved in the orbital rotation, which can be seen as mono-excitations from the inactive to the active, from inactive to the virtual, and from active to the virtual, thus contributing to the minimization of the CASSCF energy. Note that the rotation does not apply within the CAS where all possible determinants are constructed.

CASSCF is in principle able the treat static correlation, but not the dynamical one. This deficiency can be fixed by applying perturbation theory onto a multiconfigurational method, leading to the CASPT2 approach [34] as well as the so-called *N-electron valence state second order perturbation theory* (NEVPT2) [35, 36] ; or *multireference* CI (MRCI) (see for instance Ref. [37] and references therein) which consists in generating higher-excited determinants from more than one reference determinant. Despite the overall performance of the CASSCF and related methods, the exponential scaling with respect to the number of single particle states in the active space prevents its application to more than 18 electrons in 18 orbitals, which can be insufficient for the accurate treatment of highly complex systems [38].

1.1.8 Density Matrix Renormalization Group

This section aims to provide a brief overview of the *density matrix renormalization group* (DMRG) method, originally developed by S. White in 1992 [39, 40] to treat one-dimensional (1D) models. For the first time in 1999, DMRG has been applied to a molecule by mapping the molecular orbitals onto a 1D quantum lattice model [41]. Since then, DMRG has gained increasing interest in quantum chemistry due to its faculty to treat much larger active space than standard CASSCF, up to 40 electrons in 40 orbitals [42, 43] instead of 18 electrons in 18 orbitals within CASSCF, thanks to its wavefunction ansatz: the *matrix product state* (MPS) which is a low rank decomposition of the FCI tensor. DMRG codes for quantum chemistry are the spin-adapted Block code [44, 45] and the QCMaquis software [46]. The derivations made in this section are mainly based on the review by Schöllwock [47], which is a useful introductory reference for beginners in DMRG. Other DMRG reviews are provided in Refs. [42, 46, 48], and a practical guide to quantum chemists is reported in Ref. [49]. Before considering the MPS ansatz, some algebraic tools should be introduced.

Singular value decomposition

Consider an arbitrary rectangular matrix M of dimension $(N_A \times N_B)$. This matrix can be decomposed using the *singular value decomposition* (SVD),

$$M = U\Lambda V^\dagger, \qquad \Lambda = \text{diag}\{\lambda_1, \lambda_2, \ldots, \lambda_r\}, \tag{1.56}$$

where U is a rectangular matrix of dimension $(N_A \times \min(N_A, N_B))$ with orthonormal columns ($U^\dagger U = 1$), Λ is a square diagonal matrix of dimension $(\min(N_A, N_B) \times \min(N_A, N_B))$ with positive entries $\{\lambda_i\}$ called singular values, and $V^\dagger$ is a rectangular matrix of dimension $(\min(N_A, N_B) \times N_B)$ with orthonormal rows ($V^\dagger V = 1$). Note that the left (right) singular vector U (V) is unitary only if $N_A \leq N_B$ ($N_A \geq N_B$) so that $UU^\dagger = 1$ ($VV^\dagger = 1$). The number r of non zero singular values is called the Schmidt rank of M, and the singular values are sorted as $\lambda_1 \geqslant \lambda_2 \geqslant \ldots \geqslant \lambda_r > 0$. The SVD can be used to find the optimal approximation of M by a matrix $\tilde{M}$ of rank $m < r$:

$$\tilde{M} = U\tilde{\Lambda}V^\dagger, \qquad \tilde{\Lambda} = \text{diag}\{\lambda_1, \lambda_2, \ldots, \lambda_m, 0, \ldots\} \tag{1.57}$$

which is done in practice by shrinking the columns (rows) of U (V) according to m.

Schmidt decomposition

SVD is the central tool in the Schmidt decomposition of the wavefunction. Consider a bipartition of the total system in two parts A and B (for example, split the orbital space in two). The many-body Hilbert space is then spanned by the product space $\{|A_i\rangle\} \otimes \{|B_j\rangle\}$, where $\{|A_i\rangle\}_{i=1,\ldots,N_A}$ and $\{|B_j\rangle\}_{j=1,\ldots,N_B}$ are the orthonormal basis states of the many-body Hilbert spaces of subsystems A and B, containing N_A and N_B states, respectively. The general form of the wavefunction for this system is

$$|\Psi\rangle = \sum_{i}^{N_A} \sum_{j}^{N_B} C_{ij} |A_i\rangle |B_j\rangle. \tag{1.58}$$

By applying SVD onto the matrix elements C_{ij} (i and j are the row and column indices) we obtain

$$|\Psi\rangle = \sum_{i}^{N_A} \sum_{j}^{N_B} \sum_{\alpha}^{\min(N_A,N_B)} U_{i\alpha} \lambda_\alpha V_{\alpha j}^\dagger |A_i\rangle |B_j\rangle = \sum_{\alpha}^{\min(N_A,N_B)} \lambda_\alpha |\tilde{A}_\alpha\rangle |\tilde{B}_\alpha\rangle, \tag{1.59}$$

with $\sum_\alpha \lambda_\alpha^2 = 1$ for the normalization of Ψ and

$$\sum_{i}^{N_A} U_{i\alpha} |A_i\rangle = |\tilde{A}_\alpha\rangle, \qquad \sum_{j}^{N_B} V_{\alpha j}^\dagger |B_j\rangle = |\tilde{B}_\alpha\rangle. \tag{1.60}$$

Exactly like in the SVD, an approximation $|\tilde{\Psi}\rangle$ to $|\Psi\rangle$, (optimal in a least squares sense $||\,|\tilde{\Psi}\rangle - |\Psi\rangle\,||^2$) can be obtained by neglecting the smallest singular values (or Schmidt numbers) λ_α, thus leading to a smaller number of terms in the summation in Eq. (1.59). This approximation is one of the key ingredient in DMRG, as shown in the following.

Returning to DMRG, the general form of the FCI wavefunction in Eq. (1.44) can be rewritten in the occupation number representation for k orbitals:

$$|\Psi\rangle = \sum_{n_1 \ldots n_i \ldots n_k} C_{n_1 \ldots n_i \ldots n_k} |n_1 \ldots n_i \ldots n_k\rangle, \tag{1.61}$$

where $|n_1 \ldots n_i \ldots n_k\rangle$ is an occupation number vector representation of a Slater determinant [see Eq. (1.13)]:

$$|n_1 \ldots n_i \ldots n_k\rangle = \left(\hat{c}_1^\dagger\right)^{n_1} \ldots \left(\hat{c}_i^\dagger\right)^{n_i} \ldots \left(\hat{c}_k^\dagger\right)^{n_k} |\mathrm{vac}\rangle \tag{1.62}$$

and n_i denotes the d-dimensional occupation state of the ith orbital with $\{|n_i\rangle\} = \{|\mathrm{vac}\rangle, |\uparrow\rangle, |\downarrow\rangle, |\uparrow\downarrow\rangle\}$, so that $d = 4$. In contrast to Eq. (1.13) where each creation operator creates an electron in a given spin-orbital, the exponent n_i applied on the creation operator $\hat{c}_i^\dagger$ in Eq. (1.62) denotes the occupation state created in the ith spatial orbital, which can be either empty, occupied by one electron with spin up or down, or doubly occupied. We have already seen that it is common to truncate the size of the configuration space, either by considering only singles and doubles (truncated CI), or by restricting the configuration space to a given set of orbitals (CASSCF). Then, the CI coefficients are optimized according to the variational principle. The underlying idea in DMRG is to truncate the CI coefficients in the MPS representation. Let us now introduce the MPS wavefunction ansatz.

Starting with the wavefunction in Eq. (1.61), we decompose it into left (n_1) and right $(n_2 \ldots n_k)$ blocks:

$$|\Psi\rangle = \sum_{n_1} \sum_{n_2 \ldots n_k} C_{(n_1)(n_2 \ldots n_k)} |n_1\rangle |n_2 \ldots n_k\rangle, \tag{1.63}$$

where we recall that molecular orbitals are mapped onto a 1D quantum lattice model. The previously introduced state vector $C_{n_1 \ldots n_k}$ in Eq. (1.61) is now viewed as a matrix $C_{(n_1)(n_2 \ldots n_k)}$ of dimension $(d \times d^{L-1})$ where the left (n_1) and right $(n_2 \ldots n_k)$ block states are the row and column indices, respectively. Applying the SVD on this matrix, as in the Schmidt decomposition [Eq. (1.59)], leads to

$$C_{(n_1)(n_2 \ldots n_k)} = \sum_{\alpha_1}^{r_1} U_{(n_1)(\alpha_1)} \Lambda_{\alpha_1} V^{\dagger}_{(\alpha_1)(n_2 \ldots n_k)}, \tag{1.64}$$

with the rank $r_1 \leq d$, such that the wavefunction reads

$$|\Psi\rangle = \sum_{n_1} \sum_{n_2 \ldots n_k} \sum_{\alpha_1}^{r_1} U_{(n_1)(\alpha_1)} \Lambda_{\alpha_1} V^{\dagger}_{(\alpha_1)(n_2 \ldots n_k)} |n_1\rangle |n_2 \ldots n_k\rangle = \sum_{\alpha_1}^{r_1} \Lambda_{\alpha_1} |L_{\alpha_1}\rangle |R_{\alpha_1}\rangle, \tag{1.65}$$

where the left and right-singular vectors are defined as

$$|L_{\alpha_1}\rangle = \sum_{n_1} U_{(n_1)(\alpha_1)} |n_1\rangle, \qquad |R_{\alpha_1}\rangle = \sum_{n_2 \ldots n_k} V^{\dagger}_{(\alpha_1)(n_2 \ldots n_k)} |n_2 \ldots n_k\rangle, \tag{1.66}$$

respectively. Then, the matrix product $\Lambda_{\alpha_1} V^{\dagger}_{(\alpha_1)(n_2 \ldots n_k)}$ in Eq. (1.65) is rewritten as a vector $C_{\alpha_1 n_2 \ldots n_k}$ that can be decomposed into a matrix form $C_{(\alpha_1 n_2)(n_3 \ldots n_k)}$ of dimension $(r_1 d \times d^{L-2})$. By applying SVD again, it comes:

$$C_{(\alpha_1 n_2)(n_3 \ldots n_k)} = \sum_{\alpha_2}^{r_2} U_{(\alpha_1 n_2)(\alpha_2)} \Lambda_{\alpha_2} V^{\dagger}_{(\alpha_2)(n_3 \ldots n_k)}, \tag{1.67}$$

with the rank $r_2 \leq r_1 d \leq d^2$. Inserting Eq. (1.67) into (1.64) gives a new expression for the state vector,

$$C_{n_1 \ldots n_k} \equiv \sum_{\alpha_1}^{r_1} U_{(n_1)(\alpha_1)} C_{(\alpha_1 n_2)(n_3 \ldots n_k)}, \tag{1.68}$$

which leads to a Schmidt decomposition of the original wavefunction with respect to the new left and right blocks:

$$|\Psi\rangle = \sum_{\alpha_2}^{r_2} \Lambda_{\alpha_2} |L_{\alpha_2}\rangle |R_{\alpha_2}\rangle, \tag{1.69}$$

where

$$|L_{\alpha_2}\rangle = \sum_{\alpha_1 n_2} U_{(\alpha_1 n_2)(\alpha_2)} |L_{\alpha_1}\rangle |n_2\rangle, \qquad |R_{\alpha_2}\rangle = \sum_{n_3 \dots n_k} V^{\dagger}_{(\alpha_2)(n_3 \dots n_k)} |n_3 \dots n_k\rangle. \tag{1.70}$$

We reiterate these steps by growing the left block and performing further SVDs recursively, until reaching the end of the lattice:

$$|\Psi\rangle = \sum_{\alpha_{k-1}}^{r_{k-1}} \Lambda_{\alpha_{k-1}} |L_{\alpha_{k-1}}\rangle |R_{\alpha_{k-1}}\rangle, \tag{1.71}$$

with rank $r_{k-1} \leq d^{k-1}$ and

$$|L_{\alpha_i}\rangle = \sum_{\alpha_{i-1} n_i} U_{(\alpha_{i-1} n_i)(\alpha_i)} |L_{\alpha_{i-1}}\rangle |n_i\rangle, \qquad (i = 2, \dots, k-1), \tag{1.72}$$

$$|R_{\alpha_{k-1}}\rangle = \sum_{n_k} V^{\dagger}_{(\alpha_{k-1})(n_k)} |n_k\rangle. \tag{1.73}$$

Finally, these successive SVDs and Schmidt decompositions have led to a new expression for the wavefunction,

$$|\Psi\rangle = \sum_{n_1 \dots n_k} \sum_{\alpha_1 \dots \alpha_k} U_{(n_1)(\alpha_1)} U_{(\alpha_1 n_2)(\alpha_2)} U_{(\alpha_2 n_3)(\alpha_3)} \dots U_{(\alpha_{k-2} n_{k-1})(\alpha_{k-1})} V^{\dagger}_{(\alpha_{k-1})(n_k)} |n_1 \dots n_k\rangle. \tag{1.74}$$

Replacing the matrix $U_{(\alpha_{i-1} n_i)(\alpha_i)}$ of dimension $(r_{i-1} d \times r_i)$ by a set of $d (= 4)$ matrices A^{n_i} of dimension $(r_{i-1} \times r_i)$ with entries $A^{n_i}_{\alpha_{i-1}\alpha_i} = U_{(\alpha_{i-1} n_i)(\alpha_i)}$, we obtain

$$|\Psi\rangle = \sum_{n_1 \dots n_k} \sum_{\alpha_1 \dots \alpha_k} A^{n_1}_{\alpha_1} A^{n_2}_{\alpha_1 \alpha_2} \dots A^{n_{k-1}}_{\alpha_{k-2}\alpha_{k-1}} A^{n_k}_{\alpha_{k-1}} |n_1 \dots n_k\rangle, \tag{1.75}$$

where $A^{n_1}_{\alpha_1} = U_{(n_1)(\alpha_1)}$ and $A^{n_k}_{\alpha_{k-1}} = V^{\dagger}_{(\alpha_{k-1})(n_k)}$ are a set of $d (= 4)$ row vectors and columns vectors, respectively. This form can be further compacted by recognizing the sum over $\{\alpha_i\}$ as a matrix multiplication:

$$|\Psi\rangle = \sum_{n_1 \dots n_k} A^{n_1} A^{n_2} \dots A^{n_k} |n_1 \dots n_k\rangle, \tag{1.76}$$

which is nothing but the *variational* MPS ansatz of the wavefunction [50, 51], yielding a variational upper bound for the ground-state energy. This whole procedure starting from the left ($i = 1$) and finishing when the left block has reached its maximal size ($i = k - 1$) is called a sweep. Once this sweep is done, it goes back in the reverse direction, starting from the right and growing over the left side, defining a macro-iteration. The process converges after several macro-iterations (defining the number of sweeps), when a threshold value is reached for the energy.

What makes DMRG appealing in term of computational cost is the approximation of the wavefunction in Eq. (1.76) by optimally truncating the A^{n_i} matrices, keeping only the m highest singular values (so-called the *virtual* dimension) for each applied SVDs [Eq. (1.57)]. An optimal value for m is not universal, and one can resort to extrapolation techniques [52, 53]. DMRG has a polynomial scaling [53] with respect to both m and k as $O(m^2k^4 + m^3k^3)$, which considerably reduces the computational cost of the method in contrast to FCI, thus explaining why DMRG can treat an active space up to 40 electrons in 40 orbitals. Of course, m should be kept large enough to conserve as much as renormalized states as possible, but sufficiently small to reduce the computational cost. Besides, DMRG is not invariant under orbital rotations, such that the choice of the molecular orbitals as well as their ordering [49, 54] on a 1D lattice are of considerable importance, otherwise one could converge to a local minima [52, 55].

1.2 Reduced Quantity Theories

One may wonder if searching for the many-body wavefunction is the only way to reach an accurate description of the many-particle system featuring quantum effects. As mentioned in the previous section, obtaining an exact (or even highly accurate) numerical solution becomes rapidly impossible when the number of electron increases. An amusing illustration of this problem has been given by Hardy Gross[2] for the wavefunction of the oxygen atom ($1s^22s^22p^4$), hence having 24 degrees of freedom ($3N = 3 \times 8$, where N is the number of electrons). In order to plot the potential energy surface,

$$\int d\mathbf{r}_1 \int d\mathbf{r}_2 \;\dots\; \int d\mathbf{r}_N \Psi^*(\mathbf{r}_1, \mathbf{r}_2, \dots, \mathbf{r}_N)\hat{H}\Psi(\mathbf{r}_1, \mathbf{r}_2, \dots, \mathbf{r}_N), \tag{1.77}$$

the wavefunction $\Psi(\mathbf{r}_1, \mathbf{r}_2, \dots, \mathbf{r}_N)$ has to be stored. To do so, each coordinate can be discretized by 10 values, leading to 10^{24} values to store. So we would need a table with 10^{24} entries or equivalently 10^{24} bytes if one entry corresponds to one byte. Then, considering a standard DVD with a capacity of 5 GB ($5 \cdot 10^9$ bytes), it means that $2 \cdot 10^{14}$ DVDs are needed to store the wavefunction of the oxygen atom with only 10 points per coordinate. If a DVD's weight is approximately 10 grams, then

---

[2] In the IPAM (Institute of Pure and Applied Mathematics) summer school entitled *Mathematical Foundations of Density Functional Theory*, UCLA (2016).

we would need $2 \cdot 10^9$ tonnes of DVDs ! There are different points of view regarding this issue. First, one can wait for better computers to be able to treat larger and larger systems accurately using wavefunction methods and exact diagonalization (equivalent to FCI), as suggested by the empirical law of G. Moore, one of the founders of Intel enterprise, which states that the number of transistors in a microprocessor doubles every two years [56, 57]. However, this empirical law is nearing its end, as the transistors have reached the size where quantum effects play an important role [58]. Although not new [59, 60], the field of quantum information theory on the development of quantum computers and associated algorithms have gained increasing interest recently in quantum chemistry, due to their possible application to the description of quantum chemical problems out of reach by classical computers [61–63]. Of course, the development of quantum computers has its own issues which are out of the scope of this thesis. Meanwhile, one still has to find a better way to treat the electronic structure efficiently. A question arises naturally: are there methods able to reach the chemical accuracy with an affordable computational cost ? The answer to this question is yes. *In principle.* And these methods use reduced quantities as basic variable such as, for example, the electronic density, the one-particle density matrix, or the one-particle Green's function instead of the many-body wavefunction. This section is devoted to these reduced quantity theories, starting from the well-known *density functional theory* (DFT) and followed by the *reduced density matrix functional theory* (RDMFT) as well as the one-particle Green's function theory.

1.2.1 Density Functional Theory

The concept of using the electronic density as a basic variable to treat a quantum system has first been suggested by Thomas in 1927 [64], independently followed by Fermi [65]. It has led to the so-called Thomas-Fermi method, which consists in representing the Hamiltonian operator as a functional of the electron density $n(\mathbf{r})$ only. Therefore, one can bypass the construction of the complicated object that is the wavefunction and concentrate on the electronic density only, switching from $\Psi(\mathbf{x}_1, \mathbf{x}_2, \ldots, \mathbf{x}_N)$ with $(3+1)N$ coordinates to $n(\mathbf{r})$ with three spatial coordinates. Note that the electron density is obtained from the wavefunction by integrating over all but one coordinate,

$$n(\mathbf{r}) = N \sum_{\sigma} \int \mathrm{d}\mathbf{x}_2 \int \mathrm{d}\mathbf{x}_3 \ \ldots \ \int \mathrm{d}\mathbf{x}_N \left|\Psi(\mathbf{r}, \sigma, \mathbf{x}_2, \ldots, \mathbf{x}_N)\right|^2, \tag{1.78}$$

where $\mathbf{x}_i \equiv (\mathbf{r}_i, \sigma_i)$ and $\int \mathrm{d}\mathbf{x}_i \equiv \int \mathrm{d}\mathbf{r}_i \sum_{\sigma_i}$. Based on the uniform electron gas, they developed the non-interacting kinetic energy functional of the electron density $n(\mathbf{r})$,

$$T_{\mathrm{TF}}[n] = \frac{3}{10} \left(3\pi^2\right)^{2/3} \int \mathrm{d}\mathbf{r} \ n^{5/3}(\mathbf{r}), \tag{1.79}$$

which is the first local density approximation (LDA). The total energy within the Thomas–Fermi approximation is given by

$$E_{\mathrm{TF}}[n] = T_{\mathrm{TF}}[n] + V_{\mathrm{ne}}[n] + E_{\mathrm{H}}[n], \tag{1.80}$$

where $V_{\mathrm{ne}}[n] = \int \mathrm{d}\mathbf{r}\, n(\mathbf{r}) v_{\mathrm{ne}}(\mathbf{r})$ is the potential energy due to the electric attraction of the positively charged nucleus, and

$$E_{\mathrm{H}}[n] = \frac{1}{2} \iint \mathrm{d}\mathbf{r}\mathrm{d}\mathbf{r}' \frac{n(\mathbf{r})n(\mathbf{r}')}{|\mathbf{r}-\mathbf{r}'|}, \tag{1.81}$$

is the Hartree energy, corresponding to the potential energy of the electrons due to their mutual electric repulsion. However, when applied to real systems this method does not give accurate results, even qualitatively, simply because there is a huge gap between a realistic interacting system and a noninteracting uniform one. To improve on its accuracy, Dirac proposed an additional exchange density-functional energy [66],

$$E_{\mathrm{x}}[n] = -\frac{3}{4}\left(\frac{3}{\pi}\right)^{1/3} \int \mathrm{d}\mathbf{r}\; n^{4/3}(\mathbf{r}), \tag{1.82}$$

which is the exact exchange functional for a uniform electron gas. Despite this correction, the Thomas–Fermi method is still not accurate enough to describe chemical bonds qualitatively. This is not surprising, as the origin of chemical bonds is driven by the electronic repulsion. To go beyond the Thomas–Fermi approximation, one should include the electron repulsion in the density-functional kinetic energy, and an additional correlation functional of the density might also be needed. Besides, the lack of physical background establishing the uniqueness of the solution and the existence of a universal density functional has led to wonder if all of this makes any sense, and has shelved this theory until the mid-1960s, when Kohn (Nobel prize in Chemistry in 1998) answered "yes it does" and called the method DFT.

1.2.1.i Hohenberg–Kohn theorems

The aforementioned theory has been revived by two theorems which provide sound theoretical foundations of DFT, derived by Hohenberg and Kohn in 1964 [67]. For convenience, we start by rewriting the external local potential operator as

$$\hat{V} = \sum_{i=1}^{N} v(\mathbf{r}_i)\times = \sum_{i=1}^{N} \int \mathrm{d}\mathbf{r}\; v(\mathbf{r})\delta(\mathbf{r}-\mathbf{r}_i)\times = \int \mathrm{d}\mathbf{r}\; v(\mathbf{r})\hat{n}(\mathbf{r}), \tag{1.83}$$

where $\hat{n}(\mathbf{r}) \equiv \sum_{i=1}^{N} \delta(\mathbf{r}-\mathbf{r}_i)$ is the so-called density operator, with $\delta(\mathbf{r}-\mathbf{r}_i)$ the Dirac distribution. Its expression in second quantization is provided in the Appendix C. While $\hat{T}$ and $\hat{W}_{\text{ee}}$ are universal (i.e. they do not depend on the nuclei), the local potential $v(\mathbf{r})$ is molecule-dependent and its contribution to the ground-state energy $E_0[v]$ of $\hat{H}[v] = \hat{T} + \hat{W}_{\text{ee}} + \int \mathrm{d}\mathbf{r}\ v(\mathbf{r})\hat{n}(\mathbf{r})$ is the only one that depends explicitly on the ground-state electron density as follows:

$$E_0[v] = \langle \Psi_0[v] | \hat{T} + \hat{W}_{\text{ee}} + \hat{V} | \Psi_0[v] \rangle = \langle \Psi_0[v] | \hat{T} + \hat{W}_{\text{ee}} | \Psi_0[v] \rangle + \int \mathrm{d}\mathbf{r} v(\mathbf{r}) n_0(\mathbf{r}), \tag{1.84}$$

where $n_0(\mathbf{r}) = n^{\Psi_0[v]}(\mathbf{r})$ and $n_\Psi(\mathbf{r}) = \langle \Psi | \hat{n}(\mathbf{r}) | \Psi \rangle$.

The first Hohenberg–Kohn theorem establishes a one-to-one correspondence between the external local potential $v(\mathbf{r})$, up to a constant, and the non-degenerate ground-state density $n_0(\mathbf{r})$. Hence, if the density is known, one has access to the external potential, and therefore to the Hamiltonian and its associated eigenfunctions and eigenvalues. As a consequence, all the properties of the system become a functional of the ground-state electronic density. This first theorem is a proof of contradiction. Indeed, consider two local potentials $v(\mathbf{r})$ and $v'(\mathbf{r})$ that differ by more than a constant. It gives rise to two Schrödinger equations,

$$\begin{aligned} \hat{H}[v] | \Psi_0[v] \rangle &= E_0[v] | \Psi_0[v] \rangle, \\ \hat{H}[v'] | \Psi_0[v'] \rangle &= E_0[v'] | \Psi_0[v'] \rangle. \end{aligned} \tag{1.85}$$

Let us consider the case $\Psi_0[v] = \Psi_0[v']$ which leads to

$$\left(\hat{H}[v] - \hat{H}[v'] \right) | \Psi_0[v] \rangle = \left(E_0[v] - E_0[v'] \right) | \Psi_0[v] \rangle, \tag{1.86}$$

such that

$$v(\mathbf{r}) - v'(\mathbf{r}) = \frac{E_0[v] - E_0[v']}{N} = C, \tag{1.87}$$

where C is a constant. Hence $\Psi_0[v] \neq \Psi_0[v']$ if $v(\mathbf{r}) \neq v'(\mathbf{r}) + C$. Now starting with $\Psi_0[v] \neq \Psi_0[v']$ which are non-degenerate, the variational principle leads to two strict inequalities,

$$\begin{aligned} &\langle \Psi_0[v'] | \hat{H}[v] | \Psi_0[v'] \rangle > E_0[v], \\ &\langle \Psi_0[v] | \hat{H}[v'] | \Psi_0[v] \rangle > E_0[v']. \end{aligned} \tag{1.88}$$

Assuming that both wavefunctions have the same electronic density $n^{\Psi_0[v]}(\mathbf{r}) = n^{\Psi_0[v']}(\mathbf{r})$ and using Eqs. (1.85), it comes

$$\langle \Psi_0[v'] | \hat{T} + \hat{W}_{\text{ee}} | \Psi_0[v'] \rangle - \langle \Psi_0[v] | \hat{T} + \hat{W}_{\text{ee}} | \Psi_0[v] \rangle > 0, \tag{1.89}$$

and

$$\langle \Psi_0[v] | \hat{T} + \hat{W}_{\text{ee}} | \Psi_0[v] \rangle - \langle \Psi_0[v'] | \hat{T} + \hat{W}_{\text{ee}} | \Psi_0[v'] \rangle > 0, \tag{1.90}$$

which is absurd. In conclusion, if $v(\mathbf{r}) \neq v'(\mathbf{r}) + C$ then the ground-state densities of the two systems cannot be the same. They are equal to each other if $v(\mathbf{r})$ and $v'(\mathbf{r})$ differ by no more than a constant. Hence, there is indeed a one-to-one correspondence between the external local potential $v(\mathbf{r})$ and the ground-state electronic density $n_0(\mathbf{r})$. As a consequence, the nondegenerate ground-state wavefunction of a system as well as its ground-state energy can be expressed uniquely as a functional of the ground-state density,

$$n_0(\mathbf{r}) \longleftrightarrow v(\mathbf{r}) = v[n_0](\mathbf{r}) \longleftrightarrow \Psi_0[v] = \Psi_0[v[n_0]] = \Psi_0[n_0]. \tag{1.91}$$

In other words, the ground-state energy is a functional of the ground-state density, $E_0[v] = E_0[v[n_0]] = E_v[n_0]$, where

$$\begin{aligned} E_v[n] &= T[n] + W_{\text{ee}}[n] + V[n], \\ &= F[n] + \int \mathrm{d}\mathbf{r}\ v(\mathbf{r}) n(\mathbf{r}), \end{aligned} \tag{1.92}$$

and

$$F[n] = \langle \Psi_0[n] | \hat{T} + \hat{W}_{\text{ee}} | \Psi_0[n] \rangle = T[n] + W_{\text{ee}}[n] \tag{1.93}$$

is the universal Hohenberg–Kohn functional. Similarly, the other observables are also functionals of the density:

$$O = \langle \Psi_0[n] | \hat{O} | \Psi_0[n] \rangle = O[n]. \tag{1.94}$$

The second Hohenberg–Kohn theorem is the analogue for densities of the conventional wavefunction based variational principle,

$$E_0[v] \leqslant E_v[n], \tag{1.95}$$

for any trial density $n(\mathbf{r})$ such that $n(\mathbf{r}) \geqslant 0$ and $\int \mathrm{d}\mathbf{r}\ n(\mathbf{r}) = N$. The equality holds for the ground-state density $n_0(\mathbf{r})$. This leads to the following variational principle in DFT:

$$E_0[v] = \min_n \Big\{ E_v[n] \Big\} = E_v[n_0]. \tag{1.96}$$

That said, a problem remains: the explicit expression for the universal (in a sense that it does not depend on local potential and thus is the same for all electronic system) functional $F[n]$ is unknown. The domain of definition of this functional is discussed in the following.

1.2.1.ii The v- and N-representable densities

The Hohenberg–Kohn energy functional in Eq. (1.93) is defined for densities that are v-representable only. A density said to be v-representable has to be associated with the antisymmetric ground-state wavefunction $\Psi_0[v]$. As a consequence, the minimization in Eq. (1.96) is over the set of v-representable densities only.

An alternative formulation of the Hohenberg–Kohn functional is given by the so called Lieb maximization (or, equivalently, the Legendre–Fenchel transform) [68], obtained by rearranging the variational principle in Eq. (1.95). This leads to, for all $v(\mathbf{r})$,

$$F[n] \geqslant E_0[v] - \int \mathrm{d}\mathbf{r}\ v(\mathbf{r})n(\mathbf{r}), \tag{1.97}$$

or, equivalently,

$$F[n] = \sup_v \Big\{ E_0[v] - \int \mathrm{d}\mathbf{r}\ v(\mathbf{r})n(\mathbf{r}) \Big\}. \tag{1.98}$$

Note that the ground-state energy $E_0[v]$ is a concave function with respect to $v(\mathbf{r})$. For the ground-state density $n_0(\mathbf{r})$, the maximizing potential is $v[n_0](\mathbf{r})$. As Eq. (1.98) is derived from the variational principle that holds only for v-representable densities, the density in Eq. (1.98) should also be v-representable. This leads to serious difficulties as many densities have been shown to be non v-representable [68, 69].

Fortunately, it turns out that DFT can also be formulated in a way that requires the so-called N-representability conditions only for the densities. This is done by introducing the Levy–Lieb constrained search formalism [70],

$$F[n] = \min_{\Psi \to n} \Big\{ \langle \Psi | \hat{T} + \hat{W}_{\text{ee}} | \Psi \rangle \Big\}, \tag{1.99}$$

which consists in searching, in the whole set of antisymmetric wavefunctions with density $n(\mathbf{r})$ that integrates to N electrons, the one minimizing the expectation value for the operator $\hat{T} + \hat{W}_{\text{ee}}$. Since the density comes from an antisymmetric wavefunction, specifying the v-representability of the density is no more needed as the search is extended to the N-representable densities [70]:

$$n(\mathbf{r}) \geqslant 0, \qquad \int \mathrm{d}\mathbf{r}\ n(\mathbf{r}) = N, \qquad \text{and} \qquad \int \mathrm{d}\mathbf{r}\ |\nabla n(\mathbf{r})^{1/2}|^2 < \infty, \tag{1.100}$$

which is a weaker condition than the v-representability one, since the former is necessary for the latter [5]. Note that the Levy–Lieb [Eq. (1.99)] and Hohenberg–Kohn [Eq. (1.93)] functionals coincide if the N-representable density is also v-representable. In addition, this new formulation of the universal functional generalizes the first Hohenberg–Kohn theorem to degenerate states, given that the minimization will select only one wavefunction that reproduces $n(\mathbf{r})$. Combining Eq. (1.96) and (1.99) leads to the following form of the variational principle in DFT:

$$\begin{aligned} E_0[v] &= \min_{n} \left[\min_{\Psi \to n} \Big\{ \langle \Psi | \hat{T} + \hat{W}_{\text{ee}} | \Psi \rangle \Big\} + \int \mathrm{d}\mathbf{r}\ v(\mathbf{r}) n(\mathbf{r}) \right] \\ &= \min_{n} \left[\min_{\Psi \to n} \Big\{ \langle \Psi | \hat{T} + \hat{W}_{\text{ee}} | \Psi \rangle + \int \mathrm{d}\mathbf{r}\ v(\mathbf{r}) n^{\Psi}(\mathbf{r}) \Big\} \right], \end{aligned} \tag{1.101}$$

which is equivalent to the original variational principle for wavefunction methods,

$$E_0[v] = \min_{\Psi} \Big\{ \langle \Psi | \hat{T} + \hat{W}_{\text{ee}} | \Psi \rangle + \int \mathrm{d}\mathbf{r}\ v(\mathbf{r}) n^{\Psi}(\mathbf{r}) \Big\}. \tag{1.102}$$

Note that the difference between the Levy–Lieb and the Legendre–Fenchel functionals is subtle, and the reader is referred to Ref. [71] for a deeper discussion on this. One advantage of the latter formulation is that if it is easy to calculate $E_0[v]$ (for example in a model system), the potential remains a much more simpler variable than the many-body wavefunction Ψ. Hence, this formulation has been shown useful in the various improved DFT-like methods applied on simple models [72–75].

Thus far, it has not appear obvious if DFT contains any simplification over WFT. One can therefore wonder about the existence of any useful implementation of DFT. This answer is again "yes, it exists", and is the so-called Kohn–Sham (KS) DFT method.

1.2.1.iii Kohn–Sham method

Although the universal functional $F[n]$ can be found numerically through the Levy–Lieb constraint-search formalism [Eq. (1.99)] or through the Legendre–Fenchel transform [Eq. (1.98)] for a given density $n(\mathbf{r})$, its exact analytic expression is of course unknown. Hence, the DFT formulation presented in the previous section is a many-body theory which is even more expensive than WFT, given that the Schrödinger equation should be solved many times. In 1965, Kohn and Sham suggested a formulation of DFT which is a *single-electron-like theory* with an effective potential functional of the density, hence succeeding in a drastic decrease of the computational cost. This is the so-called Kohn-Sham (KS) DFT [76].

Based on the idea that only the ground-state density is needed to find all the properties of the physical system, could this density be obtained from a noninteracting electronic system ? For such a system, the first Hohenberg–Kohn theorem still holds so that there is a one-to-one correspondence between the noninteracting density and the local potential, up to a constant. In this context, the noninteracting universal functional reduces to the noninteracting kinetic energy, functional of the density. In the Levy–Lieb constrained search formalism, it is given by

$$T_{\mathrm{s}}[n] = \min_{\Phi\to n}\Big\{\langle\Phi|\hat{T}|\Phi\rangle\Big\}, \tag{1.103}$$

where the minimization is over the whole set of many-body wavefunctions giving the density $n(\mathbf{r})$. Note that the minimizing wavefunction for a noninteracting system will always be a Slater determinant, such that it is sufficient to consider Slater determinants only in the minimizing set of wavefunction. Alternatively, one can use the following Legendre–Fenchel transform:

$$T_{\mathrm{s}}[n] = \sup_{v}\Big\{\mathcal{E}[v] - \int \mathrm{d}\mathbf{r}\ v(\mathbf{r})n(\mathbf{r})\Big\}, \tag{1.104}$$

where $\mathcal{E}[v]$ is the ground-state energy of the noninteracting Hamiltonian $\hat{T} + \int \mathrm{d}\mathbf{r}\ v(\mathbf{r})\hat{n}(\mathbf{r})$. As for $F[n]$, the Levy–Lieb constrained search formalism is replaced by an unconstrained maximization over the potential. In KS-DFT, the universal functional of the interacting system can be decomposed as follows:

$$F[n] = T_{\mathrm{s}}[n] + (F[n] - T_{\mathrm{s}}[n]) = T_{\mathrm{s}}[n] + E_{\mathrm{Hxc}}[n], \tag{1.105}$$

where $T_{\mathrm{s}}[n]$ can be expressed exactly in terms of orbitals, but for which an exact explicit expression in term of the electron density remains unknown. The remaining term contains the difference in energy between the fully interacting system and the noninteracting one, and is so-called Hartree-exchange-correlation (Hxc) energy. It should not be forgotten that this term contains a correlation contribution from the kinetic energy and not only the contributions coming from the electron-electron repulsion,

$$E_{\mathrm{Hxc}}[n] = T[n] + W_{\mathrm{ee}}[n] - T_{\mathrm{s}}[n]. \tag{1.106}$$

The latter energy functional is usually decomposed into the explicitly known Hartree term [Eq. (1.81)] and the unknown exchange and correlation parts. The exchange contribution is given by the expectation value of the electron-electron repulsion for the minimizing KS determinant $\Phi^{\mathrm{KS}}[n]$ in Eq. (1.103),

$$E_{\mathrm{x}}[n] = \langle \Phi^{\mathrm{KS}}[n] | \hat{W}_{\mathrm{ee}} | \Phi^{\mathrm{KS}}[n] \rangle - E_{\mathrm{H}}[n]. \tag{1.107}$$

The correlation energy is the difference between the expectation value of the Hamiltonian $\hat{T} + \hat{W}_{\mathrm{ee}}$ associated with the exact physical wavefunction and the KS Slater determinant, both having the same density $n(\mathbf{r})$,

$$\begin{aligned} E_{\mathrm{c}}[n] &= \langle \Psi[n] | \hat{T} + \hat{W}_{\mathrm{ee}} | \Psi[n] \rangle - \langle \Phi^{\mathrm{KS}}[n] | \hat{T} + \hat{W}_{\mathrm{ee}} | \Phi^{\mathrm{KS}}[n] \rangle \\ &= \langle \Psi[n] | \hat{H}[v[n]] | \Psi[n] \rangle - \langle \Phi^{\mathrm{KS}}[n] | \hat{H}[v[n]] | \Phi^{\mathrm{KS}}[n] \rangle, \end{aligned} \tag{1.108}$$

and differs from the definition of the correlation energy in WFT. Following exactly the same steps as in the previous section, the variational principle in KS-DFT reads

$$\begin{aligned} E_0 &= \min_n \left[\min_{\Phi \to n} \left\{ \langle \Phi | \hat{T} | \Phi \rangle \right\} + E_{\mathrm{Hxc}}[n] + \int \mathrm{d}\mathbf{r} v_{\mathrm{ne}}(\mathbf{r}) n(\mathbf{r}) \right] \\ &= \min_n \left[\min_{\Phi \to n} \left\{ \langle \Phi | \hat{T} | \Phi \rangle + E_{\mathrm{Hxc}}[n^{\Phi}] + \int \mathrm{d}\mathbf{r} v_{\mathrm{ne}}(\mathbf{r}) n^{\Phi}(\mathbf{r}) \right\} \right], \end{aligned} \tag{1.109}$$

or, equivalently,

$$E_0 = \min_{\Phi} \left\{ \langle \Phi | \hat{T} | \Phi \rangle + E_{\mathrm{Hxc}}[n^{\Phi}] + \int \mathrm{d}\mathbf{r} v_{\mathrm{ne}}(\mathbf{r}) n^{\Phi}(\mathbf{r}) \right\}. \tag{1.110}$$

By comparing Eq. (1.110) with (1.102), it is clear that the Hxc energy functional does describe implicitly the interaction between the electrons, and that the explicit $1/r_{ij}$ operator has been hidden. The minimizing KS determinant Φ^{KS} in Eq. (1.110) reproduces the exact ground-state density $n_0(\mathbf{r})$. It is constructed (in a spin-restricted closed-shell formalism) from the $N/2$-lowest doubly occupied KS orbitals that fulfil the following one-electron self-consistent KS equations,

$$\left(-\frac{1}{2}\nabla^2 + v_{\mathrm{ne}}(\mathbf{r}) + \frac{\delta E_{\mathrm{Hxc}}[n^{\Phi^{\mathrm{KS}}}]}{\delta n(\mathbf{r})} \right) \varphi_i^{\mathrm{KS}}(\mathbf{r}) = \varepsilon_i^{\mathrm{KS}} \varphi_i^{\mathrm{KS}}(\mathbf{r}), \tag{1.111}$$

where

$$n^{\Phi^{\mathrm{KS}}}(\mathbf{r}) = 2\sum_{i=1}^{N/2} \left|\varphi_i^{\mathrm{KS}}(\mathbf{r})\right|^2. \tag{1.112}$$

Note that the same exponential parametrization as in Hartree–Fock theory can be used for optimizing the KS orbitals, where $\langle\Phi(\boldsymbol{\kappa})|\hat{H}|\Phi(\boldsymbol{\kappa})\rangle$ is replaced by $\langle\Phi(\boldsymbol{\kappa})|\hat{T}+\hat{V}_{\mathrm{ne}}|\Phi(\boldsymbol{\kappa})\rangle + E_{\mathrm{Hxc}}[n(\boldsymbol{\kappa})]$ in Eq. (1.27), with $|\Phi(\boldsymbol{\kappa})\rangle = e^{-\hat{\kappa}}|\Phi^{\mathrm{KS}}\rangle$ and

$$n(\boldsymbol{\kappa},\mathbf{r}) = \langle\Phi(\boldsymbol{\kappa})|\hat{n}(\mathbf{r})|\Phi(\boldsymbol{\kappa})\rangle. \tag{1.113}$$

Note also that in practical calculations, we work in a basis of atomic orbitals as in Hartree–Fock theory, and the Kohn–Sham equations in Eq. (1.111) can be rewritten as Roothaan equations in Eq. (1.24), where the Fock matrix becomes the KS matrix. The main difference between the KS self-consistent equations and the Hartree–Fock ones comes from the effective potential. In contrast to the Hartree–Fock potential, the KS one

$$v_{\mathrm{s}}(\mathbf{r}) = v_{\mathrm{ne}}(\mathbf{r}) + \frac{\delta E_{\mathrm{Hxc}}[n^{\Phi^{\mathrm{KS}}}]}{\delta n(\mathbf{r})} \tag{1.114}$$

is local instead of non local [see Eqs. (1.19) and (1.21)], contains a correlation contribution, and is constructed to reproduce the exact ground-state density of the physical system. Note that it corresponds to the maximizing potential of Eq. (1.104). However, the explicit density-dependence of the exact exchange contribution is generally unknown, and the exact exchange energy functional becomes an explicit functional of the KS orbitals [see Eq. (1.107)], themselves implicit functionals of the density:

$$E_{\mathrm{x}}[n] = -\sum_{i=1}^{N/2}\sum_{j=1}^{N/2}\iint \mathrm{d}\mathbf{r}\mathrm{d}\mathbf{r}' \frac{\varphi_i^{\mathrm{KS}*}(\mathbf{r})\varphi_j^{\mathrm{KS}*}(\mathbf{r}')\varphi_j^{\mathrm{KS}}(\mathbf{r})\varphi_i^{\mathrm{KS}}(\mathbf{r}')}{|\mathbf{r}-\mathbf{r}'|}, \tag{1.115}$$

where i and j run over spatial occupied KS orbitals. It has the same form as the exchange contribution in Hartree–Fock, but the orbitals are different. Because the exact exchange energy has no simple explicit expression in term of the density, the corresponding exchange potential $v_{\mathrm{x}}(\mathbf{r}) = \delta E_{\mathrm{x}}[n]/\delta n(\mathbf{r})$ cannot be calculated directly. It can be approximately determined using the method of *optimized effective potentials* (OEP) [77–79], which considers the functional derivative of $E_{\mathrm{x}}[n]$ with respect to the local potential $v_{\mathrm{s}}(\mathbf{r})$ and the application of the chain rule (see Appendix A for functional calculus):

$$\frac{\delta E_{\mathrm{x}}[n]}{\delta v_{\mathrm{s}}(\mathbf{r})} = \int \frac{\delta E_{\mathrm{x}}[n]}{\delta n(\mathbf{r}')}\frac{\delta n(\mathbf{r}')}{\delta v_{\mathrm{s}}(\mathbf{r})}\mathrm{d}\mathbf{r}' = \int v_{\mathrm{x}}(\mathbf{r}')\frac{\delta n(\mathbf{r}')}{\delta v_{\mathrm{s}}(\mathbf{r})}\mathrm{d}\mathbf{r}', \tag{1.116}$$

where $\delta n(\mathbf{r}')/\delta v_{\mathrm{s}}(\mathbf{r})$ is the KS static linear-response function. The determination of OEP can be formulated as an optimization problem where the energy is minimized with respect to the KS potential $v_{\mathrm{s}}(\mathbf{r})$. In practice, $v_{\mathrm{s}}(\mathbf{r})$ is expanded into an initial guess $v_0(\mathbf{r})$ and a linear combination of auxiliary functions $g_t(\mathbf{r})$ (typically Gaussian type functions for atoms and molecules) so that $v_{\mathrm{s}}(\mathbf{r}) = v_{\mathrm{ne}}(\mathbf{r}) + v_0(\mathbf{r}) + \sum_t b_t g_t(\mathbf{r})$, where $\{b_t\}_t$ are the expansion coefficients to be optimized. This leads to the "discrete" OEP equations [80–82]. It should be noted here that this optimization is not without issue and can be an ill-posed problem [79, 83]. Indeed, it can happen during the optimization of $v_{\mathrm{s}}(\mathbf{r})$ that the basis set $\{b_t\}_t$ is unbalanced in comparison to the orbital basis set $\{\chi_\mu(\mathbf{r})\}_\mu$ (for instance, some Gaussian functions $b_t(\mathbf{r})$ with much higher exponent than the ones in $\{\chi_\mu(\mathbf{r})\}_\mu$). This unbalanced basis set problem can lead to unphysical potentials, so that many potentials can produce the same numerical total energy. In this case, high oscillations can be observed during the optimization procedure, and can be fixed by including smoothness in the functional [84, 85] or by requiring a minimal change in the density upon increasing the orbital basis set [86]. Let us now turn to the exact expression for the correlation energy, which can be obtained in the adiabatic connection formalism.

1.2.1.iv Adiabatic Connection

The development of approximate xc energy functionals is a difficult task and a strategy is provided by the linear adiabatic connection (AC) [87–91]. The linear AC consists in scaling the electron-electron repulsion by a factor λ while holding the density constant. Consider the following λ-dependent Schrödinger equation:

$$\hat{H}^\lambda[v]|\Psi^\lambda[v]\rangle = \mathcal{E}^\lambda[v]|\Psi^\lambda[v]\rangle, \tag{1.117}$$

where the λ-dependent Hamiltonian reads

$$\hat{H}^\lambda[v] = \hat{T} + \lambda\hat{W}_{\mathrm{ee}} + \sum_{i=1}^{N} v(\mathbf{r}_i) \times . \tag{1.118}$$

The local potential should be λ-dependent in order to recover the exact density of the physical system ($\lambda = 1$) for any λ, i.e. $n^\lambda(\mathbf{r}) = n^{\lambda=1}(\mathbf{r}) = n(\mathbf{r})$ and $v(\mathbf{r}_i) \to v^\lambda(\mathbf{r}_i)$. The analogue of the Hohenberg–Kohn functional for a partially-interacting system is given by the Levy–Lieb constrained search formalism,

$$\begin{aligned} F^\lambda[n] &= \min_{\Psi\to n}\left\{\langle\Psi|\hat{T} + \lambda\hat{W}_{\mathrm{ee}}|\Psi\rangle\right\}, \\ &= \langle\Psi^\lambda|\hat{T} + \lambda\hat{W}_{\mathrm{ee}}|\Psi^\lambda\rangle, \end{aligned} \tag{1.119}$$

which can be alternatively written using the Legendre–Fenchel transform:

$$F^{\lambda}[n] = \sup_{v} \left\{ \mathcal{E}^{\lambda}[v] - \int \mathrm{d}\mathbf{r}\; v(\mathbf{r})n(\mathbf{r}) \right\}, \tag{1.120}$$

$$= \mathcal{E}^{\lambda}[v^{\lambda}] - \int \mathrm{d}\mathbf{r}\; v^{\lambda}(\mathbf{r})n(\mathbf{r}). \tag{1.121}$$

Note that Eqs. (1.98) and (1.104) are recovered from Eq. (1.120) for $\lambda = 1$ and $\lambda = 0$, corresponding to the Hohenberg–Kohn DFT and the KS-DFT, respectively.

Given that $F^{\lambda=0}[n] = T_{\mathrm{s}}[n]$, the KS decomposition of $F[n] = F^{\lambda=1}[n]$ leads to

$$F[n] = T_{\mathrm{s}}[n] + E_{\mathrm{Hxc}}[n] = T_{\mathrm{s}}[n] + F^{\lambda=1}[n] - F^{\lambda=0}[n], \tag{1.122}$$

so that the Hxc energy functional reads,

$$E_{\mathrm{Hxc}}[n] = \int_0^1 \mathrm{d}\lambda \frac{\mathrm{d}F^{\lambda}[n]}{\mathrm{d}\lambda} = \int_0^1 \mathrm{d}\lambda\; \langle \Psi^{\lambda} | \hat{W}_{\mathrm{ee}} | \Psi^{\lambda} \rangle, \tag{1.123}$$

where the Hellmann-Feynman theorem has been used to derive the second equality. By isolating the correlation part,

$$E_{\mathrm{c}}[n] = \int_0^1 \mathrm{d}\lambda\, \mathcal{W}_{\mathrm{c}}^{\lambda}[n], \tag{1.124}$$

one can introduce the correlation integrand

$$\mathcal{W}_{\mathrm{c}}^{\lambda}[n] = \langle \Psi^{\lambda} | \hat{W}_{\mathrm{ee}} | \Psi^{\lambda} \rangle - \langle \Phi^{\mathrm{KS}} | \hat{W}_{\mathrm{ee}}, | \Phi^{\mathrm{KS}} \rangle \tag{1.125}$$

which can also be written as

$$\mathcal{W}_{\mathrm{c}}^{\lambda}[n] = \frac{\partial E_{\mathrm{c}}^{\lambda}[n]}{\partial \lambda}, \tag{1.126}$$

where $E_{\mathrm{c}}^{\lambda}[n]$ is given by the following scaling relation [92, 93]:

$$E_{\mathrm{c}}^{\lambda}[n] = \int_0^{\lambda} \mathrm{d}\nu \left(\langle \Psi^{\nu} | \hat{W}_{\mathrm{ee}} | \Psi^{\nu} \rangle - \langle \Phi^{\mathrm{KS}} | \hat{W}_{\mathrm{ee}} | \Phi^{\mathrm{KS}} \rangle \right) = \lambda^2 E_{\mathrm{c}}[n_{1/\lambda}], \tag{1.127}$$

with $n_{1/\lambda}(\mathbf{r}) = (1/\lambda)^3 n(\mathbf{r}/\lambda)$. The adiabatic connection is built by varying continuously λ between 0 and 1 and provides some insights about the form of the Hxc energy functional, as well as possible routes for the development of improved hybrid functionals [94, 95]. In other words, the variation of λ allows to go continuously from a noninteracting KS reference system to the fully interacting one.

As readily seen in Eq. (1.125), the calculation of the integrand requires the many-body wavefunction Ψ^{λ}. Therefore, its accurate construction is very limited in practice [96], and one has to use approximation to it, such as Görling-Levy perturbation theory with respect to the coupling constant λ [97] (still keeping the ground-state density constant at each order), Padé approximation [98], interaction-strength interpolation [99] or other forms derived from coupled cluster theory [100]. An alternative kinetic-energy based adiabatic connection has also been derived and offers new possibilities for modelling correlation energy functionals [101].

The density functional approximations (DFAs) in KS-DFT – which will be discussed in the next section – are not able to treat strongly correlated systems, i.e. systems where the static correlation dominates. In order to develop more appropriate functionals able to describe such challenging systems, one can look at the $\lambda \to +\infty$ limit instead of the noninteracting $\lambda = 0$ [102, 103], leading to the *strictly correlated electron* (SCE) DFT [104–106]. When combined with the KS scheme, it is called the KS SCE DFT approach and it has been shown promising for the treatment of strongly correlated systems [107–110]. However, its application to chemical systems, which are not close enough to the strong-interaction limit, remains a challenge [111, 112].
Another interesting limit which has been considered is $\lambda \to -\infty$, corresponding to negative coupling constant (attractive electrons) and which could be appropriate to the study of supraconductivity [113].

The underlying idea of scaling the electron interaction in the adiabatic connection has been a source of inspiration for the development of new methods in which the electron-electron repulsion is separated into two part: one part treated by wavefunction theory (WFT) and the other one by DFT. It has led to in-principle exact combination of WFT and DFT theories, free of double counting problem, as discussed in more details in Sec. 1.3.

1.2.1.v Density functional approximations

This section aims to give an overview of the different DFAs. The first and significantly old DFA that have been developed is the local density approximation (LDA) [76, 114, 115] which is based on the uniform electron gas [116]. Within this approximation, the exchange-correlation energy functional reads

$$E_{\text{xc}}^{\text{LDA}}[n] = \int \mathrm{d}\mathbf{r}\, n(\mathbf{r}) \epsilon_{\text{xc}}[n], \tag{1.128}$$

where $\epsilon_{\text{xc}}[n]$ is the exchange-correlation energy per particle of a homogeneous electron gas of density $n(\mathbf{r})$. This energy can be decomposed into an exchange contribution, given in Eq. (1.82), and a correlation one for which accurate values have been calculated by QMC calculations [117], and then interpolated to provide an analytic form for $\epsilon_\mathrm{c}[n]$ [118, 119]. Going beyond LDA, the generalized gradient approximations (GGA) [76, 120] (which use the gradient of the density) have been proposed like B88 [121], LYP [122], PW91 [123–125] and PBE [126] functionals. Improvements are possible by considering higher level functionals such as meta-generalized-gradient approximations (mGGAs) implying the Laplacian of the density like the TPSS [127] and SCAN [128] functionals. The KS potential in the above DFAs is an explicit functional of the density and can be calculated easily in contrast to the OEP approach which is computationally expensive.

Note that because of the approximations made in the exchange and correlation energy functionals, the unphysical self-interaction error arising from the direct product of the densities in the Hartree functional [Eq. (1.81)] is not compensated by the exchange contribution in contrast to Hartree–Fock theory, so that a single electron can unphysically interact with itself [129]. This self-interaction error is a major drawback of a DFA for the calculation of band gaps, ionization potentials and electronic affinities due to the violation of the famous piecewise linearity of the energy between two integral numbers of electrons [130][3]. It can be fixed by using implicitly density-dependent functionals, so-called hybrid functionals. The term “hybrid” comes from the idea of mixing a fraction of Hartree–Fock exchange with density functionals. Based on arguments relying on the adiabatic connection [131], it has led to the B3LYP [132], PBE0 [133], and Coulomb attenuating method (CAM)-B3LYP [134] approximations. This exchange contribution is given in Eq. (1.115) but the orbitals are now optimized in a Hartree–Fock way with a non local exchange potential (also called generalized KS-DFT method [135]) in contrast to the OEP approach. The mixing parameters are usually determined by fitting to experimental data, or determined dynamically depending on the density of the system [136].

Another deficiency in the usual DFAs is the correct description of dispersion effects and long-range interactions such as van der Waals interactions. To overcome this issue, semiempirical dispersion corrections can be employed [137, 138]. Note that one has to be particularly careful when developing functionals based on empirical fitting, as it has been noted that the accurately obtained total energies are at the expense of the accurate recovering of the electron density [139]. Alternatively, a class of double-hybrid approximations has emerged where a fraction of MP2 correlation energy, known to recover proper dispersion effects, is used in combination with density-functional correlation approximations [140–142]. A combined HF/DFA exchange and MP2/DFA correlation functionals can also be obtained by introducing a range-separation parameter [143–151]. This idea originates from the range-separated DFT [152, 153] which will be described in Section 1.3.1.i. All these approximations

---

[3] This will be further discussed in Chap. 5, where a solution to the band gap problem in KS-DFT will be proposed using ensemble DFT.

can be sorted in different categories, forming the density functional Jacob's ladder [154] which rises up in the "heaven", where the exact universal functional is patiently waiting to be discovered. This brief summary of the various approximations emphasizes how large the collection of density functionals approximations is [155, 156].

To summarize, the KS-DFT is an in-principle exact method based on a noninteracting system, on which is applied a single-electron effective potential. The ground-state energy and density of the physical system can be recovered exactly, provided that the exact Hxc energy functional is used. While this universal functional has not been found yet, several approximations have been derived and are able to treat weakly correlated systems (i.e. systems containing dynamical correlation). Unfortunately, the functionals present in the literature are still not able to describe strongly correlated systems such as transition metal oxides [157] for which the ground-state is highly multiconfigurational (due to the d- or f-orbital manifolds, responsible for static correlation). The treatment of strong (static) correlation remains the biggest challenge in DFT, and no DFA is sufficiently accurate when applied to such system yet.

Different paths can be investigated to fix this deficiency of the current DFAs. A promising approach already mentioned in Sec. 1.2.1.iv and which conserves the DFT formalism is provided by the *strictly correlated electron* (SCE) DFT [102–110]. Another possible strategy is to merge the KS-DFT with WFT, as we have seen that the former performs well for the description of dynamical correlation, while the latter can treat static correlation (at the expense of a higher computational cost) when MCSCF-type methods are used. However, because DFT and WFT are formulated in a completely different framework, merging the two approaches without accounting for the same correlation effect twice (thus leading to the so-called double counting problem) is an extremely difficult task. This will be further discussed in Sec. 1.3, and is one of the central thematic of this thesis.

It should be noted that even if the exact functional is known, there are still some quantities which cannot be extracted exactly from KS-DFT. For instance, the description of the fundamental energy gap (referred to as the fundamental gap, or band gap for solids) cannot be equal to the KS gap. This band gap problem in DFT is commonly addressed by considering fractional number of electrons (i.e. DFT for open systems) [130, 158][4]. To improve over the description of band gaps in systems containing strongly localized d- or f-orbitals, the introduction of a Hubbard-like correction U in the Hxc functional[5] has been proposed, thus leading to the so-called DFT+U [159–161]. Although DFT+U and hybrid functionals are of course not identical [162], they share similarities in a sense that they both add a non local correction (the Hubbard U correction and the Hartree–Fock exchange, respectively) to a local

---

[4] This problem will be discussed in Chap. 5.

[5] See Sec. 2.1 for a general description of the Hubbard model

exchange potential. However, in DFT+U one has to deal with the double counting of the correlation due to this additional correction on top of a LDA or GGA density functional [163, 164]. Still, DFT+U does not always provide accurate band gaps [165, 166].

1.2.2 Reduced Density Matrix Functional Theory

The ground-state energy of the *ab-initio* Hamiltonian in Eq. (1.5) in an external nonlocal potential (e.g. the kinetic operator, the hopping in the Hubbard model, or even a potential in the presence of a magnetic field) can be written as a functional of the one-body density matrix (1RDM) and the diagonal of the two-body reduced density matrix (2RDM) only (see Appendix C):

$$\begin{aligned} E[\gamma,\Gamma^{(2)}] &= T[\gamma] + W[\Gamma^{(2)}] + V_{\text{ext}}[\gamma] \\ &= \iint \mathrm{d}\mathbf{x}\mathrm{d}\mathbf{x}'\delta(\mathbf{x}-\mathbf{x}')\left(-\frac{\nabla^2_{\mathbf{r}}}{2}\right)\gamma(\mathbf{x},\mathbf{x}') + \frac{1}{2}\iint \mathrm{d}\mathbf{x}\mathrm{d}\mathbf{x}'\frac{\Gamma^{(2)}(\mathbf{x},\mathbf{x}';\mathbf{x},\mathbf{x}')}{|\mathbf{r}-\mathbf{r}'|} \\ &\quad + \iint \mathrm{d}\mathbf{x}\mathrm{d}\mathbf{x}' v_{\text{ext}}(\mathbf{x},\mathbf{x}')\gamma(\mathbf{x},\mathbf{x}'), \end{aligned} \tag{1.129}$$

where the 2RDM reads

$$\Gamma^{(2)}(\mathbf{x}_1,\mathbf{x}_2;\mathbf{x}'_1,\mathbf{x}'_2) = N(N-1)\int \mathrm{d}\mathbf{x}_3\ \ldots\ \int \mathrm{d}\mathbf{x}_N \Psi^*(\mathbf{x}'_1,\mathbf{x}'_2,\mathbf{x}_3,\ldots,\mathbf{x}_N)\Psi(\mathbf{x}_1,\ldots,\mathbf{x}_N), \tag{1.130}$$

and the 1RDM,

$$\gamma(\mathbf{x},\mathbf{x}') = N\int \mathrm{d}\mathbf{x}_2 \int \mathrm{d}\mathbf{x}_3\ \ldots\ \int \mathrm{d}\mathbf{x}_N \Psi^*(\mathbf{x},\mathbf{x}_2,\ldots,\mathbf{x}_N)\Psi(\mathbf{x}',\mathbf{x}_2,\ldots,\mathbf{x}_N). \tag{1.131}$$

Note that the 1RDM can be obtained exactly from the 2RDM, so that the energy is only a functional of the 2RDM. Unfortunately, simple N-representability conditions do not exist as they require the knowledge of all higher order density matrices from 3- up to N-order when considering $N > 2$ electrons [167]. By not considering the N-representability constraints, the 2RDM obtained by straight minimization of the energy in Eq. (1.129) is not guaranteed to correspond to some antisymmetric N-electron wavefunction, and one could get energies lower than the exact ground-state one. This has justified the choice to keep only the 1RDM as basic variable, for which N-representability conditions are known, leading to the so-called (one-electron) reduced density matrix functional theory (RDMFT) [168, 169]. Still, note that significant progress has been achieved recently in the field of 2RDM [170–172]. Intuitively, expressing the ground-state energy as a functional of the 1RDM rather than the electronic density $n(\mathbf{r}) = \sum_\sigma \gamma(\mathbf{x},\mathbf{x})$ is appealing, because it contains more informations. Besides, the type of chemical bond is better revealed by the off-diagonal elements of the 1RDM [173, 174]. The theoretical foundation for RDMFT has been given by Gilbert [175], who extended the Hohenberg–Kohn theorem to nonlocal potentials, thus proving the one-to-one correspondence between the ground-state wavefunction and the ground-state 1RDM. This theorem guarantees the existence of an energy functional of the 1RDM, whose minimum with respect to all N-representable 1RDMs yields the exact ground-state 1RDM and energy for a given non local external potential,

$$E_0 = \min_{\gamma \in N\text{-rep}} \Big\{ E[\gamma] \Big\} = \min_{\gamma \in N\text{-rep}} \Big\{ h[\gamma] + W[\gamma] \Big\}. \tag{1.132}$$

$h[\gamma]$ is the one-particle energy functional of the 1RDM, representing the kinetic and external potential contribution,

$$h[\gamma] = \iint \mathrm{d}\mathbf{x}\mathrm{d}\mathbf{x}' \left[\delta(\mathbf{x}-\mathbf{x}') \left(-\frac{\nabla^2_{\mathbf{r}}}{2} \right) + v_{\text{ext}}(\mathbf{x},\mathbf{x}') \right] \gamma(\mathbf{x},\mathbf{x}'), \tag{1.133}$$

and $W[\gamma]$ corresponds to the two-electron repulsion energy which is also an implicit functional of the 1RDM, so-called the interaction functional. As readily seen in Eq. (1.133), a major advantage of using the 1RDM as a basic variable is that the kinetic energy can be calculated exactly if the exact 1RDM is known, in contrast to KS-DFT. However, the exact energy functional $W[\gamma] = \langle \Psi[\gamma] | \hat{W}_{\text{ee}} | \Psi[\gamma] \rangle$ is not known, in analogy with the universal Hohenberg–Kohn functional $W_{\text{ee}}[n]$ in DFT.

In Eq. (1.132), one has to ensure that the set of 1RDM over which the minimization is done contains only physical 1RDM, which are N-representables. This can be done by using the Levy–Lieb constrained search formalism which extends the domain to all pure-state N-representable 1RDMs,

$$W[\gamma] = \min_{\Psi \to \gamma} \langle \Psi | \hat{W}_{\text{ee}} | \Psi \rangle. \tag{1.134}$$

In other words, the 1RDM has to be associated with a properly anti-symmetrized wave function. Unfortunately, the pure-state N-representability conditions (also known as generalized Pauli constraints) are extremely difficult to tackle for the 1RDM, although significant progress has been reported [176–179]. To solve this problem, the constrained-search domain has been further extended to ensemble N-representable 1RDMs [180], thus leading to

$$W[\gamma] = \min_{\Gamma^{(N)} \to \gamma} \text{Tr}\Big[\hat{\Gamma}^{(N)} \hat{W}_{\text{ee}} \Big], \tag{1.135}$$

where the $\hat{\Gamma}^{(N)} = \sum_i w_i |\Psi_i\rangle\langle\Psi_i|$ is the density matrix operator describing a mixed state composed by an ensemble of pure states $|\Psi_i\rangle$ with weights w_i and with the normalization $\sum_i w_i = 1$. Tr denotes the trace, such that

$$\mathrm{Tr}\left[\hat{\Gamma}^{(N)}\hat{W}_{\mathrm{ee}}\right] = \sum_i w_i \langle \Psi_i | \hat{W}_{\mathrm{ee}} | \Psi_i \rangle. \tag{1.136}$$

In other words, there exists an ensemble of N-electron wavefunctions that together yield γ. This extension is particularly useful as the conditions for ensemble N-representability (also known as Pauli constraints) are known [181]. These conditions are commonly formulated using the basis of the eigenfunctions of the 1RDM, which are the natural spin-orbitals $\{\varphi_p\}_p$,

$$\gamma(\mathbf{x}, \mathbf{x}') = \sum_p n_p \varphi_p(\mathbf{x}) \varphi_p^*(\mathbf{x}'), \tag{1.137}$$

which form a set of orthonormal orbitals,

$$\langle \varphi_p | \varphi_q \rangle = \delta_{pq}, \tag{1.138}$$

where $\{n_p\}_p$ are the corresponding eigenvalues called the occupation numbers. The ensemble N-representability conditions for an integral number N of electrons are simple and read [181]

$$0 \leq n_p \leq 1, \qquad \sum_p n_p = N. \tag{1.139}$$

Using the spectral representation in Eq. (1.137), the 1RDM becomes a functional of the natural orbitals and their occupation numbers. Because these conditions involve eigenvalues and eigenvectors of the 1RDM, the energy functional is commonly written as a functional of the occupation numbers and natural orbitals,

$$E[\gamma] \equiv E[\{\varphi_p\}_p, \{n_p\}_p]. \tag{1.140}$$

Returning to the interaction functional expression, it can be decomposed into Hartree (H), exchange (x) and correlation (c) terms as follows:

$$W_{\mathrm{H}}[\gamma] = \frac{1}{2} \iint \frac{\gamma(\mathbf{x}, \mathbf{x})\gamma(\mathbf{x}', \mathbf{x}')}{|\mathbf{r} - \mathbf{r}'|} \mathrm{d}\mathbf{x}\mathrm{d}\mathbf{x}' \tag{1.141}$$

which is identical to $E_{\mathrm{H}}[n]$ in KS-DFT, and

$$W_{\mathrm{x}}[\gamma] = -\frac{1}{2} \iint \frac{\gamma(\mathbf{x}, \mathbf{x}')\gamma(\mathbf{x}', \mathbf{x})}{|\mathbf{r} - \mathbf{r}'|} \mathrm{d}\mathbf{x}\mathrm{d}\mathbf{x}' \tag{1.142}$$

which is exactly written as an explicit functional of the 1RDM. Only the correlation part remains unknown. Then, numerous functionals have been developed in the context of RDMFT, of the form

$$W_{\mathrm{c}}[\{\varphi_p\},\{n_p\}] = \sum_{pq} f(n_p, n_q) \iint \mathrm{d}\mathbf{x}\mathrm{d}\mathbf{x}' \frac{\varphi_p(\mathbf{x})\varphi_q(\mathbf{x}')\varphi_p^*(\mathbf{x}')\varphi_q^*(\mathbf{x})}{|\mathbf{r}-\mathbf{r}'|}. \tag{1.143}$$

The first one was introduced by Müller [182], equivalently obtained by Buijse and Baerends [183] by modelling the exchange and correlation hole of the hydrogen molecule. Since then, several corrections have been derived to improve on the correlation contribution, such as the power functional [184, 185], the Goedecker-Umrigar functional [186, 187], the corrections to Buijse and Baerends functionals (BBC) [188, 189], functionals based on the homogeneous electron gas [190] and empirical functionals [191]. Some other functionals are based on the reconstruction of the 2RDM in terms of the 1RDM, thus leading to Piris natural orbital functionals PNOFi ($i = 1, 7$) [192–203]. The latter aim at recovering the cumulant part of the 2RDM, written in the following cumulant expression [204]:

$$\Gamma_{pqrs} = \Gamma^{\mathrm{HF}}_{pqrs} + \lambda_{pqrs}[\gamma], \tag{1.144}$$

where $\Gamma^{\mathrm{HF}}_{pqrs} = n_p n_q(\delta_{pr}\delta_{qs} - \delta_{ps}\delta_{qr})$ is expressed as a functional of the occupation numbers (it has the same expression as the Hartree–Fock 2RDM but n_p and n_q can be fractional) and $\lambda_{pqrs}[\gamma]$ is the cumulant part written as a functional of the 1RDM, so that

$$W_{\mathrm{c}}[\gamma] = \frac{1}{2}\sum_{pqrs} \lambda_{pqrs}[\gamma] \iint \mathrm{d}\mathbf{x}\mathrm{d}\mathbf{x}' \frac{\varphi_r^*(\mathbf{x})\varphi_s^*(\mathbf{x}')\varphi_p(\mathbf{x})\varphi_q(\mathbf{x}')}{|\mathbf{r}-\mathbf{r}'|}. \tag{1.145}$$

Then, it is assumed that the cumulant part depends on the occupation numbers only. To simplify the construction of $\lambda_{pqrs}[\{n_p\}]$, Piris functionals generate the elements that correspond to Coulomb or exchange contributions only. Note that setting $\lambda_{pqrs} = 0$ will simply lead to the Hartree–Fock energy.

In addition to molecular dissociation curves, RDMFT has also been applied to the homogeneous electron gas [185, 205, 206] and to the description of ionization potentials, electron affinities and band gaps in solids or molecules [207–210]. A nice review of the RDMFT and its associated functional approximations can be found in Ref. [189], as well as a recent benchmarking of density matrix functional approximations in Refs. [203, 211].

Despite its promising results, RDMFT is still facing issues. Indeed, for a functional to be fully N-representable, the ensemble N-representability conditions for both the 1RDM and 2RDM have to be fulfilled. These conditions are commonly not satisfied for most of the approximate functionals [203, 211], such that too low energies can be obtained. In principle, the ensemble N-representability conditions for the 1RDM in Eq. (1.139) are sufficient [180, 212] providing that the exact functional is known, which is of course not the case. PNOFi ($i = 5,6,7$) approximations fix this problem by recovering the ensemble N-representable 2RDM, thus ensuring that the ground-state energy remains an upper bound to the true energy [213]. It is worth mentioning that even though a functional fulfils the ensemble N-representability conditions for both the 1RDM and the 2RDM, there is still no guarantee that it is associated to a given wavefunction. To my knowledge, the only functional that is associated to a given wavefunction is PNOF5, which was shown to be connected to the wavefunction of antisymmetrized product of strongly orthogonal geminal (APSG) [214][6]. Hence, the 1RDM is pure-state N-representable within PNOF5.

Another issue arises for functionals being explicit functionals of the natural orbitals and occupation numbers, instead of being explicit functionals of the full 1RDM, which is the case of most current approximations. For instance, if there are two or more degenerate natural orbitals (in terms of occupation numbers), the spectral representation of the 1RDM is no more unique. This should not be a problem if one performs a unitary transformation to change the basis in the degenerate subspace which leaves the 1RDM, and therefore the energy, unchanged. But because the functionals are explicitly dependent on the natural orbitals and occupation numbers only, they are not invariant by unitary transformations in the degenerate subspace, which can lead to size-inconsistency problems [215].

Finally, the mapping of the physical system onto a noninteracting one, like in DFT, is also missing in RDMFT. The problem is that the physically interacting 1RDM is not pure-state noninteracting v-representable [180, 216]. This is clearly understandable by looking at the property of the 1RDM of noninteracting wavefunction (i.e. a single Slater determinant). In the noninteracting case, the occupation numbers of the 1RDM are either 0 or 1 and therefore the 1RDM is idempotent, i.e. $\gamma = \gamma^2$. On the contrary, the 1RDM of an interacting system will have fractional occupation numbers[7] and will not be idempotent. It is therefore impossible to map the physical interacting system onto a pure-state noninteracting one having exactly the same 1RDM. However, one can consider an ensemble of idempotent density matrices able to reconstruct the physical one with fractional occupation numbers [218], but it leads to a completely degenerate orbital spectrum at the Fermi level energy. Then, the mapping is possible and the 1RDM is said to be ensemble non-interacting v-representable, but the molecular orbital view (essential for chemists to understand chemical processes) is completely lost. However, this degeneracy of the orbital energies is in fact a consequence of a zero temperature consideration in RDMFT and can be lifted by considering finite temperature [219]. In the latter ap-

---

[6] More details on geminal wavefunctions will be provided in Chap. 6

[7] Note that non integral occupation numbers denote a deviation for the monodeterminantal description of the system, so that all the natural orbitals having fractional occupation number should in principle be incorporated in the CAS of a CASSCF calculation [217].

proach, the authors used another reduced quantity which is very popular in condensed matter physics, namely the one-particle Green's function. They provided a systematic strategy to elaborate improved 1RDM functionals by connecting diagrammatic many-body perturbation theory to RDMFT at finite temperature. Note that at zero temperature, the corresponding Green's function of the noninteracting system in RDMFT would have degenerate poles, which is completely unphysical [219]. Like in RDMFT, ensembles have to be considered to overcome this issue.

Alternatively, one could consider mapping the physical system onto a partially-interacting one instead of a non-interacting one. This mapping would be able to reproduce the physical pure-state N-representable 1RDM from the partially interacting system. This idea was originally suggested by P. W. Ayers (not published) and will be investigated in chapter 6, where a seniority-zero wavefunction is used as a reference to get a pure-state N-representable 1RDM, while a functional of the 1RDM is employed to recover the missing correlation.

1.2.3 One-particle Green's function

This section uses the material presented in the PhD theses of Fabien Bruneval [220] and Elisa Rebolini [221]. The reader is referred to these two references for a more advanced introduction about Green's function.

Let us start from the many-body second-quantized Hamiltonian written in real space (see Appendix C):

$$\hat{H} = \int \mathrm{d}\mathbf{x}\, \hat{\Psi}^{\dagger}(\mathbf{x}) h(\mathbf{r}) \hat{\Psi}(\mathbf{x}) + \frac{1}{2} \iint \mathrm{d}\mathbf{x}\mathrm{d}\mathbf{x}' \frac{\hat{\Psi}^{\dagger}(\mathbf{x})\hat{\Psi}^{\dagger}(\mathbf{x}')\hat{\Psi}(\mathbf{x}')\hat{\Psi}(\mathbf{x})}{|\mathbf{r}-\mathbf{r}'|}, \tag{1.146}$$

where $\hat{\Psi}^{\dagger}(\mathbf{x})$ ($\hat{\Psi}(\mathbf{x})$) is the creation (annihilation) field operator of one electron with spin σ at position $\mathbf{r}$ and $h(\mathbf{r}) = (-1/2)\nabla^2 + v_{\mathrm{ne}}(\mathbf{r})$. We define the time-ordered one-particle Green's function of a system with N electrons as

$$\begin{aligned} \mathrm{i}G(1,2) &= \langle N | T\left[\hat{\Psi}(1)\hat{\Psi}^{\dagger}(2)\right] | N \rangle \\ &= \theta(t_1 - t_2)\langle N|\hat{\Psi}(1)\hat{\Psi}^{\dagger}(2)|N\rangle - \theta(t_2 - t_1)\langle N|\hat{\Psi}^{\dagger}(2)\hat{\Psi}(1)|N\rangle, \end{aligned} \tag{1.147}$$

where $|N\rangle$ is the ground state of the N-electron system. For convenience, the short-hand notation $1 \equiv (\mathbf{x}_1, t_1) = (\mathbf{r}_1, \sigma_1, t_1)$ has been introduced. T is the time-ordering operator which orders the operators with larger times on the left. In practice this is done by considering the Heaviside step function θ that reads

$$\theta(t_1 - t_2) = \begin{cases} 0, & t_1 < t_2 \\ 1, & t_1 \geq t_2 \end{cases}. \tag{1.148}$$

In contrast to the previous approaches, a time dependence is included in the field operators (so-called Heisenberg representation) as follows:

$$\hat{\Psi}(1) = e^{\mathrm{i}\hat{H}t_1}\hat{\Psi}(\mathbf{x}_1)e^{-\mathrm{i}\hat{H}t_1}, \qquad \hat{\Psi}^\dagger(2) = e^{\mathrm{i}\hat{H}t_2}\hat{\Psi}^\dagger(\mathbf{x}_2)e^{-\mathrm{i}\hat{H}t_2}. \tag{1.149}$$

Therefore, the first term in the right-hand side of Eq. (1.147) measures how an extra electron propagates from $(\mathbf{x}_2, t_2)$ to $(\mathbf{x}_1, t_1)$, while the second term measures how a missing electron (or a hole) propagates from $(\mathbf{x}_1, t_1)$ to $(\mathbf{x}_2, t_2)$. The one-particle Green's function is thus a more complex (but richer) reduced quantity than the 1RDM or the electronic density. The latter can be recovered from the Green's function in the limit $t_2 \to t_1^+ = t_1 + 0^+$ (where 0^+ is an infinitesimal positive number),

$$\gamma(\mathbf{x}_1, \mathbf{x}_2) = \langle N|\hat{\Psi}^\dagger(\mathbf{x}_1)\hat{\Psi}(\mathbf{x}_2)|N\rangle = -\mathrm{i}G(\mathbf{x}_1 t_1, \mathbf{x}_2 t_1^+), \tag{1.150}$$

and by setting $\mathbf{x}_2 = \mathbf{x}_1$ and integrating over the spin coordinates,

$$n(\mathbf{r}_1) = \sum_{\sigma_1} \gamma(\mathbf{r}_1\sigma_1, \mathbf{r}_1\sigma_1) = -\mathrm{i}\sum_{\sigma_1} G(\mathbf{r}_1\sigma_1 t_1, \mathbf{r}_1\sigma_1 t_1^+). \tag{1.151}$$

More generally, any expectation value of a one-particle operator $\hat{O}$ can be extracted from the one-particle Green's function,

$$\langle\Psi|\hat{O}|\Psi\rangle = -\mathrm{i}\iint \mathrm{d}\mathbf{x}_1\mathrm{d}\mathbf{x}_2 O(\mathbf{x}_1, \mathbf{x}_2)G(\mathbf{x}_1 t_1, \mathbf{x}_2 t_1^+). \tag{1.152}$$

To compute the expectation value of two-body operators, one would need the two-body Green's function. However, the ground-state energy of the N-electron system can be expressed by the Galitskii-Migdal formula [222] as,

$$E_0^N = -\frac{\mathrm{i}}{2}\int \mathrm{d}\mathbf{x}_1 \lim_{2\to 1^+}\left(\mathrm{i}\frac{\partial}{\partial t_1} + h(\mathbf{r}_1)\right)G(1,2), \tag{1.153}$$

thus becoming a functional of the one-particle Green's function only. Let us now look at a more explicit form of the one-particle Green's function. Because no time-dependent external potential is applied ($\hat{H}$ is time-independent), the Green's function is invariant under translation in time and we can write the Green's function as a function of the time difference $\tau = t_1 - t_2$ rather than t_1 and t_2. Additionally, by introducing the closure relation for the $(N-1)$- and $(N+1)$-electron states (denoted by i and a indices, respectively),

$$\sum_i |N-1,i\rangle\langle N-1,i|, \qquad \sum_a |N+1,a\rangle\langle N+1,a|, \tag{1.154}$$

and using Eq. (1.149), it comes

$$\begin{aligned}\mathrm{i}G(\mathbf{x}_1,\mathbf{x}_2;\tau) &= \theta(\tau)\sum_a \langle N|\hat{\Psi}(\mathbf{x}_1)|N+1,a\rangle\langle N+1,a|\hat{\Psi}^\dagger(\mathbf{x}_2)|N\rangle e^{-\mathrm{i}(E_a^{N+1}-E_0^N)\tau} \\ &\quad -\theta(-\tau)\sum_i \langle N|\hat{\Psi}^\dagger(\mathbf{x}_2)|N-1,i\rangle\langle N-1,i|\hat{\Psi}^\dagger(\mathbf{x}_1)|N\rangle e^{-\mathrm{i}(E_0^N-E_i^{N-1})\tau},\end{aligned} \tag{1.155}$$

where E_i^{N-1} and E_a^{N+1} are the energies of the ith excited state of the $(N-1)$-electron system and the ath excited state of the $(N+1)$-electron system, respectively. Then, by using the Fourier transform of the Heaviside step function,

$$\theta(\tau) = -\int_{-\infty}^{+\infty}\frac{\mathrm{d}\omega}{2\pi\mathrm{i}}\frac{e^{-\mathrm{i}\omega\tau}}{\omega+\mathrm{i}0^+}, \qquad \theta(-\tau) = \int_{-\infty}^{+\infty}\frac{\mathrm{d}\omega}{2\pi\mathrm{i}}\frac{e^{-\mathrm{i}\omega\tau}}{\omega-\mathrm{i}0^+}, \tag{1.156}$$

we obtain the following expression for the Green's function:

$$\begin{aligned}G(\mathbf{x}_1,\mathbf{x}_2;\tau) &= \int_{-\infty}^{+\infty}\frac{\mathrm{d}\omega}{2\pi}\left[\sum_a \langle N|\hat{\Psi}(\mathbf{x}_1)|N+1,a\rangle\langle N+1,a|\hat{\Psi}^\dagger(\mathbf{x}_2)|N\rangle\frac{e^{-\mathrm{i}(\omega+E_a^{N+1}-E_0^N)\tau}}{\omega+\mathrm{i}0^+}\right. \\ &\quad \left.+\sum_i \langle N|\hat{\Psi}^\dagger(\mathbf{x}_2)|N-1,i\rangle\langle N-1,i|\hat{\Psi}^\dagger(\mathbf{x}_1)|N\rangle\frac{e^{-\mathrm{i}(\omega+E_0^N-E_i^{N-1})\tau}}{\omega-\mathrm{i}0^+}\right].\end{aligned} \tag{1.157}$$

Then, by a simple change of variable and by recognizing the Fourier transform of the Green's function,

$$G(\mathbf{x}_1,\mathbf{x}_2;\tau) = \int_{-\infty}^{+\infty}\frac{\mathrm{d}\omega}{2\pi}G(\mathbf{x}_1,\mathbf{x}_2;\omega)e^{-\mathrm{i}\omega\tau}, \tag{1.158}$$

we finally obtain the Lehmann representation of the one-particle Green's function,

$$G(\mathbf{x}_1,\mathbf{x}_2;\omega) = \sum_a \frac{f_a(\mathbf{x}_1)f_a^*(\mathbf{x}_2)}{\omega-\mathcal{E}_a+i0^+} + \sum_i \frac{f_i(\mathbf{x}_1)f_i^*(\mathbf{x}_2)}{\omega-\mathcal{E}_i-\mathrm{i}0^+}, \tag{1.159}$$

where $f_a(\mathbf{x}) = \langle N|\hat{\Psi}(\mathbf{x})|N+1,a\rangle$ and $f_i(\mathbf{x}) = \langle N-1,i|\hat{\Psi}(\mathbf{x})|N\rangle$ are the Lehmann amplitudes, $\mathcal{E}_a = E_a^{N+1} - E_0^N = -A_a$ and $\mathcal{E}_i = E_0^N - E_i^{N-1} = -I_i$ correspond to minus the exact electron affinities A_a and exact ionization energies I_i, respectively. As readily seen in Eq. (1.159), the one-particle Green's function contains information about charge excitations i.e. ionization processes, such as photoemission and inverse photoemission spectroscopies). Those energies are conventionally called the poles of the one-particle Green's function. In principle, they could also be extracted within DFT, because the Green's function can be written as a functional of the density. In practice however, we don't know how to do this and DFT or time-dependent DFT are limited to the description of the N-electron system (N-electron ground-state properties and neutral excitations). The "position" of the peaks as a function of the momentum quantum number yields the band structure in solids [223]. Note that the total energy in real-space in Eq. (1.153) is expressed in the frequency domain as follows,

$$E_0^N = \frac{1}{\pi} \int_{-\infty}^{\mu} \mathrm{d}\omega \mathrm{Tr}\left[(\omega - h)\,\mathrm{Im}G(\omega)\right], \tag{1.160}$$

where μ is the chemical potential[8] and the imaginary part of the Green's function gives the spectral function, which has peaks at the poles of the Green's function.

In practice, of course, the exact charged excitations energies and excited states are not known, and one has to find another way to construct the one-particle Green's function. One can start by computing the Green's function of a noninteracting system by solving the following equation of motion:

$$\left[\mathrm{i}\frac{\partial}{\partial t_1} - h(\mathbf{r}_1)\right] G_h(1,2) = \delta(1,2), \tag{1.161}$$

where G_h is the noninteracting Green's function, which poles correspond to the orbital energies. Clearly, the spectral function of the noninteracting system differs from the interacting one. For an interacting system, the peaks are shifted and broadened and exhibit satellites (also called side-band) in extended systems, due to the coupling between excitations in the interacting system. Those features are totally absent in the noninteracting spectrum.

It can be shown that the fully-interacting Green's function can be recovered from the noninteracting one by using the so-called Dyson equation,

$$G(1,2) = G_h(1,2) + \iint \mathrm{d}3\mathrm{d}4 G_h(1,3)\Sigma_{\mathrm{Hxc}}(3,4)G(4,2), \tag{1.162}$$

or, equivalently,

$$G^{-1}(1,2) = G_h^{-1}(1,2) - \Sigma_{\mathrm{Hxc}}(1,2). \tag{1.163}$$

Σ_{Hxc} is the self-energy that contains all the effects of the electron-electron repulsion, in perfect analogy with the Hxc energy potential in DFT [see Eq. (1.164)]. Note also that $\Sigma_{\mathrm{Hxc}}[G]$ is a functional of the one-particle Green's function, like $E_{\mathrm{Hxc}}[n]$ is a functional of the density and $W[\gamma]$ is a functional of the 1RDM.

---

[8] The chemical potential will be further discussed in Chapter 4.

Instead of starting from G_h, one could compute the one-particle Green's function of the KS system, leading to G_{KS}. The two Green's functions are connected as follows,

$$G_{\mathrm{KS}}(1,2) = G_h(1,2) + \int \mathrm{d}3 G_h(1,3) v_{\mathrm{Hxc}}(\mathbf{r}_3) G_{\mathrm{KS}}(3,2), \tag{1.164}$$

or, equivalently,

$$G^{-1}_{\mathrm{KS}}(1,2) = G^{-1}_h(1,2) - v_{\mathrm{Hxc}}(1)\delta(1,2). \tag{1.165}$$

The link between the KS-DFT and the Green's function theory is provided by the Sham–Schlüter equation [224, 225]. The idea is to use the fact that the noninteracting density in the KS-DFT formalism is in principle the same as the interacting one. Hence, the diagonal of both G_{KS} and G gives the same ground-state density,

$$-\mathrm{i}G(1,1^+) = -\mathrm{i}G_{\mathrm{KS}}(1,1^+). \tag{1.166}$$

From Eqs. (1.163) and (1.165), it comes

$$G^{-1}(1,2) = G^{-1}_{\mathrm{KS}}(1,2) - \left(\Sigma_{\mathrm{Hxc}}(1,2) - v_{\mathrm{Hxc}}(1)\delta(1,2)\right), \tag{1.167}$$

or, equivalently,

$$G(1,2) = G_{\mathrm{KS}}(1,2) + \iint \mathrm{d}3\mathrm{d}4 G_{\mathrm{KS}}(1,3)\left[\Sigma_{\mathrm{Hxc}}(3,4) - v_{\mathrm{Hxc}}(3)\delta(3,4)\right] G(4,2), \tag{1.168}$$

where the double counting of the correlation is removed by subtracting the Hxc potential from the self-energy. This equation allows to recover the physical Green's function from the KS one. Using the relation in Eq. (1.166) yields an equation for the unknown Hxc potential,

$$\iint \mathrm{d}3\mathrm{d}4 G_{\mathrm{KS}}(1,3)\left[\Sigma_{\mathrm{Hxc}}(3,4) - v_{\mathrm{Hxc}}(3)\delta(3,4)\right] G(4,1^+) = 0, \tag{1.169}$$

which can be expressed in the frequency domain, thus leading to the Sham–Schlüter equation [224, 225],

$$\iint \mathrm{d}\mathbf{r}_3\mathrm{d}\mathbf{r}_4\mathrm{d}\omega e^{i\omega 0^+} G_{\mathrm{KS}}(\mathbf{r}_1,\mathbf{r}_3;\omega)\left[\Sigma_{\mathrm{Hxc}}(\mathbf{r}_3,\mathbf{r}_4;\omega) - v_{\mathrm{xc}}(\mathbf{r}_3)\delta(\mathbf{r}_3-\mathbf{r}_4)\right] G(\mathbf{r}_4,\mathbf{r}_1;\omega) = 0. \tag{1.170}$$

In analogy with DFT and RDMFT, the one-particle Green's function is used as a basic variable instead of dealing with the complicated many-body wavefunction. The functionals of these reduced quantities are yet to be found, and we are still searching for the most accurate (and universal) approximation for each of them. In Green's function theory, like in DFT or RDMFT, the self-energy needs to be approximated. It is in 1965 that Hedin proposed a set of coupled equations, so-called the Hedin's equations [226], that yields the exact self-energy, in principle. In practice, because these are non-linear equations, the determination of the self-energy remains a challenge, even numerically. This set has laid the foundation of the different self-energy approximations, like the popular GW approximation [227–229] for the description of band gaps [223, 230–234], and beyond using vertex corrections [235, 236].

1.3 Combining Density Functional Theory with Wavefunction Theory

Although DFT is in principle exact, we have seen that the many approximations developed in the literature are not adequate for the treatment of strongly correlated electrons. Since the mid-1980s, a huge collection of different DFAs has been proposed (and is still increasing), but none of them are able to treat multiconfigurational systems efficiently. One may wonder if searching for such a Hxc functional is possible, or if there are other trails to follow. One of this alternative trail is the combination of WFT with DFT. On one side, WFT is able to describe strongly correlated electrons within the MCSCF method, but the treatment of large systems remains impossible due to its high computational cost. On the other side, DFT is a very low cost approach that can handle calculations on large systems, but only the dynamical correlation effects are accurately described within the current DFAs.

Hence, merging the two approaches in order to extract the "best" of the two methods in terms of accuracy and computational cost is natural and intuitive. Unfortunately, WFT and DFT are formulated in two completely different languages. While the former uses the many-body (multideterminantal) wavefunction, the latter is based on the simple electronic density only. Although this combination is a very challenging task, it has gained much interest since the end-1990s. Depending on how the merging is performed, the resulting hybrid method could account twice for the same correlation effect, thus leading to the infamous *double counting problem*. One promising way of performing this merging is to separate the electronic interaction such that one part is treated by WFT and the other part by DFT. This separation is not unique and is one of the central questions of this thesis.

This section is organized as follows. First, the range-separation of the two-electron repulsion operator is introduced by using a linear scaling or the error function. The latter leads to the so-called multiconfigurational range-separated DFT. Alternatively, the correlation can be separated in the orbital space, where the orbitals are explicitly interacting in a given active space, while the remaining (inactive) orbitals are implicitly treated by a density functional. Finally, one can also think about a large system where a small part only would be explicitly interacting, and the rest of it treated by DFT. This strategy leads to the so-called *embedding* methods. The advantages and drawbacks of each of these distinct separations are discussed throughout this section.

1.3.1 Multiconfigurational range-separated DFT

1.3.1.i Range separation of the two-electron interaction in real space

In 1996, Savin suggested to split the electronic repulsion in real space by means of the error function, thus leading to the following range separation of the two-electron repulsion [152, 153]:

$$\frac{1}{r_{12}} = \frac{\mathrm{erf}(\mu r_{12})}{r_{12}} + \frac{1-\mathrm{erf}(\mu r_{12})}{r_{12}}, \tag{1.171}$$

where the first term in the right-hand side of Eq. (1.171) is called the long-range (lr) part and the second term is the short-range (sr) part. The error function reads

$$\mathrm{erf}(\mu r_{12}) = \frac{2}{\sqrt{\pi}} \int_0^{\mu r_{12}} e^{-t^2} \mathrm{d}t. \tag{1.172}$$

This leads to a decomposition of the electronic repulsion operator as follows:

$$\hat{W}_{\mathrm{ee}} = \hat{W}_{\mathrm{ee}}^{\mathrm{lr},\mu} + \left(\hat{W}_{\mathrm{ee}} - \hat{W}_{\mathrm{ee}}^{\mathrm{lr},\mu}\right) = \hat{W}_{\mathrm{ee}}^{\mathrm{lr},\mu} + \hat{W}_{\mathrm{ee}}^{\mathrm{sr},\mu}, \tag{1.173}$$

where only the first term of the right-hand side of Eq. (1.173) is treated explicitly. The remaining short-range contribution will be treated by a complementary short-range Hxc functional, thus leading to the ground-state energy variational expression

$$E_0[v] = \min_{\Psi} \left\{ \langle \Psi | \hat{T} + \hat{W}_{\mathrm{ee}}^{\mathrm{lr},\mu} + \hat{V} | \Psi \rangle + E_{\mathrm{Hxc}}^{\mathrm{sr},\mu}[n^{\Psi}] \right\}, \tag{1.174}$$

where the minimizing wavefunction Ψ^{μ} fulfils the following self-consistent equation:

$$\left(\hat{T} + \hat{W}_{\mathrm{ee}}^{\mathrm{lr},\mu} + \int \mathrm{d}\mathbf{r} \left[v(\mathbf{r}) + \frac{\delta E_{\mathrm{Hxc}}^{\mathrm{sr},\mu}[n^{\Psi^{\mu}}]}{\delta n(\mathbf{r})} \right] \hat{n}(\mathbf{r}) \right) |\Psi^{\mu}\rangle = \mathcal{E}^{\mu} |\Psi^{\mu}\rangle. \tag{1.175}$$

Note that Ψ^{μ} is multideterminantal as the long-range part of the repulsion is treated explicitly.

The separation is dependent on the parameter μ for which two limits can be distinguished. The

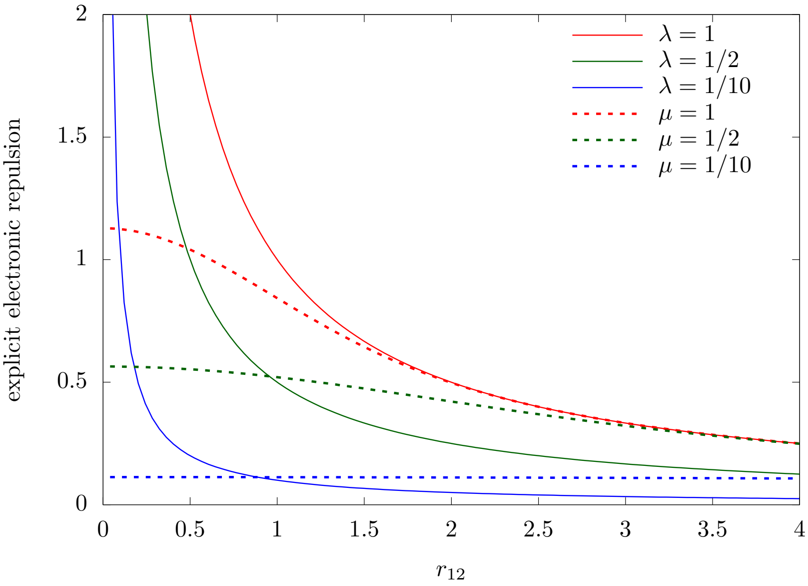

Figure 1.1: Explicit contribution of the electronic repulsion in the partially-interacting Hamiltonian in the linearly-separated DFT (full lines) and in the range-separated DFT (dashed lines).

first limit is $\mu = 0$ and corresponds to a pure KS-DFT calculation. The second limit is pure WFT and is obtained when $\mu \to +\infty$. For finite nonzero μ values, the approach is a multideterminantal range-separated DFT method (abbreviated as range-separated DFT in the following). To illustrate the difference between the linear separation λ/r_{12} (which will be further discussed in the next section) and the range separation defined by the error function, Fig. 1.1 shows the contribution of the long-range electronic repulsion as a function of the distance between two electrons. This contribution is the one present in the Hamiltonian which is treated explicitly with a many-body wavefunction. It is clear from Fig. 1.1 (dashed lines) that the Coulomb hole does not need to be described by the wavefunction in range-separated DFT (Because $\text{erf}(\mu r_{12})/r_{12}$ tends to a finite value when $r_{12} \to 0$). It is treated by the complementary short-range Hxc functional. In range-separated DFT, the long-range repulsion is taken into account by the wavefunction. For $\mu = 1$ and $\mu = 1/2$, the exact long-range electron-electron interaction (see the red curve for $\lambda = 1$) is recovered for $r_{12} > 1.5$ and $r_{12} > 3$, respectively, which is not the case with the linear separation. This is particularly interesting as long-range interactions (for instance van der Waals interactions) are usually not well described using standard DFT, such that one has to incorporate dispersion corrections [137, 138] to conventional functionals, by using MP2 [147, 237, 238] or the random phase approximation [239, 240]. It has also been shown that the range-separated DFT (finite μ) converges faster with respect to the number of configuration state functions than pure WFT ($\mu \to +\infty$) [241].

Note that standard DFAs in KS-DFT *cannot* be used directly in range-separated DFT without facing the infamous double counting problem. Hence, specific μ-dependent functionals have been developed [143–150]. In practical calculations, μ has to be fixed and its value is not universal, although it has been shown to be optimal for $\mu = 0.4$ [242].

Promising results have been obtained by combining the electronic density and the 1RDM based on the range separation of the electron-electron operator [243–245]. The idea is to recover the dynamical correlation using a short-range density functional and to treat long-range correlation effects in RDMFT. Along those lines, the range separation has also been used to handle near degeneracies in atoms and molecules [241, 246] as well as transition metal complexes with a large active space by using DMRG [247].

Extensions to the time-dependent multi-configuration regime [248–252] have also been explored, thus allowing for the description of multiple excitations [253, 254] and charge transfer excitations. The formers are simply absent in the Kohn-Sham time-dependent DFT [255] within the adiabatic approximation, while the latter are not well described [256] even by using the exact KS-DFT Hxc functional (which is frequency-independent). This is due to the lack of memory effect, meaning that the kernel should be time-dependent or, equivalently, frequency-dependent. Still dealing with the excited states, note that the Gross-Oliveira-Kohn ensemble DFT (GOK-DFT) [257–259] has also been combined with the range-separation formalism [260–266]. During my Master studies, I had the chance to work on GOK-DFT and to apply it to atoms and diatomic molecules. At the time, we suggested a strategy to get weight-independent excitation energies in GOK-DFT through a linear interpolation method [263], further improved using the extrapolation scheme of Savin [264, 267]. [9]

Returning to the range-separated DFT, although the method has the advantage of avoiding the explicit description of the Coulomb hole and the range-separated wavefunction has the corrected long-range behaviour, the construction of specific μ-dependent DFAs remains a challenging task. This can be avoided by considering the linear separation of the two-electron repulsion in real space.

1.3.1.ii Linear separation of the two-electron interaction in real space

In the spirit of the range-separated DFT, Toulouse and co-workers [141] suggested a linearly-separated DFT in which the standard DFAs can be used (with respect to a given scaling relation). This approach follows closely the standard adiabatic connection in Sec. 1.2.1.iv, where the multideterminantal Ψ^{λ} wavefunction is used instead of Φ^{KS} for the calculation of the density, therefore switching from a mapping onto a noninteracting system to a partially-interacting one for any λ in $0 \leqslant \lambda \leqslant 1$.

---

[9] These studies will *not* be described in this thesis, as they are not part of the main theme, which is the development of hybrid methods focused on the ground-state. However, the ensemble DFT will be highly discussed in Chap. 5 in another context: the extraction of the fundamental gap and first ionization potential and electronic affinity.

The Hohenberg–Kohn functional of the fully-interacting system is then decomposed into a partially-interacting one and a complementary λ-dependent Hxc energy functional,

$$F[n] = F^{\lambda}[n] + \big(F[n] - F^{\lambda}[n]\big) = F^{\lambda}[n] + \overline{E}^{\lambda}_{\mathrm{Hxc}}[n]. \tag{1.176}$$

Note that in the noninteracting limit $\lambda = 0$, the KS-DFT is recovered such that $F^{\lambda=0}[n] = T_{\mathrm{s}}[n]$ and $\overline{E}^{\lambda=0}_{\mathrm{Hxc}}[n] = E_{\mathrm{Hxc}}[n]$. In the fully-interacting limit $\lambda = 1$, the pure WFT is recovered such that $F^{\lambda=1}[n] = F[n]$ and $\overline{E}^{\lambda=1}_{\mathrm{Hxc}}[n] = 0$. The λ-dependent interaction functional is given by

$$F^{\lambda}[n] = \min_{\Psi \to n} \left\{ \langle \Psi | \hat{T} + \lambda \hat{W}_{\mathrm{ee}} | \Psi \rangle \right\} = \langle \Psi^{\lambda} | \hat{T} + \lambda \hat{W}_{\mathrm{ee}} | \Psi^{\lambda} \rangle, \tag{1.177}$$

where Ψ^{λ} is introduced in Sec. 1.2.1.iv. According to the Hellmann-Feynman theorem, the complementary λ-dependent Hxc energy functional reads

$$\overline{E}^{\lambda}_{\mathrm{Hxc}}[n] = \int_{\lambda}^{1} \mathrm{d}\nu \frac{\mathrm{d}F^{\nu}[n]}{\mathrm{d}\nu} = \int_{\lambda}^{1} \mathrm{d}\nu \langle \Psi^{\nu} | \hat{W}_{\mathrm{ee}} | \Psi^{\nu} \rangle. \tag{1.178}$$

After a few simple mathematical steps, it comes

$$\overline{E}^{\lambda}_{\mathrm{Hxc}}[n] = (1-\lambda) E_{\mathrm{Hx}}[n] + E_{\mathrm{c}}[n] - E^{\lambda}_{\mathrm{c}}[n], \tag{1.179}$$

where $E^{\lambda}_{\mathrm{c}}[n]$ is given by the uniform coordinate scaling relation in Eq. (1.127). The ground-state energy is obtained variationally as follows:

$$E_0[v] = \min_{\Psi} \left\{ \langle \Psi | \hat{T} + \lambda \hat{W}_{\mathrm{ee}} + \hat{V} | \Psi \rangle + \overline{E}^{\lambda}_{\mathrm{Hxc}}[n^{\Psi}] \right\}, \tag{1.180}$$

where the minimizing wavefunction Ψ^{λ} fulfils the self-consistent (multideterminantal) extension of the KS-DFT equation,

$$\left(\hat{T} + \lambda \hat{W}_{\mathrm{ee}} + \int \mathrm{d}\mathbf{r} \left[v(\mathbf{r}) + \frac{\delta \overline{E}^{\lambda}_{\mathrm{Hxc}}[n^{\Psi^{\lambda}}]}{\delta n(\mathbf{r})} \right] \hat{n}(\mathbf{r}) \right) |\Psi^{\lambda}\rangle = \mathcal{E}^{\lambda} |\Psi^{\lambda}\rangle. \tag{1.181}$$

In summary, this method decomposes the electronic repulsion as follows:

$$\frac{1}{r_{12}} = \frac{\lambda}{r_{12}} + \frac{(1-\lambda)}{r_{12}}, \tag{1.182}$$

where the first term in the right-hand side is treated explicitly (in WFT) and the second term is described implicitly with a density functional.

Obviously, the partial interaction λ/r_{12} diverges when $r_{12} \to 0$ even for infinitesimal values of λ so that one will have to describe a part of the Coulomb hole with WFT [see Fig. 1.1], thus leading to a slower convergence with respect to the basis set when compared with DFT (or range-separated DFT). Despite this drawback of the linearly-separated DFT in comparison to range-separate DFT, note that all the functionals already developed in the literature can be used directly thanks to the linear scaling expression of the correlation energy in Eq. (1.127).

Let us now summarize the previous subsections. Range-separated DFT is a promising method which merges WFT and DFT in-principle exactly. It is free from double counting problem. Interestingly, this range separation of the electron-electron repulsion allows to avoid the explicit description of the Coulomb hole by WFT, thus leading to a faster convergence with respect to the basis set (in comparison with pure WFT). However, such an implementation necessitates the development of μ-dependent functionals. This can be done by considering a uniform electron gas with a modified coulomb interaction, thus leading to a short-range LDA [152, 268]. A different strategy that allows the use of the already developed functionals in standard KS-DFT (and which remains free from double counting) is the linearly-separated DFT, thanks to the linear scaling expression of the correlation energy in Eq. (1.127). In return, the Coulomb hole still has to be described by WFT.

Despite the fact that these two methods are in principle exact, one may wonder if this separation of the two-electron interaction is optimal. Indeed, even though the short-range (connected with the Coulomb hole) and long-range (dispersion, van der Waals interactions) dynamical correlations are well defined in the coordinate space, this is more ambiguous for static correlation. Range-separated DFT was originally formulated to describe static correlation by reproducing the accurate long-range behaviour of the electron-electron interaction with WFT. However, static correlation can be *purely short-range*, as shown on the dissociation of the hydrogen molecule [269, 270]. This static correlation, manifested by the coupling between the $|\varphi^{\alpha}_{1\sigma_g}\varphi^{\beta}_{1\sigma_g}|$ and $|\varphi^{\alpha}_{1\sigma_u}\varphi^{\beta}_{1\sigma_u}|$ determinants, is correctly described in range-separated DFT for even an infinitesimal μ value. But this correct description is due to the residual contribution (at short-range) of the long-range interaction when $r_{12} \to 0$, and has nothing to do with the accurate recovering of the long-range behaviour [270]. Hence, the separation of the electron-electron interaction into a short- and long-range part is questionable.

Alternatively, the correlation can be separated in the orbital space, as discussed in the following section.

1.3.2 CAS-DFT

The static correlation is usually accurately treated with CASSCF, while the orbitals outside of the active space are not correlated, such that CASSCF is lacking of dynamical correlation. In analogy with range-separated DFT, this correlation could be recovered by combining CASSCF with DFT, thus leading to the so-called CAS-DFT. The CAS-DFT energy would be obtained variationally as follows [271, 272]:

$$E_0[v] = \min_{\boldsymbol{\kappa},\mathbf{S}} \Big\{ \langle \Psi^{\text{CAS}}(\boldsymbol{\kappa},\mathbf{S}) | \hat{T} + \hat{W}_{\text{ee}} + \hat{V} | \Psi^{\text{CAS}}(\boldsymbol{\kappa},\mathbf{S}) \rangle + E_{\text{c}}^{\text{CAS}}[n^{\Psi^{\text{CAS}}(\boldsymbol{\kappa},\mathbf{S})}] \Big\}, \tag{1.183}$$

where $\Psi^{\text{CAS}}(\boldsymbol{\kappa},\mathbf{S})$ is the CASSCF wavefunction in Sec. (1.1.7). Note that, in analogy with range-separated DFT, standard DFAs cannot be used directly. In order to avoid double counting problem, the complementary correlation functional $E_{\text{c}}^{\text{CAS}}[n]$ has to depend on the CAS and thus cannot be universal. As a consequence, even though this approach looks attractive at first sight, CAS-DFT is extremely difficult to implement in practice [273]. Note that a *multiconfiguration pair-density functional theory* has been recently proposed and consists in computing the kinetic energy by WFT, while the correlation energy is calculated using a functional of the electron density together with an on-top pair density correction [274].

Along those lines, a rigorous method combining CI and DFT has been explored in 1988 by Savin [275], so called CI-DFT. It consists in separating the correlation in the space of natural orbitals. The selection of the explicitly interacting orbitals is made by using a given threshold ν, with $0 \leq \nu \leq 2$. The natural orbitals with occupation greater than ν are treated by CI calculation, while the remaining part is described by a ν-dependent DFA. More recently, Gutlé and Savin [276] proposed alternative CI–DFT schemes, where the correlation energy is still split in the orbital space but through the introduction of gap shift or cut-off parameters applied to the virtual orbitals. In these approaches, a reference wavefunction is divided in two parts that are treated by different methods. The separation follows nicely the definition of the static and dynamical correlation provided by Becke [21], thus leading to three different parts,

1. a low-energy part of the one-particle spectrum involving the highest occupied molecular orbital (HOMO) and the lowest unoccupied molecular orbital (LUMO) that usually drive the chemical reactivity and properties of the system,
2. high-energy excitations, less system-specific,
3. a mixing of low- and high-excitations.

For computational reason, the CI treatment is better suited to the first part which is defined in a rather small orbital subspace. Moreover, this subspace is likely to contain nearly-degenerate partially occupied orbitals, known to be problematic in KS-DFT. On the other hand, the second part is usually well described by KS-DFT while the wavefunction calculation becomes rapidly numerically unfeasible as the size of the subspace increases.

In both CAS-DFT and in CI-DFT, the energy is split into wavefunction-functional and density-functional contributions. The separation is achieved in the orbital space.

An alternative approach has been formulated very recently by Fromager [270], where the complementary correlation is recovered by a functional of the orbital occupation instead of the electronic density. Because the static correlation is usually defined in the orbital space, one could expect the separation of the correlation energy into WFT and DFT contributions to be easier to achieve in practice. In this context, the functional becomes a CAS-dependent functionals of the orbitals occupation. The formulation of such an approach will be briefly discuss in Chapter 6.

Several different ways of merging WFT and DFT have been discussed already. All of these methods are *not* standard in quantum chemistry for two main reasons. (1) They remain computationally expensive, (2) they require the challenging development of new density functionals. Note that the second point is related to the double counting problem and the fact that the standard DFAs cannot be used. Instead of separating the electron interaction on the atoms by using a range separation, let us consider a much larger system in which the electrons are interacting only in a small area and treated by WFT. This area is “embedded” in the rest of the system treated by DFT, thus leading to so-called *embedding* methods.

1.3.3 Wavefunction in Density Functional Theory Embedding

1.3.3.i DFT-in-DFT embedding

Consider a large system (extended system or molecule) out of reach by a pure WFT calculation, for which only a small part of it contains the physics of interest. This small part could correspond to impurities, vacancies, adsorbates on a solid, or even an active center in a molecule of chemical or biological interest. Intuitively, one would like to treat only this small subsystem within a high-level correlated method and the rest of the system with a low-level method, thus allowing (hopefully) for a significant reduction of the computational cost while keeping an accurate description of the active part of the system. Usually, the system will be decomposed in two parts. One is the small part containing the active center called “cluster” and the other referred to as the environment [277]. The total energy is then decomposed as follows:

$$E_{\rm tot} = E_{\rm clu} + E_{\rm env} + E_{\rm int}, \tag{1.184}$$

where $E_{\rm int}$ is the interaction energy between the cluster and the environment. Within DFT, the total electronic density can be decomposed as $n_{\rm tot}(\mathbf{r}) = n_{\rm clu}(\mathbf{r}) + n_{\rm env}(\mathbf{r})$ [note that two out of the three densities can be considered as independent], thus leading to separate energy contributions [278–280],

$$E_{\rm A} = T_{\rm s}[n_{\rm A}] + E_{\rm H}[n_{\rm A}] + E_{\rm xc}[n_{\rm A}] + E^{\rm A}_{\rm ne}[n_{\rm A}] + E^{\rm A}_{\rm nn}, \tag{1.185}$$

where A can denote the cluster part (clu), the environment (env) or the total system (tot). $E^{\rm A}_{\rm ne}$ is the electron-nuclear attraction energy functional and $E^{\rm A}_{\rm nn}$ is the nuclear-nuclear repulsion energy of the (sub)system A. The interaction energy can be written as the difference between the total energy and the two separate subsystem energies,

$$E_{\rm int}[n_{\rm tot}, n_{\rm clu}] = T^{\rm int}_{\rm s}[n_{\rm tot}, n_{\rm clu}] + E^{\rm int}_{\rm H}[n_{\rm tot}, n_{\rm clu}] + E^{\rm int}_{\rm xc}[n_{\rm tot}, n_{\rm clu}] + E^{\rm int}_{\rm ne}[n_{\rm tot}, n_{\rm clu}] + E^{\rm int}_{\rm nn}, \tag{1.186}$$

where

$$\begin{aligned}
T^{\rm int}_{\rm s}[n_{\rm tot}, n_{\rm clu}] &= T_{\rm s}[n_{\rm tot}] - T_{\rm s}[n_{\rm clu}] - T_{\rm s}[n_{\rm env}], && (1.187)\\
E^{\rm int}_{\rm H}[n_{\rm tot}, n_{\rm clu}] &= E_{\rm H}[n_{\rm tot}] - E_{\rm H}[n_{\rm clu}] - E_{\rm H}[n_{\rm env}] = \iint \frac{n_{\rm clu}(\mathbf{r})n_{\rm env}(\mathbf{r}')}{|\mathbf{r}-\mathbf{r}'|}{\rm d}\mathbf{r}{\rm d}\mathbf{r}', && (1.188)\\
E^{\rm int}_{\rm xc}[n_{\rm tot}, n_{\rm clu}] &= E_{\rm xc}[n_{\rm tot}] - E_{\rm xc}[n_{\rm clu}] - E_{\rm xc}[n_{\rm env}], && (1.189)\\
E^{\rm int}_{\rm ne}[n_{\rm tot}, n_{\rm clu}] &= E^{\rm tot}_{\rm ne}[n_{\rm tot}] - E^{\rm clu}_{\rm ne}[n_{\rm clu}] - E^{\rm env}_{\rm ne}[n_{\rm env}] \\
&= \int {\rm d}\mathbf{r}\left(v^{\rm clu}_{\rm ne}(\mathbf{r})n_{\rm env}(\mathbf{r}) + v^{\rm env}_{\rm ne}(\mathbf{r})n_{\rm clu}(\mathbf{r})\right), && (1.190)\\
E^{\rm int}_{\rm nn} &= E^{\rm tot}_{\rm nn} - E^{\rm clu}_{\rm nn} - E^{\rm env}_{\rm nn}. && (1.191)
\end{aligned}$$

Then, we would like to solve the cluster region by taking into account the environment through the use of an embedding potential, functional of $n_{\rm tot}(\mathbf{r})$ and $n_{\rm clu}(\mathbf{r})$. This potential is updated iteratively through the following self-consistent equation:

$$\left(-\frac{1}{2}\nabla^2 + v_{\rm s}[n_{\rm clu}](\mathbf{r}) + v_{\rm emb}[n_{\rm tot}, n_{\rm clu}](\mathbf{r})\right)\varphi^{\rm clu}_i(\mathbf{r}) = \varepsilon_i\varphi^{\rm clu}_i(\mathbf{r}), \tag{1.192}$$

where the embedding potential

$$v_{\rm emb}[n_{\rm tot}, n_{\rm clu}] = v_{T_{\rm s}}[n_{\rm tot}, n_{\rm clu}] + v_{\rm H}[n_{\rm tot}, n_{\rm clu}] + v_{\rm xc}[n_{\rm tot}, n_{\rm clu}] + v_{\rm ne}[n_{\rm tot}, n_{\rm clu}] \tag{1.193}$$

is obtained by performing a functional derivative of $E_{\text{int}}[n_{\text{tot}}, n_{\text{clu}}]$ with respect to $n_{\text{clu}}(\mathbf{r})$ with $n_{\text{clu}}(\mathbf{r})$ and $n_{\text{env}}(\mathbf{r})$ are considered independent. This consideration, which is not an approximation, leads to:

$$
\begin{aligned}
v_{T_{\text{s}}}[n_{\text{tot}}, n_{\text{clu}}] &= \frac{\delta T_{\text{s}}[n_{\text{tot}}]}{\delta n_{\text{tot}}(\mathbf{r})} - \frac{\delta T_{\text{s}}[n_{\text{clu}}]}{\delta n_{\text{clu}}(\mathbf{r})}, && (1.194)\\
v_{\text{H}}[n_{\text{tot}}, n_{\text{clu}}] &= \int \frac{n_{\text{env}}(\mathbf{r}')}{|\mathbf{r}-\mathbf{r}'|}\text{d}\mathbf{r}', && (1.195)\\
v_{\text{xc}}[n_{\text{tot}}, n_{\text{clu}}] &= \frac{\delta E_{\text{xc}}[n_{\text{tot}}]}{\delta n_{\text{tot}}(\mathbf{r})} - \frac{\delta E_{\text{xc}}[n_{\text{clu}}]}{\delta n_{\text{clu}}(\mathbf{r})}, && (1.196)\\
v_{\text{ne}}[n_{\text{tot}}, n_{\text{clu}}] &= v_{\text{ne}}^{\text{env}}(\mathbf{r}). && (1.197)
\end{aligned}
$$

The Hartree, the electron-nuclear attraction potentials, and the xc contribution (which is usually approximated as an explicit functional of the density) are straightforwardly determined. However, the noninteracting kinetic energy is not known as an explicit functional of the density and is determined by the KS orbitals. Therefore, the kinetic contribution in Eq. (1.187), also called *nonadditive* kinetic energy, cannot be directly differentiated with respect to the density to get the potential in Eq. (1.194). In practice, one can use explicit DFAs like the Thomas–Fermi approximation [277] [Eq. (1.79)], gradient corrections [278–280], or the OEP technique [86, 281–283]. One way to get rid of the calculation of the nonadditive kinetic energy functional is to ensure that the densities of each subsystem are constructed from mutually orthogonal orbitals by level-shifting projections [284–287], so that $T_{\text{s}}[n_{\text{tot}}] = T_{\text{s}}[n_{\text{clu}}] + T_{\text{s}}[n_{\text{env}}]$.

This fragmentation of the system through a partitioning of the density is called DFT-in-DFT embedding (from the notation "(high-level)-in-(low-level)" embedding theory), where the cluster is treated by a high-level functional (typically a hybrid functional) while the environment is treated by a low-level functional (typically LDA or GGA). This theory has been applied to the description of chemical processes in solution by Wesolowski and Warshel [278]. Assuming that the densities $n_{\text{clu}}(\mathbf{r})$ and $n_{\text{env}}(\mathbf{r})$ are independent, one has to determine each of them separately. In the latter approach, so-called *Frozen Density Functional Embedding Theory* [278], the density $n_{\text{env}}(\mathbf{r})$ is constructed explicitly by performing a DFT calculation on the isolated environment. This density is then kept frozen so that only $n_{\text{clu}}(\mathbf{r})$ is updated in Eq. (1.192), and $n_{\text{tot}}(\mathbf{r}) = n_{\text{clu}}(\mathbf{r}) + n_{\text{env}}(\mathbf{r})$. Of course, keeping $n_{\text{env}}(\mathbf{r})$ frozen is an approximation which appears to be non negligible when $n_{\text{env}}(\mathbf{r})$ is significantly smaller than $n_{\text{tot}}(\mathbf{r})$ everywhere in space. To overcome this issue, Wesolowski and Weber suggested the freeze-and-thaw cycles [279] which consist in computing $n_{\text{clu}}(\mathbf{r})$ with the frozen $n_{\text{env}}(\mathbf{r})$, then freeze $n_{\text{clu}}(\mathbf{r})$ and determine $n_{\text{env}}(\mathbf{r})$, and do this iteratively until the densities have converged. The total electron density obtained by summation of $n_{\text{clu}}(\mathbf{r})$ and $n_{\text{env}}(\mathbf{r})$ should be the same as the one obtained from KS-DFT applied to the whole system, providing that the nonadditive kinetic energy is exactly known, which is of course not the case in practice. Although some progress on the development of this approximate functional can be noted [288], it remains an important open challenge.

1.3.3.ii WFT-in-DFT embedding

An extension of the DFT-in-DFT embedding scheme to wavefunctions has then been suggested by Carter and co-worker [280, 289], for the purpose of addressing problems such as chemisorption [280, 283, 290, 291] and point defects in semicondutors [292] which are not well described in DFT. The approach is referred to as WFT-in-DFT embedding. In this approach, the density and the energy of the cluster is determined in WFT, while the environment is still described in DFT. The embedding potential remains the same as in Eq. (1.193) and is determined self-consistently by solving the following many-body self-consistent equation [289]:

$$\left(\hat{H}_{\mathrm{clu}} + \sum_{i=1}^{N} v_{\mathrm{emb}}[n_{\mathrm{tot}}, n_{\mathrm{clu}}](\mathbf{r}_i)\times\right)\Psi_{\mathrm{clu}} = \mathcal{E}_{\mathrm{clu}}\Psi_{\mathrm{clu}}, \tag{1.198}$$

where Ψ_{clu} is a many-body wavefunction with density $n_{\mathrm{clu}}(\mathbf{r})$ and from which local properties of the cluster can be extracted accurately. $\mathcal{E}_{\mathrm{clu}}$ is the auxiliary energy of the cluster. Note that an alternative way to compute the densities has been proposed, which consists in keeping $n_{\mathrm{tot}}(\mathbf{r})$ (determined by doing a KS-DFT calculation on the whole system) frozen instead of $n_{\mathrm{env}}(\mathbf{r})$ [280]. This WFT-in-DFT scheme is more flexible than DFT-in-DFT as it allows the use of different wavefunction methods, such as MP2, CI, CASSCF [290] and Coupled Cluster [293]. In the latter, calculation of localized excited states in large systems have been performed. Note that the description of open-shell systems by using a spin-dependent embedding potential [294] has been proposed, as well as the recovering of local excited state properties by using time-dependent DFT within the DFT-in-DFT framework [295]. However, time-dependent DFT with local or semi-local approximate functionals is known to fail in describing charge-transfer excitations [255, 256, 296], which can happen inside the cluster. Hence, WFT-in-DFT is more appropriate in this context. One major problem related to the embedding potential is its non-uniqueness [281–283] (i.e. different embedding potentials for the environment and the embedded regions), because two different embedding potentials (both yielding the same density) can yield different results, like different absorption energies [297]. Nevertheless, some recent progress have been reported by constraining the embedding potentials to be the same in the cluster and the environment [283], or by using finite temperature [297], or within the so-called *partition* DFT [288, 298, 299].

The latter approach differs from DFT-in-DFT and WFT-in-DFT in a sense that each fragment can have a fractional number of electrons. Imagine a separation of the system in two where the frontier of the two subsystems is in between a covalent bond. Obviously the number of electrons would not be integer anymore in each subsystem, thus lending weight to partition DFT. In this theory, the variable becomes the collection of fragment densities $\{n_\alpha(\mathbf{r})\}_\alpha$ which are allowed to integrate to a fractional number of electrons [158]. The only constraint is that they have to sum up to the total electron density. An extension of a WFT-in-DFT type method with fractional number of electrons in each fragment remains an open question.

We have seen that the combination of WFT with DFT can be performed in several different ways. In the WFT-in-DFT method, one has to define a specific area in which the electronic repulsion will be treated by WFT. Therefore, one has to be careful when defining the partitioning of the system. This is made much clearer in model Hamiltonians, in which the area becomes a number of sites which occupations play the role of the electron density. Then, in the spirit of the adiabatic connection, a mapping of the density is made between the physical system and the partially-interacting one. This method, so-called *site-occupation embedding theory* (SOET) [72, 270, 300, 301], is the main topic of this thesis and will be largely discussed in Chapter 3. As a proof of concept, a model Hamiltonian [302] (the Hubbard model) is used rather than the realistic *ab initio* Hamiltonian. Because the model Hamiltonians are commonly used in condensed matter physics, the next chapter aims to provide an introduction to the electronic structure in this field. The so-called *dynamical mean-field theory* (DMFT) as well as the *density matrix embedding theory* (DMET), which are closely related to SOET, will be discussed as well. Another hybrid scheme is also proposed in Chapter 6, based on the separation of the electron correlation in the basis of natural orbitals, using a seniority-zero reference wavefunction.

Chapter 2

Electronic Structure Theory in Condensed-Matter Physics

Due to the presence of the electron-electron repulsion in the electronic Hamiltonian, solving the Schrödinger equation is far from trivial, as demonstrated in the previous Chapter on quantum chemistry. Although methods have been proposed to give a numerical solution with a relatively manageable computational cost, it is sometimes preferable to look at a simplified and solvable version of real complex systems. This is the concept of model. Despite their apparent simplicity, models can capture the physical effects of interest and give accurate approximations to real systems. A well-known example is the uniform electron gas, where interacting electrons are in the presence of positive charges uniformly distributed in space, which is used to construct LDA [114]. Obviously, this model is far from the idea that we have of a molecule, or even a solid consisting of different types of atoms. For instance, correlation effects induced by partially filled d- or f-bands in transition and rare-earth metals, often bounded to oxygen atoms forming transition-metal oxide complexes, cannot be described in such a model.

As stressed in Sec 1.2.1, standard KS-DFT is not adequate for the treatment of strongly correlated materials. A few examples among others are the Mott-insulator phase in nickel oxide NiO [1, 303] and titanium dioxide TiO_2 [165], the manganese oxide compounds with perovskite structure like $LaMnO_3$ [1], the vanadium(III) oxide V_2O_3 [304, 305] and the high-T_c cuprates $LaCuO_4$ [304, 306–309] discovered in 1986 by Bednorz and Müller [310, 311]. They all depict a Mott-insulator transition, i.e. they are predicted to be metallic by band theory (equivalent to molecular orbital theory for extended systems) when the temperature tends to 0, whereas they are in fact insulators [312–314]. Note that different types of metal-insulator transitions exist, see Ref. [315] for a review. In this thesis, I will be interested in the Mott insulator, where the insulating state is due to strong electron correlation. Mott-insulators are particularly interesting because a small change in the system leads to dramatic modifications in its properties. Such phase transitions, leading to high-T_c cuprates and colossal magnetoresistance in manganites, are controlled by Jahn–Teller effects, carrier doping, the applied magnetic field, pressure and chemical composition. A review of these transitions is given in Ref. [304].

Transition metal oxides are of various type, and remain an active and challenging research field, such as the development of efficient nanodevices like molecular junctions for the design of solar (or photovoltaic) cells or also in homogeneous and heterogeneous catalysis [233]. These exotic electronic and magnetic properties can be difficult to understand and to capture in theoretical physics. Therefore, models have been developed in order to describe the key physical effects in these materials. Instead of considering a model accounting for the delocalization of the electrons in the metal (large energy bands), one needs to describe the electrons in the narrow energy bands related to the localization of the *d*- or *f*-orbitals. While an atomic model would be sufficient to model *f*-electrons of rare earth metals due to their extreme localization on the metal center, *d*-electrons need to be described by a model that interpolates between delocalized (band model) and localized (atomic model) picture. Of course, such a model does not reflect the true electronic behaviour of a real material, but it contains the key ingredients to capture the right physics, at least qualitatively if not quantitatively.

Turning to the development of new methods for strongly correlated electrons, it appears important to begin with such simplified models. Indeed, even if a theory which works on a model cannot be straightforwardly applied to a real system, it is even more unlikely that a theory which does *not* provide a correct description of the model will work on the real one ! This legitimates the use of models, which remains challenging despite their apparent simplicity, like the two- or three-dimensional Hubbard model.

In Sec. 2.1, the Hubbard model will be derived from the ab-initio Hamiltonian. In order to motivate the use of this model, its connection with high-T_c superconductor cuprates (which properties are driven by the Mott transition) is discussed in Sec. 2.1.3. Various limits of the model, leading to the tight-binding, the Heisenberg and the t–J models, are given in Secs 2.1.4. DFT on the Hubbard model [so-called *site-occupation functional theory* (SOFT)] is introduced in Sec. 2.2. Then, another model mainly used in physics [so called the Anderson impurity model] which describes localized defects in a solid is introduced in Sec. 2.3. Finally, two standard embedding techniques, the *dynamical mean-field theory* (DMFT) and the *density-matrix embedding theory* (DMET), are presented in Sec. 2.4.

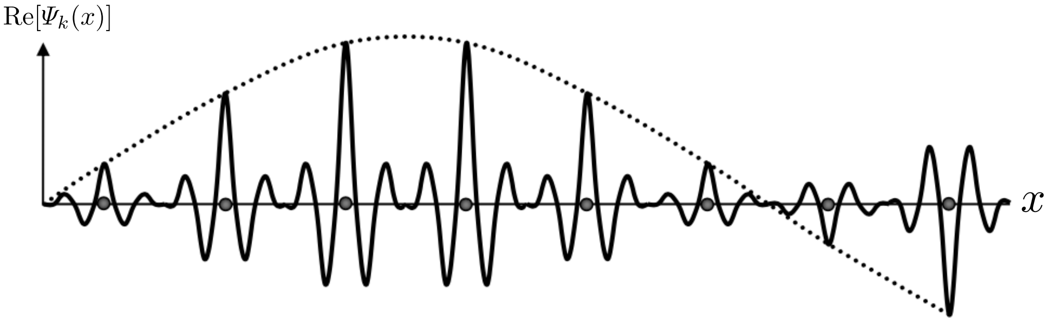

Figure 2.1: Real part of the Bloch function (full line) and of the plane wave (dotted line). Black circles represent atomic centers.

2.1 One-dimensional Hubbard model

For simplicity, only the one-dimensional Hubbard model is studied in this thesis.

2.1.1 From delocalized to localized orbitals

Starting with the model of a free electron gas in one dimension where electrons are completely delocalized, it is usual to use the "k-representation" instead of the "$\mathbf{r}$-representation",

$$|k\rangle = \frac{1}{\sqrt{2\pi}} \int_{-\infty}^{+\infty} \mathrm{d}x \, e^{\mathrm{i}kx} |x\rangle, \tag{2.1}$$

where $|k\rangle$ is the quantum state of one electron with momentum k and $|x\rangle$ is the quantum state of one electron at position x. The associated wavefunction,

$$\varphi_k(x) = \frac{1}{\sqrt{2\pi}} e^{\mathrm{i}kx}, \tag{2.2}$$

is a plane wave with momentum k. Note that if we work on a segment with length L, the renormalization factor would be $1/\sqrt{L}$ instead of $1/\sqrt{2\pi}$. While this model gives very useful physical insights about metallic materials, it is not adequate to treat a finite system such as a molecule.

For a solid described by a unit cell with an infinite number of replica, plane waves are no longer adequate and one should use Bloch functions instead,

$$\varphi_k(x) \longrightarrow \Psi_k(x) = u_k(x) e^{\mathrm{i}kx}, \tag{2.3}$$

which combine a plane wave with a function $u_k(x)$ having the same periodicity as the solid (i.e. the unit cell length). An illustration of the plane wave and the Bloch function is given in Fig. 2.1. To get even closer to an atomic description of a crystal, one can use Wannier functions $\Phi_i(x)$ since they are localized and centered on the nuclei at position i. The Wannier functions form an orthonormal basis set, i.e. $\langle \varPhi_i | \varPhi_j \rangle = \delta_{ij}$, and are obtained by applying the inverse Fourier transform to the Bloch functions:

$$\varPhi_j(x) = \frac{1}{\sqrt{2\pi}} \int \mathrm{d}k \, e^{-\mathrm{i}kj} \varPsi_k(x), \tag{2.4}$$

where the integral over k runs over the Brillouin zone (i.e. the primitive cell in the momentum k-space).

Turning to a one-dimensional lattice of L atoms with one basis function per atom, the integral over k is transformed into a finite summation. k runs over all the Brillouin zone in the range $-\pi < k \leqslant +\pi$, with $k = 2\pi m/L$ and $m = -L/2+1, -L/2+2, \ldots, L/2$. The normalization factor is also changed into $1/\sqrt{2\pi} \to 1/\sqrt{L}$, so that Eq. (2.4) becomes

$$\varPhi_j(x) = \frac{1}{\sqrt{L}} \sum_k e^{-\mathrm{i}kj} \varPsi_k(x), \tag{2.5}$$

and the Bloch functions can be recovered by Fourier transform:

$$\varPsi_k(x) = \frac{1}{\sqrt{L}} \sum_j e^{\mathrm{i}kj} \varPhi_j(x). \tag{2.6}$$

In second quantization, $\hat{c}^{\dagger}_{k\sigma}$ $(\hat{c}_{k\sigma})$ and $\hat{c}^{\dagger}_{i\sigma}$ $(\hat{c}_{i\sigma})$ denote the creation (annihilation) operators that create (annihilate) an electron in the Bloch state $|\varPsi_k, \sigma\rangle$ and in the Wannier state $|\varPhi_i, \sigma\rangle$, respectively,

$$|\varPsi_k, \sigma\rangle = \hat{c}^{\dagger}_{k\sigma} |\mathrm{vac}\rangle, \qquad |\varPhi_i, \sigma\rangle = \hat{c}^{\dagger}_{i\sigma} |\mathrm{vac}\rangle. \tag{2.7}$$

These operators are linked together by

$$\begin{cases} \hat{c}^{\dagger}_{k\sigma} = \dfrac{1}{\sqrt{L}} \sum_j e^{\mathrm{i}kj} \hat{c}^{\dagger}_{j\sigma}, & \hat{c}_{k\sigma} = \dfrac{1}{\sqrt{L}} \sum_j e^{-\mathrm{i}kj} \hat{c}_{j\sigma}, \\ \hat{c}^{\dagger}_{j\sigma} = \dfrac{1}{\sqrt{L}} \sum_k e^{-\mathrm{i}kj} \hat{c}^{\dagger}_{k\sigma}, & \hat{c}_{j\sigma} = \dfrac{1}{\sqrt{L}} \sum_k e^{\mathrm{i}kj} \hat{c}_{k\sigma}. \end{cases} \tag{2.8}$$

Note that by using the following orthogonality identities,

$$\frac{1}{L} \sum_j e^{\mathrm{i}(k-k')j} = \delta_{kk'}, \qquad \frac{1}{L} \sum_k e^{\mathrm{i}k(n-m)} = \delta_{nm}, \tag{2.9}$$

we can show that the anticommutation rules,

$$\begin{cases} \{\hat{c}_{k\sigma}, \hat{c}^\dagger_{k'\sigma'}\} = \delta_{kk'}\delta_{\sigma\sigma'}, \quad \{\hat{c}^\dagger_{k\sigma}, \hat{c}^\dagger_{k'\sigma'}\} = 0, \quad \{\hat{c}_{k\sigma}, \hat{c}_{k'\sigma'}\} = 0 \\ \{\hat{c}_{i\sigma}, \hat{c}^\dagger_{j\sigma'}\} = \delta_{ij}\delta_{\sigma\sigma'}, \quad \{\hat{c}^\dagger_{i\sigma}, \hat{c}^\dagger_{j\sigma'}\} = 0, \quad \{\hat{c}_{i\sigma}, \hat{c}_{j\sigma'}\} = 0, \end{cases} \tag{2.10}$$

still hold for these operators.

2.1.2 From the ab-initio Hamiltonian to the Hubbard model

The one-dimensional second-quantized electronic Hamiltonian reads as follows in k-space:

$$\hat{H} = \sum_{k\sigma} \varepsilon_k \hat{c}^\dagger_{k\sigma}\hat{c}_{k\sigma} + \frac{1}{2}\sum_{k_1k_2k'_1k'_2}\sum_{\sigma\sigma'} \langle k_1k_2|k'_1k'_2\rangle \hat{c}^\dagger_{k_1\sigma}\hat{c}^\dagger_{k_2\sigma'}\hat{c}_{k'_2\sigma'}\hat{c}_{k'_1\sigma}, \tag{2.11}$$

where the two-electron integral equals, in the spin-restricted formalism,

$$\langle k_1k_2|k'_1k'_2\rangle = \iint \mathrm{d}x\mathrm{d}x' \frac{\Psi^*_{k_1}(x)\Psi^*_{k_2}(x')\Psi_{k'_1}(x)\Psi_{k'_2}(x')}{|x-x'|}. \tag{2.12}$$

Turning to the lattice system, it is convenient to use Wannier functions and to rewrite the Hamiltonian in Eq. (2.11) using the inverse Fourier transform in Eq. (2.4):

$$\hat{H} = \sum_{ij}\sum_{\sigma} t_{ij}\hat{c}^\dagger_{i\sigma}\hat{c}_{j\sigma} + \frac{1}{2}\sum_{ijkl}\sum_{\sigma\sigma'}\langle ij|kl\rangle \hat{c}^\dagger_{i\sigma}\hat{c}^\dagger_{j\sigma'}\hat{c}_{l\sigma'}\hat{c}_{k\sigma}, \tag{2.13}$$

where

$$t_{ij} = -\frac{1}{2}\int \mathrm{d}x\, \Phi^*_i(x)\nabla^2\Phi_j(x), \tag{2.14}$$

is the hopping integral between lattice sites i and j, and

$$\langle ij|kl\rangle = \iint \mathrm{d}x\mathrm{d}x' \frac{\Phi^*_i(x)\Phi^*_j(x')\Phi_k(x)\Phi_l(x')}{|x-x'|}. \tag{2.15}$$

The hopping integral t_{ij} is also called the kinetic contribution, the electron itineracy, the tunnelling amplitude, or the resonance integral. In any case, it accounts for the delocalization of the electrons in the system.

No approximation has been made on the Hamiltonian in Eq. (2.13) so far. The main simplification relies on considering that the orbitals centered on the atomic positions form an atomic shell with smaller radius than the inter-atomic distance. Hence, only the largest value of $\langle ij|kl\rangle$ will be kept, and is obtained when $i = j = k = l$. This two-electron integral will be denoted by $U = \langle ii|ii\rangle$. To further simplify the Hamiltonian, the overlap of orbitals that are not centered on neighbour atoms are neglected. In addition, the hopping integral between the nearest neighbouring-sites is considered constant, thus leading to $t_{ij} = -t(\delta_{j(i+1)} + \delta_{j(i-1)})$ where $t > 0$. By applying these approximations to the Hamiltonian in Eq. (2.13), the so-called Hubbard Hamiltonian [316–319] is obtained,

$$\begin{aligned} \hat{H} &\longrightarrow \hat{T} + \hat{U} - \hat{\mu}, \\ &= -t \sum_{\langle ij \rangle} \sum_{\sigma} (\hat{c}^{\dagger}_{i\sigma} \hat{c}_{j\sigma} + \hat{c}^{\dagger}_{j\sigma} \hat{c}_{i\sigma}) + U \sum_i \hat{n}_{i\uparrow} \hat{n}_{i\downarrow} - \mu \sum_i \hat{n}_i, \end{aligned} \tag{2.16}$$

where $\hat{n}_i = \hat{n}_{i\uparrow} + \hat{n}_{i\downarrow}$ is the occupation operator on site i with $\hat{n}_{i\sigma} = \hat{c}^{\dagger}_{i\sigma} \hat{c}_{i\sigma}$. The last term in the Hamiltonian is the chemical potential μ which controls the electron filling in the system. It is considered for grand canonical calculations, and omitted otherwise. In this model, t and U will be used as parameters and are no more defined as one- and two-particle integrals. As we now work in a localized basis, it looks like real space has been discretized into a grid of points, called sites, such that $|\Phi_i\rangle \rightarrow |i\rangle$. The sites form a basis set $\{|i\rangle\}_{i=1,L}$, so that any one-electron state previously written in the continuum (in position representation) now reads

$$|k\rangle = \int \mathrm{d}x \, \varphi_k(x) |x\rangle \longrightarrow |k\rangle = \sum_i \varphi_k(i) |i\rangle, \tag{2.17}$$

where $\varphi_k(i)$ is a discrete function of the site positions $i = 1, \ldots, L$.

In general, the single-band Hubbard model is studied, meaning that only one orbital per site is considered, which is physically relevant for the description of solids with only one energy band at the Fermi surface. As a consequence, each site has only four configurations: empty ($|\mathrm{vac}\rangle$), singly-occupied ($|\uparrow\rangle$ or $|\downarrow\rangle$) and doubly-occupied ($|\uparrow\downarrow\rangle$). An illustration of this model is given in Fig. 2.2. The ratio U/t controls the importance of the localized electron picture over the delocalized one. Despite the apparent simplicity of the model, an analytic solution exists only in the half-filled case (the number of electrons equals the number of sites) in the thermodynamic limit (infinite number of sites). It is obtained from the Bethe Ansatz, as shown by Lieb and Wu in 1968 [320]. Away from half-filling, the exact solution based on the latter is found numerically.

The next section is devoted to the Mott-insulator state, responsible for the unusual properties of some transition metal oxides, which can be described in the Hubbard model.

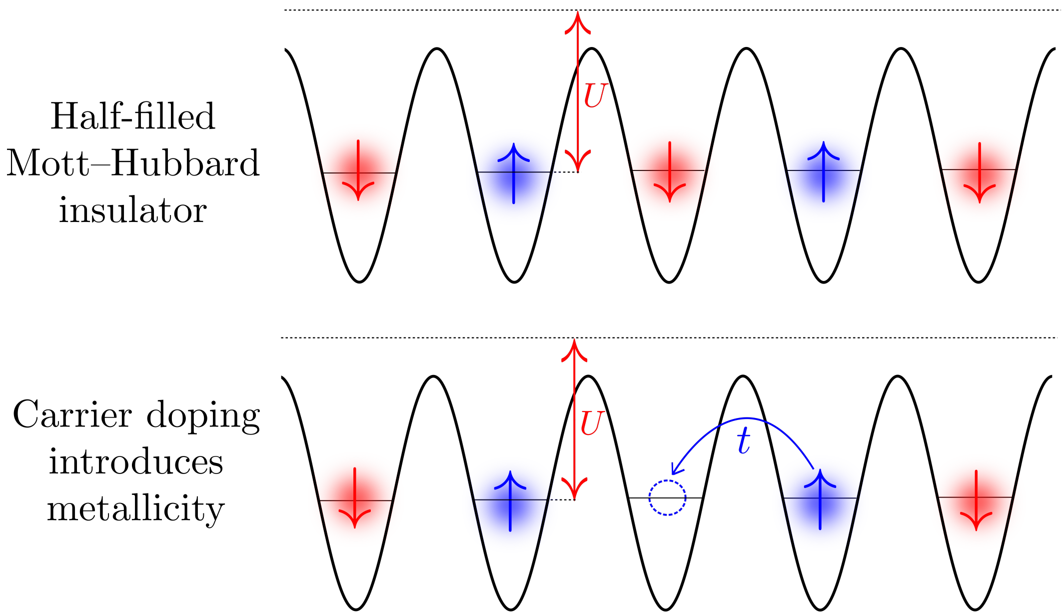

Figure 2.2: One dimensional Hubbard model at half-filling corresponding to an insulator (top panel). Carrier doping (of a hole or a particle) from the half-filled model introduces some metallicity (bottom panel).

2.1.3 Mott insulators and the Hubbard model

The difference between a metal and an insulator was given almost ninety years ago [321–324] by the theory of independent-electron (molecular orbital theory). If the highest occupied band is partially filled, the material is a metal; if it is completely filled, the material is an insulator. In other words, the Fermi level of an insulator lies in a gap between the highest filled band (valence band) and the lowest empty band (conduction band), while it lies in the valence band for a metal. However, it has been pointed out in 1937 by de Boer and Verwey that this independent-electron picture is not sufficient to describe the transition-metal oxides with a partially-filled d band such as cubic nickel oxide [303, 325], which are Mott-insulators. Several discussions have followed to explain how the Mott-insulator state is related to the electron-electron repulsion [312, 313, 326, 327]. In the following, I will focus on the Mott insulator and its description within the Hubbard model, derived in 1964 to describe electron correlation in narrow energy bands [316–319]. For pedagogical purposes, it is interesting to discuss the two-dimensional Hubbard model which is related to the high-T_c cuprates, although the one-dimensional case only is studied in this thesis. This discussion is illustrated in Fig. 2.3. According to the definition given by the independent-electron picture, the single band model should always predict a metallic state unless the valence band is completely filled. This is in fact not true, as shown in the following.

Fig. 2.3 shows the p- and the d-bands in a solid. The left panel describes a Mott–Hubbard in-

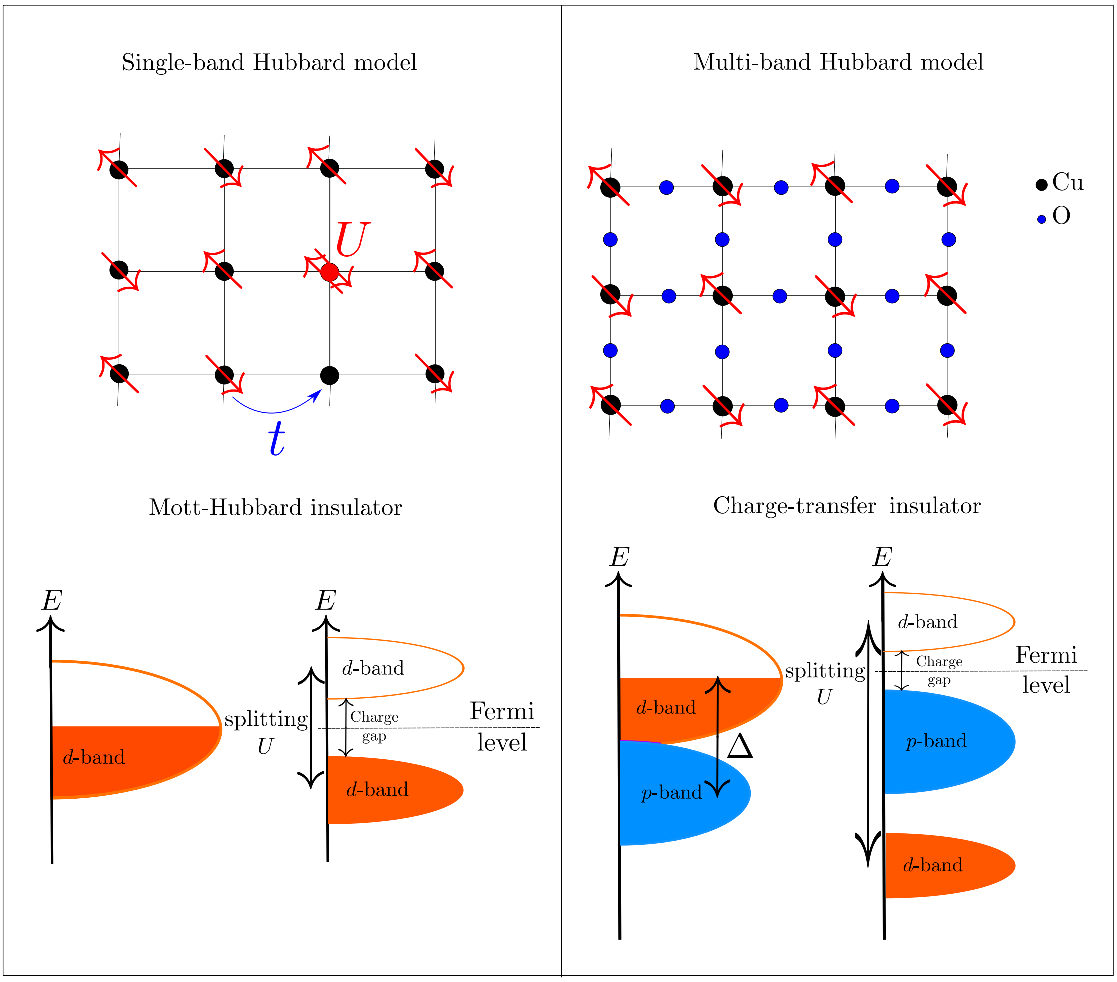

Figure 2.3: Representation of the Mott–Hubbard insulator (left panel) by the single-band Hubbard model, and the charge-transfer insulator (right panel) in CuO_2 plane by the multi-band Hubbard model. Concerning the energy band diagrams at the bottom of each panel, the one on the left corresponds to the noninteracting case while the one on the right corresponds to the interacting case ($U > 0$).

sulator, while the right panel describes a charge-transfer insulator. The distinction between the two will be explained later in this section. Let us focus on the Mott–Hubbard insulator first. In the case of the single band model, only the d-bands remain. Starting with the non interacting case ($U = 0$), the model forms a single band where electrons can move freely, and thus describes a metal. The only way to get an insulator would be to fill the band completely, until the electrons are motionless due to the Pauli principle. This is the standard metal-insulator transition. By switching on the interaction ($U > 0$), two electrons on the same site will repeal each other, thus splitting the band in two [328]. The lower band for electrons joining an empty site and the upper band for electrons joining an already occupied site, thus leading to the double occupation of a site which necessitates an energy U. If the lower band is completely filled, a competition between the delocalization induced by the hopping t and the localization of the electron induced by U will prevent the electrons to occupy the same site. The system can therefore switch from a metal to an insulator state for a given value U_c/t defining the Mott-transition. For $U > U_\mathrm{c}$, electrons are completely localized with one electron per site, and cannot move because of the energy penalty to create a doubly occupied site. So the electronic motionlessness is not due to the Pauli principle, but to the electron repulsion only. Away from half-filling, the electrons will be able to jump on empty sites even if the repulsion U is huge. Such a carrier (particle or hole) doping does introduce some metallization. Interestingly, reducing the dimension of the system will diminish the critical value U_c for which the Mott-transition appears, because a low dimension does not favour the motion of the electrons. In the drastic one-dimensional case, the Hubbard model is a Mott-insulator for any $U > 0$ [320], so that it does not manifest a Mott-insulator *transition* anymore. However, there is still a charge gap opening, present at half-filling only. Hence, the one-dimensional Hubbard model still exhibits a transition, which is called a “density-driven” Mott transition [329].

Let us now discuss the charge-transfer insulator by making a link between this simplified model and the transition metal oxides. Transition metal oxides depict narrow d- bands and the Wannier orbitals are well localized, satisfying the Hubbard assumption to neglect the non-local interactions and to consider hopping between first neighbour only. Taking high-$\mathrm{T_c}$ $\mathrm{La_2CuO_4}$ as an example, the Mott-insulating phase is dominated by the d^9 configuration of Cu. Indeed, the high-level splitting of the d-orbitals due to Jahn–Teller effect tells us that all d-band are filled except $d_{x^2-y^2}$ which is half-filled and is the only relevant orbital to be considered. Hence, considering the isolated $d_{x^2-y^2}$-band only is a good starting point for the study of high-$\mathrm{T_c}$ cuprates. In other words, the single-band approximation of the Hubbard model is relevant in this case [304]. However, this approximation does neglect the hybridization effect between the d-band of the metal and the p-band of the oxygen atoms, which appears to be important in transition metal oxides. These materials are called “charge-transfer” insulators rather than Mott-Hubbard insulators [330, 331], because the lowest excitation gap is now between the (fully occupied) p-band of the oxygen and the (unoccupied) d-band of the transition metal. As illustrated in the right panel of Fig. 2.3, the overlap between the p-bands of the oxides and the d-band of the metal cannot always be neglected. Thus, one has to consider an additional parameter $\Delta = \varepsilon_d - \varepsilon_p$, and the single-band approximation cannot give a proper description of such systems. The multi-band Hubbard model [315] has to be considered to model charge-transfer insulators. For instance, a two-band model is needed to describe the cubic nickel oxide NiO, and a three-band model for the cuprate plane CuO$_2$ (one d-band for the Cu and one p-band for each oxygen, called also the $d-p$ model [304]). Despite the fact that they are charge-transfer insulators, cuprates can still be approximated by an *effective* single-band model [331, 332].

Let us now investigate the noninteracting limit ($U = 0$) and the strongly correlated limit ($t \ll U$) of the Hubbard model.

2.1.4 Connection between Hubbard and simpler model Hamiltonians

2.1.4.i The tight-binding or Hückel model (the $U = 0$ limit)

By setting $U = 0$ in the Hubbard model [Eq. (2.16)], the tight-binding model is recovered,

$$\hat{H} \longrightarrow -t \sum_{\langle ij \rangle, \sigma} \left(\hat{c}^\dagger_{i\sigma} \hat{c}_{j\sigma} + \hat{c}^\dagger_{j\sigma} \hat{c}_{i\sigma} \right) - \mu \sum_i \hat{n}_i, \tag{2.18}$$

leading to the $(L \times L)$ Hamiltonian matrix representation in the sites basis:

$$\left[\hat{H}\right] = \begin{bmatrix} -\mu & -t & 0 & 0 & \cdots & 0 & -t \\ -t & -\mu & -t & 0 & \cdots & 0 & 0 \\ 0 & -t & -\mu & -t & \cdots & 0 & 0 \\ 0 & 0 & -t & -\mu & \cdots & 0 & 0 \\ \vdots & \vdots & \vdots & \vdots & & \vdots & \vdots \\ 0 & 0 & 0 & 0 & \cdots & -\mu & -t \\ -t & 0 & 0 & 0 & \cdots & -t & -\mu \end{bmatrix} \tag{2.19}$$

which is nothing but Hückel theory. Note that periodic boundary conditions have been used in Eq. (2.19), given by the additional $-t$ term in the upper right and lower left elements of the matrix, which is simply included in the Hamiltonian by setting $\hat{c}^\dagger_{L+1} = \hat{c}^\dagger_1$. This Hamiltonian can be diagonalized in the Bloch basis by using the canonical transformation of the creation and annihilation

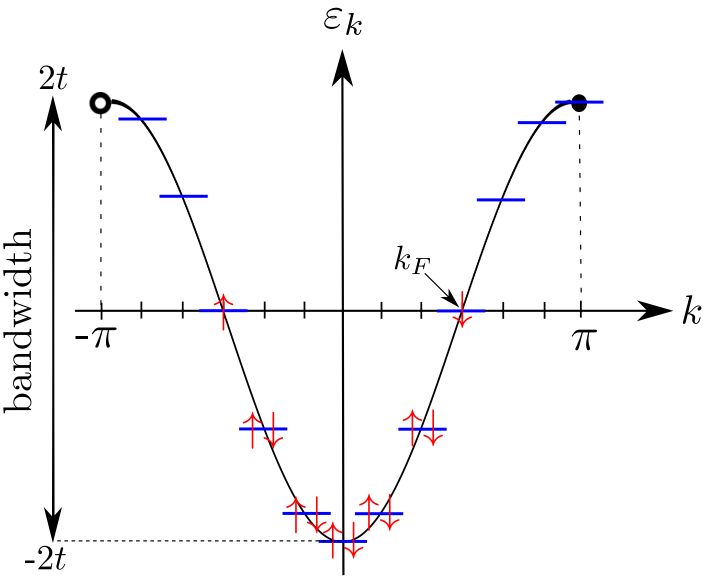

Figure 2.4: Energy dispersion $\varepsilon_k = -2t\cos(k)$ of the tight-binding model plotted in the one-dimensional Brillouin zone for 12 sites at half-filling. The Fermi momentum k_F is the momentum associated with the Fermi energy corresponding to the chemical potential μ.

operators in Eq. (2.8), together with Eq. (2.9), leading to:

$$\hat{H} = \sum_{k\sigma}(\varepsilon_k - \mu)\hat{c}^{\dagger}_{k\sigma}\hat{c}_{k\sigma}, \tag{2.20}$$

where the $\varepsilon_k = -2t\cos(k)$ is the dispersion relation. The bandwidth, defined as the difference between the maximum and the minimum of ε_k, equals to $4t$ as shown in Fig. 2.4.

2.1.4.ii t–J model and Heisenberg model for $t \ll U$

Turning to the strongly correlated limit $t \ll U$, the hopping term in the Hubbard model can be treated as a perturbation of the electronic repulsion. The second-order perturbation expansion at half-filling leads to the Heisenberg model [333, 334],

$$\hat{H}^{\text{Heisenberg}} = J\sum_{\langle ij\rangle}\mathbf{S}_i.\mathbf{S}_j = J\sum_{\langle ij\rangle}\left(\hat{S}^-_i\hat{S}^+_j + \hat{S}^+_i\hat{S}^-_j + \hat{S}^z_i\hat{S}^z_j\right), \tag{2.21}$$

where $\hat{S}^+_i = \hat{c}^{\dagger}_{i\uparrow}\hat{c}_{i\downarrow}$, $\hat{S}^-_i = \left(\hat{S}^+_i\right)^{\dagger} = \hat{c}^{\dagger}_{i\downarrow}\hat{c}_{i\uparrow}$ and $\hat{S}^z_i = \frac{1}{2}\left(\hat{n}_{i\uparrow} - \hat{n}_{i\downarrow}\right)$ are spin operators. $J = 4t^2/U$ is the antiferromagnetic exchange constant. Note that there is no more non local term in the Hamiltonian, as it would create "doubly-occupied-site" states that are prohibited in the limit $t \ll U$ for the ground state at half-filling. This model describes the super-exchange interaction between antiparallel spins, while the interaction between parallel spins is forbidden by Pauli principle (the electron-electron repulsion is only on-site in this model, and two electron of same spin cannot be in the same site). The term super-exchange comes from the process of virtual double occupation:

$$|\uparrow,\downarrow\rangle \xrightarrow{\text{hopping}} \left\{ \begin{array}{c} |\uparrow\downarrow,\text{vac}\rangle \\ |\text{vac},\uparrow\downarrow\rangle \end{array} \right\} \xrightarrow{\text{hopping}} |\downarrow,\uparrow\rangle. \tag{2.22}$$

which can be mediated by the oxygen atom separating two metallic centers in transition metal oxides. A generalization of this model away from half-filling (particularly interesting to study carrier doping leading to high-T_c cuprates for instance) is provided by the so-called t–J model, which reintroduces the hopping integral t thanks to the creation of free charge carriers (particles or holes):

$$\hat{H}^{t-J} = -t \sum_{\langle ij\rangle\sigma} \hat{\mathcal{P}} \left(\hat{c}^\dagger_{i\sigma}\hat{c}_{j\sigma} + \text{h.c.} \right) \hat{\mathcal{P}} + \hat{H}^{\text{Heisenberg}}, \tag{2.23}$$

where $\hat{\mathcal{P}}$ is a projector that prohibits the double occupation of sites. Those two Hamiltonians allow the study of magnetic properties of strongly correlated materials.

2.1.4.iii The Hubbard dimer

In order to have a better understanding of the physics involved in the Hubbard model, it is appealing to reduce the size of the system. In the thermodynamic limit at half-filling, an analytical solution is given by Bethe Ansatz [320]. Another analytical solution exits for the two-site Hubbard model, called the Hubbard dimer, for which the exact eigenvectors and eigenvalues are known. This section is first dedicated to the symmetric case, in the weakly correlated ($U = 0$) and strongly correlated ($U \gg t$) limits, followed by the study of the asymmetric Hubbard dimer. The half-filled case ($N = 2$) is considered.

Symmetric Hubbard dimer

The Hamiltonian of the symmetric Hubbard dimer is given by

$$\hat{H} = -t \sum_{\sigma} \left(\hat{c}^\dagger_{0\sigma}\hat{c}_{1\sigma} + \hat{c}^\dagger_{1\sigma}\hat{c}_{0\sigma} \right) + U \sum_{i=0,1} \hat{n}_{i\uparrow}\hat{n}_{i\downarrow}. \tag{2.24}$$

In the case of the singlet subspace ($S = 0$), the system is described by three states,

$$\frac{1}{\sqrt{2}} \left(\hat{c}^\dagger_{0\uparrow}\hat{c}^\dagger_{1\downarrow} - \hat{c}^\dagger_{0\downarrow}\hat{c}^\dagger_{1\uparrow} \right) |\text{vac}\rangle, \quad \hat{c}^\dagger_{0\uparrow}\hat{c}^\dagger_{0\downarrow}|\text{vac}\rangle, \quad \hat{c}^\dagger_{1\uparrow}\hat{c}^\dagger_{1\downarrow}|\text{vac}\rangle, \tag{2.25}$$

conveniently rewritten as

$$\frac{1}{\sqrt{2}}\left(|\uparrow_0,\downarrow_1\rangle - |\downarrow_0,\uparrow_1\rangle\right), \qquad |\uparrow\downarrow_0,\mathrm{vac}_1\rangle, \qquad |\mathrm{vac}_0,\uparrow\downarrow_1\rangle. \tag{2.26}$$

It leads to the following Hamiltonian matrix representation,

$$\left[\hat{H}\right] \equiv \begin{bmatrix} 0 & -\sqrt{2}t & -\sqrt{2}t \\ -\sqrt{2}t & U & 0 \\ -\sqrt{2}t & 0 & U \end{bmatrix}, \tag{2.27}$$

which gives after diagonalization,

$$\left[\hat{H}\right] \equiv \begin{bmatrix} \left(U-\sqrt{U^2+16t^2}\right)/2 & 0 & 0 \\ 0 & U & 0 \\ 0 & 0 & \left(U+\sqrt{U^2+16t^2}\right)/2 \end{bmatrix}. \tag{2.28}$$

Turning to $S=1$, the triplet subspace is spanned by the states:

$$\frac{1}{\sqrt{2}}\left(|\uparrow_0,\downarrow_1\rangle + |\downarrow_0,\uparrow_1\rangle\right), \qquad |\uparrow_0,\uparrow_1\rangle, \qquad |\downarrow_0,\downarrow_1\rangle, \tag{2.29}$$

which all have zero energy. In the $U=0$ limit, the whole spectrum is $\{-2t,0,2t\}$ and the associated wavefunctions are

$$\begin{aligned} |\Psi_0^{S=0}\rangle &= \frac{1}{2}\left[\Big(|\uparrow_0,\downarrow_1\rangle - |\downarrow_0,\uparrow_1\rangle\Big) + \Big(|\uparrow\downarrow_0,\mathrm{vac}_1\rangle + |\mathrm{vac}_0,\uparrow\downarrow_1\rangle\Big)\right], \\ |\Psi_1^{S=0}\rangle &= \frac{1}{\sqrt{2}}\Big(|\uparrow\downarrow_0,\mathrm{vac}_1\rangle - |\mathrm{vac}_0,\uparrow\downarrow_1\rangle\Big), \\ |\Psi_2^{S=0}\rangle &= \frac{1}{2}\left[\Big(|\uparrow_0,\downarrow_1\rangle - |\downarrow_0,\uparrow_1\rangle\Big) - \Big(|\uparrow\downarrow_0,\mathrm{vac}_1\rangle + |\mathrm{vac}_0,\uparrow\downarrow_1\rangle\Big)\right], \end{aligned} \tag{2.30}$$

where $\Psi_1^{S=0}$ is degenerate with the triplet states. Because the Coulomb repulsion U can be interpreted as an energy penalty for having two electrons on the same site, we expect the coefficients for the "doubly-occupied-site" states in $\Psi_0^{S=0}$ to decrease with U, contrary to the "singly-occupied-site" states. Indeed, in the strongly correlated regime ($U \gg t$), the diagonalized Hamiltonian matrix restricted to the singlet states reads

$$\left[\hat{H}\right] = \begin{bmatrix} -4t^2/U & 0 & 0 \\ 0 & U & 0 \\ 0 & 0 & U+4t^2/U \end{bmatrix}, \tag{2.31}$$

so that the spectrum is $\{-4t^2/U, 0, U, U + 4t^2/U\}$ in the strongly correlated limit. The energy 0 comes from the triplet while the singlet energies are $-4t^2/U$, U and $U + 4t^2/U$ with the associated wavefunctions,

$$\begin{aligned}
|\Psi_0^{S=0}\rangle &= \frac{1}{\sqrt{2}}\Big(|\uparrow_0, \downarrow_1\rangle - |\downarrow_0, \uparrow_1\rangle\Big), \\
|\Psi_1^{S=0}\rangle &= \frac{1}{\sqrt{2}}\Big(|\uparrow\downarrow_0, \mathrm{vac}_1\rangle - |\mathrm{vac}_0, \uparrow\downarrow_1\rangle\Big), \\
|\Psi_2^{S=0}\rangle &= \frac{1}{\sqrt{2}}\Big(|\uparrow\downarrow_0, \mathrm{vac}_1\rangle + |\mathrm{vac}_0, \uparrow\downarrow_1\rangle\Big), \qquad (2.32)
\end{aligned}$$

respectively. It is clear from Eqs. (2.30) and (2.32) that increasing U reduces “double-occupied-site” states in the ground state. Note also that there is no charge fluctuation in the ground state of the strongly correlated limit in contrast to the $U = 0$ case, thus revealing the connection between U and the localization of the electrons.

Asymmetric Hubbard dimer

In the symmetric model, the site occupation was equal to 1 on each site. If one wants more flexibility in the model, different on-site potentials can be introduced, thus leading to the asymmetric Hubbard dimer with Hamiltonian

$$\hat{H} = -t\sum_{\sigma}\left(\hat{c}^\dagger_{0\sigma}\hat{c}_{1\sigma} + \hat{c}^\dagger_{1\sigma}\hat{c}_{0\sigma}\right) + U\left(\hat{n}_{0\uparrow}\hat{n}_{0\downarrow} + \hat{n}_{1\uparrow}\hat{n}_{1\downarrow}\right) + v_0\hat{n}_0 + v_1\hat{n}_1. \qquad (2.33)$$

For convenience, we choose $v_0 + v_1 = 0$ and denote $\Delta v = v_1 - v_0$ which gives (for two electrons),

$$\hat{H} = -t\sum_{\sigma}\left(\hat{c}^\dagger_{0\sigma}\hat{c}_{1\sigma} + \hat{c}^\dagger_{1\sigma}\hat{c}_{0\sigma}\right) + U\left(\hat{n}_{0\uparrow}\hat{n}_{0\downarrow} + \hat{n}_{1\uparrow}\hat{n}_{1\downarrow}\right) + \Delta v(1 - \hat{n}), \qquad (2.34)$$

where $\hat{n} = \hat{n}_0 = 2 - \hat{n}_1$. This model is a very good laboratory for testing new methods. It can describe various regimes of density and correlation by varying U, t and Δv. We have already discussed the competition between localization and delocalization dictated by the ratio U/t. It is shown in Fig. 2.5 how the insertion of a new parameter Δv affects this competition for $U \gg t$. On the left panel of Fig. 2.5, $U/\Delta v > 1$ and the electron-electron repulsion prevents the electron to be on the same site, such that the occupation is strictly 1 on each site, thus featuring a Mott-Hubbard insulator state. On the right panel, $U/\Delta v < 1$ such that the difference of potential dominates and the electrons tend to be on the same site (charge-transfer insulator).

This model is solvable exactly. The exact energies E_i are determined by solving the following

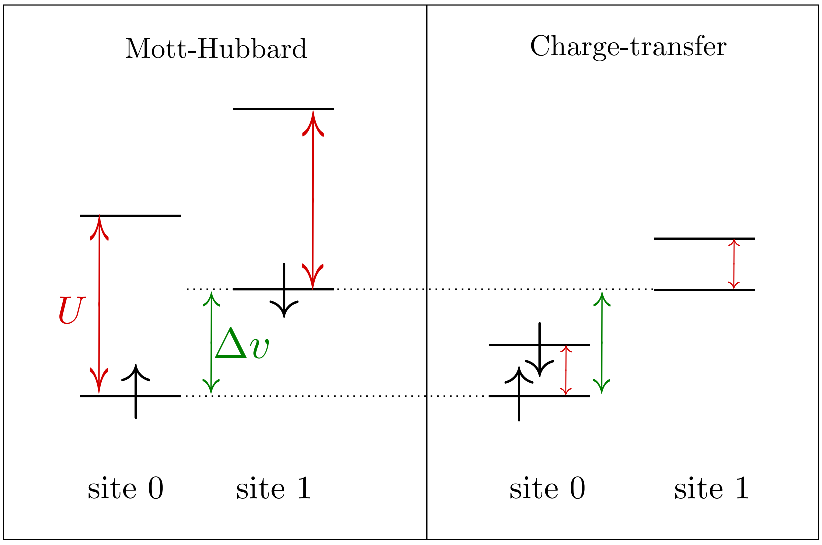

Figure 2.5: Mott-Hubbard and charge-transfer insulators depending on the ratio $U/\Delta v$ for $U \gg t$. Horizontal black lines represent *spin* orbitals. The red arrows represent the coulomb repulsion magnitude U and the green arrows the difference in on-site potential Δv. Black arrows are the electrons with spin ↑ and ↓. This figure is inspired from Ref. [335].

third-order polynomial equation,

$$-4t^2U + \left(4t^2 - U^2 + \Delta v^2\right) E_i + 2UE_i^2 = E_i^3, \tag{2.35}$$

which leads to [335]

$$\begin{aligned} E_i &= \frac{2U}{3} + \frac{2r}{3}\cos\left(\theta + \frac{2\pi}{3}(i+1)\right), \quad i = 0,1,2 \text{ (singlet states)} \\ E_i &= 0, \quad i = 3,4,5 \text{ (triplet state)}, \end{aligned} \tag{2.36}$$

where

$$r = \sqrt{3\left(4t^2 + \Delta v^2\right) + U^2}, \tag{2.37}$$

and

$$\theta = \frac{1}{3}\arccos\left[\frac{9U\left(\Delta v^2 - 2t^2\right) - U^3}{r^3}\right]. \tag{2.38}$$

According to the Hellmann-Feynman theorem, we have access to the density (i.e. the occupation on site 0) of the ith state,

$$n^i = 1 - \frac{\partial E_i}{\partial \Delta v}, \tag{2.39}$$

and the one-particle density matrix,

$$\gamma^i = \begin{bmatrix} n^i & \gamma^i_{01} \\ \gamma^i_{10} & 2-n^i \end{bmatrix}, \quad \gamma^i_{01} = -\frac{1}{2}\frac{\partial E_i}{\partial t}. \tag{2.40}$$

The double occupation are not the same on site 0 and site 1, but they can still be obtained exactly by rewriting the asymmetric Hubbard dimer with two different on-site electron-repulsion parameters U_0 and U_1,

$$\hat{H} = -t\sum_{\sigma}\left(\hat{c}^{\dagger}_{0\sigma}\hat{c}_{1\sigma} + \hat{c}^{\dagger}_{1\sigma}\hat{c}_{0\sigma}\right) + U_0\hat{n}_{0\uparrow}\hat{n}_{0\downarrow} + U_1\hat{n}_{1\uparrow}\hat{n}_{1\downarrow} + \Delta v\left(1-\hat{n}\right). \tag{2.41}$$

Its associated energies $\mathcal{E}_i(U_0, U_1, \Delta v)$ can be obtained by considering an effective physical system such that [72]:

$$\begin{aligned} U_{\text{eff}} - \Delta v_{\text{eff}} &= U_0 - \Delta v, \\ U_{\text{eff}} + \Delta v_{\text{eff}} &= U_1 + \Delta v, \end{aligned} \tag{2.42}$$

or, equivalently,

$$\begin{aligned} U_{\text{eff}} &= \frac{U_0+U_1}{2}, \\ \Delta v_{\text{eff}} &= \Delta v + \frac{U_1-U_0}{2}, \end{aligned} \tag{2.43}$$

thus leading to

$$\mathcal{E}_i(U_0, U_1, \Delta v) = E_i((U_0+U_1)/2, \Delta v + (U_1-U_0)/2). \tag{2.44}$$

According to the Hellmann–Feynman theorem, the expressions for the double occupations read

$$\left\{\begin{aligned} d^i_0 &= \langle \hat{n}_{0\uparrow}\hat{n}_{0\downarrow}\rangle = \frac{\partial \mathcal{E}_i}{\partial U_0} = \frac{1}{2}\left.\frac{\partial E_i}{\partial U}\right|_{U=(U_0+U_1)/2} - \frac{1}{2}\frac{\partial E_i}{\Delta v} = \frac{1}{2}\left(\left.\frac{\partial E_i}{\partial U}\right|_{U=(U_0+U_1)/2} - (1-n)\right), \\ d^i_1 &= \langle \hat{n}_{1\uparrow}\hat{n}_{1\downarrow}\rangle = \frac{\partial \mathcal{E}_i}{\partial U_1} = \frac{1}{2}\left.\frac{\partial E_i}{\partial U}\right|_{U=(U_0+U_1)/2} + \frac{1}{2}\frac{\partial E_i}{\Delta v} = \frac{1}{2}\left(\left.\frac{\partial E_i}{\partial U}\right|_{U=(U_0+U_1)/2} + (1-n)\right). \end{aligned}\right. \tag{2.45}$$

The various derivatives can be expressed as follows, simply obtained by differentiating Eq. (2.35):

$$\begin{aligned}\frac{\partial E_i}{\partial t} &= \frac{8t(U-E_i)}{-3E_i^2+4UE_i+4t^2-U^2+\Delta v^2},\\ \frac{\partial E_i}{\partial \Delta v} &= \frac{-2\Delta v E_i}{-3E_i^2+4UE_i+4t^2-U^2+\Delta v^2},\\ \frac{\partial E_i}{\partial U} &= \frac{4t^2+2E_i(U-E_i)}{-3E_i^2+4UE_i+4t^2-U^2+\Delta v^2}.\end{aligned} \tag{2.46}$$

In the ground state of the symmetric case, the site occupation is equal to $n = 1$, the off-diagonal density matrix element $\gamma_{01} = 4t/\mathcal{U}$ and the double occupation $d = (1 - U/\mathcal{U})/4$, where $\mathcal{U} = \sqrt{U^2 + 16t^2}$.

In addition to be solvable analytically, this model has been proven very helpful in understanding deficiencies of DFAs, for example in the description of strong electron correlation. It has also been used to test new ideas as a proof of concept. For example, one can cite the use of ensembles in RDMFT [218], the benchmark of functionals in RDMFT [203, 336, 337], and the development of alternative formulations of DFT such as lattice DFT [335, 338], site-occupation embedding theory [72, 270], thermal DFT [339], ensemble DFT [73–75, 340], and DFT beyond the Born–Oppenheimer approximation [341].

2.2 Site-Occupation Functional Theory

The *site-occupation functional theory* (SOFT), also called lattice DFT, is the discretized version of conventional real-space DFT. In this section, I will focus on the theory originally formulated by Gunnarsson and Schönhammer [342, 343] and on the *Bethe ansatz local density approximation* (BALDA). It is worth mentioning that extensions have been investigated over the past few years by including time- [344–346] and temperature-dependence [347, 348], as well as the steady current in connection with steady-state transport [349, 350].

2.2.1 Density Functional Theory on a lattice

Consider a one-dimensional lattice with L sites forming a discretized space. The sites can be associated to orthonormal orbitals centered on each nucleus (Wannier orbitals). Electron evolving on this lattice can be described by the one-band Hubbard model in Eq. (2.16) where, for sake of generality, we introduce an additional external potential $\mathbf{v} \equiv \{v_i\}_i$,

$$\begin{aligned}\hat{H} &= \hat{T} + \hat{U} + \hat{V},\\ &= -t\sum_{\langle ij\rangle}\sum_{\sigma}(\hat{c}^\dagger_{i\sigma}\hat{c}_{j\sigma} + \hat{c}^\dagger_{j\sigma}\hat{c}_{i\sigma}) + U\sum_i \hat{n}_{i\uparrow}\hat{n}_{i\downarrow} + \sum_i v_i\hat{n}_i.\end{aligned} \tag{2.47}$$

In such a system, the most intuitive analogue of the density $n(\mathbf{r})$ in real space is the collection of site occupations from which a site-occupation vector $\mathbf{n} \equiv \{n_i\}_i$ can be constructed as follows,

$$n(\mathbf{r}) = \left\langle \sum_\sigma \hat{\Psi}^\dagger(\mathbf{x})\hat{\Psi}(\mathbf{x}) \right\rangle \longrightarrow n_i = \left\langle \sum_\sigma \hat{c}^\dagger_{i\sigma}\hat{c}_{i\sigma} \right\rangle, \tag{2.48}$$

where n_i denotes the number of electrons on the ith site (or ith localized orbital). One may wonder if the Hohenberg–Kohn theorem is still valid in this context. DFT on a lattice has been first introduced by Chayes in 1985 [351], followed by the work of Gunnarsson and Schönhammer [342] in 1986 who showed that there is indeed a one-to-one correspondence between the external on-site potential and the site-occupation vector in the Hubbard model. Therefore, the variational principle,

$$E_0(\mathbf{v}) = \min_{\mathbf{n}}\Big\{ F(\mathbf{n}) + (\mathbf{v}|\mathbf{n}) \Big\}, \tag{2.49}$$

still holds, where $(\mathbf{v}|\mathbf{n}) = \sum_i v_i n_i$ and the minimization is performed over the site-occupation vector instead of the spatial density $n(\mathbf{r})$. $F(\mathbf{n})$ is the analogue of the Hohenberg–Kohn functional in DFT. It reads as follows within the Levy–Lieb constrained search formalism:

$$F(\mathbf{n}) = \min_{\Psi\rightarrow\mathbf{n}}\Big\{ \langle\Psi|\hat{T} + \hat{U}|\Psi\rangle \Big\}. \tag{2.50}$$

Strictly speaking, $F(\mathbf{n})$ is a *function* and not a *functional* of the site occupations, given that the site-occupation vector is just a collection of discrete numbers. Nevertheless, the standard DFT terminology will be used for convenience. As the Hohenberg–Kohn theorem is also valid for $U = 0$, we can decompose the Hohenberg–Kohn functional as follows (in analogy with KS-DFT):

$$F(\mathbf{n}) = T_\mathrm{s}(\mathbf{n}) + E_\mathrm{Hxc}(\mathbf{n}), \tag{2.51}$$

where the Hxc energy functional is t- and U-dependent, but it remains *universal* in a sense that it does not depend on the external potential $\mathbf{v}$. In the KS decomposition in Eq. (2.51), the hopping plays the role of a noninteracting kinetic energy,

$$T_\mathrm{s}(\mathbf{n}) = \min_{\Psi\rightarrow\mathbf{n}}\Big\{ \langle\Psi|\hat{T}|\Psi\rangle \Big\}, \tag{2.52}$$

thus leading to the alternative formulation of the variational principle,

$$E_0(\mathbf{v}) = \min_{\mathbf{n}}\Big\{ \min_{\Psi\rightarrow\mathbf{n}}\Big\{ \langle\Psi|\hat{T}|\Psi\rangle \Big\} + (\mathbf{v}|\mathbf{n}) + E_\mathrm{Hxc}(\mathbf{n}) \Big\}, \tag{2.53}$$

or, equivalently,

$$E_0(\mathbf{v}) = \min_{\Psi} \Big\{ \langle \Psi | \hat{T} | \Psi \rangle + (\mathbf{v}|\mathbf{n}^{\Psi}) + E_{\mathrm{Hxc}}(\mathbf{n}^{\Psi}) \Big\}. \tag{2.54}$$

The minimizing wavefunction in Eq. (2.54) is a monodeterminantal wavefunction satisfying the following self-consistent equation,

$$\left(\hat{T} + \sum_i \left[v_i + \frac{\partial E_{\mathrm{Hxc}}(\mathbf{n}^{\Phi^{\mathrm{KS}}})}{\partial n_i} \right] \hat{n}_i \right) |\Phi^{\mathrm{KS}}\rangle = \mathcal{E}^{\mathrm{KS}} |\Phi^{\mathrm{KS}}\rangle, \tag{2.55}$$

where $[v_i + \partial E_{\mathrm{Hxc}}(\mathbf{n})/\partial n_i]$ is the KS potential denoted by $v_i^{\mathrm{KS}}(\mathbf{n})$. This potential is responsible for the recovering of the same density than the physical system. If we denote by $\{\varphi_k\}_k$ the occupied orbitals in Φ^{KS}, they fulfil the following equation (in matrix representation):

$$\begin{bmatrix} v_0^{\mathrm{KS}} & -t & 0 & 0 & \cdots & 0 & -t \\ -t & v_1^{\mathrm{KS}} & -t & 0 & \cdots & 0 & 0 \\ 0 & -t & v_2^{\mathrm{KS}} & -t & \cdots & 0 & 0 \\ 0 & 0 & -t & v_3^{\mathrm{KS}} & \cdots & 0 & 0 \\ \vdots & \vdots & \vdots & \vdots & & \vdots & \vdots \\ 0 & 0 & 0 & 0 & \cdots & v_{L-2}^{\mathrm{KS}} & -t \\ -t & 0 & 0 & 0 & \cdots & -t & v_{L-1}^{\mathrm{KS}} \end{bmatrix} \cdot \begin{bmatrix} \varphi_k(i=0) \\ \varphi_k(i=1) \\ \varphi_k(i=2) \\ \varphi_k(i=3) \\ \vdots \\ \varphi_k(i=L-2) \\ \varphi_k(i=L-1) \end{bmatrix} = \varepsilon_k \begin{bmatrix} \varphi_k(i=0) \\ \varphi_k(i=1) \\ \varphi_k(i=2) \\ \varphi_k(i=3) \\ \vdots \\ \varphi_k(i=L-2) \\ \varphi_k(i=L-1) \end{bmatrix}, \tag{2.56}$$

where the density dependence in the KS potential has been dropped for clarity. This matrix representation can be expressed in a more compact equation that reads

$$\sum_{j=1}^{L} \left(-t_{ij} + \left[v_i + \frac{\partial E_{\mathrm{Hxc}}(\mathbf{n}^{\Phi^{\mathrm{KS}}})}{\partial n_i} \right] \delta_{ij} \right) \varphi_k(j) = \varepsilon_k \varphi_k(i), \tag{2.57}$$

with $t_{ij} = t$ for $j = i \pm 1$ and $t_{ij} = 0$ otherwise. Note that the site occupations for a closed-shell system are recovered from the KS orbitals $\varphi_k(i)$ as follows,

$$n_i = 2 \sum_k^{\mathrm{occ}} |\varphi_k(i)|^2, \tag{2.58}$$

where $\varphi_k(i)$ are either doubly or not occupied in Φ^{KS}, and form the basis in which the N-electron wavefunction is written as a single Slater determinant. However, the N-electron wavefunction in the basis of sites $\{|i\rangle\}_i$ is multideterminantal.

The one-electron state in the basis of KS orbitals are related to the one-electron state of the basis of sites as follows,

$$|\varphi_k, \sigma\rangle = \sum_{i=0}^{L-1} \varphi_k(i)|i, \sigma\rangle, \tag{2.59}$$

or, in second quantization,

$$\hat{c}^\dagger_{k\sigma} = \sum_{i=0}^{L-1} \varphi_k(i)\hat{c}^\dagger_{i\sigma}. \tag{2.60}$$

Therefore, while the KS orbitals are only not occupied or doubly occupied, the sites can be fractionally occupied.

It is important to distinguish SOFT from the other functional theories applied to the Hubbard model, where other quantities are used as basic variables [302]. In analogy with RDMFT, one can consider the 1RDM γ_{ij} as variable,

$$\gamma_{ij} = \left\langle \sum_\sigma \hat{c}^\dagger_{i\sigma}\hat{c}_{j\sigma} \right\rangle, \tag{2.61}$$

as done by Pastor and co-workers [352–357]. Interestingly, one can recover the electronic density in real space $n(\mathbf{r})$ within this formalism [216, 302] (see Appendix D),

$$n(\mathbf{r}) = \left\langle \sum_\sigma \hat{\Psi}^\dagger(\mathbf{x})\hat{\Psi}(\mathbf{x}) \right\rangle = \sum_{ij\sigma} \varphi^*_i(\mathbf{r})\varphi_j(\mathbf{r}) \left\langle \hat{c}^\dagger_{i\sigma}\hat{c}_{j\sigma} \right\rangle, \tag{2.62}$$

where $\{\varphi_i(\mathbf{r})\}_i$ are Wannier orbitals in this context. Using the whole 1RDM as a basic variable is appealing for various reasons. First of all, the kinetic energy is obtained exactly in terms of t_{ij} and γ_{ij}, in analogy with RDMFT. Therefore, the Hxc functional in this theory is t_{ij}- and $\mathbf{v}$-independent, and is in a sense more universal than the $\mathbf{v}$-independent only Hxc functional in SOFT. However, it remains U-dependent, as in standard DFT where the Hxc functional depends on the coulomb interaction. Besides, it has been shown in the early work of Schindlmayr and Godby [216] that the 1RDM is *not* noninteracting v-representable, like in RDMFT. As a consequence, the KS-type scheme cannot be straightforwardly derived. In summary, SOFT and the latter theory developed by Pastor and co-workers are the analogues of the real-space DFT and real-space RDMFT, expressed in a discretized real-space (a lattice of sites), respectively.

Returning to SOFT, the minimizing wavefunction in Eq. (2.54) is not expected to reproduce anything else than the diagonal of the 1RDM. However, the Hxc energy functional and its derivatives allow to recover all the properties of the system, in principle[1], even the two-body correlation functions such as the double occupation and of course the ground-state energy [Eq. (2.54)]. As an illustration, let us consider the uniform half-filled case where $\gamma_{ii} = 1$ for any value of U/t. For such a system, the density does not provide any information to discern between weakly and strongly correlated states. This difference is governed by the off-diagonal elements of the density matrix, representing the orbital overlaps and the competition between localization (strong correlation) and delocalization (weak correlation) of the electrons. For instance for the symmetric half-filled Hubbard dimer,

$$\hat{\gamma}^{\Psi} = \begin{bmatrix} 1 & \gamma^{\Psi}_{01} \\ \gamma^{\Psi}_{10} & 1 \end{bmatrix} \xrightarrow{U/t=0} \begin{bmatrix} 1 & 1 \\ 1 & 1 \end{bmatrix} \xrightarrow{U/t\to+\infty} \begin{bmatrix} 1 & 0 \\ 0 & 1 \end{bmatrix}, \tag{2.63}$$

where Ψ is the exact ground-state wavefunction of the dimer. As readily seen in Eq. (2.63), the off-diagonal elements depend on U/t. In SOFT, the repulsion between the electrons is effectively accounted for by a local potential, functional of the density. As a consequence, the off-diagonal elements remain unchanged when U varies, in contrast to the exact one-particle density matrix in the basis of sites,

$$\hat{\gamma}^{\Phi^{\mathrm{KS}}} = \begin{bmatrix} 1 & 1 \\ 1 & 1 \end{bmatrix}. \tag{2.64}$$

Because SOFT is a monoconfigurational method, it is also obvious that the double occupation $\langle \hat{n}_{\uparrow}\hat{n}_{\downarrow} \rangle$ cannot be reproduced directly from the KS determinant. However, any observable is in principle a functional of the density. According to the Hellmann–Feynman theorem in Eq. (2.45) for the double occupation, it comes, in KS-SOFT for the symmetric Hubbard dimer,

$$d = \frac{1}{2}\frac{\partial E_{\mathrm{Hxc}}(\mathbf{n})}{\partial U}, \tag{2.65}$$

and for the off-diagonal elements of the density matrix [see Eq. (2.40)],

$$\gamma_{01} = -\frac{1}{2}\left(\frac{\partial T_{\mathrm{s}}(\mathbf{n})}{\partial t} + \frac{\partial E_{\mathrm{c}}(\mathbf{n})}{\partial t}\right). \tag{2.66}$$

The numerical proof of these statements is given in Fig. 2.6 for the two-electron Hubbard dimer, for which a very accurate parametrization of the correlation energy has been proposed by Carrascal *et al.*

---

[1] In practice, as the theory is currently formulated, one cannot extract dynamical (time-dependent) properties but only static ground-state properties.

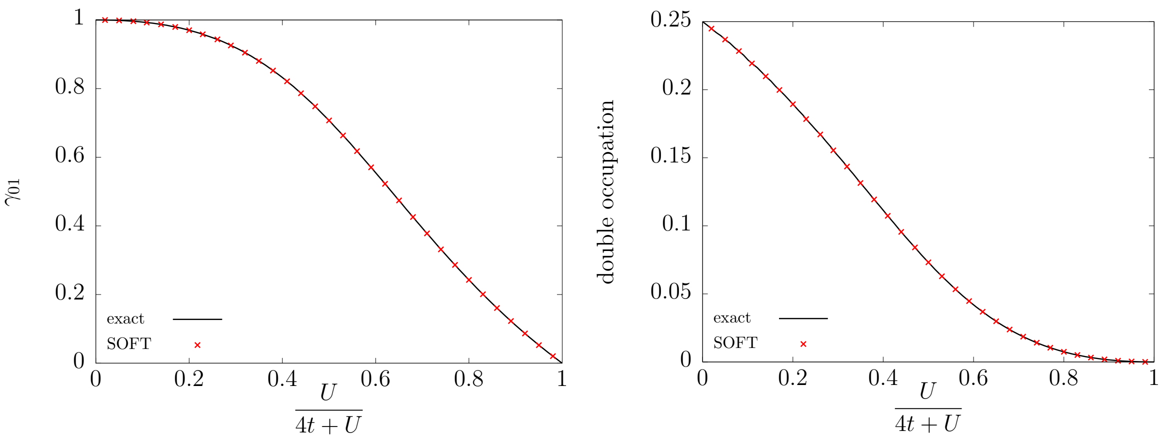

Figure 2.6: Exact off-diagonal element of the 1RDM (left) and double occupation (right) of the Hubbard dimer compared to Eqs. (2.66) and (2.65), respectively.

(see Eqs. (102)-(115) in Refs. [335, 358]). The derivatives of the Hxc energy functional with respect to U and t used to generate the curves in Fig. (2.6) are provided in the Appendix G.

Returning to the L-site uniform 1D model, the Hxc functional is simplified as follows in the mean-field approximation for the singlet ground state,

$$E_{\mathrm{Hxc}}(\mathbf{n}) \rightarrow \frac{U}{4}\sum_i n_i^2, \tag{2.67}$$

which is called the Hartree energy by physicists, so that the exchange contribution is equal to 0 for the Hubbard model. Indeed, for the one-band model, there is only one orbital per site, and given that the interaction is on-site, only electrons with opposite spin interact with each other. However, in quantum-chemical terminology, Eq. (2.67) is called the Hartree-exchange energy, which is decomposed as follows,

$$\begin{aligned} E_{\mathrm{Hx}}(\mathbf{n}) &= E_{\mathrm{H}}(\mathbf{n}) + E_{\mathrm{x}}(\mathbf{n}) = \frac{U}{4}\sum_i n_i^2, && (2.68)\\ E_{\mathrm{H}}(\mathbf{n}) &= \frac{U}{2}\sum_i n_i^2, && (2.69)\\ E_{\mathrm{x}}(\mathbf{n}) &= \frac{U}{4}\sum_i n_i^2 - E_{\mathrm{H}}(\mathbf{n}). && (2.70) \end{aligned}$$

The correlation part remains unknown, except in some particular cases, and reads

$$E_{\mathrm{c}}(\mathbf{n}) = F(\mathbf{n}) - T_{\mathrm{s}}(\mathbf{n}) - \frac{U}{4}\sum_i n_i^2. \tag{2.71}$$

2.2.2 Bethe Ansatz Local Density Approximation

In order to find approximations for the correlation energy in this context, it is useful to refer to a reference system for which exact (or highly accurate) solutions can be found. For instance, the uniform electron gas (UEG) has led to the famous local density approximation (LDA) in KS-DFT. Within LDA, the xc energy of any inhomogeneous system is approximated locally in space by that of the UEG. In the context of SOFT, the reference system is the one-dimensional uniform Hubbard model, for which an exact Bethe ansatz (BA) solution exists [320] in the thermodynamic limit. It is obtained from two coupled equations:

$$\begin{aligned}\rho(x) &= \frac{1}{2\pi} + \frac{\cos x}{\pi}\int_{-\infty}^{+\infty} \mathrm{d}y \frac{u/4}{(u/4)^2 + (y - \sin x)^2}\sigma(y), && (2.72)\\ \sigma(y) &= \frac{1}{\pi}\int_{-Q}^{+Q} \mathrm{d}x \frac{u/4}{(u/4)^2 + (y - \sin x)^2}\rho(x) - \frac{1}{\pi}\int_{-\infty}^{+\infty} \mathrm{d}y' \frac{u/2}{(u/2)^2 + (y - y')^2}\sigma(y'), && (2.73)\end{aligned}$$

where $n = N/L$ is the filling factor (the uniform density in the language of SOFT) and $u = U/t$ the dimensionless coupling constant. The parameter Q in Eq. (2.73) is determined from the normalization condition $\int_{-Q}^{+Q} \mathrm{d}x\rho(x) = n$ while $\sigma(y)$ is normalized according to $\int_{-\infty}^{+\infty} \mathrm{d}y\sigma(y) = n/2$. The ground-state per-site energy is then given by

$$e^{\mathrm{BA}}(n \leqslant 1, u) = -2t \int_{-Q}^{+Q} \mathrm{d}x\rho(x)\cos x. \tag{2.74}$$

In some particular cases, a simpler analytical expression can be obtained. In the noninteracting case ($u = 0$), the ground-state per-site energy reduces to the noninteracting per-site kinetic energy,

$$e^{\mathrm{BA}}(n \leqslant 1, u = 0) = t_{\mathrm{s}}^{\mathrm{BA}}(n \leqslant 1) = -\frac{4t}{\pi}\sin\left(\frac{n\pi}{2}\right) \tag{2.75}$$

and for any positive value of u at half-filling ($n = 1$), the system becomes a Mott insulator with per-site energy

$$e^{\mathrm{BA}}(n = 1, u) = -4t \int_{0}^{+\infty} \mathrm{d}x \frac{J_0(x)J_1(x)}{x\,(1 + \exp(xu/2))}, \tag{2.76}$$

where $J_0(x)$ and $J_1(x)$ are zero- and first-order Bessel functions. The two metallic regions $n < 1$ and $n > 1$ are connected by a hole-particle symmetry relation that reads

$$e^{\mathrm{BA}}(n > 1, u) = e^{\mathrm{BA}}(2 - n, u) + U(n - 1). \tag{2.77}$$

Regarding the expression of the correlation energy,

$$e_{\rm c}^{\rm BA}(n,u) = e^{\rm BA}(n,u) - e^{\rm BA}(n,u=0) - \frac{U}{4}n^2, \tag{2.78}$$

where $(U/4)n^2$ is the per-site Hx energy, and using Eq. (2.77), it comes

$$e_{\rm c}^{\rm BA}(2-n,u) = e_{\rm c}^{\rm BA}(n,u), \tag{2.79}$$

so that the per-site correlation energy is invariant under hole-particle symmetry.

In order to have an analytical expression for any density regime, Lima *et al.* proposed a local density approximation based on the BA. This so-called *Bethe ansatz local density approximation* (BALDA) [359–361] leads to the following per-site energy expression,

$$e^{\rm BALDA}(U,n\leq 1) = \frac{-2t\beta(U/t)}{\pi}\sin\left(\frac{\pi n}{\beta(U/t)}\right), \tag{2.80}$$

where the function $\beta(U/t)$ is determined by solving

$$\frac{-2\beta(U/t)}{\pi}\sin\left(\frac{\pi}{\beta(U/t)}\right) = -4\int_0^\infty \frac{dx}{x}\frac{J_0(x)J_1(x)}{1+\exp\left(\frac{U}{2t}x\right)}. \tag{2.81}$$

This approximation is exact in the thermodynamic limit for $U/t = 0$ and $U/t \to +\infty$ at any filling, and for any U/t at half-filling ($n = 1$). Plugging Eq. (2.80) into Eq. (2.78) gives the BALDA per-site correlation energy,

$$e_{\rm c}^{\rm BALDA}(n,u) = e^{\rm BALDA}(n,u) - e^{\rm BALDA}(n,u=0) - \frac{U}{4}n^2, \tag{2.82}$$

which has been shown to give very accurate density and energy profiles [359–361]. Promising extensions have also been developed, including the spin-dependent BALDA [362] and its fully numerical formulation [363, 364], with application on both the repulsive [365, 366] ($U > 0$) and attractive [367, 368] ($U < 0$) Hubbard models.

In spite of the aforementioned performances of the BALDA approximation, it depicts a wrong behaviour around $U = 0$ away from half-filling, which appears to be important for the calculation of the double occupation in Eq. (2.65). Indeed, since $\beta(0) = 2$ and $\partial\beta(U/t)/\partial U|_{U=0} = -\pi/(8t)$ it comes, for $n \leq 1$,

$$\left.\frac{\partial e_{\mathrm{c}}^{\mathrm{BA}}(n)}{\partial U}\right|_{U=0} = \frac{1}{4}\left[\sin\left(\frac{\pi n}{2}\right) - n^2\right] - \frac{n\pi}{8}\cos\left(\frac{\pi n}{2}\right), \tag{2.83}$$

and, consequently,

$$\frac{\partial}{\partial n}\left.\frac{\partial e_{\mathrm{c}}^{\mathrm{BA}}(n)}{\partial U}\right|_{U=0} = \frac{n\pi^2}{16}\sin\left(\frac{\pi n}{2}\right) - \frac{n}{2}. \tag{2.84}$$

As readily seen from Eqs. (2.83) and (2.84), both BALDA correlation energy and potential will vary linearly with U in the weakly correlated regime for $n < 1$, which is of course unphysical. The manifestation of this unphysical behaviour on the double occupation will be illustrated latter in Chap. 3 [see Fig. 3.16] showing that, away from half-filling, the BALDA approximation within SOFT systematically underestimates the double occupation in the weakly-correlated regime.

2.2.3 Derivative discontinuity and density-driven Mott transition

Interestingly, the exact correlation potential $\partial e_{\mathrm{c}}(n)/\partial n$ should depict a discontinuity at half-filling, which is related to the opening of the charge gap [359]. It can be shown by looking at the atomic limit ($t = 0$), where the fully-interacting L-site uniform Hubbard Hamiltonian reads,

$$\hat{H}(n) = \hat{U} + v(n)\sum_i \hat{n}_i, \tag{2.85}$$

with $v(n)$ chosen to reproduce the uniform density profile with density n. Starting from the half-filling situation (L electrons or, equivalently, $n = 1$), we can add an electron in order to investigate the behavior of $v(n)$ when $n \rightarrow 1^+$. In order to have a total number of electrons varying continuously from L to $L+1$ or, equivalently, $1 < n < (L+1)/L$, the L- and $(L+1)$-electron ground states of $\hat{H}(n)$ must be degenerate, thus leading to the following condition,

$$Lv(n) = (L+1)v(n) + U, \tag{2.86}$$

or, equivalently, $v(n) = -U$. Therefore we conclude that, in the thermodynamic limit ($L \rightarrow +\infty$),

$$v(n)|_{n=1^+} = -U. \tag{2.87}$$

On the other hand, if we consider the removal of an electron, the density can vary continuously in the range $(L-1)/L < n < 1$ if the $(L-1)$- and L-electron ground states of $\hat{H}(n)$ are degenerate, thus leading to the condition $(L-1)v(n) = Lv(n)$ and, consequently,

$$v(n)\big|_{n=1^-} = 0. \tag{2.88}$$

According to Eqs. (2.87) and (2.88), the physical potential is discontinuous at half-filling. Turning to the KS Hamiltonian with ground-state uniform density n (and $t = 0$),

$$\hat{H}^{\mathrm{KS}}(n) = v^{\mathrm{KS}}(n)\sum_i \hat{n}_i, \tag{2.89}$$

we can similarly show that, in contrast to the interacting case, the KS potential has no discontinuity at $n = 1$,

$$v^{\mathrm{KS}}(n)\big|_{n=1^+} = v^{\mathrm{KS}}(n)\big|_{n=1^-} = 0. \tag{2.90}$$

Consequently, we recover the discontinuous behavior of the correlation potential at half-filling:

$$\left.\frac{\partial e_{\mathrm{c}}(n)}{\partial n}\right|_{n=1^+} = \left.\left(v^{\mathrm{KS}}(n) - v(n) - \frac{U}{2}n\right)\right|_{n=1^+} = +U/2, \tag{2.91}$$

and

$$\left.\frac{\partial e_{\mathrm{c}}(n)}{\partial n}\right|_{n=1^-} = \left.\left(v^{\mathrm{KS}}(n) - v(n) - \frac{U}{2}n\right)\right|_{n=1^-} = -U/2. \tag{2.92}$$

In contrast to standard LDA, which is unable to describe Mott-Hubbard phenomena in realistic materials [369, 370], BALDA can model such a discontinuity by construction in the one-dimensional Hubbard model. Despite this extremely appealing feature, it may lead to convergence problems when the density gets close to half-filling. Solutions have been proposed by using finite temperature [348] or *ad-hoc* parameters [345, 346, 371]. A similar derivative discontinuity, featuring the well-known discontinuous jump in the xc potential when crossing an integral number of electron[2] [130, 158], also arises in the Anderson junction model within SOFT [372–374]. This model, consisting of two macroscopic leads coupled to an Anderson impurity, is used to describe the electron transport through a molecular junction.

---

[2] This derivative discontinuity will be discussed in Chap. 5 in detail

2.3 Single-impurity Anderson model

In this section, the single impurity Anderson model [375] (SIAM), employed to describe a magnetic impurity in a metallic host, is introduced. It is used, for instance, to model impurities in a semiconductor [376], molecular junctions [372–374], and the single-electron transistor (quantum dot coupled to two decoupled metallic leads) [377].

The SIAM Hamiltonian is given in (discretized) real space (i.e. in the basis of *sites*) as follows:

$$\hat{H}^{\text{SIAM}} = -t\sum_{\sigma}\sum_{i=1}^{L}\left(\hat{c}^{\dagger}_{i\sigma}\hat{c}_{i+1\sigma} + \text{h.c.}\right) + V\sum_{\sigma}\left[\left(\hat{c}^{\dagger}_{1\sigma}\hat{c}_{d\sigma} + \hat{c}^{\dagger}_{L\sigma}\hat{c}_{d\sigma}\right) + h.c.\right] + U\hat{n}_{0\uparrow}\hat{n}_{d\downarrow} + \varepsilon_d\hat{n}_d, \quad (2.93)$$

where the impurity is denoted by d (referring to a d-like orbital) with $\hat{n}_{d\sigma} = \hat{c}^{\dagger}_{d\sigma}\hat{c}_{d\sigma}$ and $\hat{n}_d = \sum_{\sigma}\hat{n}_{d\sigma}$, and is coupled to a noninteracting bath. The term "h.c." stands for "Hermitian conjugate". Note that this particular form of the SIAM Hamiltonian will be shown useful when compared to the SOET Hamiltonian in the next chapter.

By applying the canonical transformation of Eq. (2.8) and using periodic boundary condition $\hat{c}_{L+1\sigma} = \hat{c}_{1\sigma}$, the usual SIAM Hamiltonian expression in k-space is recovered,

$$\hat{H} = \sum_{k\sigma}\varepsilon_k\hat{c}^{\dagger}_{k\sigma}\hat{c}_{k\sigma} + \varepsilon_d\hat{n}_d + U\hat{n}_{d\uparrow}\hat{n}_{d\downarrow} + \sum_{k\sigma}\left(V_k\hat{c}^{\dagger}_{k\sigma}\hat{c}_{d\sigma} + h.c.\right), \quad (2.94)$$

where ε_k is the dispersion energy of the metallic band, like in the tight-binding model $[\varepsilon_k = -2t\cos(k)]$, ε_d is the impurity level energy, and V_k is the coupling term between the interacting impurity and the noninteracting bath,

$$V_k = 2Ve^{-ik/2}\cos(k/2)/\sqrt{L}. \quad (2.95)$$

Note that $\varepsilon_d = -U/2$ in the symmetric case. The impurity Anderson model is particularly useful to model impurities, so that it plays a major role in embedding approaches in condensed matter physics [378], like the *dynamical mean-field theory* (DMFT) which is one of the most established method for strongly correlated materials. In this approach, the physical Hamiltonian is mapped onto a SIAM, in analogy with the KS system in DFT.

2.4 Embedding techniques

In this section, two embedding theories are described: the *dynamical mean-field theory* (DMFT), formulated with Green's function, and the frequency-independent *density matrix embedding theory*

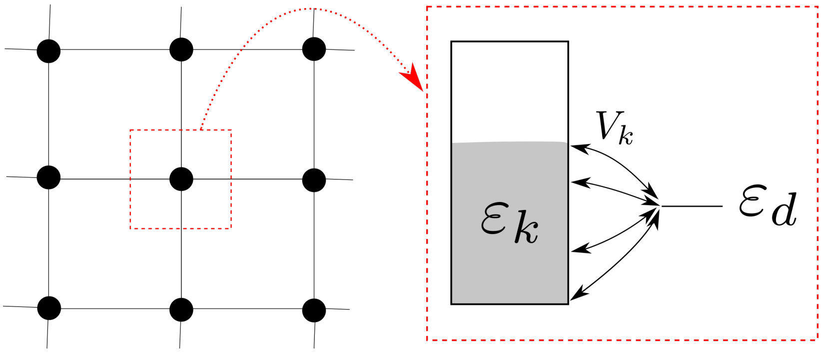

Figure 2.7: Hubbard site mapped onto a single Anderson impurity.

(DMET). They differ from the hybrid approaches described in Sec. 1.3 in a sense that they were originally formulated to solve translational invariant systems by performing a mapping onto a smaller subsystem, called the embedded system. It is worth mentioning that other promising embedding techniques exist, in particular the recently developed *self-energy embedding theory* (SEET) by Zgid and co-workers [379–384] which is also formulated in a Green's function formalism.

2.4.1 Dynamical Mean Field Theory

Dynamical mean-field theory (DMFT) [369, 378, 385–391] relies on the mapping of the fully correlated lattice problem [Eq. (2.16)] onto a correlated impurity model. In the single-site DMFT, this model is nothing else but the SIAM [Eq. (2.94)]. The idea is to separate the lattice and the impurity problems and to solve them self-consistently as follows: (i) in the impurity problem, the interacting electrons on the impurity are coupled to an effective bath determined by the lattice problem [illustrated in Fig. 2.7] (ii) the lattice problem is solved with a Green's function approach using the self-energy obtained from the impurity problem. Hence, (i) and (ii) are coupled and generate a self-consistent cycle, illustrated in Fig. 2.8 and discussed in the following. This method has been able to describe the Mott-insulator transition as well as the Kondo peak [369, 387], and is thus able to treat strongly correlated systems. First, we describe how the impurity problem is solved. Starting from the noninteracting SIAM Hamiltonian $\hat{H}^{(0)}$ [Eq. (2.94) with $U = 0$] given in matrix representation,

$$\left[\hat{H}^{(0)}\right] = \mathbf{H}^{(0)} = \begin{bmatrix} \varepsilon_d & V_{k_1} & \cdots & \cdots & V_{k_L} \\ V_{k_1}^* & \varepsilon_{k_1} & & 0 & \\ \vdots & & \ddots & & \\ \vdots & 0 & & \ddots & \\ V_{k_L}^* & & & & \varepsilon_{k_L} \end{bmatrix}, \tag{2.96}$$

we define the noninteracting Green's function, solution of the following equation:

$$\left(\omega\mathbb{1} - \mathbf{H}^{(0)}\right)\mathbf{G}^{(0)}(\omega) = \mathbb{1}, \tag{2.97}$$

leading to $\mathbf{G}^{(0)}(\omega) = (\omega\mathbb{1} - \mathbf{H}^{(0)})^{-1}$. The noninteracting Green's function of the impurity site reads [378, 392]:

$$G^{(0)}_{dd}(\omega) \equiv \mathcal{G}_0(\omega) = \frac{1}{\omega - \varepsilon_d - \Delta(\omega)}, \tag{2.98}$$

where the usual notation $\mathcal{G}_0(\omega)$ is used, and

$$\Delta(\omega) = \sum_k \frac{|V_k|^2}{\omega - \varepsilon_k} \tag{2.99}$$

is the frequency-dependent "host-impurity" hybridization function. One can then compute its associated spectral function, related to the imaginary part of the impurity Green's function, where the frequency is shifted in the complex plane by an infinitesimal constant $\eta > 0$ (thus giving the so-called "retarded" Green's function):

$$\begin{aligned} A(\omega) = -\frac{1}{\pi}\mathrm{Im}\left[\mathcal{G}_0(\omega + \mathrm{i}\eta)\right] &= -\frac{1}{\pi}\mathrm{Im}\left(\frac{1}{\omega - \varepsilon_d - \mathrm{Re}[\Delta(\omega+\mathrm{i}\eta)] - \mathrm{i}\mathrm{Im}[\Delta(\omega+\mathrm{i}\eta)]}\right) \\ &= -\frac{1}{\pi}\frac{\mathrm{Im}[\Delta(\omega+\mathrm{i}\eta)]}{\left(\omega - \varepsilon_d - \mathrm{Re}[\Delta(\omega+\mathrm{i}\eta)]\right)^2 + \left(\mathrm{Im}[\Delta(\omega+\mathrm{i}\eta)]\right)^2}. \end{aligned} \tag{2.100}$$

The real part of the retarded hybridization function $\Delta(\omega + \mathrm{i}\eta)$,

$$\begin{aligned} \mathrm{Re}[\Delta(\omega+\mathrm{i}\eta)] &= \sum_k \frac{(\omega - \varepsilon_k)|V_k|^2}{(\omega-\varepsilon_k)^2 + \eta^2} \\ &\xrightarrow{\eta\to 0^+} \sum_k \frac{|V_k|^2}{\omega - \varepsilon_k}, \end{aligned} \tag{2.101}$$

engenders a shift of the peak at position ε_d in the spectral function, while its imaginary part [378][3],

$$\begin{aligned} \Gamma(\omega) \equiv -\mathrm{Im}[\Delta(\omega+\mathrm{i}\eta)] &= \sum_k \frac{\eta|V_k|^2}{(\omega-\varepsilon_k)^2 + \eta^2} \\ &\xrightarrow{\eta\to 0} \pi\sum_k |V_k|^2\delta(\omega - \varepsilon_k), \end{aligned} \tag{2.102}$$

is responsible for the broadening of the peak, related to the life time of the states in the continuum. Note that η also plays a role in practice, as it avoids singularity in the Green's function by moving

---

[3] The limit of Eq. (2.102) comes from $\lim_{\eta\to 0}\frac{\eta}{\pi(x^2+\eta^2)} = \delta(x)$ where $\delta(x)$ is the delta function

its poles away from the real frequency axis. As an illustration to the noninteracting single-impurity Anderson model, one can imagine a single orbital (with orbital energy ε_d) in real space coupled to all the other orbitals in k-space by a hopping V_k (see Fig. 2.7), for which the k-dependence is usually neglected.

Then, let us switch on the interaction U. In analogy with the Hubbard model for U/t, the ratio U/Γ denotes the competition between the impurity to be either uncoupled or hybridized with the bath. The interacting Anderson impurity model can be solved using many-body approaches (so-called impurity-solver) such as exact diagonalization (ED) [393], Iterative Perturbation Theory (IPT) [385, 386, 394], Quantum Monte Carlo (QMC) [395–399], CISD [400], or DMRG [401, 402], thus leading to the impurity Green's function:

$$G_{dd}(\omega) \equiv G_{\text{imp}}(\omega) = \frac{1}{\omega - \varepsilon_d - \Delta(\omega) - \Sigma(\omega)}. \tag{2.103}$$

Note that in contrast to DFT+U where coulomb interaction is treated in static mean-field theory, the interactions are treated explicitly in DMFT. Indeed, the impurity Green's function contains many-body effects, accounted for by the impurity (or local) self-energy obtained from the Dyson equation,

$$\Sigma(\omega) = \mathcal{G}_0^{-1}(\omega) - G_{\text{imp}}^{-1}(\omega), \tag{2.104}$$

which will be used in step (ii).

The purpose of step (ii) is to solve the lattice problem (i.e. the Hubbard model). This is usually done by computing the interacting lattice Green's function in k-space:

$$G_k(\omega) = \frac{1}{\omega - \varepsilon_k - \Sigma_k(\omega)}, \tag{2.105}$$

where the self-energy $\Sigma_k(\omega)$ is momentum-dependent [403], except in the case of infinite dimension where the k-dependence disappears [385, 386]. Then, by using Fourier transform, the interacting local Green's function (in the basis of sites) is obtained:

$$G_{ii}(\omega) \;=\; \frac{1}{L}\sum_k G_k(\omega) = \frac{1}{L}\sum_k \frac{1}{\omega - \varepsilon_k - \Sigma_k(\omega)}. \tag{2.106}$$

Of course, the k-dependent self-energy is unknown, otherwise there would be no point in mapping the Hubbard model onto an impurity one. The DMFT approximation is first to neglect this k-dependence

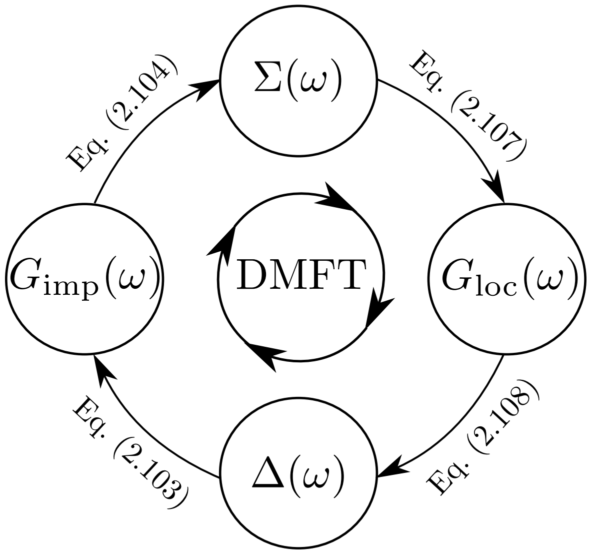

Figure 2.8: DMFT self-consistent cycle, usually initialized by setting $\Sigma(\omega) = 0$.

(such that it becomes exact in the infinite dimension [385, 386]), thus leading to

$$G_{ii}(\omega) \equiv G_{\text{loc}}(\omega) = \frac{1}{L}\sum_k \frac{1}{\omega - \varepsilon_k - \Sigma(\omega)}, \tag{2.107}$$

and then to require the local Green's function in Eq. (2.107) to be equal to the impurity one of the Anderson model,

$$\begin{aligned} G_{\text{loc}}(\omega) &= G_{\text{imp}}(\omega) \\ \frac{1}{L}\sum_k \frac{1}{\omega - \varepsilon_k - \Sigma(\omega)} &= \frac{1}{\omega - \varepsilon_d - \Delta(\omega) - \Sigma(\omega)}, \end{aligned} \tag{2.108}$$

where $\Sigma(\omega)$ is the self-energy obtained from Eq. (2.104). By solving the DMFT condition in Eq. (2.108), which is rigorously possible only for an infinite bath, one gets a new hybridization function $\Delta(\omega)$. This function describes a modified bath for the effective impurity model, that can be solved again to get the impurity interacting Green's function $G_{\text{imp}}(\omega)$ and the self-energy $\Sigma(\omega)$. These cycles continue until the self-energy does not change or, equivalently, until the calculated local Green's function is equal to the impurity one. This self-consistent cycle is illustrated in Fig. 2.8. The idea behind the equality in Eq. (2.108) is to map the physical system (represented by G_{loc}) onto a SIAM (represented by G_{imp}) where the coupling between the impurity and the noninteracting bath is optimized through the calculation of the hybridization function $\Delta(\omega)$.

Finally, DMFT suffers from limitations due to the assumption that the self-energy is purely local.

Extensions of DMFT to include nonlocal correlations are possible by considering an impurity cluster instead of just a single impurity site [329, 399, 404–409], or by combining DMFT with GW [410–414] or DFT [369, 415]. Regarding the latter approach, the double counting problem is usually removed empirically [416, 417]. For the time being, DMFT is mostly employed in condensed matter physics, although its generalization to quantum chemistry is not excluded [400].

2.4.2 Density-Matrix Embedding Theory

The basic idea of an embedding procedure is to extract properties of the physical system from a subsystem. DMET belongs to this scheme, as it separates the system into multiple fragments, each of them embedded in an approximate bath that accounts for the entanglement between itself and the rest of the system. The idea of the DMET relies on the Schmidt decomposition (see Sec. 1.1.8 on the DMRG), which is briefly reviewed here for clarity, with some different notations. Suppose that the system is divided into a *fragment* F and the rest of the system called the *environment*, E. The Hilbert space $\mathcal{H}$ of the system is then the tensor product of the ones corresponding to F and to E, $\mathcal{H} = \mathcal{H}_F \otimes \mathcal{H}_E$. The size of $\mathcal{H}_F$ ($\mathcal{H}_E$) is $N_F = 4^{L_F}$ ($N_E = 4^{L_E}$), and we denote $\{|F_i\rangle\}_i$ ($\{|E_j\rangle\}_j$) a basis of many-body states. L_F and L_E denote the number of orbitals in the fragment and in the environment, respectively. This decomposition leads to the following exact ground-state wavefunction expression:

$$|\Psi_0\rangle = \sum_i^{N_F} \sum_j^{N_E} C_{ij} |F_i\rangle |E_j\rangle, \tag{2.109}$$

which can be further simplified by applying a singular value decomposition to C_{ij},

$$\begin{aligned} |\Psi_0\rangle &= \sum_i^{N_F} \sum_j^{N_E} \sum_\alpha^{\min(N_F,N_E)} \tilde{U}_{i\alpha} \lambda_\alpha \tilde{V}^\dagger_{\alpha j} |F_i\rangle |E_j\rangle \\ &= \sum_\alpha^{N_F} \lambda_\alpha |F_\alpha\rangle |B_\alpha\rangle. \end{aligned} \tag{2.110}$$

Note that $N_F < N_E$ has been assumed in the second equality of Eq. (2.110). $\tilde{U}_{i\alpha}$ ($\tilde{V}^\dagger_{\alpha j}$) rotates the many-body basis $\{|F_i\rangle\}_i$ ($\{|E_j\rangle\}_j$) into the new many-body basis $\{|F_\alpha\rangle\}_\alpha$ ($\{|B_\alpha\rangle\}_\alpha$),

$$\sum_i^{N_E} \tilde{U}^\dagger_{i\alpha} |F_i\rangle = |F_\alpha\rangle \qquad \left(\sum_j^{N_E} \tilde{V}^\dagger_{\alpha j} |E_j\rangle = |B_\alpha\rangle \right), \tag{2.111}$$

so-called the *fragment* (*bath*) states. It is clear from Eq. (2.110) that the number of states to be considered has been reduced to N_F bath states for the environment, while the number of states remains unchanged for the fragment. The projected Hamiltonian onto this new many-body basis reads

$$\hat{H}' = \hat{P}\hat{H}\hat{P}, \tag{2.112}$$

where $\hat{P} = \sum_{\alpha\beta}^{N_F} |F_\alpha B_\beta\rangle\langle F_\alpha B_\beta|$ is the projector onto the Schmidt basis of dimension $(N_F)^2$. It is shown that the ground-state wavefunction remains invariant under this projection,

$$\begin{aligned}
\hat{P}|\Psi_0\rangle &= \sum_{\alpha\beta}^{N_F} |F_\alpha B_\beta\rangle\langle F_\alpha B_\beta|\Psi_0\rangle \\
&= \sum_{\alpha\beta}^{N_F} |F_\alpha B_\beta\rangle\langle F_\alpha B_\beta| \sum_{\gamma}^{N_F} \lambda_\gamma |F_\gamma B_\gamma\rangle \\
&= \sum_{\gamma}^{N_F} \lambda_\gamma |F_\gamma B_\gamma\rangle = |\Psi_0\rangle
\end{aligned} \tag{2.113}$$

where $|F_\alpha B_\beta\rangle$ are orthonormal, such that $\langle F_\alpha B_\beta|F_\gamma B_\gamma\rangle = \delta_{\alpha\gamma}\delta_{\beta\gamma}$. As a consequence, the embedded Hamiltonian shares the same ground-state energy with the physical one,

$$\begin{aligned}
H|\Psi_0\rangle &= E_0|\Psi_0\rangle, \\
\rightarrow PHP|\Psi_0\rangle &= PE_0P|\Psi_0\rangle, \\
\rightarrow H'|\Psi_0\rangle &= E_0|\Psi_0\rangle.
\end{aligned} \tag{2.114}$$

According to Eq. (2.114), the ground-state solution of a small embedded problem (fragment + bath) is the same as the one of the full system. This embedding is exact, but it requires the *a priori* knowledge of the exact wavefunction of the full problem, which is of course unknown. The idea of DMET is to construct an approximate one-electron projection operator, thus leading to single-particle bath states $|B_\alpha\rangle$ instead of the many-body states in Eq. (2.111). The explicit interaction will then be added on the fragment sites, such that the fragment states will remain many-body states. The embedding Hamiltonian is constructed from this approximate projection operator, as described in the following.

In this section, I will focus on the original formulation of DMET, where only one fragment (that can contain multiple impurities) is considered, with application to lattice systems with translational invariance [418]. For clarity, I will describe the theory for the uniform L-site one-dimensional Hubbard model,

$$\hat{H} = -t \sum_{\langle ij \rangle \sigma}^{L} \left(\hat{c}_{i\sigma}^{\dagger} \hat{c}_{j\sigma} + \hat{c}_{j\sigma}^{\dagger} \hat{c}_{i\sigma} \right) + U \sum_{i}^{L} \hat{n}_{i\uparrow} \hat{n}_{i\downarrow}, \tag{2.115}$$

decomposed into a fragment F and an environment E with $L_F < L_E$. Note that several equivalent derivations of DMET are available in the literature [418–424]. In addition, DMET has different formulations: the interacting bath formulation and the noninteracting one. Besides, the convergence criteria, which will be described in the following, is also not uniquely defined. In this thesis, we will focus on the noninteracting bath formulation. The derivations of Refs. [420, 424] will be used. The starting point in DMET is to determine the low-level wavefunction $|\Phi_0(u)\rangle$ which is used to construct the approximate bath orbitals. It is obtained by searching for the ground state of the following one-particle Hamiltonian,

$$\hat{h} = \hat{T} + \hat{u} = -t \sum_{\langle ij \rangle \sigma}^{L} \left(\hat{c}_{i\sigma}^{\dagger} \hat{c}_{j\sigma} + \hat{c}_{j\sigma}^{\dagger} \hat{c}_{i\sigma} \right) + \sum_{ij\sigma}^{L} u_{ij} \left(\hat{c}_{i\sigma}^{\dagger} \hat{c}_{j\sigma} + \hat{c}_{j\sigma}^{\dagger} \hat{c}_{i\sigma} \right), \tag{2.116}$$

where $\hat{u}$ is a one-body operator that contains the so-called *correlation* potential $\{u_{ij}\}_{ij}$. The 1RDM of $|\Phi_0(u)\rangle$ is idempotent and will be denoted ρ. To construct the projector P, one has to apply the Schmidt decomposition to $\Phi_0(u)$. In the following, we show how this is done in practice, following the lines of Ref. [424]. First, we diagonalize the 1RDM of $\Phi_0(u)$ to obtain the unitary transformation matrix D of size $(L \times L)$, such that

$$[\hat{h}] = D[\hat{\epsilon}]D^{\dagger}, \quad \rho = DnD^{\dagger}, \tag{2.117}$$

where $[\hat{\epsilon}]$ and n are $(L \times L)$ diagonal matrices. The diagonal elements of the matrix n are either 1 (occupied spin-orbitals) or 0 (empty spin-orbitals), and the number of occupied states will be denoted n_{occ}. We split D into its fragment and environment blocks,

$$D = \begin{bmatrix} D_F \\ D_E \end{bmatrix}, \tag{2.118}$$

where D_F is a $(L_F \times L)$ rectangular matrix. D_F is further decomposed into

$$D_F = \begin{bmatrix} D_F^{\text{occ}} & D_F^{\text{unocc}} \end{bmatrix}, \tag{2.119}$$

where D_F^{occ} is of size $(L_F \times n_{\mathrm{occ}})$. Then, a singular value decomposition is performed on D_F^{occ},

$$D_F^{\mathrm{occ}} = \tilde{U}\overline{D}_F^{\mathrm{occ}}\tilde{V}^\dagger, \tag{2.120}$$

where $\tilde{U}$ and $\tilde{V}$ are $(L_F \times L_F)$ and $(n_{\mathrm{occ}} \times n_{\mathrm{occ}})$ unitary matrices, respectively, and

$$\overline{D}_F^{\mathrm{occ}} = \{\sqrt{n^0}, 0\}, \tag{2.121}$$

is a $(L_F \times n_{\mathrm{occ}})$ diagonal matrix, with $\sqrt{n^0}$ of size $(L_F \times L_F)$. Alternatively, one can also decompose V into

$$\tilde{V} = \begin{bmatrix} \tilde{V}_F & \tilde{V}_E \end{bmatrix}, \tag{2.122}$$

where $\tilde{V}_F$ is a $(n_{\mathrm{occ}} \times L_F)$ rectangular matrix, to get the diagonal matrix $\sqrt{n^0}$,

$$D_F^{\mathrm{occ}} = \tilde{U}\sqrt{n^0}\tilde{V}_F^\dagger. \tag{2.123}$$

Note that if the fragment contains only one site, $\tilde{U}$ and $\sqrt{n^0}$ become real numbers while D_F^{occ} and $\tilde{V}_F^\dagger$ are column vectors of size n_{occ}. Finally, still following Ref. [424], the approximate projection onto the original orbital basis is given by P of size $(L \times 2L_F)$:

$$P = \begin{bmatrix} \mathbb{1} & \\ & C_B C_F^\dagger \end{bmatrix}, \tag{2.124}$$

where $\mathbb{1}$ is a $(L_F \times L_F)$ identity matrix and $C_B C_F^\dagger$ is a $(L_E \times L_F)$ rectangular matrix which is the transformation from the environment to the bath, given by

$$C_F = \tilde{U}, \quad C_B = \frac{D_E^{\mathrm{occ}} V_F}{\sqrt{1 - n^0}}. \tag{2.125}$$

As readily seen in Eq. (2.124), the transformation of the one-particle fragment states in the original basis is the identity. The fragment is therefore invariant under this projection. In the following, we will show that the electron-electron repulsion is explicitly treated in the fragment, such that the fragment part of the embedded Hamiltonian corresponds to the physical Hamiltonian, which is of course not the case for the bath.

Once this approximate one-electron projector P is obtained or, equivalently, once the Schmidt decomposition of $|\Phi_0(u)\rangle$ is performed, the embedded Hamiltonian can be determined. In the noninteracting bath formulation, the two-electron repulsion is only on the impurity sites, such that

$$\hat{H}^{\text{imp}} \quad = \quad \hat{h}^{\text{emb}} + U \sum_{i}^{L_F} \hat{n}_{i\uparrow}\hat{n}_{i\downarrow}. \tag{2.126}$$

Let us look at the derivation of the one-body operator $\hat{h}^{\text{emb}}$. In DMET, an effective one-body Hamiltonian, corresponding to the one in Eq. (2.116) but where the correlation potential acts on the environment only, is defined as

$$\hat{h}^{\text{eff}} = \hat{T} + \sum_{ij \in E,\sigma}^{L_E} u_{ij} \left(\hat{c}^{\dagger}_{i\sigma}\hat{c}_{j\sigma} + \hat{c}^{\dagger}_{j\sigma}\hat{c}_{i\sigma} \right). \tag{2.127}$$

This one-body Hamiltonian is then projected onto the fragment+bath representation by using the one-electron projection operator as follows,

$$\hat{h}^{\text{emb}} = \hat{P}^{\dagger}\hat{h}^{\text{eff}}\hat{P} = \sum_{ij\sigma}^{L_F+L_B} \tilde{h}_{ij} \left(\hat{c}^{\dagger}_{i\sigma}\hat{c}_{j\sigma} + \hat{c}^{\dagger}_{j\sigma}\hat{c}_{i\sigma} \right). \tag{2.128}$$

Finally, the on-site two-electron repulsion operator is simply added to $\hat{h}^{\text{emb}}$ to recover the embedded impurity problem of Eq. (2.126). This is why the correlation potential in Eq. (2.127) has to act on the environment only in order to avoid double counting effects. This correlation potential is determined self-consistently to enforce a particular matching condition between the low-level wavefunction $|\Phi_0(u)\rangle$ and the high-level one $|\Psi^{\text{imp}}\rangle$. The latter is obtained by solving the many-body problem in Eq. (2.126), containing $2L_F$ electrons [422], by a high-level method (typically, FCI or DMRG). Note that the correlation potential in Eq. (2.116) is involved in the determination of the approximate bath orbitals. Hence, it is implicitly taken into account in the embedded one-body part of Eq. (2.126), as well as in $|\Psi^{\text{imp}}\rangle$.

In the original DMET paper [418], the correlation potential was optimized until the following two 1RDM are matched. (i) The density matrix of the embedded problem,

$$\rho^{\text{imp}}_{ij} = \sum_{\sigma} \langle \hat{c}^{\dagger}_{i\sigma}\hat{c}_{j\sigma} \rangle_{\Psi^{\text{imp}}}, \tag{2.129}$$

and (ii) the projection of the density matrix of the reference problem, described by $|\Phi_0(u)\rangle$, onto the embedded subspace,

$$\rho^{\text{emb}} = \hat{P}^{\dagger}\rho\hat{P}. \tag{2.130}$$

Hence the name “density-matrix” embedding theory.

In order to perform such a matching, the correlation potential has to minimize the so-called cost function [420, 422]:

$$\min_{u} \text{CF}_x(u), \tag{2.131}$$

where x denotes different definitions, which are explained in the following. In the original formulation, the cost function is computed by summing the difference between all density matrix elements of Eqs. (2.129) and (2.130),

$$\text{CF}_{\text{full}}(u) = \sum_{ij}^{L_F+L_B} |\rho_{ij}^{\text{imp}} - \rho_{ij}^{\text{emb}}(u)|^2, \tag{2.132}$$

or, alternatively, in the fragment only [419, 422, 425],

$$\text{CF}_{\text{imp}}(u) = \sum_{ij}^{L_F} |\rho_{ij}^{\text{imp}} - \rho_{ij}^{\text{emb}}(u)|^2. \tag{2.133}$$

Note that the minimization of these above cost functions does usually not reach 0, as the mean-field density matrix $\rho^{\text{emb}}(u)$ is idempotent, while the high-level one ρ^{imp} is not, in principle.

This representability issue has been highlighted by Tsuchimochi *et al.* [425]. In their work, they decided to approximate the bath by the antisymmetrized geminal power correlated wavefunction (instead of Hartree-Fock like the original formulation of the theory [418]), from which any N-representable density matrix can be constructed [426], thus allowing for an exact matching between the low-level and high-level density matrices in DMET. The approximate bath states also remain many-body states. Alternatively, the matching can be performed on the diagonal of density matrices [420] on the fragment, leading to

$$\text{CF}_{\text{diag}}(u) = \sum_{i}^{L_F} |\rho_{ii}^{\text{imp}} - \rho_{ii}^{\text{emb}}(u)|^2, \tag{2.134}$$

or even by recovering the proper number of electrons by using a global chemical potential only [427], instead of the correlation potential. An illustration of the whole DMET procedure is given in Fig. 2.9 for the Hubbard model with one impurity.

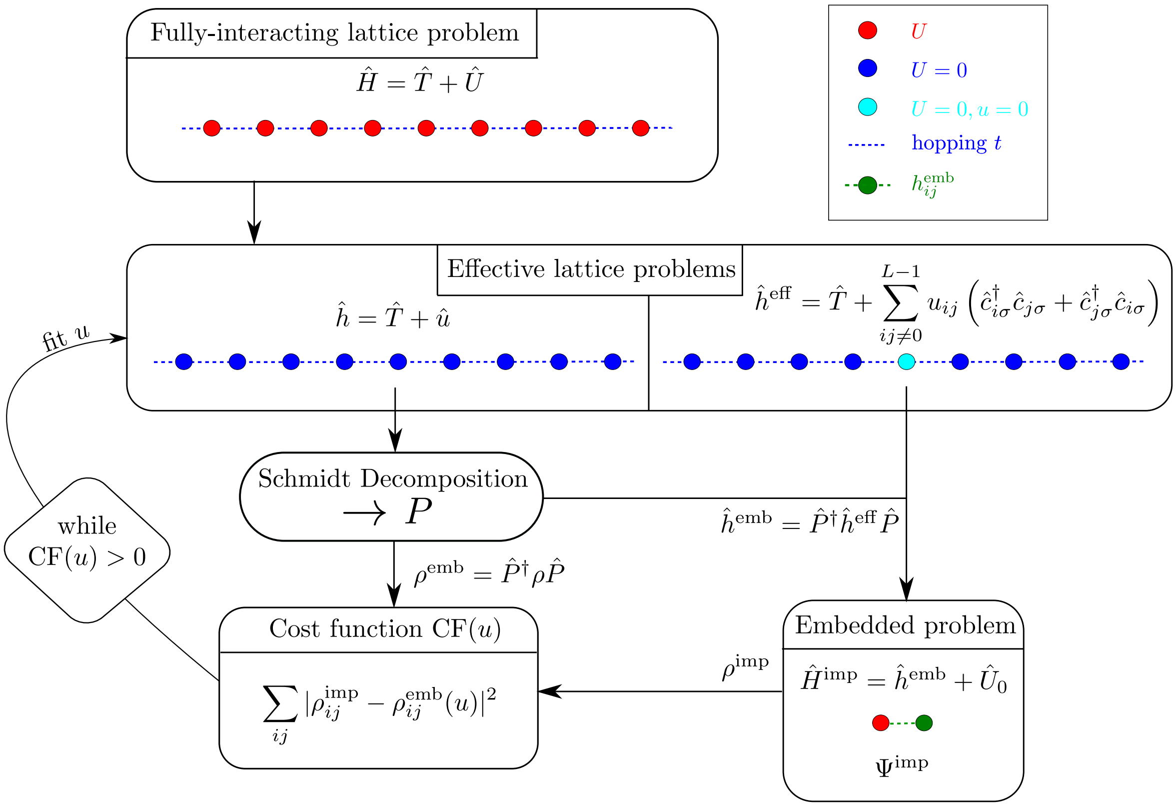

Figure 2.9: DMET procedure for the Hubbard model with a single impurity, in its non-interacting bath formulation. The impurity site is labelled as 0.

The theory presented above was developed for a lattice system with translational invariance, so that one fragment only is sufficient to compute the per-site quantities (energy and double occupation). Because of the mean-field approximation which defines the starting point of the DMET calculation, the bath states are only single-particle states so that DMET is lacking correlation effects in the bath. In order to fix this issue, one can start the DMET procedure with a spin-unrestricted Hartree-Fock wavefunction [420] or with the antisymmetrized geminal power correlated wavefunction [425].

In order to extend the method to quantum chemistry, the whole system (a molecule) has to be decomposed into multiple fragments. Each of these fragments are embedded into an environment composed of all the other fragments, which are then projected to construct new effective bath orbitals. Hence the whole system has been replaced by multiple smaller subsystems, connected by a chemical potential which ensures that the number of electrons in each of these subsystems sums up to the total number of electrons. For more details about DMET for quantum chemistry, the reader is referred to the work of Sebastian Wouters and co-workers [422]. It has also been noticed that the central part of the fragments only are very well described, as it is surrounded by interacting orbitals like in the original lattice problem. The description of the fragment edges, which are in contact with noninteracting bath orbitals, can be substantially improved by overlapping the fragments, which is also shown to improve the convergence with fragment size. The latter idea is referred to as “Bootstrap embedding” and is developed by Voorhis and co-workers [428]. It could also be interesting to look at the connection between the single-site DMET (one impurity and one effective bath sites composing the embedded problem) and the *linearized* DMFT from Bulla and Potthoff [429, 430], who have approximated the mapping in DMFT onto a two-site Anderson model, i.e. one impurity and one bath sites as well. Finally, let us stress that the embedding subspace of $2L_F$ (spatial) orbitals (with $2L_F$ electrons) can play the role of an active orbital space, thus make a connection between DMET and CASSCF [422]. Therefore, like CASSCF, dynamical correlation effects are missing in DMET. In this respect, combining DMET with DFT is appealing. To the best of our knowledge, this combination has not been developed yet. Such a comparable merging will be addressed in the following, in the context of *site-occupation embedding theory* (SOET), which is the main topic of this thesis.

Chapter 3

Site-Occupation Embedding Theory

In the spirit of the previously described embedding schemes, only a small number of sites (referred to as *impurities*) are kept interacting, while the remaining sites (referred to as the *bath*) are noninteracting. This partitioning defines our impurity-interacting system. In analogy with SOFT, a mapping is made to recover the exact density of the physical system. However, rather than considering a noninteracting fictitious system, the impurity-interacting one becomes the new reference and a complementary bath Hxc energy functional of the site occupations is used to perform the mapping. This is the so-called *site-occupation embedding theory* (SOET) [72, 270, 300, 301]. Being still in its early stage, SOET is applied to the one-dimensional Hubbard model only. Extensions to higher dimensions are of significant interest and will be investigated in a near future. In contrast to DMET and DMFT, which are exact in some particular limits only, SOET is in principle exact for any correlation and filling regimes. Of course, approximate functionals are used in practice. In this chapter, the foundations of SOET are introduced and exact SOET expressions are derived for the per-site energy and the double occupation in the uniform case. Then, some required properties that an exact functional should fulfil are discussed. Finally, we describe the approximate functionals that have been developed throughout this thesis, which are used to solve the SOET self-consistent equation. The resulting per-site energy and double occupation are extensively discussed.

3.1 In-principle exact formulation

Consider the one-dimensional L-site Hubbard model in an (not necessarily uniform) external potential with periodic conditions (if not otherwise specified, the summation runs over all sites labelled from 0 to $L-1$),

$$\hat{H} = -t\sum_{i\sigma}\left(\hat{c}^{\dagger}_{i\sigma}\hat{c}_{i+1\sigma} + \text{h.c.}\right) + U\sum_{i}\hat{c}^{\dagger}_{i\uparrow}\hat{c}_{i\downarrow}\hat{c}^{\dagger}_{i\uparrow}\hat{c}_{i\uparrow} + \sum_{i\sigma} v_i\hat{c}^{\dagger}_{i\sigma}\hat{c}_{i\sigma}. \tag{3.1}$$

If only M sites (labelled as $i = 0, 1, \ldots, M-1$) are explicitly interacting, the conventional Hohenberg–Kohn functional can be decomposed as follows [301],

$$F(\mathbf{n}) = F^{\text{imp}}_{M}(\mathbf{n}) + \overline{E}^{\text{bath}}_{\text{Hxc},M}(\mathbf{n}), \tag{3.2}$$

which introduces the analogue of the Levy–Lieb functional [Eq. (2.50)] for M interacting impurity sites,

$$F^{\text{imp}}_{M}(\mathbf{n}) = \min_{\Psi\rightarrow\mathbf{n}}\left\{\langle\Psi|\hat{T} + \hat{U}_M|\Psi\rangle\right\}, \tag{3.3}$$

where $\hat{U}_M = U\sum_{i=0}^{M-1}\hat{n}_{i\uparrow}\hat{n}_{i\downarrow}$ is the on-site M-impurity-interacting repulsion operator. In addition, the complementary contribution $\overline{E}^{\text{bath}}_{\text{Hxc},M}(\mathbf{n})$ in Eq. (3.2) is the bath Hxc energy functional of the site occupations. This functional accounts for the difference in energy between the M-impurity-interacting system and the physical one. In other words, it describes all the coupling between the interacting impurity sites and the noninteracting bath sites. The decomposition in Eq. (3.2) leads to a new expression for the ground-state energy as follows:

$$E(\mathbf{v}) = \min_{\mathbf{n}}\Big\{\min_{\Psi\rightarrow\mathbf{n}}\left\{\langle\Psi|\hat{T} + \hat{U}_M|\Psi\rangle\right\} + \overline{E}^{\text{bath}}_{\text{Hxc},M}(\mathbf{n}) + (\mathbf{v}|\mathbf{n})\Big\}, \tag{3.4}$$

thus leading to the final variational expression,

$$E(\mathbf{v}) = \min_{\Psi}\Big\{\langle\Psi|\hat{T} + \hat{U}_M|\Psi\rangle + \overline{E}^{\text{bath}}_{\text{Hxc},M}\left(\mathbf{n}^{\Psi}\right) + \left(\mathbf{v}|\mathbf{n}^{\Psi}\right)\Big\}, \tag{3.5}$$

where $\mathbf{n}^{\Psi} \equiv \{\langle\Psi|\hat{n}_i|\Psi\rangle\}_i$ is the site-occupation vector associated with the wavefunction Ψ. The minimizing M-impurity-interacting wavefunction in Eq. (3.5), denoted by Ψ^{imp}_{M}, fulfils the following self-consistent SOET equation [301],

$$\boxed{\left(\hat{T} + \hat{U}_M + \sum_{i}\left[v_i + \frac{\partial\overline{E}^{\text{bath}}_{\text{Hxc},M}\left(\mathbf{n}^{\Psi^{\text{imp}}_{M}}\right)}{\partial n_i}\right]\right)|\Psi^{\text{imp}}_{M}\rangle = \mathcal{E}^{\text{imp}}_{M}|\Psi^{\text{imp}}_{M}\rangle}, \tag{3.6}$$

where the embedding potential

$$v_{M,i}^{\mathrm{emb}}(\mathbf{n}) = v_i + \frac{\partial \overline{E}_{\mathrm{Hxc},M}^{\mathrm{bath}}(\mathbf{n})}{\partial n_i} \tag{3.7}$$

is built to reproduce the exact site occupations of the physical system.

Let us now make a brief comparison between SOET [Eq. (3.6)] and other methods that may appear very similar. The electronic repulsion on the impurity sites is treated explicitly in SOET, in contrast to DFT+U where this contribution is incorporated implicitly as a correction factor, thus making DFT+U not variational anymore. Interestingly, SOET can be seen as a lattice alternative to the range-separated DFT [Eq. (1.175)], where the electronic repulsion is now separated in the discretized real space and the electronic density is replaced by the site-occupation vector. Another interesting difference can be made between SOET and WFT-in-DFT [Eq. (1.198)]. Apart from the fact that WFT-in-DFT is applied to *ab-initio* Hamiltonian and not on a lattice, note that the kinetic operator in SOET acts on the whole system, while it acts only inside the cluster part (analogue to the impurity sites) in WFT-in-DFT. The impact of the latter difference will be further investigated in Chap. 4, where practical alternative implementations of SOET are discussed.

Let us return to the expression of the complementary Hxc energy for the bath, $\overline{E}_{\mathrm{Hxc},M}^{\mathrm{bath}}(\mathbf{n})$. The derivation of an analytical expression for this object is far from trivial as it has to (i) account for all the missing Hxc effects in the M-interacting-impurity system and (ii) map the physical system onto the impurity-interacting one by recovering the exact physical density. Let us start by writing the KS decomposition of the M-impurity-interacting Levy–Lieb functional,

$$F_M^{\mathrm{imp}}(\mathbf{n}) = T_{\mathrm{s}}(\mathbf{n}) + E_{\mathrm{Hxc},M}^{\mathrm{imp}}(\mathbf{n}). \tag{3.8}$$

$E_{\mathrm{Hxc},M}^{\mathrm{imp}}(\mathbf{n})$ is the impurity Hxc energy functional, which accounts for the difference of Hxc contributions between the non-interacting system and the M-impurity-interacting one. Plugging Eq. (3.8) into Eq. (3.3), and using the KS decomposition of the conventional Levy–Lieb functional $F(\mathbf{n}) = T_{\mathrm{s}}(\mathbf{n}) + E_{\mathrm{Hxc}}(\mathbf{n})$, it comes

$$\overline{E}_{\mathrm{Hxc},M}^{\mathrm{bath}}(\mathbf{n}) = E_{\mathrm{Hxc}}(\mathbf{n}) - E_{\mathrm{Hxc},M}^{\mathrm{imp}}(\mathbf{n}). \tag{3.9}$$

According to Eq. (3.9), the challenging task of developing the complementary bath Hxc functional has been replaced by searching for both the conventional Hxc functional and the impurity Hxc functional. For the former, The BALDA [359–361] approximation can be used, as well as other extensions already

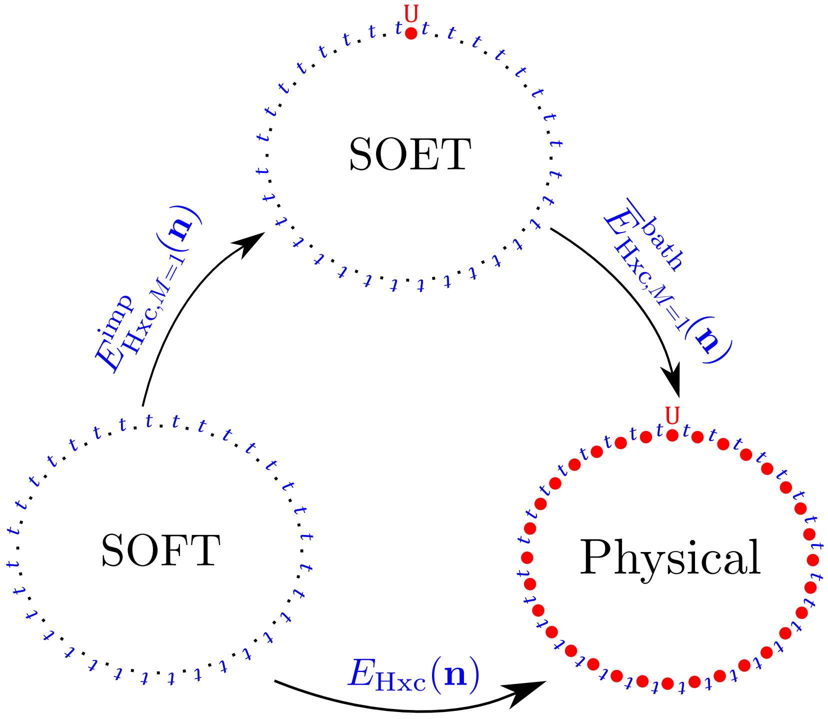

Figure 3.1: Illustration of the mappings between the physical system, the $(M{=}1)$-impurity-interacting system and the noninteracting one. The system represented is the 32-site one-dimensional Hubbard model with periodic boundary conditions.

discussed in Sec. (2.2) in the context of SOFT. Unfortunately, $E^{\mathrm{imp}}_{\mathrm{Hxc},M}(\mathbf{n})$ remains to be found as no approximation to it are given in the literature. An illustration of Eq. (3.9), which relates the mapping between the non-interacting, the impurity-interacting and the fully-interacting systems, is given in Fig. 3.1. The Hxc energies can be decomposed even further by separating the Hartree-exchange and the correlation part, such that

$$E_{\mathrm{Hxc}}(\mathbf{n}) \quad = \quad \frac{U}{4}\sum_i n_i^2 + E_{\mathrm{c}}(\mathbf{n}), \tag{3.10}$$

and

$$E^{\mathrm{imp}}_{\mathrm{Hxc},M}(\mathbf{n}) \quad = \quad \frac{U}{4}\sum_{i=0}^{M-1} n_i^2 + E^{\mathrm{imp}}_{\mathrm{c},M}(\mathbf{n}), \tag{3.11}$$

thus leading to

$$\overline{E}^{\mathrm{bath}}_{\mathrm{Hxc},M}(\mathbf{n}) = \frac{U}{4}\sum_{i=M}^{L-1} n_i^2 + \overline{E}^{\mathrm{bath}}_{\mathrm{c},M}(\mathbf{n}), \tag{3.12}$$

where

$$\overline{E}^{\mathrm{bath}}_{\mathrm{c},M}(\mathbf{n}) = E_{\mathrm{c}}(\mathbf{n}) - E^{\mathrm{imp}}_{\mathrm{c},M}(\mathbf{n}). \tag{3.13}$$

As readily seen in Eqs. (3.12) and (3.13), only the correlation energy functionals have to be approximate. In the following, the local density approximation (LDA) is considered.

3.2 Uniform case and Local Density Approximation

3.2.1 The per-site bath correlation energy

In the uniform case, the full correlation energy can be exactly expressed within LDA as follows,

$$E_{\mathrm{c}}(\mathbf{n}) = \sum_i e_{\mathrm{c}}(n_i), \tag{3.14}$$

such that, according to Eq. (3.13),

$$\overline{E}^{\mathrm{bath}}_{\mathrm{c},M}(\mathbf{n}) = \sum_i e_{\mathrm{c}}(n_i) - E^{\mathrm{imp}}_{\mathrm{c},M}(\mathbf{n}). \tag{3.15}$$

By separating the contributions of the M interacting impurity sites from the $L-M$ non-interacting bath sites, it comes

$$\overline{E}^{\mathrm{bath}}_{\mathrm{c},M}(\mathbf{n}) = \sum_{i=0}^{M-1} e_{\mathrm{c}}(n_i) + \sum_{i=M}^{L-1} e_{\mathrm{c}}(n_i) - E^{\mathrm{imp}}_{\mathrm{c},M}(\mathbf{n}). \tag{3.16}$$

If we introduce the per-site analogue of Eq. (3.13) as follows [301],

$$\boxed{\overline{e}^{\mathrm{bath}}_{\mathrm{c},M}(\mathbf{n}) = \frac{1}{M}\left[\left(\sum_{i=0}^{M-1} e_{c}(n_i)\right) - E^{\mathrm{imp}}_{\mathrm{c},M}(\mathbf{n})\right]}, \tag{3.17}$$

the final LDA expression for the bath correlation energy functional is obtained,

$$\overline{E}^{\mathrm{bath}}_{\mathrm{c},M}(\mathbf{n}) = \sum_{i=M}^{L-1} e_{\mathrm{c}}(n_i) + M\overline{e}^{\mathrm{bath}}_{\mathrm{c},M}(\mathbf{n}). \tag{3.18}$$

In the uniform case ($\mathbf{v} = 0$), the occupations are all equal to $n = N/L$, such that $\mathbf{n} \equiv \underline{n} = \{n, n, n, \ldots, n\}$. As a consequence, Eq. (3.17) can be rewritten as

$$\overline{e}^{\mathrm{bath}}_{\mathrm{c},M}(\underline{n}) = e_c(n) - \frac{E^{\mathrm{imp}}_{\mathrm{c},M}(\underline{n})}{M}. \tag{3.19}$$

As readily seen in Eq. (3.17) or (3.19), the per-site bath energy functional measures the deviation of the impurity functional from the conventional one.

3.2.2 Derivation of the exact per-site energy

The per-site energy for a uniform system is given within SOFT by [360],

$$e = E/L = t_{\mathrm{s}}(n) + \frac{U}{4}n^2 + e_{\mathrm{c}}(n), \tag{3.20}$$

where the exact expression for $t_{\mathrm{s}}(n)$ is given in Eq. (2.75) in the thermodynamic limit ($L \to +\infty$). In SOET, it is desirable to have an expression for the per-site energy that combines contributions from both (*i*) the many-body M-impurity-interacting wavefunction and (*ii*) the site-occupation functionals. To do so, Eq. (3.19) is inserted into Eq. (3.20) to give

$$e = t_{\mathrm{s}}(n) + \frac{U}{4}n^2 + \overline{e}^{\mathrm{bath}}_{\mathrm{c},M}(\underline{n}) + \frac{E^{\mathrm{imp}}_{\mathrm{c},M}(\underline{n})}{M}. \tag{3.21}$$

Then, plugging Eqs. (3.8) and (3.11) into Eq. (3.21) leads to

$$e = t_{\mathrm{s}}(n) + \frac{1}{M}\Big(F^{\mathrm{imp}}_{M}(\underline{n}) - T_{\mathrm{s}}(\underline{n})\Big) + \overline{e}^{\mathrm{bath}}_{\mathrm{c},M}(\underline{n}). \tag{3.22}$$

By applying the Hellmann–Feynman theorem to the variational energy expression in Eq. (3.5), it comes

$$t\frac{\partial E}{\partial t} = \langle \Psi^{\mathrm{imp}}_{M}|\hat{T}|\Psi^{\mathrm{imp}}_{M}\rangle + t\frac{\partial \overline{E}^{\mathrm{bath}}_{\mathrm{c},M}(\underline{n})}{\partial t}, \tag{3.23}$$

where $E = E(\mathbf{v} = 0)$. By using $E = F(\underline{n})$ together with Eqs. (3.2) and (3.23), the first term in the right hand side of Eq. (3.23) is decomposed as follows,

$$\langle \Psi^{\mathrm{imp}}_{M}|\hat{T}|\Psi^{\mathrm{imp}}_{M}\rangle = t\frac{\partial F^{\mathrm{imp}}_{M}(\underline{n})}{\partial t} \xrightarrow{\mathrm{KS}} t\frac{\partial T_{\mathrm{s}}(\underline{n})}{\partial t} + t\frac{\partial E^{\mathrm{imp}}_{\mathrm{c},M}(\underline{n})}{\partial t}, \tag{3.24}$$

thus leading to, for $U = 0$,

$$T_{\mathrm{s}}(\underline{n}) = t\frac{\partial T_{\mathrm{s}}(\underline{n})}{\partial t}. \tag{3.25}$$

By combining Eqs. (3.3), (3.24) and (3.25), an expression of the impurity Hxc energy functional which involves the impurity double occupations [$d^{\mathrm{imp}}_{M,i} = \langle \hat{n}_{i\uparrow}\hat{n}_{i\downarrow}\rangle_{\Psi^{\mathrm{imp}}_{M}} = \langle \Psi^{\mathrm{imp}}_{M}|\hat{n}_{i\uparrow}\hat{n}_{i\downarrow}|\Psi^{\mathrm{imp}}_{M}\rangle$] is obtained as follows:

$$\begin{aligned} E^{\mathrm{imp}}_{\mathrm{Hxc},M}(\underline{n}) &= F^{\mathrm{imp}}_{M}(\underline{n}) - T_{\mathrm{s}}(\underline{n}) = \langle \Psi^{\mathrm{imp}}_{M} | \hat{T} | \Psi^{\mathrm{imp}}_{M} \rangle - T_{\mathrm{s}}(\underline{n}) + U \sum_{i=0}^{M-1} d^{\mathrm{imp}}_{M,i} \\ &= t \frac{\partial E^{\mathrm{imp}}_{\mathrm{c},M}(\underline{n})}{\partial t} + U \sum_{i=0}^{M-1} d^{\mathrm{imp}}_{M,i}. \end{aligned} \tag{3.26}$$

Finally, according to Eq. (3.19), the exact expression for the per-site energy in the uniform case within SOET reads,

$$e = t_{\mathrm{s}}(n) + \frac{U}{M} \sum_{i=0}^{M-1} d^{\mathrm{imp}}_{M,i} + t \frac{\partial e_{\mathrm{c}}(n)}{\partial t} - t \frac{\partial \overline{e}^{\mathrm{bath}}_{\mathrm{c},M}(\underline{n})}{\partial t} + \overline{e}^{\mathrm{bath}}_{\mathrm{c},M}(\underline{n}). \tag{3.27}$$

Note that the per-site energy expression contains contributions coming from both the many-body impurity wavefunction and the site-occupation functionals.

However, Eq. (3.27) is not convenient in practice, because the uniform density will not be recovered anymore when approximate functionals are used. It is therefore useful to introduce another expression for the per-site energy, which can be rewritten as follows,

$$e = \frac{1}{M} \sum_{i=0}^{M-1} \left(t_{\mathrm{s}}(n_i^{\Psi^{\mathrm{imp}}_{M}}) + t \frac{\partial e_{\mathrm{c}}(n_i^{\Psi^{\mathrm{imp}}_{M}})}{\partial t} + U d^{\mathrm{imp}}_{M,i} \right) + \left(\overline{e}^{\mathrm{bath}}_{\mathrm{c},M}(\mathbf{n}^{\Psi^{\mathrm{imp}}_{M}}) - t \frac{\partial \overline{e}^{\mathrm{bath}}_{\mathrm{c},M}(\mathbf{n}^{\Psi^{\mathrm{imp}}_{M}})}{\partial t} \right), \tag{3.28}$$

such that one can use all the impurity occupations (in practice not always identical) obtained from the M-impurity-interacting wavefunction. Let us mention that in Ref. [301], we highlighted the connection between the derivatives of the per-site correlation energy with respect to t and U as follows,

$$e_{\mathrm{c}}(n) = t \frac{\partial e_{\mathrm{c}}(n)}{\partial t} + U \frac{\partial e_{\mathrm{c}}(n)}{\partial U}, \tag{3.29}$$

as well as for the impurity correlation energy,

$$E^{\mathrm{imp}}_{\mathrm{c},M}(\mathbf{n}) = t \frac{\partial E^{\mathrm{imp}}_{\mathrm{c},M}(\mathbf{n})}{\partial t} + U \frac{\partial E^{\mathrm{imp}}_{\mathrm{c},M}(\mathbf{n})}{\partial U}. \tag{3.30}$$

Consequently, according to Eq. (3.19),

$$\overline{e}^{\mathrm{bath}}_{\mathrm{c},M}(\mathbf{n}) = t \frac{\partial \overline{e}^{\mathrm{bath}}_{\mathrm{c},M}(\mathbf{n})}{\partial t} + U \frac{\partial \overline{e}^{\mathrm{bath}}_{\mathrm{c},M}(\mathbf{n})}{\partial U}. \tag{3.31}$$

By inserting the latter expression in Eq. (3.28), the per-site energy finally reads

$$\boxed{e = \frac{1}{M}\sum_{i=0}^{M-1}\left(t_{\mathrm{s}}(n_i^{\Psi_M^{\mathrm{imp}}}) + t\frac{\partial e_{\mathrm{c}}(n_i^{\Psi_M^{\mathrm{imp}}})}{\partial t} + U d_{M,i}^{\mathrm{imp}}\right) + U\frac{\partial \overline{e}_{\mathrm{c},M}^{\mathrm{bath}}(\mathbf{n}^{\Psi_M^{\mathrm{imp}}})}{\partial U}}. \tag{3.32}$$

3.2.3 Derivation of the exact double occupation

The double occupation of a uniform system is given by [302]

$$d = \frac{1}{L}\frac{\partial E}{\partial U}. \tag{3.33}$$

By applying the Hellmann–Feynman theorem to Eq. (2.54) and using the LDA, it comes

$$d = \frac{n^2}{4} + \frac{\partial e_{\mathrm{c}}(n)}{\partial U}. \tag{3.34}$$

The latter can be rewritten within SOET by inserting the decomposition of Eq. (3.19) into Eq. (3.34), thus leading to

$$d = \frac{1}{M}\frac{\partial E_{\mathrm{Hxc},M}^{\mathrm{imp}}(\underline{n})}{\partial U} + \frac{\partial \overline{e}_{\mathrm{c},M}^{\mathrm{bath}}(\underline{n})}{\partial U}. \tag{3.35}$$

Note that the above expression is exact in the uniform case, provided that the exact functionals are known. In practice, one has to use approximate functionals, and the double occupation in Eq. (3.35) does not take advantage of the explicit treatment of the interaction on the M interacting impurity sites. In order to get an exact expression which involves the many-body wavefunction, the Hellmann–Feynman theorem is applied to the variational energy in Eq. (3.5), thus leading to

$$\frac{\partial E}{\partial U} = \sum_{i=0}^{M-1} d_{M,i}^{\mathrm{imp}} + \frac{\partial \overline{E}_{\mathrm{Hxc},M}^{\mathrm{bath}}(\underline{n})}{\partial U}. \tag{3.36}$$

From the decompositions in Eqs. (3.2) and (3.8), it comes

$$\frac{\partial}{\partial U}\left[F(\underline{n}) - \overline{E}_{\mathrm{Hxc},M}^{\mathrm{bath}}(\underline{n})\right] = \frac{\partial}{\partial U}\left[E - \overline{E}_{\mathrm{Hxc},M}^{\mathrm{bath}}(\underline{n})\right] = \frac{\partial F_M^{\mathrm{imp}}(\underline{n})}{\partial U} = \frac{\partial E_{\mathrm{Hxc},M}^{\mathrm{imp}}(\underline{n})}{\partial U}, \tag{3.37}$$

such that, according to Eq. (3.36),

$$\frac{\partial E_{\mathrm{Hxc},M}^{\mathrm{imp}}(\underline{n})}{\partial U} = \sum_{i=0}^{M-1} d_{M,i}^{\mathrm{imp}}. \tag{3.38}$$

Finally, by combining Eqs. (3.35) and (3.38), the following *exact* expression for the double occupation in SOET with multiple impurities reads

$$\boxed{d = \frac{1}{M}\sum_{i=0}^{M-1} d^{\mathrm{imp}}_{M,i} + \frac{\partial \overline{e}^{\mathrm{bath}}_{\mathrm{c},M}(\mathbf{n}^{\Psi^{\mathrm{imp}}_{M}})}{\partial U}}. \tag{3.39}$$

As readily seen in Eq. (3.39), the double occupation is obtained by combining both wavefunction and density functional contributions, in analogy with the per-site energy in Eq. (3.32). Alternatively, Eq. (3.39) could have been derived from Eq. (3.35) by using Eq. (3.30), followed by Eq. (3.26). It should be noted that the double occupation of the impurity sites ($d^{\mathrm{imp}}_{M,i}$) are in principle not identical for all i in the fictitious M-impurity-interacting system described by Ψ^{imp}_{M}. Indeed, the insertion of impurities does break the translational symmetry of the system, and the embedding potential restores uniformity in the density profile only. Finally and according to Eq. (3.39), it is clear that the impurity double occupations are not reproducing the exact double occupation of the physical system, such that an additional functional contribution is required.

3.3 Exact conditions for the correlation energy functionals in SOET

In the previous section, we have seen that the correlation energy functionals should satisfy the conditions in Eqs. (3.29), (3.30) and (3.31). Before looking at approximate functionals [Sec. 3.4], more exact conditions can be investigated. Indeed, it will be shown in Sec. 3.3.1 that the impurity correlation functional has to depend on all the site occupations, even in the uniform case. Besides, the correlation functionals should also fulfil the hole-particle symmetry relation, as demonstrated in Sec. 3.3.2. Finally, we present how the correlation energy functionals can be determined numerically. These numerically exact functionals will be our references to judge the accuracy of our approximated functionals introduced in Sec. 3.4.

3.3.1 Numerical investigation of the embedding potential

The embedding potential in Eq. (3.7) is essential to ensure the in-principle-exact mapping between the physical system and the M-impurity-interacting one. Firstly, it is primordial to verify that there is no impurity-interacting v-representability problem in the one-dimensional Hubbard model. The exact embedding potential can be found numerically by solving the M-impurity-interacting Legendre–

Fenchel transform [72],

$$F_M^{\mathrm{imp}}(\mathbf{n}) = \sup_{\mathbf{v}} \left\{ \mathcal{E}_M^{\mathrm{imp}}(\mathbf{v}) - (\mathbf{v}|\mathbf{n}) \right\}, \tag{3.40}$$

where $\mathcal{E}_M^{\mathrm{imp}}(\mathbf{v})$ is the ground-state energy of $\hat{H}_M^{\mathrm{imp}}(\mathbf{v}) = \hat{T} + \hat{U}_M + \sum_i v_i \hat{n}_i$. Eq. (3.40) has been implemented and solved in Ref. [72] by exact diagonalization (FCI), by using the lanczos algorithm [431][1]. Due to the high computational cost required to compute $\mathcal{E}_M^{\mathrm{imp}}(\mathbf{v})$ exactly, a small ring of eight sites will be studied. For simplicity, one impurity only is considered. In Fig. 3.2, the maximising embedding potential (shifted so that it becomes 0 on the impurity site) is plotted (left panel). This potential is then used to solve Eq. (3.6) in order to extract the site occupations (middle panel) and the double occupations (right panel). As readily seen in the middle panel of Fig. 3.2, the uniform site occupations are recovered by using the maximising embedding potential of Eq. (3.40). Hence, no impurity-interacting v-representability problem arises. Turning to the right panel of Fig. 3.2, the impurity double occupations $d_{M=1,i}^{\mathrm{imp}}$ of the non-interacting bath sites ($i = 1, \ldots, L-1$) deviate significantly from the physical double occupation (dashed lines). However, it seems that the double occupation of the impurity site is very close to the physical one, except in the half-filled case where $d_{M=1,0}^{\mathrm{imp}} \approx 0.0715$ (instead of ≈ 0.025 for $N = 8$ [zoomed panel]). In this case, and according to the double occupation expression in SOET [Eq. (3.39)], the complementary per-site bath correlation energy derivative has a significant contribution. These observations clearly highlight the impact of the explicit treatment of the electron-electron repulsion on the impurity-interacting wavefunction.

Returning to the embedding potential (left panel of Fig. 3.2), an interesting result arises in the half-filled case. Indeed, the embedding potential in the bath is constant and equal to $U/2$. Equivalently, by applying a shift of $-U/2$, the exact expression for the single-impurity embedding potential at half-filling becomes

$$v_{M=1,i}^{\mathrm{emb}}(\underline{n} = \underline{1}) = -\frac{U}{2}\delta_{i0}. \tag{3.41}$$

On the other hand, the potential exhibits some fluctuations in the bath away from half-filling. Thus, the embedding potential is not trivial anymore, even for a uniform model. This is a direct consequence of the broken translational invariance due to the insertion of an impurity. According to the exact embedding potential expression in Eqs. (3.7) in the uniform case ($\mathbf{v} = 0$), and considering Eqs. (3.12)

---

[1] This code has been provided by Masahisa Tsuchiizu (University of Women, Nara, Japan).

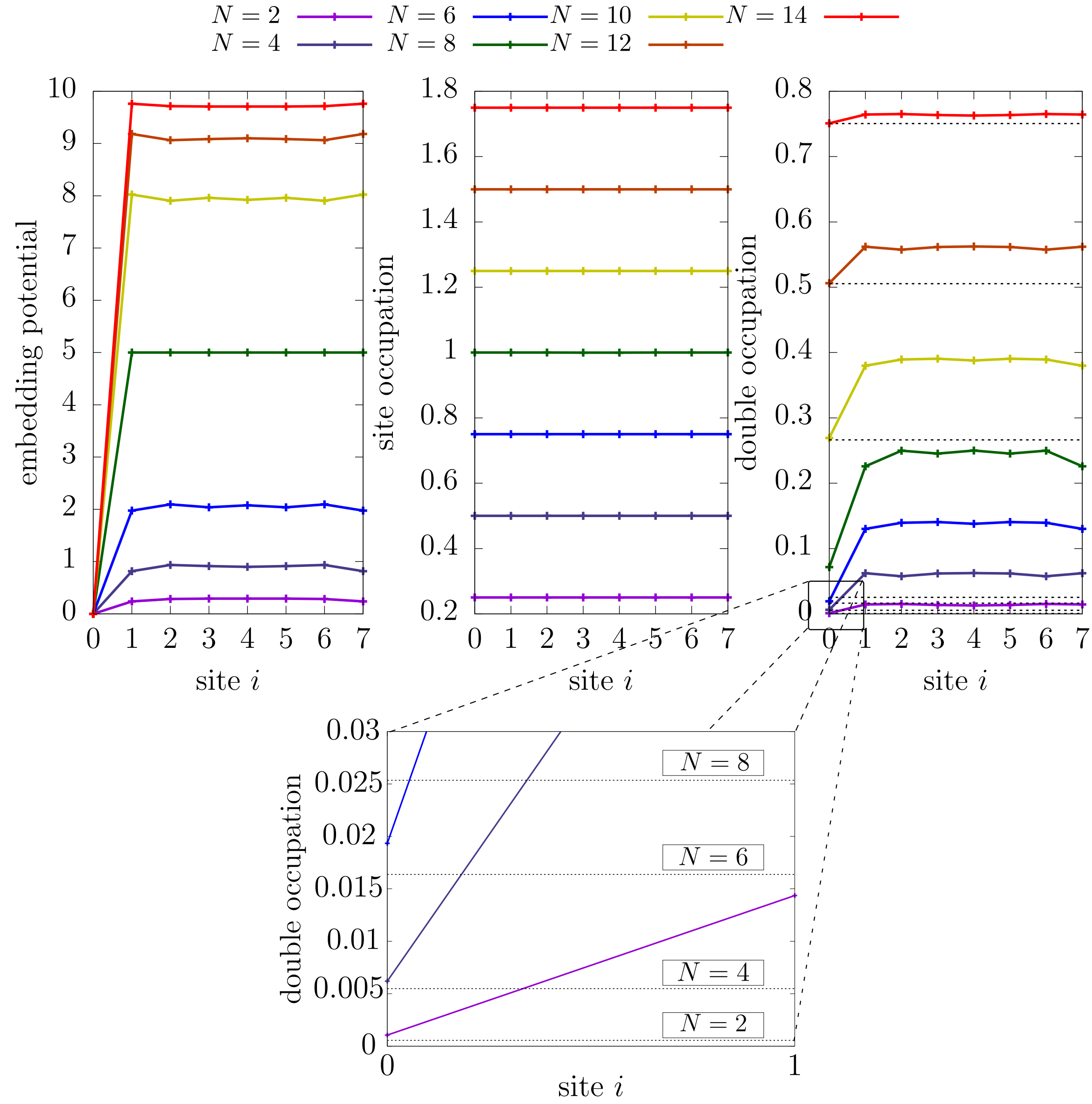

Figure 3.2: Results are shown for $U/t = 10$ and for different number of electrons in the eight-site ring Hubbard model. Left panel: embedding potential $\mathbf{v}^{\rm emb}_{M=1}(\mathbf{n}^{\Psi^{\rm imp}_{M=1}}) \equiv \{v^{\rm emb}_{M=1,i}(\mathbf{n}^{\Psi^{\rm imp}_{M=1}})\}_i$. Middle panel: site occupations $\mathbf{n}^{\Psi^{\rm imp}_{M=1}} \equiv \{n_i^{\Psi^{\rm imp}_{M=1}}\}_i$. Right panel: double occupations $d^{\rm imp}_{M=1,i} = \langle \hat{n}_{i\uparrow}\hat{n}_{i\downarrow}\rangle_{\Psi^{\rm imp}_{M=1}}$. Dashed lines: exact double occupation of the fully-interacting system. A zoom is made around the impurity site for the double occupation, in which the number of electrons corresponding to each dashed lines is specified. See text for further details.

and (3.15), it comes

$$v^{\rm emb}_{M=1,i}(\underline{n}) = \frac{U}{2}n(1-\delta_{i0}) + \left.\frac{\partial e_{\rm c}(n_i)}{\partial n_i}\right|_{n_i=n} - \left.\frac{\partial E^{\rm imp}_{{\rm c},M=1}(\mathbf{n})}{\partial n_i}\right|_{\mathbf{n}=\underline{n}} \tag{3.42}$$

By applying a shift of $-Un/2 - \left(\partial e_{\rm c}(n_i)/\partial n_i\right)|_{n_i=n}$, the expression reduces to

$$v^{\rm emb}_{M=1,i}(\underline{n}) = -\frac{U}{2}n\delta_{i0} - \left.\frac{\partial E^{\rm imp}_{{\rm c},M=1}(\mathbf{n})}{\partial n_i}\right|_{\mathbf{n}=\underline{n}}. \tag{3.43}$$

From Eq. (3.43), it comes that the impurity correlation energy functional (or, equivalently, $\overline{e}^{\rm bath}_{{\rm c},M=1}(\mathbf{n})$ according to Eq. (3.17)) has to depend on all site occupations. Otherwise, it would not account for the fluctuations of the embedding potential in the bath. This is the price the pay to achieve an exact embedding. In the particular case of half-filling where no fluctuations appear, this dependence can be neglected exactly. This assumption, so-called the “impurity local density approximation” (iLDA) [72], leads to

$$\overline{e}^{\rm bath}_{{\rm c},M=1}(\mathbf{n}) \xrightarrow{\rm iLDA} \overline{e}^{\rm bath}_{{\rm c},M=1}(n_0), \tag{3.44}$$

where the per-site bath correlation functional depends only on the occupation of the impurity site. While iLDA is exact at half-filling, it becomes an approximation in the other density regimes. This approximation will be employed in the construction of all the functional approximations developed in this thesis. In order to see the limitations of iLDA, an approximate Legendre–Fenchel transform is introduced as follows [72]:

$$F^{\rm imp}_{M=1}(n_0) = \sup_{v_0}\left\{\mathcal{E}^{\rm imp}_{M=1}(v_0) - v_0 n_0\right\}, \tag{3.45}$$

where only the potential on the impurity is optimized, while it is set to 0 in the bath. The maximising potential in Eq. (3.45) is referred to as impurity-optimised potential, and is numerically determined to recover the physical occupation on the impurity site. The site occupations obtained by solving the SOET equation [Eq. (3.6)] with this impurity-optimised potential are shown in Fig. 3.3. By construction, the impurity site occupation is indeed exact in any density and correlation regimes. In the half-filled case, the uniform occupation on all sites is recovered, demonstrating that iLDA is *not* an approximation. However, away from half-filling, the uniform occupation is not recovered and fluctuations in the bath occupations appear. Nevertheless, those fluctuations are relatively small even for large U/t values (right panel of Fig. 3.3). Therefore, iLDA seems to be a relevant approximation. Note that in practice, the embedding potentials derived from approximate functionals are not expected

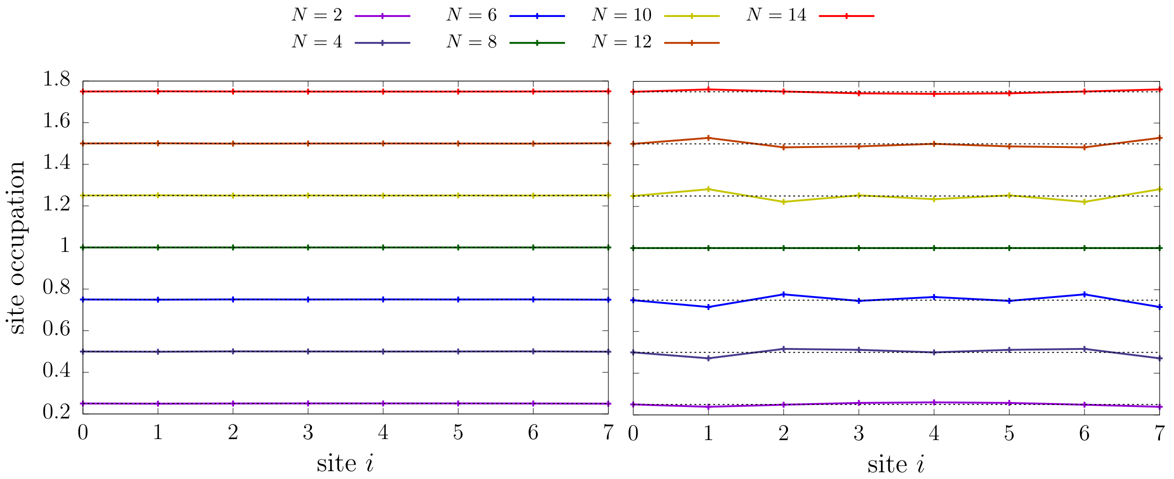

Figure 3.3: Site occupations obtained with the impurity-optimised potential for $U/t = 1$ (left panel) and $U/t = 10$ (right panel) on the uniform eight-site Hubbard ring model. Dashed lines represent the uniform site occupation $n = N/L$.

to reproduce the impurity site occupation exactly, in contrast to the impurity-optimised potential.

3.3.2 Hole-particle symmetry

As readily seen in Fig. 3.3, the right panel exhibits an axial symmetry around the green line axis corresponding to the half-filled case. It illustrates the hole-particle symmetry. In this section, we discuss the invariance of the functionals under this particular symmetry, followed by the generalized proof of Eq. (3.41) for multiple impurities [301].

Let us consider $2L - N$ electrons, so that the site-occupation vector becomes $\underline{2} - \mathbf{n} = \{2 - n_i\}_i$. Starting with the Legendre–Fenchel transform in Eq. (3.40), its hole-particle symmetric analogue reads

$$F_M^{\text{imp}}(\underline{2} - \mathbf{n}) = \sup_{\mathbf{v}} \Big\{ \mathcal{E}_M^{\text{imp},2L-N}(\mathbf{v}) - 2\sum_i v_i + (\mathbf{v}|\mathbf{n}) \Big\}, \tag{3.46}$$

where $\mathcal{E}_M^{\text{imp},2L-N}(\mathbf{v})$ is the $(2L-N)$-electron ground-state of the M-impurity-interacting Hamiltonian, which is rewritten here for convenience,

$$\hat{H}_M^{\text{imp}}(\mathbf{v}) = -t\sum_{i\sigma}\Big(\hat{c}_{i\sigma}^\dagger \hat{c}_{i+1\sigma} + \text{h.c.}\Big) + \sum_{i\sigma} v_i \hat{c}_{i\sigma}^\dagger \hat{c}_{i\sigma} + U\sum_{i=0}^{M-1} \hat{c}_{i\uparrow}^\dagger \hat{c}_{i\uparrow} \hat{c}_{i\downarrow}^\dagger \hat{c}_{i\downarrow}. \tag{3.47}$$

In order to connect the N- and the $(2L-N)$-electron systems, the following hole-particle transformation to the creation and annihilation operators is introduced:

$$\begin{aligned}\hat{c}^{\dagger}_{i\sigma} &\rightarrow \hat{b}^{\dagger}_{i\sigma}=(-1)^{i}\hat{c}_{i\sigma},\\ \hat{c}_{i\sigma} &\rightarrow \hat{b}_{i\sigma}=(-1)^{i}\hat{c}^{\dagger}_{i\sigma},\end{aligned}\tag{3.48}$$

and applied to the Hamiltonian in Eq. (3.47), thus leading to [301]

$$\begin{aligned}\hat{H}^{\mathrm{imp}}_{M}(\mathbf{v}) &= -t\sum_{i\sigma}\left(\hat{b}^{\dagger}_{i\sigma}\hat{b}_{i+1\sigma}+\mathrm{h.c.}\right)+2\sum_{i}v_i-\sum_{i\sigma}v_i\hat{b}^{\dagger}_{i\sigma}\hat{b}_{i\sigma}\\ &\quad +UM-U\sum_{i=0}^{M-1}\sum_{\sigma}\hat{b}^{\dagger}_{i\sigma}\hat{b}_{i\sigma}+U\sum_{i}\hat{b}^{\dagger}_{i\uparrow}\hat{b}_{i\uparrow}\hat{b}^{\dagger}_{i\downarrow}\hat{b}_{i\downarrow}.\end{aligned}\tag{3.49}$$

Then, by substituting and shifting the potential in Eq. (3.47) as follows:

$$\tilde{v}_i=-v_i-U\sum_{j=0}^{M-1}\delta_{ij},\tag{3.50}$$

we finally obtain

$$\hat{H}^{\mathrm{imp}}_{M}(\tilde{\mathbf{v}})=-t\sum_{i\sigma}\left(\hat{b}^{\dagger}_{i\sigma}\hat{b}_{i+1\sigma}+\mathrm{h.c.}\right)+\sum_{i\sigma}\tilde{v}_i\hat{b}^{\dagger}_{i\sigma}\hat{b}_{i\sigma}+U\sum_{i}\hat{b}^{\dagger}_{i\uparrow}\hat{b}_{i\uparrow}\hat{b}^{\dagger}_{i\downarrow}\hat{b}_{i\downarrow}+UM+2\sum_{i}v_i.\tag{3.51}$$

As readily seen from Eqs. (3.47) and (3.51), the $(2L-N)$-electron ground-state energy $\mathcal{E}^{\mathrm{imp},2L-N}_{M}(\mathbf{v})$ of $\hat{H}^{\mathrm{imp}}_{M}(\mathbf{v})$ is connected to the N-electron (or, equivalently, $(2L-N)$-hole) ground-state energy $\mathcal{E}^{\mathrm{imp},N}_{M}(\tilde{\mathbf{v}})$ of $\hat{H}^{\mathrm{imp}}_{M}(\tilde{\mathbf{v}})$ as follows,

$$\mathcal{E}^{\mathrm{imp},2L-N}_{M}(\mathbf{v})=\mathcal{E}^{\mathrm{imp},N}_{M}(\tilde{\mathbf{v}})+2\sum_{i}v_i+MU.\tag{3.52}$$

By inserting Eq. (3.52) into Eq. (3.46), the hole-particle relation for the M-impurity-interacting Levy–Lieb functional is obtained as

$$\begin{aligned}F^{\mathrm{imp}}_{M}(\underline{2}-\mathbf{n}) &= \sup_{\mathbf{v}}\left\{\mathcal{E}^{\mathrm{imp},N}_{M}(\tilde{\mathbf{v}})+(\mathbf{v}|\mathbf{n})\right\}+MU\\ &= \sup_{\tilde{\mathbf{v}}}\left\{\mathcal{E}^{\mathrm{imp},N}_{M}(\tilde{\mathbf{v}})-(\tilde{\mathbf{v}}|\mathbf{n})\right\}+U\left(M-\sum_{i=0}^{M-1}n_i\right)\\ &= F^{\mathrm{imp}}_{M}(\mathbf{n})+U\left(M-\sum_{i=0}^{M-1}n_i\right).\end{aligned}\tag{3.53}$$

In the particular case $U=0$, we recover the hole-particle symmetry relation for the non-interacting kinetic energy,

$$T_{\mathrm{s}}(\underline{2}-\mathbf{n}) = T_{\mathrm{s}}(\mathbf{n}). \tag{3.54}$$

Then, the invariance under hole-particle symmetry of the impurity correlation energy,

$$E^{\mathrm{imp}}_{\mathrm{c},M}(\underline{2}-\mathbf{n}) = E^{\mathrm{imp}}_{\mathrm{c},M}(\mathbf{n}), \tag{3.55}$$

as well as the per-site bath correlation energy using Eqs. (2.79) and (3.17),

$$\overline{e}^{\mathrm{bath}}_{\mathrm{c},M}(\underline{2}-\mathbf{n}) = \overline{e}^{\mathrm{bath}}_{\mathrm{c},M}(\mathbf{n}), \tag{3.56}$$

are derived from Eqs. (3.53) and (3.54), (3.8) and (3.11).

Let us turn to the proof of Eq. (3.41) concerning the embedding potential at half-filling. The maximising potential in the second equality of Eq. (3.53), denoted by $\tilde{\mathbf{v}}^{\mathrm{emb}}_M(\mathbf{n})$, is nothing but the exact embedding potential $\mathbf{v}^{\mathrm{emb}}_M(\mathbf{n})$ in Eq. (3.40). Therefore, the two maximising potentials are equal:

$$\mathbf{v}^{\mathrm{emb}}_M(\mathbf{n}) = \tilde{\mathbf{v}}^{\mathrm{emb}}_M(\mathbf{n}), \tag{3.57}$$

and according to the shift [Eq. (3.50)], $\tilde{\mathbf{v}}^{\mathrm{emb}}_M(\mathbf{n})$ is related to the maximising potential of Eq. (3.46) as follows:

$$\tilde{v}^{\mathrm{emb}}_{M,i}(\mathbf{n}) = -v^{\mathrm{emb}}_{M,i}(\underline{2}-\mathbf{n}) - U\sum_{j=0}^{M-1}\delta_{ij}. \tag{3.58}$$

Then, from the equality in Eq. (3.57), it comes

$$v^{\mathrm{emb}}_{M,i}(\mathbf{n}) = -v^{\mathrm{emb}}_{M,i}(\underline{2}-\mathbf{n}) - U\sum_{j=0}^{M-1}\delta_{ij}, \tag{3.59}$$

finally leading to, at half-filling [301],

$$\boxed{v^{\mathrm{emb}}_{M,i}(\mathbf{n}=\underline{1}) = -\frac{U}{2}\sum_{j=0}^{M-1}\delta_{ij}}. \tag{3.60}$$

We recognize the (previously numerically determined) result of Eq. (3.41), now generalized for a system containing multiple impurities.

3.3.3 Derivation of the exact correlation functionals and their derivatives

As readily seen in Eqs. (3.6), (3.32) and (3.39), the derivatives of the correlation functionals with respect to n, U and t are necessary to compute the self-consistent SOET equation, the double occupation, and the per-site energy, respectively. In the following, we show how these derivatives can be calculated exactly, without finite differences. As the derivatives with respect to t are intimately related to the derivatives with respect to U [see Eqs. (3.29), (3.30) and (3.31)], only the latter will be described.

Starting with the fully-interacting case, the Levy–Lieb functional in Eq. (2.50) can be rewritten as follows, as a consequence of the variational principle in SOFT [Eq. (2.49)]:

$$F(t,U,\mathbf{n}) = \sup_{\mathbf{v}} \left\{ E(t,U,\mathbf{v}) - (\mathbf{v}|\mathbf{n}) \right\}. \tag{3.61}$$

This is the fully-interacting analogue of the M-impurity-interacting Legendre–Fenchel transform [Eq. (3.40)]. Note that the t- and U-dependence have been introduced explicitly for clarity. From the KS decomposition $F(t,U,\mathbf{n}) = T_{\mathrm{s}}(t,\mathbf{n}) + E_{\mathrm{Hxc}}(t,U,\mathbf{n})$, the expression for the correlation energy is obtained as follows:

$$E_{\mathrm{c}}(t,U,\mathbf{n}) = F(t,U,\mathbf{n}) - T_{\mathrm{s}}(t,\mathbf{n}) - \frac{U}{4}\sum_i n_i^2, \tag{3.62}$$

where $T_{\mathrm{s}}(t,\mathbf{n}) = F(t,U=0,\mathbf{n})$. In the uniform case, Eq. (3.61) reduces to the ground-state energy of the fully-interacting Hamiltonian, $F(t,U,\underline{n}) = E(t,U,\mathbf{v}=0)$. Concerning the derivative with respect to U, the Hellmann–Feynman theorem is applied to Eq. (3.61), thus leading to

$$\frac{\partial F(t,U,\mathbf{n})}{\partial U} = \sum_i d_i(t,U,\mathbf{n}), \tag{3.63}$$

where $d_i(t,U,\mathbf{n}) = \langle \Psi(\mathbf{n})|\hat{n}_{i\uparrow}\hat{n}_{i\downarrow}|\Psi(\mathbf{n})\rangle$ denotes the double occupation of site i and $\Psi(\mathbf{n})$ is the ground-state wavefunction of the fully-interacting Hamiltonian $\hat{H}(t,U,\mathbf{v}(t,U,\mathbf{n}))$, with $\mathbf{v}(t,U,\mathbf{n})$ the maximising (stationary) potential of Eq. (3.61). Hence, obtaining the derivative of the correlation energy functional is straightforward and is given by

$$\frac{\partial E_{\mathrm{c}}(t,U,\mathbf{n})}{\partial U} = \sum_i d_i(t,U,\mathbf{n}) - \frac{1}{4}\sum_i n_i^2, \tag{3.64}$$

where the KS decomposition of $F(t,U,\mathbf{n})$ together with Eq. (3.63) have been used. For a uniform density profile $\mathbf{n} = \underline{n}$, the per-site analogues of Eqs. (3.62) and (3.64) are written as follows:

$$e_{\mathrm{c}}(t,U,n) = \frac{E_{\mathrm{c}}(t,U,\underline{n})}{L} = \frac{1}{L}\Big(F(t,U,\underline{n}) - T_{\mathrm{s}}(t,\underline{n})\Big) - \frac{U}{4}n^2, \tag{3.65}$$

and, according to Eq. (3.63),

$$\frac{\partial e_{\mathrm{c}}(t,U,n)}{\partial U} = d(t,U,n) - \frac{n^2}{4}, \tag{3.66}$$

where $d_i(t,U,\underline{n}) = d(t,U,n)$ is site-independent in the uniform case.

Turning to the embedded impurity problem, the impurity correlation energy is defined by

$$E_{\mathrm{c},M}^{\mathrm{imp}}(t,U,\mathbf{n}) = F_M^{\mathrm{imp}}(t,U,\mathbf{n}) - T_{\mathrm{s}}(t,\mathbf{n}) - \frac{U}{4}\sum_{i=0}^{M-1} n_i^2, \tag{3.67}$$

where $F_M^{\mathrm{imp}}(t,U,\mathbf{n})$ is given in Eq. (3.40) and $T_{\mathrm{s}}(t,\mathbf{n}) = F_M^{\mathrm{imp}}(t,U=0,\mathbf{n})$. Differentiating this impurity correlation energy with respect to U leads to

$$\frac{\partial E_{\mathrm{c},M}^{\mathrm{imp}}(t,U,\mathbf{n})}{\partial U} = \frac{\partial F_M^{\mathrm{imp}}(t,U,\mathbf{n})}{\partial U} - \frac{1}{4}\sum_{i=0}^{M-1} n_i^2, \tag{3.68}$$

where, by using the stationary potential $\mathbf{v}_M^{\mathrm{emb}}(U,t,\mathbf{n})$ in Eq. (3.40),

$$\frac{\partial F_M^{\mathrm{imp}}(t,U,\mathbf{n})}{\partial U} = \left.\frac{\partial \mathcal{E}_M^{\mathrm{imp}}(U,t,\mathbf{v})}{\partial U}\right|_{\mathbf{v}=\mathbf{v}_M^{\mathrm{emb}}(U,t,\mathbf{n})}. \tag{3.69}$$

Besides, according to the Hellmann–Feynman theorem, Eq. (3.69) becomes

$$\frac{\partial F_M^{\mathrm{imp}}(t,U,\mathbf{n})}{\partial U} = \sum_{i=0}^{M-1} d_{M,i}^{\mathrm{imp}}(\mathbf{n}), \tag{3.70}$$

where $d_{M,i}^{\mathrm{imp}}(\mathbf{n}) = \langle \Psi_M^{\mathrm{imp}}(\mathbf{n}) | \hat{n}_{i\uparrow}\hat{n}_{i\downarrow} | \Psi_M^{\mathrm{imp}}(\mathbf{n})\rangle$ and $\Psi_M^{\mathrm{imp}}(\mathbf{n})$ is the ground-state wavefunction of $\hat{H}_M^{\mathrm{imp}}(U,t,\mathbf{v}_M^{\mathrm{emb}}(U,t,\mathbf{n}))$. Finally, inserting Eq. (3.70) into (3.68) leads to

$$\frac{\partial E_{\mathrm{c},M}^{\mathrm{imp}}(t,U,\mathbf{n})}{\partial U} = \sum_{i=0}^{M-1} d_{M,i}^{\mathrm{imp}}(\mathbf{n}) - \frac{1}{4}\sum_{i=0}^{M-1} n_i^2. \tag{3.71}$$

3.4 Approximate correlation energy functionals of the site occupations

So far, exact properties of the functionals have been discussed, and the SOET equation has been solved by using numerically-optimised embedding potentials. In practice, analytical expressions for the complementary bath Hxc functional have to be developed. As already mentioned in Sec. (2.2), there are two non trivial cases for which the correlation energy is known analytically within SOFT. The first one is the one-dimensional half-filled Hubbard model in the thermodynamic limit ($n = 1$, $L \to +\infty$) [320], which has led to BALDA [359, 360]. The second one is the asymmetric Hubbard dimer for which a highly accurate parametrization has been derived [335, 358]. From the decomposition of the per-site bath correlation energy [Eq. (3.17)], it comes that both the conventional correlation energy $E_{\text{Hxc}}(\mathbf{n})$ and the impurity one $E^{\text{imp}}_{\text{Hxc},M}(\mathbf{n})$ have to be approximate. BALDA will be used to model the former, such that only the impurity correlation functional remains to be found.

3.4.1 Exact functional for the Hubbard dimer

In order to develop approximate functionals, it is advantageous to look at systems with analytical solutions. For instance, the two-electron system is considered to be a paradigm in RDMFT, as the functional of the 1RDM is exactly known in this case [189, 432, 433]. We follow the same direction by looking at the asymmetric Hubbard dimer (see Sec. 2.1.4.iii) [335, 358]. In SOET, the asymmetric Hubbard dimer is mapped onto an impurity Hubbard dimer, which ground-state energy is simply obtained by setting $U_1 = 0$ and $U_0 = U$ in Eq. (2.44), thus leading to [72]

$$\mathcal{E}^{\text{imp}}_{M=1}(U, \Delta v) = \mathcal{E}_0(U, 0, \Delta v) = E_0(U/2, \Delta v - U/2). \tag{3.72}$$

We denote the impurity occupation by $n_0 = n$ and the bath one by $n_1 = 2 - n$. The Legendre-Fenchel transforms are written as follows for the fully-interacting case,

$$F(U, n) = \sup_{\Delta v} \Big\{ E_0(U, \Delta v) + \Delta v(n-1) \Big\}, \tag{3.73}$$

and the single-impurity case,

$$F^{\text{imp}}_{M=1}(U, n) = \sup_{\Delta v} \Big\{ \mathcal{E}^{\text{imp}}_{M=1}(U, \Delta v) + \Delta v(n-1) \Big\}, \tag{3.74}$$

where the maximising potentials are denoted by $\Delta v(U, n)$ and $\Delta v^{\text{emb}}_{M=1}(U, n)$, respectively. By applying the Hellmann–Feynman theorem to Eqs. (3.73) and (3.74), and by using the stationarity of the maximising potentials, it comes

$$\left.\frac{\partial E(U,\Delta v)}{\partial \Delta v}\right|_{\Delta v=\Delta v(U,n)} = \left.\frac{\partial \mathcal{E}^{\mathrm{imp}}_{M=1}(U,\Delta v)}{\partial \Delta v}\right|_{\Delta v=\Delta v^{\mathrm{emb}}_{M=1}(U,n)} = 1-n, \tag{3.75}$$

and, according to in Eq. (3.72),

$$\left.\frac{\partial E(U/2,\Delta v)}{\partial \Delta v}\right|_{\Delta v=\Delta v(U/2,n)} = \left.\frac{\partial E(U/2,\Delta v)}{\partial \Delta v}\right|_{\Delta v=\Delta v^{\mathrm{emb}}_{M=1}(U,n)-U/2} = 1-n, \tag{3.76}$$

thus leading to the following scaling and shifting relation between the embedding potential and the conventional one:

$$\Delta v^{\mathrm{emb}}_{M=1}(U,n) = \Delta v(U/2,n) + \frac{U}{2}. \tag{3.77}$$

Then, according to this new relation together with Eq. (3.72), it comes

$$F^{\mathrm{imp}}_{M=1}(U,n) = F(U/2,n) + \frac{U}{2}(n-1) \tag{3.78}$$

and, by using the KS decompositions of both Levy–Lieb functionals of Eq. (3.78) [see Eqs. (3.8) and (2.51)],

$$E^{\mathrm{imp,2L}}_{\mathrm{Hxc},M=1}(U,n) = E^{\mathrm{2L}}_{\mathrm{Hxc}}(U/2,n) + \frac{U}{2}(n-1). \tag{3.79}$$

2L refers to as "two-level" (i.e. the Hubbard dimer). Deriving Eq. (3.79) with respect to (minus) n leads to similar scaling and shifting relation as Eq. (3.77) is obtained, but between the impurity Hxc potential and the fully-interacting Hxc potential [72]:

$$\Delta v^{\mathrm{imp,2L}}_{\mathrm{Hxc},M=1}(U,n) = \Delta v^{\mathrm{2L}}_{\mathrm{Hxc}}(U/2,n) - \frac{U}{2}, \tag{3.80}$$

where $\Delta v^{\mathrm{imp,2L}}_{\mathrm{Hxc},M=1}(U,n) = -\partial E^{\mathrm{imp,2L}}_{\mathrm{Hxc},M=1}(U,n)/\partial n$ and $\Delta v^{\mathrm{2L}}_{\mathrm{Hxc}}(U,n) = -\partial E^{\mathrm{2L}}_{\mathrm{Hxc}}(U,n)/\partial n$. Finally, from Eq. (3.79) and by separating the Hx parts,

$$\begin{aligned} E^{\mathrm{imp,2L}}_{\mathrm{Hx},M=1}(U,n) &= \frac{U}{4}n^2, \\ E^{\mathrm{2L}}_{\mathrm{Hx}}(U,n) &= \frac{U}{4}\left(n^2+(2-n)^2\right) = \frac{U}{2}\left(1+(1-n)^2\right), \end{aligned} \tag{3.81}$$

from the correlation parts, a simple scaling relation between the impurity- and the fully-interacting correlation functionals is obtained [72]:

$$E_{\mathrm{c},M=1}^{\mathrm{imp,2L}}(U,n) = E_{\mathrm{c}}^{\mathrm{2L}}(U/2,n). \tag{3.82}$$

Eq. (3.82) tells us that if the analytical expression of $E_{\mathrm{c}}^{\mathrm{2L}}(U,n)$ is known, so is the impurity correlation energy. Therefore, the parametrization of Carrascal and co-workers [335, 358] can be extended to our impurity problem by using a simple 1/2 scaling of the electronic repulsion parameter U. The derivations required to implement this correlation functional are presented in Appendix G. Consequently, the complementary bath Hxc functional is exactly known for the asymmetric Hubbard dimer and reads

$$\overline{E}_{\mathrm{Hxc},M=1}^{\mathrm{bath,2L}}(U,n) = E_{\mathrm{Hxc}}^{\mathrm{2L}}(U,n) - E_{\mathrm{Hxc},M=1}^{\mathrm{imp,2L}}(U,n) = E_{\mathrm{Hxc}}^{\mathrm{2L}}(U,n) - E_{\mathrm{Hxc}}^{\mathrm{2L}}(U/2,n). \tag{3.83}$$

3.4.2 Two-level Bethe Ansatz Local Density Approximation

Returning to a larger system ($L > 2$), the conventional correlation energy will be modelled within BALDA. If a single impurity is considered, the impurity correlation functional in Eq. (3.17) can be approximated by the impurity correlation functional of the asymmetric Hubbard dimer [Eq. (3.82)] as follows:

$$E_{\mathrm{c},M=1}^{\mathrm{imp}}(\mathbf{n}) \longrightarrow E_{\mathrm{c},M=1}^{\mathrm{imp,2L}}(U,n_0) = E_{\mathrm{c}}^{\mathrm{2L}}(U/2,n_0). \tag{3.84}$$

This is obviously an approximation, given that the exact impurity correlation functional should describe an impurity with occupation n_0, surrounded by $L-1$ noninteracting sites sharing $N-n_0$ electrons. On the contrary, the 2L impurity correlation functional describes one impurity site with occupation n_0 surrounded by one noninteracting site only with $2-n_0$ electrons. Together with BALDA, it leads to the so-called 2L-BALDA approximation,

$$\overline{e}_{\mathrm{c},M=1}^{\mathrm{bath}}(\mathbf{n}) \quad \xrightarrow{\text{2L-BALDA}} \quad e_{\mathrm{c}}^{\mathrm{BALDA}}(n_0) - E_{\mathrm{c}}^{\mathrm{2L}}(U/2,n_0). \tag{3.85}$$

Note that the dependence on the bath-site occupations is neglected. While thE dependence on the impurity occupation only is sufficient to describe the Hubbard dimer exactly, it is not the case anymore for a larger system, as shown in Sec. 3.3.1. Hence, 2L-BALDA belongs to the (more general) iLDA approximation [see Eq. (3.44)]. This will also be the case for all the functionals developed in the following.

3.4.3 Impurity Bethe Ansatz Local Density Approximation

A simple idea consists in modelling the M-impurity-interacting correlation energy within BALDA, thus leading to the so-called *M-impurity Bethe ansatz local density approximation* denoted by iBALDA(M),

$$E^{\text{imp}}_{\text{Hxc},M}(\mathbf{n}) \xrightarrow{\text{iBALDA}(M)} \sum_{i=0}^{M-1} e_{\text{c}}^{\text{BALDA}}(n_i). \tag{3.86}$$

According to Eq. (3.17), the per-site bath correlation functional measures the deviation of the impurity correlation energy from the conventional one. As both terms are expressed within BALDA, it comes

$$\overline{e}^{\text{bath}}_{\text{c},M}(\mathbf{n}) \xrightarrow{\text{iBALDA}(M)} 0, \tag{3.87}$$

and, according to Eq. (3.18),

$$\overline{E}^{\text{bath}}_{\text{Hxc},M}(\mathbf{n}) = \sum_{i=M}^{L-1} e_{\text{Hxc}}^{\text{BALDA}}(n_i) = \sum_{i=M}^{L-1} \left(\frac{U}{4} n_i^2 + e_{\text{c}}^{\text{BALDA}}(n_i)\right). \tag{3.88}$$

Obviously, if all the sites are considered as impurities ($M = L$), the SOET Hamiltonian reduces to the fully-interacting Hamiltonian and

$$\overline{E}^{\text{bath}}_{\text{c},M=L}(\mathbf{n}) = 0. \tag{3.89}$$

On the contrary, if there is no impurity, the SOFT Hamiltonian is recovered and

$$\overline{E}^{\text{bath}}_{\text{Hxc},M=0}(\mathbf{n}) = E_{\text{Hxc}}(\mathbf{n}). \tag{3.90}$$

iBALDA($M{=}L$) and iBALDA($M{=}0$) fulfil the conditions in Eqs. (3.89) and (3.90), respectively. For the latter, the Hxc functional in SOFT would be approximated within BALDA.

3.4.4 Density-functional approximations based on the SIAM

The SIAM has been briefly described in Sec. 2.3, where its Hamiltonian in the basis of sites (i.e. the discretized real space) is given in Eq. (2.93). Turning to SOET, let us consider the $(L+1)$-site SOET Hamiltonian at half-filling, for a single impurity,

$$\hat{H} = -t \sum_{\sigma} \sum_{i=0}^{L} \left(\hat{c}^{\dagger}_{i\sigma} \hat{c}_{i+1\sigma} + h.c.\right) + U \hat{n}_{0\uparrow} \hat{n}_{0\downarrow} - \frac{U}{2} \hat{n}_0, \tag{3.91}$$

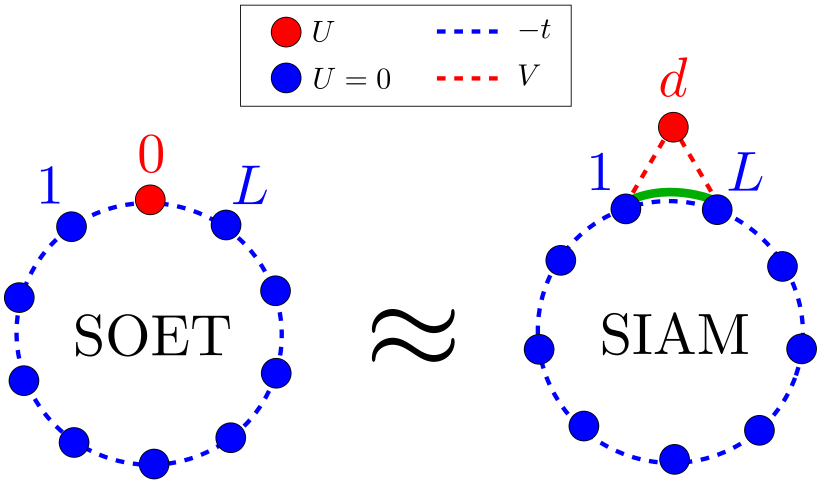

Figure 3.4: Single-impurity-interacting Hubbard model and SIAM model for $L+1$ sites, in the basis of sites. The difference between the two models is highlighted in green.

where the exact half-filling embedding potential in Eq. (3.41) has been used. This Hamiltonian and the symmetric SIAM one in Eq. (2.93) (where $\varepsilon_d = -U/2$ in the symmetric case) are essentially the same if

$$V = -t, \tag{3.92}$$

as illustrated in Fig. 3.4. Note that the single-impurity SOET Hamiltonian at half-filling and the symmetric SIAM Hamiltonian differ by the coupling term between the first neighbours of the impurity site ($i = 1$ and $i = L$). The latter (see Fig. 3.4 in green) will be ignored for simplicity. Guided by the similarities between the two models, SOET could benefit from previous works on the SIAM, such as the development of DFAs. Indeed, these DFAs could be generalized to SOET, thus providing new approximate impurity correlation functionals such as

$$E^{\text{imp}}_{\text{c},M=1}(\mathbf{n}) \longrightarrow E^{\text{SIAM}}_{\text{c}}(n_0). \tag{3.93}$$

Let us now investigate DFAs developed for the SIAM. For example, the perturbation expansion through fourth order in U/Γ, developed by Yamada [434] for the symmetric SIAM, could be used in SOET to describe the weakly correlated limit. This fourth-order correlation energy reads

$$E^{\text{SIAM}}_{\text{c},U/\Gamma\to 0}(U,\Gamma) = \frac{U^2}{\pi\Gamma}\left[-0.0369 + 0.0008\left(\frac{U}{\pi\Gamma}\right)^2\right], \tag{3.94}$$

where Γ is the (frequency-independent [434]) impurity-level-width parameter. In analogy with the Hubbard model where the ratio U/t defines the correlation strength, the ratio U/Γ in the SIAM model is used instead. Regarding the strongly correlated limit, a correlation potential relying on the BA solution to the strongly correlated SIAM [435, 436] has been proposed by Burke and co-workers [372, 373] as follows:

$$v_{\mathrm{xc}}(n) = \alpha\frac{U}{2}\left(1 - n - \frac{2}{\pi}\tan^{-1}\left(\frac{1-n}{\sigma}\right)\right), \tag{3.95}$$

where $\alpha(U,\Gamma) = U/(U + 5.68\Gamma)$ and $\sigma = 8\Gamma/(\pi^2 U)$. An impurity correlation energy functional is then obtained by integrating Eq. (3.95) with respect to the density n[2], thus leading to [300]

$$E^{\mathrm{SIAM}}_{\mathrm{c},U/\Gamma\to\infty}(U,\Gamma,n) = \alpha(U,\Gamma)\frac{U}{2}\Big[\mathcal{E}_{\mathrm{c}}(U,\Gamma,n) - \mathcal{E}_{\mathrm{c}}(U,\Gamma,0)\Big], \tag{3.96}$$

where

$$\mathcal{E}_{\mathrm{c}}(U,\Gamma,n) = n - \frac{n^2}{2} + \frac{2}{\pi}(1-n)\tan^{-1}\left[\frac{(1-n)}{\sigma}\right] - \frac{\sigma}{\pi}\ln\left[1 + \left(\frac{(1-n)}{\sigma}\right)^2\right]. \tag{3.97}$$

Note that the latter is not restricted to the symmetric case, in contrast to the correlation energy in Eq. (3.94). In order to get a correct description of the symmetric SIAM in all correlation regimes, a simple interpolation between the weakly [Eq. (3.94)] and the strongly [Eq. (3.96)] correlated limits is suggested as follows [300]:

$$E^{\mathrm{SIAM}}_{\mathrm{c}}(U,\Gamma,n=1) = \frac{1}{1+f}E^{\mathrm{SIAM}}_{\mathrm{c},U/\Gamma\to 0}(U,\Gamma) + \frac{f}{1+f}E^{\mathrm{SIAM}}_{\mathrm{c},U/\Gamma\to\infty}(U,\Gamma,n=1), \tag{3.98}$$

where $f = f(U/\Gamma) = e^{U/\Gamma - 6.876}$ (the parameter 6.876 simply corresponds to the crossing point between the two functionals). With such an interpolation, the correlation functional based on the perturbation expansion in the weakly correlated regime will dominate for $U/\Gamma < 6.876$, while the one based on the BA solution to the strongly correlated regime will dominate otherwise. Note that $E^{\mathrm{SIAM}}_{\mathrm{c}}(U,\Gamma,n=1)$ becomes positive for $U/\Gamma < 2$, which is unphysical (the correlation energy should always be negative). This artefact is actually removed by the interpolation [Eq. (3.98)] [300].

In order to generalize the DFAs based on the SIAM to SOET, we need to relate the (frequency-independent) impurity-level-width parameter Γ to the hopping parameter t of the Hubbard model. Now that the connection between the SOET and the SIAM Hamiltonians has been clarified in the basis of sites by the relation in Eq. (3.92), let us consider the SIAM Hamiltonian in k-space [Eq. (2.94)]. As mentioned in the DMFT section (Sec. 2.4.1), the coupling between the impurity and the bath

---

[2] Integration from 0 to n. To find the constant of integration, we set the energy to 0 when there is no density. This leads to a constant equal to 0.

is characterized by a frequency-dependent hybridization function [Eq. (2.99)], which imaginary part [Eq. (2.102)] is nothing but the frequency-dependent impurity level width $\Gamma(\omega)$. The latter is given in the thermodynamic limit ($L \rightarrow +\infty$) as follows:

$$\Gamma(\omega) \quad = \quad \frac{L}{2}\int_{-\pi}^{\pi} \mathrm{d}k|V_k|^2\delta(\omega-\varepsilon_k) = L\int_{0}^{\pi} \mathrm{d}k|V_k|^2\delta(\omega-\varepsilon_k) = 4V^2\int_{0}^{\pi} \mathrm{d}k\cos^2(k/2)\delta(\omega-\varepsilon_k), \tag{3.99}$$

thus leading to [3]

$$\Gamma(\omega) = \frac{V^2}{t^2}\int_{-2t}^{2t} \mathrm{d}\varepsilon \frac{t-\dfrac{\varepsilon}{2}}{\sqrt{1-\dfrac{\varepsilon^2}{4t^2}}}\delta(\omega-\varepsilon). \tag{3.100}$$

The (frequency-independent) impurity-level-width parameter Γ of the SIAM is defined as the value of the hybridization function at the Fermi level $\varepsilon_F = -2t\cos(k_F)$, such that

$$\Gamma = \Gamma(\varepsilon_F) = \frac{V^2}{t^2}\frac{t-\dfrac{\varepsilon_F}{2}}{\sqrt{1-\dfrac{\varepsilon_F^2}{4t^2}}}. \tag{3.101}$$

By using Eq. (3.92) and the relation between the uniform density $n = N/L$ in the bath and k_F,

$$\int_0^{N/4} \mathrm{d}m = \frac{Ln}{4} = \int_0^{k_F} \frac{L}{2\pi}\mathrm{d}k, \tag{3.102}$$

(or, equivalently, $n = 2k_F/\pi$) we finally obtain a t-dependent density-functional impurity level width which connects the SIAM to the original Hubbard problem,

$$\Gamma = \Gamma(t,n) = t\left(\frac{1+\cos(\pi n/2)}{\sin(\pi n/2)}\right). \tag{3.103}$$

Note that the latter expression is valid for $0 \leqslant n \leqslant 1$. In the range $1 \leqslant n \leqslant 2$, the hole-particle symmetry relation $\Gamma(t,n) = \Gamma(t,2-n)$ is used. As readily seen from Eq. (3.103), $\Gamma = t$ at half-filling.

Thanks to the relation in Eq. (3.103), it becomes now possible to develop DFAs in SOET based on the DFAs of the SIAM, as suggested in Eq. (3.93). The first approximation is given at half-filling by setting $\Gamma = t$ in Eq. (3.98). Together with BALDA, the following per-site bath correlation functional

---

[3] By using the trigonometric relations $\cos^2(x) = \dfrac{1+\cos(2x)}{2}$ and $\cos^2(x)+\sin^2(x) = 1$, together with the substitution $\varepsilon = -2t\cos(k)$.

is obtained,

$$\overline{e}_{\mathrm{c},M=1}^{\mathrm{bath}}(\mathbf{n}) \xrightarrow[\mathrm{BALDA}[n=1]]{\mathrm{SIAM}} e_{\mathrm{c}}^{\mathrm{BALDA}}(n_0) - E_{\mathrm{c}}^{\mathrm{SIAM}}(U, \Gamma = t, n = 1). \tag{3.104}$$

This functional, so-called SIAM-BALDA[n=1], is restricted to half-filling. It could be possible to extend SIAM-BALDA[n=1] away from half-filling by using Eq. (3.103). However, the interpolation formula in Eq. (3.98) depends on $f(U/t)$, which contains a parameter defined by the crossing point of the functionals at half-filling only. This function $f(U/t)$ could certainly be generalized into a n-dependent function, assuring the correct interpolation of the two correlation functionals in any density regime. This has not been investigated here.

Another DFA is obtained by replacing Γ by $\Gamma(t, n)$ in Eq. (3.94). Together with the use of BALDA for the conventional per-site correlation energy, this new functional will be referred to as SIAM-BALDA (without the suffix [n=1]) in the following,

$$\overline{e}_{\mathrm{c},M=1}^{\mathrm{bath}}(\mathbf{n}) \xrightarrow[\mathrm{BALDA}]{\mathrm{SIAM}} e_{\mathrm{c}}^{\mathrm{BA}}(n_0) - E_{\mathrm{c},U/\Gamma\to 0}^{\mathrm{SIAM}}(U, \Gamma(t, n_0)). \tag{3.105}$$

In contrast to its [n=1] analog, SIAM-BALDA is applicable to *any* density regime. At half-filling, SIAM-BALDA[n=1] is expected to be more accurate than SIAM-BALDA in the strongly correlated regime, by construction. Interestingly, the deviation from half-filling in the original Hubbard model can be interpreted, in the SIAM, as a rescaling of Γ, as readily seen in Eq. (3.103) by varying n. In the low-density regime we have $\Gamma(t, n) \approx 4t/(\pi n) \gg \Gamma(t, n = 1)$, thus leading to weaker correlation effects on the embedded impurity site, in comparison to the half-filled case.

3.5 Solution of the SOET self-consistent equations

SOET is a method which combines a many-body correlated impurity wavefunction with correlation energy functional contributions. As readily seen from Eqs. (3.28) and (3.39), the determination of the per-site energy and the double occupation expressions within SOET relies on the knowledge of the M-impurity-interacting wavefunction. This wavefunction is the one minimizing the energy, according to the variational principle in Eq. (3.5), and it fulfils the self-consistent equation in Eq. (3.6). For the clarity of this section, let us rewrite this equation for the uniform model ($\mathbf{v} = 0$),

$$\left(\hat{T} + \hat{U}_M + \sum_i \frac{\partial \overline{E}_{\mathrm{Hxc},M}^{\mathrm{bath}}\left(\mathbf{n}^{\Psi_M^{\mathrm{imp}}}\right)}{\partial n_i}\right) |\Psi_M^{\mathrm{imp}}\rangle = \mathcal{E}_M^{\mathrm{imp}} |\Psi_M^{\mathrm{imp}}\rangle. \tag{3.106}$$

In principle, any correlated method based on the explicit calculation of many-body wavefunctions or Green's functions could be employed to solve Eq. (3.106). So far in this thesis, the exact diagonalization (FCI) has been used to investigate the exact embedding potential through the implementation of the Lieb maximisation [Sec. 3.3.1]. Due to the exponential scaling of the method, only the one-dimensional eight-site Hubbard model has been studied. In order to approach more and more the thermodynamic limit, we have turned to the cheaper DMRG solver [Sec. 1.1.8] to enlarge the size of the model. From now on, the *uniform* 32-site ring Hubbard model is investigated using periodic ($\hat{c}_{L\sigma} = \hat{c}_{0\sigma}$) and antiperiodic ($\hat{c}_{L\sigma} = -\hat{c}_{0\sigma}$) boundary conditions, when $(N/2) \bmod 2 = 1$ [i.e. $N/2$ is an odd number] and $(N/2) \bmod 2 = 0$ [i.e. $N/2$ is an even number], respectively.

Note that approaching the thermodynamic limit has many interesting aspects. One of them is the possibility to study all the density regime continuously. Indeed, one could then look at the $\mathbf{n} \rightarrow \underline{1}^-$ and $\mathbf{n} \rightarrow \underline{1}^+$ limits which are essential to observe the derivative discontinuity of the exact correlation functionals [300], as well as the "density-driven" Mott-Hubbard transition that will be described in chapter 4. For the eight-site model, the available uniform occupations were $n = N/L \equiv \{0.25, 0.5, 0.75, 1, 1.25, 1.5, 1.75\}$. Note that even numbers of electrons are considered, given that the theory is currently restricted to singlet states. For 32 sites, one can approach the surrounding of half-filling by considering 30 electrons, thus leading to a uniform density $n = 0.9375$. This is much better compared to the eight-site model, even though it remains relatively far from half-filling.

In the following, Eq. (3.106) is solved with the iBALDA, 2L-BALDA, SIAM-BALDA and SIAM-BALDA[n=1] approximations. In order to be clear on the implementation of these approximations, we summarize each of them in Tab. 3.1. The SOET results are compared to the highly accurate DMRG calculation (i.e. by applying DMRG to the fully-interacting Hubbard model). The convergence criteria is imposed on the M-interacting-impurity auxiliary energy $\mathcal{E}_M^{\rm imp}$ and the occupation of one impurity site with a threshold of 10^{-5} (note that in Ref. [72], we have shown that the bath occupations converge even faster than the impurity occupation). To help convergence, the embedding potential has been updated as follows in the self-consistent cycle,

$$\left\{v_{M,i}^{\mathrm{emb},n}\right\}_i \longrightarrow \left\{(1-x)v_{M,i}^{\mathrm{emb},n-1} + xv_{M,i}^{\mathrm{emb},n}\right\}_i, \tag{3.107}$$

where n is the number of iterations and x is a coefficient between $0 < x < 1$ that mixes the potentials of the nth and $(n-1)$th iterations. In this work, x is initialized to 0.4 and incremented by 0.2 each time the convergence is reached, until $x = 1$. This scheme prevents eventual oscillations of the potential in the self-consistent procedure, such that no convergence problem has been faced in the model studied

SOET method	DFA used for $\overline{E}^{\rm bath}_{{\rm Hxc},M}(\mathbf{n})$	Correlation functional approximation
iBALDA	$\sum_{i=M}^{L}\left(\frac{U}{4}n_i^2+e_{\rm c}^{\rm BALDA}(n_i)\right)$	Eqs. (2.80)–(2.82)
SIAM-BALDA	$\sum_{i}\left(\frac{U}{4}n_i^2+e_{\rm c}^{\rm BALDA}(n_i)\right)-\frac{U}{4}n_0^2-E^{\rm SIAM}_{{\rm c},U/\Gamma\rightarrow 0}\left(U,\Gamma(t,n_0)\right)$	Eqs. (2.80)–(2.82), (3.94) and (3.103)
SIAM-BALDA[n=1]	$\sum_{i}\left(\frac{U}{4}+e_{\rm c}^{\rm BALDA}(n=1)\right)-\frac{U}{4}-E_{\rm c}^{\rm SIAM}(U,\Gamma=t,n=1)$	Eqs. (2.80)–(2.82), (3.98) with (3.94), (3.96) and (3.97)
2L-BALDA	$\sum_{i}\left(\frac{U}{4}n_i^2+e_{\rm c}^{\rm BALDA}(n_i)\right)-\frac{U}{4}n_0^2-E_{\rm c}^{\rm imp,2L}(n_0)$	Eqs. (2.80)–(2.82), (103)

Table 3.1: Summary of the DFAs used for $\overline{E}^{\rm bath}_{{\rm Hxc},M}(\mathbf{n})$ in the practical SOET calculations [Eq (3.106)]. The corresponding approximate bath Hxc potentials on site i are simply obtained by taking the derivative with respect to n_i. In the half-filled case, we used the exact potential in Eq. (3.60).

in this chapter (i.e. the uniform one-dimensional 32-site Hubbard model). The convergence is reached for approximately 10 or 20 iterations, depending on the correlation strength and the density regime. At half-filling, the exact embedding potential [Eq. (3.60)] is used such that one iteration only is needed to converge.

3.5.1 Density profiles

In Sec. 3.3.1, the exact embedding potential able to recover the uniform density has been calculated, showing the absence of impurity-interacting v-representability problem in the Hubbard model within SOET. Besides, it has been shown that an impurity-optimised potential could reproduce the exact impurity occupation, at the expense of the uniform occupation in the bath. One may wonder if the different approximations are able or not to reproduce a correct density profile. At half-filling, the exact embedding potential is used so that the answer is definitely *yes*.

The density profiles obtained by solving the SOET equation [Eq. (3.106)] are shown in Fig. 3.5 for $N = 8$ and $N = 24$ electrons, and a single impurity site. When no embedding potential is used, it is clear that the uniform density profile cannot be reproduced due to the impurity site which breaks the translational invariance of the system. As expected, the exact uniformity is *not* reproduced by the

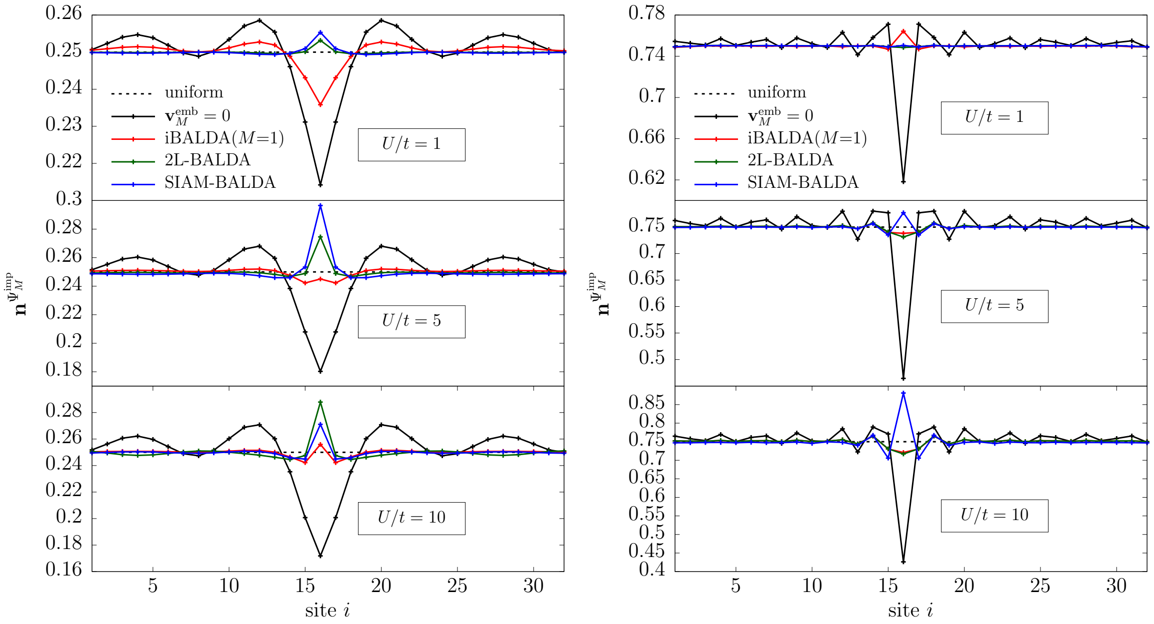

Figure 3.5: Density profile obtained after solving the SOET equations self-consistently. Left panel: $N = 8$ electrons. Right panel: $N = 24$ electrons. The impurity located on site 16. See text for further details.

approximate functionals in SOET, for any correlation and density regime studied in Fig. 3.5. In spite of that, the uniformity in the bath sites is usually well recovered within all the approximations, in contrast to the impurity site on which the strongest deviation from the exact site-occupation arises, and is somehow echoed on its closest neighbours. Nevertheless, this deviation remains relatively small in most cases.

To conclude, the DFAs in SOET can correctly reproduce the uniform bath occupation, even away from half-filling. The recovering of an accurate occupation on the impurity and its closest neighbour sites is more challenging, due to the presence of the explicit repulsion between the electrons. Nevertheless, the final occupations are very encouraging and they do not differ too much from the exact one.

We now discuss the resulting per-site energy and double occupation within SOET.

3.5.2 Per-site energy and double occupation at half-filling

3.5.2.i Per-site energy at half-filling

Let us focus on the half-filled case, for which the exact embedding potential is used. Solving the SOET equation [Eq. (3.106)] leads to the site-occupation vector $\left(\mathbf{n}^{\Psi_M^{\text{imp}}} \equiv \left\{\langle \Psi_M^{\text{imp}} | \hat{n}_i | \Psi_M^{\text{imp}} \rangle\right\}_i\right)$ and the double occupations $\left(d_{M,i}^{\text{imp}} = \langle \Psi_M^{\text{imp}} | \hat{n}_{i\uparrow} \hat{n}_{i\downarrow} | \Psi_M^{\text{imp}} \rangle\right)$. They are used to compute the physical per-site energy and the physical double occupation, for which exact expressions are given in Eqs. (3.28) and (3.39), respectively. Given that the exact embedding potential is used, the exact uniform density is reproduced and $\Psi_M^{\rm imp}$ (as well as $\{d_{M,i}^{\rm imp}\}_i$) will be the same for any DFAs and will only depend on M. In addition, BALDA is exact at half-filling in the thermodynamic limit for the conventional per-site correlation energy. In other words, the errors in the per-site energy and the double occupation within SOET at half-filling are directly caused by the error in the approximate impurity correlation functionals, which is the so-called functional-driven error [437].

We start by noticing that all the correlation functionals studied in Sec. 3.4 are of the form $t\times\mathcal{G}(U/t)$. As a consequence, they all automatically satisfy the conditions in Eqs. (3.29), (3.30) and (3.31). Hence, passing from Eq. (3.28) to Eq. (3.32) does not induce any additional error [301]. By inserting Eq. (3.19) into Eq. (3.32), the following convenient expression for the per-site energy is obtained:

$$e = \frac{1}{M}\sum_{i=0}^{M-1}\left(t_{\rm s}(n_i^{\Psi_M^{\rm imp}}) + e_{\rm c}(n_i^{\Psi_M^{\rm imp}}) + U\langle \hat{n}_{i\uparrow}\hat{n}_{i\downarrow}\rangle_{\Psi_M^{\rm imp}}\right) - U\frac{\partial E_{{\rm c},M}^{\rm imp}(\mathbf{n}^{\Psi_M^{\rm imp}})}{\partial U}. \tag{3.108}$$

This expression simplifies the understanding of the following results, as the derivative of the impurity correlation energy with respect to U only has to be considered (everything else is exact in the thermodynamic limit at half-filling). Results are shown in Fig. 3.6 for the various aforementioned approximations. The derivatives of the impurity correlation energies with respect to U are also provided in Fig. 3.7 to assist the discussion. According to Eq. (3.108), Fig. 3.7 is entirely sufficient to rationalize the results in Fig. 3.6, apart from a scaling factor $-U$.

Let us start the discussion with the per-site energy obtained with iBALDA(M=1). For one impurity ($M = 1$), it is clear from Fig. 3.7 that the derivative of the iBALDA(M=1) correlation energy is exactly equal to the exact conventional per-site one (dashed black lines). This was expected as the iBALDA(M=1) impurity correlation energy is modelled by BALDA, which gives the exact conventional per-site correlation energy at half-filling in the thermodynamic limit. We conclude that errors due to the size are negligible here. However, the exact per-site correlation energy is not the same as the exact impurity one (full black lines). The deviation of iBALDA(M=1) from the latter is echoed on the per-site energy in Fig. 3.21 with a scaling factor $-U$, giving a poor description of the energy. In other words, setting the per-site bath correlation energy $\overline{e}_{{\rm c},M=1}^{\rm bath}(\mathbf{n})$ to 0, as done by construction within iBALDA(M), is insufficient here.

Improvements over iBALDA(M=1) can be done in two distinct manners. (i) By using functionals that provide a non-zero contribution for $\overline{e}_{{\rm c},M=1}^{\rm bath}(\mathbf{n})$ while conserving a single-impurity, or (ii) by

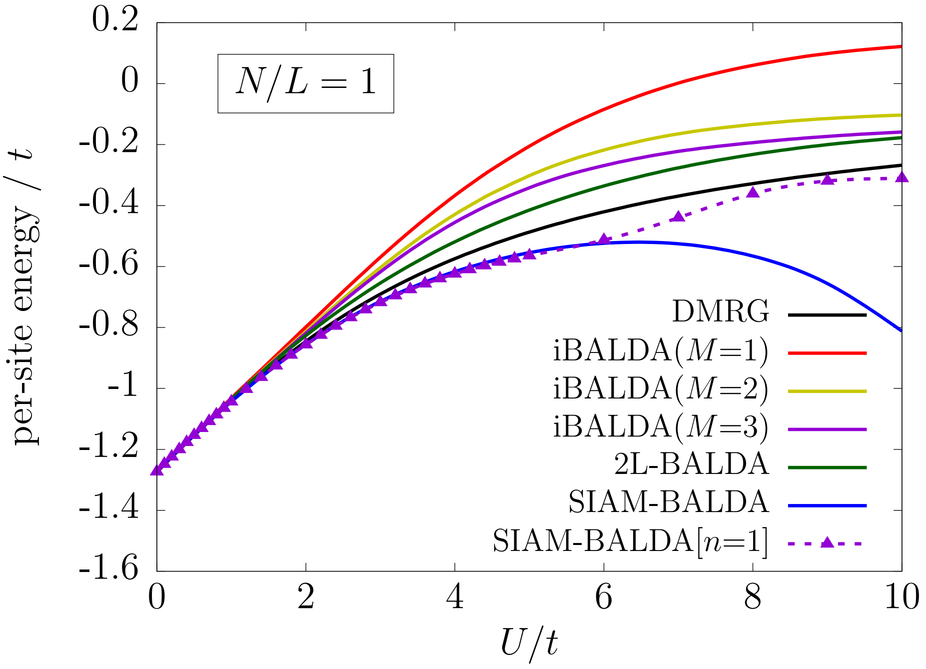

Figure 3.6: Per-site energy at half-filling for the various SOET approximations as a function of U/t. See text for further details.

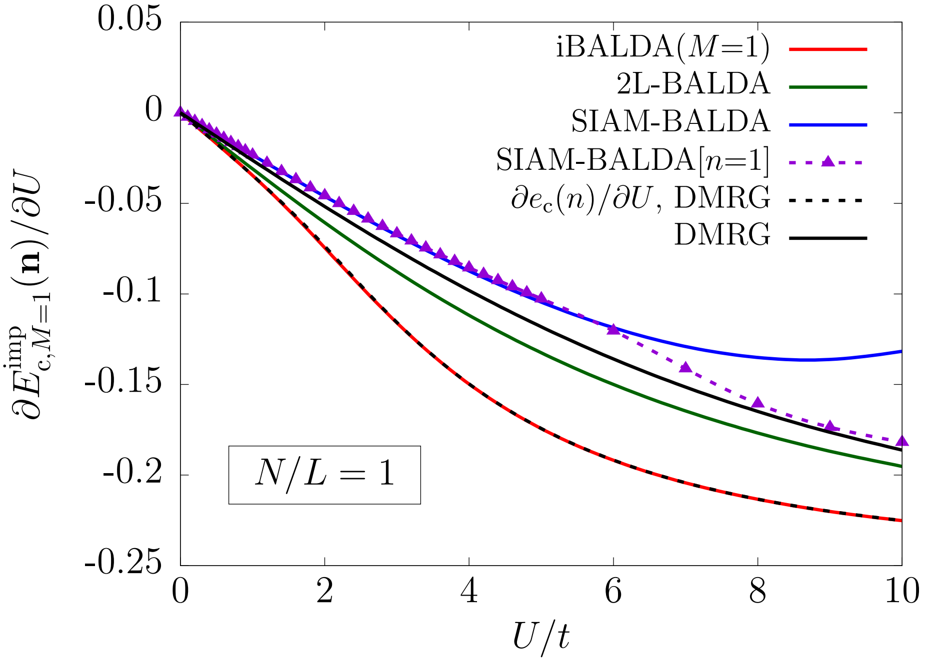

Figure 3.7: Derivative of the impurity correlation energy with respect to U for $n = 1$ as a function U/t. The exact derivatives (labelled by DMRG) are obtained following Sec. 3.3.3. The dashed black line is on top of the iBALDA(M=1) curve.

increasing the number of impurity sites within iBALDA(M). Indeed, and as already mentioned in Sec. 3.4.3, if all sites are interacting iBALDA(M) becomes exact. In Fig. 3.6, $M = 2$ and $M = 3$ impurities have been considered. While iBALDA(M=2) clearly improves over iBALDA(M=1), the per-site energy within iBALDA(M=3) does not change much in comparison with iBALDA(M=2). This slow convergence towards the exact solution with respect to the number of impurities has also been observed in the context of DMET, and has been further investigated by Welborn *et al.* [428], who showed that the convergence speed is given by $1/M$ (see Fig. 4 in Ref. [428]). In addition, the precision gained by increasing the number of impurities is at the expense of a higher computational cost. The above argument suggests that increasing the number of impurities might not be the route to pursue in the context of SOET.

Turning to the first solution (i), 2L-BALDA and SIAM-BALDA can be used to improve over iBALDA(M=1). Impressively, the 2L-BALDA per-site energy is even better than the iBALDA(M=3) one in all the correlation range of Fig. 3.6. This lends weight to the development of single-impurity-interacting functionals rather than increasing the number of impurities. The good accuracy of 2L-BALDA is quite impressive as this functional is exact for the Hubbard dimer only. Concerning the approximations based on the SIAM, SIAM-BALDA gives an extremely accurate per-site energy in the weakly correlated regime ($U \leqslant 4t$, where $4t$ is the bandwidth). This trend confirms the connection between SOET and the SIAM model, as discussed in Sec. 3.4.4. Then, the approximation starts to deviate from the exact result, which is expected as SIAM-BALDA is based on a perturbation expansion in the weakly correlated limit ($U/t \to 0$). Around $U \approx 6t$, the SIAM-BALDA[n=1] functional, based on the interpolation between the weakly and the strongly correlated regimes, takes over from SIAM-BALDA to catch up with the correct per-site energy for $U \geqslant 6t$.

3.5.2.ii Double occupation at half-filling

The exact expression of the double occupation in SOET is given in Eq. (3.39) and, in analogy with the per-site energy discussed above, will be rewritten for a uniform model as follows by using Eq. (3.17):

$$d = \frac{1}{M}\sum_{i=0}^{M-1}\left(\langle \hat{n}_{i\uparrow}\hat{n}_{i\downarrow}\rangle_{\Psi_M^{\text{imp}}} + \frac{\partial e_c(n_i^{\Psi_M^{\text{imp}}})}{\partial U}\right) - \frac{\partial E_{\text{c},M}^{\text{imp}}(\mathbf{n}^{\Psi_M^{\text{imp}}})}{\partial U}. \tag{3.109}$$

The double occupation obtained with the various SOET approximations is shown in Fig. 3.8. Again, in the particular case of half-filling, only the derivative of the approximate impurity correlation energy with respect to U is responsible of any error in the double occupation. This observation is in complete analogy with the per-site energy, except that the error in the double occupation is given by the error

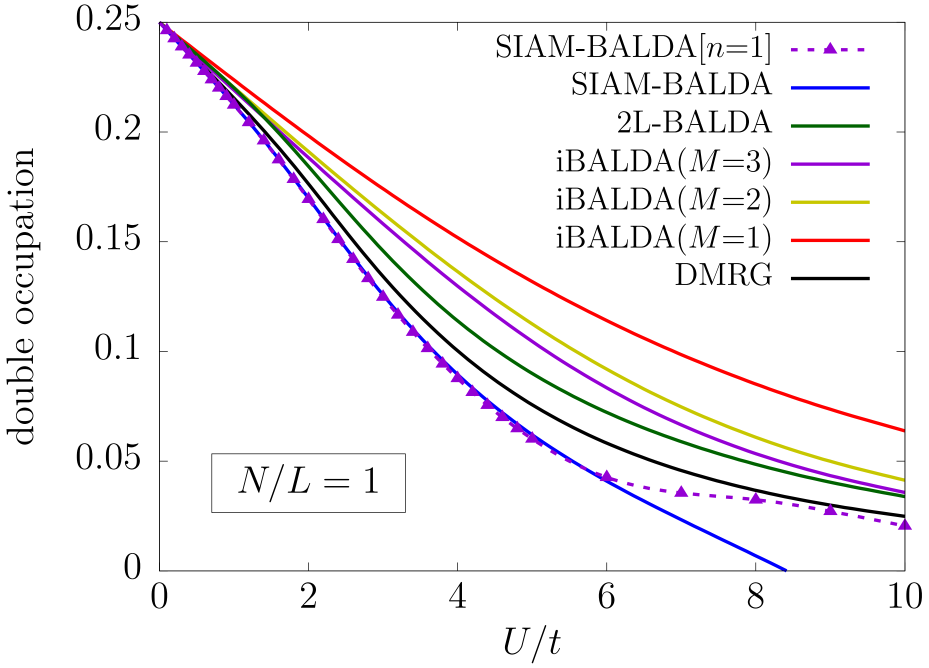

Figure 3.8: Double occupation at half-filling for the various DFAs in SOET, as a functional of U/t.

in the impurity derivative correlation energy with a scaling factor -1, instead of $-U$. Consequently, there is no need to discuss this result differently from the previous discussion on the per-site energy, as one can directly use Fig. 3.7 to explain Fig. 3.8. As readily seen in Fig. 3.8, increasing the number of impurities within iBALDA(M) improves the description of the double occupation. In other words, according to Eq. (3.39), the double occupation on the impurity sites $\left(\{d^{\mathrm{imp}}_{M,i}\}_{i=0,\ldots,M-1}\right)$ is getting closer to the physical double occupation, and $\partial\overline{e}^{\mathrm{bath}}_{\mathrm{c},M}(\mathbf{n})/\partial U$ decreases with the number of impurities.

3.5.3 Per-site energy and double occupation away from half-filling

Although half-filling, which corresponds to the Mott–Hubbard insulator state, is one of the most challenging cases, it is also interesting to look at its surrounding. For instance, in the high-T$_{\mathrm{c}}$ cuprates the superconductivity arises due to carrier doping of the half-filled system. In contrast to the previous section, the BALDA per-site correlation energy will not be exact anymore away from half-filling. Hence, the derivative of the impurity correlation functional with respect to U [Fig. 3.7] alone will not be sufficient to rationalize the results. Besides, none of the DFAs developed in this thesis can reproduce the exact uniformity away from half-filling, as already illustrated in Fig. 3.5. The deviation from uniformity thus leads to the so-called density-driven errors [437], which can either compensate the functional-driven errors (so-called error cancellation) or accumulate onto it.

3.5.3.i Per-site energy away from half-filling

Let us start with the per-site energy, given in Fig. 3.9 in the most challenging site-occupation domain $0.6 \leqslant n = N/L \leqslant 1$. Only the $U/t = 1$ and $U/t = 5$ cases will be shown, as the qualitative discussion of the results do not change by passing from $U/t = 5$ to $U/t = 10$, except for SIAM-BALDA which is not physical anymore in the strongly correlated regime [300, 301]. It appears that the results are easier to analyse by using the exact SOET expression for the per-site energy in Eq. (3.28), that we recall here for convenience,

$$e = \frac{1}{M}\sum_{i=0}^{M-1}\left(t_{\mathrm{s}}(n_i^{\Psi_M^{\mathrm{imp}}}) + t\frac{\partial e_{\mathrm{c}}(n_i^{\Psi_M^{\mathrm{imp}}})}{\partial t} + U d_{M,i}^{\mathrm{imp}}\right) + \left(\overline{e}_{\mathrm{c},M}^{\mathrm{bath}}(\mathbf{n}^{\Psi_M^{\mathrm{imp}}}) - t\frac{\partial \overline{e}_{\mathrm{c},M}^{\mathrm{bath}}(\mathbf{n}^{\Psi_M^{\mathrm{imp}}})}{\partial t}\right). \quad (3.110)$$

According to Eq. (3.110), the correlation energy functionals as well as their derivative with respect to t are needed to have a full understanding of the result in Fig. 3.9. They are provided in Figs. 3.10 and 3.11, respectively. Let us stress that the iBALDA(M=1) curves in Figs. 3.10 and 3.11 are equivalent to the BALDA approximation to the conventional per-site correlation energy and its derivative with respect to t, respectively.

Functional-driven error away from half-filling

In a first step, we discuss the per-site energies obtained by plugging the exact density $\mathbf{n} = \underline{n} \equiv \{n_i = n = N/L\}_i$ in the functional contributions in Eq. (3.110) (see full lines in Fig. 3.9), so that the total error is interpreted as a functional-driven error only. As readily seen in the weakly correlated regime of Fig. 3.9 (top panel), the iBALDA(M) approximation is the most accurate in the domain $0.6 \leqslant N/L \leqslant 0.75$, being almost on top of the exact per-site energy. On the contrary, the 2L-BALDA and SIAM-BALDA approximations slightly underestimate the per-site energy. At first glance, this result is counter intuitive. Indeed, as readily seen in the top panels of Figs. 3.10 and 3.11, the iBALDA(M=1) impurity correlation energy and its derivative with respect to t are far from accurate in contrast to the 2L-BALDA and SIAM-BALDA ones. The accuracy of iBALDA(M) can be explained by error cancellation. Indeed, both the per-site bath correlation functional and its derivative appear in the expression of the per-site energy in Eq. (3.110). For the iBALDA(M=1) approximation, those contributions are set to zero by construction. Then, judging by Figs. 3.10 and 3.11, the exact per-site correlation energy and the exact impurity one are very close to each other away from half-filling, as well as their derivatives. Hence, the difference of the two quantities [according to Eq. (3.19)] leads to per-site bath correlation functional which is almost equal to 0, lending weight to the iBALDA(M) approximation. Indeed, the errors on the impurity correlation energy within iBALDA(M=1) are al-

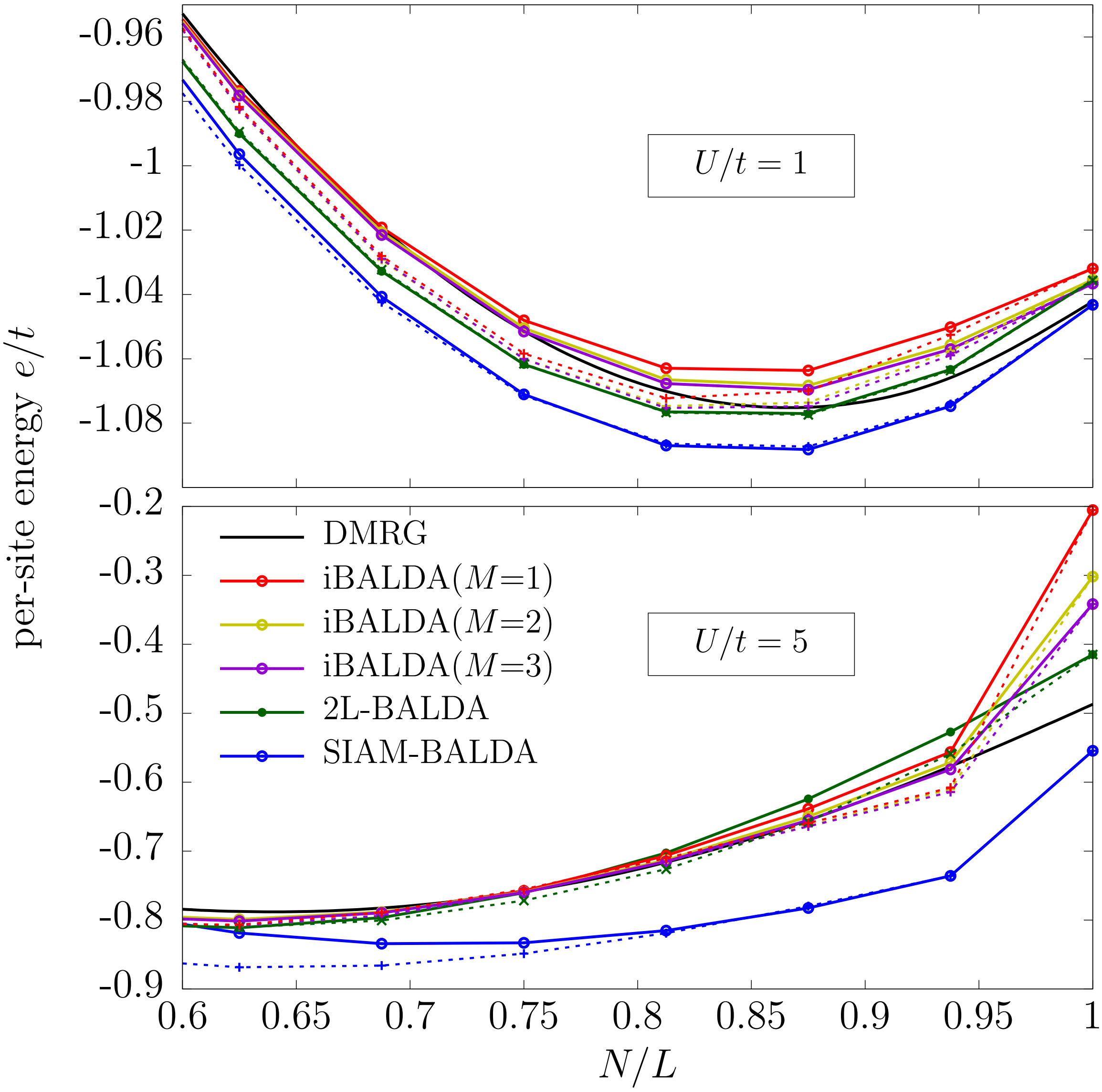

Figure 3.9: Per-site energy for the various DFAs in SOET, as a function of N/L for $U/t = 1$ (top panel) and $U/t = 5$ (bottom panel). Full lines correspond to the per-site energies obtained with the exact occupation $n = N/L$, while the dashed lines are the per-site energies obtained with the converged occupations.

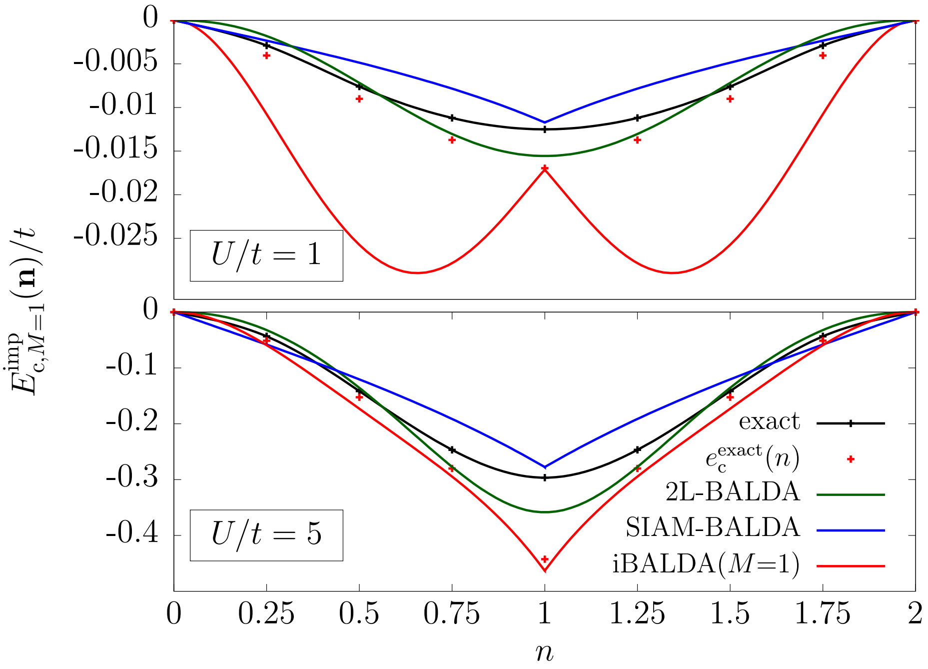

Figure 3.10: Impurity correlation energy as a function of $n = N/L$. The exact derivatives of $e_c(n)$ and $E_{c,M=1}^{\text{imp}}(\mathbf{n})$ are obtained following Sec. 3.3.3 on the eight-site ring model by exact diagonalization.

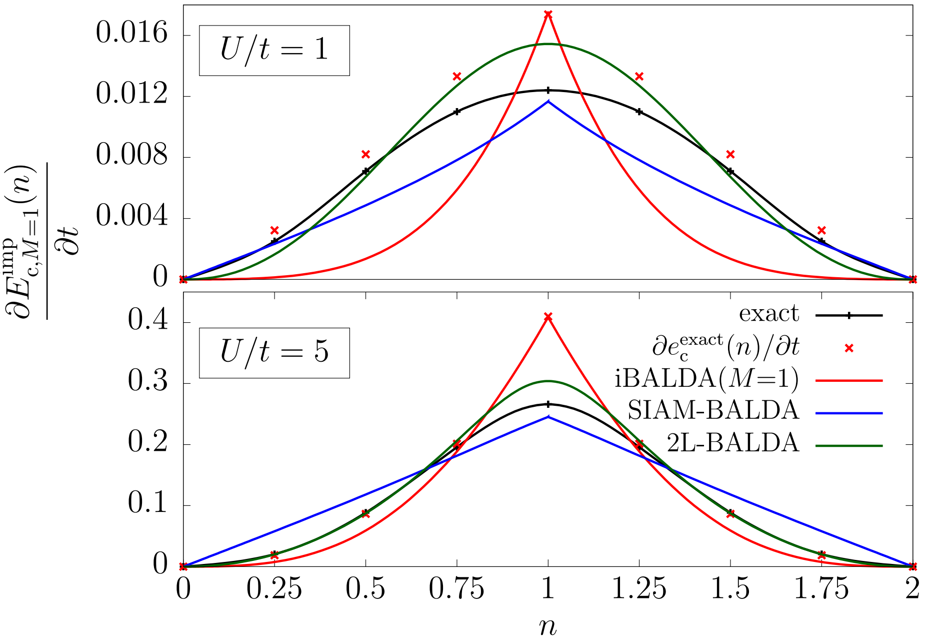

Figure 3.11: Derivative of the impurity correlation energy with respect to t as a function of $n = N/L$. The exact derivatives of $e_c(n)$ and $E_{c,M=1}^{\text{imp}}(\mathbf{n})$ are obtained by exact diagonalization following Sec. 3.3.3 on the eight-site ring model.

most exactly compensated by the errors made by BALDA on the conventional per-site correlation energy. The same happens for their derivatives. On the contrary, within 2L-BALDA, the error made on the conventional per-site correlation energy is absolutely *not* compensated by the one made on the impurity correlation energy. As a consequence, and despite its better accuracy for the impurity correlation energy, 2L-BALDA is less accurate than iBALDA(M=1) away from half-filling.

Still in the domain $0.6 \leqslant N/L \leqslant 0.75$, let us increase the correlation strength to $U/t = 5$ (bottom panels of Figs 3.9, 3.10 and 3.11). In this regime of correlation and density, both iBALDA(M) and 2L-BALDA per-site energies are very close to each other. This can be simply explain by looking at the bottom panels of Figs. 3.10 and 3.11, where BALDA (labelled by iBALDA(M=1)) is now becoming very accurate for the description of both the full per-site correlation energy and the impurity correlation energy. This is also the case for 2L-BALDA, which is even on top of the exact impurity correlation functional in this regime. Obviously, SIAM-BALDA does not exhibit the same feature. As a consequence, iBALDA(M) and 2L-BALDA are reproducing the correct per-site energy (and with almost no error cancellation), while SIAM-BALDA underestimates the per-site energy. Note that, in contrast to the half-filling case discussed previously, increasing the number of impurities has no true impact on the per-site energy, because $\overline{e}_{\mathrm{c},M}^{\mathrm{bath}}(\mathbf{n})$ is close to zero already for $M = 1$.

Turning to the density regime $0.75 \geqslant N/L \geqslant 1$ in Fig. 3.9, the per-site energy within iBALDA(M=1) starts to deviate from the exact curve, both for $U/t = 1$ (top panel) and $U/t = 5$ (bottom panel). By looking at the exact results for the full per-site correlation and the impurity correlation functionals in Fig. 3.10 (and 3.11 for their derivatives with respect to t), it becomes clear that they differ more and more from each other as the density moves towards $n = 1$ (half-filling). This tendency shows that the bath correlation functional $\overline{e}_{\mathrm{c},M=1}^{\mathrm{bath}}(\mathbf{n})$ is not negligible anymore. Therefore, iBALDA(M=1) is not appropriate and deteriorates the per-site energy within SOET. In this domain of density, and above all very close to the half-filling case, increasing the number of impurities improves the description of the per-site energy. Alternatively, 2L-BALDA also improves over iBALDA(M) by providing a better approximation to $\overline{e}_{\mathrm{c},M=1}^{\mathrm{bath}}(\mathbf{n})$ in the very close vicinity of half-filling. This is also the case of SIAM-BALDA at half-filling, but as soon as we deviate from the half-filled case, SIAM-BALDA has the poorer performance.

Self-consistent results

For now, only the functional-driven error has been discussed. The total error is the sum of this error with the so-called “density-driven error”. The latter defines the error in energy due to the deviation of the occupation from the exact one. This deviation can arise as soon as we solve the

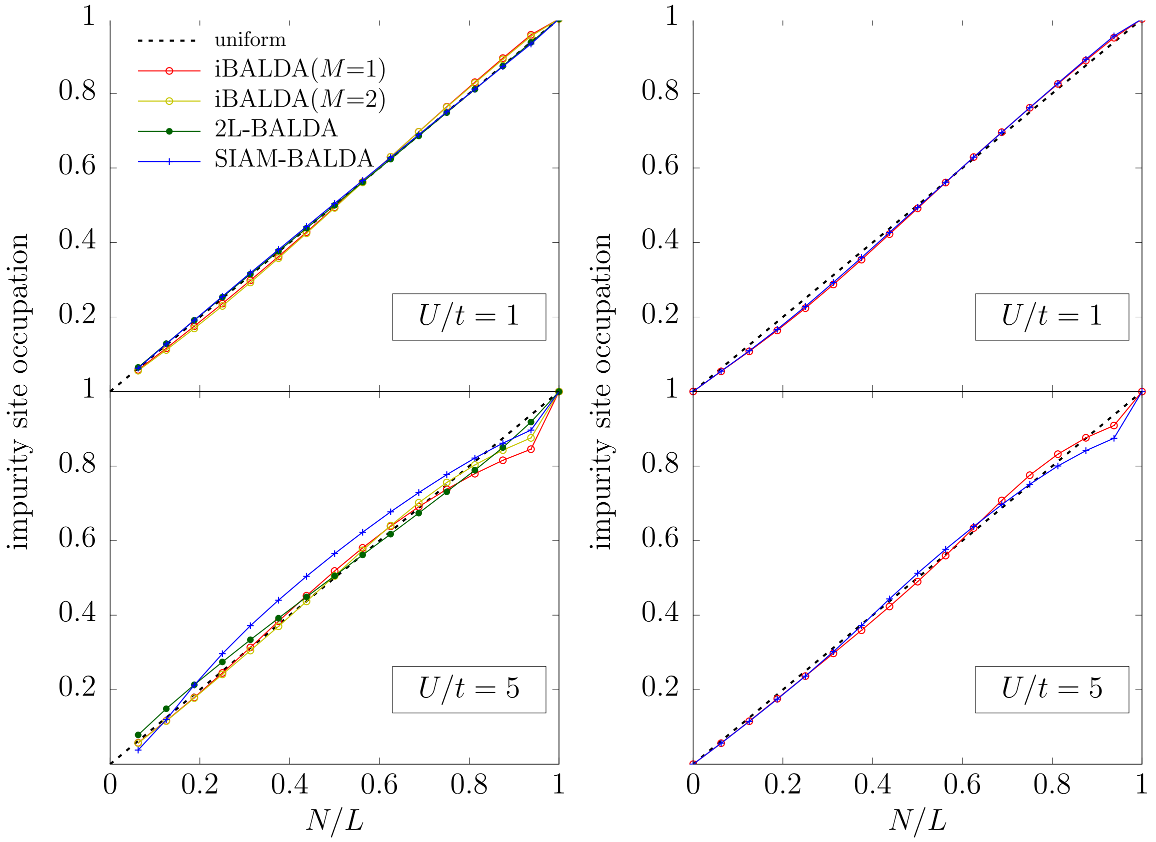

Figure 3.12: Left panel: impurity occupation obtained self-consistently. For the iBALDA(M=2), the two impurities have the same occupation by symmetry. Right panel: Same as left panel for the iBALDA(M=3) approximation. The occupation of the central impurity site ($n_1^{\Psi^{\rm imp}_{M=3}}$, in red) is not equal to the occupation of its first neighbour impurity sites ($n_0^{\Psi^{\rm imp}_{M=3}} = n_2^{\Psi^{\rm imp}_{M=3}}$, in blue).

SOET equation self-consistently with an approximate functional. The per-site energy obtained self-consistently is shown in Fig. 3.9 (dashed lines). The difference between those lines and the DMRG per-site energy corresponds to the total error. The density-driven error is the difference between this total error and the functional-driven error (which itself is the difference between the full lines and the DMRG results). Therefore, if the total error appears to be smaller than the functional-driven one, it means that the self-consistency has improved over the not converged results (i.e., using the exact density). This is manifested by a negative density-driven error. Starting with the weaker correlation regime (top panel of Fig. 3.9), only the per-site energy within the iBALDA approximation contains density-driven errors. For SIAM-BALDA and 2L-BALDA, the full and dashed lines are almost on top of each other, which means that the error is driven by the energy functional only.

This can be rationalized with the help of the converged impurity occupation and the impurity correlation potential in Figs. 3.12 and 3.13, respectively. As readily seen in Fig. 3.12, the impurity occupation is generally well reproduced in the weakly correlated regime (top left panel) for all oc-

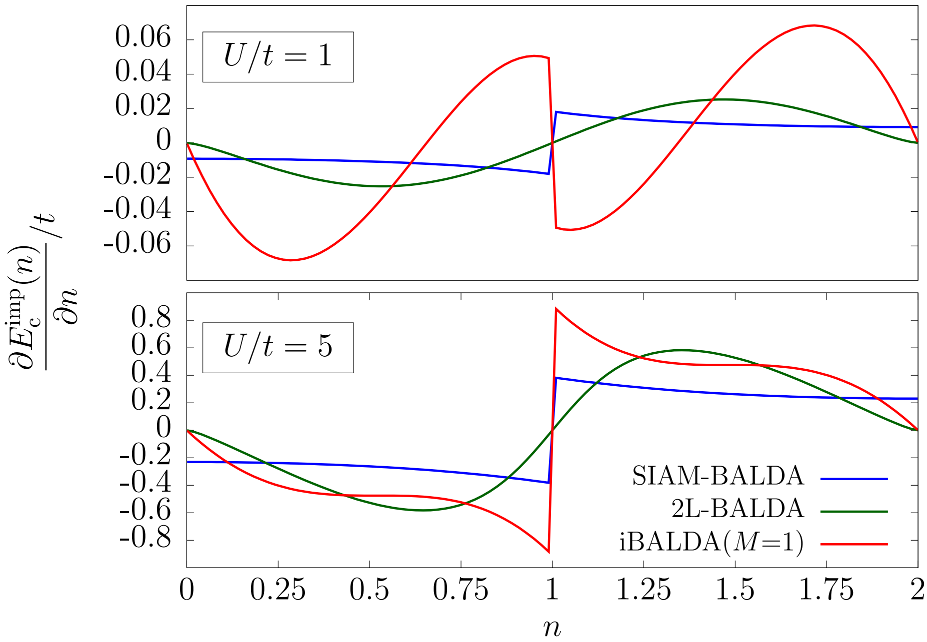

Figure 3.13: Impurity correlation potential. The exact potential at half-filling ($n = 1$) has been used, so that all potentials are crossing 0 at $n = 1$. Note that the iBALDA(M=1) curve does also correspond to the BALDA approximation modelling the conventional correlation potential $\partial e_c(n)/\partial n$.

cupation filling. However, by taking a closer look to the impurity occupation within iBALDA(M), we see that it is underestimated for $N/L \leqslant 0.6$ and overestimated otherwise. This explains why the per-site energy contains density-driven errors within iBALDA(M) and not within 2L-BALDA and SIAM-BALDA. This deviation from uniformity can be rationalized by looking at the impurity correlation potential in Fig. 3.13. The impurity correlation potential is part of the embedding correlation potential, which reads as follows for all the DFAs considered in this thesis:

$$v_{c,i}^{\text{emb}}(n_i) = \frac{\partial e_c(n_i)}{\partial n_i} - \sum_{j=0}^{M-1} \delta_{ij} \frac{\partial E_{c,M}^{\text{imp}}(n_j)}{\partial n_j}. \tag{3.111}$$

Within iBALDA(M), this correlation potential is always equal to 0 on the impurity sites, and to $\partial e_c(n_i)/\partial n_i$ in the bath. I recall that the iBALDA(M=1) correlation potentials in Fig. 3.13 also correspond to BALDA, used to model the conventional correlation potential. Focusing on the weakly correlated regime (top panel of Fig. 3.13), the correlation potential is strongly attractive (negative) in the bath for $n \leqslant 0.6$, thus leading to a charge transfer between the impurities and the bath, inducing a depletion of the density on the impurity sites [301]. The opposite situation happens for $0.6 \leqslant n < 1$, as reflected in the impurity occupation in the top panels of Fig. 3.12. Such an unphysical feature of the BALDA potential in the weakly correlated regime (already observed in Ref. [366]) is also present in the 2L-BALDA and SIAM-BALDA embedding potentials. However, $\partial e_c(n)/\partial n$ appears on all sites, and is not cancelled on the impurity like in iBALDA(M). This has strong consequences, as we could in principle shift the potential by $-\partial e_{\mathrm{c}}(n)/\partial n$ in the uniform case, hence keeping only the impurity correlation potential in Eq. (3.111). If the latter is accurate (like in 2L-BALDA and SIAM-BALDA) the correct occupation is recovered on the impurity. In the case of iBALDA(M), the impurity correlation potential is not accurate for $U/t = 1$.

Let us now look at the moderate correlation regime ($U/t = 5$). By construction, the exact occupation is recovered for $N/L = 1$ for all DFAs. The impurity occupation (bottom panel of Fig. 3.13) within iBALDA(M) remains relatively accurate except in the vicinity of half-filling. On the contrary, the 2L-BALDA impurity occupation is accurate around half-filling, in this regime of correlation. In the case of SIAM-BALDA, the impurity occupation deviates strongly from the exact one in the mid-range occupation filling, while it remains very accurate around half-filling. All these informations extracted from Fig. 3.12 are in complete adequacy with Fig. 3.9 for the per-site energy. A more detailed discussion is provided in Ref. [301].

3.5.3.ii Double occupation away from half-filling

In analogy with the per-site energy, it is interesting to look at the double occupation away from half-filling, as shown in Fig. 3.14. For clarity, we recall the exact double occupation expression within SOET:

$$d = \frac{1}{M}\sum_{i=0}^{M-1}\langle \hat{n}_{i\uparrow}\hat{n}_{i\downarrow}\rangle_{\Psi_M^{\mathrm{imp}}} + \frac{\partial \overline{e}_{\mathrm{c},M}^{\mathrm{bath}}(\mathbf{n}^{\Psi_M^{\mathrm{imp}}})}{\partial U}, \tag{3.112}$$

where $\overline{e}_{\mathrm{c},M}^{\mathrm{bath}}(\mathbf{n})$ measures the coupling between the impurities and the bath, and is given in Eq. (3.17). To facilitate the interpretation of the results, we also provide the derivative of the impurity correlation energy functionals with respect to U in Fig. 3.15. Starting with the iBALDA(M) approximation, the density-functional contribution in Eq. (3.112) reduces to zero by construction, so that only the bare impurity double occupations remain. It could be seen as a drastic approximation. However, as readily seen in Fig. 3.15 for $U/t = 1$ (top panel), the derivative of the conventional per-site correlation energy ($\partial e_{\mathrm{c}}(n)/\partial U$) is almost equivalent to the impurity one ($\partial E_{\mathrm{c},M=1}^{\mathrm{imp}}(\mathbf{n})/\partial U$), making the iBALDA approximation relevant. This observation has already been made for the per-site energy, with the derivative with respect to t. Hence, the bare impurity double occupation is sufficient to properly describe the physical double occupation away from half-filling. As a consequence, iBALDA(M) will be accurate for any M such that there is absolutely no need to increase the number of impurities.

Returning to a single impurity, the 2L-BALDA and SIAM-BALDA approximations do not generally

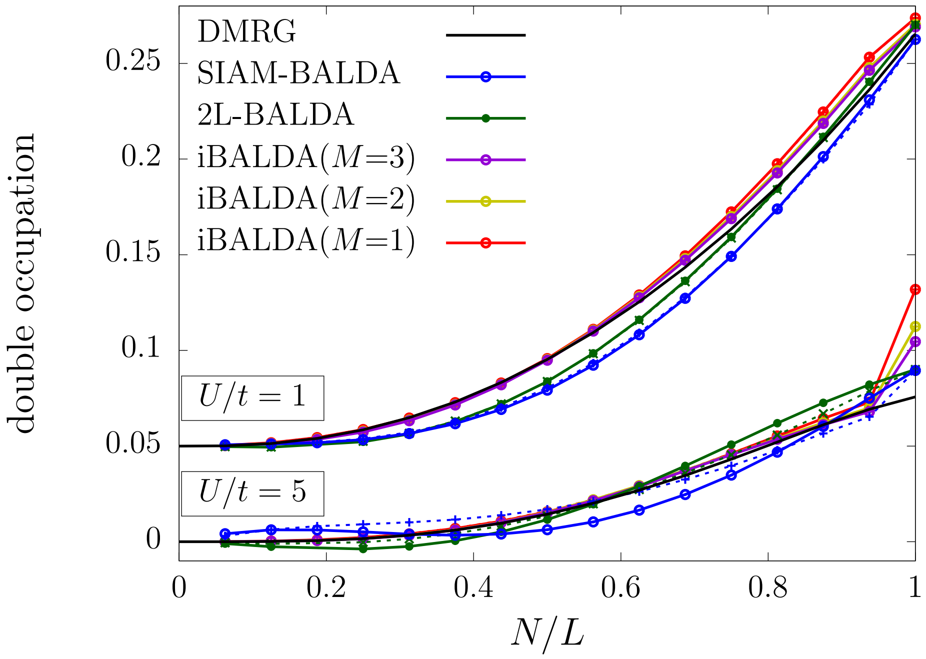

Figure 3.14: Top panel: Double occupation as a function of the filling $n = N/L$ for $U/t = 1$ and $U/t = 5$. For readability, the double occupation for $U/t = 1$ has been positively shifted by 0.05. Full lines correspond to the iteration 0, using the exact density in the correlation functionals. Dashed lines represent the double occupation after convergence (with the converged density). For iBALDA, the two of them are always on top of each others, as same as for 2L-BALDA and SIAM-BALDA, but for $U/t = 1$ only.

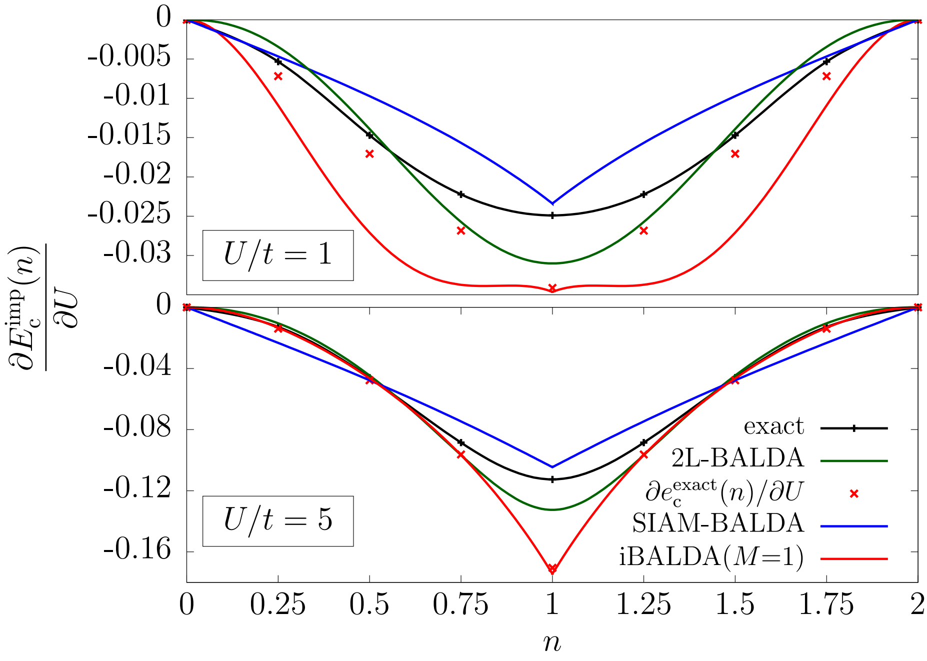

Figure 3.15: Derivative of the impurity correlation energy functionals with respect to U as a function of $n = N/L$. The exact derivatives of $e_c(n)$ and $E^{imp}_{c,M=1}(\mathbf{n})$ are obtained following Sec. 3.3.3 on the eight-site ring model by exact diagonalization.

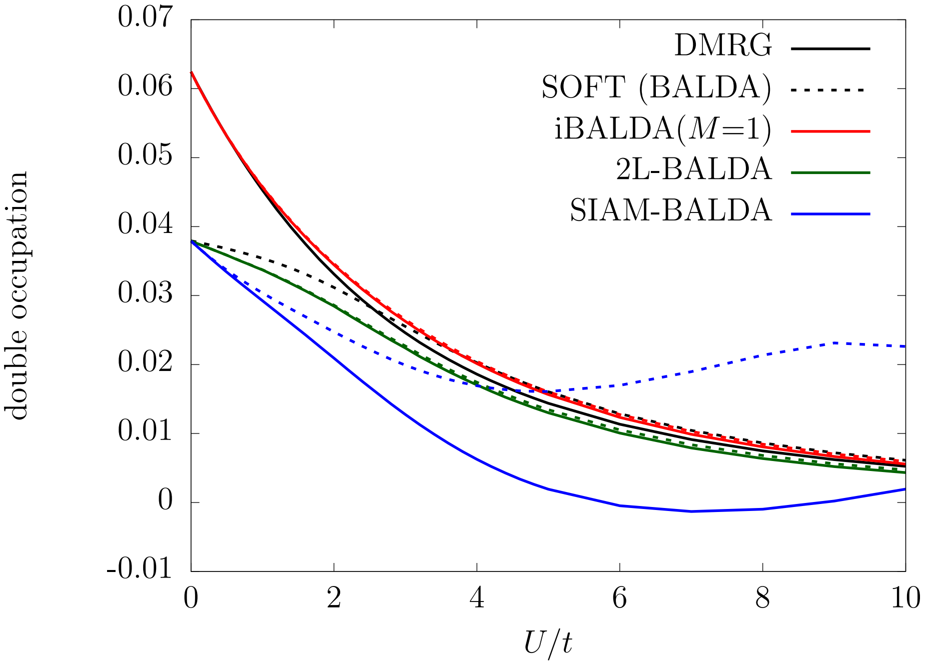

Figure 3.16: Double occupation at quarter filling ($N = 16$, $n = 0.5$) as a function of U/t. Full lines correspond to the iteration 0, using the exact density in the correlation functionals. Dashed lines represent the self-consistently determined double occupation.

improve over iBALDA, except at half-filling. Again, and in complete analogy with the per-site energy, the deficiency of 2L-BALDA here is *not* the 2L approximation to the impurity correlation energy, but the BALDA one for the conventional per-site correlation energy. By construction, 2L-BALDA does not benefit from the error cancellation which is present in iBALDA. This is the exact reason why the double occupation is poorly reproduced by both SIAM-BALDA and 2L-BALDA for the weakly correlated regime. Indeed, as shown in Fig. 3.16, the double occupation within SOFT (BALDA) cannot reproduce the exact double occupation even for $U/t = 0$, due to the wrong behaviour of BALDA in the weakly correlated limit, mentioned in Sec. 2.2.2 [Eq. (2.83)]. Unfortunately, all the functionals for which the impurity correlation functional is not based on BALDA will inherit this deficiency, which is the case of every functionals developed in this thesis apart from iBALDA(M). Indeed, the double occupation within iBALDA(M=1) is almost on top of the physical one in Fig. 3.16 for any U/t. This is one of the main improvement of SOET over SOFT, because SOET takes advantage of the explicit treatment of the electronic repulsion on the impurity sites. For the 2L-BALDA approximation, the correct double occupation is recovered when entering the strongly correlated regime ($U/t > 4$), at least in the quarter-filling shown in Fig. 3.16. Finally, the effect of self-consistency can be rather strong in the 2L-BALDA and SIAM-BALDA double occupation for $U/t = 5$, in contrast to iBALDA(M) for which no density-driven error is observed. For the latter, the double occupation is approximate by the bare double occupation on the impurity sites only, without any site-occupation functional contribution. We can conclude that the change in density does not have a significant impact on the M-impurity-interacting wavefunction Ψ_M^{imp} (as same as on $d_{M,i}^{\text{imp}}$) in contrast to the DFAs. Interestingly, judging by Fig. 3.14, the self-consistency improves the resulting double occupation in 2L-BALDA. No similar conclusion can be made about SIAM-BALDA, which is the DFA that leads to the poorer double occupation.

3.5.4 Derivative discontinuity at half-filling

Returning to the correlation potential, we proved in Sec. 2.2.3 that $e_{\text{c}}(n)$ depicts a derivative discontinuity at half-filling in the thermodynamic limit. A similar proof has been provided in Appendix D of Ref. [300], showing that $\overline{e}_{\text{c},M=1}^{\text{bath}}(\mathbf{n})$ does not contain a derivative discontinuity neither on the impurity site, nor in the bath. Alternatively, according to the expression of $\overline{e}_{\text{c},M}^{\text{bath}}(\mathbf{n})$ in Eq. (3.17), the impurity correlation energy functional exhibits a derivative discontinuity on the impurity site, but not in the bath. From the exact expression of the embedding potential in Eq. (3.7) and the decomposition of the bath Hxc energy functional in Eq. (3.18), we conclude that the embedding correlation potential should be discontinuous in the bath and smooth on the interacting impurity sites. An intuitive explanation of this result could be that the derivative discontinuity, which is related to the opening of the Mott-gap [360], is already taken into account by the explicit treatment of the electron-electron interaction on the impurity sites, while it has to be described by discontinuous correlation potentials in the bath. According to Fig. 3.13, iBALDA(M=1) and SIAM-BALDA exhibit such a discontinuity at half-filling due to the hole-particle symmetry condition, as soon as $U > 0$. On the other hand, even though the 2L-BALDA impurity correlation potential also fulfils the hole-particle symmetry condition, it smoothly tends to 0 when approaching $n = 1$. As a consequence, the potential does not manifest a derivative discontinuity at half-filling when U/t is *finite*. It only does when $U/t \to +\infty$ (See Ref. [72] for $U/t = 100$, which is close enough to the atomic limit to reveal the presence of a discontinuity). As discussed by Dimitrov *et al.* [438], the dimer functional reproduces an intra-system steepening and not an inter-system derivative discontinuity. In other words, the change in density in the dimer (2L) functional does not correspond to a change in the total number of electrons. The latter is indeed fixed to $N = 2$ in the dimer. Only the number of electrons on the impurity site varies. The problem becomes equivalent to describing an inter-system derivative discontinuity only when the impurity can be treated as an isolated system, which is indeed the case in the atomic limit.

Nevertheless, from a practical point of view, exhibiting a derivative discontinuity is not necessarily an advantage. Indeed, it may lead to convergence issues around half-filling, as already observed in KS-SOFT in the description of inhomogeneous models [360]. Practical solutions to this problem have been proposed for conventional KS calculations by using either a finite temperature [348] or *ad-hoc* parameters [345, 346, 371], and could be considered also in SOET. This is left for future work. One could think that 2L-BALDA would not be concerned by convergence issues as it does not exhibit a discontinuity in the impurity correlation potential (except in the atomic limit). However, the BALDA correlation potential is still employed on the bath sites within 2L-BALDA, which means that convergence problems will appear as soon as bath occupations are close to 1. For now, no such situation has been observed in SOET, simply because only 32 sites were considered, such that the closest uniform occupation to half-filling is obtained for 30 electrons, i.e. $n = 0.9375$. This occupation is far enough from the half-filling to avoid any problem.

Convergence issues are expected to arise when approaching the thermodynamic limit since the density can then be much closer to 1. Unfortunately, this limit cannot be reached as the current implementation of SOET does not allow a decrease of the computational cost in comparison to a fully many-body treatment of the problem. Nevertheless, because only the impurity sites are explicitly interacting, we expect SOET to be cheaper than WFT. The following chapter deals with alternative implementations of SOET, by using a SIAM-solver or a projection method based of the Schmidt decomposition, possibly enabling the treatment of much larger Hubbard rings.

Chapter 4

Towards an efficient implementation of the self-consistent impurity problem in SOET

In contrast to the usual embedding approaches, SOET treats all the bath sites explicitly as the kinetic operator in Eq. (3.6) acts on the whole system. Although this explicit treatment is appealing, the current implementation of SOET in the previous chapter did not allow a decrease in computational cost in comparison to WFT. This can be contrasted with WFT-in-DFT [Eq. (1.198)] for which the wavefunction is only built on the cluster, thus reducing the size of the Hilbert space and the computational cost. Given that only a small number of sites are explicitly interacting within SOET, it could be possible to find a more efficient impurity solver, thus leading to a computational cost in between DFT and WFT. In this chapter, two different implementations are discussed. The first one is a reformulation of the impurity problem in SOET into a (not necessarily symmetric) SIAM, which can be solved by using Green's function methods, as discussed in Sec. 4.1. The second one presented in Sec. 4.2 makes use of the Schmidt decomposition (in analogy with DMET) thus leading to the so-called *projected* SOET (P-SOET).

4.1 Single-Impurity Anderson Model solver

In the previous chapter, we investigated the connection between the SOET Hamiltonian at half-filling and the symmetric SIAM (see Sec. 3.4.4). Note that this connection was not exact as the coupling term between the two neighbours ($i = 1$ and $i = L$) of the impurity site in the SIAM was ignored.

In this section, a rigorous transformation of the SOET Hamiltonian into the SIAM Hamiltonian is provided. By doing so, SIAM-solver (also called impurity-solver) can then be employed to solve the SOET equations by using Green's function techniques. Note that this work is currently in progress and a draft is in preparation, in collaboration with Matthieu Saubanère in Montpellier (France).

4.1.1 From the SOET to the SIAM Hamiltonian

Let us start by rewriting the SOET Hamiltonian for a single impurity as follows,

$$\begin{aligned}\hat{H}^{\text{SOET}} &= -t\sum_{i\sigma}(\hat{c}^{\dagger}_{i\sigma}\hat{c}_{i+1\sigma} + \text{h.c.}) + \sum_{i}\left[v_i + \frac{\partial \overline{E}^{\text{bath}}_{\text{Hxc}}(\mathbf{n})}{\partial n_i}\right]\hat{n}_i + \hat{U}_0 \qquad (4.1)\\ &= \hat{h}_0 + \hat{h}_{0\text{b}} + \hat{h}_{\text{b}} + \hat{U}_0, \qquad (4.2)\end{aligned}$$

where $\hat{U}_0 = U\hat{n}_{0\uparrow}\hat{n}_{0\downarrow}$ is the on-site repulsion operator on the impurity,

$$\hat{h}_0 = \left[v_0 + \frac{\partial \overline{E}^{\text{bath}}_{\text{Hxc}}(\mathbf{n})}{\partial n_0}\right]\hat{n}_0 \qquad (4.3)$$

is the one-body embedding potential operator on the impurity,

$$\hat{h}_{0\text{b}} = -t\sum_{\sigma}(\hat{c}^{\dagger}_{0\sigma}\hat{c}_{1\sigma} + \text{h.c.}) \qquad (4.4)$$

is the hopping Hamiltonian between the impurity and its nearest neighbouring sites, and

$$\hat{h}_{\text{b}} = -t\sum_{i\neq 0,\sigma}(\hat{c}^{\dagger}_{i\sigma}\hat{c}_{i+1\sigma} + \text{h.c.}) + \sum_{i\neq 0}\left[v_i + \frac{\partial \overline{E}^{\text{bath}}_{\text{Hxc}}(\mathbf{n})}{\partial n_i}\right]\hat{n}_i \qquad (4.5)$$

is the remaining part that contains only bath contributions, with the embedding potential $v^{\text{emb}}_i(\mathbf{n}) = v_i + \partial\overline{E}^{\text{bath}}_{\text{Hxc}}(\mathbf{n})/\partial n_i$. Note that the reference to the number of impurities (M) has been omitted for convenience, given that only one impurity site is considered in this section. Getting rid of the two-body part of the Hamiltonian, only the one-body part,

$$\hat{h}^{\text{SOET}} = \hat{h}_0 + \hat{h}_{0\text{b}} + \hat{h}_{\text{b}}, \qquad (4.6)$$

remains, which matrix representation is of size $L \times L$ and reads

$$\left[\hat{h}^{\mathrm{SOET}}\right] = \begin{pmatrix} \mathbf{h_0} & \mathbf{h_{0b}^\dagger} \\ \mathbf{h_{0b}} & \mathbf{h_b} \end{pmatrix} = \left(\begin{array}{c|ccccc} \mathbf{h_0} & & & \mathbf{h_{0b}^\dagger} & & \\ \hline & v_1^{\mathrm{emb}} & -t & & & \mathbf{0} \\ & -t & v_2^{\mathrm{emb}} & -t & & \\ \mathbf{h_{0b}} & & -t & \ddots & \ddots & \\ & & & \ddots & & -t \\ & \mathbf{0} & & & -t & v_{L-1}^{\mathrm{emb}} \end{array}\right). \tag{4.7}$$

Now, the idea is to recover the SIAM Hamiltonian in the "k-space". To do so, a canonical transformation using a unitary matrix $\mathbf{P_b}$ is employed to diagonalize the block matrix of the bath,

$$\mathbf{P_b h_b P_b^\dagger} = \mathbf{D}, \tag{4.8}$$

thus leading to a new one-body Hamiltonian, keeping the impurity site unchanged,

$$\begin{aligned} \left[\hat{h}_P^{\mathrm{SOET}}\right] &= \mathbf{P}\left[\hat{h}^{\mathrm{SOET}}\right]\mathbf{P}^\dagger \\ &= \begin{pmatrix} 1 & \mathbf{0} \\ \mathbf{0} & \mathbf{P_b} \end{pmatrix} \begin{pmatrix} \mathbf{h_0} & \mathbf{h_{0b}^\dagger} \\ \mathbf{h_{0b}} & \mathbf{h_b} \end{pmatrix} \begin{pmatrix} 1 & \mathbf{0} \\ \mathbf{0} & \mathbf{P_b^\dagger} \end{pmatrix} \\ &= \begin{pmatrix} 1 & \mathbf{0} \\ \mathbf{0} & \mathbf{P_b} \end{pmatrix} \begin{pmatrix} \mathbf{h_0} & \mathbf{h_{0b}^\dagger P_b^\dagger} \\ \mathbf{h_{0b}} & \mathbf{h_b P_b^\dagger} \end{pmatrix} = \begin{pmatrix} \mathbf{h_0} & \mathbf{h_{0b}^\dagger P_b^\dagger} \\ \mathbf{P_b h_{0b}} & \underbrace{\mathbf{P_b h_b P_b^\dagger}}_{\mathbf{D}} \end{pmatrix}. \end{aligned} \tag{4.9}$$

The eigenvalues of the diagonal matrix $\mathbf{D}$ are denoted by $\tilde{\varepsilon}_k$. In addition, the column vector $\mathbf{P_b h_{0b}}$ contains the couplings between the impurity and the bath, denoted by $\tilde{V}_k$, in analogy with the SIAM. The transformed one-body Hamiltonian now reads

$$\hat{h}_P^{\mathrm{SOET}} = \sum_{k\sigma} \tilde{\varepsilon}_k \hat{c}_{k\sigma}^\dagger \hat{c}_{k\sigma} + \varepsilon_d \hat{n}_d + \sum_k \tilde{V}_k (\hat{c}_{d\sigma}^\dagger \hat{c}_{k\sigma} + \mathrm{h.c.}), \tag{4.10}$$

which is nothing but the one-body part of the SIAM Hamiltonian [see Eq. (2.94)], with the substitutions $\varepsilon_k \rightarrow \tilde{\varepsilon}_k$, $V_k \rightarrow \tilde{V}_k$ and $\varepsilon_d \rightarrow v_0^{\mathrm{emb}}$. To adopt the same notation as in the SIAM, we used $\hat{c}_{d\sigma} = \hat{c}_{0\sigma}$, with $\hat{n}_d = \hat{n}_{d\uparrow} + \hat{n}_{d\downarrow}$ and $\hat{n}_{d\sigma} = \hat{c}_{d\sigma}^\dagger \hat{c}_{d\sigma}$. By using the canonical transformation given by the unitary matrix $\mathbf{P}$ on the two-body impurity-interacting SOET Hamiltonian [Eq. (4.1)], it comes

$$\hat{H}_P^{\mathrm{SOET}} = \hat{P}\hat{H}^{\mathrm{SOET}}\hat{P}^\dagger = \hat{P}\left(\hat{h}^{\mathrm{SOET}} + \hat{U}_0\right)\hat{P}^\dagger = \hat{h}_P^{\mathrm{SOET}} + \hat{U}_0, \tag{4.11}$$

where the transformation does not affect the impurity site. The full expression of the transformed Hamiltonian thus reads

$$\hat{H}_P^{\mathrm{SOET}} = \sum_{k\sigma} \tilde{\varepsilon}_k \hat{c}^\dagger_{k\sigma} \hat{c}_{k\sigma} + \varepsilon_d \hat{n}_d + \sum_k \tilde{V}_k (\hat{c}^\dagger_{d\sigma} \hat{c}_{k\sigma} + \mathrm{h.c.}) + U \hat{n}^\dagger_d \hat{n}_d. \tag{4.12}$$

Note that the Hamiltonian in Eq. (4.12) is the same as the Hamiltonian in Eq. (4.1), written in a new basis. This basis is analogue to the basis of k-states. As one can pass from the Hamiltonian in Eq. (4.12) to the SOET Hamiltonian by applying the unitary transformation in the bath, and vice-versa, solving one or the other is completely equivalent and no information is lost. Therefore, once the analytical embedding potentials are calculated, one has to apply the canonical transformation to get a SIAM-like Hamiltonian, where the band energies $\tilde{\varepsilon}_k$ and coupling values $\tilde{V}_k$ are determined numerically by the transformation. This Hamiltonian could then be solved by any impurity-solver method, also used in DMFT (see Sec. 2.4.1). In practice, due to the use of DFAs for the embedding potential, this procedure has to be reiterated until occupations in the bath and on the impurity are converged. Also, if the impurity-solver is not exact, additional errors might appear.

4.1.2 Second-order perturbation theory

In Sec. 2.4.1, we have shown how the SIAM Hamiltonian can be solved by using Green's function techniques in the DMFT framework. The procedure described here is different, as there is no mapping on an impurity Green's function. This section provides the basic idea to be implemented, as well as an explicit expression for the self-energy based on *second-order perturbation theory* (SOPT). We want to build the retarded impurity-interacting Green's function, from which the occupations and the double occupation are obtained. In the following, I will always consider the retarded quantities (Green's functions, self-energies and hybridization functions). Let us separate the impurity-interacting Hamiltonian into an unperturbed part, corresponding to the one-particle Hamiltonian, and a perturbation containing the electron-electron repulsion operator,

$$\hat{H} = \hat{H}_0 + \hat{H}_1, \tag{4.13}$$

with

$$\hat{H}_0 = \sum_{k\sigma} \tilde{\varepsilon}_k \hat{c}^\dagger_{k\sigma} \hat{c}_{k\sigma} + \sum_k \tilde{V}_k (\hat{c}^\dagger_{d\sigma} \hat{c}_{k\sigma} + \mathrm{h.c.}) + \varepsilon_d \hat{n}_d \tag{4.14}$$

and

$$\hat{H}_1 = U\hat{c}^{\dagger}_{d\uparrow}\hat{c}_{d\uparrow}\hat{c}^{\dagger}_{d\downarrow}\hat{c}_{d\downarrow}. \tag{4.15}$$

As a starting point, the noninteracting Green's function is considered. This Green's function is solution of the noninteracting SIAM. Consider the following impurity (or host) noninteracting Green's function:

$$G^{(0)}_{dd}(z) = \frac{1}{z - \tilde{\varepsilon}_d - \Delta(z)}, \tag{4.16}$$

where $z = \omega + i\eta$ with $\eta \to 0^+$ is a infinitesimal positive number, and

$$\Delta(z) = \sum_k \frac{|\tilde{V}_k|^2}{z - \tilde{\varepsilon}_k} = \sum_k \frac{|\tilde{V}_k|^2}{\omega - \tilde{\varepsilon}_k} - i\pi \sum_k |\tilde{V}_k|^2 \delta(\omega - \tilde{\varepsilon}_k) \tag{4.17}$$

is the "host-impurity" retarded hybridization function, already discussed in Sec. 2.4.1. Usually, the k-dependence of the coupling term $\tilde{V}_k$ is neglected, which will not be the case in our theory. The host Green's function is then used to compute the following conduction electron Green's function:

$$G^{(0)}_{kk'}(z) = \frac{\delta_{kk'}}{z - \tilde{\varepsilon}_k} + \frac{\tilde{V}^*_k}{z - \tilde{\varepsilon}_k} G^{(0)}_{dd}(z) \frac{\tilde{V}_{k'}}{z - \tilde{\varepsilon}_{k'}}, \tag{4.18}$$

as well as the Green's function of the conducting electrons coupled to the impurity,

$$G^{(0)}_{kd}(z) = \frac{\tilde{V}_k}{z - \tilde{\varepsilon}_k} G^{(0)}_{dd}(z), \tag{4.19}$$

for each frequency z. This is different from DMFT where only the impurity Green's function was calculated. In practice, two grids have to be defined. One for the k-values,

$$k \in [-\pi, \pi], \quad k = 2\pi m/L, \quad m = -\frac{L}{2}, \dots, \frac{L}{2}, \quad \delta_k = \frac{2\pi}{L-1}, \tag{4.20}$$

which is as large as the number of sites L, and δ_k is the interval between two k-points. The second one corresponds to the frequency domain of ω,

$$\omega \in [E_{\min}, E_{\max}], \quad \delta_E = \frac{E_{\max} - E_{\min}}{N_E - 1}, \tag{4.21}$$

where N_E is the number of points on the grid, and δ_E is the interval between two points on the frequency grid. Eqs. (4.16), (4.18) and (4.19) give the matrix elements of the Green's function in "k-space", denoted by $\mathbf{G}^{(0)}_{\mathrm{k}}(z)$. Once this zeroth-order Green's function is calculated, correlation coming from the perturbed Hamiltonian has to be included. This is done by computing the impurity-interacting Green's function, given by the Dyson equation as follows:

$$[\mathbf{G}_{\mathrm{Rel}}(z)]^{-1} = \left[\mathbf{G}^{(0)}_{\mathrm{Rel}}(z)\right]^{-1} - \mathbf{\Sigma}_{\mathrm{Rel}}(z), \tag{4.22}$$

or, equivalently,

$$\mathbf{G}_{\mathrm{Rel}}(z) = \mathbf{G}^{(0)}_{\mathrm{Rel}}(z) + \mathbf{G}^{(0)}_{\mathrm{Rel}}(z)\mathbf{\Sigma}_{\mathrm{Rel}}(z)\mathbf{G}_{\mathrm{Rel}}(z). \tag{4.23}$$

The real-space Green's function is related to the k-space one by the previously introduced canonical transformation,

$$\mathbf{G}_{\mathrm{Rel}}(z) = \mathbf{P}^{\dagger}\mathbf{G}_{\mathrm{k}}(z)\mathbf{P}, \tag{4.24}$$

and $\mathbf{\Sigma}_{\mathrm{Rel}}(z)$ is the real-space self-energy that accounts for all the missing impurity correlation effects, further described in the following. Note that the site occupations are given by

$$n_i = 2\int_{-\infty}^{\mu} \rho_{ii}(\omega)\mathrm{d}\omega, \tag{4.25}$$

where the factor 2 originates from the spin, and $\rho_{ii}(\omega)$ is the diagonal part of the spectral function

$$\rho_{ij}(\omega) = -\frac{1}{\pi}\mathrm{Im}G^{\mathrm{Rel}}_{ij}(z). \tag{4.26}$$

This density is then introduced again in the DFAs to compute the embedding potential in the SOET Hamiltonian [Eq. (4.1)] which is then transformed into the SIAM-like Hamiltonian and solved again by the impurity solver. This procedure is repeated until convergence is reached.

Turning to the expression of the self-energy, note that a non-local (k-dependent) self-energy is in principle needed to solve the Hamiltonian in Eq. (4.12). It is common to make a local (k-independent) approximation to the self-energy, which is an exact assumption in infinite dimension, like in DMFT (see Sec. 2.4.1). We don't make this assumption here. A non-local self-energy has been proposed by Schweitzer and Czycholl [439], who have used the limit of infinite dimension to determine the k-dependence, by taking into account corrections from nearest neighbour contributions to the self-energy. They introduced a notation $\mathbf{R}$ representing the distance between the impurity site and a bath site, such that

$$\mathbf{\Sigma}_{\mathrm{Rel}} = \begin{pmatrix} \Sigma^{\mathrm{Rel}}_{\mathbf{R=0}} & \Sigma^{\mathrm{Rel}}_{\mathbf{R=1}} & \cdots & \Sigma^{\mathrm{Rel}}_{\mathbf{R=N}} \\ \Sigma^{\mathrm{Rel}}_{-\mathbf{R=1}} & & & \\ \vdots & & 0 & \\ \Sigma^{\mathrm{Rel}}_{-\mathbf{R=N}} & & & \end{pmatrix} = \begin{pmatrix} \Sigma^{\mathrm{Rel}}_{00} & \Sigma^{\mathrm{Rel}}_{01} & \cdots & \Sigma^{\mathrm{Rel}}_{0N} \\ \Sigma^{\mathrm{Rel}}_{10} & & & \\ \vdots & & 0 & \\ \Sigma^{\mathrm{Rel}}_{N0} & & & \end{pmatrix}, \tag{4.27}$$

where $\Sigma^{\mathrm{Rel}}_{ji} = \Sigma^{\mathrm{Rel}*}_{ij}$. From Eq. (SC-17) in Ref. [439], the SOPT self-energy is given by

$$\begin{aligned} \Sigma^{\mathrm{Rel}}_{\mathbf{R}}(z) &= U^2 \int \mathrm{d}\xi_1 \int \mathrm{d}\xi_2 \int \mathrm{d}\xi_3 \, \rho_{\mathbf{R}}(\xi_1)\rho_{\mathbf{R}}(\xi_2)\rho_{-\mathbf{R}}(\xi_3) \\ &\quad \times \frac{f(\xi_1)f(\xi_2)(1-f(\xi_3)) + (1-f(\xi_1))(1-f(\xi_2))f(\xi_3)}{z-\xi_1-\xi_2+\xi_3}, \end{aligned} \tag{4.28}$$

where $f(\xi)$ is the Fermi function at $T = 0K$,

$$f(\xi) = \begin{cases} 1 & \text{if } \xi \leq \mu \\ 0 & \text{otherwise} \end{cases}, \tag{4.29}$$

and μ is the chemical potential. The calculation of μ is subtle. Although it is well known in the noninteracting (electron independent) picture like in metals, it is not uniquely defined for semi-conductors or insulators due to the opening of the band gap. Indeed, if all the valence band is filled, the chemical potential can take any value inside the gap. In other words, it lies in between the valence and the conduction bands. In practice, it could be defined thank to the following function,

$$N(\xi) = -\int_{-\infty}^{\xi} \frac{2}{\pi} \mathrm{Im}\mathrm{Tr}\left[G_{\mathrm{Rel}}(\omega)\right] \mathrm{d}\omega \tag{4.30}$$

which gives the total number of electrons N when $\xi = \mu$. Another definition is the average of the LUMO and HOMO orbital energies of the noninteracting system. Note that Eq. (4.28) requires a triple integral over the frequencies, which is computationally expensive. One can reduce this computational cost by employing another expression of the self-energy, in Eq. (SC-18) of Ref. [439],

$$\Sigma^{\mathrm{Rel}}_{\mathbf{R}}(z) = U^2(-\mathrm{i}) \int \mathrm{d}\lambda \, e^{\mathrm{i}\lambda z} \left(A^2_{\mathbf{R}}(\lambda)B_{-\mathbf{R}}(-\lambda) + B^2_{\mathbf{R}}(\lambda)A_{-\mathbf{R}}(-\lambda)\right), \tag{4.31}$$

with

$$A_{\mathbf{R}}(\lambda) = \int_{-\infty}^{+\infty} \mathrm{d}\xi\, \rho_{\mathbf{R}}(\xi) f(\xi) e^{-\mathrm{i}\lambda\xi}, \tag{4.32}$$

$$B_{\mathbf{R}}(\lambda) = \int_{-\infty}^{+\infty} \mathrm{d}\xi\, \rho_{\mathbf{R}}(\xi)(1 - f(\xi)) e^{-\mathrm{i}\lambda\xi}, \tag{4.33}$$

or, equivalently, for $T = 0K$,

$$A_{\mathbf{R}}(\lambda) = \int_{-\infty}^{\mu} \mathrm{d}\xi\, \rho_{\mathbf{R}}(\xi) e^{-\mathrm{i}\lambda\xi}, \tag{4.34}$$

$$B_{\mathbf{R}}(\lambda) = \int_{\mu}^{+\infty} \mathrm{d}\xi\, \rho_{\mathbf{R}}(\xi) e^{-\mathrm{i}\lambda\xi}. \tag{4.35}$$

In practice, the implementation is initialized by using the noninteracting Green's function to compute the spectral functional in Eq. (4.26).

Note that the k-space and the real-space self-energies are related as follows, as same as for the Green's function in Eq. (4.24):

$$\mathbf{\Sigma}_{\mathrm{k}}(z) = \mathbf{P}\mathbf{\Sigma}_{\mathrm{Rel}}(z)\mathbf{P}^{\dagger}. \tag{4.36}$$

To summarize the above discussion, an algorithm is provided in Fig. 4.1 and illustrated in Fig. 4.2. This algorithm has been implemented and tested. For the time being, decent density profiles have been obtained in the weakly correlated regime $U/t \approx 1$ only. This is due to the SOPT approximation. In order to check if the above implementation is correct, it would be interesting to improve the self-energy calculation by considering more involved impurity solvers, like in DMFT. Actually, another PhD student in our lab, Laurent Mazouin, is working on the formulation of SOET using Green's function, and on the development of self-energies adapted to the impurity problem in SOET. With his help, a more detailed and formal connection between SOET and DMFT could be derived.

4.2 Projected Site-Occupation Embedding Theory

Let us now turn to another strategy to reduce the computational cost of SOET. We have seen in Sec. 2.4.2 that DMET uses the Schmidt decomposition to project the original lattice problem onto a much smaller embedded one. This decomposition is appropriate for the development of embedding schemes, as it is based on the separation of the whole system into two subsystems. In analogy with DMET, the Schmidt decomposition will be incorporated in our SOET scheme, leading to the so-called *projected* SOET (P-SOET).

Algorithm 1 SOET/SIAM solver

```
input : $L, N, t, U, \mathbf{v}, \mathbf{n}$
do while $\Delta n_0, \Delta E \geq$ threshold
    $\mathbf{v}^{\text{emb}}(\mathbf{n})$
    $\mathbf{H}_P^{\text{SOET}} = \mathbf{P}\mathbf{H}^{\text{SOET}}\mathbf{P}^\dagger$, Eq. (4.11)
    do for $\omega$ in frequency grid, Eq. (4.21)
        $\mathbf{G}_{\text{k}}^{(0)}(z)$, Eqs. (4.16),(4.18),(4.19)
        $\mathbf{G}_{\text{Rel}}^{(0)}(z) = \mathbf{P}^\dagger\mathbf{G}_{\text{k}}^{(0)}(z)\mathbf{P}$, Eq. (4.24)
        $\rho_{\mathbf{R}}^{(0)}(\omega)$, Eq. (4.26)
        $\mathbf{\Sigma}_{\text{Rel}}(z)$, Eq. (4.31)
        $\mathbf{G}_{\text{Rel}}(z)$, Dyson Eq. (4.22)
        $\rho_{ii}(\omega)$, Eq. (4.26)
    end do
    $n_i$, Eq. (4.25)
    $E$, $\langle \hat{n}_\uparrow \hat{n}_\downarrow \rangle$ Ref. [440]
end do
```

Figure 4.1: Algorithm to solve the SOET equation using a SIAM solver. Δn_0 and ΔE denote the difference in the impurity occupation and the energy between two successive iterations, respectively.

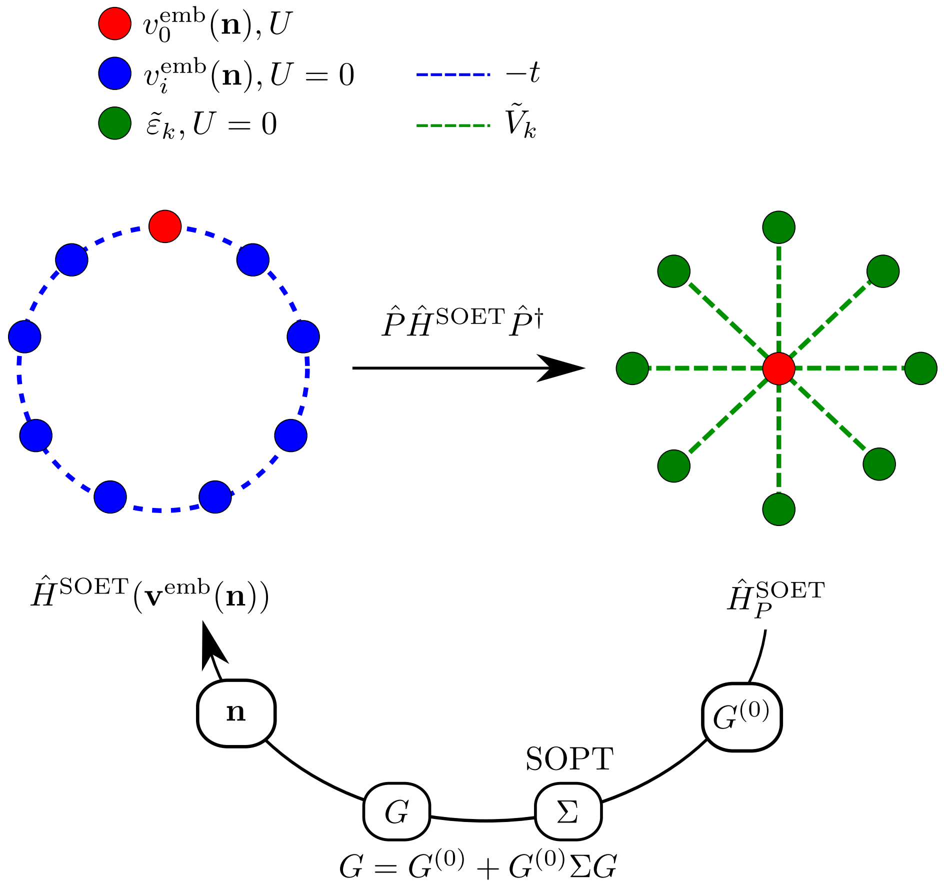

Figure 4.2: Illustration of the self-consistent SOET procedure based on the SIAM solver (see algorithm in Fig. 4.1 and text for further details).

4.2.1 Construction of the embedded-impurity problem

In complete analogy with DMET, the first thing to do is to compute the bath states by performing the Schmidt decomposition on a given wavefunction. Given that SOET is a DFT-based method, it seems natural to use the KS-SOFT wavefunction as a starting point, in contrast to the Hartree-Fock one in DMET. The procedure to obtain this projector is the same as in DMET and is detailed in Sec. 2.4.2. In the particular case of the uniform Hubbard model, the bath states coming from the KS Slater determinant or the Hartree–Fock one are identical. Obviously, the projector is therefore also identical in both method in this case. We start by projecting the SOET Hamiltonian onto the new embedded-impurity problem as follows,

$$\hat{H}^{\rm imp} = \hat{P}^{\dagger} \hat{H}^{\rm SOET} \hat{P}, \tag{4.37}$$

where, in the uniform case, the SOET Hamiltonian reads,

$$\hat{H}^{\rm SOET} = \hat{T} + \hat{U}_M + \sum_{i=0}^{L-1} \left[\left. \frac{\partial \overline{E}^{\rm bath}_{{\rm Hxc},M}(\mathbf{n})}{\partial n_i} \right|_{\mathbf{n}=\underline{n}_0^{\Psi_M^{\rm imp}}} \right] \hat{n}_i, \tag{4.38}$$

where M is the number of impurities.

In contrast to the SOET Hamiltonian in Eq. (3.6), note that the bath Hxc potential is now calculated by setting $\mathbf{n} = \underline{n}_0^{\Psi_M^{\rm imp}} \equiv \left\{ n_0^{\Psi_M^{\rm imp}}, n_0^{\Psi_M^{\rm imp}}, \dots, n_0^{\Psi_M^{\rm imp}} \right\}$, instead of the usual site-occupation vector $\left\{ n_0^{\Psi_M^{\rm imp}}, n_1^{\Psi_M^{\rm imp}}, \dots, n_{L-1}^{\Psi_M^{\rm imp}} \right\}$. In other words, only the occupation on the impurity site labelled as 0 is used, which is convenient in an embedding formalism. Indeed, like in DMET, the projection leads to an embedded-impurity problem of $2 \times M$ sites. When this embedded-impurity problem is solved, only the occupation of the $2 \times M$ sites will be accessible. In order to formulate a self-consistent procedure similar to SOET, we decided to select a given occupation between these $2 \times M$ sites, chosen to be the impurity site "0", and to assume $\mathbf{n} = \underline{n}_0^{\Psi_M^{\rm imp}}$. In the uniform case, note that setting $\mathbf{n} = \underline{n}_0^{\Psi_M^{\rm imp}}$ in Eqs. (3.6) and (4.38) leads to the same embedding potential, providing that the exact bath Hxc functional is known. Indeed, all sites have the same occupation in the uniform case (in principle) such that $\mathbf{n} \equiv \{n_0, n_1, \dots, n_{L-1}\} = \{n, n, \dots, n\}$. However, when it comes to practical use of DFAs, the embedding potential will not be the same in both Hamiltonians simply because the resulting density profile is (unfortunately) not uniform anymore.

Let us rewrite the projected Hamiltonian in Eq. (4.37) as

$$\hat{H}^{\rm imp} \quad = \quad \hat{h}^{\rm emb} + \hat{U}_M = \sum_{ij=0}^{2M-1} \sum_{\sigma} h^{\rm emb}_{ij} \left(\hat{c}^{\dagger}_{i\sigma} \hat{c}_{j\sigma} + {\rm h.c.} \right) + U \sum_{i=0}^{M-1} \hat{n}_{i\uparrow} \hat{n}_{i\downarrow}, \tag{4.39}$$

where $\hat{h}^{\mathrm{emb}} = \hat{P}^{\dagger}\hat{h}^{\mathrm{SOET}}\hat{P}$ is the projection of $\hat{h}^{\mathrm{SOET}}$, which is the one-body part of the impurity-interacting SOET Hamiltonian containing the kinetic energy operator, as well as the density-functional embedding potential operator. In the particular case of a single impurity ($M = 1$), the embedded problem consists of one interacting site embedded into one bath site only (describing the environment). In other words, an impurity-interacting Hubbard dimer (equivalent to an Anderson dimer) is obtained and can be solved analytically. Indeed, according to Ref. [72] and Sec. 3.4.1, the impurity-interacting ground-state energy of the dimer is related to the physical one by a simple scaling and shifting relation [Eq. (3.72)],

$$\mathcal{E}^{\mathrm{imp}}_{M=1}(U, t, \Delta v) = E_0(U/2, t, \Delta v - U/2), \tag{4.40}$$

where E_0 is given in Eq. (2.36). Given that our Hubbard dimer is obtained by projection, we have $\Delta v \equiv h^{\mathrm{emb}}_{11} - h^{\mathrm{emb}}_{00}$ and $t \equiv -h^{\mathrm{emb}}_{01} > 0$. The impurity occupation is recovered by applying the Hellmann–Feynman theorem as follows (in analogy with Sec. 2.1.4.iii for the conventional Hubbard dimer):

$$\begin{aligned} n_0 &= 1 - \left.\frac{\partial \mathcal{E}^{\mathrm{imp}}_{M=1}(U, t, \Delta v)}{\partial \Delta v}\right|_{t=-h^{\mathrm{emb}}_{01}}, \\ &= 1 - \left.\frac{\partial E(U, t, \Delta v)}{\partial \Delta v}\right|_{U=U/2, t=-h^{\mathrm{emb}}_{01}, \Delta v = \Delta\overline{v}}, \end{aligned} \tag{4.41}$$

where $\Delta\overline{v} = \Delta v - U/2$. Similarly, and according to Eq. (2.45), the double occupation on the impurity site reads

$$d^{\mathrm{imp}} = \frac{1}{2}\left(\left.\frac{\partial E(U, t, \Delta v)}{\partial U}\right|_{U=U/2, t=-h^{\mathrm{emb}}_{01}, \Delta v = \Delta\overline{v}} - (1-n) \right). \tag{4.42}$$

For more than one impurity, the system cannot be solved analytically anymore, and DMRG will be employed as an impurity solver. Once the impurity occupation $n_0^{\Psi^{\mathrm{imp}}_M} = \langle \Psi^{\mathrm{imp}}_M | \hat{n}_0 | \Psi^{\mathrm{imp}}_M \rangle$ is obtained, it is inserted into the embedding potential in the SOET Hamiltonian in Eq. (4.38), and the procedure is reiterated until the impurity occupation converges.

The P-SOET approach is illustrated in Fig. 4.3. As readily seen in this figure, two starting points are considered. The first one is the fully-interacting Hubbard model. It defines the true physical system to be solved, for a given U and t and N electrons. This problem is mapped onto an impurity-interacting Hubbard model, given by the Hamiltonian in Eq. (4.38) where the embedding potential is always calculated by using the occupation of the impurity site. Then, a projector is calculated

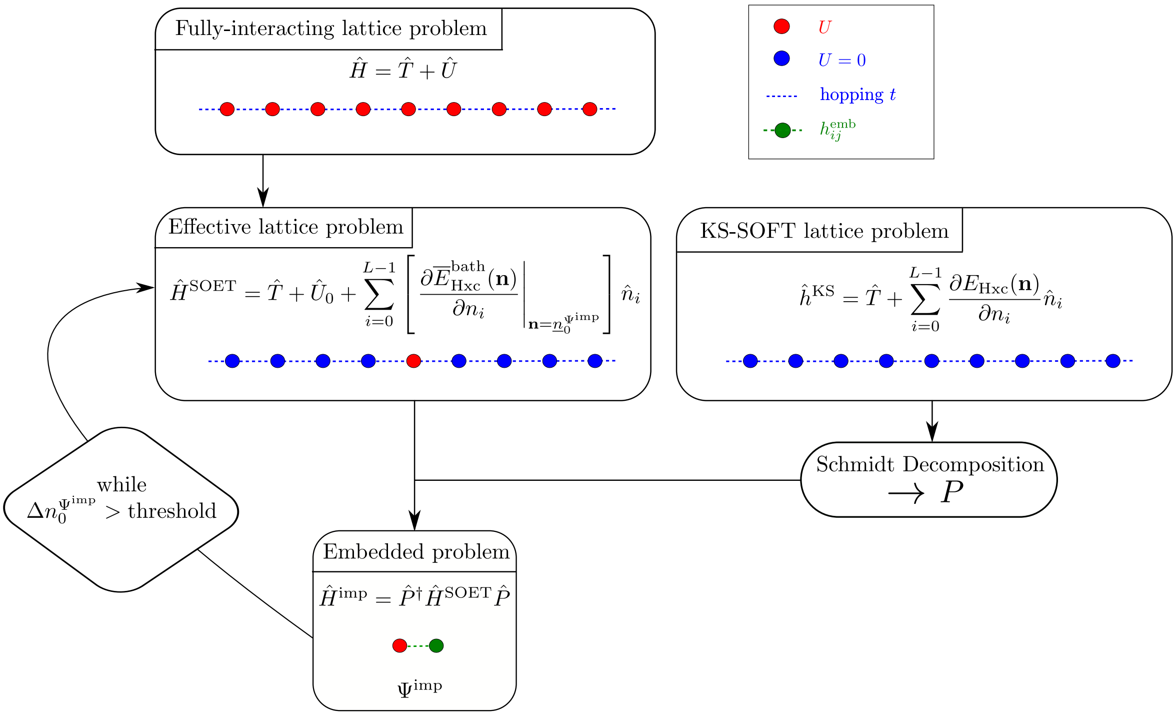

Figure 4.3: Projected-SOET procedure for a single impurity site labelled as 0. The projector is computed only once, by performing the Schmidt decomposition on the KS-SOFT lattice problem with the exact uniform density.

only once, by performing the Schmidt decomposition on the KS-SOFT lattice problem. This projector is then applied on Eq. (4.38) to obtain the embedded-impurity Hamiltonian in Eq. (4.39). The occupation and the double occupation of the impurity sites are then obtained by solving the embedded-impurity problem, either analytically for $M = 1$ by using Eqs. (4.41) and (4.42), or numerically using the DMRG solver for $M > 1$. Finally, the occupation on the impurity site 0 is inserted into Eq. (4.38), such that the procedure can be reiterated until the impurity occupation converges. Note that the exact uniform density of the physical problem is used to initialize the embedded potential at iteration 0. For a more general case (not studied in this thesis), the exact density is unknown and we could use the density obtained from the KS-SOFT calculation, which is in principle exact.

Let us now investigate the performance of P-SOET. The 400-site uniform Hubbard model is studied, hence demonstrating that P-SOET is a very low-cost approach able to treat large systems. Indeed, one iteration in P-SOET has exactly the same computational cost than one DMET iteration. In the regimes where P-SOET converges, the number of iterations needed to reach convergence is small, usually less than 10 iterations for iBALDA, and less than 20 for 2L-BALDA. My guess is that DMET needs much more iterations to optimize the correlation potential. Note that the expressions for the per-site energy and the double occupation in Eqs. (3.28) and (3.39), respectively, will be used.

Nbr. electrons	$N=2$	$N=4$	$N=6$	$N=8$	$N=10$	$N=12$
Uniform occ. $n=$	0.16667	0.33333	0.5	0.66667	0.83333	1
$U=t$	0.16559	0.33174	0.49883	0.66618	0.83329	1
$U=2t$	0.16377	0.32854	0.49613	0.66488	0.83305	1
$U=3t$	0.16209	0.32520	0.49296	0.66307	0.83251	1
$U=4t$	0.16068	0.32223	0.48990	0.66104	0.83167	1
$U=5t$	0.15954	0.31972	0.48719	0.65904	0.83057	1
$U=6t$	0.15861	0.31765	0.48489	0.65718	0.82930	1
$U=7t$	0.15784	0.31593	0.48296	0.65553	0.82796	1
$U=8t$	0.15720	0.31449	0.48134	0.65409	0.82663	1
$U=9t$	0.15666	0.31327	0.47997	0.65284	0.82537	1
$U=10t$	0.15621	0.31224	0.47881	0.65177	0.82421	1
$U=100t$	0.15141	0.30184	0.46785	0.63440	0.81267	1

Table 4.1: Occupation of the impurity site obtained within P-SOET by using the exact embedding potential from SOET for the 12-site Hubbard ring with a single impurity.

4.2.2 Errors due to the projection

In contrast to the original formulation of SOET, P-SOET is not in-principle exact anymore, due to the approximate description of the bath states. In order to quantify the error due to this projection, let us start by using the exact embedding potential, obtained numerically by Legendre–Fenchel transform on the 12-site ring Hubbard model (see Sec. 3.3.1 for the 8-site ring model), and see if the uniform density is recovered when solving the (projected) embedded-impurity problem. The resulting density is given in Tab. 4.1. Interestingly, by using the exact embedding potential from SOET, the half-filling occupation can be exactly recovered when applying P-SOET. However, this is not the case away from half-filling, as readily seen in Tab. 4.1. The deviation of the impurity occupation from the exact uniform one increases with U/t, showing that the exact embedding potential in SOET does not reproduce the uniform density when it is projected onto the embedded subsystem. Despite this unfortunate result, the error in the occupation is around 2×10^{-2} or less for $U=10t$ and up to 4×10^{-2} for $U=100t$, which remains relatively small in comparison to the final density obtained by solving the embedded problem within SOET and its various DFAs (chapter 3).

Let us investigate the effect of the projection on the impurity double occupation d^{imp}, which is an essential quantity involved in the calculation of the per-site energy and the true physical double occupation in SOET. In the case of half-filling for a single impurity, d^{imp} has been calculated within SOET using the exact diagonalization, and within P-SOET according to Eq. (4.42). The exact embedding potential has been used in both cases. Results are shown in Fig. 4.4 for the 12-site Hubbard ring. Note that the impurity double occupation has been plotted with respect to $U/(4t+U)$, which is equal to 0 for $U=0$, equal to 1 for $t=0$, and equal to $1/2$ for $U=4t$, so that the noninteracting limit,

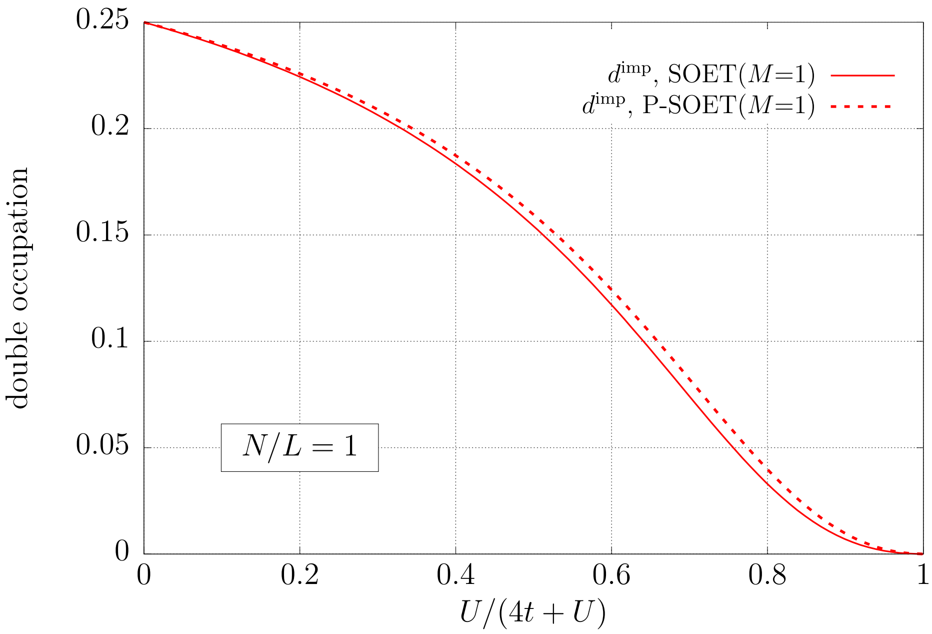

Figure 4.4: Impurity double occupation in SOET and in P-SOET for a single-impurity at half-filling. The exact diagonalization has been used within SOET.

the atomic limit and the medium correlation strength are considered, respectively. Given that the exact diagonalization is used to solve the SOET Hamiltonian with the exact potential, the resulting impurity double occupation is exact as well (in a sense that it is calculated from the exact impurity wavefunction, but it does still not correspond to the true physical double occupation). In contrast to the impurity occupation [Tab. 4.1], the impurity double occupations obtained in SOET and in P-SOET are not identical at half-filling. Nevertheless, the difference remains small.

4.2.3 BALDA potential at half-filling

In the previous chapter, the exact embedding potential has been used in the half-filled case, for a *finite* system. Let us recall that this potential is equal to 0 on the impurity sites and $U/2$ in the bath (or, equvialently, $-U/2$ on the impurity sites and 0 in the bath). According to Eq. (3.43), satisfying this condition is equivalent to set the impurity correlation potential to 0 at half-filling. For the 2L-BALDA approximation, based on the asymmetric Hubbard dimer, this condition is fulfilled. But for functionals which are developed in the thermodynamic limit, such as iBALDA(M) and SIAM-BALDA, the impurity correlation potential at half-filling is not defined due to the presence of a derivative discontinuity in the impurity correlation energy functional.

For convenience, the BALDA (or equivalently, iBALDA) correlation potential,

$$\frac{\partial e_{\rm c}^{\rm BALDA}(n<1)}{\partial n} = -2t\cos\left(\frac{\pi n}{\beta(U/t)}\right) + 2t\cos\left(\frac{\pi n}{2}\right) - \frac{Un}{2}, \tag{4.43}$$

will take the following value at half-filling,

$$\left.\frac{\partial e_{\mathrm{c}}^{\mathrm{BALDA}}(n \leqslant 1)}{\partial n}\right|_{n=1} \rightarrow \left.\frac{\partial e_{\mathrm{c}}^{\mathrm{BALDA}}(n \leqslant 1)}{\partial n}\right|_{n=1^-} = -2t\cos\left(\frac{\pi}{\beta(U/t)}\right) - \frac{U}{2}, \tag{4.44}$$

which is equal to 0 for $U = 0$ only (with $\beta(0) = 2$). This choice is made in order to have a continuous embedding potential in the range $0 \leq n \leq 1$, and not in the range $0 \leq n < 1$ only like in chapter 3. Indeed, the half-filling iBALDA correlation potential was previously set to the exact correlation potential for a *finite* system, i.e. $\partial e_{\mathrm{c}}^{\mathrm{BALDA}}(n \leqslant 1)/\partial n|_{n=1} = 0$. This choice was made for practical reason. As mentioned in the very end of chapter 3, convergence issues may arise around half-filling, when either the impurity *or* the bath occupations are very close to 1. If the iBALDA correlation potential in Eq. (4.44) were used to solve the SOET self-consistent equation, the occupations in the whole system would have fluctuated around 1 and no convergence would have been reached.

In P-SOET, the situation is different. All the bath occupations are set to the impurity occupation in the theory. Hence, there are no fluctuations and all occupations are the same, such that this particular convergence issue at half-filling can be avoided (as shown in the following section). Therefore, we can use the definition of the correlation potential in Eq. (4.44) at half-filling. In order to make a difference between the latter potential and the (exact) one used in iBALDA at half-filling, we referred to it as the $\overline{\text{iBALDA}}$ approximation. The difference between the two approximations is made clear in Fig. 4.5.

Also, let us stress that enlarging the size of the system to 400 sites allows us to study the whole range of the density regime. Therefore, we can approach the $\mathbf{n} = \underline{1}^-$ limit very accurately. Indeed, taking 398 electrons in 400 sites leads to $n = 0.995$, against $n = 0.9375$ for the 32-site Hubbard model studied in SOET. As already mentioned, approaching the half-filled case can lead to convergence issues due to the derivative discontinuity in the embedding potential, even within P-SOET. This will be shown in the next section, where per-site energies and double occupations are calculated in different correlation and density regimes.

4.2.4 Double occupation and per-site energy at half-filling

4.2.4.i Double occupation at half-filling

Turning to the exact double occupation expression in SOET [Eq. (3.39)], the 2L-BALDA, iBALDA(M) and the new $\overline{\text{iBALDA}}(M)$ functionals are tested on the 400-site ring Hubbard model. The Bethe Ansatz (BA) [320] results obtained by solving Eq (2.74) are used as a reference[1]. Let us focus on the half-filled case, which is the only case where iBALDA(M) and $\overline{\text{iBALDA}}(M)$ differ. In Fig. 4.6, the

---

[1] The BA code has been written by Matthieu Saubanère, CNRS at the Institut Charles Gerhardt Montpellier (FRANCE).

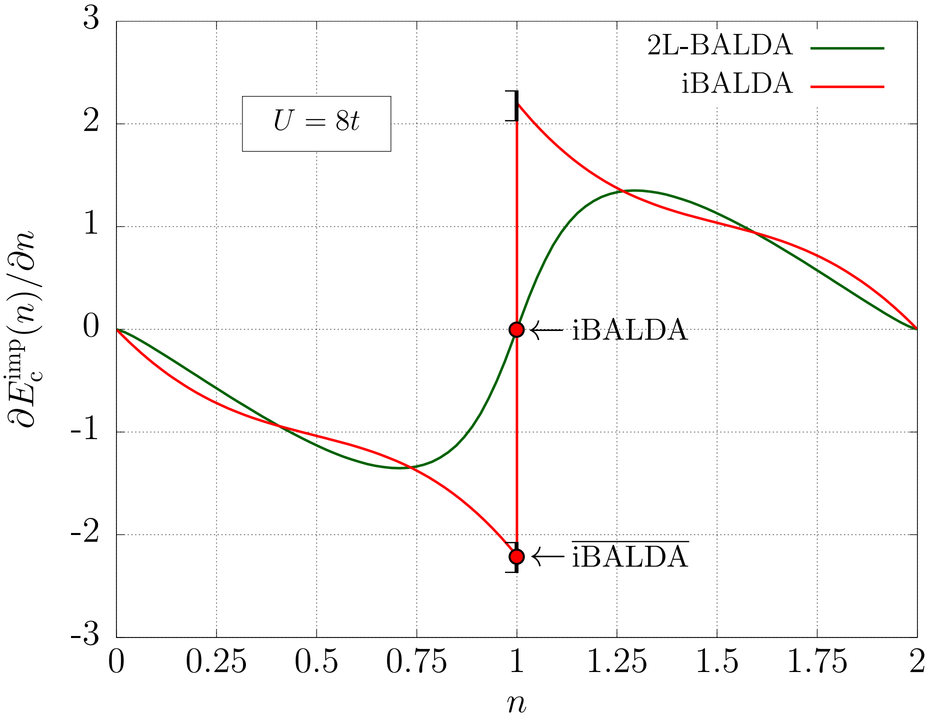

Figure 4.5: 2L-BALDA and iBALDA correlation potential with respect to n for $U/t = 8$. At half-filling, the iBALDA correlation potential is exact and equal to 0, while the $\overline{\mathrm{iBALDA}}$ correlation potential is given in Eq. (4.44). Note that this BALDA potential is also used in the bath.

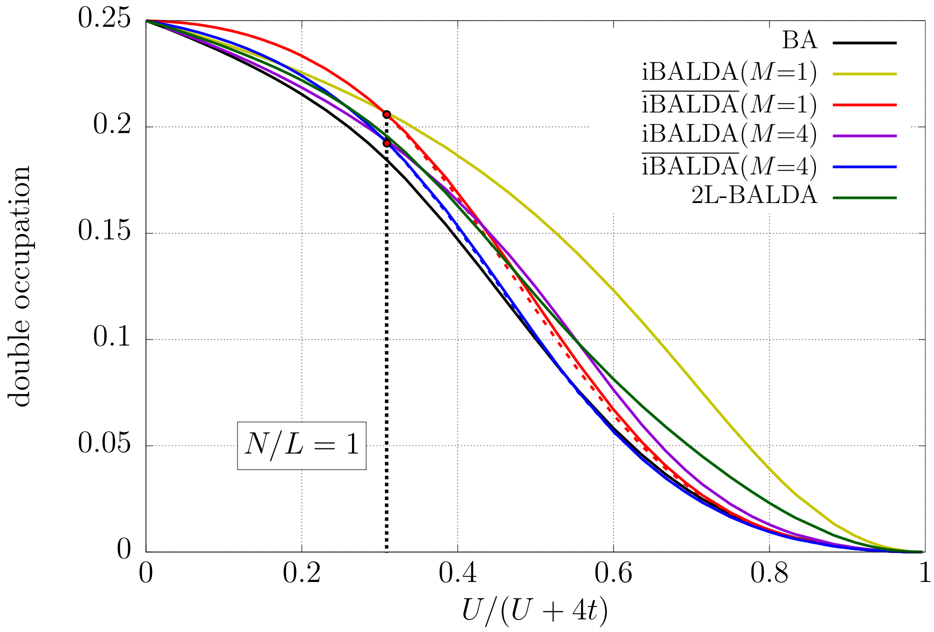

Figure 4.6: Double occupation for the various functionals at half-filling, within P-SOET. For the $\overline{\mathrm{iBALDA}}(M)$ approximation, the full lines represent the result at the first iteration while the dashed lines are the one obtained after convergence. The red dot and the black dashed line correspond to the correlation regime from which $\overline{\mathrm{iBALDA}}(M)$ starts to converge.

double occupation has been plotted with respect to the correlation strength. First of all, it is clear that all approximations are exact in the $U = 0$ and $t = 0$ limits. Then, the iBALDA(M) and 2L-BALDA double occupations are quasi identical to the SOET results [Fig. 3.8] presented in the previous chapter. Hence, the same conclusions still hold, e.g. the double occupation is improved when using non-zero per-site bath correlation functional (2L-BALDA here, as compared to iBALDA(M=1)), and when increasing the number of impurities. For the latter, the improvement is at the expense of a much higher computational cost, as passing from $M = 1$ to $M = 4$ is equivalent to solve a 8-site Hubbard model instead of a Hubbard dimer for the embedded problem.

Note that for 2L-BALDA and iBALDA(M), the exact embedding potential is used such that there are no density-driven errors and the problem converges to the exact density in one iteration only (see Tab. 4.1). For this reason, and because there is no bath correlation energy functional of the density in DMET, the iBALDA(M=1) double occupation (corresponding to $d^{\mathrm{imp}}_{M=1}$) is exactly the same as the single-impurity DMET one [418, 420]. Indeed, in both P-SOET and DMET theories, the correlation potential is the same at half-filling for a single impurity, so that there is absolutely no difference between the two approaches. In other words, the impurity wavefunctions are identical in both methods at half-filling. Then, if bath correlation functionals are used, P-SOET improves over DMET, as shown by the 2L-BALDA double occupation. If the matching is performed on the diagonal of the 1RDM of the fragment only, DMET [see the noninteracting (NI) bath formulation in Ref. [420] and the Fig. 2 therein] is similar to iBALDA(M) for the calculation of the double occupation. To improve over iBALDA(M) (or, equivalently, NI in Ref. [420]), DMET can match not only the diagonal but all the 1RDM of the fragment, while the improvement of P-SOET relies on the development of new M-dependent functionals. Alternatively, constructing more accurate bath orbitals by starting with the antisymmetrized geminal power wavefunction [425] or the unrestricted Hartree-Fock one [420] is also a way to increase the performance of DMET as well as P-SOET.

Let us now turn to the new $\overline{\text{iBALDA}}$ approximation for $M = 1$. The only difference with iBALDA(M) is in the embedding potential at half-filling. This potential is still 0 on the impurity by construction, but instead of being $U/2$ in the bath it becomes equal to the one in Eq. (4.44) computed with the occupation of the impurity, and is thus no more exact for a finite system. Surprisingly, at the first iteration using the exact uniform density (full lines in Fig. 4.6), $\overline{\text{iBALDA}}$(M=1) performs better than iBALDA(M=1) for $U/(4t + U) > 0.3$ (or, equivalently, $U > 1.8t$), and even better than 2L-BALDA and iBALDA(M=4) in the strongly correlation regime $U > 4t$. Given that there is no functional contribution in the expression of the double occupation within iBALDA(M) or

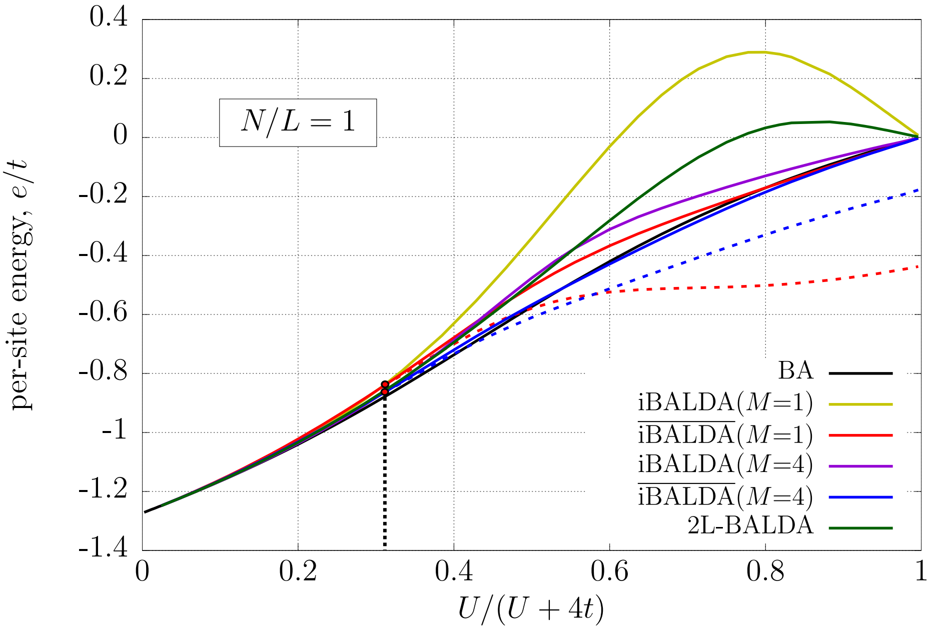

Figure 4.7: Same as Fig. 4.6 but for the per-site energy.

$\overline{\text{iBALDA}}(M)$ [see Eq. (3.39)], it means that the impurity double occupation $d^{\text{imp}}_{M=1}$ gets much closer to the true physical double occupation when using the potential in Eq. (4.44). Therefore, the embedding potential has a strong influence on the resulting impurity double occupation. For $U < 1.8t$, $\overline{\text{iBALDA}}(M)$ is however not better than iBALDA(M) (for $M = 1$ and $M = 4$). Interestingly, as shown in Fig. 4.6 by the red dots and the dashed black line, this is exactly the regime in which the $\overline{\text{iBALDA}}(M)$ shows self-consistent convergence problems. This can be explained as follows: in the weakly correlated regime, the deviation from the half-filling is small, so that the embedding potential remains close to the discontinuity and starts to oscillate. On the contrary, in the strongly correlated regime, the deterioration of the density is strong enough to remain far from the discontinuity, so that it becomes possible to converge. Impressively, $\overline{\text{iBALDA}}(M{=}4)$ gives the best double occupation for $U > 1.8t$, and is even on top of the exact double occupation for $U > 4t$. In analogy with the SOET results presented in the previous chapter, the density-driven error is almost absent in the double occupation. This is because the double occupation within $\overline{\text{iBALDA}}(M)$ does consider the bare M-interacting-impurity double occupation only, without any contribution from a complementary functional of the density.

4.2.4.ii Per-site energy at half-filling

Let us now turn to the per-site energy at half-filling, shown in Fig. 4.7. We start by analysing the per-site energy [Eq. (3.28)] in which the exact uniform density has been inserted (full lines). In analogy with the double occupation, we notice that P-SOET is exact in both the non-interacting and the atomic limits, for all functionals. The 2L-BALDA and iBALDA(M) results are very similar to the per-site energy obtained within SOET [see Fig. 3.6 in the previous chapter]. For a single impurity, both of them feature a positive per-site energy in the strongly correlated regime, although 2L-BALDA remains constantly better than iBALDA$(M{=}1)$. By increasing the number of impurities in iBALDA$(M{=}4)$, we recover a negative per-site energy. It should be noted that, in contrast to the double occupation, the per-site energy within iBALDA(M) is not calculated the same way in P-SOET and in DMET, such that they are not directly comparable. Returning to P-SOET, even though iBALDA$(M{=}4)$ is already relatively accurate in all the correlation regime, it is outperformed by $\overline{\text{iBALDA}}(M{=}1)$ with a single impurity only, as soon as $U/(4t+U) > 0.4$. Impressively, $\overline{\text{iBALDA}}(M{=}1)$ is highly accurate in the strongly correlated regime ($U/(4t+U) > 0.7$), and increasing the number of impurities to $M = 4$ leads to a per-site energy which is almost on top of the exact one in all regimes of correlation, from $U = 0$ to $U \to +\infty$.

Turning to the per-site energy obtained by using the converged density for $\overline{\text{iBALDA}}(M)$ (I recall that the other approximations have no density-driven error at half-filling, because the exact embedding potential is employed), the density starts to deviate from the half-filled one as soon as $U/(4t{+}U) > 0.4$, and does not converge for $U < 1.8t$. It is clear from the dashed lines in Fig. 4.7 that the deterioration of the density is not in favour of a better accuracy. Indeed, huge density-driven errors arise when the correlation increases, thus making $\overline{\text{iBALDA}}(M)$ not exact anymore in the atomic limit after convergence. Note that by increasing the number of impurities, this error is less pronounced.

4.2.5 Double occupation and per-site energy away from half-filling

4.2.5.i Double occupation away from half-filling

Away from half-filling ($0 \leqslant n < 1$), the iBALDA(M) and $\overline{\text{iBALDA}}(M)$ approximations are exactly the same. In order to have smooth potentials in the range $0 \leqslant n \leqslant 1$, $\overline{\text{iBALDA}}(M)$ is used instead of iBALDA(M). Therefore, we focus on the $\overline{\text{iBALDA}}(M)$ approximation in the following. Let us first take a look at the 2L-BALDA double occupation in Fig. 4.8. We start by using the exact density at iteration 0 (full lines). The physical 2L-BALDA double occupation [see Eq. (3.39)] (in green) and its bare double occupation d^{imp} (in yellow) differ by $\partial \overline{e}^{\text{bath}}_{\text{c},M=1}(\mathbf{n})/\partial U$. The latter leads to a significant overestimation of the double occupation. In other words, it does not account for enough correlation effects. Very surprisingly, this is not anymore the case when considering the $\overline{\text{iBALDA}}(M)$ double occupation (which is only given by the bare impurity double occupation). Indeed, the impurity double occupation becomes highly accurate in the whole density domain, and overcomes the performance of the physical 2L-BALDA double occupation (in green), which is already relatively good considering

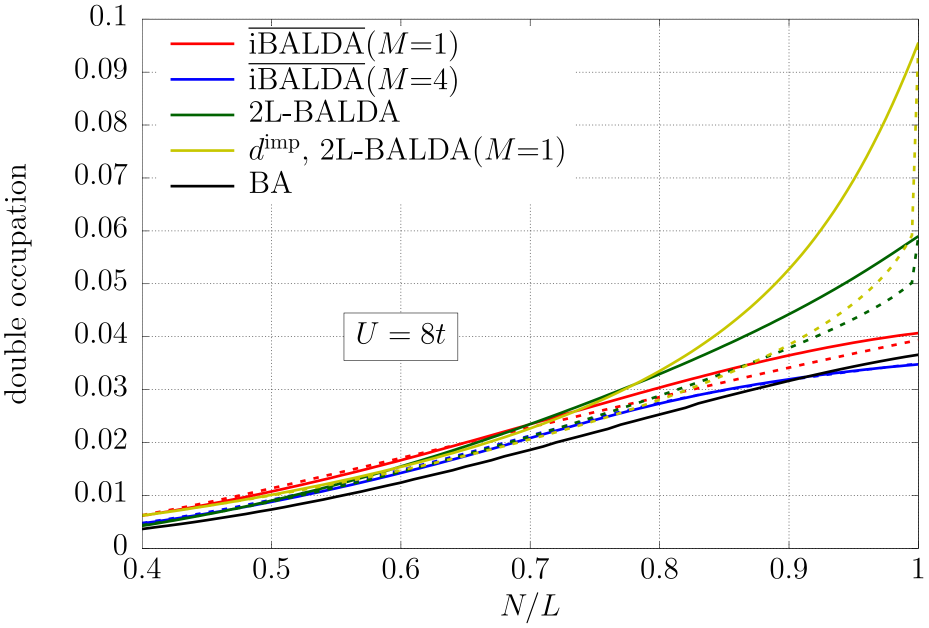

Figure 4.8: Double occupation for the 2L-BALDA and $\overline{\text{iBALDA}}(M)$ approximations in P-SOET ($L = 400$). The bare impurity double occupation of 2L-BALDA (yellow lines) is plotted as a comparison to the bare impurity double occupation of $\overline{\text{iBALDA}}(M{=}1)$. Full lines: results obtained at iteration 0 using the exact density. Dashed lines: results obtained after reaching convergence. See text for further details.

only one impurity. I recall that this behaviour could not been really observed previously, as the number of sites was not sufficient to sample the whole density domain.

Increasing the number of impurities does slightly improves the double occupation. However, this small improvement is not worth it, considering the already high accuracy and the low computational cost of $\overline{\text{iBALDA}}(M{=}1)$. The good performance of $\overline{\text{iBALDA}}(M{=}1)$ can be rationalized as follows. According to Fig. 4.5, the impurity correlation potential in $\overline{\text{iBALDA}}(M{=}1)$ is becoming more and more negative when approaching $n = 1$, while the 2L-BALDA one increases towards 0 for $0.75 \lesssim n \leq 1$. Therefore, and according to Eq. (3.43), the embedding potential is much more repulsive on the impurity site within $\overline{\text{iBALDA}}(M{=}1)$ than within 2L-BALDA, leading to a decrease of the impurity double occupation in the density domain $0.75 \lesssim n \leq 1$ [see Fig. 4.8].

Considering the final converged results (dashed lines) in Fig. 4.8, the impurity double occupation in $\overline{\text{iBALDA}}(M)$ is not much affected by density-driven errors. For $M = 4$, this error on the double occupation is even very close to zero, as the dashed line and the full line are almost indiscernible. This has to be distinguished from the 2L-BALDA double occupation, for which the error in the density significantly improve the double occupation in the vicinity of half-filling, even for the bare impurity double occupation. This error in the impurity occupation is indeed very large in this case, as shown in Fig. 4.9 which shows the densities obtained self-consistently. Within 2L-BALDA, the impurity

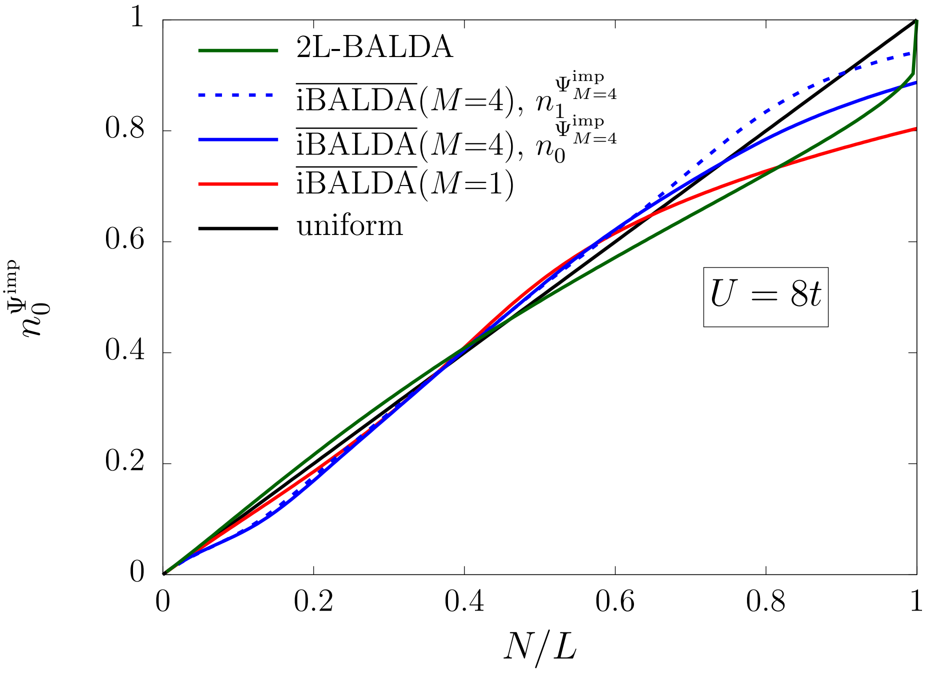

Figure 4.9: Self-consistent impurity occupation(s) for 2L-BALDA and $\overline{\text{iBALDA}}(M)$ approximations in P-SOET ($L = 400$). For $\overline{\text{iBALDA}}(M{=}4)$, the two central impurities are $n_1^{\Psi^{\text{imp}}_{M=4}} = n_2^{\Psi^{\text{imp}}_{M=4}}$ with their two neighbours $n_0^{\Psi^{\text{imp}}_{M=4}} = n_3^{\Psi^{\text{imp}}_{M=4}}$.

occupation deviates from the exact uniform occupation, and is significantly underestimated. This underestimation of the impurity occupation close to the half-filled case also leads to an underestimation of the impurity correlation potential in Fig. 4.5, functional of the density. In other words, the impurity correlation potential becomes more attractive or, according to Eq. (3.111), the embedding potential becomes more repulsive. This leads to a decrease of the impurity double occupation which gets closer to the exact one.

4.2.5.ii Per-site energy away from half-filling

Let us now discuss the per-site energy [Eq. (3.27)] in Fig. 4.10. Starting with the iteration 0 using the exact density (full lines), the same conclusions than for the double occupation can be made. Although 2L-BALDA gives relatively accurate results, it is significantly outperformed by $\overline{\text{iBALDA}}(M)$ in the vicinity of half-filling. Indeed, $\overline{\text{iBALDA}}(M{=}1)$ is an excellent approximation to the per-site energy. $\overline{\text{iBALDA}}(M{=}4)$ is even better, as it becomes almost indiscernible from the exact per-site energy in the range of $0.6 \leqslant N/L \leqslant 1$.

However, and as already discussed in the context of SOET in the previous chapter, the density-driven errors can be important for the per-site energy. Turning to the converged results in Fig. 4.10 (dashed lines), the density-driven error is now becoming very important for the $\overline{\text{iBALDA}}(M)$ approx-

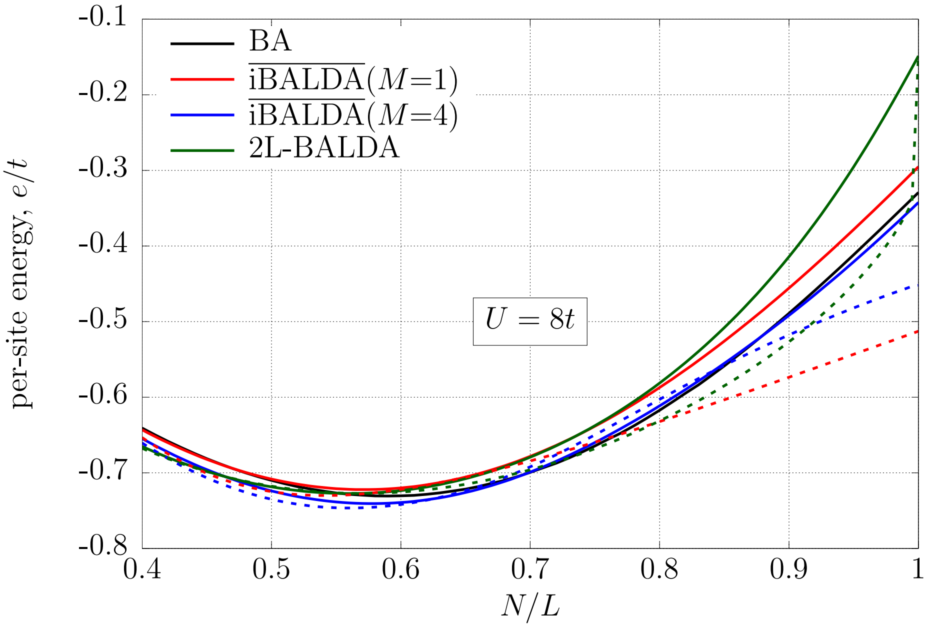

Figure 4.10: 2L-BALDA and $\overline{\text{iBALDA}}(M)$ per-site energies in P-SOET ($L = 400$). Full lines: results obtained at iteration 0 using the exact density. Dashed lines: results obtained after reaching convergence. See text for further details.

imation in the vicinity of half-filling, even for $M = 4$. Indeed, in contrast to the double occupation, the per-site energy within $\overline{\text{iBALDA}}(M)$ does include density-functional contributions. According to Fig. 4.9, it is clear that the density-driven error in the per-site energy follows the same trends as the error in the impurity occupation, which is quite expected. For all functionals, it leads to a decrease of the per-site energy close to half-filling. While it improves the performance of 2L-BALDA, it deteriorates the $\overline{\text{iBALDA}}(M)$ energies.

4.2.6 Opening of the charge gap at half-filling

The question we now wish to address is whether one could describe the opening of the charge gap at half-filling. In the 1D Hubbard model, no Mott transition arises as a function of U, as the model becomes an insulator at half-filling for any $U > 0$. However, there is another Mott transition which is a “density-driven” Mott transition, i.e. the transition from a metal ($n < 1$) to an insulator ($n = 1$), for any finite non zero value of U [329]. In order to see this transition, we plot the density as a function of the chemical potential. The chemical potential is a shift in the external potential that fixes the number of electrons in the system,

$$\hat{H} \longrightarrow \hat{H}(\mu) = \hat{H} - \mu\hat{N}, \tag{4.45}$$

where $\hat{N} = \sum_i \hat{n}_i$ is the counting operator. The total number of electrons varies with μ, except if μ is in the charge gap. Indeed, the half-filled one-dimension Hubbard model is an insulator, such that it depicts the splitting of the d band in semi-conductors (see Fig. 2.3). Assuming that we are in the thermodynamic limit, if the chemical potential varies inside of the valence band, the number of electrons will vary continuously with it. But if the chemical potential varies in the band gap, then the number of electrons will always be the one that fills the valence band completely (so $n = 1$ in the Hubbard model), such that the chemical potential is not uniquely defined anymore. This is also related to the discontinuity in the correlation potential at half-filling. Alternatively, this behaviour can be observed by looking at the compressibility $\mathrm{d}N/\mathrm{d}\mu$ [418], which vanishes when entering the charge gap. In order to find the number of electrons associated with a given chemical potential, it comes from Eq. (4.45) that we have to solve the following (per-site) minimization within P-SOET:

$$\min_{N} \left\{ e^{\text{P-SOET}}(N/L) - \mu N/L \right\}, \tag{4.46}$$

where the exact density $n = N/L$ in the P-SOET per-site energy is used in a first step. The minimizing number of electrons in Eq. (4.46) is the one corresponding to the given and fixed chemical potential μ, denoted by $N(\mu)$. Therefore, for each value of μ, we perform the minimization in Eq. (4.46) to find the minimizing density $n(\mu) = N(\mu)/L$, where $L = 400$ in our case. Given that the per-site energy in P-SOET has been calculated for any even electron number N, the minimization is done over 200 points. Note that such a minimization would have been irrelevant in the original implementation of SOET, where only the 32-site Hubbard model was studied. The results are shown in Fig. 4.11 for $U = 8t$, such that it can be directly compared to the DMET results in Figs. 3 and 4 of Refs. [418] and [420], respectively. First, let us discuss the exact curve of this plot, obtained with BA calculations. As readily seen in the BA curve, increasing the chemical potential leads to a continuous increase of the number of electrons in the metallic domain $N/L < 1$. As soon as the system becomes half-filled ($N/L = 1$), the number of electrons is not influenced by the change in chemical potential anymore. Hence, the compressibility $\mathrm{d}N(\mu)/\mathrm{d}\mu$ vanishes, thus manifesting the opening of the gap. The size of the gap is then determined by the size of the plateau at $N/L = 1$. Turning to P-SOET at iteration 0 with the exact density (full lines), $\overline{\text{iBALDA}}(M)$ is almost on top of the BA curve, even for a single impurity. This is one of the most important result in this thesis, in my opinion. Indeed, this density-driven gap opening is neither obtained in single-site DMFT [329] nor in single-site DMET [418, 420] for the one-dimensional Hubbard model, while it is obtained almost exactly in P-SOET within $\overline{\text{iBALDA}}(M{=}1)$ (using the exact density). This very nice feature of P-SOET (and, more generally, SOET) is clearly due to the fact that all the missing correlation in

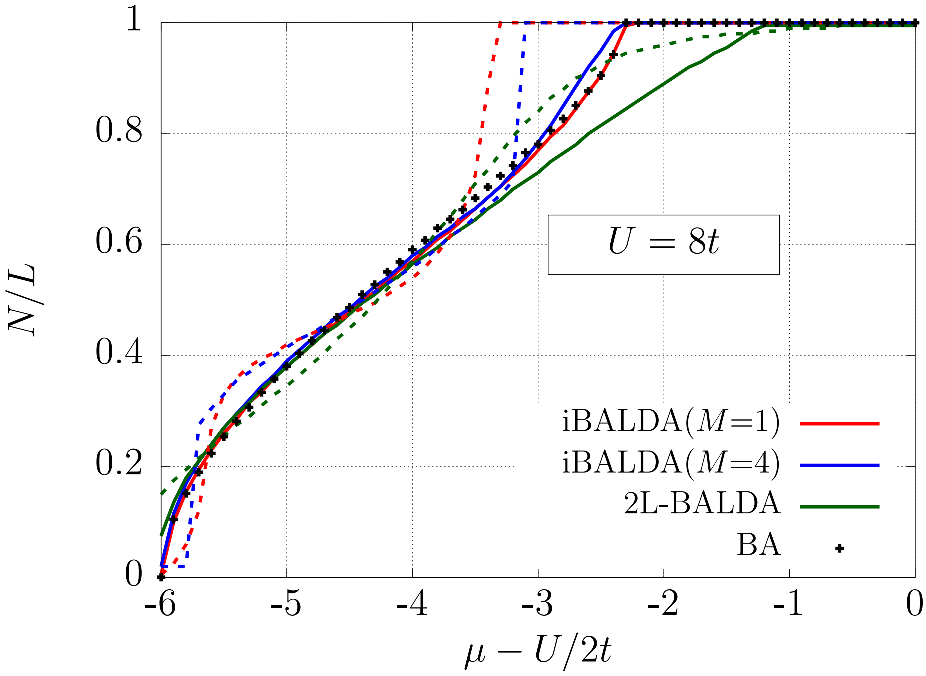

Figure 4.11: Variation of the density filling as a function of the chemical potential for $U/t = 8$, according to Eq. (4.46) using the exact density for $e^{\text{P-SOET}}(N/L)$ (full lines), and the converged one (dashed lines). See text for further details.

single-site DMET and single-site DMFT can in principle be included in the SOET bath correlation functional. In contrast to $\overline{\text{iBALDA}}(M)$, 2L-BALDA is faced to difficulties when approaching half-filling. At first sight, it seems that it does describe the opening of the gap, even though the position of the gap is displaced. In fact, it does not describe a gap at half-filling. Indeed, the constant plateau is reached for $N = 398$, equivalent to $n = 0.995$! Note that this would also be the case if one uses the iBALDA(M) approximation instead of $\overline{\text{iBALDA}}(M)$ (not shown). Apparently, iBALDA(M) and 2L-BALDA approximations do not describe the insulating state with enough precision to account for the density-driven Mott transition correctly. This is most certainly due to the fact that 2L-BALDA does not depict any discontinuity in the potential, and that iBALDA(M) set the impurity correlation potential to 0 at half-filling, instead of using Eq. (4.44) [see Fig. 4.5). A deeper analysis is still in progress.

Let us now look at the results obtained with the converged density (obtained self-consistency), inserted in Eq. (4.46) as follows,

$$\min_N \left\{ e_M^{\text{P-SOET}}(n_0^{\Psi_M^{\text{imp}}}) - \mu N/L \right\}, \tag{4.47}$$

where $e_M^{\text{P-SOET}}(n_0^{\Psi_M^{\text{imp}}})$ denotes the per-site energy obtained by solving the N-electron/M-impurity-interacting problem self-consistently within P-SOET. The results are shown in dashed lines in Fig. 4.11.

Clearly, the density-driven error has a huge impact on the compressibility. In contrast to DMET and DMFT which always give a good representation of the compressibility in the doped region ($n \lesssim 0.7$) [329, 418, 420], the P-SOET compressibility is subject to strong density-driven errors. As a consequence, even though $\overline{\text{iBALDA}}(M)$ exhibits a plateau at $N/L = 1$, the position of the density-driven Mott transition is misplaced and is strongly overestimated. For 2L-BALDA, it is not even clear if a plateau is reached or not here. In order to check the opening of a Mott gap in 2L-BALDA, we could treat a much larger system to have more precision around half-filling.

4.3 Summary and Perspectives

Let us highlight what SOET and its alternative formulations bring to the condensed matter physics community. To summarize, SOET in its original formulation (Chap. 3) is an in-principle exact theory, that relies on a mapping of the physical fully-interacting problem onto an embedded one, composed of interacting impurities surrounded by noninteracting effective bath sites. Within the exact formalism and using Legendre transforms, we have seen some very interesting features of the embedding potential. Away from half-filling, the breaking of translational symmetry due to the explicit treatment of the impurity sites leads to fluctuations of the embedding potential in the bath. While this statement is quite intuitive, it highlights the fact that the bath correlation functional (or, equivalently, the impurity one) has to depend on all sites occupation, and not only on the impurity one(s), as it has been assumed throughout the various approximations developed in this thesis. This gives an idea of the difficult task of achieving an exact embedding, even for a uniform model. Then, exact expressions for the double occupation and per-site energy have been derived for the uniform model within SOET, involving both wavefunction and density-functional contributions, hence showing that SOET is indeed a true combination of the two approaches. We have also seen how significant is the per-site bath correlation contribution around the half-filled case, where the density-driven Mott transition arises. This contribution, for which we provided some exact numerical values and approximate analytical expressions, can actually help in understanding the missing correlation in DMET. A connection with the single-impurity Anderson model has also been investigated, throughout the development of SIAM-based functionals. This connection has been further investigated by transforming the SOET Hamiltonian onto a SIAM Hamiltonian, which can then be solved by impurity-solver techniques using Green's function. However, despite this rewriting of the SOET Hamiltonian, it is not obvious if it leads to a decrease of the computational cost, except if we use approximate solver like second-order perturbation theory. In our group, Laurent Mazouin is actually working on a Green's function-based formulation of SOET, and we hope to get a mapping of the type of DMFT (with a single impurity

Green's function), but where the mapping is performed on the density. This is currently in progress. A clearer connection with DMFT could then be investigated, in the spirit of the projected version of SOET, which is closely related to DMET. Within this projected formulation, the computational cost has become almost negligible, as the problem now reduces to the diagonalization of a $(L \times L)$ matrix to create the projector, used to project the physical problem onto a $2L_F$ size problem (where L_F is the number of impurities). This (now approximate) formulation of SOET has been shown very promising, and highly accurate results for the per-site energy, the double occupation, and the density-driven Mott Hubbard transition have been obtained.

Let us now turn to future works. First of all, it is clear that new functionals should be developed. This could be done by looking, for example, at the perturbation expansion of the embedding potential by Görling-Levy perturbation theory [78, 97], or by adapting the Sham-Schlüter equation [224] to SOET. The latter approach has been recently investigated by Laurent Mazouin up to second-order, and the obtained embedding potential is shown to partially compensate the Friedel-like oscillations of the density that arise when interacting impurities are "inserted" in the model [Fig. 3.5]. A second-order correlation energy functional could then be obtained from the self-energy. This would only be sufficient in the weakly correlated regime, but it would be the first step toward the development of a functional that depends on all the site occupations. This is currently in progress.

Also, multiple-impurity functionals that account for the per-site bath correlation functional (in contrast to iBALDA) could also be developed. This is left for future work. Of course, it would also be interesting to extend SOET to higher dimensions like the 2D Hubbard model that contains a Mott–Hubbard transition as a function of U/t, as well as superconducting states to model the high-$\mathrm{T_c}$ cuprates. But this extension requires the development of appropriate functionals that we have not investigated yet. For this purpose, an automated way of constructing functionals in SOET is of major importance, and is also left for future work. Finally, a grand canonical formulation of SOET (to be contrasted to the canonical formulation of SOET) is also of interest. The so-called partition DFT [299] could bring an answer to this problem.

Chapter 5

Unified formulation of fundamental and optical gap problems in ensemble DFT

In the previous chapters, the Mott transition has been introduced in the context of the Hubbard model, and is manifested by the opening of a gap between the valence and the conduction band. This chapter deals with the fundamental gap (or, equivalently, twice the hardness [441]), which is one of the most challenging quantities to describe in quantum chemistry for molecules [2], as well as in condensed matter physics for solids [442]. There are several sorts of gaps, which has sometimes led to confusion in the literature [443]. For instance, the optical gap, given by the lowest excitation energy (neutral excitation) is completely different from the fundamental gap, obtained by the difference between the ionization potential and the electronic affinity (charge excitations). We can find different terminology in the literature, such as the transport gap, the electronic gap, the band gap (for solids) and the charge gap, all identical to the fundamental gap. These energy gaps between the highest occupied and lowest unoccupied electronic levels determine the electronic, optical, redox, and transport properties of a material, such as semiconductors and photovoltaic materials. The determination of the fundamental gap remains one of the biggest challenge in density-functional theory (DFT) [2].

In this chapter, we first review how the optical and fundamental gap can be extracted from a DFT calculation, followed by an unified formulation of these two different gaps at a formal level, in the context of ensemble DFT.

5.1 Optical gap in ensemble DFT

This section focuses on the extraction of the exact optical gap in ensemble DFT, which is essential to understand the outcomes of the approach presented in the following, so-called N-centered ensemble DFT [75].

In DFT, the KS gap is given by the difference between the *lowest unoccupied molecular orbital* (LUMO, denoted by L) and the *highest occupied molecular orbital* (HOMO, denoted by H),

$$E_{\mathrm{g}}^{\mathrm{KS}} = \varepsilon_{\mathrm{L}}^{\mathrm{KS}} - \varepsilon_{\mathrm{H}}^{\mathrm{KS}}. \tag{5.1}$$

Although this gap gives a first and relatively good approximation to the optical gap in molecules, it contributes only to about 60% of the optical gap in solids [444]. The correction is commonly provided by linear response, i.e. the xc kernel in time-dependent DFT (TDDFT) [445], which has been widely and successfully employed over the last thirty years (see for instance reviews in Refs. [255, 296] and references therein). Unfortunately, TDDFT does not give an accurate description of charge transfer excitations [446] when local or semi-local functionals are used. Even worse, multiple excitations are completely absent from the spectra [254]. Note that some progress regarding these issues have been made recently [447–449]. Alternatively, and originated from solids state physics, the more involved *many-body perturbation theory* (MPBT) within GW together with the Bethe Salpeter equation [450, 451], which relies on the two-particle Green's function, can be used.

It is desirable to have access to the whole excited spectrum of the system by a time-independent approach that remains computationally cheap. The Gross–Oliveira–Kohn (GOK) DFT for canonical ensemble [257–259] is such a theory, proposed in the late 1980s and which generalizes the seminal work of Theophilou [452]. In the following, we focus on ensembles consisting of two nondegenerate states,

$$E^w = (1-w)E_0 + wE_1, \tag{5.2}$$

where $w_0 = 1 - w$ is the weight associated to the ground-state energy E_0 and $w_1 = w$ is the one associated to the first excited state E_1. E^w is called the ensemble energy and can be expressed variationally as follows,

$$E^w = \min_{\hat{\Gamma}^w} \mathrm{Tr}\left[\hat{\Gamma}^w \hat{H}\right] = \mathrm{Tr}\left[\hat{\Gamma}_0^w \hat{H}\right]. \tag{5.3}$$

where $\hat{\Gamma}^w = (1-w)|\overline{\Psi}_0\rangle\langle\overline{\Psi}_0| + w|\overline{\Psi}_1\rangle\langle\overline{\Psi}_1|$ is the ensemble density matrix operator, and $\overline{\Psi}_0$ and $\overline{\Psi}_1$ denote ground- and first-excited state orthonormal trial wavefunctions, respectively. This energy is linear with respect to w and its derivative gives rise to the first excitation energy, i.e. the optical gap,

$$\Omega = E_1 - E_0 = \frac{\mathrm{d}E^w}{\mathrm{d}w}. \tag{5.4}$$

Turning to GOK-DFT, the exact ensemble energy in Eq. (5.3) can be rewritten as follows [257–259],

$$E^w = \min_n \left\{ F^w[n] + \int \mathrm{d}\mathbf{r} v_{\mathrm{ext}}(\mathbf{r}) n(\mathbf{r}) \right\}, \tag{5.5}$$

where

$$F^w[n] = \min_{\hat{\Gamma}^w \to n} \left\{ \mathrm{Tr}\left[\hat{\Gamma}^w \left(\hat{T} + \hat{W}_{\mathrm{ee}} \right) \right] \right\} \tag{5.6}$$

is the analogue of the Levy–Lieb functional for ensembles. Note that the minimization is over the whole set of ensemble density matrix operators with density $n(\mathbf{n})$. Then, the noninteracting ensemble kinetic energy and the ensemble *weight-dependent* Hxc energy are introduced by performing the KS decomposition as follows,

$$F^w[n] = T_{\mathrm{s}}^w[n] + E_{\mathrm{Hxc}}^w[n]. \tag{5.7}$$

The noninteracting ensemble kinetic energy can be rewriting in a Legendre–Fenchel transform,

$$T_{\mathrm{s}}^w[n] = \sup_v \left\{ \mathcal{E}_{\mathrm{KS}}^w[v] - \int \mathrm{d}\mathbf{r} v(\mathbf{r}) n(\mathbf{r}) \right\}, \tag{5.8}$$

and $\mathcal{E}_{\mathrm{KS}}^w[v]$ is the ensemble energy, obtained by averaging the N-electron ground- and first-excited-state energies of $\hat{T} + \int \mathrm{d}\mathbf{r} v(\mathbf{r}) n(\mathbf{r})$ as follows,

$$\mathcal{E}_{\mathrm{KS}}^w[v] = (1-w)\sum_{i=1}^{N} \varepsilon_i[v] + w\left(\sum_{i=1}^{N-1} \varepsilon_i[v] + \varepsilon_{\mathrm{L}}[v] \right) = \sum_{i=1}^{N-1} \varepsilon_i[v] + (1-w)\varepsilon_{\mathrm{H}}[v] + w\varepsilon_{\mathrm{L}}[v]. \tag{5.9}$$

Returning to the KS expression for the exact ensemble energy, combining Eqs. (5.5) and (5.7) gives the variational expression

$$E^w = \min_{\hat{\Gamma}^w} \left\{ \mathrm{Tr}\left[\hat{\Gamma}^w \left(\hat{T} + \hat{V}_{\mathrm{ext}} \right) \right] + E_{\mathrm{Hxc}}^w[n_{\hat{\Gamma}^w}] \right\}, \tag{5.10}$$

where $\hat{V}_{\mathrm{ext}} = \int \mathrm{d}\mathbf{r} v_{\mathrm{ext}}(\mathbf{r}) \hat{n}(\mathbf{r})$, and the minimizing noninteracting ensemble density matrix operator

$\hat{\Gamma}^w_{\rm KS}$ reproduces the physical interacting density $n_{\hat{\Gamma}^w_{\rm KS}}(\mathbf{r}) = n_{\hat{\Gamma}^w_0}(\mathbf{r})$. It is constructed from a single set of orbitals which fulfil the following self-consistent KS equations,

$$\left(-\frac{\nabla^2}{2} + v_{\rm ext}(\mathbf{r}) + \frac{\delta E^w_{\rm Hxc}[n_{\hat{\Gamma}^w_{\rm KS}}]}{\delta n(\mathbf{r})}\right)\varphi^w_i(\mathbf{r}) = \varepsilon^w_i \varphi^w_i(\mathbf{r}). \tag{5.11}$$

Finally, using Eq. (5.10) together with the Hellmann–Feynman theorem, followed by Eq. (5.11) leads to the final GOK-DFT expression for the optical gap [258],

$$\Omega = \varepsilon^w_{\rm L} - \varepsilon^w_{\rm H} + \Delta^w_{\rm xc}, \tag{5.12}$$

where $\Delta^w_{\rm xc} = \partial E^\alpha_{\rm xc}[n^w]/\partial\alpha|_{\alpha=w}$ is so-called derivative discontinuity (DD) contribution to the optical gap [453, 454]. The Hartree contribution is weight-independent. When $w \to 0$,

$$\Omega = \varepsilon_{\rm L} - \varepsilon_{\rm H} + \Delta^{w\to 0}_{\rm xc} = E^{\rm KS}_{\rm g} + \Delta^{\rm opt}_{\rm xc}, \tag{5.13}$$

and $\Delta^{\rm opt}_{\rm xc}$ is the DD that corresponds to the jump in the xc potential when moving from $w = 0$ (N-electron ground-state) to $w \to 0$ (ensemble of N-electron ground and excited states), and should not be confused with the conventional ground-state DD, which will be extensively discussed in the following. As readily seen in Eq. (5.12), the KS gap for ensembles is weight-dependent. This dependency has to be counterbalanced by the ensemble DD to obtain a physically relevant weight-independent optical gap.

Despite the in-principle exact and time-independent formulation of GOK-DFT, the theory is not standard in quantum chemistry or in condensed matter physics, due to the highly complicated task of developing weight-dependent xc energy functionals. It has however gained increasing interest recently, first of all by considering the weight-independent functional as a first approximation [261], leading to curvature in the ensemble energy with respect to w (or, equivalently, to a weight-dependent optical gap, which is unphysical). A way to deal with this problem is to find an optimal w value [455], or to use Boltzmann weights [261] (which is not mandatory). Alternatively, we have recently suggested a linear interpolation between the ground-state ($w = 0$) and equi-ensemble state ($w = 1/2$), which circomvent the selection of a given weight [263, 264]. This interpolation method has been shown to give very accurate excitation energies on atoms and small molecules, and to catch charge transfer and double excitation energies (see also Ref. [340]). To go beyond weight-independent functionals, the so-called *generalised adiabatic connection for ensembles* (GACE) has been proposed by Franck and Fromager [260]. Since the last two years, the number of papers on ensemble DFT is increasing significantly. For instance to fix the infamous problem of "ghost-interaction" [266, 456, 457] (which is the ensemble analogue to the self-interaction in KS-DFT), to extract individual energies from GOK-DFT [458], and to develop weight-dependent functionals from the Hubbard dimer [73, 74], based on perturbation expansions to the weakly correlated limit and to the symmetric case [74]. Finally, note that a general formula for the weight-dependent Hx functional has been proposed [459] and was shown to provide accurate charge transfer excitations [460] on an asymmetric two-electron diatomic model.

5.2 Fundamental gap and the derivative discontinuity

Let us turn to charge excitations instead of neutral excitations, leading to the famous fundamental gap. This gap is defined as the difference between the ionization potential,

$$I^N = E_0^{N-1} - E_0^N, \tag{5.14}$$

and the electronic affinity,

$$A^N = E_0^N - E_0^{N+1} = I^{N+1}, \tag{5.15}$$

thus leading to

$$E_g^N = I^N - A^N = E_0^{N-1} + E_0^{N+1} - 2E_0^N. \tag{5.16}$$

In contrast to the optical gap, for which the number of electrons remains constant (hence the term "neutral" excitation), the fundamental gap describes ionization processes (so-called "charge" excitations) Experimentally, this gap can be determined via photoelectron spectroscopy and electron attachment spectroscopy [443]. In contrast, the optical gap is a measure of the absorption spectroscopy, as it describes the lowest possible neutral excitation in the system. The difference is subtle, and is made clearer by looking at Fig. 5.1. In this illustration, we see that the optical gap is obtained by exciting one electron from the valence band to the conduction band thanks to a photon absorption. In this case, the jump of the electron creates a hole behind, that is bound to the electron, forming what we call an exciton. This exciton-binding energy is the difference between the optical and the fundamental gap. In the latter, the hole and the electron are not bound together. Indeed, this gap is defined by ionization processes, such that the electron is first entirely removed from the system (ionization potential, thus creating an unbinding hole) and then added in the conduction band (electronic affinity, thus creating an unbinding electron). Note that in molecules, we usually refer to the *hardness*, which

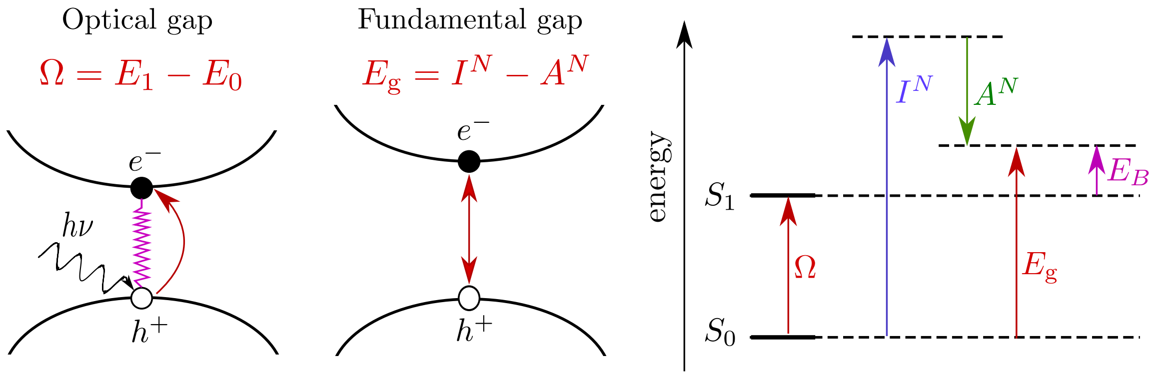

Figure 5.1: Left: Artistic view of the optical gap and the fundamental gap in solids. Right: Illustration of the energy gaps in molecules. The discrete energy levels S_0 and S_1 denote the singlet ground-state and the lowest singlet excited state, respectively. This figure is inspired from Ref. [443].

corresponds to half of the fundamental gap [441]. Now, we shall see how this gap can be obtained through DFT calculation.

As readily seen in Eq. (5.16), three $\mathcal{N}$-electron ground-state energies (with $\mathcal{N} \equiv \{N-1, N, N+1\}$) are in principle needed to compute the fundamental gap. In practice, we know (as discussed in the first chapter) that an accurate determination of the energy is expensive in term of computational cost, such that WFT can be applied to very small systems only. One could also do three different calculations using DFT or Hartree–Fock, thus leading to the so-called ΔSCF [461] method that produces reasonable results for atoms and molecules. But concerning the calculation of the band gap in solids, it cannot be straightforwardly applied. Indeed, a solid is considered by a unit cell which is infinitely replicated. Removing or adding an electron to that unit cell is also repeated on all the replica, such that the $N-1$- and $N+1$- ground-state energies are not possible to compute directly. This issue is usually avoided by introducing a compensating uniform background to the unit cell [462].

Therefore, it is desirable to extract the fundamental gap from one calculation on the neutral system only. In Hartree–Fock theory and DFT, this is done by approximating the fundamental gap by the simple difference between the LUMO and the HOMO orbital energies, like the KS gap in Eq. (5.1). Hence, the optical gap and the fundamental gap are totally equivalent in both theories, which is of course not the case in reality, as extensively discussed in Refs. [443, 444]. According to Eq. (5.13), the KS gap differs from the optical gap by a DD. In fact, the term "derivative discontinuity" in KS-DFT originates from the seminal work of Perdew and Levy in 1983 [130] on the fundamental gap, in the continuity of the DFT for fractional number of electrons [158]. In the latter work, they showed that the energy should be piecewise linear with respect to the number of electrons M where M is fractional,

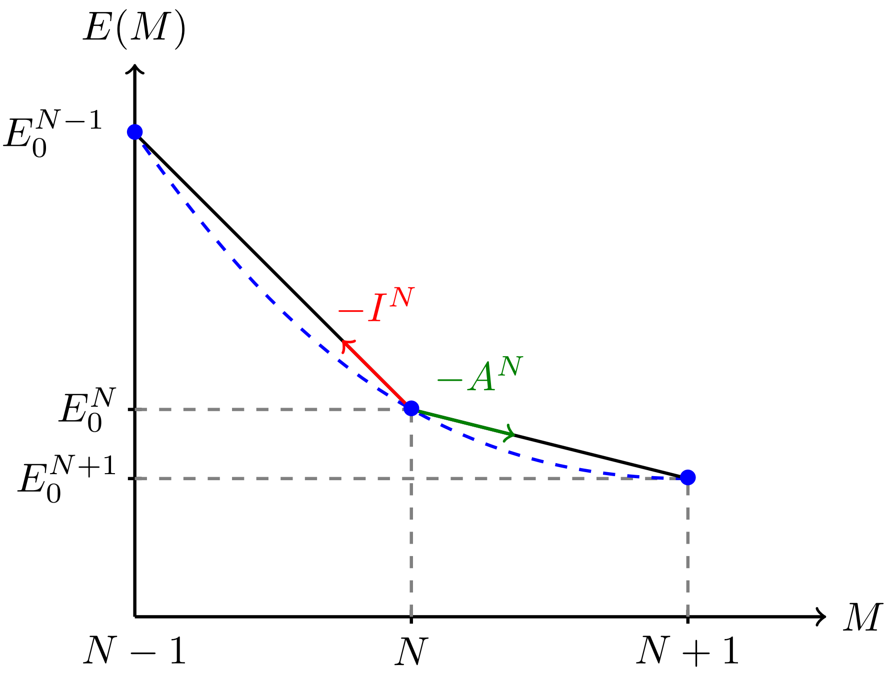

Figure 5.2: Piecewise linearity of the energy with respect to the (fractional) number of electrons. The slope when approaching N from the left gives the ionization potential, while approaching from the right gives the electronic affinity. The blue dashed line corresponds to the convex behaviour of local and semi-local DFAs.

and that its slope between $N-1 < M < N$ gives rise to (minus) the ionization potential, while its slope between $N < M < N+1$ is (minus) the electronic affinity. This is illustrated in Fig. 5.2. As readily seen in Fig. 5.2, the derivative of the energy with respect to the number of electrons (which is nothing but the chemical potential) is discontinuous at each integral number of electrons. In KS-DFT, this discontinuity is manifested in the xc potential, such that the fundamental gap for a N-electron system reads

$$E_{\rm g}^N = \varepsilon_{\rm L}^N - \varepsilon_{\rm H}^N + \left.\frac{\delta E_{\rm Hxc}[n]}{\delta n(\mathbf{r})}\right|_{N-\delta} - \left.\frac{\delta E_{\rm Hxc}[n]}{\delta n(\mathbf{r})}\right|_{N+\delta} = E_{\rm g}^{\rm KS} + \Delta_{\rm xc}^N, \tag{5.17}$$

where $\Delta_{\rm xc}^N$ is the infamous xcDD, which is not equal to $\Delta_{\rm xc}^{\rm opt}$. Standard xc functionals do not exhibit such a DD, such that this discontinuous behaviour has been the subject of extensive discussions in the literature [130, 224, 438, 463–476]. According to Eq. (5.17), it is in principle sufficient to extend the domain of definition of the conventional xc functional to fractional electron numbers in order to account for the DD. Unfortunately, this task is far from trivial and, despite significant progress [442, 477–491], no clear strategy has emerged over the past decades. It is even argued that invoking fractional number of electrons is maybe not the correct route to pursue [444, 475, 476]. In the latter works by Baerends and co-workers [444, 475, 476], an extensive discussion is made on the exact and approximate KS gap for both molecules and solids. It is stressed that this gap should not be interpreted as a representation of the fundamental gap. Baerends also suggests to compute the correction $\Delta_{\rm xc}^N$ from the response part of the xc potential, based on an integral number of electrons approach [475].

In practice, both chemistry and physics communities have turned to generally more expensive "post-DFT" for the computation of the charged excitations, such as DFT+U [159–161, 492–494] or the even more involved Green's function-based methods like GW [223, 231–234, 495]. Hybrid functionals can also be used [496–499], as they correct for the delocalization error (related to the self-interaction error) in DFT due to their portion of Hartree–Fock exchange [442, 477]. Note that this correction is due to an error cancellation between convex (DFT, delocalization error) and concave (HF, localization error) components, which does not provide a general solution for the description of the band gap [477], and can even give poorer optical gaps than without HF exchange [444].

5.3 Fundamental gap in N-centered ensemble DFT

Quite recently, Kraisler and Kronik made the formal connection between non-neutral excitations and GOK-DFT more explicit by introducing a grand canonical ensemble weight, thus paving the way to the construction of more reliable xc functionals for ionization and affinity processes [500, 501]. Unfortunately, as the total (fractional) number of electrons varies with the weight, the analogy with GOK-DFT can only be partial. It will be shown below that with an appropriate choice of grand canonical ensemble, informations about non-neutral excitations can be extracted, in principle exactly, from a canonical (time-independent) formalism. As a remarkable result, the optical and fundamental gap problems become formally identical, even though the physics they describe is completely different. Although it had not been realized yet, advances in GOK-DFT should therefore be beneficial to the description of fundamental gaps too.

5.3.1 Single-weight N-centered ensemble DFT

In the conventional DFT formulation of the fundamental gap problem, a grand canonical ensemble consisting of $(N-1)$- and N-electron ground states is considered, thus leading to a total number of electrons that can be fractional. By analogy with the time-ordered one-particle Green's function, which contains information about the $(N-1)$-, N-, and $(N+1)$-electron systems, we propose instead to consider what we will refer to as an *N-centered* grand canonical ensemble. The latter will be characterized by a *central* number N of electrons and an ensemble weight ξ, in the range $0 \leq \xi \leq 1/2$, that is assigned to *both* $(N-1)$- and $(N+1)$-electron states. In the following, the ensemble will be denoted as $\{N,\xi\}$. It is formally described by the following ensemble density matrix operator,

$$\hat{\Gamma}^{\{N,\xi\}} = \xi\hat{\Gamma}^{N_-} + \xi\hat{\Gamma}^{N_+} + (1-2\xi)\hat{\Gamma}^{N}, \tag{5.18}$$

which is a convex combination of $\mathcal{N}$-electron density matrix operators $\hat{\Gamma}^{\mathcal{N}}$ with $\mathcal{N} \in \{N_-, N, N_+\}$. Note that, for sake of compactness, we used the shorthand notations $N_- = N-1$ and $N_+ = N+1$ (not to be confused with left- and right-hand limits). If pure states are used (which is not compulsory) then $\hat{\Gamma}^{\mathcal{N}} = |\Psi^{\mathcal{N}}\rangle\langle\Psi^{\mathcal{N}}|$ where $\Psi^{\mathcal{N}}$ is an $\mathcal{N}$-electron many-body wavefunction. Although the N-centered ensemble describes the addition (*and* removal) of an electron to (from) an N-electron system, the corresponding N-centered ensemble density,

$$n_{\hat{\Gamma}^{\{N,\xi\}}}(\mathbf{r}) = \xi n_{\Psi^{N_-}}(\mathbf{r}) + \xi n_{\Psi^{N_+}}(\mathbf{r}) + (1-2\xi)n_{\Psi^{N}}(\mathbf{r}), \tag{5.19}$$

integrates to the central *integral* number of electrons N. Thus we generate a canonical density from a grand canonical ensemble. This is the fundamental difference between conventional DFT for open systems and the N-centered ensemble DFT derived in the following. Note that, in a more chemical language, the deviation of the N-centered ensemble density from the N-electron one $n_{\Psi^N}(\mathbf{r})$ is nothing but the difference between right and left Fukui functions [502] scaled by the ensemble weight ξ.

For a given external potential $v_{\text{ext}}(\mathbf{r})$, we can construct, in analogy with Eq. (5.18), the following N-centered ground-state ensemble energy,

$$E_0^{\{N,\xi\}} = \xi E_0^{N_-} + \xi E_0^{N_+} + (1-2\xi)E_0^{N}, \tag{5.20}$$

where $E_0^{\mathcal{N}}$ is the $\mathcal{N}$-electron ground-state energy of $\hat{H} = \hat{T} + \hat{W}_{\text{ee}} + \int d\mathbf{r}\; v_{\text{ext}}(\mathbf{r})\hat{n}(\mathbf{r})$, and $\hat{n}(\mathbf{r})$ is the density operator. The operators $\hat{T}$ and $\hat{W}_{\text{ee}}$ describe the electronic kinetic and repulsion energies, respectively. Note that the N-centered ground-state ensemble energy is linear in ξ and its slope is nothing but the fundamental gap. From the following extension of the Rayleigh–Ritz variational principle,

$$E_0^{\{N,\xi\}} = \min_{\hat{\Gamma}^{\{N,\xi\}}} \text{Tr}\left[\hat{\Gamma}^{\{N,\xi\}}\hat{H}\right] = \text{Tr}\left[\hat{\Gamma}_0^{\{N,\xi\}}\hat{H}\right], \tag{5.21}$$

where Tr denotes the trace, we conclude that the Hohenberg–Kohn theorem [67] applies to N-centered ground-state ensembles for any *fixed* value of ξ. Let us stress that, unlike in DFT for fractional electron numbers, the one-to-one correspondence between the N-centered ensemble density and the external potential holds *up to a constant*, simply because the former density integrates to a fixed central number N of electrons. We can therefore extend DFT to N-centered ground-state ensembles and obtain the energy variationally as follows,

$$E_0^{\{N,\xi\}} = \min_{n \rightarrow N} \left\{ F^{\{N,\xi\}}[n] + \int \mathrm{d}\mathbf{r}\, v_{\mathrm{ext}}(\mathbf{r}) n(\mathbf{r}) \right\}, \tag{5.22}$$

where the minimization is restricted to densities that integrate to N. As readily seen from Eq. (5.20), conventional (N-electron) ground-state DFT is recovered when $\xi = 0$. The analog of the Levy–Lieb functional for N-centered ground-state ensembles reads

$$F^{\{N,\xi\}}[n] = \min_{\hat{\Gamma}^{\{N,\xi\}} \rightarrow n} \mathrm{Tr}\left[\hat{\Gamma}^{\{N,\xi\}} \left(\hat{T} + \hat{W}_{\mathrm{ee}} \right) \right], \tag{5.23}$$

where the minimization is restricted to N-centered ensembles with density n. Let us consider the KS decomposition,

$$F^{\{N,\xi\}}[n] = T_{\mathrm{s}}^{\{N,\xi\}}[n] + E_{\mathrm{Hxc}}^{\{N,\xi\}}[n], \tag{5.24}$$

where

$$T_{\mathrm{s}}^{\{N,\xi\}}[n] = \min_{\hat{\Gamma}^{\{N,\xi\}} \rightarrow n} \mathrm{Tr}\left[\hat{\Gamma}^{\{N,\xi\}} \hat{T} \right] \tag{5.25}$$

is the non-interacting kinetic energy contribution and

$$E_{\mathrm{Hxc}}^{\{N,\xi\}}[n] = \frac{1}{2} \iint \mathrm{d}\mathbf{r}\mathrm{d}\mathbf{r}' \,\frac{n(\mathbf{r})n(\mathbf{r}')}{\mid \mathbf{r} - \mathbf{r}' \mid} + E_{\mathrm{xc}}^{\{N,\xi\}}[n] \tag{5.26}$$

is the ξ-dependent analog of the Hartree-xc (Hxc) functional for N-centered ground-state ensembles. Interestingly, even though the electronic excitations described in N-centered ensemble DFT and GOK-DFT [258] are completely different, the two theories are formally identical. Indeed, by rewriting the noninteracting kinetic energy in Eq. (5.25) into the following Lieb maximisation,

$$T_{\mathrm{s}}^{\{N,\xi\}}[n] = \sup_{v} \left\{ \mathcal{E}_{\mathrm{KS}}^{\{N,\xi\}}[v] - \int \mathrm{d}\mathbf{r} v(\mathbf{r}) n(\mathbf{r}) \right\}, \tag{5.27}$$

where $\mathcal{E}_{\mathrm{KS}}^{\{N,\xi\}}[v]$ is the N-centered ground-state ensemble energy of $\hat{T} + \int \mathrm{d}\mathbf{r}\; v(\mathbf{r})\hat{n}(\mathbf{r})$, and using Eq. (5.20), it comes

$$\mathcal{E}_{\mathrm{KS}}^{\{N,\boldsymbol{\xi}\}}[v] = \sum_{i=1}^{N-1} \varepsilon_i[v] + (1-\xi)\, \varepsilon_{\mathrm{H}}[v] + \xi \varepsilon_{\mathrm{L}}[v]. \tag{5.28}$$

According to Eqs. (5.9) and (5.28), the non-interacting kinetic energy functionals used in both theories are actually equal. This is simply due to the fact that, in a non-interacting system, the fundamental and optical gaps boil down to the same quantity. This is of course not the case for interacting electrons, which means that each theory requires the construction of a *specific* weight-dependent xc functional.

For that purpose, we propose to extend to N-centered ground-state ensembles the generalized adiabatic connection formalism for ensembles (GACE) which was originally introduced in the context of GOK-DFT [73, 260]. In contrast to standard DFT for grand canonical ensembles [500], the ensemble weight ξ can in principle vary in N-centered ensemble DFT while holding the density *constant*. Consequently, we can derive the following GACE formula,

$$E_{\rm xc}^{\{N,\xi\}}[n] = E_{\rm xc}[n] + \int_0^{\xi} {\rm d}\alpha\, \Delta_{\rm xc}^{\{N,\alpha\}}[n], \tag{5.29}$$

where, unlike in conventional adiabatic connections [503], we integrate over the ensemble weight rather than the two-electron interaction strength. The GACE integrand $\Delta_{\rm xc}^{\{N,\alpha\}}[n] = \partial E_{\rm xc}^{\{N,\alpha\}}[n]/\partial\alpha$ quantifies the deviation of the N-centered ground-state ensemble xc functional from the conventional (weight-independent) ground-state one $E_{\rm xc}[n] = E_{\rm xc}^{\{N,\xi=0\}}[n]$. As shown in Ref. [75], the GACE integrand is simply equal to the difference in fundamental gap between the interacting and non-interacting systems with N-centered ground-state ensemble density n (and weight α):

$$\Delta_{\rm xc}^{\{N,\alpha\}}[n] = E_{\rm g}^{\{N,\alpha\}}[n] - \left(\varepsilon_{\rm L}^{\{N,\alpha\}}[n] - \varepsilon_{\rm H}^{\{N,\alpha\}}[n]\right). \tag{5.30}$$

Let us now return to the variational ensemble energy expression in Eq. (5.22). Combining the latter with Eqs. (5.24) and (5.25) leads to

$$E_0^{\{N,\xi\}} = \min_{\hat{\Gamma}^{\{N,\xi\}}} \left\{ {\rm Tr}\left[\hat{\Gamma}^{\{N,\xi\}}\left(\hat{T} + \hat{V}_{\rm ext}\right)\right] + E_{\rm Hxc}^{\{N,\xi\}}[n_{\hat{\Gamma}^{\{N,\xi\}}}]\right\}, \tag{5.31}$$

where $\hat{V}_{\rm ext} = \int {\rm d}\mathbf{r}\, v_{\rm ext}(\mathbf{r})\hat{n}(\mathbf{r})$. Note that the minimizing density matrix operator $\hat{\Gamma}_{\rm KS}^{\{N,\xi\}}$ in Eq. (5.31) is the non-interacting N-centered ground-state ensemble one whose density equals the physical interacting one $n_{\hat{\Gamma}_0^{\{N,\xi\}}}(\mathbf{r})$. It can be constructed from a *single* set of orbitals which fulfill the following self-consistent KS equations [the latter are simply obtained from the stationarity condition associed to Eq. (5.31)],

$$\left[-\frac{\nabla^2}{2} + v_{\rm KS}^{\{N,\xi\}}(\mathbf{r})\right]\varphi_i^{\{N,\xi\}}(\mathbf{r}) = \varepsilon_i^{\{N,\xi\}}\varphi_i^{\{N,\xi\}}(\mathbf{r}), \tag{5.32}$$

where $v_{\mathrm{KS}}^{\{N,\xi\}}(\mathbf{r}) = v_{\mathrm{ext}}(\mathbf{r}) + v_{\mathrm{Hxc}}^{\{N,\xi\}}[n_{\hat{\Gamma}_0^{\{N,\xi\}}}](\mathbf{r})$ and $v_{\mathrm{Hxc}}^{\{N,\xi\}}[n](\mathbf{r}) = \delta E_{\mathrm{Hxc}}^{\{N,\xi\}}[n]/\delta n(\mathbf{r})$. In the particular case of pure non-interacting $\mathcal{N}$-electron states,

$$n_{\hat{\Gamma}_0^{\{N,\xi\}}}(\mathbf{r}) = \sum_{i=1}^{N_-} \left|\varphi_i^{\{N,\xi\}}(\mathbf{r})\right|^2 + (1-\xi)\left|\varphi_{\mathrm{H}}^{\{N,\xi\}}(\mathbf{r})\right|^2 + \xi\left|\varphi_{\mathrm{L}}^{\{N,\xi\}}(\mathbf{r})\right|^2, \tag{5.33}$$

where L ($i = N_+$) and H ($i = N$) refer to the LUMO and HOMO of the N-electron KS system, respectively. By inserting the latter density into Eq. (5.30) and taking $\alpha = \xi$, we finally deduce from Eq. (5.32) the analog of the GOK-DFT optical gap expression for the fundamental gap,

$$\boxed{E_{\mathrm{g}}^N = \varepsilon_{\mathrm{L}}^{\{N,\xi\}} - \varepsilon_{\mathrm{H}}^{\{N,\xi\}} + \left.\frac{\partial E_{\mathrm{xc}}^{\{N,\xi\}}[n]}{\partial\xi}\right|_{n=n_{\hat{\Gamma}_0^{\{N,\xi\}}}}}. \tag{5.34}$$

This is the central result of this chapter. Note that, when $\xi = 0$, the famous formula of Perdew and Levy [130][Eq. (5.17)] is recovered with a much more explicit density-functional expression for the DD.

5.3.2 Two-weight generalization of the theory

5.3.2.i Extending the Levy–Zahariev shift-in-potential procedure to ensembles

In order to establish a connection between N-centered ensemble DFT and the standard formulation of the fundamental gap problem in DFT (which relies on fractional electron numbers), we propose in the following to extend the theory to N-centered ensembles where the removal and the addition of an electron can be controlled independently. For that purpose, we introduce the generalized *two-weight* N-centered ensemble density matrix operator,

$$\hat{\Gamma}^{\{N,\boldsymbol{\xi}\}} = \sum_{\nu=\pm} \xi_\nu \hat{\Gamma}^{N_\nu} + \left[1 - \sum_{\nu=\pm} \xi_\nu \frac{N_\nu}{N}\right] \hat{\Gamma}^N, \tag{5.35}$$

where $\boldsymbol{\xi} \equiv (\xi_-, \xi_+)$ and the convexity conditions $\xi_- \geq 0$, $\xi_+ \geq 0$, and $\xi_- N_- + \xi_+ N_+ \leq N$ are fulfilled. Note that, by construction, the N-centered ensemble density associated to $\hat{\Gamma}^{\{N,\boldsymbol{\xi}\}}$ still integrates to N, and the single-weight formulation of N-centered ensemble DFT discussed previously is simply recovered when $\xi_- = \xi_+ = \xi$. The ensemble energy now reads

$$E_0^{\{N,\boldsymbol{\xi}\}} = \sum_{\nu=\pm} \xi_\nu E_0^{N_\nu} + \left[1 - \sum_{\nu=\pm} \xi_\nu \frac{N_\nu}{N}\right] E_0^N. \tag{5.36}$$

Interestingly, if we extend the Levy–Zahariev shift-in-potential procedure [504] to N-centered ground-state ensembles as follows [note that the superscripts ξ in Eq. (5.32) should now be replaced by $\boldsymbol{\xi}$ in the generalized two-weight theory],

$$\varepsilon_i^{\{N,\boldsymbol{\xi}\}} \rightarrow \tilde{\varepsilon}_i^{\{N,\boldsymbol{\xi}\}} = \varepsilon_i^{\{N,\boldsymbol{\xi}\}} + C^{\{N,\boldsymbol{\xi}\}}\left[n_{\hat{\Gamma}_0^{\{N,\boldsymbol{\xi}\}}}\right], \tag{5.37}$$

where the density-functional shift reads

$$C^{\{N,\boldsymbol{\xi}\}}[n] = \frac{E_{\mathrm{Hxc}}^{\{N,\boldsymbol{\xi}\}}[n] - \int \mathrm{d}\mathbf{r}\; v_{\mathrm{Hxc}}^{\{N,\boldsymbol{\xi}\}}[n](\mathbf{r})n(\mathbf{r})}{\int \mathrm{d}\mathbf{r}\; n(\mathbf{r})}, \tag{5.38}$$

the N-centered ground-state ensemble energy can be written as a simple weighted sum of shifted KS orbital energies. Indeed, according to Eq. (5.31) [where ξ is replaced by $\boldsymbol{\xi}$], the N-centered ground-state ensemble energy can be written as follows,

$$\begin{aligned} E_0^{\{N,\boldsymbol{\xi}\}} &= \mathrm{Tr}\left[\hat{\Gamma}_{\mathrm{KS}}^{\{N,\boldsymbol{\xi}\}}\left(\hat{T}+\hat{V}_{\mathrm{ext}}\right)\right] + E_{\mathrm{Hxc}}^{\{N,\boldsymbol{\xi}\}}\left[n_{\hat{\Gamma}_{\mathrm{KS}}^{\{N,\boldsymbol{\xi}\}}}\right] \\ &= \mathrm{Tr}\left[\hat{\Gamma}_{\mathrm{KS}}^{\{N,\boldsymbol{\xi}\}}\left(\hat{T}+\hat{V}_{\mathrm{KS}}^{\{N,\boldsymbol{\xi}\}}\right)\right] + E_{\mathrm{Hxc}}^{\{N,\boldsymbol{\xi}\}}\left[n_{\hat{\Gamma}_{\mathrm{KS}}^{\{N,\boldsymbol{\xi}\}}}\right] - \int d\mathbf{r}\; v_{\mathrm{Hxc}}^{\{N,\boldsymbol{\xi}\}}\left[n_{\hat{\Gamma}_0^{\{N,\boldsymbol{\xi}\}}}\right](\mathbf{r})\; n_{\hat{\Gamma}_{\mathrm{KS}}^{\{N,\boldsymbol{\xi}\}}}(\mathbf{r}), \end{aligned} \tag{5.39}$$

where

$$\hat{V}_{\mathrm{KS}}^{\{N,\boldsymbol{\xi}\}} = \int d\mathbf{r}\; v_{\mathrm{KS}}^{\{N,\boldsymbol{\xi}\}}(\mathbf{r})\,\hat{n}(\mathbf{r}) \tag{5.40}$$

and $n_{\hat{\Gamma}_{\mathrm{KS}}^{\{N,\boldsymbol{\xi}\}}}(\mathbf{r}) = \mathrm{Tr}\left[\hat{\Gamma}_{\mathrm{KS}}^{\{N,\boldsymbol{\xi}\}}\hat{n}(\mathbf{r})\right]$. Since the two densities $n_{\hat{\Gamma}_{\mathrm{KS}}^{\{N,\boldsymbol{\xi}\}}}$ and $n_{\hat{\Gamma}_0^{\{N,\boldsymbol{\xi}\}}}$ are equal and integrate to N, we obtain from Eqs. (5.32) and (5.38),

$$E_0^{\{N,\boldsymbol{\xi}\}} = \sum_{\nu=\pm}\xi_\nu\sum_{i=1}^{N_\nu}\varepsilon_i^{\{N,\boldsymbol{\xi}\}} + \left[1-\sum_{\nu=\pm}\frac{\xi_\nu N_\nu}{N}\right]\sum_{i=1}^{N}\varepsilon_i^{\{N,\boldsymbol{\xi}\}} + NC^{\{N,\boldsymbol{\xi}\}}\left[n_{\hat{\Gamma}_0^{\{N,\boldsymbol{\xi}\}}}\right]. \tag{5.41}$$

Finally, by rewriting the last term in the right-hand side of Eq. (5.41) as follows,

$$NC^{\{N,\boldsymbol{\xi}\}}\left[n_{\hat{\Gamma}_0^{\{N,\boldsymbol{\xi}\}}}\right] = \sum_{\nu=\pm}\xi_\nu\sum_{i=1}^{N_\nu}C^{\{N,\boldsymbol{\xi}\}}\left[n_{\hat{\Gamma}_0^{\{N,\boldsymbol{\xi}\}}}\right] + \left(1-\sum_{\nu=\pm}\frac{\xi_\nu N_\nu}{N}\right)\sum_{i=1}^{N}C^{\{N,\boldsymbol{\xi}\}}\left[n_{\hat{\Gamma}_0^{\{N,\boldsymbol{\xi}\}}}\right], \tag{5.42}$$

and by using the definition of the shifted KS orbital energies in Eq. (5.37), it comes

$$E_0^{\{N,\boldsymbol{\xi}\}} = \left[1+\frac{\xi_- - \xi_+}{N}\right]\sum_{i=1}^{N}\tilde{\varepsilon}_i^{\{N,\boldsymbol{\xi}\}} - \xi_-\tilde{\varepsilon}_{\mathrm{H}}^{\{N,\boldsymbol{\xi}\}} + \xi_+\tilde{\varepsilon}_{L}^{\{N,\boldsymbol{\xi}\}}. \tag{5.43}$$

In the non-interacting limit, it is readily seen from Eq. (5.43) that, unless $\xi_- = \xi_+ = \xi$, the N-centered ensemble does not describe a single-electron excitation from the HOMO to the LUMO. In other words, the generalized two-parameter N-centered ensemble non-interacting kinetic energy is not equal anymore to its GOK-DFT analog. Interestingly, in the (very) particular case $N = 2$, the latter is actually recovered if the weight assigned to the first excited state is set to ξ_+ (see Appendix A in Ref. [75]).

5.3.2.ii Exact extraction of individual energies

We will now show that, by using the shift-in-potential procedure introduced previously and exploiting the linearity in $\boldsymbol{\xi}$ of the ensemble energy, it becomes possible to extract individual $\mathcal{N}$-electron ground-state energies. Starting from Eq. (5.36) and noticing that $E_0^N = E_0^{\{N,\boldsymbol{\xi}=0\}}$, we can express the exact N-electron energy in terms of $E_0^{\{N,\boldsymbol{\xi}\}}$ and its derivatives as follows,

$$E_0^N = E_0^{\{N,\boldsymbol{\xi}\}} - \sum_{\nu=\pm} \xi_\nu \frac{\partial E_0^{\{N,\boldsymbol{\xi}\}}}{\partial \xi_\nu}. \tag{5.44}$$

Moreover, as readily seen from Eq. (5.36), the N_+- and N_--electron energies can be extracted separately from the ensemble energy as follows,

$$E_0^{N_\pm} = \frac{N_\pm}{N} E_0^N + \frac{\partial E_0^{\{N,\boldsymbol{\xi}\}}}{\partial \xi_\pm}. \tag{5.45}$$

Note that, for convenience, Eqs. (5.44) and (5.45) will be compacted into a single equation,

$$E_0^{\mathcal{N}} = \frac{\mathcal{N}}{N} E_0^{\{N,\boldsymbol{\xi}\}} + \sum_{\nu=\pm} \left[\frac{(\mathcal{N} - N)(\mathcal{N} - N_{-\nu})}{2} - \frac{\mathcal{N}\xi_\nu}{N} \right] \frac{\partial E_0^{\{N,\boldsymbol{\xi}\}}}{\partial \xi_\nu}, \tag{5.46}$$

where $\mathcal{N} \in \{N_-, N, N_+\}$.

Applying the Hellmann–Feynman theorem to the variational ensemble energy expression in Eq. (5.31) [with the substitution $\xi \to \boldsymbol{\xi}$] gives

$$\frac{\partial E_0^{\{N,\boldsymbol{\xi}\}}}{\partial \xi_\pm} = \mathrm{Tr}\left[\left[\partial_{\xi_\pm} \hat{\Gamma}_{\mathrm{KS}}^{\{N,\boldsymbol{\xi}\}} \right] \left(\hat{T} + \hat{V}_{\mathrm{KS}}^{\{N,\boldsymbol{\xi}\}} \right) \right] + \left. \frac{\partial E_{\mathrm{xc}}^{\{N,\boldsymbol{\xi}\}}[n]}{\partial \xi_\pm} \right|_{n = n_{\hat{\Gamma}_0^{\{N,\boldsymbol{\xi}\}}}}, \tag{5.47}$$

where

$$\partial_{\xi_\pm}\hat{\Gamma}_{\rm KS}^{\{N,\boldsymbol{\xi}\}} = \left|\Phi_{N_\pm}^{\{N,\boldsymbol{\xi}\}}\right\rangle\left\langle\Phi_{N_\pm}^{\{N,\boldsymbol{\xi}\}}\right| - \frac{N_\pm}{N}\left|\Phi_{N}^{\{N,\boldsymbol{\xi}\}}\right\rangle\left\langle\Phi_{N}^{\{N,\boldsymbol{\xi}\}}\right|, \tag{5.48}$$

and the KS potential operator is defined in Eq. (5.40). Note that the $\mathcal{N}$-electron Slater determinants $\Phi_{\mathcal{N}}^{\{N,\boldsymbol{\xi}\}}$ in Eq. (5.48) are constructed from the KS orbitals $\varphi_i^{\{N,\boldsymbol{\xi}\}}(\mathbf{r})$ in Eq. (5.32). Consequently, Eq. (5.47) can be simplified as follows,

$$\frac{\partial E_0^{\{N,\boldsymbol{\xi}\}}}{\partial \xi_\pm} = \pm\frac{1}{N}\sum_{i=1}^{N}\left(\varepsilon_{N+\frac{1}{2}\pm\frac{1}{2}}^{\{N,\boldsymbol{\xi}\}} - \varepsilon_i^{\{N,\boldsymbol{\xi}\}}\right) + \left.\frac{\partial E_{\rm xc}^{\{N,\boldsymbol{\xi}\}}[n]}{\partial \xi_\pm}\right|_{n=n_{\hat{\Gamma}_0^{\{N,\boldsymbol{\xi}\}}}}. \tag{5.49}$$

Since the shift introduced in Eq. (5.37) does not affect KS orbital energy differences,

$$\varepsilon_j^{\{N,\boldsymbol{\xi}\}} - \varepsilon_i^{\{N,\boldsymbol{\xi}\}} = \tilde{\varepsilon}_j^{\{N,\boldsymbol{\xi}\}} - \tilde{\varepsilon}_i^{\{N,\boldsymbol{\xi}\}}, \tag{5.50}$$

we finally deduce from Eqs. (5.43), (5.46), and (5.49) the following exact expressions,

$$E_0^{\mathcal{N}} = \sum_{i=1}^{\mathcal{N}}\tilde{\varepsilon}_i^{\{N,\boldsymbol{\xi}\}} + \sum_{\nu=\pm}\left[\frac{(\mathcal{N}-N)(\mathcal{N}-N_{-\nu})}{2} - \frac{\mathcal{N}\xi_\nu}{N}\right] \times \left.\frac{\partial E_{\rm xc}^{\{N,\boldsymbol{\xi}\}}[n]}{\partial \xi_\nu}\right|_{n=n_{\hat{\Gamma}_0^{\{N,\boldsymbol{\xi}\}}}}. \tag{5.51}$$

Eq. (5.51) is the second key result of this work. As a direct consequence, the ionization potential (IP), denoted I^N, and the electron affinity (EA), denoted $A^N = I^{N_+}$, can now be extracted, in principle exactly, as follows,

$$I^{N+\frac{1}{2}\pm\frac{1}{2}} = \pm\left(E^N - E^{N_\pm}\right) = -\tilde{\varepsilon}_{N+\frac{1}{2}\pm\frac{1}{2}}^{\{N,\boldsymbol{\xi}\}} + \sum_{\nu=\pm}\left(\frac{\xi_\nu}{N} + \frac{N_{-\nu}-N_\pm}{2}\right)\left.\frac{\partial E_{\rm xc}^{\{N,\boldsymbol{\xi}\}}[n]}{\partial \xi_\nu}\right|_{n=n_{\hat{\Gamma}_0^{\{N,\boldsymbol{\xi}\}}}}. \tag{5.52}$$

As readily seen from Eq. (5.51), individual state properties can be extracted exactly from the ensemble density. There is in principle no need to use individual state densities for that purpose. Nevertheless, in practice, it might be convenient to construct N-centered ground-state ensemble xc DFAs using individual densities, in the spirit of the ensemble-based approach of Kraisler and Kronik [500]. Since the individual densities are implicit functionals of the ensemble density, an optimized effective potential would be needed. A similar strategy would apply if we want to remove ghost-interaction-type errors [456] by using an N-centered ensemble exact exchange (EEXX) energy.

Finally, if we consider the conventional N-electron ground-state KS-DFT limit of Eq. (5.51), i.e.

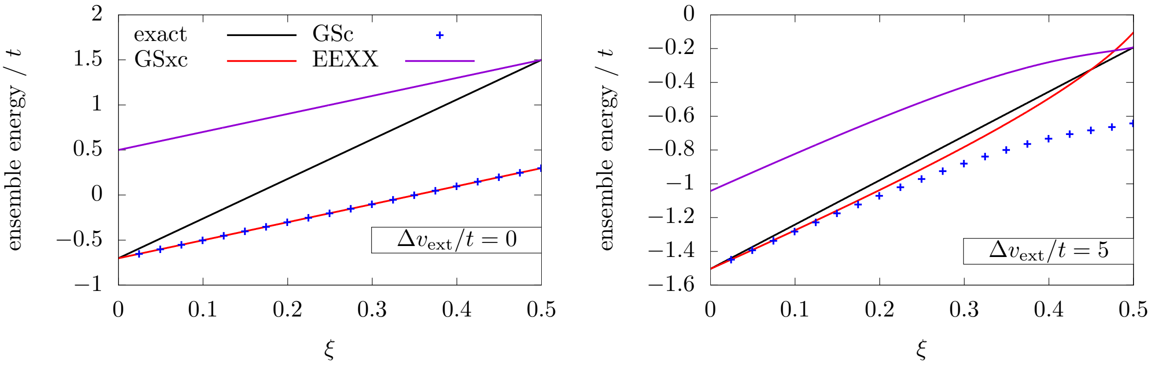

Figure 5.3: Exact and approximate N-centered ground-state ensemble energies plotted as a function of ξ for $N = 2$ and $U/t = 5$ in the symmetric (left panel) and asymmetric (right panel) Hubbard dimers. See text for further details.

$\boldsymbol{\xi} = 0$, we recover the Levy–Zahariev expression $E_0^N = \sum_{i=1}^{N} \tilde{\varepsilon}_i^{\{N,\boldsymbol{\xi}=0\}}$ [504] for the N-electron energy and, in addition, we obtain the following compact expressions for the anionic and cationic energies,

$$\boxed{E_0^{N_\pm} = \sum_{i=1}^{N_\pm} \left(\tilde{\varepsilon}_i^{\{N,\boldsymbol{\xi}=0\}} + \frac{1}{N_\pm} \left. \frac{\partial E_{\rm xc}^{\{N,\boldsymbol{\xi}\}}[n_{\Psi_0^N}]}{\partial \xi_\pm} \right|_{\boldsymbol{\xi}=0} \right)}, \tag{5.53}$$

where $n_{\Psi_0^N}$ denotes the exact N-electron ground-state density. As well known and now readily seen from Eq. (5.53), it is impossible to describe all $\mathcal{N}$-electron ground-state energies with the *same* potential. When an electron is added (+)/removed (−) to/from an N-electron system, an additional shift (second term in the right-hand side of Eq. (5.53)) is applied to the already shifted KS orbital energies. Interestingly, we also recover from Eq. (5.52) a more explicit form of the Levy–Zahariev IP expression [504],

$$I^N = -\tilde{\varepsilon}_{\rm H}^{\{N,\boldsymbol{\xi}=0\}} + \left. \frac{\partial E_{\rm xc}^{\{N,\boldsymbol{\xi}\}}[n_{\Psi_0^N}]}{\partial \xi_-} \right|_{\boldsymbol{\xi}=0}, \tag{5.54}$$

where the second term in the right-hand side can be interpreted as the shifted Hxc potential at position $\mathbf{r} \to \infty$ [504]. Similarly, the electronic affinity reads

$$A^N = -\tilde{\varepsilon}_{\rm L}^{\{N,\boldsymbol{\xi}=0\}} - \left. \frac{\partial E_{\rm xc}^{\{N,\boldsymbol{\xi}\}}[n_{\Psi_0^N}]}{\partial \xi_+} \right|_{\boldsymbol{\xi}=0}. \tag{5.55}$$

5.3.3 Application to the asymmetric Hubbard dimer

As a proof of concept, we apply in the following N-centered ensemble DFT to the asymmetric Hubbard dimer (see Sec. 2.1.4.iii), Thus, we illustrate the fact that the theory applies not only to exact *ab initio*

Hamiltonians but also to lattice ones, which might be of interest for modeling extended systems. In this case, the density reduces to a single number $n = n_0$ which is the occupation of site 0, and $n_1 = N - n$. In the following, the central number of electrons will be set to $N = 2$ so that the convexity condition reads $\xi_+ \leq (2 - \xi_-)/3$. It can be shown that the N-centered non-interacting kinetic and EEXX energies can be expressed analytically as follows [75],

$$\begin{aligned} T_{\rm s}^{\{N,\boldsymbol{\xi}\}}(n) &= -2t\sqrt{(\xi_+ - 1)^2 - (n-1)^2}, \\ E_{\rm x}^{\{N,\boldsymbol{\xi}\}}(n) &= \frac{U}{2}\left[1 + \frac{\xi_+ - \xi_-}{2} + \left(1 - \frac{3\xi_+ + \xi_-}{2}\right)\left(\frac{n-1}{\xi_+ - 1}\right)^2\right] - E_{\rm H}(n), \end{aligned} \tag{5.56}$$

where the Hartree energy reads $E_{\rm H}(n) = U\left(1 + (n-1)^2\right)$. On the other hand, the correlation energy can be computed exactly by Lieb maximization [73, 75]. As readily seen from Eq. (5.56), an N-centered ensemble density n is non-interacting v-representable if $|n - 1| \leq 1 - \xi_+$. In Fig. 5.3, the total N-centered ground-state ensemble energy is plotted as a function of $\xi_- = \xi_+ = \xi$ for various approximate density-functional xc energies [exact densities were used]: $E_{\rm x}^{\{N,\xi\}}(n)$ only [EEXX], the "conventional" weight-independent N-electron ground-state (GS) xc functional $E_{\rm xc}^{\{N,\xi=0\}}(n)$ [GSxc], and $E_{\rm x}^{\{N,\xi\}}(n) + E_{\rm c}^{\{N,\xi=0\}}(n)$ [GSc]. The accurate parameterization of Carrascal *et al.* [335, 358] was used for $E_{\rm c}^{\{N,\xi=0\}}(n)$ (see Appendix G.1). In the symmetric case, all energy contributions are linear in ξ since $n = 1$ [see Eq. (5.56)]. Nevertheless, the correct slope is reproduced only when the weight dependence is taken into account in both exchange and correlation energies. This becomes even more critical in the asymmetric case [bottom panel] where approximations in the xc energy induce curvature, thus leading to a weight-dependent fundamental gap, which is of course unphysical. More insight into the weight dependence is given by the GACE integrand in Eq. (5.30), and is not shown in this thesis. The reader is referred to as Ref. [75] for a more detailed discussion on the GACE integrand.

Turning to the calculation of the IP, Eq. (5.54) was verified by calculating each (density-functional) contribution separately [75]. Results obtained for the asymmetric dimer are shown in Fig. 5.4. As soon as the on-site repulsion is switched on (and up to $U/t \approx 4$), both the shifted KS HOMO energy and the DD (second term in the right-hand side of Eq. (5.54)) contribute substantially to the IP. Interestingly, in this regime of correlation and density, the shift-in-potential procedure is not crucial. The unshifted KS HOMO energy varies with U through the density. Note that the situation would be completely different in the symmetric case [not shown] where $I^N(\Delta v_{\rm ext} = 0) = -t - E_0^N(\Delta v_{\rm ext} = 0)$ and the unshifted KS HOMO energy equals $-t$. By construction, the latter energy becomes $\frac{1}{2}E_0^N(\Delta v_{\rm ext} = 0)$ [which is U-dependent] after shifting. As a result, in the symmetric case, the shift and the DD equally contribute [by $-(\frac{1}{2}E_0^N(\Delta v_{\rm ext} = 0) + t)$] to the IP. Returning to the asymmetric case in Fig. 5.4, the

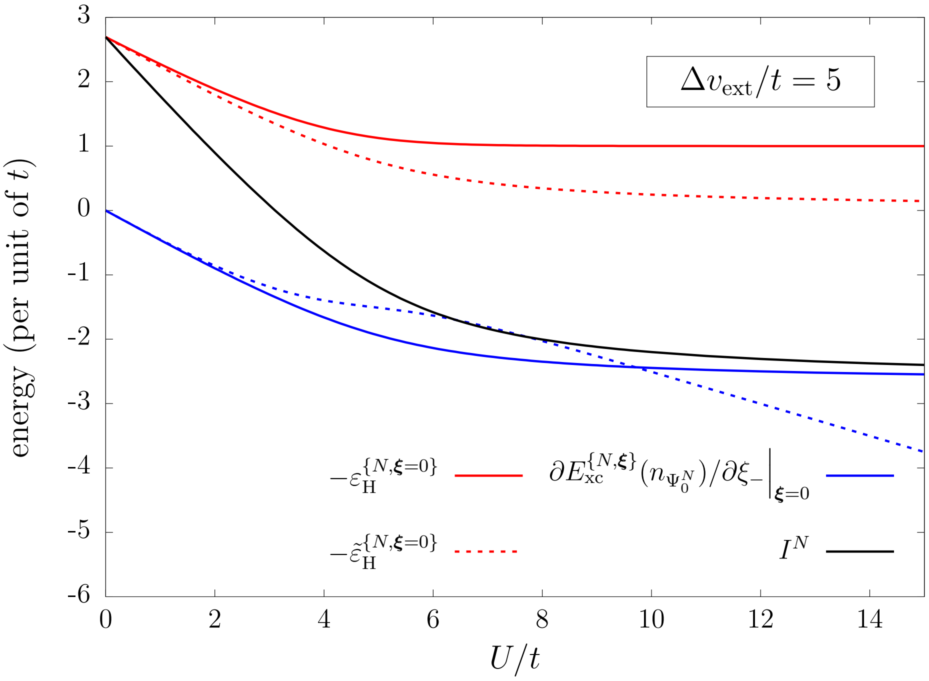

Figure 5.4: Exact shift-in-potential (difference between dashed and full red lines) and density-functional DD (full blue line) contributions to the IP [see Eq. (5.54)] plotted as a function of U/t for $\Delta v_{\rm ext}/t = 5$. The EEXX contribution to the DD is shown in dashed blue line.

IP reduces to the DD in the strongly correlated regime ($U/t \geqslant 10$), thus illustrating the importance of weight dependence in both exchange and correlation energies.

5.4 Summary and perspectives

We have shown that the fundamental gap problem, which is traditionally formulated in grand canonical ensemble DFT, can be recast into a canonical problem where the xc functional becomes ensemble weight dependent. As a remarkable result, modeling the infamous DD becomes equivalent to modelling the weight dependence, exactly like in the optical gap problem. This key result, which is depicted in Eq. (5.34), opens up a new paradigm in the development of DFAs for gaps which are computationally much cheaper than conventional time-dependent post-DFT treatments. Fig. 5.5 is a summary illustration of the difference between DFT for fractional number of electrons and the N-centered ensemble DFT. As readily seen in Fig. 5.5 and as already mentioned, the jump in the xc potential has to be modelled in DFT in order to recover the fundamental gap with only one calculation. This is still a major challenge in DFT. Otherwise, one can do two DFT calculations to get the ionization potentials I^N and $I^{N+1} = A^N$, which are in-principle exactly given by (minus) the HOMO KS orbital energy of the N- and $N+1$-electron systems, respectively, according to the ionization potential theorem. In the herein proposed N-centered ensemble DFT, this xcDD is simply modelled by a weight-derivative

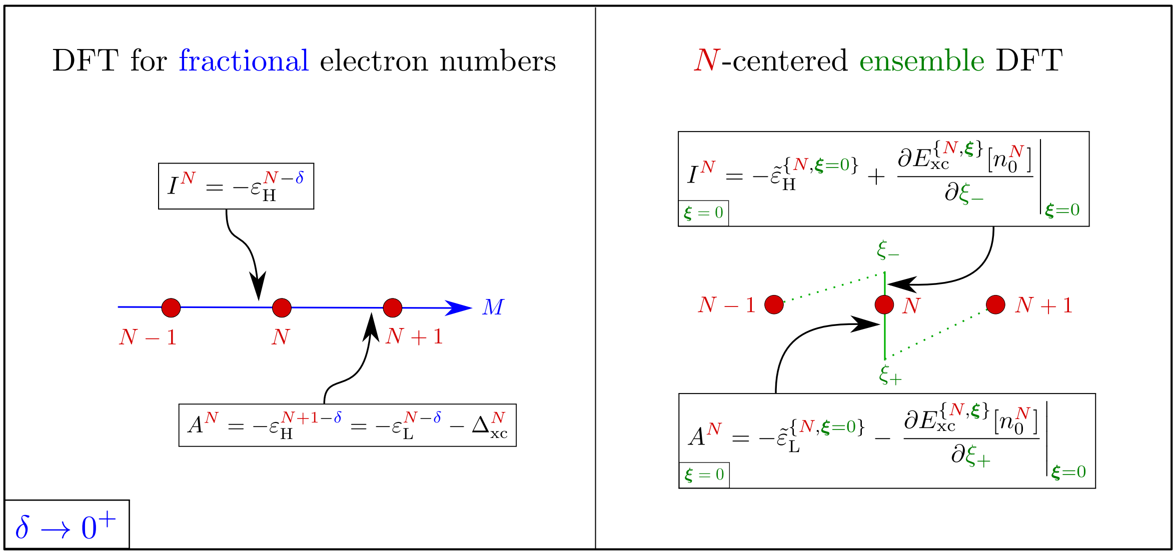

Figure 5.5: Left panel: DFT for fractional number of electrons. The fundamental gap is obtained by looking at the left limit of the N- and $N+1$-electron energy, which defines the xcDD in Eq. (5.17). The xc potential is uniquely defined for fractional number of electrons [158]. Right panel: N-centered ensemble DFT. The fundamental gap is obtained through the weight-dependence of the xc energy functional, whose ensemble density integrates to the central number of electrons N. The KS orbital energies are fixed by the shift introduced in Eq. (5.37).

of the ensemble xc energy functional. Therefore, accounting for the DD is straightforward, providing that weight-dependent functionals are accessible. In the spirit of our previous work in GOK-DFT [74], in the context of the Hubbard dimer, weight-dependent correlation energy functionals can be developed by performing Taylor expansions around the noninteracting ($U = 0$) and the symmetric ($n = 1$) limits. Seeking further into GOK-DFT, a linear interpolation [263] could also be considered, even by using weight-independent functionals. A natural step forward would be to apply the approach, for example, to a finite uniform electron gas [505], thus providing an *ab initio* local DFA that incorporates DDs through its weight dependence. Work is currently in progress in this direction.

Chapter 6

SOET and the ab-initio Hamiltonians

In the spirit of his predecessors, e.g. DMFT [400], DMET [419, 422] as well as SEET [380], the extension to quantum chemistry will be investigated in SOET. Such an extension is not straightforward, as it faces several fundamental issues like representability problems, the universality of the functionals, and the dependence on the molecular orbital basis. This chapter intends to give general thoughts and perspectives about this generalization to quantum chemistry, which has finally led us to an exact formulation of RDMFT based on a seniority-zero wavefunction, for which an article is currently in preparation.

6.1 Extension of SOET to Quantum Chemistry

The extension of SOET to quantum chemistry has been formally explored by Fromager, leading to the *complete active space site-occupation functional theory* (CASSOFT) [270]. In this context, the impurities in SOET play the role of the active orbitals in the CAS. I recall that the basic variable in SOFT and in SOET is the site-occupation vector, which corresponds to the diagonal of the 1RDM, i.e. the orbital-occupation vector in quantum chemistry.

Let us start by rewriting the second-quantized form of the Hamiltonian in the basis of molecular orbitals $\{\varphi_p(\mathbf{r})\}_p$,

$$\hat{H} = \hat{h} + \hat{W}_{\rm ee} = \sum_{pq}\sum_{\sigma} h_{pq}\hat{c}^\dagger_{p\sigma}\hat{c}_{q\sigma} + \frac{1}{2}\sum_{pqrs}\sum_{\sigma\sigma'}\langle pq|rs\rangle \hat{c}^\dagger_{p\sigma}\hat{c}^\dagger_{q\sigma'}\hat{c}_{s\sigma'}\hat{c}_{r\sigma}, \tag{6.1}$$

where $\hat{c}^\dagger_{p\sigma}$ ($\hat{c}_{p\sigma}$) is the creation (annihilation) operator of an electron of spin σ in the pth orbital, and

$$\langle pq|rs\rangle = \iint {\rm d}\mathbf{r}{\rm d}\mathbf{r}' \frac{\varphi_p^*(\mathbf{r})\varphi_q^*(\mathbf{r}')\varphi_r(\mathbf{r})\varphi_s(\mathbf{r}')}{|\mathbf{r}-\mathbf{r}'|}. \tag{6.2}$$

Then, a CAS is introduced in which the interactions between the active orbitals are treated explicitly, like the impurity sites in SOET,

$$\hat{W}_{\rm ee} \longrightarrow \hat{W}^{\rm CAS} = \frac{1}{2}\sum_{uvxy}^{\rm active}\sum_{\sigma\sigma'}\langle uv|xy\rangle \hat{c}^\dagger_{u\sigma}\hat{c}^\dagger_{v\sigma'}\hat{c}_{y\sigma'}\hat{c}_{x\sigma}. \tag{6.3}$$

In the spirit of SOET, a complementary functional of the orbital occupation should be introduced in order to recover the missing (dynamical) correlation. This is not an easy task, already because SOET can be formulated in any orbital basis [270]. Hence, the complementary functional will depend on the choice of the orbitals, as well as on the active space such that it is not universal anymore and seems highly complicated to model. One has to choose a given orbital basis in which this generalization of SOET will be formulated. A "natural" choice would be the natural orbitals which diagonalize the 1RDM. Indeed, all the informations of the 1RDM are now concentrated into the occupation numbers of these orbitals, corresponding to the basic variable in SOET. In addition, we would benefit from previous works in RDMFT (usually formulated in the natural orbital basis as well, see Sec. 1.2.2). Of course, one first needs to optimise the orbitals to find the natural orbital basis that diagonalizes the 1RDM, such that the whole 1RDM can be constructed. In conclusion, the generalization of SOET to quantum chemistry requires to work within RDMFT. Let us recall that, in RDMFT, the universal interaction functional [70] is given by

$$W(\boldsymbol{D}) = \min_{\Psi\rightarrow\boldsymbol{D}}\langle\Psi|\hat{W}_{\rm ee}|\Psi\rangle, \tag{6.4}$$

and the ground-state energy is obtained variationally as follows,

$$E(\boldsymbol{h}) = \min_{\boldsymbol{D}}\Big\{(\boldsymbol{h}|\boldsymbol{D}) + W(\boldsymbol{D})\Big\}, \tag{6.5}$$

where $\boldsymbol{D} \equiv \{D_{pq}\}_{pq} = \big\{\langle\sum_\sigma \hat{c}^\dagger_{p\sigma}\hat{c}_{q\sigma}\rangle\big\}_{pq}$ and $(\boldsymbol{h}|\boldsymbol{D}) = \sum_{pq} h_{pq}D_{pq}$.

It has already been mentioned in Sec. 1.2.2 that the 1RDM is not pure-state noninteracting v-representable [180, 216] because of its idempotent property. Let us assume that the 1RDM is pure-state CAS-representable, such that a CAS-interacting functional could be introduced as follows,

$$W^{\rm CAS}(\boldsymbol{D}) = \min_{\Psi\rightarrow\boldsymbol{D}}\langle\Psi|\hat{W}^{\rm CAS}|\Psi\rangle, \tag{6.6}$$

as well as the following decomposition in the spirit of SOET,

$$W(\boldsymbol{D}) = W^{\rm CAS}(\boldsymbol{D}) + \overline{W}^{\rm CAS}(\boldsymbol{D}), \tag{6.7}$$

where $\overline{W}^{\rm CAS}(\boldsymbol{D})$ is the complementary functional of the 1RDM. According to Eqs. (6.5), (6.6) and (6.7), the following exact expression for the ground-state energy is obtained,

$$E(\boldsymbol{h}) = \min_{\boldsymbol{D}} \Big\{ (\boldsymbol{h}|\boldsymbol{D}) + W^{\rm CAS}(\boldsymbol{D}) + \overline{W}^{\rm CAS}(\boldsymbol{D}) \Big\}, \tag{6.8}$$

or, equivalently,

$$E(\boldsymbol{h}) = \min_{\Psi} \Big\{ \langle \Psi | \hat{h} + \hat{W}^{\rm CAS} | \Psi \rangle + \overline{W}^{\rm CAS}(\boldsymbol{D}^{\Psi}) \Big\}. \tag{6.9}$$

Turning to the natural orbital representation $\boldsymbol{D} \equiv (\boldsymbol{\kappa}, \mathbf{n})$, where $\boldsymbol{\kappa}$ denotes the orbital rotation (see Sec. 1.1.4) and $\mathbf{n}$ is the natural orbital-occupation vector given by the diagonal of the 1RDM, Eq. (6.9) can be rewritten as

$$E(\boldsymbol{h}) = \min_{\Psi} \Big\{ \langle \Psi | \hat{h} + \hat{W}^{\rm CAS} | \Psi \rangle + \overline{W}^{\rm CAS}(\boldsymbol{\kappa}^{\Psi}, \mathbf{n}^{\Psi}) \Big\}. \tag{6.10}$$

It is still unclear how such an approach could be implemented. However, if the exact natural orbitals were known, they could be used as a basis such that

$$E(\boldsymbol{h}) = \min_{\mathbf{C}} \Big\{ \langle \Psi(\mathbf{C}) | \sum_p h_{pp} \hat{n}_p + \hat{W}^{\rm CAS} | \Psi(\mathbf{C}) \rangle + \overline{W}^{\rm CAS}(\mathbf{n}^{\Psi(\mathbf{C})}) \Big\}, \tag{6.11}$$

where $|\Psi(\mathbf{C})\rangle = \sum_I C_I |I\rangle$ is a normalized wavefunction expanded in the basis of Slater determinants $\{|I\rangle\}_I$ constructed in the fixed natural orbital basis. Therefore, the minimization in Eq. (6.10) is reduced to optimize the CI coefficients $\{C_i\}_i$ only. The minimizing wavefunction $\Psi^{\rm emb}$ in Eq. (6.11) describes a fictitious system whose CAS has been embedded in order to reproduce the exact occupation numbers of the natural orbitals, and fulfils the SOET-like self-consistent equation:

$$\boxed{\left(\sum_p h_{pp} \hat{n}_p + \hat{W}^{\rm CAS} + \sum_p \frac{\partial W^{\rm CAS}(\mathbf{n}^{\Psi^{\rm emb}})}{\partial n_p} \hat{n}_p \right) |\Psi^{\rm emb}\rangle = \mathcal{E}^{\rm emb} |\Psi^{\rm emb}\rangle}. \tag{6.12}$$

In practice, however, the exact natural orbitals are not known (except for the uniform electron gas and the symmetric Hubbard dimer, for instance). In addition, the previous assumption that the 1RDM is pure-state CAS-representable, leading to Eq. (6.6), is most certainly not valid. Indeed, $\hat{W}^{\rm CAS}$ allows for the hopping of the electrons inside the CAS, but not on the totality of the orbital space. Hence the noninteracting orbitals outside the CAS will have occupation equal to 0 (virtual orbitals) or 2 (core orbitals), thus leading to pure-state v-representability problem. Ensembles are thus needed to recover the fractional occupation numbers of the exact physical 1RDM, which we would like to avoid.

Indeed, using ensembles, we would have many degenerate determinants to handle which would be a nightmare to implement and to solve numerically.

In practice, one could think about matching the active part of the 1RDM only, which would be pure-state CAS-representable, in the spirit of the iLDA approximation in SOET [see Eq. (3.44)]. In order to add more flexibility, multiple CAS could be defined and solved separately, but would still be coupled together in some manner, in the spirit of DMET for quantum chemistry where multiple fragments are defined using localized orbitals [419, 422]. This has not been investigated yet and deserves more thinking. Of course, the most challenging part would still be the development of complementary functionals that are CAS- and orbital-dependent. Another way to look at the problem is to add partial interactions in the whole molecular orbital space. This has been investigated by using a seniority-zero interacting Hamiltonian, as shown in the following.

6.2 Seniority-zero Hamiltonian

Before entering into the newly formulated approach which will be detailed in the next section, it is important to provide a brief overview of the existing methods based on geminals, which describe the physical behaviour of a pair of electrons. We have seen in the first chapter that the mean-field approximation is insufficient to describe strongly correlated systems. An alternative consists in excitation-based configuration selection procedures (CISD, CCSD, ...) based on a single-determinant reference as a zeroth-order wavefunction, which have been proven highly accurate in the description of dynamical correlation. However, when strong static correlation arises, due to the multiconfigurational character of the system, these methods are not accurate anymore and the orbital picture breaks down. One example of strongly correlated system is a superconductor, which is not correctly described by a single Slater determinant, but can be alternatively described by a wavefunction built from Cooper pairs [506], which are geminals. This idea of using two-electron functions as building block for many-body wavefunctions is old, and the reader is referred to Ref. [507] which gives a good chronological overview of the theory of geminals, from the early 1950s to the late 1990s. In order to go beyond the independent particle scheme, given by the product of orbitals forming a Slater determinant, a product of geminals forming a more general wavefunction termed *antisymmetrized product of geminals* (APG) [508, 509] is considered as follows,

$$|\Psi^{\text{APG}}\rangle = \prod_{x}^{N_P} \sum_{pq}^{K} G_{pq}^{x} \hat{c}_{p\uparrow}^{\dagger} \hat{c}_{q\downarrow}^{\dagger} |\text{vac}\rangle, \tag{6.13}$$

where N_P is the number of electron pairs (labelled by x), $\hat{c}^\dagger_{p\uparrow}\hat{c}^\dagger_{q\downarrow}$ is the electron-pair creation operator with associated geminal coefficient G^x_{pq}, and K is the number of basis functions. Unfortunately, the APG method remains extremely expensive in term of computational cost, due to factorial scaling.

Then, many wavefunction ansätze have been derived to reduce the computational cost of the method, while keeping its most interesting feature, i.e. the description of strong correlation. Most of them are seniority-zero wavefunctions. In quantum chemistry, the concept of seniority has been introduced recently by Scuseria and co-workers [510], and it consists in partitioning the FCI Fock space into subspaces defined by the seniority number operator,

$$\hat{\Omega} = \sum_{p}^{K} \left(\hat{n}_{p\uparrow} + \hat{n}_{p\downarrow} - 2\hat{n}_{p\uparrow}\hat{n}_{p\downarrow} \right). \tag{6.14}$$

This operator simply counts the number of unpaired electrons. In Ref. [510], the authors have shown that the seniority-zero sector $\left(\langle\hat{\Omega}\rangle = 0\right)$ contributes significantly to the static correlation energy. A FCI calculation in the seniority-zero subspace, which consists in all possible configurations in which orbitals are either empty or doubly occupied (i.e., wavefunctions constructed solely by closed-shell determinants), leads to the so-called *doubly occupied configuration interaction* (DOCI) [511]. The DOCI (or, equivalently, seniority-zero) Hamiltonian reads

$$\hat{H}^{\mathcal{S}_0} = \sum_{p} h_{pp}\hat{n}_p + \sum_{p>q} \langle pq|pq\rangle \hat{n}_p \hat{n}_q - \sum_{p>q}\sum_{\sigma} \langle pq|qp\rangle \hat{n}_{p\sigma}\hat{n}_{q\sigma} + \sum_{pq} \langle pp|qq\rangle \hat{P}^\dagger_p \hat{P}_q, \tag{6.15}$$

where $\hat{n}_p = \hat{n}_{p\uparrow} + \hat{n}_{p\downarrow}$, $\hat{n}_{p\sigma} = \hat{c}^\dagger_{p\sigma}\hat{c}_{p\sigma}$, and $\hat{P}^\dagger_p = \hat{c}^\dagger_{p\uparrow}\hat{c}^\dagger_{p\downarrow}$ is the creation operator of a pair of electrons in the pth orbital. During the last decade, several wavefunction ansätze have been proposed to solve this Hamiltonian in the most efficient manner. Starting with the *antisymmetric product of interacting geminals* (APIG) proposed by Silver in 1969 [512], which is an excellent approximation to DOCI [513], one had to find better practical and tractable ways to solve the problem, for instance by using the *antisymmetrized geminal power* (AGP) wavefunction [514]. Another promising approximation to APIG is the so-called *antisymmetric product of one-reference-orbital geminals* (AP1roG) [214, 513], which has been shown to be exactly equivalent to the *pair-coupled cluster* (pCCD) method with pair-excitations only [515–517]. Together with orbital-optimization, AP1roG (or pCCD) is a size-consistent approach for which accurate energies have been obtained in the strongly correlated regime [518]. Although they are based on a single closed-shell reference determinant, they have been shown to be a very good approximation to the APIG and DOCI references, in contrast to CCD, CCSD and CCSD(T) when not restricted to the seniority-zero subspace [515]. In spite of this extremely satisfying results, AP1roG and related geminal-based wavefunctions are not appropriate to describe dynamical correlation. Indeed, this type of correlation cannot be described by electron-pair states and need to be included *a posteriori* using perturbation theory [507, 519–524], coupled-cluster [525, 526], extended random phase approximation [527], or DFT [528, 529]. For the latter, the double counting problem is handled by separating the Coulomb repulsion in two parts, one treated by the pCCD wavefunction, while the other is treated by DFT, thus leading to a hybrid scheme (such as presented in the last section of Chap. 1). One of the main advantage of this multideterminantal DFT approach is that pCCD has a low polynomial scaling, in contrast to usual multiconfigurational wavefunction methods, such that it is expected to treat relatively large systems.

In the following, an in-principle exact combined WFT-RDMFT theory is introduced, where the physical *ab-initio* problem is mapped onto a seniority-zero interacting wavefunction which, thanks to an appropriate interaction energy functional of the 1RDM, reproduces the physical natural orbitals and occupation numbers of the fully-interacting system exactly.

6.3 RDMFT based on a Seniority-zero wavefunction

The following work is still in progress, in collaboration with Naoki Nakatani (Tokyo, Japan) [530]. A draft is currently in preparation.

6.3.1 Theory

Let us consider the seniority-zero analogue of the interaction functional,

$$W^{\mathcal{S}_0}(\boldsymbol{D}) = \min_{\Psi \in \mathcal{S}_0 \rightarrow \boldsymbol{D}} \langle \Psi | \hat{W}_{\rm ee} | \Psi \rangle, \tag{6.16}$$

where the minimization is now restricted to (normalized) seniority-zero wavefunctions. If we denote

$$\overline{W}^{\mathcal{S}_0}(\boldsymbol{D}) = W(\boldsymbol{D}) - W^{\mathcal{S}_0}(\boldsymbol{D}) \tag{6.17}$$

the complementary interaction energy contribution which is not described by a seniority-zero wavefunction (like, for example, interpair nondynamic correlation [201]), it comes from Eqs (6.4) and (6.5) that, for any trial seniority-zero wavefunction Ψ,

$$\langle \Psi | \hat{W}_{\rm ee} | \Psi \rangle + \overline{W}^{\mathcal{S}_0}\left(\boldsymbol{D}^{\Psi}\right) + {\rm Tr}\left[\boldsymbol{h}\boldsymbol{D}^{\Psi}\right] \geq W\left(\boldsymbol{D}^{\Psi}\right) + {\rm Tr}\left[\boldsymbol{h}\boldsymbol{D}^{\Psi}\right] \geq E_0, \tag{6.18}$$

thus leading to the exact variational expression for the ground-state energy,

$$E_0 = \min_{\Psi \in \mathcal{S}_0} \left\{ \langle \Psi | \hat{H} | \Psi \rangle + \overline{W}^{\mathcal{S}_0} \left(\boldsymbol{D}^{\Psi} \right) \right\}. \tag{6.19}$$

Let us now use the natural orbital representation $\boldsymbol{D} \equiv (\boldsymbol{\kappa}, \mathbf{n})$. In such a representation, Eq. (6.16) is rewritten as follows,

$$\begin{aligned} W^{\mathcal{S}_0}(\boldsymbol{\kappa}, \mathbf{n}) &= \min_{\Psi \in \mathcal{S}_0(\boldsymbol{\kappa}) \to \mathbf{n}} \langle \Psi | \hat{W}_{\text{ee}} | \Psi \rangle, \\ &= \min_{\Psi \in \mathcal{S}_0(0) \to \mathbf{n}} \langle \Psi(\boldsymbol{\kappa}) | \hat{W}_{\text{ee}} | \Psi(\boldsymbol{\kappa}) \rangle, \end{aligned} \tag{6.20}$$

where $|\Psi(\boldsymbol{\kappa})\rangle = e^{-\hat{\kappa}}|\Psi\rangle$, and $\boldsymbol{\kappa} = 0$ denotes the unrotated molecular orbital basis. The minimization on the first line of Eq. (6.20) is restricted to seniority-zero wavefunctions $|\Psi(\boldsymbol{\kappa})\rangle = \sum_{I(\boldsymbol{\kappa})} C_{I(\boldsymbol{\kappa})} |I(\boldsymbol{\kappa})\rangle$, where $|I(\boldsymbol{\kappa})\rangle$ are closed-shell Slater determinants that are constructed in a molecular orbital basis which rotates with $\boldsymbol{\kappa}$. Such wavefunctions belong to the seniority-zero subspace denoted by $\mathcal{S}_0(\boldsymbol{\kappa})$, and fulfil the following density constraint,

$$\mathbf{n}^{\Psi(\boldsymbol{\kappa})} \equiv \left\{ \langle \Psi(\boldsymbol{\kappa}) | \hat{n}_{p(\boldsymbol{\kappa})} | \Psi(\boldsymbol{\kappa}) \rangle = n_p \right\}_p . \tag{6.21}$$

Turning to the second line of Eq. (6.20), the minimization is now restricted to linear combinations $|\Psi\rangle = \sum_{I \in \mathcal{S}_0(0)} C_I |I\rangle$ of closed-shell determinants $\{|I\rangle\}_I$ that are constructed in the *unrotated* molecular orbital basis. The wavefunctions $|\Psi\rangle$ belong to the seniority-zero subspace $\mathcal{S}_0(0)$. Note that the orbital occupation constraint should then be considered in the *unrotated* orbital basis, $\mathbf{n}^{\Psi} \equiv \{\langle \Psi | \hat{n}_p | \Psi \rangle = n_p\}_p$, which is equivalent to the constraint in the rotated basis. Indeed,

$$\begin{aligned} \langle \Psi(\boldsymbol{\kappa}) | \hat{n}_{p(\boldsymbol{\kappa})} | \Psi(\boldsymbol{\kappa}) \rangle &= \sum_{\sigma} \langle \Psi(\boldsymbol{\kappa}) | \hat{c}^{\dagger}_{p(\boldsymbol{\kappa})\sigma} \hat{c}_{p(\boldsymbol{\kappa})\sigma} | \Psi(\boldsymbol{\kappa}) \rangle = \sum_{\sigma} \langle \Psi | e^{\hat{\kappa}} e^{-\hat{\kappa}} \hat{c}^{\dagger}_{p\sigma} e^{\hat{\kappa}} e^{-\hat{\kappa}} \hat{c}_{p\sigma} e^{\hat{\kappa}} e^{-\hat{\kappa}} | \Psi \rangle \\ &= \langle \Psi | \hat{n}_p | \Psi \rangle. \end{aligned} \tag{6.22}$$

Let us now see if the domain of minimization can be extended to any trial wavefunctions, and not only the one restricted to seniority-zero wavefunctions. We start with the following equivalent expression of Eq. (6.20),

$$W^{\mathcal{S}_0}(\boldsymbol{\kappa}, \mathbf{n}) = \min_{\Psi \in \mathcal{S}_0(0) \to \mathbf{n}} \langle \Psi | \hat{W}_{\text{ee}}(\boldsymbol{\kappa}) | \Psi \rangle, \tag{6.23}$$

where

$$\hat{W}_{\mathrm{ee}}(\boldsymbol{\kappa}) \quad = \quad e^{\hat{\kappa}}\,\hat{W}_{\mathrm{ee}}\,e^{-\hat{\kappa}} = \frac{1}{2}\sum_{pqrs}\langle pq|rs\rangle^{\boldsymbol{\kappa}}\sum_{\sigma\sigma'}\hat{c}^{\dagger}_{p\sigma}\hat{c}^{\dagger}_{q\sigma'}\hat{c}_{s\sigma'}\hat{c}_{r\sigma}, \tag{6.24}$$

and $\langle pq|rs\rangle^{\boldsymbol{\kappa}} = \langle p(\boldsymbol{\kappa})q(\boldsymbol{\kappa})|r(\boldsymbol{\kappa})s(\boldsymbol{\kappa})\rangle$. According to Eq. (6.24), the rotation has been incorporated into the electronic integrals, while the creation and annihilation operators act in the unrotated molecular orbital basis.

By introducing the projection of $\hat{W}_{\mathrm{ee}}(\boldsymbol{\kappa})$ onto $\mathcal{S}_0(0)$,

$$\hat{W}^{\mathcal{S}_0}_{\mathrm{ee}}(\boldsymbol{\kappa}) = \sum_{I,J\in\mathcal{S}_0(0)}\langle I|\hat{W}_{\mathrm{ee}}(\boldsymbol{\kappa})|J\rangle|I\rangle\langle J|, \tag{6.25}$$

it comes

$$W^{\mathcal{S}_0}(\boldsymbol{\kappa},\mathbf{n}) = \min_{\Psi\in\mathcal{S}_0(0)\rightarrow\mathbf{n}}\left\langle\Psi\middle|\hat{W}^{\mathcal{S}_0}_{\mathrm{ee}}(\boldsymbol{\kappa})\middle|\Psi\right\rangle. \tag{6.26}$$

Interestingly, the ground-state wavefunction of $\hat{W}^{\mathcal{S}_0}_{\mathrm{ee}}(\boldsymbol{\kappa}) + \sum_p \varepsilon_p\hat{n}_p$ (where $\hat{n}_p$ acts in the unrotated molecular orbital basis) belongs to $\mathcal{S}_0(0)$ and, by analogy with DFT, we should have a one-to-one correspondence between the occupation of the unrotated orbitals and the one-electron energies $\{\varepsilon_p\}_p$. Consequently, for *any* normalized wavefunction Ψ (including those that do not belong to $\mathcal{S}_0(0)$), the following inequality is fulfilled,

$$\left\langle\Psi\middle|\hat{W}^{\mathcal{S}_0}_{\mathrm{ee}}(\boldsymbol{\kappa}) + \sum_p\varepsilon_p(\mathbf{n})\hat{n}_p\middle|\Psi\right\rangle \geq \left\langle\Psi^{\mathcal{S}_0(0)}_{\boldsymbol{\kappa}}(\mathbf{n})\middle|\hat{W}^{\mathcal{S}_0}_{\mathrm{ee}}(\boldsymbol{\kappa}) + \sum_p\varepsilon_p(\mathbf{n})\hat{n}_p\middle|\Psi^{\mathcal{S}_0(0)}_{\boldsymbol{\kappa}}(\mathbf{n})\right\rangle, \tag{6.27}$$

where $\Psi^{\mathcal{S}_0(0)}_{\boldsymbol{\kappa}}(\mathbf{n})$ is the minimizing wavefunction of Eq. (6.26), and $\{\varepsilon_p(\mathbf{n})\}_p$ are the one-electron energies, functionals of the density $\mathbf{n}$. Note that the natural orbitals of $\Psi^{\mathcal{S}_0(0)}_{\boldsymbol{\kappa}}(\mathbf{n})$ are the unrotated orbitals, by construction. Since

$$W^{\mathcal{S}_0}(\boldsymbol{\kappa},\mathbf{n}) = \langle\Psi^{\mathcal{S}_0(0)}_{\boldsymbol{\kappa}}(\mathbf{n})|\hat{W}^{\mathcal{S}_0}_{\mathrm{ee}}(\boldsymbol{\kappa})|\Psi^{\mathcal{S}_0(0)}_{\boldsymbol{\kappa}}(\mathbf{n})\rangle, \tag{6.28}$$

inserting the condition $\Psi\rightarrow\mathbf{n}$ into Eq. (6.27) leads to

$$W^{\mathcal{S}_0}(\boldsymbol{\kappa},\mathbf{n}) = \min_{\Psi\rightarrow\mathbf{n}}\langle\Psi|\hat{W}^{\mathcal{S}_0}_{\mathrm{ee}}(\boldsymbol{\kappa})|\Psi\rangle, \tag{6.29}$$

where, as pointed out previously, the occupation constraint is written in the *unrotated* orbital basis. In contrast to Eq. (6.26), the domain of the minimization is now extended to any trial wavefunction

Ψ that reproduces $\mathbf{n}$. Note that this minimization could have been written over the CI coefficient $\mathbf{C} \equiv \{C_I\}_I$ instead of the wavefunction, given that the orbitals are fixed. We now have everything we need to formulate a variational principle where the minimization is performed over both orbital rotations and trial wavefunctions Ψ (or, equivalently, $\mathbf{C}$).

The following exact variational expression for the energy is then obtained,

$$E_0 = \min_{\boldsymbol{\kappa},\mathbf{n}} \left\{ W^{\mathcal{S}_0}(\boldsymbol{\kappa},\mathbf{n}) + \overline{W}^{\mathcal{S}_0}(\boldsymbol{\kappa},\mathbf{n}) + (\boldsymbol{h}(\boldsymbol{\kappa})|\mathbf{n}) \right\} \tag{6.30}$$

where $(\boldsymbol{h}(\boldsymbol{\kappa})|\mathbf{n}) = \sum_p h_{p(\boldsymbol{\kappa})p(\boldsymbol{\kappa})} n_p$. Inserting Eq. (6.29) into Eq. (6.30), it comes

$$E_0 = \min_{\boldsymbol{\kappa},\mathbf{n}} \left\{ \min_{\Psi\rightarrow\mathbf{n}} \left\{ \langle \Psi | \hat{W}_{\text{ee}}^{\mathcal{S}_0}(\boldsymbol{\kappa}) | \Psi \rangle \right\} + \overline{W}^{\mathcal{S}_0}(\boldsymbol{\kappa},\mathbf{n}) + (\boldsymbol{h}(\boldsymbol{\kappa})|\mathbf{n}) \right\}, \tag{6.31}$$

or, equivalently,

$$E_0 = \min_{\boldsymbol{\kappa},\mathbf{n}} \left\{ \min_{\Psi\rightarrow\mathbf{n}} \left\{ \langle \Psi | \hat{W}_{\text{ee}}^{\mathcal{S}_0}(\boldsymbol{\kappa}) | \Psi \rangle + \overline{W}^{\mathcal{S}_0}(\boldsymbol{\kappa},\mathbf{n}^{\Psi}) + \big(\boldsymbol{h}(\boldsymbol{\kappa})\big|\mathbf{n}^{\Psi}\big) \right\} \right\}. \tag{6.32}$$

By introducing the operators

$$\hat{h}^{\mathcal{S}_0}(\boldsymbol{\kappa}) = \sum_p h_{p(\boldsymbol{\kappa})p(\boldsymbol{\kappa})} \hat{n}_p \tag{6.33}$$

and $\hat{H}^{\mathcal{S}_0}(\boldsymbol{\kappa}) = \hat{h}^{\mathcal{S}_0}(\boldsymbol{\kappa}) + \hat{W}_{\text{ee}}^{\mathcal{S}_0}(\boldsymbol{\kappa})$ [see Eqs. (6.15) and (6.25)], we obtain the final variational expression for the energy,

$$E_0 = \min_{\boldsymbol{\kappa}} \left\{ \min_{\Psi} \left\{ \langle \Psi | \hat{H}^{\mathcal{S}_0}(\boldsymbol{\kappa}) | \Psi \rangle + \overline{W}^{\mathcal{S}_0}(\boldsymbol{\kappa},\mathbf{n}^{\Psi}) \right\} \right\}. \tag{6.34}$$

where $\boldsymbol{\kappa}$ and Ψ are *independent* variables. Thus, the minimizations in Eq. (6.34) leads to a set of two equations. The first one is obtained by searching for the minimizing wavefunction denoted by $\Psi^{\mathcal{S}_0}$, which fulfils the following self-consistent equation,

$$\boxed{\left(\hat{H}^{\mathcal{S}_0}(\boldsymbol{\kappa}) + \sum_p \left. \frac{\partial \overline{W}^{\mathcal{S}_0}(\boldsymbol{\kappa},\mathbf{n})}{\partial n_p} \right|_{\mathbf{n}=\mathbf{n}^{\Psi^{\mathcal{S}_0}}} \hat{n}_p \right) \left| \Psi^{\mathcal{S}_0} \right\rangle = \mathcal{E}^{\mathcal{S}_0} \left| \Psi^{\mathcal{S}_0} \right\rangle}. \tag{6.35}$$

The second one is the stationarity condition, fulfilled when the orbitals are optimized,

$$\frac{\partial \hat{H}^{\mathcal{S}_0}(\boldsymbol{\kappa})}{\partial \kappa_{pq}} + \left. \frac{\partial \overline{W}^{\mathcal{S}_0}(\boldsymbol{\kappa},\mathbf{n})}{\partial \kappa_{pq}} \right|_{\mathbf{n}=\mathbf{n}^{\Psi^{\mathcal{S}_0}}} = 0. \tag{6.36}$$

Although this method has not been implemented yet, due to the lack of any analytical form of the complementary functional, it could be done by following these steps:

1. Solve the system with Hartree–Fock to get the starting natural orbitals and occupation numbers
2. Solve Eq. (6.35) to get the CI coefficients, the seniority-zero wavefunction and the new set of occupation numbers
3. Optimise the natural orbitals by solving the stationarity condition in Eq. (6.36). which is fulfilled for $\boldsymbol{\kappa} = 0$ (for convenience)
4. Go back to step 2 with the new sets of natural orbitals and occupation numbers until convergence is reached.

Note that steps 2 and 3 are similar to a MCSCF calculation. Within this theory, the exact 1RDM should in-principle be recovered provided that the exact complementary functional is known, which is a long-term undertaking.

6.3.2 Adiabatic Connection

The adiabatic connection [see Sec. 1.2.1.iv] is an appropriate tool that gives some informations about the form of the complementary functional and its importance. Let us consider the λ-dependent Hamiltonian expressed in the natural orbital basis of the true physical system,

$$\hat{H}^{\lambda}(\boldsymbol{\varepsilon}) \quad = \quad \hat{H}^{\mathcal{S}_0} + \lambda\left(\hat{H} - \hat{H}^{\mathcal{S}_0}\right) = \sum_{p} \varepsilon_p \hat{n}_p + \hat{W}_{\rm ee}^{\mathcal{S}_0} + \lambda\left(\sum_{p\neq q} h_{pq}\hat{n}_{pq} + \hat{W}_{\rm ee} - \hat{W}_{\rm ee}^{\mathcal{S}_0}\right), \quad (6.37)$$

where $\hat{n}_{pq} = \sum_\sigma \hat{c}^\dagger_{p\sigma}\hat{c}_{q\sigma}$. Note that $D_{pq}^{\lambda=1} = D_{pq}^{\lambda=0} = 0$ in this basis, but this is not anymore true for intermediate values of λ. The ground-state wavefunction $\Psi^\lambda(\mathbf{n})$ of the Hamiltonian $\hat{H}^\lambda(\boldsymbol{\varepsilon}^\lambda)$ reproduces the exact natural occupation numbers $\mathbf{n}$ of the physical system for any λ, and $\boldsymbol{\varepsilon}^\lambda$ can be obtained from the following Legendre–Fenchel transform [68] (see, for instance, Eq. (1.104) for the noninteracting kinetic energy functional in KS-DFT),

$$W^\lambda(\mathbf{n}) = \sup_{\boldsymbol{\varepsilon}}\left\{\mathcal{E}^\lambda(\boldsymbol{\varepsilon}) - (\boldsymbol{\varepsilon}|\mathbf{n})\right\} = \mathcal{E}^\lambda(\boldsymbol{\varepsilon}^\lambda) - (\boldsymbol{\varepsilon}^\lambda|\mathbf{n}), \quad (6.38)$$

where $\mathcal{E}^\lambda(\boldsymbol{\varepsilon})$ is the ground-state energy of $\hat{H}^\lambda(\boldsymbol{\varepsilon})$. Note that this construction reproduces the diagonal of the density matrix $\boldsymbol{D}_{pp}^{\lambda=1}$. For $\lambda = 1$, it represents the occupation numbers of the physical system in the natural orbital basis and $\varepsilon_p^{\lambda=1} = h_{pp}$. When $\lambda = 0$, the seniority-zero wavefunction $\Psi^{\mathcal{S}_0}$

with natural orbital occupancies $\mathbf{n}$ is recovered. By construction, it also shares the same set of natural orbitals with the physical wavefunction, which is in principle not the case for the previously described seniority zero wavefunction ansatz (DOCI, APIG, AP1roG). For $0 < \lambda < 1$, the 1RDM is not constrained to be diagonal. Indeed, the system is considered in the natural orbital basis of the fully-interacting system, which is *a priori* not the natural orbital basis of the partially-interacting system.

Let us now investigate the adiabatic path that connects the seniority-zero system to the physical fully-interacting one, by considering the physical interaction energy,

$$\begin{aligned} W(\boldsymbol{D}) \equiv W(\mathbf{n}) &= W^{\lambda=1}(\mathbf{n}) = W^{\lambda=0}(\mathbf{n}) + \left(W^{\lambda=1}(\mathbf{n}) - W^{\lambda=0}(\mathbf{n})\right) \\ &= W^{\lambda=0}(\mathbf{n}) + \int_0^1 \mathrm{d}\lambda \frac{\mathrm{d}W^{\lambda}(\mathbf{n})}{\mathrm{d}\lambda} \\ &= \left\langle \Psi^{\mathcal{S}_0}(\mathbf{n}) \middle| \hat{W}_{\mathrm{ee}}^{\mathcal{S}_0} \middle| \Psi^{\mathcal{S}_0}(\mathbf{n}) \right\rangle + \int_0^1 \mathrm{d}\lambda \, \overline{\mathcal{W}}_{\mathrm{c}}^{\lambda}(\mathbf{n}), \end{aligned} \tag{6.39}$$

where, according to the Hellmann–Feynman theorem, the complementary correlation integrand equals

$$\overline{\mathcal{W}}_{\mathrm{c}}^{\lambda}(\mathbf{n}) = \langle \Psi^{\lambda}(\mathbf{n}) | \hat{W}_{\mathrm{ee}} - \hat{W}^{\mathcal{S}_0} | \Psi^{\lambda}(\mathbf{n}) \rangle + \sum_{p \neq q} h_{pq} \langle \Psi^{\lambda}(\mathbf{n}) | \hat{n}_{pq} | \Psi^{\lambda}(\mathbf{n}) \rangle. \tag{6.40}$$

Therefore, according to Eqs. (6.17) and (6.28), the complementary energy functional is given by

$$\overline{W}^{\mathcal{S}_0}(\mathbf{n}) = \int_0^1 \mathrm{d}\lambda \, \overline{\mathcal{W}}_{\mathrm{c}}^{\lambda}(\mathbf{n}). \tag{6.41}$$

By construction, $\overline{\mathcal{W}}_{\mathrm{c}}^{\lambda=0}(\mathbf{n}) = 0$. Note the presence of the nonzero contribution from the off-diagonal part of the 1RDM. We have observed that this contribution is negligible, as assumed by Pernal in a similar context in Ref. [531].

Let us highlight some similarities and differences between this work and the recent one of Pernal [531]. In the latter work, the density matrix is assumed to be diagonal and equal to $D_{pq}^{\lambda=0} = \delta_{pq} n_p$ along the whole adiabatic connection path, such that the natural orbitals are assumed to be the same set of orbitals as the seniority zero reference system. In our approach, we want to reproduce the exact occupation numbers of the physical system, $D_{pp}^{\lambda} = D_{pp}^{\lambda=1} = n_p$, while the off-diagonal elements are free to vary (and be non-zero) except when $\lambda = 0$, by construction. The integrand in Ref. [531] is obtained by the extended random phase approximation. In our work, this quantity is exactly determined through the determination of the potential restoring the occupation number [Eq. (6.38)]. The Lieb maximization of Eq. (6.38) is calculated within the highly accurate DMRG method. We will show that the integrand has a quadratic behaviour with respect to λ in our context. The linear approximation in λ of the integrand proposed in Ref. [531] could be used in practice.

6.3.3 Results

Let us now look at the correlation integrand as a function of the coupling constant λ. Because the Legendre–Fenchel transform in Eq. (6.38) is evaluated by the highly accurate DMRG method, we are limited to small systems as well as relatively small basis sets. Geminals are exact for a 2 electrons system, like the hydrogen molecule. In order to get a non-zero form of the complementary interacting functional, we need to study system which are not well described by the seniority-zero Hamiltonian [Eq. (6.15)], i.e. those for which dynamical correlation effects are important. Therefore, we are currently looking at the Beryllium atom, the Helium dimer [24] the transition of H_4 from D_{2h} to D_{4h} geometry [201], the H_2 dimer, the LiH, the N_2 and hydrogen molecular chains. Given that the work is still in progress, only few results on the Helium dimer and the chain of eight hydrogens H_8 are shown in this thesis.

Eq. (6.38) has been solved for different λ values in both of these systems, using DMRG. It leads to the maximizing "local" potentials $\left\{\varepsilon_p^\lambda\right\}_\lambda$ that reproduce the exact occupation number of the true physical natural orbitals, as well as the eigenfunction $\Psi^\lambda(\mathbf{n})$ of $\hat{H}^\lambda(\boldsymbol{\varepsilon}^\lambda)$. Hence, the integrand in Eq. (6.40) can be computed and is plotted in Figs. 6.1 and 6.2 for the H_8 molecular chain and the Helium dimer in the cc-pVDZ basis set (see Appendix H), respectively. According to Figs 6.1 and 6.2, the integrand is quadratic in λ, which somehow shows that the assumption of Pernal in Ref. [531] is not always valid. Interestingly, the integrand for H_8 is much larger than in Fig. 2 of Ref. [531]. This can be explained by the orbital basis that we use. Indeed, it is known that the optimization of the orbitals in seniority-zero approaches has huge importance [518, 532]. Hence, using the (frozen and delocalized) natural orbitals of the fully-interacting Hamiltonian as a basis set for our seniority-zero Hamiltonian is not optimal, and does not minimize the energy. This is of course not a problem in the exact theory, since the complementary functional of the occupation numbers is supposed to contain the missing correlation energy. Hence, the complementary functional, given by the integration of the correlation integrand according to Eq. (6.41), contributes significantly to the energy. As a consequence, using the natural orbital basis of the fully-interacting Hamiltonian could be problematic in practice, when approximate functionals are used. This feature also arises in Fig. 6.3, representing the dissociation curve of the Helium dimer in the natural orbital basis of the fully-interacting Hamiltonian. $\lambda = 1$ (left panel) corresponds to the DMRG energy of the fully-interacting system, while $\lambda = 0$ (right panel) is the DMRG energy in the seniority-zero subspace only. The latter is completely unable to describe the small dissociation energy of He_2, and gives a particularly wrong (overestimated) energy.

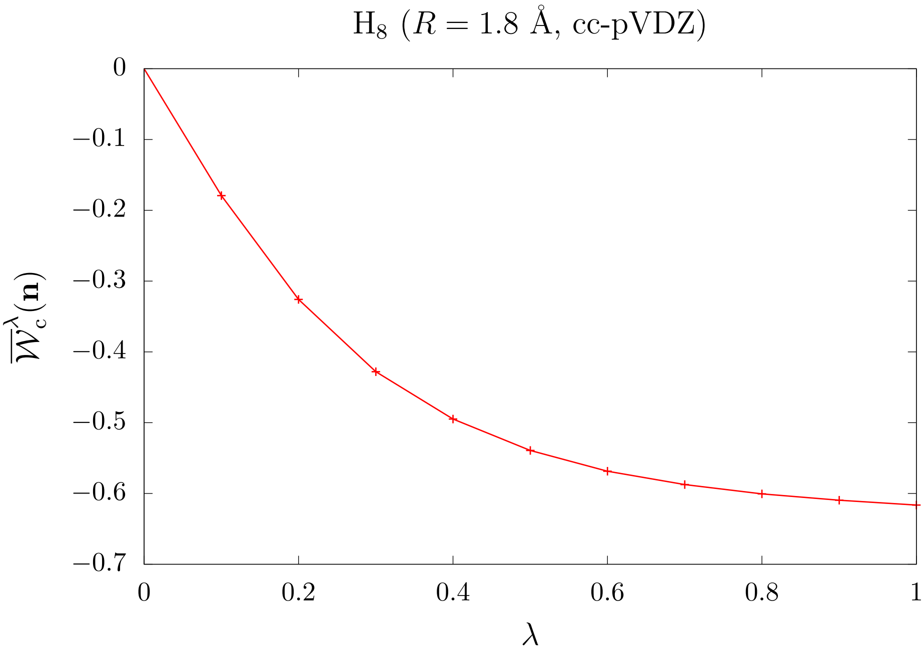

Figure 6.1: Correlation integrand [Eq. (6.40)] for the H_8 molecular chain with interatomic distance $R = 1.8$ Å in the cc-pVDZ basis. The energy is in atomic unit (hartree).

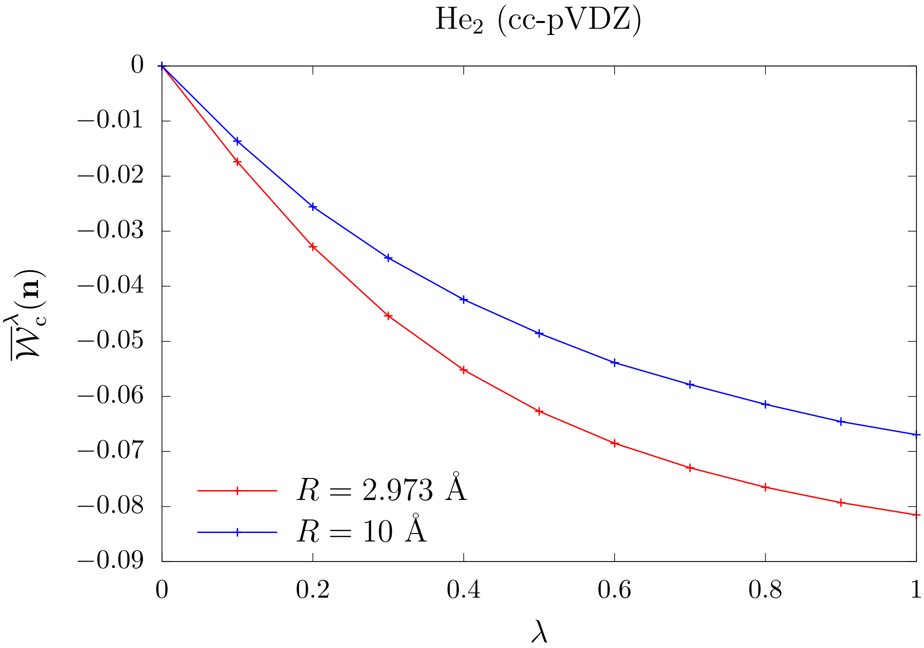

Figure 6.2: Correlation integrand [Eq. (6.40)] for the He_2 molecule with interatomic distance at equilibrium $R_{\text{eq}} = 2.973$ Å and close to dissociation $R = 10$ Å, in the cc-pVDZ basis. The energy is in atomic unit (hartree).

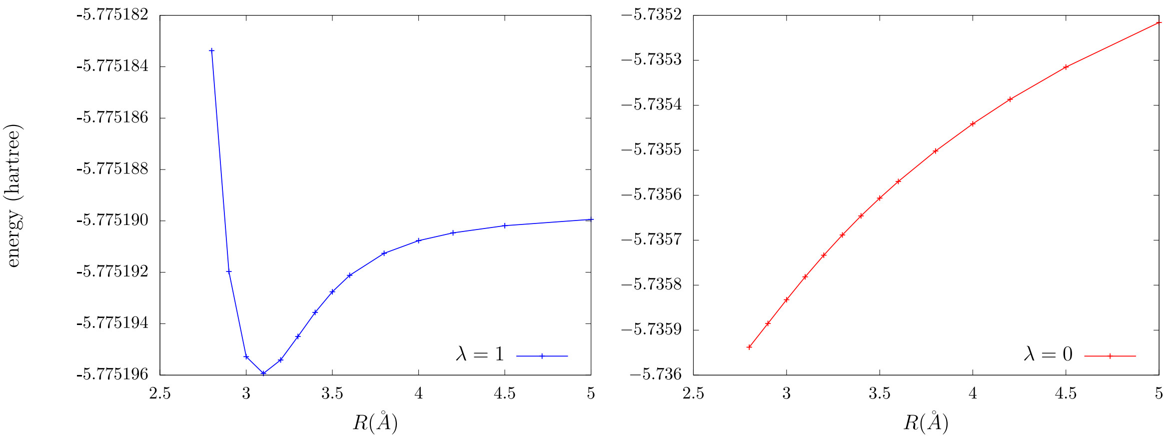

Figure 6.3: Dissociation energy curve of the Helium dimer obtained by solving Eq. (6.37) in the natural orbital basis of the fully-interacting Hamiltonian, for $\lambda = 1$ (left panel) and $\lambda = 0$ (right panel) in cc-pVDZ basis set.

As a consequence, the complementary energy functional should in-principle compensate for this huge error. At first sight, this result is very surprising. Indeed, as seen in Fig. 1 of Ref. [526], it is clear that the energy obtained from the *antisymmetrized product of strongly orthogonal geminals* (APSG) remains in the scope of the exact energy, even though the dissociation energy is not well described. Consequently, the wrong energy in our Fig. 6.3 (right panel) is clearly due to the fact that the true exact natural orbitals are used instead of being reoptimized. It remains unclear if the herein approach, as formulated in this section, could be successfully implemented, as the reference wavefunction is not good enough when the physical natural orbitals are used.

The reoptimization of the natural orbitals in our scheme should be investigated, and is left for future work. In the spirit of Pernal's approach [531], we could also apply the extended random phase approximation [531]. Turning to the development of the complementary functionals of the 1RDM that contain intergeminal correlation, one could look at the recent work of van Meer *et al.* [533], which aims at generating new functionals containing non-geminal dynamical correlation, in the context of RDMFT. Alternatively, another kind of adiabatic connection could be formulated, by gradually increasing the seniority number until the full configuration space is recovered, in the spirit of Refs [510, 534].

To end this last chapter, I would say that having a variational multi-configurational method able to treat both static and dynamical correlation effects with a cheap computational cost remains the holy grail of quantum chemistry. Numerous novel ideas and directions are still emerging, but no method has yet appeared as *the* method of choice for describing strongly correlated molecular systems.

Conclusion

The description of strong electronic correlation effects in both quantum chemistry and condensed matter physics has been extensively discussed throughout this thesis. The combination of *wavefunction theory* (WFT) with methods based on reduced quantities as a basic variable (electronic density, one-particle reduced density matrix, or Green's function) has been investigated. In particular, we focused on the combination of WFT with *density functional theory* (DFT), which aims to treat both static and dynamical correlations at a reasonable computational cost. Indeed, WFT is computationally expensive and is usually lacking of dynamical correlation [535], while the low-cost Kohn–Sham DFT together with density-functional approximations miss static correlation effects [2]. Given that the two approaches are formulated in a completely different language, it remains extremely challenging to merge them in an efficient manner, and to avoid any double counting of the correlation. Despite the increasing gain of interest in hybrid methods, none of them has emerged as the true solution yet.

During this thesis, we have brought our own contributions to this large and active field of research, in both fields of quantum chemistry and condensed matter physics. The methods presented herein do not claim to be a general solution to the treatment of strongly correlated systems. Nevertheless, they pave the way towards the efficient description of such systems. The first method that we described is the so-called *site-occupation embedding theory* (SOET). The formulation of SOET relies on the in-principle-exact mapping of the physical system onto a partially-interacting one, thus leading to a rigorous combination of WFT with DFT [Eq. (3.6)]. Being in its early stages, the theory has been applied to the one-dimensional uniform Hubbard model only, and an exact expression has been derived for both the per-site energy [Eq. (3.32)] and the double occupation [Eq. (3.39)]. Several approximate functionals have been developed in this context, by looking at the exact analytical expressions to the Hubbard dimer, the one-dimensional half-filled Hubbard model and the symmetric single-impurity Anderson model (SIAM). Promising results have been obtained in the whole range of correlation and density.

In spite of these successful results, more efficient implementations of SOET needed to be explored in order to reduce the computational cost. First, we transformed the SOET Hamiltonian onto the SIAM

Hamiltonian, which can then be solved by using impurity-solvers. Second, we employed the Schmidt decomposition, thus leading to the so-called *projected* SOET (P-SOET). The latter share similarities (as well as differences in many aspects) with the *density matrix embedding theory* (DMET), but SOET contains an additional contribution coming from a functional of the density. Thanks to this analytic functional, the density-driven Mott–Hubbard transition, which denotes the opening of the charge gap, has been successfully described with a single impurity only. In my opinion, this is one of the most striking results in SOET. The next step forward would be to study the two-dimensional Hubbard model, which contains a Mott–Hubbard transition in U/t and can model the physics in the high-$\mathrm{T_c}$ cuprates. In order to move in this direction, new functionals have to be considered. As in standard DFT, an automated way of developing functionals would definitely increase the domain of application of SOET, which would eventually become a standard and popular embedding approach [4].

The charge gap (or fundamental gap) has then been studied within the ensemble DFT formalism. By considering a particular choice of ensemble, we provided a complete reformulation of the fundamental gap problem in DFT. This reformulation consists in rewriting the derivative discontinuity (previously formulated within DFT for fractional number of electrons) into a derivative of the weight-dependent exchange-correlation functional [Eq. (5.34)], in complete analogy with the extraction of the optical gap in ensemble DFT for excited states.

In other words, the fundamental gap problem (traditionally formulated in grand canonical ensemble DFT) has been recast into a canonical problem where the xc functional is ensemble-weight-dependent. We called this theory the N-centered ensemble DFT. When combined with the ensemble analogue of Levy–Zahariev shift in the potential, and together with a generalization of the ensemble weights, the extraction of individual energies [Eq. (5.53)] (as well as ionization potential and electronic affinity) has been rendered possible. As a proof of principle, the method has only been applied to the Hubbard dimer yet. An obvious step forward would be the development of weight-dependent functionals for model Hamiltonian as well as *ab-initio* Hamiltonian.

Finally, we discussed the extension of SOET to quantum chemistry. This would in principle lead to a *complete active space* DFT (CAS-DFT) approach defined in the orbital space only [Eq. (6.12)], where the active orbitals play the role of the interacting impurities in the original formulation of SOET. However, this formulation is facing difficulties, such as the CAS-dependence of the functional, as well as pure-state v-representability issues. Alternatively, a new theory based on a seniority-zero reference wavefunction has been proposed, in which a complementary functional of the natural orbitals and occupation numbers should in-principle recover all the missing correlation effects [Eq. (6.35)]. We have derived an adiabatic connection and shown the quadratic behaviour in λ of the correlation integrand. The importance of the orbital optimization has also been highlighted.

To conclude, new ideas and in-principle-exact methods have been derived throughout this thesis, dealing with significant and actual problems in DFT: the description of strongly correlated systems and the extraction of the fundamental gap. These methods shed a new light on the treatment of strongly correlated systems. By extending and investigating them further, we feel in our bones that they could be useful for the large community of theoretical chemists and physicists. Many challenging tasks must however be faced, in particular the development of appropriate functionals.

Appendices

A Functional calculus

Let F be a function of f, itself a function of x. Hence, F is called a functional of f. The functional derivative is given by:

$$\delta F[f] = F[f + \delta f] - F[f] = \int \frac{\delta F[f]}{\delta f(x)} \delta f(x) \mathrm{d}x. \tag{42}$$

If f is also a functional of another function $g(x)$, then $F\Big[f[g]\Big]$ has a functional derivative given by the chain rule:

$$\frac{\delta F[f]}{\delta g(x)} = \int \frac{\delta F[f]}{\delta f(x')} \frac{\delta f(x')}{\delta g(x)} \mathrm{d}x'. \tag{43}$$

If F is a function of $f(x)$, then the functional derivative with respect to $f(x')$ is

$$\frac{\delta F(f(x))}{\delta f(x')} = \frac{\mathrm{d}F(f(x))}{\mathrm{d}f} \delta(x - x'), \tag{44}$$

where $\delta(x - x')$ is the delta function.

B Lagrangian multipler method

In DFT, the ground-state energy is given by the following variational principle:

$$E_0 = \min_{\Phi} \Big\{ \langle \Phi | \hat{T} + \hat{V}_{\mathrm{ne}} | \Phi \rangle + E_{\mathrm{Hxc}}[n^{\Phi}] \Big\} = \min_{\Phi} \Big\{ E[\{\varphi_i\}] \Big\}, \tag{45}$$

where

$$E[\{\varphi_i\}] = \sum_{i=1}^{N} \int \varphi_i^*(\mathbf{r}) \left(-\frac{1}{2}\nabla^2 + v_{\mathrm{ne}}(\mathbf{r}) \right) \varphi_i(\mathbf{r}) + E_{\mathrm{Hxc}}[n], \tag{46}$$

and $n(\mathbf{r}) = \sum_{i=1}^{N} |\varphi_i(\mathbf{r})|^2 = \sum_{i=1}^{N} \varphi_i^*(\mathbf{r})\varphi(\mathbf{r})$. The minimization consists in finding the set of KS orbitals that minimizes the energy E_0, with the orthonormal constraint $\langle \Phi_i | \Phi_j \rangle = \delta_{ij}$. Because the KS orbitals are eigenfunctions of a self-adjoint operator, one can always find an orthogonal set of orbitals, so that only to normalization constraint can be considered by writting the following Lagrangian:

$$\mathcal{L}[\{\varphi_i\}] = E[\{\varphi_i\}] - \sum_{i=1}^{N} \varepsilon_i \left(\int \varphi_i^*(\mathbf{r})\varphi_i(\mathbf{r})\mathrm{d}\mathbf{r} - 1 \right). \tag{47}$$

Considering the stationarity of the Lagrangian with respect to a small change in the orbitals $\{\varphi_i\} \to \{\varphi_i + \delta\varphi_i\}$ leads to

$$\delta\mathcal{L}[\{\varphi_i\}] = \mathcal{L}[\{\varphi_i + \delta\varphi_i\}] - \mathcal{L}[\{\varphi_i\}] = 0. \tag{48}$$

Considering a small change $\varphi_k^* \to \varphi_k^* + \delta\varphi_k^*$, we get

$$\begin{aligned}
\delta\mathcal{L}[\{\varphi_i\}] &= \int (\varphi_k^*(\mathbf{r}) + \delta\varphi_k^*(\mathbf{r})) \left(-\frac{1}{2}\nabla^2 + v_{\mathrm{ne}}(\mathbf{r}) \right) \varphi_k(\mathbf{r})\mathrm{d}\mathbf{r} \\
&\quad - \int \varphi_k^*(\mathbf{r}) \left(-\frac{1}{2}\nabla^2 + v_{\mathrm{ne}}(\mathbf{r}) \right) \varphi_k(\mathbf{r})\mathrm{d}\mathbf{r} + E_{\mathrm{Hxc}}[n^{\{\varphi_k + \delta\varphi_k\}}] - E_{\mathrm{Hxc}}[n^{\{\varphi_k\}}] \\
&\quad - \varepsilon_k \left(\int (\varphi_k^*(\mathbf{r}) + \delta\varphi_k^*(\mathbf{r}))\, \varphi_k(\mathbf{r})\mathrm{d}\mathbf{r} - \int \varphi_k^*(\mathbf{r})\varphi_k(\mathbf{r})\mathrm{d}\mathbf{r} \right) \\
&= \int \delta\varphi_k^*(\mathbf{r}) \left(-\frac{1}{2}\nabla^2 + v_{\mathrm{ne}}(\mathbf{r}) \right) \varphi_k(\mathbf{r})\mathrm{d}\mathbf{r} + E_{\mathrm{Hxc}}[n^{\{\varphi_k + \delta\varphi_k\}}] - E_{\mathrm{Hxc}}[n^{\{\varphi_k\}}] \\
&\quad - \varepsilon_k \int \delta\varphi_k^*(\mathbf{r})\varphi_k(\mathbf{r})\mathrm{d}\mathbf{r}.
\end{aligned} \tag{49}$$

Then, by identifying

$$\begin{aligned}
E_{\mathrm{Hxc}}[n^{\{\varphi_k + \delta\varphi_k\}}] - E_{\mathrm{Hxc}}[n^{\{\varphi_k\}}] &= \delta E_{\mathrm{Hxc}}[n[\{\varphi_k\}]] \\
&= \int \frac{\delta E_{\mathrm{Hxc}}[n]}{\delta\varphi_k^*(\mathbf{r})} \delta\varphi_k^*(\mathbf{r})\mathrm{d}\mathbf{r},
\end{aligned} \tag{50}$$

we obtain

$$\delta\mathcal{L}[\{\varphi_i\}] = \int \left[\left(-\frac{1}{2}\nabla^2 + v_{\mathrm{ne}}(\mathbf{r}) - \varepsilon_k \right) \varphi_k(\mathbf{r}) + \frac{\delta E_{\mathrm{Hxc}}[n]}{\delta\varphi_i^*(\mathbf{r})} \right] \delta\varphi_i^*(\mathbf{r}) = 0. \tag{51}$$

Using the formula for the functional derivative in Eq. (42), one gets

$$\delta\mathcal{L}[\{\varphi_i\}_i] = \int \frac{\delta\mathcal{L}[\{\varphi_i\}]}{\delta\varphi_i^*(\mathbf{r})} \delta\varphi_i^*(\mathbf{r})\mathrm{d}\mathbf{r}, \tag{52}$$

so that

$$\left(-\frac{1}{2}\nabla^2 + v_{\mathrm{ne}}(\mathbf{r}) - \varepsilon_k\right)\varphi_k(\mathbf{r}) + \frac{\delta E_{\mathrm{Hxc}}[n]}{\delta\varphi_i^*(\mathbf{r})} = 0. \tag{53}$$

Finally, using the chain rules in Eq. (43), we have

$$\frac{\delta E_{\mathrm{Hxc}}[n]}{\delta\varphi_k^*(\mathbf{r})} = \int \frac{\delta E_{\mathrm{Hxc}}[n]}{\delta n(\mathbf{r}')}\frac{\delta n(\mathbf{r}')}{\delta\varphi_k^*(\mathbf{r})}\mathrm{d}\mathbf{r}', \tag{54}$$

where $n = \sum_{i=1}^{N}|\varphi_i(\mathbf{r})|^2$ so that

$$\frac{\delta n(\mathbf{r}')}{\delta\varphi_k^*(\mathbf{r})} = \varphi_k(\mathbf{r})\delta(\mathbf{r}-\mathbf{r}'), \tag{55}$$

with $\delta(\mathbf{r}-\mathbf{r}')$ is the delta function. Therefore, Eq. (54) becomes

$$\frac{\delta E_{\mathrm{Hxc}}[n]}{\delta\varphi_k^*(\mathbf{r})} = \frac{\delta E_{\mathrm{Hxc}}[n]}{\delta n(\mathbf{r})}\varphi_k(\mathbf{r}), \tag{56}$$

and Eq. (53) turns to the self-consistent KS equations:

$$\left(-\frac{1}{2}\nabla^2 + v_{\mathrm{ne}}(\mathbf{r}) + \frac{\delta E_{\mathrm{Hxc}}[n]}{\delta n(\mathbf{r})}\right)\varphi_i(\mathbf{r}) = \varepsilon_i\varphi_i(\mathbf{r}). \tag{57}$$

C Real-space and orbital-space Second Quantization

Starting with the Schödinger theory, the quantum state of a single electron in the so-called "**r**-representation" is written as:

$$|\Psi\rangle = \int \mathrm{d}\mathbf{r}\Psi(\mathbf{r})|\mathbf{r}\rangle, \tag{58}$$

where $\Psi(\mathbf{r}) = \langle\mathbf{r}|\Psi\rangle$ is the one-electron wavefunction which is continuous in the coordinate space, and $|\mathbf{r}\rangle$ is the quantum state describing the electron at position $\mathbf{r}$. In Pauli theory where the spin σ of the electron is considered as an additional degree of freedom, the quantum state of a single electron is written as:

$$|\Psi_\sigma\rangle = \int \mathrm{d}\mathbf{r}\Psi(\mathbf{r})|\mathbf{r},\sigma\rangle, \tag{59}$$

where $|\mathbf{r},\sigma\rangle$ denotes the quantum state describing the electron at position $\mathbf{r}$ with spin σ, with $\sigma = \{\uparrow,\downarrow\}$. In Eq. (1.5), the electronic Hamiltonian has been written in the first quantization formalism.

An alternative and more compact formulation is provided by the second quantization [3, 536]. This second quantization can be formulated in different manner. First of all, we focus on the real-space second quantization, where the creation and annihilation operators are field operators $\hat{\Psi}^\dagger_\sigma(\mathbf{r})$ and $\hat{\Psi}_\sigma(\mathbf{r})$, which creates or destroys an electron at position $\mathbf{r}$ with spin σ, respectively, so that

$$|\Psi_\sigma\rangle = \int \mathrm{d}\mathbf{r} \Psi(\mathbf{r})|\mathbf{r}, \sigma\rangle = \int \mathrm{d}\mathbf{r} \Psi(\mathbf{r})\hat{\Psi}^\dagger_\sigma(\mathbf{r})|\mathrm{vac}\rangle, \tag{60}$$

with $\hat{\Psi}^\dagger_\sigma(\mathbf{r})|\mathrm{vac}\rangle = |\mathbf{r}, \sigma\rangle$. These operators are satisfying several rules, such as $\hat{\Psi}^\dagger_\sigma(\mathbf{r})|\mathbf{r}, \sigma\rangle = \hat{\Psi}_\sigma(\mathbf{r})|\mathrm{vac}\rangle = 0$: it is impossible to create an electron at position $\mathbf{r}$ with spin σ if one is already there, as well as it is impossible to destroy an electron that does not exist. In order to enforce the Pauli exclusion principle, these operators fulfill the following anticommutation relations:

$$\begin{aligned}
\Big[\hat{\Psi}^\dagger_\sigma(\mathbf{r}), \hat{\Psi}^\dagger_{\sigma'}(\mathbf{r}')\Big]_+ &= 0, \\
\Big[\hat{\Psi}_\sigma(\mathbf{r}), \hat{\Psi}_{\sigma'}(\mathbf{r}')\Big]_+ &= 0, \\
\Big[\hat{\Psi}^\dagger_\sigma(\mathbf{r}), \hat{\Psi}_{\sigma'}(\mathbf{r}')\Big]_+ &= \delta(\mathbf{r}-\mathbf{r}')\delta_{\sigma\sigma'},
\end{aligned} \tag{61}$$

where $\delta_{\sigma\sigma'}$ and $\delta(\mathbf{r}-\mathbf{r}')$ are the Kronecker delta and the Dirac delta function, respectively. Within the real-space second quantization, the Hamiltonian reads:

$$\begin{aligned}
\hat{H} &= \hat{T} + \hat{V}_{\mathrm{ne}} + \hat{W}_{\mathrm{ee}}, \\
\hat{T} &= -\frac{1}{2}\int\int \mathrm{d}\mathbf{r}\mathrm{d}\mathbf{r}'\delta(\mathbf{r}-\mathbf{r}')\nabla^2 \sum_\sigma \hat{\Psi}^\dagger_\sigma(\mathbf{r})\hat{\Psi}_\sigma(\mathbf{r}'), \\
\hat{V}_{\mathrm{ne}} &= \int \mathrm{d}\mathbf{r}\, v_{\mathrm{ne}}(\mathbf{r}) \sum_\sigma \hat{\Psi}^\dagger_\sigma(\mathbf{r})\hat{\Psi}_\sigma(\mathbf{r}), \\
\hat{W}_{\mathrm{ee}} &= \int\int \mathrm{d}\mathbf{r}\mathrm{d}\mathbf{r}' \sum_{\sigma,\sigma'} \frac{\hat{\Psi}^\dagger_\sigma(\mathbf{r})\hat{\Psi}^\dagger_{\sigma'}(\mathbf{r}')\hat{\Psi}_{\sigma'}(\mathbf{r}')\hat{\Psi}_\sigma(\mathbf{r})}{|\mathbf{r}-\mathbf{r}'|},
\end{aligned} \tag{62}$$

where we define the density matrix operator:

$$\hat{\gamma}(\mathbf{r}, \mathbf{r}') = \sum_\sigma \hat{\Psi}^\dagger_\sigma(\mathbf{r})\hat{\Psi}_\sigma(\mathbf{r}'), \tag{63}$$

the density operator:

$$\hat{n}(\mathbf{r}) = \hat{\gamma}(\mathbf{r}, \mathbf{r}) = \sum_\sigma \hat{\Psi}^\dagger_\sigma(\mathbf{r})\hat{\Psi}_\sigma(\mathbf{r}), \tag{64}$$

and the pair density operator:

$$\hat{n}(\mathbf{r},\mathbf{r}') = \sum_{\sigma,\sigma'} \hat{\Psi}^{\dagger}_{\sigma}(\mathbf{r})\hat{\Psi}^{\dagger}_{\sigma'}(\mathbf{r}')\hat{\Psi}_{\sigma'}(\mathbf{r}')\hat{\Psi}_{\sigma}(\mathbf{r}), \tag{65}$$

in real-space second quantization. The expectation value of each of these operators gives the one-particle density matrix,

$$\gamma(\mathbf{r},\mathbf{r}') = \sum_{\sigma} \langle \Psi | \hat{\Psi}^{\dagger}_{\sigma}(\mathbf{r})\hat{\Psi}_{\sigma}(\mathbf{r}') | \Psi \rangle, \tag{66}$$

the electronic density,

$$n(\mathbf{r}) = \sum_{\sigma} \langle \Psi | \hat{\Psi}^{\dagger}_{\sigma}(\mathbf{r})\hat{\Psi}_{\sigma}(\mathbf{r}) | \Psi \rangle, \tag{67}$$

and the pair density (which is the diagonal of the 2RDM in real-space),

$$n(\mathbf{r},\mathbf{r}') = \sum_{\sigma,\sigma'} \langle \Psi | \hat{\Psi}^{\dagger}_{\sigma}(\mathbf{r})\hat{\Psi}^{\dagger}_{\sigma'}(\mathbf{r}')\hat{\Psi}_{\sigma'}(\mathbf{r}')\hat{\Psi}_{\sigma}(\mathbf{r}) | \Psi \rangle, \tag{68}$$

respectively. The expectation value of the Hamiltonian is given in Sec. 1.2.2 in the context of RDMFT [Eq. (1.129)].

Alternatively when working in a given orbital basis set $\{|\varphi_i\rangle\}_i$ one can use creation ($\hat{c}^{\dagger}_{i\sigma}$) and annihilation ($\hat{c}_{i\sigma}$) operators to create or destroy an electron of spin σ in the ith orbital, respectively, so that $\hat{c}^{\dagger}_{i\sigma}|\text{vac}\rangle = |\varphi_{\text{i}}\rangle \otimes |\sigma\rangle = |\varphi_{\text{i}}, \sigma\rangle$. These operators are orbital-space operators and also fulfill the anticommutation rules:

$$\begin{aligned}
\left[\hat{c}^{\dagger}_{i\sigma}, \hat{c}^{\dagger}_{j\sigma'}\right]_+ &= 0, \\
\left[\hat{c}_{i\sigma}, \hat{c}_{j\sigma'}\right]_+ &= 0, && (69) \\
\left[\hat{c}^{\dagger}_{i\sigma}, \hat{c}_{j\sigma'}\right]_+ &= \delta_{ij}\delta_{\sigma\sigma'}. && (70)
\end{aligned}$$

In contrast to the field operator which act in the real space by creating or annihilating electrons at a given position, these new operators create and annihilate electrons in orbitals which are delocalized in space. The quantum state of one electron can therefore be rewritten as

$$|\Psi_\sigma\rangle = \sum_i C_i |\varphi_i, \sigma\rangle. \tag{71}$$

In this basis, the wavefunction is now represented by the coefficients C_i forming a vector column. In principle, the basis set should be infinite, but in practice it will be finite so that the column vector will have a finite dimension. Note that in the "**r**-representation", the wavefunction cannot be written as a vector column as it is continuous in the coordinate space. Within this orbital-space second quantization, the Hamiltonian reads:

$$\begin{aligned}
\hat{H} &= \hat{h} + \hat{W}_{\mathrm{ee}}, \\
\hat{h} &= \sum_{ij\sigma} h_{ij} \hat{c}^\dagger_{i\sigma} \hat{c}_{j\sigma}, \\
\hat{W}_{\mathrm{ee}} &= \frac{1}{2} \sum_{ijkl\sigma\sigma'} U_{ijkl} \hat{c}^\dagger_{i\sigma} \hat{c}^\dagger_{k\sigma'} \hat{c}_{l\sigma'} \hat{c}_{j\sigma}
\end{aligned} \tag{72}$$

where $\hat{h}$ denotes the one-electron operator of the Hamiltonian, containing the kinetic operator and the nuclei potential operator, and

$$h_{ij} = \langle \varphi_i | \hat{h} | \varphi_j \rangle = \int \mathrm{d}\mathbf{r} \varphi_i^*(\mathbf{r}) \hat{h} \varphi_j(\mathbf{r}), \tag{73}$$

$$U_{ijkl} = \langle ij | kl \rangle = \iint \mathrm{d}\mathbf{r}\mathrm{d}\mathbf{r}' \frac{\varphi_i^*(\mathbf{r}) \varphi_j^*(\mathbf{r}') \varphi_k(\mathbf{r}) \varphi_l(\mathbf{r}')}{|\mathbf{r} - \mathbf{r}'|} \tag{74}$$

are the one and two-electron integrals, respectively. The summations and indices in the Hamiltonian in Eq. (1.5), written in first quantization, refer to the electrons, such that this Hamiltonian depends on the number of electrons in the system. On the contrary, the indices in Eq. (72), written in orbital-space second quantization, are orbital indices and the number of electrons is no more specified. The former formalism (first quantization) can be seen as an answer to the question : "Who occupies what ?", while the latter (second quantization) rather answers to "What is occupied ?"[1].

D Passing from the real space to the orbital space

Based on the second quantization presented in the previous section, the connection between the real space and the orbital space is studied, through the expression of the real-space density and the real-

---

[1] From a lecture of Emmanuel Fromager in the ISTPC Summer School, Aussois (FRANCE), 2017

space one-particle density matrix in the orbital space. Thanks to the identity relation,

$$\sum_i |\varphi_i\rangle\langle\varphi_i| = \mathbb{1}, \tag{75}$$

we define $|\mathbf{r}\rangle = \sum_i |\varphi_i\rangle\langle\varphi_i|\mathbf{r}\rangle = \sum_i \varphi_i^*(\mathbf{r})|\varphi_i\rangle$ which connects the real-space to the orbital-space second quantized operators:

$$\begin{aligned} \hat{\Psi}_\sigma^\dagger(\mathbf{r})|\text{vac}\rangle &= |\mathbf{r},\sigma\rangle = |\mathbf{r}\rangle \otimes |\sigma\rangle \\ &= \sum_p \varphi_i^*(\mathbf{r})|\varphi_i\rangle \otimes |\sigma\rangle = \sum_p \varphi_i^*(\mathbf{r})|\varphi_i,\sigma\rangle = \sum_p \varphi_i^*(\mathbf{r})\hat{c}_{i\sigma}^\dagger|\text{vac}\rangle. \end{aligned} \tag{76}$$

One can therefore pass from one space to another by a simple change of basis:

$$\hat{\Psi}_\sigma^\dagger(\mathbf{r}) = \sum_i \varphi_i^*(\mathbf{r})\hat{c}_{i\sigma}^\dagger, \qquad \hat{\Psi}_\sigma(\mathbf{r}) = \sum_i \varphi_i(\mathbf{r})\hat{c}_{i\sigma}. \tag{77}$$

Note that plugging this change of basis in Eq. (60) allows one to recover Eq. (71) where $C_i = \int \mathrm{d}\mathbf{r}\varphi_i^*(\mathbf{r})\Psi(\mathbf{r}) = \langle\varphi_i|\Psi\rangle$. The reverse transformation is of course possible and reads:

$$\hat{c}_{i\sigma}^\dagger = \int \mathrm{d}\mathbf{r}\varphi_i(\mathbf{r})\hat{\Psi}_\sigma^\dagger(\mathbf{r}), \qquad \hat{c}_{i\sigma} = \int \mathrm{d}\mathbf{r}\varphi_i^*(\mathbf{r})\hat{\Psi}_\sigma(\mathbf{r}). \tag{78}$$

Plugging Eq. (77) into the real-space electronic density in Eq. (67),

$$\begin{aligned} \hat{n}(\mathbf{r}) &= \sum_\sigma \hat{\Psi}_\sigma^\dagger(\mathbf{r})\hat{\Psi}_\sigma(\mathbf{r}) \\ &= \sum_\sigma \sum_{ij} \varphi_i^*(\mathbf{r})\varphi_j(\mathbf{r})\hat{c}_{i\sigma}^\dagger\hat{c}_{j\sigma}, \end{aligned} \tag{79}$$

we find that the real-space density is defined by taking all the density matrix elements $D_{ij} = \langle\Psi|\sum_\sigma \hat{c}_{i\sigma}^\dagger\hat{c}_{j\sigma}|\Psi\rangle$,

$$n(\mathbf{r}) = \sum_{ij} \varphi_i^*(\mathbf{r})\varphi_j(\mathbf{r})D_{ij}. \tag{80}$$

Therefore, we need the whole orbital-space density matrix to recover the real-space density. Please note that D_{ij} is the analog of $\gamma(\mathbf{r},\mathbf{r}')$ but in the orbital-space. Indeed, plugging Eq. (77) into the real-space density matrix in Eq. (66) leads to

$$\hat{\gamma}(\mathbf{r},\mathbf{r}') = \sum_\sigma \sum_{ij} \varphi_i^*(\mathbf{r})\varphi_j(\mathbf{r}')\hat{c}_{i\sigma}^\dagger\hat{c}_{j\sigma}, \tag{81}$$

so that

$$\gamma(\mathbf{r},\mathbf{r}') \quad = \quad \sum_{ij}\varphi_i^*(\mathbf{r})\varphi_j(\mathbf{r}')D_{ij}. \tag{82}$$

Passing from $\gamma(\mathbf{r},\mathbf{r}')$ to D_{ij} is also possible using Eq. (78):

$$\sum_\sigma \hat{a}_i^\dagger \hat{a}_{j\sigma} = \sum_\sigma \int \mathrm{d}\mathbf{r} \int \mathrm{d}\mathbf{r}' \varphi_i(\mathbf{r})\varphi_j^*(\mathbf{r}')\hat{\Psi}_\sigma^\dagger(\mathbf{r})\hat{\Psi}_\sigma(\mathbf{r}'), \tag{83}$$

so that

$$D_{ij} \quad = \quad \int \mathrm{d}\mathbf{r} \int \mathrm{d}\mathbf{r}' \varphi_i(\mathbf{r})\varphi_j^*(\mathbf{r}')\gamma(\mathbf{r},\mathbf{r}'). \tag{84}$$

The only case where the diagonal of the orbital-space density matrix is sufficient is when the basis set is composed of natural orbitals. For instance, in KSDFT, the basis set is constituted of orthonormal KS orbitals forming a single Slater determinant. In this basis, the density matrix is diagonal and its diagonal coefficients are the occupation number of the KS orbitals, that are either equal to 2 or 0 in the spin-restricted formalism. Because it is diagonal, the density of the KS system is written as

$$n(\mathbf{r}) = 2\sum_{i=1}^{N/2} |\varphi_i^{\mathrm{KS}}(\mathbf{r})|. \tag{85}$$

The summation goes up to all the occupied orbitals, so $N/2$ orbitals in the case of a spin-restricted closed-shell system. This is the case for any theory written in the basis forming a single Slater determinant.

E Derivatives of BALDA

E.1 Derivative with respect to U and t

As readily seen in Eq. (3.39), the derivative of the complementary bath per-site correlation energy functional with respect to U is necessary to compute double occupation in SOET. According to Eq. (3.19), it implies the derivative of the conventional per-site correlation energy, modelled with BALDA, which reads

$$\frac{\partial e_{\mathrm{c}}^{\mathrm{BALDA}}(n \leqslant 1, U/t)}{\partial U} = \frac{\partial \beta(U/t)}{\partial U}\left[\frac{-2t}{\pi}\sin\left(\frac{\pi n}{\beta(U/t)}\right) + \frac{2tn}{\beta(U/t)}\cos\left(\frac{\pi n}{\beta(U/t)}\right)\right] - \frac{n^2}{4}, \tag{86}$$

and then for $n > 1$,

$$\begin{aligned}\frac{\partial e_{\mathrm{c}}^{\mathrm{BALDA}}(n>1,U/t)}{\partial U} &= \frac{\partial\beta(U/t)}{\partial U}\left[\frac{-2t}{\pi}\sin\left(\frac{\pi(2-n)}{\beta(U/t)}\right)+\frac{2t(2-n)}{\beta(U/t)}\cos\left(\frac{\pi(2-n)}{\beta(U/t)}\right)\right]\\ &+(n-1)-\frac{n^2}{4},\end{aligned} \tag{87}$$

where $\partial\beta(U/t)/\partial U = (\partial\beta(U/t)/\partial(U/t))/t$, is computed with finite differences by solving Eq. (2.81) for $\beta(U/t)$.

The derivative with respect to t are calculated according to Eq. (3.29).

E.2 Derivative with respect to n

To get the correlation embedding potential, the derivatives of the correlation functionals with respect to n is necessary. The derivative of the convention per-site density-functional correlation energy reads

$$\frac{\partial e_{\mathrm{c}}^{\mathrm{BALDA}}(n\leqslant 1)}{\partial n} = -2t\cos\left(\frac{\pi n}{\beta(U/t)}\right)+2t\cos\left(\frac{\pi n}{2}\right)-\frac{Un}{2}, \tag{88}$$

and

$$\frac{\partial e_{\mathrm{c}}^{\mathrm{BALDA}}(n>1)}{\partial n} = 2t\cos\left(\frac{\pi(2-n)}{\beta(U/t)}\right)-2t\cos\left(\frac{\pi(2-n)}{2}\right)+U-\frac{Un}{2}. \tag{89}$$

F Derivatives of SIAM-BALDA

The derivatives of the SIAM-BALDA impurity correlation functional [Eq. (3.94) combined with Eq. (3.103)] are given with respect to U for $n \leqslant 1$ as follows,

$$\frac{\partial E_{\mathrm{c},U/\Gamma\to 0}^{\mathrm{SIAM}}(U,\Gamma(t,n))}{\partial U} = -\frac{2\times 0.0369}{\pi}\left(\frac{U}{\Gamma(t,n)}\right)+\frac{4\times 0.0008}{\pi^3}\left(\frac{U}{\Gamma(t,n)}\right)^3. \tag{90}$$

The derivative with respect to t is given according to Eq. (3.30). Then, the impurity correlation potential is determined by the derivative of the functional with respect to the occupation number n,

$$\frac{\partial E_{\mathrm{c},U/\Gamma\to 0}^{\mathrm{SIAM}}(U,\Gamma(t,n))}{\partial n} = \frac{\partial\Gamma(t,n)}{\partial n}\left.\frac{\partial E_{\mathrm{c},U/\Gamma\to 0}^{\mathrm{SIAM}}(U,\Gamma)}{\partial\Gamma}\right|_{\Gamma=\Gamma(t,n)}, \tag{91}$$

where

$$\frac{\partial E_{\mathrm{c},U/\Gamma\to 0}^{\mathrm{SIAM}}(U,\Gamma)}{\partial\Gamma} = \frac{0.0369}{\pi}\left(\frac{U}{\Gamma}\right)^2-\frac{3\times 0.0008}{\pi^3}\left(\frac{U}{\Gamma}\right)^4, \tag{92}$$

and

$$\begin{aligned}\frac{\partial\Gamma(t,n)}{\partial n} &= t\left(\frac{-\frac{\pi}{2}\sin^2(\pi n/2)-(1+\cos(\pi n/2))\frac{\pi}{2}\cos(\pi n/2)}{\sin^2(\pi n/2)}\right)\\ &= -\frac{\pi t}{2}\left(\frac{1+\cos(\pi n/2)}{\sin^2(\pi n/2)}\right)=-\frac{\pi\Gamma(t,n)}{2\sin(\pi n/2)}.\end{aligned} \tag{93}$$

If $n > 1$, the particle-hole formalism imposes to use $\Gamma(t, 2-n)$ instead of $\Gamma(t, n)$. The derivatives with respect to n should be changed accordingly.

G Derivatives of 2L-BALDA

G.1 Parametrization of the correlation energy of the dimer

In this section, we summarize the parametrization of the Hubbard dimer correlation energy by Carrascal and co-workers [335, 358], necessary to understand the following derivations. The equations coming from their paper are referred to as (&N), where N is the number of the equation. We start from the definition of the correlation energy, where n is the occupation of the site 0 and $u = U/2t$ is a dimensionless parameter,

$$E_{\rm c}^{\rm 2L}(U,n)=f(g,\rho)\Big|_{\substack{g=g(\rho,u)\\ \rho=|n-1|}}-T_{\rm s}(n)-E_{\rm Hx}(U,n), \tag{94}$$

where 2L refers to “two-level”, and

$$T_{\rm s}(n)=-2t\sqrt{n(2-n)},\qquad E_{\rm Hx}(U,n)=U\left(1-n\left(1-\frac{n}{2}\right)\right). \tag{95}$$

To account for particle-hole symmetry of the functional, the variable $\rho = |n-1|$ is used rather than n directly. We now simply follow the guidelines from Eq.(&102) to (&107), leading to

$$f(g,\rho)=-2tg+Uh(g,\rho), \tag{96}$$

and

$$h(g,\rho)=\frac{g^2\left(1-\sqrt{1-\rho^2-g^2}\right)+2\rho^2}{2(g^2+\rho^2)}. \tag{97}$$

Then, they proposed a first approximation to $g(\rho, u)$, denoted by the label 0:

$$g_0(\rho, u) = \sqrt{\frac{(1-\rho)(1+\rho(1+(1+\rho)^3 u a_1(\rho, u)))}{1+(1+\rho)^3 u a_2(\rho, u)}}, \tag{98}$$

where

$$a_i(\rho, u) = a_{i1}(\rho) + u a_{i2}(\rho), \quad i = 1, 2 \tag{99}$$

and

$$a_{21}(\rho) = \frac{1}{2}\sqrt{\frac{\rho(1-\rho)}{2}}, \quad a_{12}(\rho) = \frac{1}{2}(1-\rho), \quad a_{11}(\rho) = a_{12}\left(1+\frac{1}{\rho}\right), \quad a_{22}(\rho) = \frac{a_{12}(\rho)}{2}. \tag{100}$$

Plugging $g = g_0(\rho, u)$ into $f(g, \rho)$ leads to the first parametrization of $E_{\mathrm{c}}^{2L}(n)$ in Eq. (94). In this work, we implemented the more accurate parametrization, given in Eq.(&114) [358]:

$$g_1(\rho, u) = g_0(\rho, u) + \left(u \left.\frac{\partial h(g, \rho)}{\partial \rho}\right|_{g=g_0(\rho, u)} - 1\right) q(\rho, u), \tag{101}$$

and where $q(\rho, u)$ is given in Eq. (&115) by [358]:

$$q(\rho, u) = \frac{(1-\rho)(1+\rho)^3 u^2[(3\rho/2 - 1 + \rho(1+\rho)^3 u a_2(\rho, u))a_{12}(\rho) - \rho(1+(1+\rho)^3 u a_1(\rho, u))a_{22}(\rho)]}{2g_0(\rho, u)(1+(1+\rho)^3 u a_2(\rho, u))^2}. \tag{102}$$

The accurate parametrization of $E_{\mathrm{c}}^{2L}(n)$ is obtained by plugging this $g_1(\rho, u)$ into $f(g, \rho)$, instead of $g_0(\rho, u)$.

In order to obtain the impurity correlation energy, a simple scaling of the interaction parameter U has to be applied on the conventional correlation energy, as demonstrated in Ref. [72], leading to

$$E_{\mathrm{c}}^{\mathrm{imp,2L}}(U, n) = E_{\mathrm{c}}^{2L}(U/2, n) = f(g, \rho)\Big|_{\substack{g=g(\rho, u/2)\\ \rho=|n-1|}} - T_{\mathrm{s}}(n) - E_{\mathrm{Hx}}(U/2, n). \tag{103}$$

G.2 Derivative with respect to U and t

We compute the derivative with respect to the dimensionless parameter $u = U/2t$. The ρ- and u-dependence of $g(\rho, u)$ will be omitted for readability. Besides, many functions will be introduced, aiming to make the implementation and its numerical verification easier. Starting with

$$\frac{\partial E_{\mathrm{c}}^{2\mathrm{L}}(n)}{\partial U} = \frac{1}{2t} \left.\frac{\partial f(g, \rho)}{\partial u}\right|_{\substack{g=g(\rho, u)\\ \rho=|n-1|}} - \left(1 + n\left(\frac{1}{2}n - 1\right)\right), \tag{104}$$

the impurity correlation functional reads, according to Eq. (103),

$$\frac{\partial E_{\rm c}^{\rm imp,2L}(n)}{\partial U} = \frac{1}{4t}\left.\frac{\partial f(g,\rho)}{\partial u}\right|_{\substack{g=g(\rho,u/2)\\ \rho=|n-1|}} - \frac{1}{2}\left(1+n\left(\frac{1}{2}n-1\right)\right), \tag{105}$$

with

$$\frac{\partial f(g,\rho)}{\partial u} = -2t\left(\frac{\partial g}{\partial u} - h(g,\rho) - u\times\frac{\partial h(g,\rho)}{\partial u}\right). \tag{106}$$

The derivative of $h(g,\rho)$ is quite easy, as its only u-dependence is contained in g, so that:

$$\frac{\partial h(g,\rho)}{\partial u} = \frac{\partial g}{\partial u}\frac{\partial h(g,\rho)}{\partial g}, \tag{107}$$

with

$$\frac{\partial h(g,\rho)}{\partial g} = g\frac{g^4+3g^2\rho^2+2\rho^2\left(\rho^2-1-Y(g,\rho)\right)}{2\left(g^2+\rho^2\right)^2 Y(g,\rho)}, \tag{108}$$

where the function $Y(g,\rho)=\sqrt{1-g^2-\rho^2}$ has been introduced. For the first approximation, $g=g_0$ and

$$\frac{\partial g_0(\rho,u)}{\partial u} = \frac{\partial\sqrt{G(\rho,u)}}{\partial u} = \frac{\partial G(\rho,u)/\partial u}{2\sqrt{G(\rho,u)}}, \tag{109}$$

where $G(\rho,u)=N(\rho,u)/D(\rho,u)$ and

$$N(\rho,u) = (1-\rho)\left[1+\rho\left(1+(1+\rho)^3ua_1(\rho,u)\right)\right], \tag{110}$$

$$D(\rho,u) = 1+(1+\rho)^3ua_2(\rho,u). \tag{111}$$

Their respective derivative with respect to u reads

$$\frac{\partial N(\rho,u)}{\partial u} = (1-\rho)\rho(1+\rho)^3\left(a_1(\rho,u)+u\frac{\partial a_1(\rho,u)}{\partial u}\right), \tag{112}$$

$$\frac{\partial D(\rho,u)}{\partial u} = (1+\rho)^3\left(a_2(\rho,u)+u\frac{\partial a_2(\rho,u)}{\partial u}\right), \tag{113}$$

with

$$\frac{\partial a_2(\rho,u)}{\partial u} = a_{22}(\rho), \qquad \frac{\partial a_1(\rho,u)}{\partial u} = a_{12}(\rho). \tag{114}$$

Turning to the second approximation $g = g_1$ implemented in this work, one get from the derivative of Eq. (101),

$$\frac{\partial g_1}{\partial u} = \frac{\partial g_0}{\partial u} + \left(\left.\frac{\partial h(g,u)}{\partial g}\right|_{g=g_0} + u\frac{\partial}{\partial u}\left(\left.\frac{\partial h(g,u)}{\partial g}\right|_{g=g_0}\right)\right) q(\rho,u) + \left(u\left.\frac{\partial h(g,u)}{\partial g}\right|_{g=g_0} - 1\right)\frac{\partial q(\rho,u)}{\partial u}. \tag{115}$$

For convenience, we introduce two functions $w(g,u)$ and $v(g,u)$ so that

$$\frac{\partial}{\partial u}\left(\frac{\partial h(g,u)}{\partial g}\right) = \left(\frac{\partial w(g,u)}{\partial u}v(g,u) - w(g,u)\frac{\partial v(g,u)}{\partial u}\right)\Big/ w(g,u)^2, \tag{116}$$

with

$$w(g,u) = g\left[g^4 + 3g^2\rho^2 + 2\rho^2\left(\rho^2 - 1 - Y(g,\rho)\right)\right], \tag{117}$$

$$v(g,u) = 2Y(g,\rho)\left(g^2+\rho^2\right)^2, \tag{118}$$

and

$$\frac{\partial w(g,u)}{\partial u} = \frac{\partial g}{\partial u}\left[g^4 + 3g^2\rho^2 + 2\rho^2\left(\rho^2 - 1 - Y(g,\rho)\right) + g\left(4g^3 + 6g\rho^2 + \frac{2\rho^2 g}{Y(g,\rho)}\right)\right], \tag{119}$$

$$\frac{\partial v(g,u)}{\partial u} = g\left(g^2+\rho^2\right)\frac{\partial g}{\partial u}\left[\frac{-2\left(g^2+\rho^2\right)}{Y(g,\rho)} + 8Y(g,\rho)\right]. \tag{120}$$

Finally, the last term in Eq. (115) reads, for $q(\rho,u) = j(\rho,u)k(\rho,u)/l(\rho,u)$:

$$\frac{\partial q(\rho,u)}{\partial u} = \frac{\left(\frac{\partial j(\rho,u)}{\partial u}k(\rho,u) + j(\rho,u)\frac{\partial k(\rho,u)}{\partial u}\right) l(\rho,u) - j(\rho,u)k(\rho,u)\frac{\partial l(\rho,u)}{\partial u}}{l(\rho,u)^2} \tag{121}$$

with

$$j(\rho,u) = (1-\rho)(1+\rho)^3u^2, \tag{122}$$

$$k(\rho,u) = \left(3\rho/2 - 1 + \rho(1+\rho)^3ua_2(\rho,u)\right)a_{12}(\rho) - \rho\left(1 + (1+\rho)^3\lambda u a_1(\rho,u)\right)a_{22}(\rho) \tag{123}$$

$$l(u) = 2g_0(u)\left[1 + (1+\rho)^3\lambda u a_2(\rho,u,\lambda)\right]^2, \tag{124}$$

and their derivative with respect the u:

$$\begin{aligned}
\frac{\partial j(\rho,u)}{\partial u} &= 2(1-\rho)(1+\rho)^3\lambda u \\
\frac{\partial k(u)}{\partial u} &= a_{12}(\rho)\left[\rho(1+\rho)^3\left(a_2(\rho,u)+u\frac{\partial a_2(\rho,u)}{\partial u}\right)\right]-a_{22}(\rho)\left[\rho(1+\rho)^3\left(a_1(\rho,u)+u\frac{\partial a_1(\rho,u)}{\partial u}\right)\right] \\
\frac{\partial l(u)}{\partial u} &= 4g_0(u)\left[1+(1+\rho)^3ua_2(\rho,u)\right](1+\rho)^3\left(a_2(\rho,u)+u\frac{\partial a_2(\rho,u)}{\partial u}\right) \\
&\quad +2\frac{\partial g_0}{\partial u}\left[1+(1+\rho)^3\lambda ua_2(\rho,u)\right]^2 .
\end{aligned} \tag{125}$$

The derivative with respect to t is given according to Eq. (3.30).

G.3 Derivative with respect to n

Regarding the derivative with respect to n which is necessary to get the embedded correlation potential, it comes

$$\frac{\partial E_{\mathrm{c}}^{\mathrm{imp,2L}}(n)}{\partial n}=\frac{\partial\rho}{\partial n}\left.\frac{f(g,\rho)}{\partial\rho}\right|_{\substack{g=g(\rho,u/2)\\ \rho=|n-1|}}-\frac{\partial\mathcal{T}_s(n)}{\partial n}-\frac{U}{2} \tag{126}$$

where $\partial\rho/\partial n=\mathrm{sign}(n-1)$ and

$$\frac{\partial\mathcal{T}_s(n)}{\partial n}=-\frac{2t(1-n)}{\sqrt{n(2-n)}}. \tag{127}$$

We start with

$$\frac{\partial f(g,\rho)}{\partial\rho}=-2t\frac{\partial g}{\partial\rho}+U\frac{\partial h(g,\rho)}{\partial\rho}, \tag{128}$$

where, for the first parametrization using $g=g_0(\rho,u)$,

$$\frac{\partial g_0}{\partial\rho} \quad = \quad =\frac{1}{2g_0D(\rho,u)}\left(\frac{\partial N(\rho,u)}{\partial\rho}-g_0^2\frac{\partial D(\rho,u)}{\partial\rho}\right), \tag{129}$$

with

$$\begin{aligned}
\frac{\partial N(\rho,u)}{\partial\rho} &= -1+(1-2\rho)\left(1+(1+\rho)^3ua_1(\rho,u)\right)+\rho u(1-\rho)(1+\rho)^2\left(3a_1(\rho,u)+(1+\rho)\frac{\partial a_1(\rho,u)}{\partial\rho}\right), \\
\frac{\partial D(\rho,u)}{\partial\rho} &= u(1+\rho)^2\left(3a_2(\rho,u)+(1-\rho)\frac{\partial a_2(\rho,u)}{\partial\rho}\right),
\end{aligned} \tag{130}$$

and

$$
\begin{aligned}
\frac{\partial a_1(\rho,u)}{\partial\rho} &= \frac{\partial a_{11}(\rho)}{\partial\rho} + u\frac{\partial a_{12}(\rho)}{\partial\rho}, && (131)\\
\frac{\partial a_2(\rho,u)}{\partial\rho} &= \frac{\partial a_{21}(\rho)}{\partial\rho} + u\frac{\partial a_{22}(\rho)}{\partial\rho} && (132)\\
\frac{\partial a_{12}(\rho)}{\partial\rho} &= 2\frac{\partial a_{22}(\rho)}{\partial\rho} = -\frac{1}{2}, && (133)\\
\frac{\partial a_{21}(\rho)}{\partial\rho} &= \frac{1-2\rho}{2\sqrt{(1-\rho)\rho/2}}, && (134)\\
\frac{\partial a_{11}(\rho)}{\partial\rho} &= \frac{\partial a_{21}(\rho)}{\partial\rho}\left(1+\frac{1}{\rho}\right) - \frac{1}{\rho^2}a_{21}(\rho). && (135)\\
& && (136)
\end{aligned}
$$

Then, the right term in the right hand side of Eq. (128) is derived as:

$$
\begin{aligned}
\frac{\partial h(g,\rho)}{\partial\rho} = {} & \frac{1}{2(g^2+\rho^2)}\left(4\rho + 2g\frac{\partial g}{\partial\rho}\left(1-Y(g,\rho)\right) + g^2\frac{g(\partial g/\partial\rho)+\rho}{Y(g,\rho)}\right)\\
& -\frac{g(\partial g/\partial\rho)+\rho}{(g^2+\rho^2)^2}\left(2\rho^2 + g^2\left(1-Y(g,\rho)\right)\right). \qquad (137)
\end{aligned}
$$

Turning to the second parametrization $g = g_1$, the derivative with respect to ρ leads to

$$
\frac{\partial g_1}{\partial\rho} = \frac{\partial g_0}{\partial\rho} + \left(u\left.\frac{\partial h(g,\rho)}{\partial g}\right|_{g=g_0} - 1\right)\frac{\partial q(\rho,u)}{\partial\rho} + u\frac{\partial}{\partial\rho}\left(\left.\frac{\partial h(g,\rho)}{\partial g}\right|_{g=g_0}\right)q(\rho,u) \qquad (138)
$$

with

$$
\begin{aligned}
\frac{\partial}{\partial\rho}\left(\frac{\partial h(g,\rho)}{\partial g}\right) = {} & \frac{-(\partial g/\partial\rho)(g^2+\rho^2) + 4g(g(\partial g/\partial\rho)+\rho)}{(g^2+\rho^2)^3}\left(2\rho^2 + g^2(1-Y(g,\rho))\right)\\
& -\frac{g}{(g^2+\rho^2)^2}\left(4\rho + 2g\frac{\partial g}{\partial\rho}\left(1-Y(g,\rho)\right) + g^2\frac{g(\partial g/\partial\rho)+\rho}{Y(g,\rho)}\right)\\
& -\frac{g(\partial g/\partial\rho)+\rho}{(g^2+\rho^2)^2}\left(2g(1-Y(g,\rho)) + \frac{g^3}{Y(g,\rho)}\right)\\
& +\frac{1}{2(g^2+\rho^2)}\left(2\frac{\partial g}{\partial\rho}(1-Y(g,\rho)) + \frac{2g\rho}{Y(g,\rho)} + \frac{5g^2(\partial g/\partial\rho)}{Y(g,\rho)} + g^3\frac{g(\partial g/\partial\rho)+\rho}{Y(g,\rho)^3}\right).\\
& \qquad (139)
\end{aligned}
$$

Finally,

$$
\frac{\partial q(\rho,u)}{\partial\rho} = \left(\frac{\partial P(\rho,u)}{\partial\rho}Q(\rho,u) - P(\rho,u)\frac{\partial Q(\rho,u)}{\partial\rho}\right)\Big/ Q(\rho,u)^2, \qquad (140)
$$

with

$$\begin{aligned}
\frac{\partial P(\rho,u)}{\partial\rho} &= \left(3(1-\rho)(1+\rho)^2-(1+\rho)^3\right)u^2\left[\left(\frac{3\rho}{2}-1+\rho(1+\rho)^3ua_2(\rho,u)\right)a_{12}(\rho)\right. \\
&\left.-\rho\left(1+(1+\rho)^3ua_1(\rho,u)\right)a_{22}(\rho)\right] \\
&+(1-\rho)(1+\rho)^3u^2\left[\left(\frac{3}{2}+3u(1+\rho)^2\rho a_2(\rho,u)+u(1+\rho)^3\left(a_2(\rho,u)+\rho\frac{\partial a_2(\rho,u)}{\partial\rho}\right)\right)a_{12}(\rho)\right. \\
&+\left(\frac{3\rho}{2}-1+\rho(1+\rho)^3ua_2(\rho,u)\right)\frac{\partial a_{12}(\rho)}{\partial\rho}-\left(\rho\frac{\partial a_{22}(\rho)}{\partial\rho}+a_{22}(\rho)\right)\left(1+(1+\rho)^3ua_1(\rho,u)\right) \\
&\left.-\rho a_{22}(\rho)\left(3(1+\rho)^2ua_1(\rho,u)+(1+\rho)^3u\frac{\partial a_1(\rho,u)}{\partial\rho}\right)\right] \qquad (141) \\
\frac{\partial Q(\rho,u)}{\partial\rho} &= 2\frac{\partial g_0}{\partial\rho}\left(1+(1+\rho)^3ua_2(\rho,u)\right)^2+4g_0\left(1+(1+\rho)^3\right. \\
&\left.\times\, ua_2(\rho,u)\right)u\left(3(1+\rho)^2a_2(\rho,u)+(1+\rho)^3\frac{\partial a_2(\rho,u)}{\partial\rho}\right). \qquad (142)
\end{aligned}$$

H Atomic orbitals and Basis set

An exact analytic solution of the Schrödinger equation for an atom or a molecule with more than one electron is not known. In order to approach numerically the exact solution for such systems, one has to construct molecular orbitals $\varphi_i(\mathbf{r})$ based on a linear combination of atomic orbitals (LCAO) $\chi_\mu(\mathbf{r})$:

$$\varphi_i(\mathbf{r})=\sum_{\mu=1}^{m}c_{\mu i}\chi_\mu(\mathbf{r}). \tag{143}$$

For instance, the $1s$ atomic orbital of the hydrogen atom is given by a Slater-type orbitals function $\chi_{1s}(\mathbf{r})=(1/\sqrt{\pi})e^{-r}$. Slater-type orbitals (STO) centered on the nucleus at position $\mathbf{R}_A$ are usually a better approximation to the atomic orbital:

$$f_{lm}^S(\xi;\mathbf{r}-\mathbf{R}_A)=N_l^S(\xi)p_{lm}(x,y,z)e^{-\xi|\mathbf{r}-\mathbf{R}_A|}, \tag{144}$$

where $N_l^S(\xi)$ is a normalization constant and $p_{lm}(x,y,z)$ is a polynom representing spherical harmonics. Atomic orbitals described by such functions form a so-called STO basis set. The STO have the advantage to correctly describe the nuclear cusp. However, it directly leads to computational issues, which are usually solved by approximating the STO by Gaussian-type orbitals (GTO):

$$f_{lm}^S\sim\sum_{i=1}^{k}f_{lm}^G \tag{145}$$

with

$$f_{lm}^{G}(\alpha; \mathbf{r} - \mathbf{R}_A) = N_l^G(\alpha) p_{lm}(x, y, z) e^{-\alpha|\mathbf{r}-\mathbf{R}_A|^2}, \qquad (146)$$

where $N_l^G(\alpha)$ is a normalization constant and the exposant α (as well as ξ in Eq. (144)) results from an optimisation of isolated atoms. Such an assembling of primitive Gaussian functions leads to a so-called contracted function. The whole set of contracted functions describing the atomic orbitals is called the contracted basis set, which is easier to handle numerically in comparison to the (larger) basis set composed of primitive functions. The approximated functions in Eq. (145) form a basis set called STO-kG, where k is the number of Gaussian functions used to describe the STO. Usually, $k = 3$ and go up to $k = 6$ and the basis is called minimal basis, because each atomic orbital is described by only one (approximate) STO. Those basis sets are however not sufficiently efficient to describe electronic correlation, and are only used for very big systems (in huge organic molecules or biochemical systems) where larger basis are out of reach in term of computational cost. To improve the performance of the basis, the next step is to multiply the number of approximate STO to describe the valence atomic orbitals. This leads to the valence double zeta (VDZ), triple zeta (VTZ), quadruple zeta (VTZ) basis set, etc. In a different notation introduced by Popler and coworkers, the VDZ basis set can be written as k-mnG, where k, m and n are contraction length of the core atomic orbitals and of the each "zeta" of the valence atomic orbitals, respectively. This notation has the advantage to specify the different contraction lengths used in the approximate STO functions describing valence atomic orbitals. One example is the VDZ basis 6-31G or the VTZ basis 6-311G. The improvement over the STO-kG basis sets is significant, but is often still insufficient. To add more flexibility, polarisation function are added, which are functions corresponding to a higher angular momentum l. Such corrections leads to the pVDZ, pVTZ and pVQZ basis sets. Using Popler's notation, one can specify the type of polarization function added, for instance 6-31G(d) for the carbon atom (or, equivalently, 6-31G*). Other improvements can be considered by adding diffuse functions (with a weak exponent α) and using atomic basis that already contain correlation effects between the electrons of the same atom leading to aug-cc-pVDZ, etc, where "aug" means augmented by diffuse functions and "cc" means correlation consistent.

Bibliography

[1] Y. Tokura, N. Nagaosa, *Science* **2000**, *288*, 462–468.

[2] A. J. Cohen, P. Mori-Sánchez, W. Yang, *Chem. Rev.* **2011**, *112*, 289–320.

[3] T. Helgaker, P. Jorgensen, J. Olsen, *Molecular electronic-structure theory*, John Wiley & Sons, **2014**.

[4] Q. Sun, G. K.-L. Chan, *Acc. Chem. Res.* **2016**, *49*, 2705–2712.

[5] R. G. Parr, W. Yang, Density-Functional Theory of Atoms and Molecules, vol. 16 of International series of monographs on chemistry, **1989**.

[6] S. Langhoff, *Quantum mechanical electronic structure calculations with chemical accuracy*, *Vol. 13*, Springer Science & Business Media, **2012**.

[7] M. Born, R. Oppenheimer, *Ann. Phys.* **1927**, *389*, 457.

[8] E. A. Hylleraas, *Z. Phys.* **1929**, *54*, 347–366.

[9] H. M. James, A. S. Coolidge, *J. Chem. Phys.* **1933**, *1*, 825–835.

[10] J. S. Sims, S. Hagstrom, *Phys. Rev. A* **1971**, *4*, 908–916.

[11] B. L. Hammond, W. A. Lester, P. J. Reynolds, *Monte Carlo methods in ab initio quantum chemistry*, *Vol. 1*, World Scientific, **1994**.

[12] D. R. Hartree in Mathematical Proceedings of the Cambridge Philosophical Society, *Vol. 24*, Cambridge University Press, **1928**, pp. 89–110.

[13] D. R. Hartree, *The calculation of atomic structures*, Wiley, **1957**.

[14] W. Pauli in *Writings on Physics and Philosophy*, Springer, **1994**, pp. 165–181.

[15] J. C. Slater, *Phys. Rev.* **1929**, *34*, 1293.

[16] J. C. Slater, *Phys. Rev.* **1930**, *35*, 210.

[17] V. Fock, *Z. Phys.* **1930**, *61*, 126–148.

[18] C. Møller, M. S. Plesset, *Phys. Rev.* **1934**, *46*, 618.

[19] M. A. Buijse, PhD thesis, Centrale Huisdrukkerij Vrije Universiteit Amsterdam, **1991**.

[20] D. K. Mok, R. Neumann, N. C. Handy, *J. Phys. Chem.* **1996**, *100*, 6225–6230.

[21] A. D. Becke, *J. Chem. Phys.* **2013**, *138*, 074109.

[22] E. Ramos-Cordoba, P. Salvador, E. Matito, *Phys. Chem. Chem. Phys.* **2016**, *18*, 24015.

[23] C. L. Benavides-Riveros, N. N. Lathiotakis, M. A. L. Marques, *Phys. Chem. Chem. Phys.* **2017**, *19*, 12655.

[24] Ł. Mentel, X. Sheng, O. Gritsenko, E. Baerends, *J. Chem. Phys.* **2012**, *137*, 204117.

[25] J. A. Pople, R. K. Nesbet, *J. Chem. Phys.* **1954**, *22*, 571–572.

[26] C. A. Coulson, I. Fischer, *Lond. Edinb. Dubl. Phil. Mag.* **1949**, *40*, 386–393.

[27] G. H. Booth, A. J. Thom, A. Alavi, *J. Chem. Phys.* **2009**, *131*, 054106.

[28] J. A. Pople, R. Seeger, R. Krishnan, *Int. J. Quantum Chem.* **1977**, *12*, 149–163.

[29] R. J. Bartlett, *Annu. Rev. Phys. Chem.* **1981**, *32*, 359–401.

[30] P. R. Taylor in *Lecture Notes in Quantum Chemistry II: European Summer School in Quantum Chemistry*, (Ed.: B. O. Roos), Springer Berlin Heidelberg, Berlin, Heidelberg, **1994**, pp. 125–202.

[31] M. Nooijen, K. Shamasundar, D. Mukherjee, *Mol. Phys.* **2005**, *103*, 2277–2298.

[32] R. J. Bartlett, M. Musiał, *Rev. Mod. Phys.* **2007**, *79*, 291.

[33] C. J. Stein, M. Reiher, *J. Chem. Theory Comput.* **2016**, *12*, 1760–1771.

[34] K. Andersson, P.-Å. Malmqvist, B. O. Roos, *J. Chem. Phys.* **1992**, *96*, 1218.

[35] C. Angeli, R. Cimiraglia, S. Evangelisti, T. Leininger, J.-P. Malrieu, *J. Chem. Phys.* **2001**, *114*, 10252.

[36] C. Angeli, R. Cimiraglia, J.-P. Malrieu, *J. Chem. Phys.* **2002**, *117*, 9138.

[37] P. G. Szalay, T. Müller, G. Gidofalvi, H. Lischka, R. Shepard, *Chem. Rev.* **2011**, *112*, 108–181.

[38] K. H. Marti, I. M. Ondik, G. Moritz, M. Reiher, *J. Chem. Phys.* **2008**, *128*, 014104.

[39] S. R. White, *Phys. Rev. Lett.* **1992**, *69*, 2863.

[40] S. R. White, *Phys. Rev. B* **1993**, *48*, 10345.

[41] S. R. White, R. L. Martin, *J. Chem. Phys.* **1999**, *110*, 4127–4130.

[42] S. Wouters, D. Van Neck, *Eur. Phys. J. D* **2014**, *68*, 272.

[43] N. Nakatani, S. Guo, *J. Chem. Phys.* **2017**, *146*, 094102.

[44] G. K.-L. Chan, S. Sharma, *Annu. Rev. Phys. Chem.* **2011**, *62*, 465–481.

[45] S. Sharma, G. K.-L. Chan, *J. Chem. Phys.* **2012**, *136*, 124121.

[46] S. Keller, M. Dolfi, M. Troyer, M. Reiher, *J. Chem. Phys.* **2015**, *143*, 244118.

[47] U. Schollwöck, *Ann. Phys.* **2011**, *326*, 96–192.

[48] G. K.-L. Chan, A. Keselman, N. Nakatani, Z. Li, S. R. White, *J. Chem. Phys.* **2016**, *145*, 014102.

[49] R. Olivares-Amaya, W. Hu, N. Nakatani, S. Sharma, J. Yang, G. K.-L. Chan, *J. Chem. Phys.* **2015**, *142*, 034102.

[50] S. Östlund, S. Rommer, *Phys. Rev. Lett.* **1995**, *75*, 3537.

[51] S. Rommer, S. Östlund, *Phys. Rev. B* **1997**, *55*, 2164.

[52] K. H. Marti, M. Reiher, *Mol. Phys.* **2010**, *108*, 501–512.

[53] G. K.-L. Chan, M. Head-Gordon, *J. Chem. Phys.* **2002**, *116*, 4462–4476.

[54] G. Moritz, B. A. Hess, M. Reiher, *J. Chem. Phys.* **2005**, *122*, 024107.

[55] S. F. Keller, M. Reiher, *CHIMIA Int. J. Quantum Chem.* **2014**, *68*, 200–203.

[56] G. E. Moore, *IEEE solid-state circuits society newsletter* **2006**, *20*, 33–35.

[57] R. R. Schaller, *IEEE spectrum* **1997**, *34*, 52–59.

[58] M. M. Waldrop, *Nature News* **2016**, *530*, 144.

[59] B. M. Boghosian, W. Taylor IV, *Physica D: Nonlinear Phenomena* **1998**, *120*, 30–42.

[60] C. Zalka in Proc. Royal Soc. Lond. A, *Vol. 454*, The Royal Society, **1998**, pp. 313–322.

[61] J. D. Whitfield, J. Biamonte, A. Aspuru-Guzik, *Mol. Phys.* **2011**, *109*, 735–750.

[62] J. R. McClean, J. Romero, R. Babbush, A. Aspuru-Guzik, *New J. Phys.* **2016**, *18*, 023023.

[63] M. Reiher, N. Wiebe, K. M. Svore, D. Wecker, M. Troyer, *Proc. Natl. Acad. Sci.* **2017**, 201619152.

[64] L. H. Thomas in Mathematical Proceedings of the Cambridge Philosophical Society, *Vol. 23*, Cambridge University Press, **1927**, pp. 542–548.

[65] E. Fermi, *Rend. Accad. Naz. Lincei* **1927**, *6*, 32.

[66] P. A. Dirac in Mathematical Proceedings of the Cambridge Philosophical Society, *Vol. 26*, Cambridge University Press, **1930**, pp. 376–385.

[67] P. Hohenberg, W. Kohn, *Phys. Rev.* **1964**, *136*, B864.

[68] E. H. Lieb, *Int. J. Quantum Chem.* **1983**, *24*, 243.

[69] M. Levy, *Phys. Rev. A* **1982**, *26*, 1200.

[70] M. Levy, *Proc. Natl. Acad. Sci.* **1979**, *76*, 6062–6065.

[71] P. W. Ayers, *Phys. Rev. A* **2006**, *73*, 012513.

[72] B. Senjean, M. Tsuchiizu, V. Robert, E. Fromager, *Mol. Phys.* **2017**, *115*, 48–62.

[73] K. Deur, L. Mazouin, E. Fromager, *Phys. Rev. B* **2017**, *95*, 035120.

[74] K. Deur, L. Mazouin, B. Senjean, E. Fromager, *Eur. Phys. J. B* **2018**, *91*, 162.

[75] B. Senjean, E. Fromager, *Phys. Rev. A* **2018**, *98*, 022513.

[76] W. Kohn, L. Sham, *Phys. Rev.* **1965**, *140*, A1133.

[77] J. D. Talman, W. F. Shadwick, *Phys. Rev. A* **1976**, *14*, 36.

[78] A. Görling, M. Levy, *Phys. Rev. A* **1994**, *50*, 196.

[79] S. Hirata, S. Ivanov, I. Grabowski, R. J. Bartlett, K. Burke, J. D. Talman, *J. Chem. Phys.* **2001**, *115*, 1635–1649.

[80] W. Yang, Q. Wu, *Phys. Rev. Lett.* **2002**, *89*, 143002.

[81] Q. Wu, W. Yang, *J. Chem. Phys.* **2003**, *118*, 2498–2509.

[82] Q. Wu, A. J. Cohen, W. Yang, *J. Chem. Phys.* **2005**, *123*, 134111.

[83] V. Staroverov, G. Scuseria, E. Davidson, *J. Chem. Phys.* **2006**, *124*, 141103–141103.

[84] T. Heaton-Burgess, F. A. Bulat, W. Yang, *Phys. Rev. Lett.* **2007**, *98*, 256401.

[85] F. A. Bulat, T. Heaton-Burgess, A. J. Cohen, W. Yang, *J. Chem. Phys.* **2007**, *127*, 174101.

[86] C. R. Jacob, *J. Chem. Phys.* **2011**, *135*, 244102.

[87] J. Harris, R. Jones, *J. Phys. F: Metal Physics* **1974**, *4*, 1170.

[88] D. C. Langreth, J. P. Perdew, *Solid State Commun.* **1975**, *17*, 1425–1429.

[89] O. Gunnarsson, *Phys. Rev. B* **1976**, *13*, 4274.

[90] J. Harris, *Phys. Rev. A* **1984**, *29*, 1648.

[91] A. Savin, F. Colonna, R. Pollet, *Int. J. Quantum Chem.* **2003**, *93*, 166–190.

[92] M. Levy, *Phys. Rev. A* **1991**, *43*, 4637.

[93] M. Levy, J. P. Perdew, *Phys. Rev. B* **1993**, *48*, 11638.

[94] K. Burke, M. Ernzerhof, J. P. Perdew, *Chem. Phys. Lett.* **1997**, *265*, 115–120.

[95] Y. Cornaton, O. Franck, A. M. Teale, E. Fromager, *Mol. Phys.* **2013**, *111*, 1275–1294.

[96] A. Teale, S. Coriani, T. Helgaker, *J. Chem. Phys.* **2009**, *130*, 104111.

[97] A. Görling, M. Levy, *Phys. Rev. B* **1993**, *47*, 13105.

[98] M. Ernzerhof, *Chem. Phys. Lett.* **1996**, *263*, 499–506.

[99] M. Seidl, J. P. Perdew, S. Kurth, *Phys. Rev. Lett.* **2000**, *84*, 5070.

[100] A. Teale, S. Coriani, T. Helgaker, *J. Chem. Phys.* **2010**, *132*, 164115.

[101] A. M. Teale, T. Helgaker, A. Savin, *J. Chin. Chem. Soc.* **2016**, *63*, 121–128.

[102] M. Seidl, J. P. Perdew, M. Levy, *Phys. Rev. A* **1999**, *59*, 51.

[103] M. Seidl, *Phys. Rev. A* **1999**, *60*, 4387.

[104] M. Seidl, P. Gori-Giorgi, A. Savin, *Phys. Rev. A* **2007**, *75*, 042511.

[105] P. Gori-Giorgi, M. Seidl, G. Vignale, *Phys. Rev. Lett.* **2009**, *103*, 166402.

[106] P. Gori-Giorgi, M. Seidl, *Phys. Chem. Chem. Phys.* **2010**, *12*, 14405–14419.

[107] F. Malet, P. Gori-Giorgi, *Phys. Rev. Lett.* **2012**, *109*, 246402.

[108] F. Malet, A. Mirtschink, J. C. Cremon, S. M. Reimann, P. Gori-Giorgi, *Phys. Rev. B* **2013**, *87*, 115146.

[109] A. Mirtschink, M. Seidl, P. Gori-Giorgi, *Phys. Rev. Lett.* **2013**, *111*, 126402.

[110] F. Malet, A. Mirtschink, C. Mendl, J. Bjerlin, E. Karabulut, S. Reimann, P. Gori-Giorgi, *Phys. Rev. Lett.* **2015**, *115*, 033006.

[111] F. Malet, A. Mirtschink, K. J. Giesbertz, L. O. Wagner, P. Gori-Giorgi, *Phys. Chem. Chem. Phys.* **2014**, *16*, 14551–14558.

[112] S. Vuckovic, L. O. Wagner, A. Mirtschink, P. Gori-Giorgi, *J. Chem. Theory Comput.* **2015**, *11*, 3153–3162.

[113] M. Seidl, P. Gori-Giorgi, *Phys. Rev. A* **2010**, *81*, 012508.

[114] P. A. M. Dirac, *Math. Proc. Camb. Philos. Soc* **1930**, *26*, 376.

[115] J. C. Slater, *Phys. Rev.* **1951**, *81*, 385.

[116] P.-F. Loos, P. M. Gill, *Wiley Interdiscip. Rev. Comput. Mol. Sci.* **2016**, *6*, 410–429.

[117] D. M. Ceperley, B. Alder, *Phys. Rev. Lett.* **1980**, *45*, 566.

[118] S. H. Vosko, L. Wilk, M. Nusair, *Can. J. Phys.* **1980**, *58*, 1200–1211.

[119] J. P. Perdew, Y. Wang, *Phys. Rev. B* **1992**, *45*, 13244.

[120] J. . Perdew, W. Yue, *Phys. Rev. B* **1986**, *33*, 8800.

[121] A. D. Becke, *Phys. Rev. A* **1988**, *38*, 3098.

[122] C. Lee, W. Yang, R. G. Parr, *Phys. Rev. B* **1988**, *37*, 785.

[123] J. P. Perdew, *Unified theory of exchange and correlation beyond the local density approximation*, *Vol. 11*, Akademie Verlag, Berlin, **1991**.

[124] J. P. Perdew, J. A. Chevary, S. H. Vosko, K. A. Jackson, M. R. Pederson, D. J. Singh, C. Fiolhais, *Phys. Rev. B* **1992**, *46*, 6671–6687.

[125] K. Burke, J. P. Perdew, Y. Wang in *Electronic Density Functional Theory*, Springer, **1998**, pp. 81–111.

[126] J. P. Perdew, K. Burke, M. Ernzerhof, *Phys. Rev. Lett.* **1996**, *77*, 3865.

[127] J. Tao, J. P. Perdew, V. N. Staroverov, G. E. Scuseria, *Phys. Rev. Lett.* **2003**, *91*, 146401.

[128] J. Sun, A. Ruzsinszky, J. P. Perdew, *Phys. Rev. Lett.* **2015**, *115*, 036402.

[129] J. P. Perdew, A. Zunger, *Phys. Rev. B* **1981**, *23*, 5048.

[130] J. P. Perdew, M. Levy, *Phys. Rev. Lett.* **1983**, *51*, 1884.

[131] A. D. Becke, *J. Chem. Phys.* **1993**, *98*, 1372–1377.

[132] A. Becke, *J. Chem. Phys.* **1993**, *98*, 5648–5652.

[133] C. Adamo, V. Barone, *J. Chem. Phys.* **1999**, *110*, 6158–6170.

[134] T. Yanai, D. P. Tew, N. C. Handy, *Chem. Phys. Lett.* **2004**, *393*, 51–57.

[135] A. Seidl, A. Görling, P. Vogl, J. Majewski, M. Levy, *Phys. Rev. B* **1996**, *53*, 3764.

[136] M. A. Marques, J. Vidal, M. J. Oliveira, L. Reining, S. Botti, *Phys. Rev. B* **2011**, *83*, 035119.

[137] M. Dion, H. Rydberg, E. Schröder, D. C. Langreth, B. I. Lundqvist, *Phys. Rev. Lett.* **2004**, *92*, 246401.

[138] S. Grimme, *J. Comp. Chem.* **2004**, *25*, 1463–1473.

[139] M. G. Medvedev, I. S. Bushmarinov, J. Sun, J. P. Perdew, K. A. Lyssenko, *Science* **2017**, *355*, 49–52.

[140] S. Grimme, *J. Chem. Phys.* **2006**, *124*, 034108.

[141] K. Sharkas, J. Toulouse, A. Savin, *J. Chem. Phys.* **2011**, *134*, 064113.

[142] E. Fromager, *J. Chem. Phys.* **2011**, *135*, 244106.

[143] H. Iikura, T. Tsuneda, T. Yanai, K. Hirao, *J. Chem. Phys.* **2001**, *115*, 3540–3544.

[144] J. Toulouse, F. Colonna, A. Savin, *Phys. Rev. A* **2004**, *70*, 062505.

[145] J. Toulouse, F. Colonna, A. Savin, *J. Chem. Phys.* **2005**, *122*, 014110.

[146] I. C. Gerber, J. G. Angyán, *Chem. Phys. Lett.* **2005**, *415*, 100–105.

[147] J. G. Angyán, I. C. Gerber, A. Savin, J. Toulouse, *Phys. Rev. A* **2005**, *72*, 012510.

[148] O. A. Vydrov, G. E. Scuseria, *J. Chem. Phys.* **2006**, *125*, 234109.

[149] J.-D. Chai, M. Head-Gordon, *Phys. Chem. Chem. Phys.* **2008**, *10*, 6615–6620.

[150] E. Goll, M. Ernst, F. Moegle-Hofacker, H. Stoll, *J. Chem. Phys.* **2009**, *130*, 234112.

[151] J. Heyd, G. E. Scuseria, M. Ernzerhof, *J. Chem. Phys.* **2003**, *118*, 8207.

[152] A. Savin, *Recent Developments and Applications of Modern Density Functional Theory*, Elsevier, Amsterdam, **1996**, p. 327.

[153] T. Leininger, H. Stoll, H.-J. Werner, A. Savin, *Chem. Phys. Lett.* **1997**, *275*, 151.

[154] J. P. Perdew, K. Schmidt in AIP Conference Proceedings, *Vol. 577*, AIP, **2001**, pp. 1–20.

[155] M. A. L. Marques, M. J. T. Oliveira, T. Burnus, *Computer Physics Communications* **2012**, *183*, 2272–2281.

[156] N. Mardirossian, M. Head-Gordon, *Mol. Phys.* **2017**, *115*, 2315–2372.

[157] C. J. Cramer, D. G. Truhlar, *Phys. Chem. Chem. Phys.* **2009**, *11*, 10757–10816.

[158] J. P. Perdew, R. G. Parr, M. Levy, J. L. Balduz Jr, *Phys. Rev. Lett.* **1982**, *49*, 1691.

[159] V. I. Anisimov, J. Zaanen, O. K. Andersen, *Phys. Rev. B* **1991**, *44*, 943.

[160] A. I. Liechtenstein, V. I. Anisimov, J. Zaanen, *Phys. Rev. B* **1995**, *52*, R5467.

[161] M. Cococcioni, S. de Gironcoli, *Phys. Rev. B* **2005**, *71*, 035105.

[162] P. Verma, D. G. Truhlar, *Theoretical Chemistry Accounts* **2016**, *135*, 182.

[163] B. Himmetoglu, A. Floris, S. Gironcoli, M. Cococcioni, *Int. J. Quantum Chem.* **2014**, *114*, 14–49.

[164] S. Ryee, M. J. Han, *arXiv:1709.03214* **2017**.

[165] X. Han, K. Song, L. Lu, Q. Deng, X. Xia, G. Shao, *J. Mater. Chem. C* **2013**, *1*, 3736–3746.

[166] Y.-C. Wang, Z.-H. Chen, H. Jiang, *J. Chem. Phys.* **2016**, *144*, 144106.

[167] D. A. Mazziotti, *Phys. Rev. Lett.* **2012**, *108*, 263002.

[168] R. A. Donnelly, R. G. Parr, *J. Chem. Phys.* **1978**, *69*, 4431–4439.

[169] R. A. Donnelly, *J. Chem. Phys.* **1979**, *71*, 2874–2879.

[170] A. E. DePrince III, *J. Chem. Phys.* **2016**, *145*, 164109.

[171] D. A. Mazziotti, *Phys. Rev. Lett.* **2016**, *117*, 153001.

[172] D. A. Mazziotti, *Phys. Rev. A* **2016**, *94*, 032516.

[173] D. Vanfleteren, D. Van Neck, P. Bultinck, P. W. Ayers, M. Waroquier, *J. Chem. Phys.* **2010**, *132*, 164111.

[174] J. Sandoval-Lira, M. Hô, R. Hernández-Esparza, J. C. Ramirez, J. M. Hernández-Pérez, *Theor. Chem. Acc.* **2016**, *135*, 1–10.

[175] T. L. Gilbert, *Phys. Rev. B* **1975**, *12*, 2111.

[176] P. W. Ayers, S. Golden, M. Levy, *J. Chem. Phys.* **2006**, *124*, 054101.

[177] A. A. Klyachko, *J. Phys.: Conference Series* **2006**, *36*, 72.

[178] M. Altunbulak, A. Klyachko, *Commun. Math. Phys.* **2008**, *282*, 287–322.

[179] R. Chakraborty, D. A. Mazziotti, *Int. J. Quantum Chem.* **2015**, *115*, 1305–1310.

[180] S. M. Valone, *J. Chem. Phys.* **1980**, *73*, 1344–1349.

[181] A. J. Coleman, *Rev. Mod. Phys.* **1963**, *35*, 668.

[182] A. Müller, *Phys. Lett. A* **1984**, *105*, 446.

[183] M. Buijse, E. Baerends, *Mol. Phys.* **2002**, *100*, 401–421.

[184] S. Sharma, J. K. Dewhurst, N. N. Lathiotakis, E. K. U. Gross, *Phys. Rev. B* **2008**, *78*, 201103.

[185] N. N. Lathiotakis, S. Sharma, J. K. Dewhurst, F. G. Eich, M. A. L. Marques, E. K. U. Gross, *Phys. Rev. A* **2009**, *79*, 040501.

[186] S. Goedecker, C. Umrigar, *Phys. Rev. Lett.* **1998**, *81*, 866.

[187] A. Holas, *Phys. Rev. A* **1999**, *59*, 3454.

[188] O. Gritsenko, K. Pernal, E. J. Baerends, *J. Chem. Phys.* **2005**, *122*, 204102.

[189] K. Pernal, K. J. Giesbertz in *Density-Functional Methods for Excited States*, Springer, **2015**, pp. 125–183.

[190] N. N. Lathiotakis, N. Helbig, A. Zacarias, E. K. U. Gross, *J. Chem. Phys.* **2009**, *130*, 064109.

[191] M. A. Marques, N. Lathiotakis, *Phys. Rev. A* **2008**, *77*, 032509.

[192] M. Piris, P. Otto, *Int. J. Quantum Chem.* **2003**, *94*, 317–323.

[193] P. Leiva, M. Piris, *J. Mol. Struct. THEOCHEM* **2005**, *719*, 63–67.

[194] M. Piris, *Int. J. Quantum Chem.* **2006**, *106*, 1093–1104.

[195] M. Piris, X. Lopez, J. Ugalde, *J. Chem. Phys.* **2007**, *126*, 214103.

[196] M. Piris, J. M. Ugalde, *J. Comput. Chem.* **2009**, *30*, 2078–2086.

[197] M. Piris, X. Lopez, F. Ruipérez, J. Matxain, J. Ugalde, *J. Chem. Phys.* **2011**, *134*, 164102.

[198] M. Piris, *Int. J. Quantum Chem.* **2013**, *113*, 620–630.

[199] M. Piris, *J. Chem. Phys.* **2014**, *141*, 044107.

[200] M. Piris, J. M. Ugalde, *Int. J. Quantum Chem.* **2014**, *114*, 1169–1175.

[201] E. Ramos-Cordoba, X. Lopez, M. Piris, E. Matito, *J. Chem. Phys.* **2015**, *143*, 164112.

[202] X. Lopez, M. Piris, F. Ruipérez, J. M. Ugalde, *J. Phys. Chem. A* **2015**, *119*, 6981–6988.

[203] I. Mitxelena, M. Piris, M. Rodriguez-Mayorga, *J. Phys. Condens. Matter* **2017**, *29*, 425602.

[204] W. Kutzelnigg, D. Mukherjee, *J. Chem. Phys.* **1999**, *110*, 2800–2809.

[205] J. Cioslowski, K. Pernal, *J. Chem. Phys.* **1999**, *111*, 3396–3400.

[206] N. N. Lathiotakis, N. Helbig, E. K. U. Gross, *Phys. Rev. B* **2007**, *75*, 195120.

[207] N. Helbig, N. N. Lathiotakis, M. Albrecht, E. K. U. Gross, *Europhys. Lett.* **2007**, *77*, 67003.

[208] N. Helbig, N. N. Lathiotakis, E. K. U. Gross, *Phys. Rev. A* **2009**, *79*, 022504.

[209] S. Sharma, S. Shallcross, J. K. Dewhurst, E. K. U. Gross, *arXiv:0912.1118v2* **2009**.

[210] E. N. Zarkadoula, S. Sharma, J. K. Dewhurst, E. K. U. Gross, N. N. Lathiotakis, *Phys. Rev. A* **2012**, *85*, 032504.

[211] M. Rodriguez-Mayorga, E. Ramos-Cordoba, M. Via-Nadal, M. Piris, E. Matito, *Phys. Chem. Chem. Phys.* **2017**, *19*, 24029–24041.

[212] T. T. Nguyen-Dang, E. V. Ludena, Y. Tal, *J. Mol. Struct. THEOCHEM* **1985**, *120*, 247–264.

[213] I. Mitxelena, M. Rodriguez-Mayorga, M. Piris, *Eur. Phys. J. B* **2018**, *91*, 109.

[214] P. A. Johnson, P. W. Ayers, P. A. Limacher, S. De Baerdemacker, D. Van Neck, P. Bultinck, *Comp. Theor. Chem.* **2013**, *1003*, 101.

[215] N. Lathiotakis, N. Gidopoulos, N. Helbig, *J. Chem. Phys.* **2010**, *132*, 084105.

[216] A. Schindlmayr, R. W. Godby, *Phys. Rev. B* **1995**, *51*, 10427.

[217] J. M. Bofill, P. Pulay, *J. Chem. Phys.* **1989**, *90*, 3637–3646.

[218] R. Requist, O. Pankratov, *Phys. Rev. B* **2008**, *77*, 235121.

[219] K. J. Giesbertz, A.-M. Uimonen, R. van Leeuwen, *arXiv:1804.09921* **2018**.

[220] F. Bruneval, PhD thesis, **2005**.

[221] E. Rebolini, PhD thesis, Paris 6, **2014**.

[222] V. Galitskii, A. Migdal, *Sov. Phys. JETP* **1958**, *7*.

[223] L. Reining, *WIREs Comput. Mol. Sci.* **2018**, *8*, e1344.

[224] L. J. Sham, M. Schlüter, *Phys. Rev. Lett.* **1983**, *51*, 1888.

[225] L. Sham, M. Schlüter, *Phys. Rev. B* **1985**, *32*, 3883.

[226] L. Hedin, *Phys. Rev.* **1965**, *139*, A796.

[227] F. Aryasetiawan, O. Gunnarsson, *Rep. Prog. Phys.* **1998**, *61*, 237.

[228] B. Holm, U. von Barth, *Phys. Rev. B* **1998**, *57*, 2108.

[229] P. Garcia-González, R. W. Godby, *Phys. Rev. B* **2001**, *63*, 075112.

[230] M. Gatti, F. Bruneval, V. Olevano, L. Reining, *Phys. Rev. Lett.* **2007**, *99*, 266402.

[231] F. Bruneval, *J. Chem. Phys.* **2012**, *136*, 194107.

[232] H. Jiang, *Int. J. Quantum Chem.* **2015**, *115*, 722–730.

[233] G. Pacchioni, *Catal. Lett.* **2015**, *145*, 80–94.

[234] Q. Ou, J. E. Subotnik, *J. Phys. Chem. A* **2016**, *120*, 4514–4525.

[235] R. Del Sole, L. Reining, R. Godby, *Phys. Rev. B* **1994**, *49*, 8024.

[236] P. Romaniello, S. Guyot, L. Reining, *J. Chem. Phys.* **2009**, *131*, 154111.

[237] I. C. Gerber, J. G. Ángyán, *J. Chem. Phys.* **2007**, *126*, 044103.

[238] E. Fromager, H. J. Aa. Jensen, *Phys. Rev. A* **2008**, *78*, 022504.

[239] J. Toulouse, I. C. Gerber, G. Jansen, A. Savin, J. G. Ángyán, *Phys. Rev. Lett.* **2009**, *102*, 096404.

[240] J. Toulouse, W. Zhu, J. G. Ángyán, A. Savin, *Phys. Rev. A* **2010**, *82*, 032502.

[241] R. Pollet, A. Savin, T. Leininger, H. Stoll, *J. Chem. Phys.* **2002**, *116*, 1250.

[242] E. Fromager, J. Toulouse, H. J. A. Jensen, *J. Chem. Phys.* **2007**, *126*, 074111.

[243] K. Pernal, *Phys. Rev. A* **2010**, *81*, 052511.

[244] D. R. Rohr, J. Toulouse, K. Pernal, *Phys. Rev. A* **2010**, *82*, 052502.

[245] K. Pernal, *J. Chem. Phys.* **2012**, *136*, 184105.

[246] A. Stoyanova, A. M. Teale, J. Toulouse, T. Helgaker, E. Fromager, *J. Chem. Phys.* **2013**, *139*, 134113.

[247] E. D. Hedegård, S. Knecht, J. S. Kielberg, H. J. Aa. Jensen, M. Reiher, *J. Chem. Phys.* **2015**, *142*, 224108.

[248] E. Fromager, S. Knecht, H. J. Aa. Jensen, *J. Chem. Phys.* **2013**, *138*, 084101.

[249] E. D. Hedegård, F. Heiden, S. Knecht, E. Fromager, H. J. A. Jensen, *J. Chem. Phys.* **2013**, *139*, 184308.

[250] E. Rebolini, J. Toulouse, A. M. Teale, T. Helgaker, A. Savin, *J. Chem. Phys.* **2014**, *141*, 044123.

[251] E. Rebolini, J. Toulouse, A. M. Teale, T. Helgaker, A. Savin, *Phys. Rev. A* **2015**, *91*, 032519.

[252] E. Rebolini, A. M. Teale, T. Helgaker, A. Savin, J. Toulouse, *Mol. Phys.* **2018**, 1–9.

[253] O. V. Gritsenko, S. J. A. Van Gisbergen, A. Gorling, E. J. Baerends, *J. Chem. Phys.* **2000**, *113*, 8478.

[254] N. T. Maitra, F. Zhang, R. J. Cave, K. Burke, *J. Chem. Phys.* **2004**, *120*, 5932.

[255] M. Casida, M. Huix-Rotllant, *Annu. Rev. Phys. Chem.* **2012**, *63*, 287.

[256] A. Dreuw, M. Head-Gordon, *J. Am. Chem. Soc.* **2004**, *126*, 4007–4016.

[257] E. K. U. Gross, L. N. Oliveira, W. Kohn, *Phys. Rev. A* **1988**, *37*, 2805.

[258] E. K. U. Gross, L. N. Oliveira, W. Kohn, *Phys. Rev. A* **1988**, *37*, 2809.

[259] L. Oliveira, E. Gross, W. Kohn, *Phys. Rev. A* **1988**, *37*, 2821.

[260] O. Franck, E. Fromager, *Mol. Phys.* **2014**, *112*, 1684.

[261] E. Pastorczak, N. I. Gidopoulos, K. Pernal, *Phys. Rev. A* **2013**, *87*, 062501.

[262] K. Pernal, N. I. Gidopoulos, E. Pastorczak in *Adv. Quantum Chem. Vol. 73*, Elsevier, **2016**, pp. 199–229.

[263] B. Senjean, S. Knecht, H. J. Aa. Jensen, E. Fromager, *Phys. Rev. A* **2015**, *92*, 012518.

[264] B. Senjean, E. D. Hedegård, M. M. Alam, S. Knecht, E. Fromager, *Mol. Phys.* **2016**, *114*, 968.

[265] M. M. Alam, S. Knecht, E. Fromager, *Phys. Rev. A* **2016**, *94*, 012511.

[266] M. M. Alam, K. Deur, S. Knecht, E. Fromager, *J. Chem. Phys.* **2017**, *147*, 204105.

[267] A. Savin, *J. Chem. Phys.* **2014**, *140*, 18A509.

[268] J. Toulouse, A. Savin, H.-J. Flad, *Int. J. Quantum Chem.* **2004**, *100*, 1047–1056.

[269] P. Gori-Giorgi, A. Savin, *Int. J. Quantum Chem.* **2009**, *109*, 1950–1961.

[270] E. Fromager, *Mol. Phys.* **2015**, *113*, 419.

[271] B. B. Miehlich, H. Stoll, A. Savin, *Mol. Phys.* **1997**, *91*, 527–536.

[272] J. Gräfenstein, D. Cremer, *Chem. Phys. Lett.* **1999**, *316*, 569.

[273] Y. Kurzweil, K. V. Lawler, M. Head-Gordon, *Mol. Phys.* **2009**, *107*, 2103–2110.

[274] P. Sharma, D. G. Truhlar, L. Gagliardi, *J. Chem. Theory Comput.* **2018**, *14*, 660–669.

[275] A. Savin, *Int. J. Quantum Chem.* **1988**, *34*, 59.

[276] C. Gutlé, A. Savin, *Phys. Rev. A* **2007**, *75*, 032519.

[277] P. Cortona, *Phys. Rev. B* **1991**, *44*, 8454.

[278] T. A. Wesolowski, A. Warshel, *J. Phys. Chem.* **1993**, *97*, 8050–8053.

[279] T. A. Wesolowski, J. Weber, *Chem. Phys. Lett.* **1996**, *248*, 71–76.

[280] N. Govind, Y. A. Wang, E. A. Carter, *J. Chem. Phys.* **1999**, *110*, 7677–7688.

[281] O. Roncero, A. Zanchet, P. Villarreal, A. Aguado, *J. Chem. Phys.* **2009**, *131*, 234110.

[282] S. Fux, C. R. Jacob, J. Neugebauer, L. Visscher, M. Reiher, *J. Chem. Phys.* **2010**, *132*, 164101.

[283] C. Huang, M. Pavone, E. A. Carter, *J. Chem. Phys.* **2011**, *134*, 154110.

[284] F. R. Manby, M. Stella, J. D. Goodpaster, T. F. Miller III, *J. Chem. Theory Comput.* **2012**, *8*, 2564–2568.

[285] R. C. Pennifold, S. J. Bennie, T. F. Miller III, F. R. Manby, *J. Chem. Phys.* **2017**, *146*, 084113.

[286] F. Libisch, M. Marsman, J. Burgdörfer, G. Kresse, *J. Chem. Phys.* **2017**, *147*, 034110.

[287] D. V. Chulhai, J. D. Goodpaster, *J. Chem. Theory Comput.* **2018**, *14*, 1928–1942.

[288] K. Jiang, J. Nafziger, A. Wasserman, *J. Chem. Phys.* **2018**, *148*, 104113.

[289] P. Huang, E. A. Carter, *Annu. Rev. Phys. Chem.* **2008**, *59*, 261–290.

[290] T. Klüner, N. Govind, Y. A. Wang, E. A. Carter, *J. Chem. Phys.* **2002**, *116*, 42–54.

[291] P. Huang, E. A. Carter, *J. Chem. Phys.* **2006**, *125*, 084102.

[292] K. Yu, F. Libisch, E. A. Carter, *J. Chem. Phys.* **2015**, *143*, 102806.

[293] A. S. P. Gomes, C. R. Jacob, L. Visscher, *Phys. Chem. Chem. Phys.* **2008**, *10*, 5353–5362.

[294] J. D. Goodpaster, T. A. Barnes, F. R. Manby, T. F. Miller III, *J. Chem. Phys.* **2012**, *137*, 224113.

[295] J. Neugebauer, M. J. Louwerse, E. J. Baerends, T. A. Wesolowski, *J. Chem. Phys.* **2005**, *122*, 094115.

[296] M. A. L. Marques, E. K. U. Gross, *Annu. Rev. Phys. Chem.* **2004**, *55*, 427.

[297] C. Huang, *J. Chem. Phys.* **2016**, *144*, 124106.

[298] M. H. Cohen, A. Wasserman, *J. Stat. Phys.* **2006**, *125*, 1121–1139.

[299] P. Elliott, K. Burke, M. H. Cohen, A. Wasserman, *Phys. Rev. A* **2010**, *82*, 024501.

[300] B. Senjean, N. Nakatani, M. Tsuchiizu, E. Fromager, *Phys. Rev. B* **2018**, *97*, 235105.

[301] B. Senjean, N. Nakatani, M. Tsuchiizu, E. Fromager, *arXiv:1806.06057* **2018**.

[302] K. Capelle, V. L. Campo Jr., *Phys. Rep.* **2013**, *528*, 91.

[303] J. H. de Boer, E. J. Verwey, *Proc. Phys. Soc.* **1937**, *49*, 59.

[304] M. Imada, A. Fujimori, Y. Tokura, *Rev. Mod. Phys.* **1998**, *70*, 1039.

[305] C. Grygiel, PhD thesis, Université de Caen, **2008**.

[306] J. Orenstein, A. Millis, *Science* **2000**, *288*, 468–474.

[307] T. Yanagisawa, M. Miyazaki, *EPL* **2014**, *107*, 27004.

[308] T. Yanagisawa, *Physics Procedia* **2015**, *65*, 5–8.

[309] T. Yanagisawa, *Adv. Cond. Matter Phys.* **2015**, *2015*.

[310] J. G. Bednorz, K. A. Müller, *Z. Phys. B Condensed Matter* **1986**, *64*, 189–193.

[311] J. G. Bednorz, K. A. Müller, *Rev. Mod. Phys.* **1988**, *60*, 585.

[312] N. F. Mott, *Proc. Phys. Soc. A* **1949**, *62*, 416.

[313] W. Kohn, *Phys. Rev.* **1964**, *133*, A171.

[314] N. Mott, *Rev. Mod. Phys.* **1968**, *40*, 677.

[315] F. Gebhard, *The Mott Metal-Insulator Transition*, Springer, **1997**.

[316] J. Hubbard, *Proc. R. Soc. London A* **1963**, *276*, 238–257.

[317] J. Hubbard, *Proc. R. Soc. London A* **1964**, *277*, 237–259.

[318] J. Hubbard, *Proc. R. Soc. London A* **1964**, *281*, 401.

[319] J. Hubbard, *Proc. R. Soc. London A* **542-560**, *285*, 238–257.

[320] E. H. Lieb, F. Y. Wu, *Phys. Rev. Lett.* **1968**, *20*, 1445.

[321] H. Bethe, *Ann. Phys.* **1928**, *392*, 55–129.

[322] A. Sommerfeld, *Z. Phys.* **1928**, *47*, 1–32.

[323] F. Bloch, *Z. Phys.* **1929**, *57*, 545–555.

[324] A. H. Wilson, *Proc. R. Soc. Lond. A* **1931**, *133*, 458–491.

[325] N. Mott, R. Peierls, *Proc. Phys. Soc.* **1937**, *49*, 72.

[326] N. Mott, *Can. J. Phys.* **1956**, *34*, 1356–1368.

[327] N. Mott, *Philos. Mag.* **1961**, *6*, 287–309.

[328] N. Mott, Metal-insulator Transition, **1990**.

[329] M. Capone, M. Civelli, S. Kancharla, C. Castellani, G. Kotliar, *Phys. Rev. B* **2004**, *69*, 195105.

[330] A. Fujimori, F. Minami, *Phys. Rev. B* **1984**, *30*, 957.

[331] J. Zaanen, G. Sawatzky, J. Allen, *Phys. Rev. Lett.* **1985**, *55*, 418.

[332] K.-O. Backlund, Deriving an extended one-band Hubbard model for cuprate superconductors, **2011**.

[333] A. Auerbach, *Interacting electrons and quantum magnetism*, Springer, **1994**.

[334] G. Morandi, P. Sodano, A. Tagliacozzo, V. Tognetti, *Field Theories for Low-Dimensional Condensed Matter Systems: Spin Systems and Strongly Correlated Electrons*, *Vol. 131*, Springer Science & Business Media, **2013**.

[335] D. J. Carrascal, J. Ferrer, J. C. Smith, K. Burke, *J. Phys. Condens. Matter* **2015**, *27*, 393001.

[336] S. Di Sabatino, J. A. Berger, L. Reining, P. Romaniello, *J. Chem. Phys.* **2015**, *143*, 024108.

[337] E. Kamil, R. Schade, T. Pruschke, P. E. Blöchl, *Phys. Rev. B* **2016**, *93*, 085141.

[338] D. J. Carrascal, J. Ferrer, N. Maitra, K. Burke, *arXiv:1802.09988* **2018**.

[339] J. C. Smith, A. Pribram-Jones, K. Burke, *Phys. Rev. B* **2016**, *93*, 245131.

[340] F. Sagredo, K. Burke, *arXiv:1806.03392* **2018**.

[341] C. Li, R. Requist, E. K. U. Gross, *J. Chem. Phys.* **2018**, *148*, 084110.

[342] O. Gunnarsson, K. Schönhammer, *Phys. Rev. Lett.* **1986**, *56*, 1968.

[343] K. Schönhammer, O. Gunnarsson, R. Noack, *Phys. Rev. B* **1995**, *52*, 2504.

[344] C. Verdozzi, *Phys. Rev. Lett.* **2008**, *101*, 166401.

[345] S. Kurth, G. Stefanucci, E. Khosravi, C. Verdozzi, E. K. U. Gross, *Phys. Rev. Lett.* **2010**, *104*, 236801.

[346] D. Karlsson, A. Privitera, C. Verdozzi, *Phys. Rev. Lett.* **2011**, *106*, 116401.

[347] G. Stefanucci, S. Kurth, *Phys. Rev. Lett.* **2011**, *107*, 216401.

[348] G. Xianlong, A.-H. Chen, I. Tokatly, S. Kurth, *Phys. Rev. B* **2012**, *86*, 235139.

[349] G. Stefanucci, S. Kurth, *Nano Lett.* **2015**, *15*, 8020–8025.

[350] S. Kurth, G. Stefanucci, *Phys. Rev. B* **2016**, *94*, 241103.

[351] J. Chayes, L. Chayes, M. B. Ruskai, *J. Stat. Phys.* **1985**, *38*, 497.

[352] R. López-Sandoval, G. Pastor, *Phys. Rev. B* **2000**, *61*, 1764.

[353] R. López-Sandoval, G. Pastor, *Phys. Rev. B* **2002**, *66*, 155118.

[354] R. López-Sandoval, G. Pastor, *Phys. Rev. B* **2004**, *69*, 085101.

[355] M. Saubanère, G. Pastor, *Phys. Rev. B* **2009**, *79*, 235101.

[356] M. Saubanère, G. Pastor, *Phys. Rev. B* **2011**, *84*, 035111.

[357] W. Töws, M. Saubanère, G. Pastor, *Theor. Chem. Acc.* **2014**, *133*, 1–15.

[358] D. Carrascal, J. Ferrer, J. Smith, K. Burke, *J. Phys. Condens. Matter* **2016**, *29*, 019501.

[359] N. Lima, L. Oliveira, K. Capelle, *Europhys. Lett.* **2002**, *60*, 601.

[360] N. A. Lima, M. F. Silva, L. N. Oliveira, K. Capelle, *Phys. Rev. Lett.* **2003**, *90*, 146402.

[361] K. Capelle, N. Lima, M. Silva, L. Oliveira in *The Fundamentals of Electron Density, Density Matrix and Density Functional Theory in Atoms, Molecules and the Solid State*, Springer, **2003**, p. 145.

[362] V. V. Franca, D. Vieira, K. Capelle, *New J. Phys.* **2012**, *14*, 073021.

[363] G. Xianlong, M. Polini, M. Tosi, V. L. Campo Jr, K. Capelle, M. Rigol, *Phys. Rev. B* **2006**, *73*, 165120.

[364] G. Xianlong, M. Rizzi, M. Polini, R. Fazio, M. P. Tosi, V. L. Campo Jr, K. Capelle, *Phys. Rev. Lett.* **2007**, *98*, 030404.

[365] M. Silva, N. Lima, A. L. Malvezzi, K. Capelle, *Phys. Rev. B* **2005**, *71*, 125130.

[366] A. Akande, S. Sanvito, *Phys. Rev. B* **2010**, *82*, 245114.

[367] V. Campo Jr, K. Capelle, *Phys. Rev. A* **2005**, *72*, 061602.

[368] G. Xianlong, *Phys. Rev. B* **2008**, *78*, 085108.

[369] G. Kotliar, S. Y. Savrasov, K. Haule, V. S. Oudovenko, O. Parcollet, C. A. Marianetti, *Rev. Mod. Phys.* **2006**, *78*, 865.

[370] Z.-J. Ying, V. Brosco, G. M. Lopez, D. Varsano, P. Gori-Giorgi, J. Lorenzana, *Phys. Rev. B* **2016**, *94*, 075154.

[371] Z.-J. Ying, V. Brosco, J. Lorenzana, *Phys. Rev. B* **2014**, *89*, 205130.

[372] J. P. Bergfield, Z.-F. Liu, K. Burke, C. A. Stafford, *Phys. Rev. Lett.* **2012**, *108*, 066801.

[373] Z.-F. Liu, J. P. Bergfield, K. Burke, C. A. Stafford, *Phys. Rev. B* **2012**, *85*, 155117.

[374] Z.-F. Liu, K. Burke, *Phys. Rev. B* **2015**, *91*, 245158.

[375] P. W. Anderson, *Phys. Rev.* **1961**, *124*, 1.

[376] M. R. Galpin, D. E. Logan, *Phys. Rev. B* **2008**, *77*, 195108.

[377] K. Zawadzki, L. N. Oliveira, *arXiv:1803.07112* **2018**.

[378] A. Georges, *C. R. Phys.* **2016**, *17*, 430–446.

[379] A. A. Kananenka, E. Gull, D. Zgid, *Phys. Rev. B* **2015**, *91*, 121111.

[380] T. N. Lan, A. A. Kananenka, D. Zgid, *J. Chem. Phys.* **2015**, *143*, 241102.

[381] T. N. Lan, A. A. Kananenka, D. Zgid, *J. Chem. Theory Comput.* **2016**, *12*, 4856.

[382] D. Zgid, E. Gull, *New J. Phys.* **2017**, *19*, 023047.

[383] T. N. Lan, A. Shee, J. Li, E. Gull, D. Zgid, *Phys. Rev. B* **2017**, *96*, 155106.

[384] T. N. Lan, S. Iskakov, D. Zgid, *arXiv:1806.01950* **2018**.

[385] A. Georges, G. Kotliar, *Phys. Rev. B* **1992**, *45*, 6479.

[386] A. Georges, G. Kotliar, W. Krauth, M. J. Rozenberg, *Rev. Mod. Phys.* **1996**, *68*.

[387] G. Kotliar, D. Vollhardt, *Phys. Today* **2004**, *57*, 53.

[388] K. Held, *Adv. Phys.* **2007**, *56*, 829.

[389] D. Vollhardt, K. Byczuk, M. Kollar in *Strongly Correlated Systems*, Springer, **2012**, pp. 203–236.

[390] P. Werner, M. Casula, *J. Phys. Condens. Matter* **2016**, *28*, 383001.

[391] R. M. Martin, L. Reining, D. M. Ceperley, *Interacting Electrons*, Cambridge University Press, **2016**.

[392] A. C. Hewson, *The Kondo problem to heavy fermions*, *Vol. 2*, Cambridge university press, **1997**.

[393] M. Caffarel, W. Krauth, *Phys. Rev. Lett.* **1994**, *72*, 1545.

[394] X. Y. Zhang, M. J. Rozenberg, G. Kotliar, *Phys. Rev. Lett.* **1993**, *70*, 1666–1669.

[395] M. Rozenberg, X. Zhang, G. Kotliar, *Phys. Rev. Lett.* **1992**, *69*, 1236.

[396] A. N. Rubtsov, V. V. Savkin, A. I. Lichtenstein, *Phys. Rev. B* **2005**, *72*, 035122.

[397] A. Fuhrmann, D. Heilmann, H. Monien, *Phys. Rev. B* **2006**, *73*, 245118.

[398] P. Werner, A. Comanac, L. De'Medici, M. Troyer, A. J. Millis, *Phys. Rev. Lett.* **2006**, *97*, 076405.

[399] K. Haule, *Phys. Rev. B* **2007**, *75*, 155113.

[400] D. Zgid, G. K.-L. Chan, *J. Chem. Phys.* **2011**, *134*, DOI `10.1063/1.3556707`.

[401] D. J. Garcia, K. Hallberg, M. J. Rozenberg, *Phys. Rev. Lett.* **2004**, *93*, 246403.

[402] M. Karski, C. Raas, G. S. Uhrig, *Phys. Rev. B* **2008**, *77*, 075116.

[403] T. Miyake, C. Martins, R. Sakuma, F. Aryasetiawan, *Phys. Rev. B* **2013**, *87*, 115110.

[404] M. Hettler, A. Tahvildar-Zadeh, M. Jarrell, T. Pruschke, H. Krishnamurthy, *Phys. Rev. B* **1998**, *58*, R7475.

[405] M. Hettler, M. Mukherjee, M. Jarrell, H. Krishnamurthy, *Phys. Rev. B* **2000**, *61*, 12739.

[406] A. Lichtenstein, M. Katsnelson, *Phys. Rev. B* **2000**, *62*, R9283.

[407] G. Kotliar, S. Y. Savrasov, G. Pálsson, G. Biroli, *Phys. Rev. Lett.* **2001**, *87*, 186401.

[408] O. Parcollet, G. Biroli, G. Kotliar, *Phys. Rev. Lett.* **2004**, *92*, 226402.

[409] T. Maier, M. Jarrell, T. Pruschke, M. H. Hettler, *Rev. Mod. Phys.* **2005**, *77*, 1027.

[410] P. Sun, G. Kotliar, *Phys. Rev. B* **2002**, *66*, 085120.

[411] S. Biermann, F. Aryasetiawan, A. Georges, *Phys. Rev. Lett.* **2003**, *90*, 086402.

[412] K. Karlsson, *J. Phys. Condens. Matter* **2005**, *17*, 7573.

[413] L. Boehnke, F. Nilsson, F. Aryasetiawan, P. Werner, *Phys. Rev. B* **2016**, *94*, 201106.

[414] F. Nilsson, F. Aryasetiawan, *Computation* **2018**, *6*, 26.

[415] F. Lechermann, A. Georges, A. Poteryaev, S. Biermann, M. Posternak, A. Yamasaki, O. Andersen, *Phys. Rev. B* **2006**, *74*, 125120.

[416] M. Karolak, G. Ulm, T. Wehling, V. Mazurenko, A. Poteryaev, A. Lichtenstein, *J. Electron Spectros. Relat. Phenomena* **2010**, *181*, 11–15.

[417] H. Park, A. J. Millis, C. A. Marianetti, *Phys. Rev. B* **2014**, *89*, 245133.

[418] G. Knizia, G. K.-L. Chan, *Phys. Rev. Lett.* **2012**, *109*, 186404.

[419] G. Knizia, G. K.-L. Chan, *J. Chem. Theory Comput.* **2013**, *9*, 1428–1432.

[420] I. W. Bulik, G. E. Scuseria, J. Dukelsky, *Phys. Rev. B* **2014**, *89*, 035140.

[421] B.-X. Zheng, G. K.-L. Chan, *Phys. Rev. B* **2016**, *93*, 035126.

[422] S. Wouters, C. A. Jiménez-Hoyos, Q. Sun, G. K.-L. Chan, *J. Chem. Theory Comput.* **2016**, *12*, 2706–2719.

[423] S. Wouters, C. A. Jiménez-Hoyos, G. K.-L. Chan in *Fragmentation*, Wiley-Blackwell, **2017**, Chapter 8, pp. 227–243.

[424] T. Ayral, T.-H. Lee, G. Kotliar, *Phys. Rev. B* **2017**, *96*, 235139.

[425] T. Tsuchimochi, M. Welborn, T. Van Voorhis, *J. Chem. Phys.* **2015**, *143*, 024107.

[426] D. A. Mazziotti, *J. Chem. Phys.* **2000**, *112*, 10125–10130.

[427] I. W. Bulik, W. Chen, G. E. Scuseria, *J. Chem. Phys.* **2014**, *141*, 054113.

[428] M. Welborn, T. Tsuchimochi, T. Van Voorhis, *J. Chem. Phys.* **2016**, *145*, 074102.

[429] R. Bulla, M. Potthoff, *Eur. Phys. J. B* **2000**, *13*, 257–264.

[430] M. Potthoff, *Phys. Rev. B* **2001**, *64*, 165114.

[431] E. Dagotto, *Rev. Mod. Phys.* **1994**, *66*, 763.

[432] P.-O. Löwdin, H. Shull, *Phys. Rev.* **1956**, *101*, 1730.

[433] W. Kutzelnigg, *Theoretica chimica acta* **1963**, *1*, 327–342.

[434] K. Yamada, *Prog. Theo. Phys.* **1975**, *53*, 970–986.

[435] P. Wiegmann, A. Tsvelick, *J. Phys. C: Solid State Phys.* **1983**, *16*, 2281.

[436] R. Konik, H. Saleur, A. Ludwig, *Phys. Rev. Lett.* **2001**, *87*, 236801.

[437] M.-C. Kim, E. Sim, K. Burke, *Phys. Rev. Lett.* **2013**, *111*, 073003.

[438] T. Dimitrov, H. Appel, J. I. Fuks, A. Rubio, *New J. Phys.* **2016**, *18*, 083004.

[439] H. Schweitzer, G. Czycholl, *Solid State Commun* **1990**, *74*, 735–742.

[440] D. Sénéchal, D. Perez, D. Plouffe, *Phys. Rev. B* **2002**, *66*, 075129.

[441] R. G. Parr, R. G. Pearson, *J. Am. Chem. Soc.* **1983**, *105*, 7512.

[442] P. Mori-Sánchez, A. J. Cohen, W. Yang, *Phys. Rev. Lett.* **2008**, *100*, 146401.

[443] J.-L. Bredas, *Mater. Horizons* **2014**, *1*, 17.

[444] E. Baerends, O. Gritsenko, R. Van Meer, *Phys. Chem. Chem. Phys.* **2013**, *15*, 16408–16425.

[445] E. Runge, E. K. Gross, *Phys. Rev. Lett.* **1984**, *52*, 997.

[446] J. I. Fuks, N. T. Maitra, *Phys. Chem. Chem. Phys.* **2014**, *16*, 14504–14513.

[447] N. T. Maitra, *J. Chem. Phys.* **2016**, *144*, 220901.

[448] N. T. Maitra, *J. Phys. Condens. Matter* **2017**, *29*, 423001.

[449] S. Kümmel, *Adv. Energy Mater.* **2017**, *7*, 1700440.

[450] G. Onida, L. Reining, A. Rubio, *Rev. Mod. Phys.* **2002**, *74*, 601.

[451] F. Sottile, M. Marsili, V. Olevano, L. Reining, *Phys. Rev. B* **2007**, *76*, 161103.

[452] A. K. Theophilou, *J. Phys. C: Solid State Phys.* **1979**, *12*, 5419.

[453] M. Levy, *Phys. Rev. A* **1995**, *52*, R4313.

[454] Z.-h. Yang, J. R. Trail, A. Pribram-Jones, K. Burke, R. J. Needs, C. A. Ullrich, *Phys. Rev. A* **2014**, *90*, 042501.

[455] Á. Nagy, *J. Phys. B: At. Mol. Opt. Phys.* **1996**, *29*, 389.

[456] N. I. Gidopoulos, P. G. Papaconstantinou, E. K. U. Gross, *Phys. Rev. Lett.* **2002**, *88*, 033003.

[457] E. Pastorczak, K. Pernal, *J. Chem. Phys.* **2014**, *140*, 18A514.

[458] Z.-h. Yang, A. Pribram-Jones, K. Burke, C. A. Ullrich, *Phys. Rev. Lett.* **2017**, *119*, 033003.

[459] T. Gould, S. Pittalis, *Phys. Rev. Lett.* **2017**, *119*, 243001.

[460] T. Gould, L. Kronik, S. Pittalis, *J. Chem. Phys.* **2018**, *148*, 174101.

[461] R. O. Jones, O. Gunnarsson, *Rev. Mod. Phys.* **1989**, *61*, 689.

[462] M. K. Y. Chan, G. Ceder, *Phys. Rev. Lett.* **2010**, *105*, 196403.

[463] R. G. Parr, L. J. Bartolotti, *J. Phys. Chem.* **1983**, *87*, 2810–2815.

[464] R. W. Godby, M. Schlüter, L. J. Sham, *Phys. Rev. B* **1987**, *36*, 6497.

[465] R. W. Godby, M. Schlüter, L. J. Sham, *Phys. Rev. B* **1988**, *37*, 10159.

[466] R. K. Nesbet, *Phys. Rev. A* **1997**, *56*, 2665.

[467] M. K. Harbola, *Phys. Rev. A* **1998**, *57*, 4253.

[468] G. K.-L. Chan, *J. Chem. Phys.* **1999**, *110*, 4710–4723.

[469] A. M. Teale, F. De Proft, D. J. Tozer, *J. Chem. Phys.* **2008**, *129*, 044110.

[470] E. M. Stoudenmire, L. O. Wagner, S. R. White, K. Burke, *Phys. Rev. Lett.* **2012**, *109*, 056402.

[471] W. Yang, A. J. Cohen, P. Mori-Sánchez, *J. Chem. Phys.* **2012**, *136*, 204111.

[472] T. Gould, J. Toulouse, *Phys. Rev. A* **2014**, *90*, 050502.

[473] A. Benitez, C. R. Proetto, *Phys. Rev. A* **2016**, *94*, 052506.

[474] M. J. P. Hodgson, E. Kraisler, E. K. U. Gross, *arXiv:1706.00586* **2017**.

[475] E. Baerends, *Phys. Chem. Chem. Phys.* **2017**, *19*, 15639–15656.

[476] E. J. Baerends, *J. Chem. Phys.* **2018**, *149*, 054105.

[477] A. J. Cohen, P. Mori-Sánchez, W. Yang, *Science* **2008**, *321*, 792–794.

[478] A. J. Cohen, P. Mori-Sánchez, W. Yang, *Phys. Rev. B* **2008**, *77*, 115123.

[479] N. Sai, P. F. Barbara, K. Leung, *Phys. Rev. Lett.* **2011**, *106*, 226403.

[480] L. Kronik, T. Stein, S. Refaely-Abramson, R. Baer, *J. Chem. Theory Comput.* **2012**, *8*, 1515–1531.

[481] S. Refaely-Abramson, S. Sharifzadeh, N. Govind, J. Autschbach, J. B. Neaton, R. Baer, L. Kronik, *Phys. Rev. Lett.* **2012**, *109*, 226405.

[482] R. A. Miranda-Quintana, P. W. Ayers, *Phys. Chem. Chem. Phys.* **2016**, *18*, 15070–15080.

[483] C. Li, J. Lu, W. Yang, *J. Chem. Phys.* **2017**, *146*, 214109.

[484] J. P. Perdew, W. Yang, K. Burke, Z. Yang, E. K. U. Gross, M. Scheffler, G. E. Scuseria, T. M. Henderson, I. Y. Zhang, A. Ruzsinszky, et al., *Proc. Natl. Acad. Sci.* **2017**, *114*, 2801–2806.

[485] F. Zhou, V. Ozolins, *arXiv:1710.08973* **2017**.

[486] X. Zheng, A. J. Cohen, P. Mori-Sánchez, X. Hu, W. Yang, *Phys. Rev. Lett.* **2011**, *107*, 026403.

[487] X. Zheng, T. Zhou, W. Yang, *J. Chem. Phys.* **2013**, *138*, 174105.

[488] C. Li, X. Zheng, A. J. Cohen, P. Mori-Sánchez, W. Yang, *Phys. Rev. Lett.* **2015**, *114*, 053001.

[489] X. Andrade, A. Aspuru-Guzik, *Phys. Rev. Lett.* **2011**, *107*, 183002.

[490] A. Görling, *Phys. Rev. B* **2015**, *91*, 245120.

[491] A. Thierbach, C. Neiss, L. Gallandi, N. Marom, T. Körzdörfer, A. Görling, *J. Chem. Theory Comput.* **2017**, *13*, 4726–4740.

[492] W. E. Pickett, S. C. Erwin, E. C. Ethridge, *Phys. Rev. B* **1998**, *58*, 1201.

[493] H. J. Kulik, M. Cococcioni, D. A. Scherlis, N. Marzari, *Phys. Rev. Lett.* **2006**, *97*, 103001.

[494] H. J. Kulik, N. Marzari, *J. Chem. Phys.* **2010**, *133*, 114103.

[495] F. Bruneval, M. A. Marques, *J. Chem. Theory Comput.* **2012**, *9*, 324–329.

[496] Y. Imamura, R. Kobayashi, H. Nakai, *J. Chem. Phys.* **2011**, *134*, 124113.

[497] V. Atalla, I. Y. Zhang, O. T. Hofmann, X. Ren, P. Rinke, M. Scheffler, *Phys. Rev. B* **2016**, *94*, 035140.

[498] T. Stein, H. Eisenberg, L. Kronik, R. Baer, *Phys. Rev. Lett.* **2010**, *105*, 266802.

[499] T. Stein, J. Autschbach, N. Govind, L. Kronik, R. Baer, *J. Chem. Phys. Lett.* **2012**, *3*, 3740–3744.

[500] E. Kraisler, L. Kronik, *Phys. Rev. Lett.* **2013**, *110*, 126403.

[501] E. Kraisler, L. Kronik, *J. Chem. Phys.* **2014**, *140*, 18A540.

[502] R. G. Parr, W. Yang, *J. Am. Chem. Soc.* **1984**, *106*, 4049–4050.

[503] Á. Nagy, *Int. J. Quantum Chem.* **1995**, *56*, 225.

[504] M. Levy, F. Zahariev, *Phys. Rev. Lett.* **2014**, *113*, 113002.

[505] P.-F. Loos, P. M. W. Gill, *Phys. Rev. Lett.* **2009**, *103*, 123008.

[506] L. N. Bardeen, L. N. Cooper, J. R. Schrieffer, *Phys. Rev.* **1957**, *108*, 1175–1204.

[507] P. R. Surján in *Correlation and localization*, Springer, **1999**, p. 63.

[508] A. C. Hurley, J. E. Lennard-Jones, J. A. Pople, *Proc. R. Soc. Lond. A* **1953**, *220*, 446.

[509] W. Kutzelnigg, *J. Chem. Phys.* **1964**, *40*, 3640.

[510] L. Bytautas, T. M. Henderson, C. A. Jiménez-Hoyos, J. K. Ellis, G. E. Scuseria, *J. Chem. Phys.* **2011**, *135*, 044119.

[511] F. Weinhold, E. B. Wilson Jr, *J. Chem. Phys.* **1967**, *46*, 2752–2758.

[512] D. M. Silver, *J. Chem. Phys.* **1969**, *50*, 5108.

[513] P. A. Limacher, P. W. Ayers, P. A. Johnson, S. De Baerdemacker, D. Van Neck, P. Bultinck, *J. Chem. Theory Comput.* **2013**, *9*, 1394.

[514] A. J. Coleman, *J. Math. Phys.* **1965**, *6*, 1425–1431.

[515] T. Stein, T. M. Henderson, G. E. Scuseria, *J. Chem. Phys.* **2014**, *140*, 214113.

[516] T. M. Henderson, I. W. Bulik, G. E. Scuseria, *J. Chem. Phys.* **2015**, *142*, 214116.

[517] I. W. Bulik, T. M. Henderson, G. E. Scuseria, *J. Chem. Theory Comput.* **2015**, *11*, 3171.

[518] K. Boguslawski, P. Tecmer, P. W. Ayers, P. Bultinck, S. De Baerdemacker, D. Van Neck, *Phys. Rev. B* **2014**, *89*, 201106.

[519] I. Røeggen in *Correlation and Localization*, Springer, **1999**, pp. 89–103.

[520] E. Rosta, P. R. Surján, *J. Chem. Phys.* **2002**, *116*, 878.

[521] M. Kobayashi, Á. Szabados, H. Nakai, P. R. Surján, *J. Chem. Theory Comput.* **2010**, *6*, 2024.

[522] M. Piris, *J. Chem. Phys.* **2013**, *139*, 064111.

[523] K. Boguslawski, P. Tecmer, *J. Chem. Theory Comput.* **2017**, *13*, 5966.

[524] M. Piris, *Phys. Rev. Lett.* **2017**, *119*, 063002.

[525] W. Kutzelnigg, *Chem. Phys.* **2012**, *401*, 119.

[526] T. Zoboki, Á. Szabados, P. R. Surján, *J. Chem. Theory Comput.* **2013**, *9*, 2602–2608.

[527] K. Pernal, *J. Chem. Theory Comput.* **2014**, *10*, 4332.

[528] A. J. Garza, I. W. Bulik, T. M. Henderson, G. E. Scuseria, *J. Chem. Phys.* **2015**, *142*, 044109.

[529] A. J. Garza, I. W. Bulik, T. M. Henderson, G. E. Scuseria, *Phys. Chem. Chem. Phys.* **2015**, *17*, 22412.

[530] B. Senjean, N. Nakatani, E. Fromager, *to be submitted* **2018**.

[531] K. Pernal, *Phys. Rev. Lett.* **2018**, *120*, 013001.

[532] P. A. Limacher, T. D. Kim, P. W. Ayers, P. A. Johnson, S. De Baerdemacker, D. Van Neck, P. Bultinck, *Mol. Phys.* **2014**, *112*, 853.

[533] R. van Meer, O. V. Gritsenko, E. J. Baerends, *J. Chem. Phys.* **2018**, *148*, 104102.

[534] R. Gebauer, M. H. Cohen, R. Car, *arXiv:1309.3929* **2013**.

[535] F. A. Evangelista, *J. Chem. Phys.* **2018**, *149*, 030901.

[536] A. Szabo, N. S. Ostlund, *Modern quantum chemistry: introduction to advanced electronic structure theory*, Courier Dover Publications, **2012**.